Review Article

A Systematic Review on Biochemical and Pharmacological Properties of the Active Phytochemicals Present in *Aegle marmelos* (L).

Mrudhulla Sivakumar[1], Pariyaporn Itsaranuwat[2], Narendhirakannan RT[1,*]

[1]Department of Biochemistry, Kongunadu Arts and Science College (Autonomous), G.N. Mills, Coimbatore, Tamil Nadu, INDIA.
[2]Department of Biotechnology, Mahasarakham University, Mahasarakham, THAILAND.

Submission Date: 09-05-2024; Revision Date: 14-06-2024; Accepted Date: 25-07-2024.

ABSTRACT

Aim: Medicinal plant research is becoming increasingly prevalent since it is devoid of pollution, toxins and adverse effects. In recent years, it has come to light that a variety of ailments can be treated with plant-derived compounds from fruits, seeds, leaves, bark, etc. *Aegle marmelos* (Bael tree) is an important medicinal as well as a sacred tree with diverse therapeutic values. This review is to present current knowledge on the ethnomedicinal applications, nutritional composition, bioactive constituents and pharmacological activity of *A. marmelos* to validate its therapeutic potential. **Materials and Methods:** Out of 120 articles identified, 62 met the inclusion criteria, forming the basis for synthesizing data on ethnomedicinal uses, bioactive constituents and pharmacological activities of *A. marmelos*, contributing to a holistic understanding of its therapeutic potential. The study employed a robust methodology, including a comprehensive literature search across prominent databases using keywords related to *Aegle marmelos* and also its medicinal properties. **Results:** These research and review articles provided about the pharmacological properties of *A. Marmelos*. It has been utilized to treat several health issues in ancient medicinal system, including diarrhea, diabetes, fever, ulcers, inflammations and bacterial infections. The bioactive metabolites including alkaloids, terpenoids, saponins, pectins, steroids, flavonoids, tannins, carotenoids and phenolics. **Conclusion:** Based on our studies, *in vitro* as well as *in vivo* investigations revealed that *A. marmelos* has therapeutic benefits such as antioxidant, analgesic, anti-inflammatory, antidiarrheal, cardioprotective, anticancer and antimicrobial properties that proved its historical uses.

Keywords: *Aegle marmelos*, Bael, Phytochemicals, Medicinal plant.

Correspondence:
Dr. Narendhirakannan RT
Assistant Professor, Department of Biochemistry, Kongunadu Arts and Science College (Autonomous), G.N. Mills, Coimbatore-641029, Tamil Nadu, INDIA.

Email: rtnaren@kongunaducollege.ac.in

INTRODUCTION

Aegle marmelos (Linn.), belongs to the family Rutaceae, which is one of the prominent and underutilized aromatic medicinal trees of Indian heritage.[1] It is popularly known as the Bael fruit tree and the other common names include Indian quince, Bengal quince, golden apple and holy fruit. It is a moderate-sized, slender, slow-growing, tough tropical tree. It grows to an elevation of 1200 m in the western Himalayas and is found on Andaman Island and it is dispersed across deciduous woods of India.[2] *A. marmelos* is endemic to Northern India, although it can also be found in Bangladesh, Ceylon, Burma, Indo-China and Thailand.[3] Hindus often regard this tree as sacred because they offer its leaves when they worship Lord Shiva. Different parts of this tree at various stages of maturation are utilized as ethnomedicine to treat a variety of human as well as animal diseases. As far back as 800 B.C., this tree is recorded in prehistoric literature. It is planted all over India because of its mythological significance and is primarily grown close

SCAN QR CODE TO VIEW ONLINE

www.ajbls.com

DOI: 10.5530/ajbls.2024.13.32

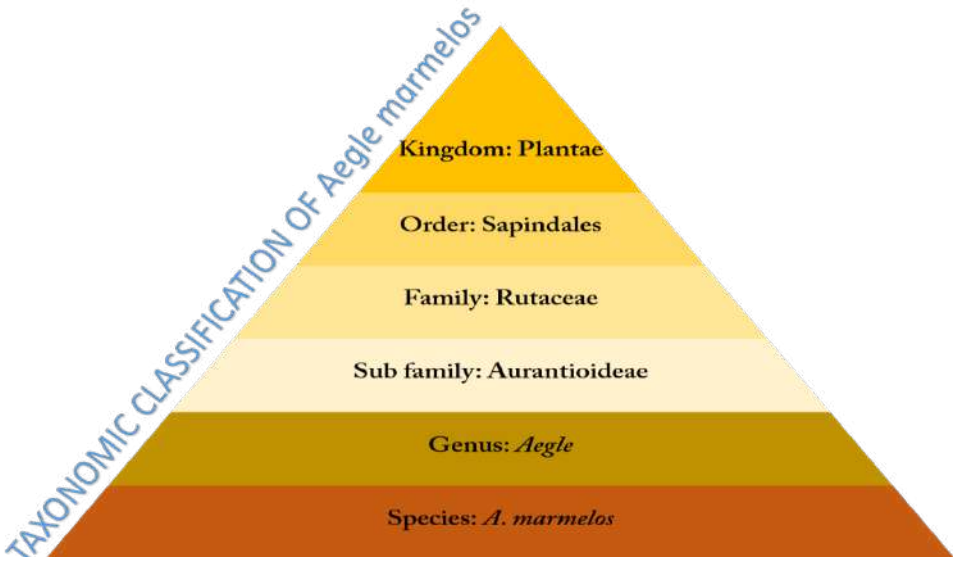

Figure 1: Taxonomic classification of *A. marmelos.*

to temples.[4] In this review, we have summarized the botanical description, therapeutic uses, non-therapeutic uses, phytochemistry and pharmacological activities of *A. marmelos*. Figure 1 represents the taxonomic classification of *A. marmelos*.

MATERIALS AND METHODS

Literature Search Strategy

A broad search was executed across multiple online databases, comprising Scopus, Web of Science, PubMed and Google Scholar. The search strategy involved keywords related to *Aegle marmelos*, ethnomedicinal applications, nutritional composition, bioactive constituents and pharmacological activity.

Eligibility criteria

Eligibility of articles was determined based on predefined criteria for inclusion and exclusion. Inclusion criteria encompassed studies focusing on ethnomedicinal uses, phytochemical composition and pharmacological properties of *A. marmelos*. Only peer-reviewed articles written in English were taken into consideration.

Data Extraction

Data relevant to ethnomedicinal applications, bioactive constituents and pharmacological activities of *A. marmelos* were extracted from selected articles. Information on methodologies, results and conclusions was systematically recorded to ensure accuracy and completeness. The compiled data were synthesized to offer a holistic perspective into the ethnomedicinal applications and pharmacological prospects of *A. marmelos*. Data synthesis involved categorization based on the types of bioactive compounds identified and the observed pharmacological activities. The findings were critically analyzed to validate the therapeutic potential of *A. marmelos* and identify areas for further research.

RESULTS

The exploration of Google Scholar, Web of Science, PubMed and Scopus resulted in the identification of 120 articles. Following the assessment of eligibility, 62 articles were identified as meeting the inclusion criteria and were thus included in the review. These articles collectively provided comprehensive insights into the ethnomedicinal applications, nutritional composition, bioactive constituents and pharmacological activities of *A. marmelos*.

Nutritional Properties

The nutrients of *A. marmelos* are particularly advantageous to human health, as evidenced by numerous research investigations. Recent studies have examined the nutritional advantages of *A. marmelos* as well as its low-cost manufacturing and marketing to promote environmental health. The major part of *A. marmelos* is water, ranges from 60% to 65%, followed by carbohydrate, sugars, fibers and other compositions includes vitamins, minerals, amino acids and various fatty acids.[5] Bael helps prevent rancidity and colour loss since as it holds a significant quantity of vitamin A, B and C all and these can serve as antioxidants.[6]

A. marmelos, like other fruits, provides varying nutritional contents based on the maturation stages. Bael seed contains a greater percentage of fat (14.94%).[7]

PHYTOCHEMISTRY

The GCMS profiling of alcoholic extract of *A. marmelos* leaves showed the existence of the bioactive compounds such as p-cymene, 1-dodecanol, Cyclooctasiloxane, Dotriacontane, Phthalic acid, Hexadecanoic acid, Cyclodecasiloxane, Oleic acid, Octadecanoic acid, Alpha-Neodene, Phenol, Nonahexacontanoic acid, Nonacosane, Benzoic acid, 13-docosenoic acid, Retinoic acid and Farnesyl acetone.[8] The fatty acid- derivatives like decanoic acid, methyl ester, octanoic acid ester, Pentadecanoic acid, methyl ester, 9-Hexadecanoic acid, methyl ester, Octadecatrienoic acid, ethyl ester, Eicosanoic acid, methyl ester were reported in *A. marmelos* seed oil.[9] The hydro-alcoholic extract of *A. marmelos* unripe fruit contains gallic acid and quercetin.[10] The study done by Shakya war *et al*.[11] concluded that the phytochemicals such as tannins, alkaloids, proteins, carbohydrates, starch, resin, coumarins, tannins, phlobatannins, polyphenols, vitamin C, steroids and glycosides have existed in the different parts of *A. marmelos* fruits such as pericarp and pulp.

PHARMACOLOGICAL ACTIVITIES

The pharmacological potential of *A. marmelos*, encompassing antioxidant, inflammation-suppressing, hypoglycemic, anti-cancer, insecticidal, anti-diarrheal properties, offers a multifaceted approach to therapeutic interventions (Figure 2).

ANTIOXIDANT EFFECTS

The methanol extracts of leaves, seeds, ripe fruit and half-ripe fruit of *A. marmelos* were found to scavenge DPPH and Nitric oxide radicals in a dose-dependent manner. Maximum DPPH radical scavenging activity (IC_{50}=251.2 µg/mL) was shown by a methanol extract from a half-ripe fruit.[12] From the earlier research, it was able to draw the conclusion that *A. marmelos* enhances the antioxidant state in the tissues of diabetic rats. It may be suggested that the mechanism of action of *A. marmelos* seems to be similar to glibenclamide action.[13] Furthermore, in an effort to discover an alternate form of treatment for different ailments, the therapeutic value of this plant is being investigated extensively.[14] A previous work revealed that *A. marmelos* showed a neuroprotective effect against STZ-induced oxidative imbalance and cognitive deficits in male rats, which has proven its anti-oxidant activity.[15] According to Surolia

- ANTIOXIDANT EFFECTS
- ANTI-INFLAMMATORY EFFECTS
- ANTI-CANCER EFFECTS
- ANTI-GLYCEMIC EFFECTS
- ANALGESIC EFFECTS
- ANTIMICROBIAL EFFECTS
- HEPATOPROTECTIVE EFFECTS
- CARDIOPROTECTIVE EFFECTS

Figure 2: Pharmacological activities.

et al.[16] *A. marmelos* pulp pectin has the highest percentage of DPPH radical inhibition when compared to *A. marmelos* shell and seed pectin at all concentrations.

ANTICANCER EFFECTS

The anticancer activity against gastric cancer cells was studied previously by Sampath *et al.*[17] showed an IC_{50} value of 40.33 µg/mL that concluded the synthesized AgNPs from *A. marmelos* can act as a novel anticancer agent. The anti-cancer potency of the *A. marmelos* fruit pulp (aqueous extract) was evaluated using an MTT assay, which shed light on the inhibitory activity (IC_{50}=47.92 µg/mL) against the Breast cancer cells (MCF-7). The study provided promising guidelines regarding the potential uses of *A. marmelos* as an anticancer agent.[18] The substantial anti-cancer benefits of methanol and acetone extracts from *A. marmelos* on HEp-2 and MDA-MB-231, while protecting normal Vero cells.[19] The ethanol extract of fruit pulp of *A. marmelos* exhibited remarkable anti-oncogenic effects against the DMBA-induced breast cancer mice model. This study also demonstrated that the pulp had considerably reduced the size of the mammary tumour along with a significant decrease in biomarkers in serum like malondialdehyde, glucose and TNF-α level.[20]

Topical application of *A. marmelos* bark extract resulted in a considerable increase in the average latent period of tumour development, a significant decrease in tumor volume, tumour frequency and the overall number of papillomas and also a substantial reduction in the concentration of glutathione, were observed in 7,12-dimethylbenz[a]anthracene-induced skin papilloma mice model.[21] The results of the study carried out by Kumar *et al.*,[22] demonstrated the anti-ocnogenic property of the leaves of *A. marmelos* extracted using methanol against MCF-7 cells. The therapeutic effectiveness of an anticancer drug depends on its capacity to prevent the growth of tumours both in their early and later stages of formation.

ANTI-BACTERIAL EFFECTS

A. marmelos plays a vital in herbal medicine and is far more beneficial and secure than synthetic compounds. The *A. marmelos* fruits extracted using various solvents inhibited the growth of *Bacillus subtilis*, *Escherichia coli* and *Staphylococcus aureus*.[23] The methanol as well as chloroform derived leaves extracts showed excellent bactericidal effects against the gram-positive as gram-negative bacteria. The study suggested concentration-dependent anti-bacterial activity.[24] The *A. marmelos* leaves methanolic and acetone extract revealed substantial anti-bacterial action against tested microorganisms. *Serratia marcescens* exhibited the highest sensitivity among the tested organisms, as indicated by significant zones of inhibition across all four *A. marmelos* leaf extracts.[19] Interestingly, the bactericidal property of the synthesized nanoparticles was effective against the microorganisms like *Staphylococcus aureus*, *Escherichia coli*, *Aeromonas hydrophila*, *Pseudomonas aeruginosa* and *Streptococcus pyogenes*.[25] The extraction of *A. marmelos* leaves and fruit was carried out using ethanol, hexane and distilled water respectively. This study elicited that the ethanol extract had effectively inhibited the multi-drug resistant *Escherichia coli* than the aqueous and hexane extracts.[26]

ANTI-FUNGAL EFFECTS

The acetone, aqueous, methanol and chloroform extract of *A. marmelos* fruits exhibited fungicidal activity against *Candida albicans* (MTCC-227) and *Aspergillus brasiliensis* (MTCC-1344).[23] The essential oil extracted from the *A. marmelos* leaves possess anti-fungal activity, which was proven by the zone of inhibition with a diameter of 30 mm formed against the test organisms such as *Candida albicans* and *Aspergillus niger* respectively.[22] Significant fungicidal activity was exhibited against the *Fusarium oxysporum*, followed by *Pestalotia foe dans* and *Paecilomyces variotii* by the various concentrations (25, 50 and 75 µg/mL) of *A. marmelos* leaves extract.[28] *A. marmelos* extract completely inhibited the mycelial formation of *Pythium debaryanum* at the concentration of 1 mL concentration and so the methanol extract of *A. marmelos* leaves and fruits were recorded with a maximum inhibition of fungal growth.[29] The previous reports of Sriramulu and Sumathi[30] demonstrated the fungicidal effects of Iron oxide nanoparticles synthesized from *A. marmelos* against the phytopathogen *Fusarium solani* (12±0.53 mm), isolated from soil.

ANTI-VIRAL EFFECTS

The Seselin isolated from *A. marmelos* showed promising antiviral activity against (BmNPV) *Bombyx mori nucleopolyhedrovirus*.[31] *In silico* studies by Andleeb *et al.*,[32] revealed the good binding affinity of Quercetin, catechin and marmenol found in *A. marmelos* towards the HN Protein of NDV (Newcastle Disease Virus). The compound seselin of *A. marmelos* demonstrated the strongest receptor interaction with spike protein, main protease and its free enzymes of SARS CoV-2.[33]

ANTI-ULCER EFFECTS

A. marmelos have been shown to possess antiulcer activity against experimentally induced ulcer models. The anti-ulcer activity of an aqueous extract of *A. marmelos* leaves was examined in Wistar rats with ulcers induced using indomethacin. The effects of 175 mg/kg and 350 mg/kg of *A. marmelos* extract on gastrointestinal volume, acidity as well as ulcer index were noted, which was statistically significant ($p<0.01$) than the control group.[34] The ulcer protection percentage of ethanolic extract of *A. marmelos* leaves was found to be 56.33% in the ethanol-induced gastric ulcer model, which was higher than the standard drug Omeprazole (50.44%).[35] *A. marmelos* fruit extract has protective effects against the Aspirin-Induced Gastro-Duodenal ulcer in Albino mice Model.[36] The findings of Sharma *et al*.[37] showed the anti-ulcer action of aqueous and methanol extract of *A. marmelos* seed against the Indomethacin Induced and Stress-induced Ulceration models respectively.

ANTI-GLYCEMIC EFFECTS

Patients with Non-Insulin Dependent Diabetes Mellitus who were taking sulfonylurea at a dose of 5 or 10 mg/day had a decrease in their blood and urine glucose levels after taking *A. marmelos* extract for eight weeks.[38] Furthermore, the previous study of Arumugam *et al*.,[38] also evidenced the potent anti-diabetic activity of *A. marmelos* extract. Significant reductions the glycemic index were achieved in streptozotocin-induced diabetes in rabbits treated with extracts of *A. marmelos* leaves and calluses. Moreover, the bark extract of *A. marmelos* also showed anti-diabetic activity in the diabetic rats.[40] Likewise, the fruit extract of *A. marmelos* exhibited hypoglycemic activity in alloxan-induced diabetes in Male Sprague Dawley rats.[41] An aqueous extract of *A. marmelos* fruit administered orally two times a day for four weeks at a dosage of 250 mg/kg body weight effectively lowered the blood glucose levels of streptozotocin-induced diabetic rats. Comparing this dosage to the usual medication glibenclamide, the findings were effective.[42]

ANTI-DIARRHEAL EFFECTS

Many medications are prepared using fruit, roots, bark, leaves, ripe fruit rind and flowers. *A. marmelos* has been employed historically for a variety of ethnobotanical uses. Based on the data gathered, it appears that *A. marmelos* has anti-diarrheal properties.[43] *A. marmelos* decoction proved beneficial in treating a range of infectious diarrheal diseases brought on by *Vibrio cholerae, Shigella flexneri*, Enteropathogenic *Escherichia coli*, *Enter invasive Escherichia coli*, Heat-labile toxin producing enterotoxigenic *Escherichia coli* and, to a lesser degree, rotaviral infections and giardiasis.[44]

ANTI-INFLAMMATORY EFFECTS

A. marmelos root bark aqueous extract significantly decreased inflammation in paw edema induced by carrageenan and granuloma induced by cotton pellets, with the percentage of inhibition of 46% and 9.2%, respectively.[45] Young (2 and 3-year-old) roots from Gujarat and young (1-year-old) roots from Odisha displayed the maximum anti-inflammatory effects by inhibiting pro-inflammatory cytokines and enhanced the anti-inflammatory cytokines like IL-2. *A. marmelos* extracts' anti-inflammatory properties were found to be similar to those of mature stem and root barks when tested *in vivo* on roots, stems and leaves.[46] The phytocompound Marmelosin, from the *A. marmelos* elicited anti-inflammatory effects.[47] The study by Kumari *et al*.[48] demonstrated that the dried flowers extract of *A. marmelos* displayed a notable increase in the infiltrating of peritoneal cells in rats, reduction of Nitric oxide generation by rat peritoneal cells and suppression of urticaria on the rat's skin following histamine injection.

INSECTICIDAL EFFECTS

The essential oil extracted from the *A. marmelos* showed insecticidal effects against the stored grain pests.[49] Interestingly, the ovicidal, larvicidal, adulticidal and repellant effects of the essential oil from the *A. marmelos* leaves were examined against the insects *Aedes aegypti* and *Culex quinquefasciatus*.[50] Various concentrations of the petroleum ether, aqueous, methanol and ethanol extract of *A. marmelos* leaves dramatically decreased the oviposition and adult emergence of *Callosobruchus chinensis*.[51]

ANALGESIC EFFECTS

The study done by Shankarananth *et al*.[52] demonstrated the analgesic activity of *A. marmelos*. The acetic acid-induced writhing was greatly diminished by the methanolic leaves extract of *A. marmelos* whereas, the analgesic efficacy was significantly increased at doses of 200 and 300 mg/kg of methanolic extract of *A. marmelos* leaves in the tail flick test. The analgesic efficacy of the aqueous extract of *A. marmelos* stem bark was found to be dose-dependent in acetic acid-induced writhing and tail flick test in mice models.[53] The ethanol extract of *A.*

marmelos leaves (200 mg/kg) and fruit pulp (200 mg/kg) demonstrated their analgesic property by the reduced number of writhing and the period was increased in Eddy's hot plate method.[54]

CARDIOPROTECTIVE EFFECTS

Methanol extract of *A. marmelos* leaves pre-treated mice model showed a substantial reduction in serum indicators like creatinine phosphokinase MB, serum glutamate oxaloacetate transaminase and serum glutamate pyruvate transaminase in a dosage-related manner, indicating cardiac protection. Histopathological findings also further confirmed the cardioprotective effects and benefits of *A. marmelos*.[55] Likewise, the aqueous extract of *A. marmelos* leaves exhibited excellent cardioprotective action against the Isoproterenol induced Myocardial injury in adult male Albino Wistar rats.[56] The research of Jagetia and Venkatesh,[57] also confirmed the cardioprotective activities of the hydroalcoholic extract of *A. marmelos* against the Doxorubicin hydrochloride-induced cardiotoxicity in mice.

HEPATOPROTECTIVE EFFECTS

Methanolic extract of *A. marmelos* leaves also confirmed its hepatoprotective benefits against Carbon tetrachloride-treated albino Wistar rats.[58] *A. marmelos* treatment significantly reduced the impacts of paracetamol in a dose-related manner. The maximum hepatoprotective action of *A. marmelos* was observed at 100 mg/kg.[59] Interestingly, another work by Rathee *et al*.[60] demonstrated that the hepatotoxicity was dramatically reversed in the carbon tetrachloride-treated Wistar rat models by the oral administration of the substantially low dose of *A. marmelos* (25 mg/kg) combined with piperine.

WOUND HEALING EFFECTS

The methanolic extract of *A. marmelos* was applied topically twice daily for 12 days in a row, the excision wound area in mice was dramatically decreased (0.03 ± 0.02 mm^2) and healed.[61] The report of Gautam *et al*.[62] evidenced the remarkable wound-healing potency of the 50% ethanolic extract of *A. marmelos* fruit pulp in the excision, incision and dead wound models. *A. marmelos* treated groups showed complete constriction and epithelization of wounds on the 20th day, which was observed on the 24th day for the control group.

CONCLUSION

The above evidence shed a light on the folklore uses and various therapeutic potential of *A. marmelos*. It has been enriched with immense phytochemicals like alkaloids, tannins, coumarins, saponins, terpenoids, etc., The whole tree or any of its parts like stem, leaves, flowers, fruits, etc. can be used for several health ailments like diabetes, microbial infection, inflammation and as painkillers. Based on its relevance in folk medicine and the promise it has shown in preliminary studies, the *A. marmelos* fruit can also be consumed as a functional food, which merits a wide range of health advantages. *A. marmelos* continues to be a crucial natural medicine for a variety of health ailments since many of its traditional uses have been supported by research over time. However, a significant amount of work is still necessary to comprehend the role of *A. marmelos* in various therapeutic mechanisms and also to isolate the specific lead compounds effective against a variety of serious and chronic disorders.

ACKNOWLEDGEMENT

The authors are grateful to the management as well as the faculty members in the , Department of Biochemistry, Kongunadu Arts and Science College (Autonomous), G.N. Mills P.O, Coimbatore, Tamil Nadu-641029, India for providing the support to fulfil this work.

FUNDING STATEMENT

The authors did not receive support from any organization for the submitted work.

AUTHORS CONTRIBUTIONS

All the authors were contributed equally for concept making, data acquiring, investigating and writing the manuscript.

CONFLICT OF INTEREST

All of the authors had no any personal, financial, commercial, or academic conflicts of interest separately.

ABBREVIATIONS

DPPH: 2,2-diphenyl-1-picrylhydrazyl; **STZ:** Streptozotocin; **IL-1β:** Interleukin-1β; **MIP1:** α-Macrophage inflammatory protein-1 alpha; **IL-6:** Interleukin-6; **TNF α:** Tumour Necrosis Factor

alpha; **MTT:** 3-[4,5-dimethylthiazol-2-yl]-2,5 diphenyl tetrazolium bromide.

SUMMARY

A. marmelos (Bael tree) holds significant therapeutic value in traditional medicine, addressing ailments like diarrhea, diabetes, fever and bacterial infections. This review aims to consolidate current knowledge on its ethnomedicinal applications, nutritional content, bioactive constituents and pharmacological activities. The work utilized an extensive search in major databases using *A. marmelos*-related terms. Out of 120 publications found, 62 were eligible, laying the groundwork for investigating the pharmacological properties of *A. marmelos*. Phytochemical screening revealed diverse compounds, including alkaloids, flavonoids and terpenoids. *In vitro* as well as *in vivo* studies underscore its antioxidant, analgesic, anti-inflammatory and antimicrobial properties, validating its historical medicinal uses and highlighting its potential for future therapeutic interventions.

REFERENCES

1. Jindal M, Kumar V, Rana V, Tiwary AK. *A. marmelos* fruit pectin for food and pharmaceuticals: Physico-chemical, rheological and functional performance. Carbohydrate polymers. 2013;93(2):386-94. https://doi.org/10.1016/j.carbpol.2012.12.012
2. Sharma GN, Dubey SK, Sati N, Sanadya J. Ulcer healing potential of *A. marmelos* fruit seed. Asian J Pharm Life Sci. 2011;1(2):172-8.
3. Rahman S, Parvin R. Therapeutic potential of *A. marmelos* (L.)-An overview. Asian Pacific journal of tropical disease. 2014;4(1):71-7. https://doi.org/10.1016%2FS2222-1808(14)60318-2
4. Sharma N, Dubey W. History and taxonomy of *A. marmelos*: a review. International Journal of Pure and Applied Bioscience. 2013;1(6):7-13.
5. Gupta D, John PP, Kumar P, Jain J. Evaluation of antioxidant activity of unripe *A. marmelos* corr. Fruits. Journal of Applied Pharmaceutical Sciences and Research. 2018:4-7.
6. Murthy HN, Bhat MA, Dalawai D. Bioactive compounds of bael (*A. marmelos* (L.) correa). Bioactive compounds in underutilized fruits and nuts. 2020:459-86. https://doi.org/10.1007/978-3-030-30182-8_35
7. Mahato H, Kumar B. Medicinal Uses with Immense Economic Potential and Nutritional Properties of *A. marmelos*: A Concise Review. Biocomposites; Books on Demand: Norderstedt, Germany. 2022:133.
8. Ahmad W, Amir M, Ahmad A, Ali A, Ali A, Wahab S, *et al*. *A. marmelos* leaf extract phytochemical analysis, cytotoxicity, *in vitro* antioxidant and antidiabetic activities. Plants. 2021;10(12):2573. https://doi.org/10.3390/plants10122573
9. Bajaniya VK, Kandoliya UK, Bodar NH, Bhadja NV, Golakiya BA. Fatty acid profile and phytochemical characterization of bael seed (*A. marmelos* L.) oil. International Journal of Current Microbiology and Applied Sciences. 2015;4(2):97-102.
10. Mahesare SS, Waghmare SP, Thorat MG, Hajare SW, Itankar PR. Quantitative analysis of biomarkers in hydro-ethanolic extract of *A. marmelos* by High-Performance Thin Layer Chromatography (HPTLC). International Journal of Chemical Studies. 2020;8(3):1479-82.DOI: 10.22271/chemi.2020.v8.i3t.9404
11. Shakyawar SL, Rahman MA, Sundaram S, Alok S. Preliminary Qualitative Phytochemical, Physico-Chemical and Phyto-Pharmacognostical Standardisation Evaluation of the Pulp (Without Seed), Pericarp, Leaves and Seed of *A. marmelos* L.(Bael). Int. J. Pharm. Sci. Res. 2020;11(7):3489-506.
12. Bristy NJ, Hasan AN, Alam MN, Wahed TB, Roy P, Alam KK. Characterization of antioxidant and cytotoxic potential of methanolic extracts of different parts of *A. marmelos* (L.). International Journal of Pharmaceutical Sciences and Research. 2017;8(3):1476.
13. Narendhirakannan RT, Subramanian S. Biochemical evaluation of the protective effect of *A. marmelos* (L.), Corr. leaf extract on tissue antioxidant defense system and histological changes of pancreatic β-cells in streptozotocin-induced diabetic rats. Drug and chemical toxicology. 2010;33(2):120-30. https://doi.org/10.3109/01480540903203984
14. Raja WW, Khan SH. Estimation of some phytoconstituents and evaluation of antioxidant activity in *A. marmelos* leaves extract. Journal of Pharmacognosy and Phytochemistry. 2017;6(1):37-40.
15. Raheja S, Girdhar A, Kamboj A, Lather V, Pandita D. *A. marmelos* leaf extract ameliorates the cognitive impairment and oxidative stress induced by intracerebroventricular streptozotocin in male rats. Life sciences. 2019;221:196-203. https://doi.org/10.1016/j.lfs.2019.02.032
16. Surolia R, Singh A, Bhatnagar T. Comparative Study on the Characterization and Antioxidant Properties of Bael (*A. marmelos*) Pulp. Shell and Seed Pectin. 2022. https://doi.org/10.21203/rs.3.rs-1586407/v1
17. Sampath G, Govarthanan M, Rameshkumar N, Vo DV, Krishnan M, Sivasankar P, Kayalvizhi N. Eco-friendly biosynthesis metallic silver nanoparticles using *A. marmelos* (Indian bael) and its clinical and environmental applications. Applied Nanoscience. 2023;13(1):663-74.https://doi.org/10.1007/s13204-021-01883-8
18. Vardhini SP, Sivaraj C, Arumugam P, Ranjan H, Kumaran T, Baskar M. Antioxidant, anticancer, antibacterial activities and GCMS analysis of aqueous extract of pulps of *A. marmelos* (L.) Correa. The Journal of Phytopharmacology. 2018;7(1):72-8.
19. Seemaisamy R, Faruck LH, Gattu S, Neelamegam R, Bakshi HA, Rashan L, Al-Buloshi M, Hasson SS, Nagarajan K. Anti Microbial and Anti Cancer activity of *A. marmelos* and Gas Chromatography Coupled Spectrometry Analysis of their Chemical Constituents. International Journal of Pharmaceutical Sciences and Research. 2019 ;10(1):373-80.http://researchonline.ljmu.ac.uk/id/eprint/16357/
20. Akhouri V, Kumari M, Kumar A. Therapeutic effect of *A. marmelos* fruit extract against DMBA induced breast cancer in rats. Scientific reports. 2020;10(1):18016.https://doi.org/10.1038/s41598-020-72935-2
21. Gupta N, Agrawal RC, Sharma P, Narwariya A. Anticancer potential of *A. marmelos* bark extract against DMBA induced skin papillomagenesis with reference to oxidative stress. Eur. J. Pharm. Med. Res. 2016;3(4):309-14.
22. Kumar PY, Parimalam M, Kumar D, Joseph E, David D, Vinolia R. Screening of phytochemicals, *in vitro* assessment of antioxidant, anti-inflammatory, Tlc profiling and anticancer activity of *A. marmelos* (L.) leaves. Annals of the Romanian Society for Cell Biology. 2021:18061-71.
23. Dahiya R, Tomar RS, Shrivastava V. Evaluation of Antimicrobial potential of *A. marmelos* fruit extract against selected microorganisms. Journal of Pharmaceutical Sciences and Research. 2015;7(9):681.
24. Yadav SS, Dahiya KU, Ganie SA, Gulia SK. Antibacterial activity of *A. marmelos* (L.) Correa. Int J Pharm Pharm Sci. 2015;7(3):462-4.
25. Patil S, Sivaraj R, Rajiv P, Venckatesh R, Seenivasan R. Green synthesis of silver nanoparticle from leaf extract of *A. marmelos* and evaluation of its antibacterial activity. Int J Pharm Pharm Sci. 2015;7(6):169-73.
26. Ganapathy S, Karpagam S. *In vitro* antibacterial and phytochemical potential of *A. marmelos* against multiple drug resistant (MDR) *Escherichia coli*. Journal of Pharmacognosy and Phytochemistry. 2016;5(1):253-5.
27. Ibrahim NA, El-Sakhawy FS, Mohammed MM, Farid MA, AbdelWahed NA, Deabes DA. Chemical composition, antimicrobial and antifungal activities of essential oils of the leaves of *A. marmelos* (L.) Correa growing in Egypt. Journal of Applied Pharmaceutical Science. 2015;5(2):001-5. DOI: 10.7324/JAPS.2015.50201
28. Abirami SG, Vivekanandhan K, Hemanthkumar R, Prasanth S, Kumar JR. Study of antimicrobial potential of *A. marmelos*. Journal of Medicinal Plants Studies. 2014;2(2):113-6.
29. More YD, Gade RM, Shitole AV. *In vitro* Antifungal Activity of *A. marmelos*, *Syzygium cumini* and *Pongamia pinnata* Extracts against *Fusarium oxysporum* f. sp. cicero. Indian Journal of Pharmaceutical Sciences. 2017;79(3):457-62.

30. Sriramulu M, Balaji, Sumathi S. Photo catalytic, antimicrobial and antifungal activity of biogenic iron oxide nanoparticles synthesised using *A. marmelos* extracts. Journal of Inorganic and Organometallic Polymers and Materials. 2021;31:1738-44.
31. Somu C, Karuppiah H, Sundaram J. Antiviral activity of seselin from *A. marmelos* against nuclear polyhedrosis virus infection in the larvae of silkworm, *Bombyx mori*. Journal of ethnopharmacology. 2019;245:112155. https://doi.org/10.1016/j.jep.2019.112155
32. Andleeb R, Ijaz MU, Rafique A, Ashraf A, Bano N, Zafar N, *et al*. Biological activities of methanolic extract of *A. marmelos* against HN protein of newcastle disease virus. Agronomy. 2021 Sep 6;11(9):1784. https://doi.org/10.3390/agronomy11091784
33. Nivetha R, Bhuvaragavan S, Muthu Kumar T, Ramanathan K, Janarthanan S. Inhibition of multiple SARS-CoV-2 proteins by an antiviral biomolecule, seselin from *A. marmelos* deciphered using molecular docking analysis. Journal of Biomolecular Structure and Dynamics. 2022;40(21):11070-81. https://doi.org/10.21203/rs.3.rs-31134/v1
34. Madhu C, Hindu K, Sudeepthi CD, Maneela P, Reddy KV, Sree BB. Anti ulcer activity of aqueous extract of *A. marmelos* leaves on rats. Asian Journal of Pharmaceutical Research. 2012;2(4):132-5.
35. Sharmin Rahman D, Quader MR, Sharmin R, Momtaz A, Sharmin K, Eva EO, Mosaddek AS. Evaluation of Anti Ulcer Activity of Ethanolic Extract of *A. marmelos* Leaves on Rats. ARC J. Dent. Sci. 2016;1:23-6.
36. Das SK, Roy C. The protective role of *A. marmelos* on aspirin–induced gastro-duodenal ulceration in albino rat model: a possible involvement of antioxidants. Saudi Journal of Gastroenterology. 2012;18(3):188-94.https://doi.org/10.4103%2F1319-3767.96452
37. Sharma GN, Dubey SK, Sati N, Sanadya J. Ulcer healing potential of *A. marmelos* fruit seed. Asian J Pharm Life Sci. 2011;1(2):172-8.
38. Sankhla A, Sharma S, Sharma N. Hypoglycemic effect of bael patra (*A. marmelos*) in NIDDM patients. Journal of Dairying, Foods and Home Sciences. 2009;28(3 and 4):233-6.
39. Arumugam S, Kavimani S, Kadalmani B, Ahmed AB, Akbarsha MA, Rao MV. Antidiabetic activity of leaf and callus extracts of *A. marmelos* in rabbit. Sci Asia. 2008;34(3):317-21.
40. Gandhi GR, Ignacimuthu S, Paulraj MG. Hypoglycemic and β-cells regenerative effects of *A. marmelos* (L.) Corr. bark extract in streptozotocin-induced diabetic rats. Food and chemical toxicology. 2012;50(5):1667-74. doi:10.1016/j.fct.2012.01.030
41. Abdallah IZ, Salem I, El-Salam A, Nayrouz AS. Evaluation of anti-diabetic and antioxidant activity of *A. marmelos* L. Correa fruit extract in diabetic rats. The Egyptian Journal of Hospital Medicine. 2017;67(2):731-41. DOI : 10.12816/0037829
42. Bindu Jacob BJ, Narendhirakannan RT. Role of medicinal plants in the management of diabetes mellitus: a review. 3 Biotech, 9, 1-17. https://doi.org/10.1007/s13205-018-1528-0
43. Rakulini R, Sounthararajan K. A review of anti–diarrheal activity of *A. marmelos*. Journal of Complementary and Alternative Medical Research, 6, 1-10.
44. Brijesh, S., Daswani, P., Tetali, P., Antia, N., and Birdi, T. Studies on the anti-diarrheal activity of *A. marmelos* unripe fruit: Validating its traditional usage. BMC complementary and alternative medicine, 209;9(1):1-12.
45. Benni JM, Jayanthi MK, Suresha RN. Evaluation of the anti-inflammatory activity of *A. marmelos* (Bilwa) root. Indian journal of pharmacology. 2011;43(4):393-7.https://doi.org/10.4103%2F0253-7613.83108
46. Rajaram A, Vanaja GR, Vyakaranam P, Rachamallu A, Reddy GV, Anilkumar K, *et al*. Anti-inflammatory profile of *A. marmelos* (L) Correa (Bilva) with special reference to young roots grown in different parts of India. Journal of Ayurveda and integrative medicine. 2018;9(2):90-8.https://doi.org/10.1016/j.jaim.2017.03.006
47. Pynam H, Dharmesh SM. Antioxidant and anti-inflammatory properties of marmelosin from Bael (*A. marmelos* L.); Inhibition of TNF-α mediated inflammatory/tumor markers. Biomedicine and Pharmacotherapy. 2018 Oct 1;106:98-108. https://doi.org/10.1016/j.biopha.2018.06.053
48. Kumari KD, Weerakoon TC, Handunnetti SM, Samarasinghe K, Suresh TS. Anti-inflammatory activity of dried flower extracts of *A. marmelos* in Wistar rats. Journal of ethnopharmacology. 2014;151(3):1202-8. https://doi.org/10.1016/j.jep.2013.12.043
49. Kumar R, Kumar A, Prasal CS, Dubey NK, Samant R. Insecticidal activity *A. marmelos* (L.) Correa essential oil against four stored grain insect pests. International Journal of Food Safety. 2008;10:39-49.
50. Sarma R, Mahanta S, Khanikor B. Insecticidal activities of the essential oil of *A. marmelos* (Linnaeus, 1800) against *Aedes aegypti* (Linnaeus, 1762) and *Culex quinquefasciatus* (Say, 1823). Universal Journal of Agricultural Research. 2017;5(5):304-11.DOI: 10.13189/ujar.2017.050508
51. Murasing C, Das P, Sathish K, Hazarika LK. Bio efficacy of Bael (*A. marmelos*) Correa (Rutaceae) leaf extracts against pulse beetle (*Callosobruchus chinensis* L.) in stored green gram seed (*Vigna radiata* L.). Int. J. Curr. Microbiol. App. Sci. 2017;6(8):2067-75. http://dx.doi.org/10.20546/ijcmas.2017.603.246
52. Shankarananth V, Balakrishnan N, Suresh D, Sureshpandian G, Edwin E, Sheeja E. Analgesic activity of methanol extract of *A. marmelos* leaves. Fitoterapia. 2007;78(3):258-9. https://doi.org/10.1016/j.fitote.2006.12.004
53. Ghodki SG, Borade SB, Pise H, Motghare V, Mehani RS, Wadgbalkar P. Evaluation of analgesic activity of *A. marmelos* steam bark in experimental animals. International Journal of Basic and Clinical Pharmacology. 2016;5(3):1081. http://dx.doi.org/10.18203/2319-2003.ijbcp20161572
54. Krishnakanth K, Abhilash BG, Neeraja K, Rao GH, Cheekavolu C. Analgesic and anti-inflammatory activity of ethanolic extracts of leaf and fruit pulp of *A. marmelos* in albino rats. International Journal of Basic and Clinical Pharmacology. 2017 Jul 1;6(7):1596. http://dx.doi.org/10.18203/2319-2003.ijbcp20172634
55. Vishwakarma P, Divekar P, Goel RK, Sharma M, Saini M, Saxena KK. Evaluation of cardioprotective effect of *A. marmelos* on doxorubicin induced cardiotoxicity: an experimental study. International Journal of Basic and Clinical Pharmacology. 2018;7(7):1309-14.http://dx.doi.org/10.18203/2319-2003.ijbcp20182674
56. Ramachandra Y, Ashajyothi C, Padmalatha R. Cardio protective effect of *A. marmelos* on isoproterenol induced myocardial infarction in rats. International journal of Biology, Pharmnacy and Applied sciences. 2012;1:718-29.
57. Jagetia GC, Venkatesh P. An indigenous plant bael (*A. marmelos* (L.) Correa) extract protects against the doxorubicin-induced cardiotoxicity in mice. Biochem physiol. 2015;4(3): 1000163. doi: 10.4172/2168-9652.1000163
58. Siddique NA, Mujeeb M, Najmi AK, Aftab A, Aslam J. Free radical scavenging and hepatoprotective activity of *A. marmelos* (Linn.) corr leaves against carbon tetrachloride. International Journal of Comprehensive Pharmacy. 2011;2(08):1-6.
59. Rathee D, Kamboj A, Sachdev RK, Sidhu S. Hepatoprotective effect of *A. marmelos* augmented with piperine co-administration in paracetamol model. Revista Brasileira de Farmacognosia. 2018;28:65-72. https://doi.org/10.1016/j.bjp.2017.11.003
60. Rathee D, Kamboj A, Sidhu S. Augmentation of hepatoprotective potential of *A. marmelos* in combination with piperine in carbon tetrachloride model in wistar rats. Chemistry Central Journal. 2018;12:1-3. https://doi.org/10.1186/s13065-018-0463-9
61. Arunachalam KD, Subhashini S, Annamalai SK. Wound healing and antigenotoxic activities of *A. marmelos* with relation to its antioxidant properties. J Pharm Res. 2012;5(3):1492-502.
62. Gautam MK, Purohit V, Agarwal M, Singh A, Goel RK. *In vivo* healing potential of *A. marmelos* in excision, incision and dead space wound models. The Scientific World Journal. 2014;2014. https://doi.org/10.1155/2014/740107

Cite this article: Mrudhulla S, Itsaranuwat P, Narendhirakannan RT. A Systematic Review on Biochemical and Pharmacological Properties of the Active Phytochemicals Present in *Aegle marmelos* (L). Asian J Biol Life Sci. 2024;13(2):250-7.

plants

MDPI

Review

A Review of the Role of an Anthocyanin, Cyanidin-3-*O*-*β*-glucoside in Obesity-Related Complications

Ponnuvel Deepa [1], Minji Hong [1], Kandhasamy Sowndhararajan [2] and Songmun Kim [1,*]

[1] School of Natural Resources and Environmental Science, Kangwon National University, Chuncheon 24341, Republic of Korea; taanishadeepa@gmail.com (P.D.); alswl0356@kangwon.ac.kr (M.H.)
[2] Department of Botany, Kongunadu Arts and Science College, Coimbatore 641029, India; sowndhar1982@gmail.com
* Correspondence: perfume@kangwon.ac.kr; Tel.: +82-33-250-6447

Abstract: Obesity has become a major health issue worldwide and obese individuals possess higher levels of adipose tissue when compared with healthy individuals. Obesity is highly associated with the development of different chronic diseases, such as diabetes, cardiovascular diseases, hypertension, cancers, etc. Previous studies established that anthocyanin compounds play an important role in attenuating obesity-related consequences. Among various anthocyanin compounds, cyanidin-3-*O*-*β*-glucoside (C3G) is the most important component and is widely distributed in various colored edible plant materials, especially berries, cherries, black rice, purple corn, etc. In recent decades, several studies have reported the therapeutical properties of C3G. C3G has various biological properties and health benefits, such as antioxidant, antimicrobial, anti-inflammatory, antidiabetic, anti-obesity, neuroprotective, anticancer, etc. In this review, we summarized the in vitro and in vivo studies in relation to the role of C3G in obesity-related complications. Several mechanistic studies demonstrated that C3G maintains the metabolism of glucose, fatty acids, and lipids by regulating different genes and signaling pathways. It could be concluded that the consumption of C3G protects healthy individuals from obesity-related issues by maintaining body weight and regulating their metabolism and energy balance. This review provides some important signaling pathways/targets of C3G to facilitate the prevention and treatment of obesity, leading to the development of important food supplements.

Keywords: anthocyanin; cyanidin-3-*O*-*β*-glucoside; cyanidin-3-glucoside; obesity; adipogenesis; adipocyte

Citation: Deepa, P.; Hong, M.; Sowndhararajan, K.; Kim, S. A Review of the Role of an Anthocyanin, Cyanidin-3-*O*-*β*-glucoside in Obesity-Related Complications. *Plants* **2023**, *12*, 3889. https://doi.org/10.3390/plants12223889

Academic Editors: Sebastian Granica, Ochuko Lucky Erukainure and Chika Ifeanyi Chukwuma

Received: 9 October 2023
Revised: 7 November 2023
Accepted: 16 November 2023
Published: 17 November 2023

1. Introduction

Obesity is one of the most important health problems worldwide with considerable illness and mortality. According to the WHO, more than 2.8 million deaths occur every year due to obesity-related consequences. In 2016, approx. 1.9 billion adults were obese [1,2]. If secular trends continue, it is estimated that 38% of the world's adult population will be overweight by 2030 and an additional 20% will be obese exclusively in underdeveloped countries [3]. Genetic mechanisms, endocrine, appetite disorders, and diabetes-associated diseases are major factors that trigger obesity [4,5]. Obesity is a high-risk factor for developing numerous chronic diseases, including diabetes, heart disease, liver disease, and hypertension [6]. Lipid and energetic metabolisms comprise a sequence of biosynthetic and oxidative reactions required for the energy supply and differentiation of adipocytes. In these, lipogenesis activates mitochondrial biogenesis, the production of reactive oxygen species, and inflammatory responses that are highly correlated with obesity [5]. The major causative factor for obesity is the consumption of more calories accompanied by the accumulation of excessive fat. Although lifestyle changes and improving physical activity are the best strategies for preventing obesity, it can be difficult to continue these activities in the long term [7]. Some treatment strategies that can be followed to prevent obesity

are thermogenesis of brown adipose tissue, genetics and epigenetics, physical exercise, and diet, including foods with bioactive components [8]. Therefore, developing a novel effective approach to prevent obesity-related complications is essential for the scientific community [6,7].

Anthocyanins are widely found in colored fruits and vegetables. [4]. They are important flavonoid compounds in terms of food as well as medicine due to the availability of numerous structurally different bioactive components [9,10]. Anthocyanin components offer potential health-promoting functions due to their strong antioxidant effects [9,11]. Anthocyanin components are rich in colored fruits, vegetables, and cereals, including berries, cherries, grapes, black beans, purple cabbage, purple corn, black rice, etc. In addition, anthocyanins are generally treated as colorants in beverages, fruit fillings, and dairy products. Hence, anthocyanins play a significant role in the diet of humans [5,12]. Diets supplemented with anthocyanin-rich berries can significantly affect gastrointestinal bacterial communities with respect to obligate anaerobes by decreasing the gastrointestinal luminal oxygen and oxidative stress [13]. In particular, cyanidin and its derivatives can exhibit a protective effect on DNA cleavage [14]. The administration and consumption of cyanidin glycosides are effective in reducing reactive oxygen species (ROS)-mediated cell and tissue damage [15,16].

In recent times, there has been significant attention in the research of anthocyanin derivatives. Approx. 635 different anthocyanin components have been identified in various plants. In particular, pelargonidin, cyanidin, delphinidin, peonidin, petunidin, and malvidin are important aglycones in foods [5]. Among them, cyanidin-3-*O*-*β*-glucoside (C3G) is an important biologically active component (Figure 1). Numerous studies have confirmed that anthocyanins provide various therapeutic effects, especially C3G, which significantly increases energy expenditure as well as decreases weight gain [10,17]. Further, C3G is considered to be the main component in terms of the bioavailability and active form of cyanidin in human tissues [18]. C3G markedly reduces lipogenesis, oxidative stress, and inflammation, thereby improving the obesity-mediated dysregulation of metabolism. C3G has the potential to speed up lipolysis and thermogenesis and to reduce body fat accumulation. A study found that a master regulator of energy metabolism, namely peroxisome proliferator-activated receptors (PPARs), is activated by C3G [19].

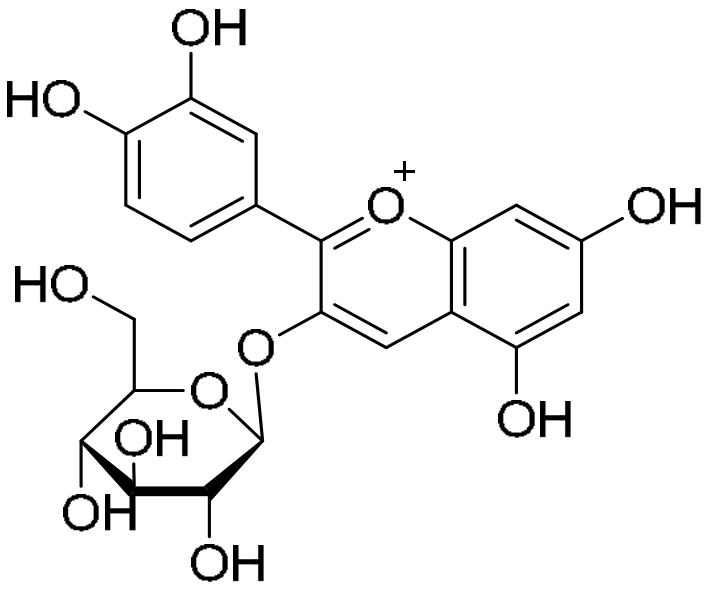

Figure 1. The chemical structure of cyanidin-3-*O*-*β*-glucoside.

C3G and its metabolites have better absorption and bioavailability, and their interaction with gut microbiota may improve their positive health effects. Several studies on C3G have been published in the past decades. However, no detailed review has been published

regarding the role of C3G in obesity-related complications. In this context, the present review aims to discuss the possible therapeutical properties of C3G for preventing and treating obesity based on in vitro and in vivo studies. For this purpose, a literature search was performed in electronic databases using "obesity" as the major term, together with "C3G", and mainly comprised articles in English. This review mainly focused on the role of C3G in obesity with its underlying mechanisms, leading to the development of potent food supplements for preventing obesity-related health issues.

2. The Occurrence and Color Characteristics of C3G

Anthocyanin content in colored fruits and vegetables varies remarkably, according to different species. In addition, numerous factors influence the level of anthocyanin content, such as the cultivar, geographical location, environmental conditions, cultural practices, harvest time and methods, processing and storage conditions, etc. [20–22]. Berries are a rich source of anthocyanins, including strawberries, blueberries, blackberries, black elderberries, bilberries, blackcurrants, chokeberries, redcurrants, and raspberries [22]. In these, the highest anthocyanin content is found in elderberries (1.4 g) and chokeberries (1.8 g) per 100 g of product [23,24]. Moreover, purple corn, cherries, plums, pomegranates, eggplant, wine, grapes, and colored vegetables such as black carrots, red cabbage, and purple cauliflower contain appreciable amounts of anthocyanin compounds [24,25]. Among the different anthocyanins, C3G is widely found in colorful berries, blue and red fruits, and vegetables. In particular, pomegranates, blackberries, bilberries, elderberries, and mulberries possess a higher bioavailability of C3G. In addition, C3G is commonly found in black rice, black beans, and purple potatoes [26,27].

The color of the anthocyanin pigments usually ranges from pale yellow to blue, but are primarily responsible for the red, purple, and blue colors of different plant organs. In general, C3G is normally found in vegetables and fruits as a red pigment. However, the pH, light, temperature, and structure play a critical role in the color and stability of anthocyanins. At an alkaline pH, anthocyanins are blue pigments, whereas they are red at an acidic pH. However, these pigments are highly unstable and oxidized into dark brown compounds at alkaline conditions due to degradation [28]. In their structure, the B-ring and the presence of hydroxyl or methoxyl groups also influence the stability of anthocyanins. Further, the presence of an oxonium ion adjacent to carbon 2, metal ions, temperature, light, and oxygen may also influence the stability of the anthocyanin pigments [22,28]. In the flowers and fruits of some plants, the colors may depend on the combined effect of the light absorbance of chlorophylls and anthocyanins [29,30].

3. The Chemistry of C3G

Anthocyanins are anthocyanidin glycosides (aglycones). They are formed by a flavylium cation backbone that is hydroxylated in different positions to produce diverse anthocyanidins [29]. Cyanidin is one of the extensively distributed pigments in plants. In these, C3G is the most characterized anthocyanin in edible plants, followed by delphinidin, pelargonidin, and peonidin glucosides. These aglycones differ according to their B-ring substitution pattern [28]. C3G is a monomeric anthocyanin and a water-soluble pigment with a molecular weight of 449.4 g/mol. It is derived from the aglycone cyanidin and is more hydrophilic than cyanidin. C3G consists of an *O*-glycosylated anthocyanidin with two hydroxyls on the third aromatic ring. In acidic conditions, C3G occurs in the flavylium form. On the other hand, in alkaline conditions, C3G occurs in the carbinol form through the hydration of the flavylium cation or in the quinoidal form through the loss of a proton [31]. In plants, C3G is biosynthesized through the flavan-3-ol pathway. Previously, pharmacokinetics studies in humans demonstrated that >20 kinds of C3G metabolites have been identified [32]. The main bioactive metabolites of C3G are protocatechuic acid, phloroglucinaldehyde, vanillic acid, and ferulic acid. Furthermore, the stability of C3G is improved when it is acylated with lauric acid, owing to its ester group [33,34].

4. In Vitro Studies on the Role of C3G in Obesity-Related Complications

The excessive consumption of energy-rich foods and an inactive lifestyle are believed to be the main causes of obesity-related insulin resistance and abnormal glucose metabolism. Scientific studies confirmed that anthocyanins may lower the metabolic risks linked with obesity due to their potent antioxidant and anti-inflammatory properties. The dysfunction of adipocytes is highly correlated with the onset of obesity and insulin resistance. It is believed that obesity and the improvement of insulin sensitivity can be prevented by regulating the secretion of adipocytokine and the expression of adipocyte-specific genes. Table 1 shows the mechanisms of C3G for preventing obesity-related complications under different in vitro conditions.

Table 1. The effects of cyanidin-3-*O*-*β*-glucoside on the obesity-associated mechanisms under in vitro conditions.

Model	Concentration	Mechanism(s)	Year of Publication	References
Rat adipocytes	100 μM	• Enhanced adiponectin and leptin secretion • Upregulated adipocyte-specific gene expressions	2004	[35]
Human preadipocytes	100 μM	• Upregulated adiponectin and downregulated PAI-1 and IL-6	2006	[36]
3T3-L1 adipocytes and RAW 264.7 cells	10, 50, and 100 μM	• Inhibited the release of MCP-1 and MRP-2	2007	[37]
H_2O_2- and TNF-α-induced insulin resistance in 3T3-L1 adipocytes	10, 20, and 40 μM	• Inhibited the JNK signal pathway	2008	[38]
Primary brown preadipocytes	100 μM	• Decreased the insulin-induced ROS production	2010	[39]
3T3-L1 adipocytes	20 and 100 μM	• Upregulated the GLUT4 gene expression	2011	[40]
Skeletal muscle cells and adipocytes from female KK-Ay mice	10, 50, and 100 μmol/L	• Activated LPL in plasma and skeletal muscle • Inhibited LPL in adipose tissue by activating pAMPK	2011	[41]
Human omental adipocytes and 3T3-L1 cells.	Human omental adipocytes—50 and 100 μmol/L; 3T3-L1 cells—10 and 100 μmol/L	• Increased the adipocyte glucose uptake and GLUT4 translocation • Increased nuclear PPARγ, adiponectin, and the GLUT4 expressions	2011	[42]
Preadipocytes from human adipose explant tissue	50 μM	• Inhibited the expression of ChREBP	2012	[43]
Human HepG2 cells	100 μM	• Increased cellular AMPK activity. • Induced AMPK downstream target ACC phosphorylation and inactivation • Decreased malonyl CoA contents	2012	[44]
3T3-L1 adipocytes	50 μM	• Increased the activity of AMPK and decreased the activity of GFAT • Decreased the expression of adipose triglyceride lipase by attenuating the O-glycosylation of the transcription factor FoxO1	2012	[45]

Table 1. *Cont.*

Model	Concentration	Mechanism(s)	Year of Publication	References
Preadipocyte 3T3-L1 cells	Black soybean anthocyanins; 12.5 and 50 μg/mL	• Inhibited the proliferation of preconfluent preadipocytes and maturing postconfluent adipocytes • Reduced the number of viable cells • Increased epinephrine-induced lipolysis • Reduced lipid accumulation and suppressed the expression of PPARγ	2012	[46]
3T3 adipocytes	12.5, 25, and 50 μM	• Induced the adiponectin expression and secretion by Foxo1	2014	[47]
3T3-L1 fibroblasts	5 or 20 μM	• Decreased fat accumulation in 3T3-L1 adipocytes by increasing CPT-1 • Decreased FAS and the SREBP-1c expression	2015	[48]
3T3-L1 adipocytes	20 and 100 μM	• Increased the PPARγ and C/EBPα gene expressions • Increased adiponectin secretion, decreased TNF-α secretion, activated insulin signaling, and increased the glucose uptake • Increased the expression of the PGC-1α, SIRT1, and UCP-3 genes	2015	[49]
Primary human preadipocytes	100 μM	• Decreased the TNFα secretion and increased insulin-stimulated lipogenesis	2016	[50]
3T3-L1 adipocytes	10 and 50 μM	• Activated the PI3K/Akt pathways	2017	[51]
3T3-L1 adipocytes	50 μM	• Prevented adipocyte differentiation, lipid accumulation, and reduced PPAR-γ activity • Activated insulin signaling and enhanced GLUT4 translocation	2017	[52]
3T3-L1 adipocytes	50 and 100 μM	• Increased cAMP levels and the expression of the mitochondrial genes (TFAM, SOD2, UCP-1 and UCP-2), UCP-1 protein, and beige adipocyte markers (CITED1 and TBX1)	2017	[53]
Brown adipose tissue C3H10T1/2 clone 8 cells induced by palmitate	Isolated from mulberry; 100 and 200 μg/mL	• Inhibited the release of adipokines • Reduced lipid accumulation	2018	[54]
Palmitic acid-induced 3T3-L1 adipocytes	Anthocyanin-rich extract; 10 and 20 μg/mL	• Inhibited the activation of the NF-κB pathway • Regulated the PI3K/Akt, GLUT-1, and adiponectin mRNA levels	2019	[55]
Macrophage–adipocyte interaction, using mono- and co-culture	1.0 mg/mL of the anthocyanin-rich extracts of purple and red maize or 50 μM of pure anthocyanins	• Reduced the production of pro-inflammatory cytokines • Inhibited the activation of NF-κB and JNK	2019	[2]
Pancreatic lipase and cholesterol esterase Caco-2 cells	12.5–100 μM	• Inhibited pancreatic lipase and pancreatic cholesterol esterase activity • Inhibited the formation of cholesterol micelles • Reduced cholesterol uptake • Suppressed the mRNA expression of NPC1L1	2019	[56]

Table 1. *Cont.*

Model	Concentration	Mechanism(s)	Year of Publication	References
Pancreatic lipase activity	50 to 350 μM	• Cyanidin—IC50 at 28.29 μM • C3G—IC50 at 188.28 μM	2019	[57]
Human adipose tissue	25 μM	• Inhibited adipogenesis and downregulated adiponectin genes • Induced a higher accumulation of calcium deposits • Upregulated the osteocyte-specific gene BMP-2, Runx-2 expression, and BMP-2 secretion	2019	[58]
RAW 264.7 macrophages and 3T3-L1 adipocytes	Anthocyanin-rich water extracts (PMWs) from purple maize; 1 mg/mL	• Downregulated the production of pro-inflammatory mediators and improved insulin sensitivity	2019	[59]
3T3-L1 hypertrophic adipocytes exposed to palmitic acid	5–10 μM	• Reduced lipid accumulation and the PPARγ and NF-κB pathways • Improved the adiponectin mRNA levels • Ameliorated adipose tissue dysfunction	2020	[60]
Palmitic acid-induced proximal tubular cells	2, 10, and 20 μM	• Inhibited the activation of NF-kB and the expression of inflammatory cytokine	2020	[61]
HepG2 cells and C2C12 myotubes	10 and 50 μM	• Increased glucose uptake • Induced the rate of hepatic fatty acid oxidation • Activated PPARs with the highest affinity for PPARα	2020	[19]
C3H/10T1/2 brown adipose cells	10–40 μM	• Regulated the UCP1 protein	2021	[62]
Human SGBS adipocytes and murine 3T3-L1 cells.	1–20 μM	• Reduced mRNA levels and prevented lipotoxicity in dysfunctional adipocytes	2021	[63]
Human amniotic epithelial cells (hAECs)	20 μM	• In differentially expressed genes, 109 genes were upregulated and 232 were downregulated.	2021	[64]
3T3-L1 preadipocytes	50–200 μM	• Reduced the formation of insulin fibrils • Attenuated insulin fibril-induced cytotoxicity	2022	[65]
3T3-L1 preadipocytes	30–100 μM	• Downregulated PPARγ, C/EBPα, adiponectin, and aP2 • Inhibited adipocyte formation	2023	[66]
Pancreatic lipase inhibitory assay	0.05 to 0.35 mg/mL	• C3G inhibited pancreatic lipase at IC50—0.268 mg/mL	2023	[67]
3T3-L1 preadipocytes	5 and 10 μM	• Reduced the C/EBPβ, PPARγ, FAS expressions, and activated the AMPK pathway in the early phase of adipogenesis	2023	[68]

An excessive amount of circulating free fatty acids has been proven to be potentially associated with obesity, insulin resistance, and diabetes. In this context, lipolysis inhibition is the main target for reducing free fatty acids and improving insulin sensitivity. A study reported that C3G effectively suppressed the release of free fatty acids and glycerol from 3T3-L1 adipocytes during hyperglycemia. C3G treatment downregulated the hexosamine

biosynthetic pathway by increasing the AMP-activated protein kinase activity, decreasing the glutamine:fructose 6-phosphate aminotransferase activity (GFAT), and reducing the production of cellular UDP-N-acetylglucosamine. Furthermore, C3G downregulated the adipose triglyceride lipase expression by attenuating the forkhead box O1 (FoxO1) transcription factor [45]. C3G efficiently improved insulin resistance in 3T3-L1 adipocytes by upregulating the expression of the glucose transporter type 4 (GLUT4) gene [40].

C3G markedly inhibited basal adipocyte lipolysis in differentiated human fat cells. A mixture of docosahexaenoic acid and C3G reduced the tumor necrosis factor-α (TNF-α) secretion and enhanced insulin-induced lipogenesis [50]. Matsukawa et al. [49] demonstrated that C3G treatment differentiated the 3T3-Ll cells into smaller adipocytes by upregulating the gene expressions of PPARγ and C/EBPα, increasing the adiponectin secretion, decreasing the TNF-α secretion, activating insulin signaling, and increasing the glucose uptake. Further, C3G effectively upregulated the expression of PGC-1α, sirtuin-1 (SIRT1), and the uncoupling protein (UCP)-3 genes in C2C12 myotubes. Jia et al. [19] found that C3G effectively enhanced the uptake of glucose in HepG2 cells as well as C2C12 myotubes. Further, C3G stimulated the hepatic fatty acid oxidation rate. The results revealed that C3G upregulated the main regulators of energy metabolism, i.e., PPARs. In rat adipocytes, C3G increased the secretion of adipocytokines, such as adiponectin and leptin. Further, the adipocyte-specific gene expression was upregulated by C3G treatment without PPARγ activation [35]. In human adipocytes, C3G or cyanidin treatment significantly upregulated the gene expression of adiponectin as well as downregulated plasminogen activator inhibitor-1 and IL-6. C3G or cyanidin treatment also activated the lipid metabolism-associated genes, such as uncoupling protein2, acyl-CoA oxidase1, and perilipin [36].

One of the promising approaches for treating obesity is to convert white adipocytes into brown-like adipocytes. In 3T3-L1 adipocytes, C3G stimulated phenotypic modifications into white adipocytes, such as higher levels of multilocular lipid droplets and mitochondrial content. In addition, C3G treatment increased the expression of the mitochondrial genes in 3T3-L1. Moreover, C3G improved the differentiation of preadipocytes by activating the CCAAT/enhancer-binding protein β (C/EBPβ) via increasing the level of intracellular cyclic adenosine 3′5′-monophosphate (cAMP) [53]. Recently, Han et al. [62] found that Prdm16 bound to the promoter region (−500 to −150 bp) of UCP1 to stimulate its transcription with the presence of C3G in C3H10T12 brown adipose cells, thereby facilitating brown adipose tissue programming. In differentiated palmitate-induced C3H10T1/2 clone8 cells, C3G suppressed the release of adipokines, such as extracellular nicotinamide phosphoribosyltransferase and fibroblast growth factor 21 [54].

A study indicated that C3G treatment significantly regulated protein kinase B (Akt) phosphorylation, the sensitivity of adipocytes to palmitic acid, GLUT-1 and GLUT-4 glucose transporters, and hexokinase-II in palmitic acid-induced human SGBS adipocytes. In addition, the cells pretreated with C3G exhibited a significant reduction in the mRNA levels of pro-inflammatory cytokines (TNF-α, interleukin (IL)-6, IL-8, and monocyte chemoattractant protein-1 (MCP-1)) in palmitic acid-induced human SGBS adipocytes [63]. C3G markedly reduced the accumulation of lipids, PPARγ, and the nuclear factor kappa B (NF-κB) pathways in palmitic acid-induced 3T3-L1 adipocytes, and enhanced insulin sensitivity via the restoration of the insulin receptor substrate 1 (IRS-1)/phosphatidylinositol 3-kinase (PI3K)/Akt pathway. Moreover, C3G improved the mRNA levels of adiponectin in palmitic acid-induced 3T3-L1 and SGBS human adipocytes [60]. C3G treatment efficiently triggered the expression and secretion of adiponectin in 3T3 adipocytes through the transcription factor forkhead box O1 (FoxO1). The authors found that C3G upregulated FoxO1 by enhancing its deacetylation through silent mating type information regulation 2 homolog 1 [47].

In 3T3-L1 adipocytes, a study found that C3G treatment effectively reverted the insulin resistance induced by H_2O_2- or TNF-α via the downregulation of the c-Jun N-terminal kinases (JNK) signaling pathway [38]. C3G and its metabolite protocatechuic acid improved the uptake of adipocyte glucose and GLUT4 membrane translocation in human

omental adipocytes and 3T3-L1 cells. Further, these components markedly increased the nuclear PPARγ activity and the expression of GLUT4 [42]. In macrophage-conditioned media-treated adipocytes, C3G and pelargonidin-3-O-glucoside suppressed the activation of the NF-κB and JNK pathways by regulating the phosphorylation of IκBα and JNK, respectively [2]. In 3T3-L1 adipocytes, anthocyanins extracted from colored corn blocked the adipocyte differentiation and the accumulation of lipids, and attenuated the transcription of PPAR-γ. In 3T3-L1 cells, black soybean anthocyanins decreased the accumulation of lipids and inhibited the expression of PPARγ [46]. Further, anthocyanins improved inflammation induced by TNF-α and insulin resistance in adipocytes by activating insulin signaling and enhanced translocation of GLUT4 [52].

Further, AMPK plays a key role in preventing hepatic lipid metabolism by regulating the downstream acetyl CoA carboxylase and carnitine palmitoyl transferase 1 pathways. A study indicated that C3G regulated hepatic lipid homeostasis through an AMPK-dependent signaling pathway [44]. In 3T3-L1 preadipocytes, cyanidin treatment suppressed adipogenesis via the downregulation of gene expressions, such as PPARγ, C/EBPα, adiponectin, and aP2. In addition, intracellular Ca^{2+} was increased in the cyanidin-stimulated cells [66]. Cyanidin-3-rutinoside (C3R) significantly upregulated the uptake of glucose and the expression of plasma membrane glucose transporter type 4 (GLUT4) by triggering the PI3K/Akt pathways [51]. In mesenteric adipose tissue-cultured medium-induced RAW 264.7 cells, cyanidin and C3G markedly inhibited the migration and production of inflammatory chemokines, such as MCP-1 and MRP-2 [37]. Zhang et al. [59] investigated the effect of anthocyanin-rich water extracts obtained from 20 different purple corn genotypes on RAW 264.7 macrophages and 3T3-L1 adipocytes. These extracts efficiently decreased the production of the pro-inflammatory mediators, regulated the diabetes-associated key enzymes, and improved insulin sensitivity. In the early phase of adipogenesis, C3G exposure markedly suppressed the expression of (C/EBPβ), PPARɣ, and FAS, and activated the AMPK pathway when compared to late-phase exposure [68].

Saulite et al. [58] investigated the effect of malvidin, cyanidin, and delphinidin against adipose tissue-derived human mesenchymal stem cells. The results revealed that delphinidin suppressed adipogenesis and decreased fatty acid-binding protein 4 (FABP4) and the adiponectin genes. Malvidin stimulated a higher level of calcium accumulation in the cells. Further, the osteocyte-specific gene BMP-2 and Runx-2 expression were upregulated in addition to the stimulation of BMP-2 secretion by malvidin. According to suitable stimuli, adipocytes can be proliferated and differentiated. The important transcription factor responsible for lipogenesis is the carbohydrate response element-binding protein (ChREBP) chiefly found in lipogenic organs. Pompei et al. [43] found that cyanidin diminished the differentiation by 20% as well as the ChREBP expression in preadipocytes. The authors suggested that cyanidin exhibited an inhibitory activity on adipogenesis by interfering with the extracellular matrix [43]. Takahashi et al. [64] reported that C3G showed significant induction in adipocyte differentiation in human amniotic epithelial cells.

Pancreatic lipase is one of the most essential digestive enzymes for metabolism as well as for the absorption of triglycerides to monoglycerides and free fatty acids. In the body, the level of total cholesterol is decreased when inhibiting the lipase enzyme activity [69]. In this context, different authors investigated the inhibitory potential of C3G against lipase enzymes. Their studies showed that C3G markedly inhibited the pancreatic lipase activity with IC_{50} values of 188.28 μM [57] and 0.268 mg/mL [67]. A recent study demonstrated that the development of insulin fibrils was attenuated by anthocyanins, such as cyanidin, C3G, C3R, malvidin, and malvidin-3-glucoside [65]. In another study, the results exhibited that C3R effectively inhibited pancreatic lipase (IC_{50} at 59.4 μM). Further, C3R showed a considerable reduction in the cholesterol uptake in free cholesterol as well as mixed micelles in addition to the suppression of the NPC1L1 expression in Caco-2 cells [56]. Chen et al. [70] found that C3G from *Aronia melanocarpa* exhibited the strongest inhibitory activity against α-amylase and lipase. However, cyanidin 3-galactoside, cyanidin-3-arabinoside, and cyanidin 3-xyloside did not show any effect on the α-amylase and lipase enzymes. Further,

Xie et al. [71] suggested that the structures of the B-ring and glycosyl group were mainly associated with the inhibitory potentials of monomeric anthocyanins.

5. In Vivo Studies on the Role of C3G in Obesity-Related Complications

Similar to the in vitro studies, numerous in vivo studies have been carried out to determine the effect of C3G on obesity-associated mechanisms (Table 2). The C3G-rich purple corn color effectively reduced body weight gain as well as the weights of white and brown adipose tissue in high-fat (HF) diet-induced mice. Further, the purple corn color downregulated the mRNA levels of the enzymes responsible for the synthesis of fatty acid triacylglycerol and reduced the mRNA level of sterol regulatory element-binding protein-1 in white adipose tissue [72]. In another study, the dietary intake of anthocyanin upregulated the adiponectin expression in white adipose tissue and suggested that the activation of AMPK was a possible mechanism for these changes [35].

Table 2. The effect of cyanidin-3-*O*-*β*-glucoside on the obesity-associated mechanisms under in vivo conditions.

Model	Dose	Mechanism(s)	Year of Publication	References
HFD-induced C57BL/6J mice	Purple corn extract; 2 g/kg diet	• Suppressed the mRNA levels of the enzymes involved in fatty acid and triacylglycerol synthesis • Lowered the SREBP-1 level in white adipose tissue	2003	[72]
HFD-induced C57/Bl6 mice	90 mg/kg/day	• Reduced body weight gain and fat accumulation	2010	[39]
HFD-induced C57BLK/6J mice	C3G-rich grape pomace extract; 250 mg/kg b.w. per day	• Lowered plasma C-reactive protein levels	2010	[73]
KK-Ay mice	10, 50, and 100 µmol/L; 1 g/kg	• Reduced obesity, the accumulation of fat, and the plasma triglyceride levels	2011	[41]
HFD-induced C57BL/6 mice	3G-rich black soybean seed coat extract for 14 weeks	• Suppressed fat accumulation, reduced the plasma glucose level, and enhanced insulin sensitivity • Upregulated UCP-1 in brown adipose tissue and UCP-2 in white adipose tissue • Downregulated inflammatory cytokines, TNF-α, and MCP-1 in white adipose tissue	2011	[74]
Sprague-Dawley rats—ovariectomized (OVX)	5% and 10% (*w*/*w*) black berries	• Decreased hepatic NF-κB, and the cyclooxygenase-2 expression levels	2012	[75]
HFD-fed C57BL/6J mice and db/db and db/+ mice	0.2%	• Reduced the white adipose tissue mRNA levels and inflammatory cytokines • Decreased the c-JNK activation and promoted the phosphorylation of FoxO1	2012	[76]
HFD-fed C57BL/6 mice	40 and 200 mg/kg food for 12 weeks	• Inhibited body weight gain, reduced insulin resistance, lowered the size of adipocytes, and reduced lipid accumulation and leptin secretion	2013	[77]

Table 2. *Cont.*

Model	Dose	Mechanism(s)	Year of Publication	References
HFD-induced rats	100 mg/kg	• Decreased body weight, visceral adiposity, the average feed efficiency ratio, triglyceride, total cholesterol, low density lipoprotein cholesterol, fasting glucose, and the insulin resistance index • Normalized the serum adiponectin and high-density lipoprotein cholesterol levels	2014	[78]
db/db mice	2 g/kg diet	• Restored endothelium-dependent relaxation of the aorta	2014	[47]
Estrogen-deficient animals with diet-induced obesity in OVX rats	Black carrot extract; 2% for 12 weeks	• Reduced fat mass and weight gain • Normalized HOMA-IR • Prevented the increase in the serum total and LDL cholesterol and triglycerides • Upregulated the gene expressions of CPT-1 and PPAR-α and downregulated the expressions of FAS and SREBP-1c	2015	[48]
HFD-induced C57BL/6J mice	Cyanidin-based anthocyanin-rich blackcurrant extract; 1% for 8 weeks	• Reduced body weight gain and improved glucose metabolism	2015	[79]
HFD-induced C57BL/6J mice	Anthocyanin-rich black elderberry extract; 20–40 mg and 100–200 mg/kg b.w. for 16 weeks	• Reduced liver weights, serum triglycerides, and MCP-1 • Decreased serum insulin and TNFα • Attenuated the mRNA level of FAS,PARγ2, and liver cholesterol	2015	[80]
Diabetes model in KK-Ay mice	C3G-rich aronia juice; free intake	• Reduced body weights and blood glucose levels • Reduced weights of white adipose tissues	2016	[81]
HFD-induced mice	Purple corn anthocyanin; 200 mg/kg	• Increased the fecal butyric acid levels, elevated hepatic SOD and GPx activities, and decreased lipid peroxidation • Downregulated the expression levels of TNFα, IL-6, iNOS, and NF-κB	2017	[82]
db/db mice	1 mg/mL for 16 weeks	• Increased energy expenditure, limited weight gain, maintained glucose homeostasis, reversed hepatic steatosis, improved cold tolerance, and enhanced BAT activity • Regulated the transcription of UCP1	2017	[17]
C57BL/6 J mice fed with a high-fat high-cholesterol diet	200 mg/kg	• Regulated the activation of brown adipose tissue and the expression of adipokines • Alleviated diet-induced fatty liver	2018	[54]
HFD-induced obese mice	Haskap Berry; 0.192% C3G-rich extract	• Decreased body weight gain • Decreased glucose excursion and exhibited lower glycemia	2018	[83]

Table 2. *Cont.*

Model	Dose	Mechanism(s)	Year of Publication	References
Human primary myotubes derived from obese and obese T2DM participants	10 and 100 μM	• Enhanced glucose uptake • Downregulated the expression of AGTR-1, and upregulated the expression of IRS-1 and GLUT4	2018	[84]
HFD-fed C57BL/6J mice	AC-rich blend; 2, 20, or 40 mg/kg body weight	• Mitigated obesity, dyslipidemia, and insulin resistance • Attenuated increased liver lipid deposition and inflammation • Suppressed oxidative stress, NF-κB and JNK activation, and PTP1B overexpression	2018	[85]
HF and high-fructose diet-induced mice	1 mg/mL	• Enhanced energy expenditure and thermogenic capacity • Increased the expression of UCP1 and other thermogenic genes	2018	[86]
Diet-induced mouse model	0.02 g/kg BW/ day	• Reduced systolic and diastolic blood pressure • Reduced the percentage of body fat and improved glucose tolerance	2019	[87]
HFD-induced C57BL/6N mice	*Aronia melanocarpa* extract (70% ethanol extract); 50, 100, and 200 mg/kg body weight/day	• Reduced the serum levels of leptin, insulin, triglyceride, total cholesterol, and LDL cholesterol • Decreased the CCAAT/enhancer-binding protein, PPAR, sterol regulatory element-binding protein-1c, PPARγ coactivator-1, acetyl-CoA carboxylase 1, ATP-citrate lyase, fatty acid synthase, and adipocyte protein mRNA expressions	2019	[88]
C57BL/6 J mice	50 mg/day/body weight for 8 weeks	• Reduced plasma and hepatic triglycerides, glucose tolerance, and adiposity	2020	[19]
HFD-induced C57BL/6J mice	Lingonberry (5% *w*/*w*) and its anthocyanin; C3G for 12 weeks	• Enhanced the plasma lipid and glucose profiles and reduced the plasma inflammatory cytokine levels	2020	[61]
HF and high-fructose diet-induced db/db mice	1 mg/mL	• Increased the expression of the UCP1 gene of BAT	2021	[62]
HFD-induced mice	Purple corn anthocyanin; 400 mg/kg	• Downregulated the expression of PPARγ, C/EBPα, and SREBP-1c • Upregulated the expression of PPARα, PGC1α, PRDM16, and FGF21 • Promoted the hepatic AMPK activity	2021	[4]
High-fat high-sucrose diet-indued mice	45.2 mg/kg for 10 weeks	• Attenuated liver steatosis, insulin resistance, and chronic inflammation	2021	[89]

Table 2. *Cont.*

Model	Dose	Mechanism(s)	Year of Publication	References
HFD Sprague-Dawley rats	Isolated from *Aronia melanocarpa*, Haicheng, China; 100 and 200 mg/kg bw/day) for 8 weeks.	• Inhibited body weight gain and reduced serum lipids and fat accumulation • Decreased the levels of TNF-α, IL-6, and IL-1β in serum • Alleviated obesity by promoting the phosphorylation of AMPK • Promoted the phosphorylation of STAT3 and suppressed NF-κB p65	2021	[90]
HF-high-carbohydrate diet-induced obesity model	0.02 g/kg BW/d	• Downregulated AGTR-1 and upregulated the GLUT4 mRNA expression	2022	[91]
High-fat meal in healthy humans	Cyanidin- and delphinidin-rich extract (1 g consisted of 150 mg bilberry extract, 230 mg black currant extract, and 620 mg black rice extract)	• Mitigated endotoxemia and reduced increases in plasma LPS and the LPS-binding protein • Attenuated plasma glucose and triglyceride increases, TNFα and NOX4 upregulation, and JNK1/2 activation	2022	[92]
HFD-fed C57BL/6 mice	Casein/C3G nanoparticles	• Ameliorated fat accumulation and liver oxidative stress	2023	[93]

It is well known that brown adipose tissue burns energy to generate heat. The previous studies found that C3G can improve the thermogenic ability of brown adipose tissue. Han et al. [62] evaluated the effect of C3G on the UCP1 gene expression in db/db mice induced with a HF, high-fructose diet and found that Prdm16 is directly bound to the promoter region of UCP1. In another study, C3G efficiently regulated the transcription of UCP1 in brown adipose tissue as well as in subcutaneous white adipose tissue by enhancing mitochondrial number and function [17]. In the diet-induced obesity mice model, the purple corn cob extract treatment upregulated the M2 markers (ArgI, Fizz1, and TGFβ) and downregulated the inflammatory mediators (TNF-α, IL-6, IL-1β, and COX-2) by suppressing NF-kB signaling [94]. Jia et al. [19] reported that the dietary supplementation of C3G upregulated the PPARs in the HF-diet-induced mice. In the KK-Ay mice, C3G significantly enhanced obesity and triglyceride metabolism by partly activating lipoprotein lipase in the plasma and skeletal muscle. The inhibition of lipoprotein lipase (LPL) in adipose tissue following the activation of pAMPK might have been attributed to the inhibition of lipoprotein lipase [41]. Guo et al. [76] reported that C3G regulated the signaling pathway, c-Jun N-terminal kinase/foxO1, and its associated inflammatory adipocytokines. Ren-Qiang et al. [78] also reported that C3G diminished obesity-related dyslipidemia and insulin resistance in HF-diet-induced rats by enhancing the level of serum adiponectin. Biswas et al. [83] reported that C3G supplementation in the diet reduced weight gain, and improved food intake and metabolism during obesity.

The combination of peptides and C3G markedly improved the glucose uptake with or without insulin. In addition, this combination suppressed the expression of the angiotensin II receptor, type 1 (AGTR-1), and activated the insulin receptor substrate 1 and GLUT4 expressions [84]. In diet-induced obese mice, the mixture of C3G and peptides efficiently decreased systolic as well as diastolic blood pressure. Further, this combination significantly reduced body fat levels and enhanced glucose tolerance [87]. In diet-induced obese mice, the combination of C3G and peptides regulated the expression of the genes associated with glucose metabolism [91]. The administration of anthocyanins from purple corn remarkably reduced body weight gain, fat mass, total cholesterol, and triglyceride levels in the HF-diet-induced mice. The data demonstrated that the anthocyanin extract suppressed the

expression of PPARγ, C/EBPα, and SREBP-1c, subsequently activating the expression of PPARα, PGC1α, PRDM16, and FGF21 [4].

Titta et al. [39] demonstrated that the anthocyanin-rich extract from Moro oranges marginally affected the accumulation of fats in C57/Bl6 mice induced with a HF diet. Anthocyanin black carrots fermented with *Aspergillus oryzae* inhibited lipid and glucose metabolism via the activation of hepatic insulin signaling and the AMPK pathways in OVX rats [48]. A study demonstrated that anthocyanins from black rice, black soybeans, and purple corn alleviated oxidative stress and inflammation-related obesity in HF-diet-induced mice by suppressing the expression of TNFα, IL-6, inducible nitric oxide synthase (iNOS), and NF-κB, and increasing the hepatic superoxide dismutase (SOD) and glutathione peroxidase (GPx) activities [82]. Blackberries containing 87% of the C3G diet downregulated the expression levels of hepatic NF-κB and cyclooxygenase-2 in ovariectomized rats [75]. A C3G-enriched *Aronia melanocarpa* extract inhibited adipogenesis by downregulating the expressions of the CCAAT/enhancer-binding protein, PPAR, sterol regulatory element-binding protein-1c, PPARγ coactivator-1, acetyl-CoA carboxylase 1, ATP-citrate lyase, fatty acid synthase, and adipocyte protein 2 [88]. The anthocyanin-rich extract from aronia fruit reduced the accumulation of visceral fat and hyperglycemia via the inhibition of pancreatic lipase activity and the adsorption of intestinal lipids [95]. In HF-diet-induced rats, C3G isolated from *Aronia melanocarpa* treatment expressively decreased the levels of TNF-α, IL-6, and IL-1β in the serum. Further, C3G improved HFD-induced obesity by activating AMPK and suppressed HFD-induced inflammation by activating the phosphorylation of STAT3 and suppressing NF-κB p65 in the nucleus [90].

Anthocyanins, such as C3G, C3R, and pelargonidin-3-glucoside, isolated from Chinese mulberry significantly inhibited body weight gain, reduced insulin resistance, lowered the size of adipocytes, and attenuated the accumulation of lipids and the secretion of leptin [77]. The supplementation of cyanidin and delphinidin effectively controlled overweight, obesity, and type 2 diabetes by modulating the activity of inflammatory mediators, oxidative stress, and NF-κB/JNK activation [85]. Esposito et al. [79] suggested that the gut microbiome and the kind of anthocyanin aglycone moiety could influence the preventive role of anthocyanins in obesity and their associated insulin resistance. The supplementation of cyanidin- and delphinidin-rich extracts also exhibited beneficial effects on unhealthy diets [92]. The administration of C3G from Saskatoon berries diminished liver steatosis, insulin resistance, and chronic inflammation in HF and high-sucrose-induced mice [89].

The improvement in the thermogenesis of brown adipose tissue is an efficient strategy for alleviating obesity. A study exhibited that C3G improved the energy expenditure and thermogenesis of brown adipose tissue in mice induced with HF diet obesity. Additionally, C3G upregulated the UCP1 expression as well as other thermogenic genes in inguinal white adipose tissue and brown adipose tissue [86]. In db/db mice, C3G treatment restored the endothelium-dependent relaxation of the aorta [47]. C3G controlled the adipokine expression in brown adipose tissue in high-fat-cholesterol diet-induced mice [54]. A recent study demonstrated that treatment with casein/C3G nanoparticles ameliorated the HFD-induced accumulation of fats and liver oxidative stress in C57BL/6 mice [93]. In a recent study, Meleleo et al. [96] demonstrated that anthocyanins, such as cyanidin, C3G quercetin, and quercetin-*O*-glucoside, interacted with planar lipid membranes and formed conductive units.

6. Conclusions and Future Perspectives

C3G is an important anthocyanin compound and is widely found in various fruits and vegetables. Previous studies established that C3G supplementation offers numerous health benefits to the consumer. In this review, we discussed the effect of C3G treatment on obesity-associated mechanisms under different in vitro and in vivo models. The mechanisms preventing obesity highly depend on their capacity to control the consumption of food and energy metabolism and improve inflammatory response, insulin resistance, and glucose metabolism. In addition, C3G can effectively inhibit the pancreatic lipase enzyme. A

variety of pathways and gene expressions play a crucial role in preventing obesity-related consequences. In particular, AMPK is an important pathway, attributed to the prevention of hepatic lipid metabolism, and PPARs play a key role in energy metabolism. The IRS-1/PI3K/Akt pathway and GLUT4 gene expression are mainly responsible for insulin sensitivity and the NF-κB signaling pathway is for inflammatory response. The published papers clearly showed that C3G could be a potential agent for facilitating the prevention and treatment of obesity-associated complications owing to its multi-targeted activities. Although C3G can effectively attenuate obesity-associated complications, further clinical studies leading to the development of C3G-enriched functional foods are required.

Author Contributions: Conceptualization, S.K.; methodology, S.K. and P.D.; writing—original draft preparation, P.D. and K.S.; writing—review and editing, M.H., K.S. and S.K. All authors have read and agreed to the published version of the manuscript.

Funding: This research received no external funding.

Data Availability Statement: Not applicable.

Acknowledgments: This work was supported by the "Quality characteristics of health function and development of breeding material lines of purple corn (PJ015140)" from the Rural Development Administration, Korea.

Conflicts of Interest: The authors declare no conflict of interest.

Abbreviations

ACC	Acetyl-CoA carboxylase
AGTR-1	Angiotensin II Receptor Type 1
Akt	Protein Kinase B
AMPK	Adenosine monophosphate-activated protein kinase
aP2	Adipocyte Protein 2
ATP	Adenosine triphosphate
BMP-2	Bone Morphogenetic Protein-2
C/EBPα	CCAAT/enhancer-binding protein α
C3G	Cyanidin-3-*O*-*β*-glucoside
C3R	Cyanidin-3-rutinoside
cAMP	Cyclic adenosine 3′,5′-monophosphate
ChREBP	Carbohydrate response element-binding protein
COX-2	Cyclooxygenase 2
CPT-1	Carnitine palmitoyltransferase I
FABP4	Fatty acid-binding protein 4
FAS	Fatty acid synthase
FGF21	Fibroblast growth factor 21 i
FoxO1	Forkhead box protein O1
GFAT	Glutamine:fructose-6-phosphate aminotransferase
GLUT4	Glucose transporter type 4
GPx	Glutathione peroxidase
H_2O_2	Hydrogen peroxide
hAECs	Human aortic endothelial cells
HFD	High-fat diet
IL-1β	Interleukin-1 beta
IL-6	Interleukin-6
iNOS	Inducible nitric oxide synthase
IRS-1	Insulin receptor substrate 1
IκBα	Inhibitor of nuclear factor kappa B
JNK	c-Jun N-terminal kinase
LPL	Lipoprotein lipase
malonyl CoA	Malonyl coenzyme A
MCP-1	Monocyte chemoattractant protein-1

mRNA	Messenger RNA
MRP-2	Macrophage inflammatory protein-related protein-2
NF-κB	Nuclear factor kappa B
NPC1L1	Niemann-Pick C1-Like 1
OVX	Ovariectomy
PAI-1	Plasminogen activator inhibitor-1
PGC1α	Peroxisome proliferator-activated receptor-γ coactivator 1-α
PI3K	Phosphoinositide 3-kinase
PPARs	Peroxisome proliferator-activated receptors
PPARα	Peroxisome proliferator-activated receptor alpha
PPARγ	Peroxisome proliferator-activated receptor gammaa
PRDM16	PR/SET Domain 16
PTP1B	Protein tyrosine phosphatase 1B
ROS	Reactive oxygen species
Runx-2	Runt-related transcription factor 2
SIRT1	Sirtuin1
SOD	Superoxide dismutase
SOD2	Superoxide dismutase-2
SREBP-1c	Sterol regulatory element-binding protein 1c
STAT3	Signal transducer and activator of transcription 3
TFAM	Mitochondrial transcription factor A
TNF-α	Tumor necrosis factor alpha
UCP	Uncoupling protein
WHO	World Health Organization

References

1. Wharton, S.; Lau, D.C.W.; Vallis, M.; Sharma, A.M.; Biertho, L.; Campbell-Scherer, D. Obesity in adults: A clinical practice guideline. *Can. Med. Assoc. J.* **2020**, *192*, E875–E891. [CrossRef]
2. Zhang, Q.; Vital, D.L.; Mejia, E.G.D. Anthocyanins from colored maize ameliorated the inflammatory paracrine interplay between macrophages and adipocytes through regulation of NF-κB and JNK-dependent MAPK pathways. *J. Funct. Foods* **2019**, *54*, 175–186. [CrossRef]
3. Hruby, A.; Hu, F.B. The Epidemiology of Obesity: A Big Picture. *Pharmacoeconomics* **2015**, *33*, 673–689. [CrossRef]
4. Xu, H.; Liu, M.; Liu, H.; Zhao, B.; Zheng, M.; Liu, J. Anthocyanins from purple corn ameliorated obesity in high fat diet-induced obese mice through activating hepatic AMPK. *J. Funct. Foods* **2021**, *84*, 104582. [CrossRef]
5. Gomes, J.V.P.; Rigolon, T.C.B.; Souza, M.S.D.S. Antiobesity effects of anthocyanins on mitochondrial biogenesis, inflammation, and oxidative stress: A systematic review. *Nutrition* **2019**, *66*, 192–202. [CrossRef]
6. Wolfenden, L.; Ezzati, M.; Larijani, B.; Dietz, W. The challenge for global health systems in preventing and managing obesity. *Obes. Rev.* **2019**, *20*, 185–193. [CrossRef]
7. Bluher, M. Obesity: Global epidemiology and pathogenesis. *Nat. Rev. Endocrinol.* **2019**, *15*, 288–298. [CrossRef]
8. Palou, A.; Bonet, M.L. Challenges in obesity research. *Nutr. Hosp.* **2013**, *5*, 144–153.
9. Lao, F.; Sigurdson, G.T.; Giusti, M.M. Health benefits of purple corn (*Zea mays* L.) phenolic compounds. *Compr. Rev. Food Sci. Food Saf.* **2017**, *16*, 234–246. [CrossRef]
10. Cuevas Montilla, E.; Hillebrand, S.; Antezana, A.; Winterhalter, P. Soluble and bound phenolic compounds in different Bolivian purple corn (*Zea mays* L.) cultivars. *J. Agric. Food Chem.* **2011**, *59*, 7068–7074. [CrossRef]
11. Yang, Z.; Zhai, W. Identification and antioxidant activity of anthocyanins extracted from the seed and cob of purple corn (*Zea mays* L.). *Innov. Food Sci. Emerg. Technol.* **2010**, *11*, 169–176. [CrossRef]
12. You, Y.; Zhou, F.; Huang, D. Eating the right color: Dietary anthocyanins and obesity control. *Food Beverage Asia* **2018**, *12*, 57–59.
13. Overall, J.; Bonney, S.A.; Wilson, M.; Beermann, A.; Grace, M.H.; Esposito, D.; Lila, M.A.; Komarnytsky, S. Metabolic Effects of Berries with Structurally Diverse Anthocyanins. *Int. J. Mol. Sci.* **2017**, *18*, 422. [CrossRef]
14. Acquaviva, R.; Russo, A.; Galvano, F.; Galvano, G.; Barcellona, M.L.; Li Volti, G.; Vanella, A. Cyanidin and cyanidin 3-O-beta-D-glucoside as DNA cleavage protectors and antioxidants. *Cell Biol. Toxicol.* **2003**, *19*, 243–252. [CrossRef]
15. Galvano, F.; La Fauci, L.; Lazzarino, G.; Fogliano, V.; Ritieni, A.; Ciappellano, S.; Battistini, N.C.; Tavazzi, B.; Galvano, G. Cyanidins: Metabolism and biological properties. *J. Nutr. Biochem.* **2004**, *15*, 2–11. [CrossRef]
16. Zhu, W.; Jia, Q.; Wang, Y.; Zhang, Y.; Xia, M. The anthocyanin cyanidin-3-*O*-*β*-glucoside, a flavonoid, increases hepatic glutathione synthesis and protects hepatocytes against reactive oxygen species during hyperglycemia: Involvement of a cAMP-PKA-dependent signaling pathway. *Free Radic. Biol. Med.* **2012**, *52*, 314–327. [CrossRef]
17. You, Y.; Yuan, X.; Liu, X.; Liang, C.; Meng, M.; Huang, Y.; Han, X.; Guo, J.; Guo, Y.; Ren, C.; et al. Cyanidin-3-glucoside increases whole body energy metabolism by upregulating brown adipose tissue mitochondrial function. *Mol. Nutr. Food Res.* **2017**, *61*, 1700261. [CrossRef]

18. Zannou, O.; Oussou, K.F.; Chabi, I.B.; Awad, N.M.H.; Aïssi, M.V.; Goksen, G.; Mortas, M.; Oz, F.; Proestos, C.; Kayodé, A.P.P. Nanoencapsulation of Cyanidin 3-O-Glucoside: Purpose, technique, bioavailability, and stability. *Nanomaterials* **2023**, *13*, 617. [CrossRef]
19. Jia, Y.; Wu, C.; Kim, Y.S.; Yang, S.O.; Kim, Y.; Kim, J.S.; Jeong, M.Y.; Lee, J.H.; Kim, B.; Lee, S.; et al. A dietary anthocyanin cyanidin-3-*O*-glucoside binds to PPARs to regulate glucose metabolism and insulin sensitivity in mice. *Commun. Biol.* **2020**, *3*, 514. [CrossRef]
20. Spinardi, A.; Cola, G.; Gardana, C.S.; Mignani, I. Variation of Anthocyanin Content and Profile Throughout Fruit Development and Ripening of Highbush Blueberry Cultivars Grown at Two Different Altitudes. *Front. Plant Sci.* **2019**, *10*, 1045. [CrossRef]
21. Liu, Z.; Dong, B.; Liu, C.; Zong, Y.; Shao, Y.; Liu, B.; Yue, H. Variation of anthocyanin content in fruits of wild and cultivated *Lycium ruthenicum*. *Ind. Crops Prod.* **2020**, *146*, 11220. [CrossRef]
22. Mattioli, R.; Francioso, A.; Mosca, L.; Silva, P. Anthocyanins: A Comprehensive Review of Their Chemical Properties and Health Effects on Cardiovascular and Neurodegenerative Diseases. *Molecules* **2020**, *25*, 3809. [CrossRef]
23. de Pascual-Teresa, S.; Sanchez-Ballesta, M.T. Anthocyanins: From plant to health. *Phytochem. Rev.* **2008**, *7*, 281–299. [CrossRef]
24. Wu, X.; Beecher, G.R.; Holden, J.M.; Haytowitz, D.B.; Gebhardt, S.E.; Prior, R.L. Concentrations of anthocyanins in common foods in the United States and estimation of normal consumption. *J. Agric. Food Chem.* **2006**, *54*, 4069–4075. [CrossRef]
25. Neveu, V.; Perez-Jimenez, J.; Vos, F.; Crespy, V.; du Chaaut, L.; Mennen, L.; Knox, C.; Eisner, R.; Cruz, J.; Wishart, D.; et al. Phenol-Explorer: An online comprehensive database on polyphenol contents in foods. *Database* **2010**, *2010*, bap024. [CrossRef]
26. Cheng, Z.; Si, X.; Tan, H.; Zang, Z.; Tian, J.; Shu, C.; Sun, X.; Li, Z.; Jiang, Q.; Meng, X.; et al. Cyanidin-3-*O*-glucoside and its phenolic metabolites ameliorate intestinal diseases via modulating intestinal mucosal immune system: Potential mechanisms and therapeutic strategies. *Crit. Rev. Food Sci. Nutr.* **2023**, *63*, 1629–1647. [CrossRef]
27. Frountzas, M.; Karanikki, E.; Toutouza, O.; Sotirakis, D.; Schizas, D.; Theofilis, P.; Tousoulis, D.; Toutouzas, K.G. Exploring the Impact of Cyanidin-3-Glucoside on Inflammatory Bowel Diseases: Investigating New Mechanisms for Emerging Interventions. *Int. J. Mol. Sci.* **2023**, *24*, 9399. [CrossRef]
28. Khoo, H.E.; Azlan, A.; Tang, S.T.; Lim, S.M. Anthocyanidins and anthocyanins: Colored pigments as food, pharmaceutical ingredients, and the potential health benefits. *Food Nutr. Res.* **2017**, *61*, 1361779. [CrossRef]
29. Castañeda-Ovando, A.; de Lourdes Pacheco-Hernández, M.; Páez-Hernández, M.E.; Rodríguez, J.A.; Galán-Vidal, C.A. Chemical studies of anthocyanins: A review. *Food Chem.* **2009**, *113*, 859–871. [CrossRef]
30. He, J.; Giusti, M.M. Anthocyanins: Natural colorants with health-promoting properties. *Annu. Rev. Food Sci. Technol.* **2010**, *1*, 163–187. [CrossRef]
31. Olivas-Aguirre, F.J.; Rodrigo-García, J.; Martínez-Ruiz, N.D.R.; Cárdenas-Robles, A.I.; Mendoza-Díaz, S.O.; Álvarez-Parrilla, E.; González-Aguilar, G.A.; De la Rosa, L.A.; Ramos-Jiménez, A.; Wall-Medrano, A. Cyanidin-3-*O*-glucoside: Physical-Chemistry, Foodomics and Health Effects. *Molecules* **2016**, *21*, 1264. [CrossRef]
32. De Ferrars, R.M.; Czank, C.; Zhang, Q.; Botting, N.P.; Kroon, P.A.; Cassidy, A.; Kay, C.D. The pharmacokinetics of anthocyanins and their metabolites in humans. *Br. J. Pharmacol.* **2014**, *171*, 3268–3282. [CrossRef]
33. Zhao, X.; Yuan, Z.; Feng, L.; Fang, Y. Cloning and expression of anthocyanin biosynthetic genes in red and white pomegranate. *J. Plant Res.* **2015**, *128*, 687–696. [CrossRef]
34. Tan, J.; Li, Y.; Hou, D.X.; Wu, S. The Effects and Mechanisms of Cyanidin-3-Glucoside and Its Phenolic Metabolites in Maintaining Intestinal Integrity. *Antioxidants* **2019**, *8*, 479. [CrossRef]
35. Tsuda, T.; Ueno, Y.; Aoki, H.; Koda, T.; Horio, F.; Takahashi, N.; Kawada, T.; Osawa, T. Anthocyanin enhances adipocytokine secretion and adipocyte-specific gene expression in isolated rat adipocytes. *Biochem. Biophys. Res. Commun.* **2004**, *316*, 149–157. [CrossRef]
36. Tsuda, T.; Ueno, Y.; Yoshikawa, T.; Kojo, H.; Osawa, T. Microarray profiling of gene expression in human adipocytes in response to anthocyanins. *Biochem. Pharmacol.* **2006**, *71*, 1184–1197. [CrossRef]
37. Choe, M.R.; Kang, J.H.; Yoo, H.; Choe, S.Y.; Yang, C.H.; Kim, M.O.; Yu, R. Cyanidin and Cyanidin-3-*O*-*β*-D-glucoside suppress the inflammatory responses of obese adipose tissue by inhibiting the release of chemokines MCP-1 and MRP-2. *J. Food Sci. Nutr.* **2007**, *12*, 148–153. [CrossRef]
38. Guo, H.; Ling, W.; Wang, Q.; Liu, C.; Hu, Y.; Xia, M. Cyanidin 3-glucoside protects 3T3-L1 adipocytes against H2O2- or TNF-alpha-induced insulin resistance by inhibiting c-Jun NH2-terminal kinase activation. *Biochem. Pharmacol.* **2008**, *75*, 1393–1401. [CrossRef]
39. Titta, L.; Trinei, M.; Stendardo, M.; Berniakovich, I.; Petroni, K.; Tonelli, C.; Riso, P.; Porrini, M.; Minucci, S.; Pelicci, P.G.; et al. Blood orange juice inhibits fat accumulation in mice. *Int. J. Obes.* **2010**, *34*, 578–588. [CrossRef]
40. Inaguma, T.; Han, J.; Isoda, H. Improvement of insulin resistance by Cyanidin 3-glucoside, anthocyanin from black beans through the up-regulation of GLUT4 gene expression. *BMC Proc.* **2011**, *5* (Suppl. S8), P21. [CrossRef]
41. Wei, X.; Wang, D.; Yang, Y.; Xia, M.; Li, D.; Li, G.; Zhu, Y.; Xiao, Y.; Ling, W. Cyanidin-3-*O*-*β*-glucoside improves obesity and triglyceride metabolism in KK-Ay mice by regulating lipoprotein lipase activity. *J. Sci. Food Agric.* **2011**, *91*, 1006–1013. [CrossRef]
42. Scazzocchio, B.; Vari, R.; Filesi, C.; Archivio, M.D.; Santangelo, C.; Giovannini, C.; Lacovelli, A.; Silecchia, G.; Volti, G.L.; Galvano, F.; et al. Cyanidin-3-*O*-*β*-glucoside and protocatechuic acid exert insulin-like effects by upregulating PPARγ activity in human omental adipocytes. *Diabetes* **2011**, *60*, 2234–2244. [CrossRef]

43. Pompei, A.; Toniato, E.; Innocenti, P.D.; Alimonte, I.; Cellini, C.; Mattoscio, D.; Cotellese, R.; Bosco, D.; Ciccarelli, R.; Dadorante, V.D.; et al. Cyanidin reduces preadipocyte differentiation and relative ChREBP expression. *J. Biol. Regul. Homeost. Agents* **2012**, *26*, 253–264.
44. Guo, H.; Liu, G.; Zhong, R.; Wang, Y.; Wang, D.; Xia, M. Cyanidin-3-*O*-*β*-glucoside regulates fatty acid metabolism via an AMP-activated protein kinase-dependent signaling pathway in human HepG2 cells. *Lipids Health Dis.* **2012**, *11*, 10. [CrossRef]
45. Guo, H.; Guo, J.; Jiang, X.; Li, Z.; Ling, W. Cyanidin-3-*O*-*β*-glucoside, a typical anthocyanin, exhibits antilipolytic effects in 3T3-L1 adipocytes during hyperglycemia: Involvement of FoxO1-mediated transcription of adipose triglyceride lipase. *Food Chem. Toxicol.* **2012**, *50*, 3040–3047. [CrossRef]
46. Kim, H.K.; Kim, J.N.; Han, S.N.; Nam, J.H.; Na, H.N.; Ha, T.J. Black soybean anthocyanins inhibit adipocyte differentiation in 3T3-L1 cells. *Nutr. Res.* **2012**, *32*, 770–777. [CrossRef]
47. Liu, Y.; Li, D.; Zhang, Y.; Sun, R.; Xia, M. Anthocyanin increases adiponectin secretion and protects against diabetes-related endothelial dysfunction. *Am. J. Physiol. Endocrinol. Metab.* **2014**, *306*, E975–E988. [CrossRef]
48. Park, S.; Kang, S.; Jeong, D.Y.; Jeong, S.Y.; Park, J.J.; Yun, H.S. Cyanidin and malvidin in aqueous extracts of black carrots fermented with *Aspergillus oryzae* prevent the impairment of energy, lipid and glucose metabolism in estrogen-deficient rats by AMPK activation. *Genes Nutr.* **2015**, *10*, 455. [CrossRef]
49. Matsukawa, T.; Inaguma, T.; Han, J.; Villareal, M.O.; Isoda, H. Cyanidin-3-glucoside derived from black soybeans ameliorate type 2 diabetes through the induction of differentiation of preadipocytes into smaller and insulin-sensitive adipocytes. *J. Nutr. Biochem.* **2015**, *26*, 860–867. [CrossRef]
50. Bjork, C.; Wilhelm, U.; Mandrup, S.; Larsen, B.D.; Bordoni, A.; Heden, P.; Ryden, M.; Arner, P.; Laurencikiene, J. Effects of selected bioactive food compounds on human white adipocyte function. *Nutr. Metab.* **2016**, *13*, 4. [CrossRef]
51. Choi, K.H.; Lee, H.A.; Park, M.H.; Han, J.S. Cyanidin-3-rutinoside increases glucose uptake by activating the PI3K/Akt pathway in 3T3-L1 adipocytes. *Environ. Toxicol. Pharmacol.* **2017**, *54*, 1–6. [CrossRef]
52. Luna-Vital, D.; Weiss, M.; Mejia, E.G.D. Anthocyanins from purple corn ameliorated tumor necrosis factor-α-induced inflammation and insulin resistance in 3T3-L1 adipocytes via activation of insulin signaling and enhanced GLUT4 translocation. *Mol. Nutr. Food Res.* **2017**, *61*, 1700362. [CrossRef]
53. Matsukawa, T.; Villareal, M.O.; Motojima, H.; Isoda, H. Increasing cAMP levels of preadipocytes by cyanidin-3-glucoside treatment induces the formation of beige phenotypes in 3T3-L1 adipocytes. *J. Nutr. Biochem.* **2017**, *40*, 77–85. [CrossRef]
54. Pei, L.; Wan, T.; Wang, S.; Ye, M.; Qiu, Y.; Jiang, R.; Pang, N.; Huang, Y.; Zhou, Y.; Jiang, X.; et al. Cyanidin-3-*O*-*β*-glucoside regulates the activation and the secretion of adipokines from brown adipose tissue and alleviates diet induced fatty liver. *Biomed. Pharmacother.* **2018**, *105*, 625–632. [CrossRef]
55. Muscarà, C.; Molonia, M.S.; Speciale, A.; Bashllari, R.; Cimino, F.; Occhiuto, C.; Saija, A.; Cristani, M. Anthocyanins ameliorate palmitate-induced inflammation and insulin resistance in 3T3-L1 adipocytes. *Phytother. Res.* **2019**, *33*, 1888–1897. [CrossRef]
56. Thilavech, T.; Adisakwattana, S. Cyanidin-3-rutinoside acts as a natural inhibitor of intestinal lipid digestion and absorption. *BMC Complement. Altern. Med.* **2019**, *19*, 242. [CrossRef]
57. Vijayaraj, P.; Nakagawa, H.; Yamaki, K. Cyanidin and cyanidin-3-glucoside derived from *Vigna unguiculata* act as noncompetitive inhibitors of pancreatic lipase. *J. Food Biochem.* **2019**, *43*, e12774. [CrossRef]
58. Saulite, L.; Jekabsons, K.; Klavins, M.; Muceniece, R.; Riekstina, U. Effects of malvidin, cyanidin and delphinidin on human adipose mesenchymal stem cell differentiation into adipocytes, chondrocytes and osteocytes. *Phytomedicine* **2019**, *53*, 86–95. [CrossRef]
59. Zhang, Q.; Mejia, E.G.D.; Vital, D.L.; Tao, T.; Chandrasekaran, S.; Chatham, L.; Juvik, J.; Singh, V.; Kumar, D. Relationship of phenolic composition of selected purple maize (*Zea mays* L.) genotypes with their anti-inflammatory, anti-adipogenic and anti-diabetic potential. *Food Chem.* **2019**, *289*, 739–750. [CrossRef]
60. Molonia, M.S.; Occhiuto, C.; Muscara, C.; Speciale, A.; Bashllari, R.; Villarroya, F.; Saija, A.; Cimino, F.; Cristani, M. Cyanidin-3-*O*-glucoside restores insulin signaling and reduces inflammation in hypertrophic adipocytes. *Arch. Biochem. Biophys.* **2020**, *691*, 108488. [CrossRef]
61. Madduma Hewage, S.; Prashar, S.; Debnath, S.C.; Karmin, O.; Siow, Y.L. Inhibition of Inflammatory Cytokine Expression Prevents High-Fat Diet-Induced Kidney Injury: Role of Lingonberry Supplementation. *Front. Med.* **2020**, *7*, 80. [CrossRef]
62. Han, S.; Yang, Y.; Lu, Y.; Guo, J.; Han, X.; Gao, Y.; Huang, W.; You, Y.; Zhan, J. Cyanidin-3-*O*-glucoside regulates the expression of Ucp1 in brown adipose tissue by activating Prdm16 gene. *Antioxidants* **2021**, *10*, 1986. [CrossRef] [PubMed]
63. Molonia, M.S.; Quesada-Lopez, T.; Speciale, A.; Muscara, C.; Saija, A.; Villarroya, F.; Cimino, F. In vitro effects of Cyanidin-3-*O*-Glucoside on inflammatory and insulin-sensitizing genes in human adipocytes exposed to palmitic acid. *Chem. Biodivers.* **2021**, *12*, e2100607. [CrossRef] [PubMed]
64. Takahashi, S.; Ferdousi, F.; Zheng, Y.-W.; Oda, T.; Isoda, H. Human amniotic epithelial cells as a tool to investigate the effects of cyanidin 3-O-Glucoside on cell differentiation. *Int. J. Mol. Sci.* **2021**, *22*, 3768. [CrossRef]
65. Channuwong, P.; Salae, K.; Chongruchiroj, S.; Cheng, H.; Suantawee, T.; Thilavech, T.; Adisakwattana, S. Dietary anthocyanins inhibit insulin fibril formation and cytotoxicity in 3T3-L1 preadipocytes. *Int. J. Biol. Macromol.* **2022**, *223*, 1578–1585. [CrossRef]
66. Kongthitilerd, P.; Barras, E.; Rong, W.; Thibodeaux, A.; Rigdon, M.; Yao, S.; Adisakwattana, S.; Suantawee, T.; Cheng, H. Cyanidin inhibits adipogenesis in 3T3-L1 preadipocytes by activating the PLC-IP3 pathway. *Biomed. Pharmacother.* **2023**, *162*, 114677. [CrossRef]

67. Wang, Y.; Chen, L.; Liu, H.; Xie, J.; Yin, W.; Xu, Z.; Ma, H.; Wu, W.; Zheng, M.; Liu, M.; et al. Characterization of the synergistic inhibitory effect of cyanidin-3-*O*-glucoside and catechin on pancreatic lipase. *Food Chem.* **2023**, *404*, 134672. [CrossRef]
68. Molonia, M.S.; Salamone, F.L.; Muscarà, C.; Costa, G.; Vento, G.; Saija, A.; Speciale, A.; Cimino, F. Regulation of mitotic clonal expansion and thermogenic pathway are involved in the antiadipogenic effects of cyanidin-3-*O*-glucoside. *Front. Pharmacol.* **2023**, *14*, 1225586. [CrossRef]
69. Vangoori, Y.; Dakshinamoorthi, A.; Kavimani, S. Prominent Pancreatic Lipase Inhibition and Free Radical Scavenging Activity of a *Myristica fragrans* Ethanolic Extract in vitro. Potential Role in Obesity Treatment. *Maedica* **2019**, *14*, 254–259.
70. Chen, L.; Chen, W.; Li, D.; Liu, X. Anthocyanin and proanthocyanidin from *Aronia melanocarpa* (Michx.) Ell.: Purification, fractionation, and enzyme inhibition. *Food Sci. Nutr.* **2023**, *11*, 3911–3922. [CrossRef]
71. Xie, L.; Xie, J.; Xu, Y.; Chen, W. Discovery of anthocyanins from cranberry extract as pancreatic lipase inhibitors using a combined approach of ultrafiltration, molecular simulation and spectroscopy. *Food Funct.* **2020**, *11*, 8527–8536. [CrossRef]
72. Tsuda, T.; Horio, F.; Uchida, K.; Aoki, H.; Osawa, T. Dietary cyanidin 3-O-beta-D-glucoside-rich purple corn color prevents obesity and ameliorates hyperglycemia in mice. *J. Nutr.* **2003**, *133*, 2125–2130. [CrossRef]
73. Hogan, S.; Canning, C.; Sun, S.; Sun, X.; Zhou, K. Effects of grape pomace antioxidant extract on oxidative stress and inflammation in diet induced obese mice. *J. Agric. Food Chem.* **2010**, *58*, 11250–11256. [CrossRef] [PubMed]
74. Kanamoto, Y.; Yamashita, Y.; Nanba, F.; Yoshida, T.; Tsuda, T.; Fukuda, I.; Nakamura-Tsuruta, S.; Ashida, H. A black soybean seed coat extract prevents obesity and glucose intolerance by up-regulating uncoupling proteins and down-regulating inflammatory cytokines in high-fat diet-fed mice. *J. Agric. Food Chem.* **2011**, *59*, 8985–8993. [CrossRef]
75. Kaume, L.; Gilbert, W.C.; Brownmiller, C.; Howard, L.R.; Devareddy, L. Cyanidin 3-O-β-D-glucoside-rich blackberries modulate hepatic gene expression, and anti-obesity effects in ovariectomized rats. *J. Funct. Foods* **2012**, *4*, 480–488. [CrossRef]
76. Guo, H.; Xia, M.; Zou, T.; Ling, W.; Zhong, R.; Zhang, W. Cyanidin 3-glucoside attenuates obesity-associated insulin resistance and hepatic steatosis in high-fat diet-fed and db/db mice via the transcription factor FoxO1. *J. Nutr. Biochem.* **2012**, *23*, 349–360. [CrossRef] [PubMed]
77. Wu, T.; Qi, X.; Liu, Y.; Guo, J.; Zhu, R.; Chen, W.; Zheng, X.; Yu, T. Dietary supplementation with purified mulberry (*Morus australis* Poir) anthocyanins suppresses body weight gain in high-fat diet fed C57BL/6 mice. *Food Chem.* **2013**, *141*, 482–487. [CrossRef] [PubMed]
78. Ren-Qiang, Y.; Xiao-You, Q.; Xiang, Z.; Jing, Z.; Lu-Yi, M. Cyanidin-3-glucoside attenuates body weight gain, serum lipid concentrations and insulin resistance in high-fat diet-induced obese rats. *Chin. J. Contemp. Pediatr.* **2014**, *16*, 534–538.
79. Esposito, D.; Damsud, T.; Wilson, M.; Grace, M.H.; Strauch, R.; Li, X.; Lila, M.A.; Komarnytsky, S. Black Currant Anthocyanins Attenuate Weight Gain and Improve Glucose Metabolism in Diet-Induced Obese Mice with Intact, but Not Disrupted, Gut Microbiome. *J. Agric. Food Chem.* **2015**, *63*, 6172–6180. [CrossRef]
80. Farrell, N.J.; Norris, G.H.; Ryan, J.; Porter, C.M.; Jiang, C.; Blesso, C.N. Black elderberry extract attenuates inflammation and metabolic dysfunction in diet-induced obese mice. *Br. J. Nutr.* **2015**, *114*, 1123–1131. [CrossRef]
81. Yamane, T.; Kozuka, M.; Konda, D.; Nakano, Y.; Nakagaki, T.; Ohkubo, I.; Ariga, H. Improvement of blood glucose levels and obesity in mice given aronia juice by inhibition of dipeptidyl peptidase IV and α-glucosidase. *J. Nutr. Biochem.* **2016**, *31*, 106–112. [CrossRef]
82. Wu, T.; Guo, X.; Zhang, M.; Yang, L.; Liu, R.; Yin, J. Anthocyanins in black rice, soybean and purple corn increase fecal butyric acid and prevent liver inflammation in high fat diet-induced obese mice. *Food Funct.* **2017**, *8*, 3178–3186. [CrossRef]
83. Biswas, D.; Sarkar, S.; De Silva, A.B.K.H.; D'Souza, K.; Kienesberger, P.; Rupasinghe, H.P.V.; Pulinilkunnil, T. Cyanidin-3-*O*-Glucoside rich extract from haskap berry improves glucose homeostasis and insulin sensitivity in diet-induced obese mice. *Can. J. Diabetes* **2018**, *42*, S24–S61. [CrossRef]
84. Shi, M.; O'Keefe, L.; Simcocks, A.C.; Su, X.Q.; McAinch, A.J. The effect of cyanidin-3-*O*-*β*-glucoside and peptides extracted from yoghurt on glucose uptake and gene expression in human primary skeletal muscle myotubes from obese and obese diabetic participants. *J. Funct. Foods* **2018**, *51*, 55–64. [CrossRef]
85. Daveri, E.; Cremonini, E.; Mastaloudis, A.; Hester, S.N.; Wood, S.M.; Waterhouse, A.L.; Anderson, M.; Fraga, C.G.; Oteiza, P.I. Cyanidin and delphinidin modulate inflammation and altered redox signaling improving insulin resistance in high fat-fed mice. *Redox Biol.* **2018**, *18*, 16–24. [CrossRef]
86. You, Y.; Han, X.; Guo, J.; Guo, Y.; Yin, M.; Liu, G.; Huang, W.; Zhan, J. Cyanidin-3-glucoside attenuates high-fat and high-fructose diet-induced obesity by promoting the thermogenic capacity of brown adipose tissue. *J. Funct. Foods* **2018**, *41*, 62–71. [CrossRef]
87. Shi, M.; Mathai, M.L.; Xu, G.; McAinch, A.J.; Su, X.Q. The effects of supplementation with blueberry, cyanidin-3-*O*-*β*-glucoside, yoghurt and its peptides on obesity and related comorbidities in a diet-induced obese mouse model. *J. Funct. Foods* **2019**, *56*, 92–101. [CrossRef]
88. Lim, S.-M.; Lee, H.S.; Jung, J.I.; Kim, S.M.; Kim, N.Y.; Seo, T.S.; Bae, J.-S.; Kim, E.J. Cyanidin-3-*O*-Galactoside-enriched *Aronia melanocarpa* extract attenuates weight gain and adipogenic pathways in high-fat diet-induced obese C57BL/6 mice. *Nutrients* **2019**, *11*, 1190. [CrossRef]
89. Zhao, R.; Xiang, B.; Dolinsky, V.W.; Xia, M.; Shen, G.X. Saskatoon berry powder reduces hepatic steatosis and insulin resistance in high fat-high sucrose diet-induced obese mice. *J. Nutr. Biochem.* **2021**, *95*, 108778. [CrossRef]

90. Jiao, X.; Shen, Y.; Deng, H.; Zhang, Q.; Zhao, J. Cyanidin-3-*O*-galactoside from *Aronia melanocarpa* attenuates high-fat diet-induced obesity and inflammation via AMPK, STAT3, and NF-κB p65 signaling pathways in Sprague-Dawley rats. *J. Funct. Foods* **2021**, *85*, 104616. [CrossRef]
91. Shi, M.; Mathai, M.L.; Xu, G.; Su, X.Q.; McAinch, A.J. The effect of dietary supplementation with blueberry, cyanidin-3-*O*-*β*-glucoside, yoghurt and its peptides on gene expression associated with glucose metabolism in skeletal muscle obtained from a high-fat-high-carbohydrate diet induced obesity model. *PLoS ONE* **2022**, *17*, e0270306. [CrossRef]
92. Cremonini, E.; Daveri, E.; Iglesias, D.E.; Kang, J.; Wang, Z.; Gray, R.; Mastaloudis, A.; Kay, C.D.; Hester, S.N.; Wood, S.M.; et al. A randomized placebo-controlled cross-over study on the effects of anthocyanins on inflammatory and metabolic responses to a high-fat meal in healthy subjects. *Redox Biol.* **2022**, *51*, 102273. [CrossRef]
93. Lyu, Q.; Deng, H.; Wang, S.; El-Seedi, H.; Cao, H.; Chen, L.; Teng, H. Dietary supplementation with casein/cyanidin-3-*O*-glucoside nanoparticles alters the gut microbiota in high-fat fed C57BL/6 mice. *Food Chem.* **2023**, *412*, 135494. [CrossRef]
94. Tomay, F.; Marinelli, A.; Leoni, V.; Caccia, C.; Matros, A.; Mock, H.P.; Tonelli, C.; Petroni, K. Purple corn extract induces long-lasting reprogramming and M2 phenotypic switch of adipose tissue macrophages in obese mice. *J. Transl. Med.* **2019**, *17*, 237. [CrossRef]
95. Takahashi, A.; Shimizu, H.; Okazaki, Y.; Sakaguchi, H.; Taira, T.; Suzuki, T.; Chiji, H. Anthocyanin-rich Phytochemicals from Aronia Fruits Inhibit Visceral Fat Accumulation and Hyperglycemia in High-fat Diet-induced Dietary Obese Rats. *J. Oleo. Sci.* **2015**, *64*, 1243–1250. [CrossRef]
96. Meleleo, D.; Avato, P.; Conforti, F.; Argentieri, M.P.; Messina, G.; Cibelli, G.; Mallamaci, R. Interaction of Quercetin, Cyanidin, and Their O-Glucosides with Planar Lipid Models: Implications for Their Biological Effects. *Membranes* **2023**, *13*, 600. [CrossRef]

frontiers | Frontiers in Plant Science

TYPE Editorial
PUBLISHED 28 March 2024
DOI 10.3389/fpls.2024.1400006

OPEN ACCESS

EDITED AND REVIEWED BY
Brigitte Mauch-Mani,
Université de Neuchâtel, Switzerland

*CORRESPONDENCE
Archana Singh
archanasingh@pmb.du.ac.in
Dhandapani Gurusamy
gdhandapani@kongunaducollege.ac.in
Indrakant K. Singh
iksingh@db.du.ac.in

RECEIVED 12 March 2024
ACCEPTED 22 March 2024
PUBLISHED 28 March 2024

CITATION
Singh A, Gurusamy D and Singh IK (2024) Editorial: Calcium signaling: an early plant defense response against pests and pathogens.
Front. Plant Sci. 15:1400006.
doi: 10.3389/fpls.2024.1400006

Editorial: Calcium signaling: an early plant defense response against pests and pathogens

Archana Singh[1,2,3]*, Dhandapani Gurusamy[4]* and Indrakant K. Singh[5]*

[1]Department of Plant Molecular Biology, University of Delhi, New Delhi, India, [2]Department of Botany, Hansraj College, University of Delhi, Delhi, India, [3]Delhi School of Climate Change and Sustainability, Institution of Eminence, Maharishi Karnad Bhawan, University of Delhi, Delhi, India, [4]Department of Botany, Kongunadu Arts and Science College (Autonomous), Bharathiar University, Coimbatore, Tamil Nadu, India, [5]Molecular Biology Research Lab, Department of Zoology, Deshbandhu College & Delhi School of Public Health, Institution of Eminence, University of Delhi, Delhi, India

KEYWORDS

Ca^{2+} signaling, cyclic-nucleotide-gated channels (CNGCs), calmodulin, biotic stress, crop production

Editorial on the Research Topic
Calcium signaling: an early plant defense response against pests and pathogens

Plants are exposed to biotic stresses caused by interactions with other living organisms. This leads to adverse effects on their growth, development and productivity. Plants have evolved sophisticated defense mechanisms to protect themselves, including sensing biotic cues, signal transduction, reprogramming at transcript, protein as well as metabolite levels to strengthen their defense status. One important macronutrient for plants is calcium, which plays a significant role in the early signaling pathways that govern plant-biotic interactions. Plants produce a calcium signature in response to pest or pathogen attack, which acts as a signal. In order to activate the defense mechanism, these signals are detected by calcium sensors and then sent on to downstream signaling components. Our comprehension of the biochemical and molecular elements of calcium signaling, such as Calmodulin (CaM), CaM-like proteins (CML), Calcineurin B-like proteins (CBL), Calcium dependent protein kinases (CDPKs) and their transporters viz Cyclic nucleotide gated channels (CNGCs), two pore channels (TPCs), Annexins, Glutamate-like receptor channels, Ca^{2+}/cation exchangers (CCXs), Ca^{2+}-ATPases, Ca^{2+}/H^{+} exchangers (CAXs), has advanced recently. Even though a number of cutting-edge studies have been carried out, little is known about the decoding of the full components of the calcium signaling pathway and how it interacts with other relevant pathways, such as the Reactive Oxygen Species (ROS) and Mitogen-Activated Protein Kinase (MAPK) pathways, when a pathogen and pest interact. Through genome editing and genetic engineering, scientists will be able to modify the calcium signaling system and its components, which are essential in plant defense, to create plants that are more resistant to pests and diseases.

In the present Research Topic, Neelam et al. highlighted the critical involvement of calcium signaling pathways in plant responses to harmful and helpful microorganisms, illuminating the complex dynamics of these interactions. Defense signaling systems are

triggered and relayed by modulating calcium signaling, especially by microbial effectors in pathogenic environments. Since many different Ca2+ binding and decoding proteins are involved in the complex process of Ca2+-dependent signaling, it is important to identify the genes that control the Ca2+ surge, especially when it comes to agricultural plants. Additionally, authors stress the importance of calcium signaling in establishing symbiotic partnerships between plants and beneficial bacteria, particularly in the development of arbuscular mycorrhizal (AM) and rhizobia interactions. For nutrient uptake, stress resistance, and general plant health, this relationship is essential. It has been proposed that calcium-based fertilizers could be useful instruments to improve these symbiotic relationships and eventually increase crop yields.

Similarly, Bhar et al. evaluated the importance of the Calcium signaling pathway, emphasizing its critical function in the signal transduction machinery and its significance as a pivotal event in pathogenic plant biotic interactions. A praiseworthy feature of the research is how well the authors have explained the notion of "calcium signature". The paper focuses on the interactions between various signaling pathways rather than just explaining the calcium signaling pathway. This inclusion is essential because it clarifies how different routes are connected to one another, which eventually helps to establish an efficient and natural resistance response. The authors shed important light on the holistic nature of plant defense mechanisms by expanding on this crosstalk. The work recognizes the complex relationship between ROS and MAPK with calcium signaling and addresses this relationship correctly. This study's finding highlights the dynamic character of signal transduction networks and adds to the complexity of plant defense mechanisms.

Furthermore, Hamouzová et al. suggested and reported the role of Ca2+ signaling in weeds stressed by herbicides. The authors investigate the potential sensing and molecular communication via Ca2+ signals in weeds under such stress conditions, and they suggest that Ca2+signaling may result in transcriptional reprogramming during herbicide stress. Stress-responsive genes like GSTs and CYP450s are overexpressed in weeds that are resistant to herbicides. The authors put forth a theory on the potential for herbicide resistance to be conferred by a Ca2+-mediated signal network. The scientists point out how important it is to keep an eye on Ca2+ signal patterns linked to herbicide stress responses and speculate that weeds may be affected by Ca2+ signal-regulated alternative splicing. Herbicide processes and the herbicide stress signaling network remain poorly understood, despite advances in our knowledge of Ca2+-mediated signal networks in crops and plants under a variety of environmental stressors. To clarify the roles of Ca2 + signaling in weeds under herbicide stress, the authors call for additional research efforts that include obtaining reference weed genomes, RNA-seq transcriptome studies, modelling approaches based on bioinformatics, and gene editing experiments (using RNAi and/or CRISPR/Cas systems).

Additionally, calcium cyanamide (CaCN2) has been shown by Xie et al. to have the potential to be a dual-purpose agricultural agent that serves as a soil cleanser and fertilizer. The capacity of CaCN2 to reduce Corynespora blight and prevent the establishment of pathogens in soil derived from plant debris are indications of its fungicidal activity. Furthermore, one reason for the soil's efficacy in suppressing soil-borne pathogens is the conversion of CaCN2 into hydrogen cyanamide. The fact that CaCN2 lessens pathogens' prevalence in soil residues rather than totally eliminating them is one noteworthy finding of this study. With its ability to prevent soil-borne pathogens as well as soil wastes, CaCN2 may be an important factor in controlling plant diseases and preserving the health of the soil. Additionally, it has been found that the combination of CaCN2 and polyethylene film (PE) treatment—specifically, PE—is more successful in preventing the transfer of disease residues from soil to the atmosphere. This data implies that a major decrease in cucumber leaf disease may result from the integration of these technologies into agricultural operations, particularly in the growing of protected vegetables.

Plants frequently face both biotic and abiotic stresses at the same time, and a crucial component of their survival and adaptability is how they sort and combine these cues. Xu et al. examined the integration of various stress conditions in signaling responses and the function of calcium (Ca2+) signals in sensing abiotic environmental cues while taking into account the various pressures placed on plants. Abiotic stresses include elements like temperature, salt, drought, and other environmental variables, whereas biotic stresses are caused by living things like pathogens and pests. The report explores new developments that provide insight into the processes by which plants use Ca2+ signaling to sense and react to abiotic stressors. Developing solutions to improve crop stress tolerance requires an understanding of these systems, which is crucial given the influence of climate change on global agriculture.

This compilation highlights the importance of Ca2+ signaling during plant-biotic interactions and adds to our understanding of complex signaling networks. With a deeper comprehension of Calcium signaling and the elements of the plant defense pathway, scientists will be able to use genome editing and genetic engineering to modify the process and increase plant resistance to pests and diseases. The integration of the detection of various stress situations and the ensuing signaling reactions that require attention are also included in this Research Topic. This information may facilitate the creation of focused methods to control calcium signaling for better crop protection and strengthened symbiotic connections.

Author contributions

AS: Conceptualization, Data curation, Writing – review & editing. DG: Writing – review & editing. IS: Writing – review & editing.

Funding

The author(s) declare financial support was received for the research, authorship, and/or publication of this article. AS and IKS

are thankful to the Science and Engineering Research Board (SERB), Govt. of India for research funding.

Conflict of interest

The authors declare that the research was conducted in the absence of any commercial or financial relationships that could be construed as a potential conflict of interest.

Publisher's note

Received: 9 June 2023 | Revised: 29 June 2023 | Accepted: 5 July 2023

DOI: 10.1002/arch.22036

RESEARCH ARTICLE

Archives of INSECT BIOCHEMISTRY AND PHYSIOLOGY WILEY

Inefficient uptake of small interfering RNAs is responsible for their inability to trigger RNA interference in Colorado potato beetle cells

Jinmo Koo[1] | Dhandapani Gurusamy[1,2] | Subba Reddy Palli[1]

[1]Department of Entomology, University of Kentucky, Lexington, Kentucky, USA

[2]Department of Botany, Kongunadu Arts and Science College (Autonomous), Bharathiar University, Coimbatore, India

Correspondence
Subba Reddy Palli, Department of Entomology, College of Agriculture, University of Kentucky, Lexington, KY 40546, USA.
Email: rpalli@uky.edu

Funding information
National Institutes of Health, Grant/Award Number: R01GM070559; National Institute of Food and Agriculture; National Science Foundation I/UCRC; Center for Arthropod Management Technologies, Grant/Award Number: IIP-1821936; US Department of Agriculture, Grant/Award Number: 2351177000

Abstract

There has been limited success in the usage of exogenous small interference RNA (siRNA) or small hairpin RNA (shRNA) to trigger RNA interference (RNAi) in insects. Instead, long double-stranded RNAs (dsRNA) are used to induce knock-down of target genes in insects. Here, we compared the potency of si/sh RNAs and dsRNA in Colorado potato beetle (CPB) cells. CPB cells showed highly efficient RNAi response to dsRNA. However, si/sh RNAs were inefficient in triggering RNAi in CPB cells. Confocal microscopy observations of Cy3 labeled-si/sh RNA cellular uptake revealed reduced si/sh RNA uptake compared to dsRNA. si/sh RNAs were stable in the conditioned media of CPB cells. Although in a small amount, when internalized by CPB cells, the si/sh RNAs were processed by the Dicer enzyme. Lipid-mediated transfection and chimeric dsRNA approaches were used to improve the delivery of si/sh RNAs. Our results suggest that the uptake of si/sh RNAs is inefficient in CPB cells, resulting in ineffective RNAi response. However, with the help of effective delivery methods, si/sh RNA could be a useful option for developing target-specific RNAi-mediated biopesticides.

KEYWORDS
cellular uptake, RNAi, shRNA, siRNA

Research Highlights

- Colorado potato beetle (CPB) cells do not efficiently uptake small interference RNA (siRNA) molecules, which

is the main reason for their lower RNA interference (RNAi) response.
- Improvement of siRNA delivery into CPB cells increased RNAi response.

1 | INTRODUCTION

RNA interference (RNAi) is a reverse genetic technique that has been used in functional genomics (Bargmann, 2001), therapeutics (Setten et al., 2019), and plant protection (De Schutter et al., 2022; Palli, 2014, 2023; Zhu & Palli, 2020). Double-stranded RNA (dsRNA) with the sequence complementary to the target gene is delivered to the cells to trigger RNAi response. Different lengths and structures of dsRNAs could be designed for different purposes. dsRNA is usually designed at 200–800 p length (Li & Zamore, 2019a). Small interference RNA (siRNA) and small hairpin RNA (shRNA) are usually designed with the shortest length (19–27 bp) that RNAi machinery can recognize (Pushparaj et al., 2008). The use of these three different RNAi triggers can vary depending on the target organisms and the delivery methods. dsRNAs longer than 30 bp activate the immune response in mammals (Elbashir et al., 2001). This involves induction of the interferon signaling pathway, leading to nonspecific gene expression inhibition (Wang & Carmichael, 2004). To minimize this immune response, siRNA is normally used instead of long dsRNA in mammalian systems (Marques & Williams, 2005). Long dsRNAs are routinely used in insects for functional genomics studies and biopesticide development. Although, dsRNA-mediated immune responses have been reported in several insects, including honey bees (Flenniken & Andino, 2013) and silkworms (Liu et al., 2013). shRNA has been widely used to construct transgenic cell lines or animals in which stably expressed shRNA enforces stable and heritable gene silencing (Paddison et al., 2002).

In insects, long dsRNAs are used to trigger RNAi. siRNA failed to induce RNAi in the following insects; *Drosophila melanogaster* (Saleh et al., 2006), *Diabrotica virgifera* (Bolognesi et al., 2012; Miyata et al., 2014; Zhang et al., 2012), and *Tribolium castaneum* (Miller et al., 2012), and a nematode, *Caenorhabditis elegans* (Mcewan et al., 2012; Parrish et al., 2000). Significant knockdown of target genes using siRNAs has been reported in the following insects; *Manduca sexta* (Levin et al., 2005), *Helicoverpa armigera* (Kumar et al., 2009), *Plutella xylostella* (He et al., 2012), *Acyrthosiphon pisum* (Mutti et al., 2006), *Bactericerca cockerelli* (Wuriyanghan et al., 2011), *Bemisia tabaci* (Upadhyay et al., 2011), *Apis mellifera* (Jarosch & Moritz, 2011), *Reticulitermes flavipes* (Zhou et al., 2006), and *Aedes aegypti* (Abbasi et al., 2020). Other than those reports, the use of siRNA in insects is limited. siRNA often needs a more complex design and is usually less efficient than dsRNA.

Why is siRNA not as effective as long dsRNA? First, siRNA efficiency is highly variable depending on its target site. Even within the same gene, knockdown efficiency can vary greatly between different sequence sites that siRNAs target (Reynolds et al., 2004). Since long dsRNAs produce multiple siRNAs targeting different sites of mRNA, the combined response of siRNAs results in efficient knockdown of the target gene. That is why using dsRNA is often simpler to knockdown target genes than relying on a single site targeting siRNA. Second, the siRNAs are not taken up by cells as efficiently as longer dsRNAs (Bolognesi et al., 2012; Miller et al., 2012; Saleh et al., 2006). Third, since siRNAs have fewer base pairs that can form hydrogen bonds, the strength of a double-stranded structure may not be as strong as long dsRNA, where hundreds of nucleotides form complementary hydrogen bonds (Zhang et al., 2015). The Colorado potato beetle (CPB) cell line exhibits a robust RNAi response to dsRNA treatment (Yoon et al., 2016, 2018). Using this CPB cell line, we checked the sensitivity of CPB cells to si/sh RNA treatment. We also addressed reasons siRNA is less effective than dsRNA in CPB cells. Finally, we propose ways to improve siRNA efficiency in CPB cells.

2 | MATERIALS AND METHODS

2.1 | Cell line

CPB cell line (BCIRL-Lepd-SL1; Long et al., 2002) obtained from the Biological Control of Insects Research Laboratory (USDA-ARS) was cultured in EX-CELL 420 (Sigma-Aldrich) medium supplemented with 10% fetal bovine serum (R&D Systems) at 27°C.

2.2 | RNA isolation, cDNA synthesis, and quantitative real-time polymerase chain reaction

Total RNA was isolated using TRIzol reagent (Molecular Research Center Inc.). To synthesize cDNA, M-MLV Reverse Transcriptase (Invitrogen™) kit was used. One microgram of total RNA, dNTP, random primer, and oligo primer was mixed in 13 µL. The mixture was incubated at 65°C for 5 min. Then, 5× buffer, DTT, and reverse transcriptase were added to 20 µL. The mixture was incubated at 37°C for 1 h, followed by 70°C for 15 min for enzyme inactivation. Quantitative real-time polymerase chain reaction (qRT-PCR) reaction (10 µL final volume) contained 5 µL of 2× SYBR Mix (Bio-Rad), 2 µL of fivefold diluted cDNA, 2.6 µL of nuclease-free water, and 0.2 µL each of 10 µM forward and reverse gene-specific primers. An initial incubation of 95°C for 3 min, followed by 40 cycles of 95°C for 5 s, and 60°C for 60 s settings were used. A melt curve was generated at the end of the run to confirm primer specificity. qRT-PCR reactions were performed in Applied Biosystems Step One Plus™ Real-Time PCR System. The relative mRNA levels were calculated using the Delta-Delta Ct method. Ribosomal protein 4 (RP4) was used as a housekeeping gene.

2.3 | dsRNA, siRNA, and shRNA synthesis

Total RNA isolated from CPB cells was used to synthesize cDNA. Using cDNA as a template, fragments of the target gene with 5′ T7 promoter sequence were amplified using PCR. PCR amplifications were conducted in 50 µL reactions containing 5 µM concentration of each primer (Supporting Information: Table S1), 25 µL of *Taq* 2× Master Mix (New England Biolabs), and 5 µL of synthesized cDNA. PCR conditions were 95°C for 3 min, followed by 35 cycles of 95°C for 30 s, 57°C for 30 s, and 68°C for 1 min, finishing with an extension step at 68°C for 5 min. PCR products were purified using the QIAquick PCR purification kit (QIAGEN). The purified PCR products were used as templates to synthesize dsRNAs using the Megascript T7 RNA synthesis kit (Life Technologies).

To synthesize siRNA, sense and antisense single-stranded RNA was synthesized from two different templates. To generate DNA template for the sense strand, 10 µL of 100 µM Top sense primer (TS), 10 µL of 100 µM Bottom sense primer (BS), 10 µL of Buffer 3.1 (New England Biolabs), and 70 µL of water were mixed and incubated in 90°C for 4 min and let it slowly cool down in room temperature. DNA template for the antisense strand was prepared using the same method, using Top antisense primer and Bottom antisense primer. The Megascript T7 RNA synthesis kit was used to synthesize single-stranded RNA using annealed sense and antisense templates. Synthesized single-stranded RNAs are complementary to each other and annealed to form dsRNA. siRNA target site was selected using the BLOCK-iT™ RNAi Designer website (Thermo Fisher Scientific Inc.).

To synthesize shRNA, the templates were annealed with Top (T) and Bottom (B) oligos using the same method mentioned above. Megascript T7 RNA synthesis kit was employed to synthesize RNA using the annealed template. The complementary sequence within synthesized RNA binds to make a hairpin structure with a 9 bp loop (Supporting Information: Figure S1a). The loop length and sequence were designed based on the information from

the publications (Mcmanus et al., 2002). Synthesized siRNA and shRNA were checked using 4% agarose gels (Supporting Information: Figure S1b).

2.4 | Confocal microscopy

To label RNA with Cy3 dye, Cyanine 3-UTP (enhanced; Enzo Life Sciences Inc.) was used instead of UTP from Megascript T7 RNA synthesis kit for transcription of RNA. QIAquick PCR purification kit (QIAGEN) was used to purify the labeled products. One siLuc molecule has 13 uridines in total of 42 nucleotides (31%). One shLuc molecule has 13 uridines in total of 47 nucleotides (27.7%). One dsLuc molecule has 190 uridines in total of 710 nucleotides (26.8%). The percentage of uridine incorporation into ds/si/sh Luc is similar. Therefore, using an equal amount (ng) of those RNA molecules should have comparable amount of Cy3 molecules as well. CPB cells were seeded in eight-well chamber slides. Cy3 labeled-dsRNA, siRNA, or shRNA was treated and incubated for 5 h. Incubated cells were washed with 1× phosphate-buffered saline three times. Washed cells were fixed with 4% paraformaldehyde and mounted with DAPI-containing medium. Leica TCS SP8 DLS instrument was used for confocal microscopy observations.

Images containing 50–100 cells were used for quantification. The total red intensity of the image was divided by the total number of cells in the same image to calculate Cy3 intensity per cell. The total red intensity of the image was measured using ImageJ software. To account for the red background signal, the red intensity from the control (no Cy3 labeled RNA treated) was subtracted from the red intensity from Cy3 labeled RNA treated cells.

2.5 | Stability assay in conditioned media

CPB cells seeded in six-well plates containing 2 mL medium/well were incubated for 3 days. The medium was collected and processed by taking supernatant after centrifuging at 5000*g* for 10 min to remove cell debris. One µg dsLuc, siLuc, or shLuc was incubated with 19 µL of the conditioned medium at 28°C for various lengths. The products were run on 1% agarose gels for dsLuc and 2% agarose gels for siLuc and shLuc.

2.6 | ^{32}P labeled RNA

^{32}P-UTP was used in place of UTP in the Megascript T7 RNA synthesis kit to synthesize ^{32}P labeled-dsRNA, siRNA, and shRNA. QIAquick PCR purification kit (QIAGEN) was used to purify the labeled products. 0.14 million CPM (count per million) of ^{32}P-labeled dsLuc, siLuc, or shLuc was added to CPB cells seeded in six-well plates. After 48 h of incubation, the cells were harvested, and RNA was isolated. Three houndred CPM of total RNA was resolved on 8 M urea-16% polyacrylamide gels. The gels were dried and exposed overnight to a phosphorImager screen, and the screen was scanned in a phosphorImager (Typhoon 9500, GE Healthcare Life Sciences). ImageJ software was used to process the image.

2.7 | Transfection

FuGENE® HD Transfection Reagent (Promega) was used to help deliver si/sh RNA into CPB cells. In 10 µL of EX-CELL 420 media, 0.5 µg of siRNA or shRNA and 0.5 µL of FuGENE were mixed to make the complex. The complex was vortexed and incubated at room temperature for 15 min. Ten µL complex was added to a well of 96-well plates seeded with CPB cells in 100 µL of medium.

2.8 | Long dsGFP fused si/sh IAP synthesis

To fuse siIAP sequence into long dsGFP, a modified forward primer with 19 bp siIAP sequence inserted between T7 and GFP gene-specific sequence was designed. The reverse primer was identical to what was used to amplify normal dsGFP templates. Using these primers, a hybrid template was generated with 19 bp IAP sequence attached to 5′ of GFP fragment with PCR. The Megascript T7 RNA synthesis kit was used to synthesize long dsGFP fused siIAP using the amplified template. To fuse shIAP sequence into long dsGFP, a modified forward primer with a 47 bp shIAP sequence inserted between T7 and GFP gene-specific sequence was designed.

2.9 | Statistics

To compare the means between the two groups (control and treatment), a two-tailed *t* test was used. Three replicates of cells seeded in different wells were processed as individual samples for each treatment. To verify the normal distribution of the replicates, the Shapiro–Wilk test was performed using a tool from the Statistics Kingdom website (https://www.statskingdom.com/shapiro-wilk-test-calculator.html). *F* test with *p* value of 0.05 was used to determine equal variance among the treatment. *t* test and *F* test were done in Excel Version 2211 (Microsoft).

3 | RESULTS

3.1 | si/sh RNA are inefficient in inducing RNAi in CPB cells

The inhibitor of apoptosis (IAP) gene was used as a target gene to check RNAi efficiency in CPB cells. IAP knockdown triggers apoptosis in CPB cells (Yoon et al., 2016, 2018). Characteristics of apoptosis phenotype include cell death with apoptotic body formation. Apoptotic bodies are types of extracellular vesicles that are the remnants of cells having undergone apoptosis (Battistelli & Falcieri, 2020). When dsIAP (5 ng/μL) was added to the CPB cells, efficient RNAi response was detected based on the apoptosis phenotype. In contrast, the si/sh IAP-treated cells (5 ng/μL) did not show cellular apoptosis (Figure 1a). A higher concentration of si/sh IAP (40 ng/μL) also failed to affect CPB cells, whereas a lower concentration of dsIAP (0.2 ng/μL) was sufficient to trigger apoptosis (Supporting Information: Figure S2). It has been reported that RNAi efficiency can vary significantly depending on the siRNA target site within the gene (Reynolds et al., 2004). To rule out this position effect, we digested 402 bp long dsIAP with RNase III to produce a heterogeneous mix of siRNAs (18–25 bp). The digested products were run on a gel and purified to remove long residual dsRNA (Figure 1b). No apoptosis was observed when the digested and purified heterogeneous mix of siIAPs were added to the CPB cells medium (Figure 1c). These results indicate that si/sh RNAs are inefficient in inducing RNAi in CPB cells.

3.2 | Uptake of si/sh RNA in CPB cells is not as efficient as dsRNA

Cy3-labeled RNA molecules can be used to visualize their uptake into the cells using a confocal microscope (Dhandapani et al., 2019; Gurusamy et al., 2020). We labeled dsRNA, siRNA, and shRNA with Cy3 (Supporting Information: Figure S3) to compare their cellular uptake efficiency. dsRNA uptake in CPB cells was visualized by the red signal (Cy3). However, little Cy3 signal was detected in Cy3 labeled-siRNA or -shRNA treated cells (Figure 2a). Indeed, Cy3 signal intensity per cell was significantly lower in Cy3 labeled-siRNA and -shRNA treated cells compared to Cy3 labeled-dsRNA (Figure 2b and Supporting Information: Figure S4). These results suggest that, unlike dsRNA, si/sh RNAs are not taken up efficiently by CPB cells.

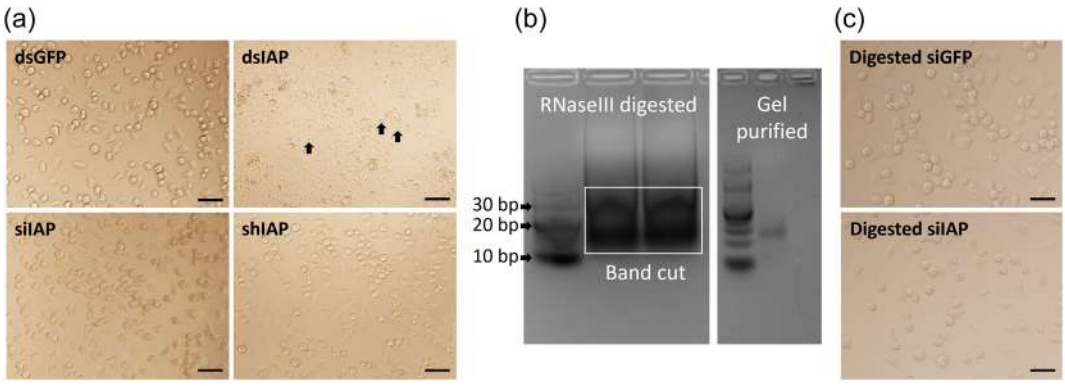

FIGURE 1 Insensitivity of Colorado potato beetle (CPB) cells to si/sh RNA mediated RNAi. (a) 5 ng/μL of dsIAP, siIAP, or shIAP was added to CPB cells. dsGFP was used as a control. Photos were taken 24 h after treatment. Some of the apoptotic bodies are indicated with black arrows. (b) 402 bp dsIAP was digested with RNase III to make a heterogenous mix of 18–25 bp siRNAs. Digested products were run on 2% agarose gel, and 18–25 bp gel region was cut, and the RNA was purified to remove undigested dsRNA. (c) 2 ng/μL of digested and purified siRNA was added to CPB cells. Photos were taken 24 h after treatment. The scale bar is 50 μm.

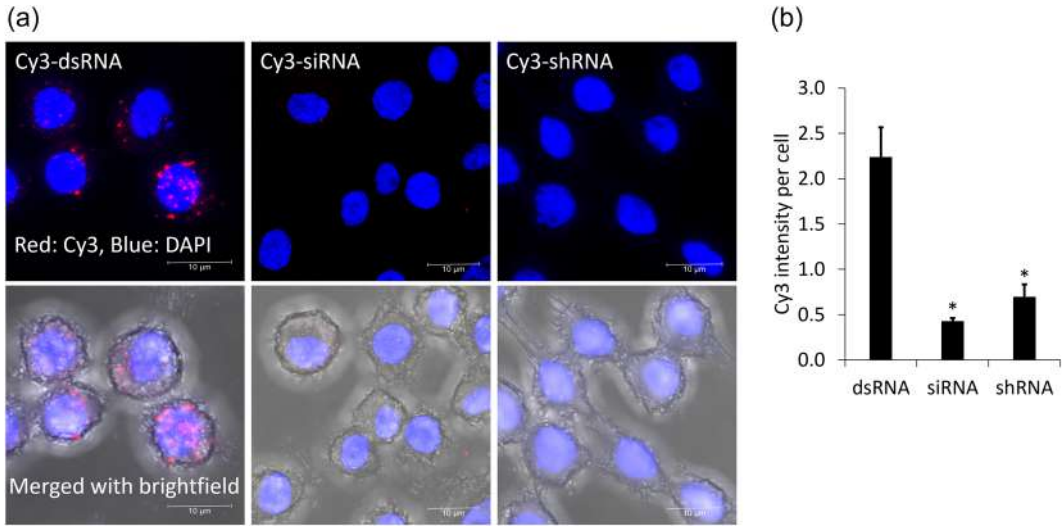

FIGURE 2 Inefficient uptake of si/sh RNA into Colorado potato beetle (CPB) cells. (a) Confocal images of dsRNA uptake. Half ng/μL of Cy3 labeled dsRNA, siRNA, or shRNA (targeting the luciferase gene) was added to CPB cells. After 5 h incubation, the cells were washed, fixed, and imaged with a confocal microscope. Red dots indicate internalized Cy3 signal and blue circles indicate DAPI-labeled nuclei. The fluorescent image merged with Brightfield is shown at the bottom to confirm that all the Cy3 signals are inside the cells. (b) Quantification of Cy3 signal intensity in cells. Mean ± SE ($N = 3$) is shown. "*" denotes significant differences between control (dsRNA) and treatments (siRNA or shRNA) ($p < 0.05$).

3.3 | si/sh RNAs are stable in the conditioned media of CPB cells, and si/sh RNAs are processed by Dicer when entered inside the cell

It is possible that si/sh RNA is not stable in the extracellular conditions, so there were not enough molecules left to be taken up by the CPB cells. To address this issue, we checked si/sh RNA stability in conditioned media of CPB

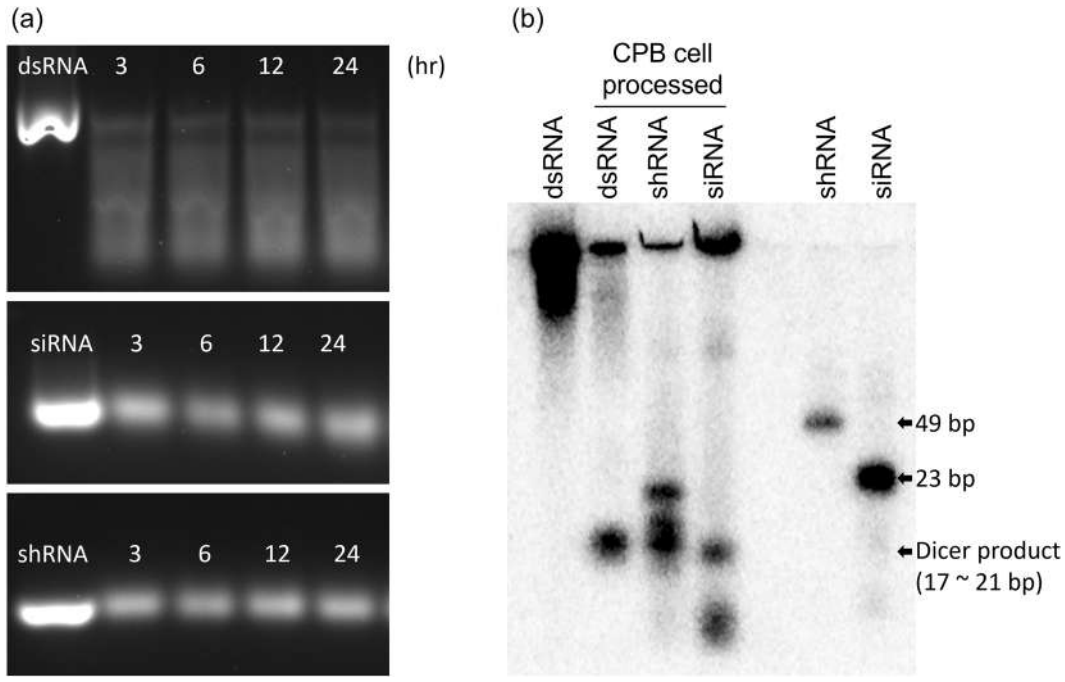

FIGURE 3 Extracellular stability and intracellular processing of si/sh RNA in Colorado potato beetle (CPB) cells. (a) si/sh RNA stability in the extracellular environment. dsRNA, siRNA, or shRNA (targeting the luciferase gene) was incubated with conditioned media from CPB cells for different lengths of time (3, 6, 12, and 24 h). The dsRNA samples were run on 1% agarose gels and siRNA and shRNA samples were run on 2% agarose gels. (b) Fate of si/sh RNA in CPB cells. ^{32}P labeled dsRNA, siRNA, or siRNA (targeting the luciferase gene) were added to CPB cells. After 2 days of incubation, total RNA was extracted from the treated cells. 300 CPM of total RNA was resolved on 8 M urea-16% polyacrylamide gels. The gels were dried and imaged in a phosphorImager.

cells. si/sh RNA was stable for up to 24 h in the conditioned media. This stability was comparable to dsRNA (Figure 3a). These results confirmed that the reduced uptake of si/sh RNA in CPB cells was indeed caused by the inability of cells to internalize the molecules.

Even though in a less amount, some si/sh RNA internalization was detected in the confocal analysis (Figure 2b), we wanted to know what happens to the si/sh RNA internalized into CPB cells. To answer the question, the CPB cells were treated with ^{32}P labeled si/sh RNA, and the fate of labeled RNA inside the cell was tracked. As reported previously (Yoon et al., 2018), ^{32}P-dsRNA treated CPB cells produce 17–21 bp Dicer product. Interestingly, ^{32}P-si/sh RNA-treated CPB cells also showed similar size Dicer products (Figure 3b). These products are smaller than their original size, represented by 49 and 23 bp bands from naked shRNA and siRNA, respectively, in urea-containing denaturing gel. These results suggest that RNAi machinery proteins can process si/sh RNAs once internalized. The band signal present at the top of the gel in the wells loaded with RNA isolated from si/sh RNA-treated CPB cells may be due to nontarget interaction with si/sh RNA and a trace of protein present in isolated RNA.

3.4 | Improved delivery increases the efficiency of si/sh RNA in CPB cells

Internalization of the si/sh RNA appears to be the major limiting factor that causes inefficient RNAi in CPB cells. Hence, if we can improve the delivery of si/sh RNA into CPB cells, they may be able to trigger RNAi response.

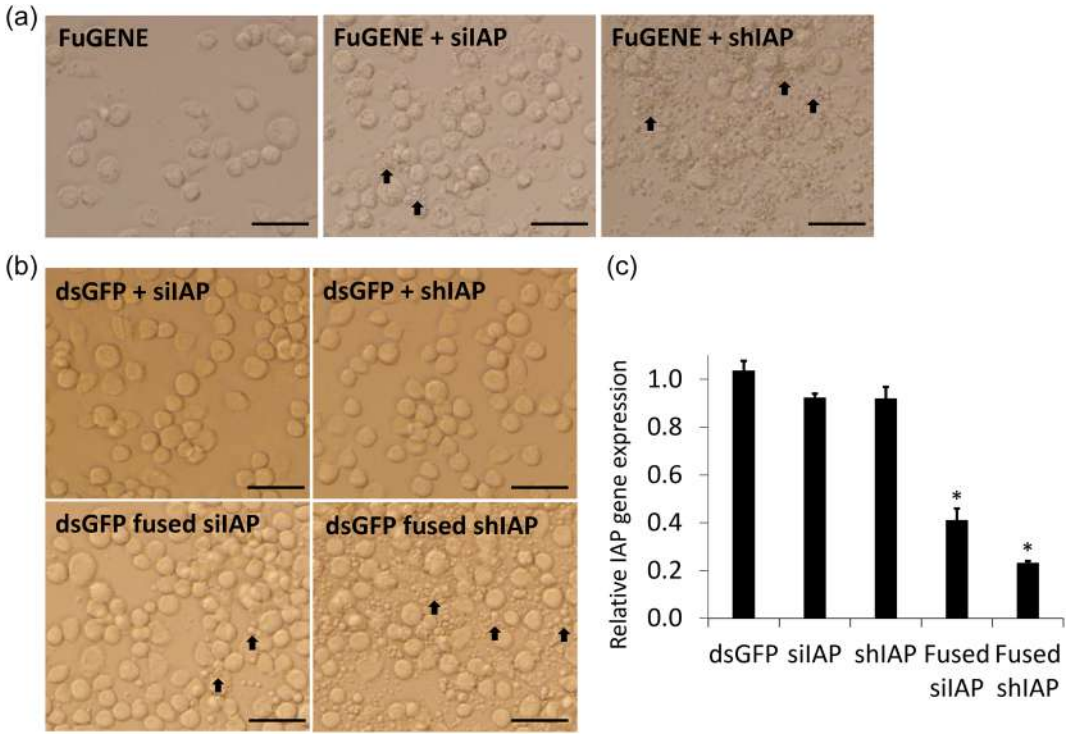

FIGURE 4 Cellular delivery methods to increase the efficiency of si/sh RNA induced RNAi in CPB cells. (a) Delivery of si/sh IAP into CPB cells using transfection reagent, FuGENE. (b) Enhanced delivery of long dsGFP fused si/sh IAP into CPB cells. Some of the apoptotic bodies are indicated with black arrows. Scale bar is 50 µm. (c) IAP gene mRNA knockdown efficiency in CPB cells by dsGFP fused si/sh RNA treatment was quantified with qRT-PCR. Mean ± SE ($N = 4$) is shown. "*" denotes significant differences in the expression levels of IAP gene between control (dsGFP) and treatments ($p < 0.05$). CPB, Colorado potato beetle; IAP, inhibitor of apoptosis; RNAi, RNA interference; qRT-PCR, quantitative real-time polymerase chain reaction.

When a transfection reagent was used to enhance the delivery of si/sh RNA into CPB cells, the IAP knockdown phenotype was detected (Figure 4a). Also, the hybrid fusion of siIAP and dsGFP designed to improve uptake (Supporting Information: Figure S5) showed IAP knockdown phenotype (Figure 4b) with significant knockdown efficiency (Figure 4c).

4 | DISCUSSION

Consistent with our results, targeting the Actin gene with 60 bp dsRNA only induced a low RNAi response, whereas 200 bp and longer dsRNA caused high mortality in CPB larva (He et al., 2020). In addition, we propose that inefficient uptake of siRNA leads to inefficient RNAi response in CPB cells. This agrees with previous reports from other insects. In *D. melanogaster* S2 cells, length (between 31 and 211 bp) dependent silencing efficiency of dsRNA was observed. Reduced uptake of 21 bp siRNA was observed, and siRNA failed to induce RNAi response in S2 cells (Saleh et al., 2006). Confocal microscope observation showed that *D. virgifera* midgut cells could not take up siRNA (Bolognesi et al., 2012). In *T. castaneum*, siRNA injection into larval hemocoel failed to trigger RNAi. When siRNA was injected into embryos at the syncytial blastoderm stage, where the cell wall has not been formed yet, significant knockdown of target mRNA occurred. This implies that siRNA cannot go through the cell wall (Miller et al., 2012).

Although it seems clear that uptake efficiency of siRNA is significantly lower than dsRNA in above-mentioned insects, whether siRNA takes different uptake route compared to dsRNA is unknown. dsRNA uptake in insects is known to be mediated by multiple routes, with clathrin-mediated endocytosis being the primary uptake mechanism (Pinheiro et al., 2018; Saleh et al., 2006; Ulvila et al., 2006; Yoon et al., 2016). In *A. aegypti*, inhibition of clathrin-mediated endocytosis was sufficient to suppress the uptake of dsRNA, siRNA, and shRNA, suggesting si/sh RNA also use clathrin-mediated endocytosis for cellular uptake (Abbasi et al., 2020). Further research is needed to determine whether this is also true for other insects.

si/sh RNAs were stable in the conditioned media of CPB cells. Different insects and tissues have different nuclease activity that degrades dsRNA. Nuclease activity in coleopteran insects, including CPB, is weaker than in lepidopteran insects (Singh et al., 2017). CPB cells used in our study may not produce sufficient nuclease to differentiate stability between dsRNA and si/sh RNA. Further studies are needed to verify si/sh RNA stability in different conditions. Sf9 cells, derived from *Spodoptera frugiperda* and known to have high nuclease activity against dsRNA (Koo & Palli, 2023), could be a good cell line for such studies. The stability of siRNA has been analyzed in *B. tabaci* feeding assays, and siRNA recovered from the diet 7 days after feeding assays were stable (Borgio, 2010; Upadhyay et al., 2011). In therapeutics, modification of siRNA with improved stability has proved to increase target knockdown efficiency (Elmén et al., 2005; Hu et al., 2020). This indicates that the stability of siRNA in the target system is a crucial factor that determines RNAi efficiency. However, stability does not seem to be the limiting factor in CPB cells. siRNA was stable for up to 24 h, comparable to dsRNA stability (Figure 3a).

According to the previous report, siRNA designed with a 25–30 bp length was 100 times more potent than 21 bp. This greater potency was suggested to depend on the function of Dicer (Kim et al., 2005). Other reports showed that in addition to cleaving dsRNA into siRNA, Dicer also plays functions in loading cleaved siRNA into RISC assembly (Lee et al., 2004; Sontheimer, 2005). These observations imply that RNAi potency can be increased when siRNA is designed long enough to be processed by Dicer. Our designed siRNA (23 bp, including both 5′ and 3′ overhangs) and shRNA (21 bp + 9 bp loop; Supporting Information: Figure S1a) seem to be long enough to be processed by Dicer into smaller siRNA, presumably with a length of 17–21 bp (Figure 3b). The size of siRNA generated by Dicer processing is known to be species-specific (Santos et al., 2019).

Lipid-mediated transfection is widely used to deliver siRNA in mammalian cells (Li & Zamore, 2019b). Transfection of siRNA effectively induced silencing in *Drosophila* S2 cells (Saleh et al., 2006). We also report that the transfection agent successfully delivered siRNA into CPB cells (Figure 4a). In another attempt to deliver siRNA into CPB cells, we used a fusion of siIAP and dsGFP to increase the length of the product (Supporting Information: Figure S5). The chimeric dsRNA approach has been used to target multiple genes and species with a single type of dsRNA (Chen et al., 2021; Wang et al., 2021). Chimeric dsRNA was also used to target multiple RNAi pathways (siRNA and miRNA pathways; Jannot et al., 2008). Our dsGFP fused siIAP approach adds to the proof of concept that chimeric dsRNA can also be used to enhance the delivery of siRNA targeting a short length of the sequence.

Currently, long dsRNAs are primarily pursued as biopesticides (Christiaens et al., 2020). However, siRNA has some advantages over dsRNA. First, siRNA is highly specific. Longer dsRNA has a higher risk of nontarget effects because long dsRNA sequences can contain multiple siRNA matching sites with non-targets (Chen et al., 2021). Second, siRNA can minimize the immune response, which can be especially beneficial to nontarget insects. Although it is underrated, dsRNA does trigger immune responses in insects (Flenniken & Andino, 2013; Haller et al., 2019; Liu et al., 2013). Similar to what has been observed in the mammalian system, using siRNA may mitigate insect immune response. Therefore, with the help of effective delivery methods, such as the use of nanoparticles, siRNA can be a useful option for developing RNAi-mediated bio-insecticides.

AUTHOR CONTRIBUTIONS

Jinmo Koo and Subba Reddy Palli designed research; Jinmo Koo and Dhandapani Gurusamy performed research; Jinmo Koo, Dhandapani Gurusamy, and Subba Reddy Palli analyzed data; Jinmo Koo and Subba Reddy Palli wrote the paper.

ACKNOWLEDGMENTS

Research reported in this publication was supported by the National Institute of General Medical Sciences of the National Institutes of Health under Award number R01GM070559 and the National Institute of Food and Agriculture, the National Science Foundation I/UCRC, the Center for Arthropod Management Technologies (under grant no. IIP-1821936, and by industry partners), and US Department of Agriculture (under HATCH Project 2351177000).

CONFLICT OF INTEREST STATEMENT

The authors declare no conflict of interest.

DATA AVAILABILITY STATEMENT

The data that supports the findings of this study are available in the Supporting Information of this article.

ORCID

Subba Reddy Palli http://orcid.org/0000-0002-0873-3247

REFERENCES

Abbasi, R., Heschuk, D., Kim, B. & Whyard, S. (2020) A novel paperclip double-stranded RNA structure demonstrates clathrin-independent uptake in the mosquito *Aedes aegypti*. *Insect Biochemistry and Molecular Biology*, 127, 103492.

Bargmann, C.I. (2001) High-throughput reverse genetics: RNAi screens in *Caenorhabditis elegans*. *Genome Biology*, 2, reviews1005.1–reviews1005.3.

Battistelli, M. & Falcieri, E. (2020) Apoptotic bodies: particular extracellular vesicles involved in intercellular communication. *Biology*, 9, 21.

Bolognesi, R., Ramaseshadri, P., Anderson, J., Bachman, P., Clinton, W., Flannagan, R. et al. (2012) Characterizing the mechanism of action of double-stranded RNA activity against western corn rootworm *(Diabrotica virgifera virgifera* LeConte). *PLoS One*, 7, e47534.

Borgio, J.F. (2010) RNAi mediated gene knockdown in sucking and chewing insect pests. *Journal of Biopesticides*, 3, 386–393.

Chen, J., Peng, Y., Zhang, H., Wang, K., Zhao, C., Zhu, G. et al. (2021) Off-target effects of RNAi correlate with the mismatch rate between dsRNA and non-target mRNA. *RNA Biology*, 18, 1747–1759.

Christiaens, O., Whyard, S., Vélez, A.M. & Smagghe, G. (2020) Double-stranded RNA technology to control insect pests: current status and challenges. *Frontiers in Plant Science*, 11, 451.

De Schutter, K., Taning, C.N.T., Van Daele, L., Van Damme, E.J.M., Dubruel, P. & Smagghe, G. (2022) RNAi-based biocontrol products: market status, regulatory aspects, and risk assessment. *Frontiers in Insect Science*, 1, 818037.

Dhandapani, R.K., Gurusamy, D., Howell, J.L. & Palli, S.R. (2019) Development of CS-TPP-dsRNA nanoparticles to enhance RNAi efficiency in the yellow fever mosquito, *Aedes aegypti*. *Scientific Reports*, 9, 8775.

Elbashir, S.M., Harborth, J., Lendeckel, W., Yalcin, A., Weber, K. & Tuschl, T. (2001) Duplexes of 21-nucleotide RNAs mediate RNA interference in cultured mammalian cells. *Nature*, 411, 494–498.

Elmén, J. (2005) Locked nucleic acid (LNA) mediated improvements in siRNA stability and functionality. *Nucleic Acids Research*, 33, 439–447.

Flenniken, M.L. & Andino, R. (2013) Non-specific dsRNA-mediated antiviral response in the honey bee. *PLoS One*, 8, e77263.

Gurusamy, D., Mogilicherla, K., Shukla, J.N. & Palli, S.R. (2020) Lipids help double-stranded RNA in endosomal escape and improve RNA interference in the fall armyworm, *Spodoptera frugiperda*. *Archives of Insect Biochemistry and Physiology*, 104, e21678.

Haller, S., Widmer, F., Siegfried, B.D., Zhuo, X. & Romeis, J. (2019) Responses of two ladybird beetle species (Coleoptera: Coccinellidae) to dietary RNAi. *Pest Management Science*, 75, 2652–2662.

He, G., Sun, Y. & Li, F. (2012) RNA interference of two acetylcholinesterase genes in *Plutella xylostella* reveals their different functions. *Archives of Insect Biochemistry and Physiology*, 79, 75–86.

He, W., Xu, W., Xu, L., Fu, K., Guo, W., Bock, R. et al. (2020) Length-dependent accumulation of double-stranded RNAs in plastids affects RNA interference efficiency in the Colorado potato beetle. *Journal of Experimental Botany*, 71, 2670–2677.

Hu, B., Zhong, L., Weng, Y., Peng, L., Huang, Y. & Zhao, Y. et al. (2020) Therapeutic siRNA: state of the art. *Signal Transduction and Targeted Therapy*, 5, 101.

Jannot, G., Boisvert, M.E.L., Banville, I.H. & Simard, M.J. (2008) Two molecular features contribute to the Argonaute specificity for the microRNA and RNAi pathways in *C. elegans*. *RNA*, 14, 829–835.

Jarosch, A. & Moritz, R.F.A. (2011) Systemic RNA-interference in the honeybee *Apis mellifera*: tissue dependent uptake of fluorescent siRNA after intra-abdominal application observed by laser-scanning microscopy. *Journal of Insect Physiology*, 57, 851–857.

Kim, D.-H., Behlke, M.A., Rose, S.D., Chang, M.-S., Choi, S. & Rossi, J.J. (2005) Synthetic dsRNA Dicer substrates enhance RNAi potency and efficacy. *Nature Biotechnology*, 23, 222–226.

Koo, J. & Palli, S.R. (2023) dsRNase1 contribution to dsRNA degradation activity in the Sf9 cells conditioned medium. *Frontiers in Insect Science*, 3, 1118775.

Kumar, M., Gupta, G.P. & Rajam, M.V. (2009) Silencing of acetylcholinesterase gene of *Helicoverpa armigera* by siRNA affects larval growth and its life cycle. *Journal of Insect Physiology*, 55, 273–278.

Lee, Y.S., Nakahara, K., Pham, J.W., Kim, K., He, Z., Sontheimer, E.J. et al. (2004) Distinct roles for *Drosophila* Dicer-1 and Dicer-2 in the siRNA/miRNA silencing pathways. *Cell*, 117, 69–81.

Levin, D.M., Breuer, L.N., Zhuang, S., Anderson, S.A., Nardi, J.B. & Kanost, M.R. (2005) A hemocyte-specific integrin required for hemocytic encapsulation in the tobacco hornworm, *Manduca sexta*. *Insect Biochemistry and Molecular Biology*, 35, 369–380.

Li, C. & Zamore, P.D. (2019a) Preparation of dsRNAs for RNAi by in vitro transcription. *Cold Spring Harbor Protocols*, 3, 209–214.

Li, C. & Zamore, P.D. (2019b) RNAi in mammalian cells by siRNA duplex transfection. *Cold Spring Harbor Protocols*, 4, 286–288.

Liu, J., Smagghe, G. & Swevers, L. (2013) Transcriptional response of BmToll9-1 and RNAi machinery genes to exogenous dsRNA in the midgut of *Bombyx mori*. *Journal of Insect Physiology*, 59, 646–654.

Long, S.H., Mcintosh, A.H., Grasela, J.J. & Goodman, C.L. (2002) The establishment of a Colorado potato beetle (Coleoptera: Chrysomelidae) pupal cell line. *Applied Entomology and Zoology*, 37, 447–450.

Marques, J.T. & Williams, B.R.G. (2005) Activation of the mammalian immune system by siRNAs. *Nature Biotechnology*, 23, 1399–1405.

Mcewan, D.L., Weisman, A.S. & Hunter, C.P. (2012) Uptake of extracellular double-stranded RNA by SID-2. *Molecular Cell*, 47, 746–754.

Mcmanus, M.T., Petersen, C.P., Haines, B.B., Chen, J. & Sharp, P.A. (2002) Gene silencing using micro-RNA designed hairpins. *RNA*, 8, 842–850.

Miller, S.C., Miyata, K., Brown, S.J. & Tomoyasu, Y. (2012) Dissecting systemic RNA interference in the red flour beetle *Tribolium castaneum*: parameters affecting the efficiency of RNAi. *PLoS One*, 7, e47431.

Miyata, K., Ramaseshadri, P., Zhang, Y., Segers, G., Bolognesi, R. & Tomoyasu, Y. (2014) Establishing an in vivo assay system to identify components involved in environmental RNA interference in the western corn rootworm. *PLoS One*, 9, e101661.

Mutti, N.S., Park, Y., Reese, J.C. & Reeck, G.R. (2006) RNAi knockdown of a salivary transcript leading to lethality in the pea aphid, *Acyrthosiphon pisum*. *Journal of Insect Science*, 6, 1–7.

Paddison, P.J., Caudy, A.A., Bernstein, E., Hannon, G.J. & Conklin, D.S. (2002) Short hairpin RNAs (shRNAs) induce sequence-specific silencing in mammalian cells. *Genes & Development*, 16, 948–958.

Palli, S.R. (2014) RNA interference in Colorado potato beetle: steps toward development of dsRNA as a commercial insecticide. *Current Opinion in Insect Science*, 6, 1–8.

Palli, S.R. (2023) RNAi turns 25: contributions and challenges in insect science. *Frontiers in Insect Science - Insect Molecular Genetics*, 3, 1209478.

Parrish, S., Fleenor, J., Xu, S., Mello, C. & Fire, A. (2000) Functional anatomy of a dsRNA trigger. *Molecular Cell*, 6, 1077–1087.

Pinheiro, D.H., Vélez, A.M., Fishilevich, E., Wang, H., Carneiro, N.P., Valencia-Jiménez, A. et al. (2018) Clathrin-dependent endocytosis is associated with RNAi response in the western corn rootworm, *Diabrotica virgifera* virgifera LeConte. *PLoS One*, 13, e0201849.

Pushparaj, P.N., Aarthi, J.J., Manikandan, J. & Kumar, S.D. (2008) siRNA, miRNA, and shRNA: in vivo applications. *Journal of Dental Research*, 87, 992–1003.

Reynolds, A., Leake, D., Boese, Q., Scaringe, S., Marshall, W.S. & Khvorova, A. (2004) Rational siRNA design for RNA interference. *Nature Biotechnology*, 22, 326–330.

Saleh, M.C., Van Rij, R.P., Hekele, A., Gillis, A., Foley, E., O'Farrell, P.H. et al. (2006) The endocytic pathway mediates cell entry of dsRNA to induce RNAi silencing. *Nature Cell Biology*, 8, 793–802.

Santos, D., Mingels, L., Vogel, E., Wang, L., Christiaens, O. & Cappelle, K. et al. (2019) Generation of virus- and dsRNA-derived siRNAs with species-dependent length in insects. *Viruses*, 11, 738.

Setten, R.L., Rossi, J.J. & Han, S. (2019) The current state and future directions of RNAi-based therapeutics. *Nature Reviews Drug Discovery*, 18, 421–446.

Singh, I.K., Singh, S., Mogilicherla, K., Shukla, J.N. & Palli, S.R. (2017) Comparative analysis of double-stranded RNA degradation and processing in insects. *Scientific Reports*, 7, 17059.

Sontheimer, E.J. (2005) Assembly and function of RNA silencing complexes. *Nature Reviews Molecular Cell Biology*, 6, 127–138.

Ulvila, J., Parikka, M., Kleino, A., Sormunen, R., Ezekowitz, R.A., Kocks, C. et al. (2006) Double-stranded RNA is internalized by scavenger receptor-mediated endocytosis in *Drosophila* S2 cells. *Journal of Biological Chemistry*, 281, 14370–14375.

Upadhyay, S.K., Chandrashekar, K., Thakur, N., Verma, P.C., Borgio, J.F., Singh, P.K. et al. (2011) RNA interference for the control of whiteflies (*Bemisia tabaci*) by oral route. *Journal of Biosciences*, 36, 153–161.

Wang, K., Cheng, H., Chen, J., Zhu, G., Tang, P. & Han, Z. (2021) Chimeric double-stranded RNAs could act as tailor-made pesticides for controlling storage insects. *Journal of Agricultural and Food Chemistry*, 69, 6166–6171.

Wang, Q. & Carmichael, G.G. (2004) Effects of length and location on the cellular response to double-stranded RNA. *Microbiology and Molecular Biology Reviews*, 68, 432–452.

Wuriyanghan, H., Rosa, C. & Falk, B.W. (2011) Oral delivery of double-stranded RNAs and siRNAs induces RNAi effects in the potato/tomato Psyllid, *Bactericerca cockerelli*. *PLoS One*, 6, e27736.

Yoon, J.-S., Mogilicherla, K., Gurusamy, D., Chen, X., Chereddy, S.C.R.R. & Palli, S.R. (2018) Double-stranded RNA binding protein, Staufen, is required for the initiation of RNAi in coleopteran insects. *Proceedings of the National Academy of Sciences of the United States of America*, 115, 8334–8339.

Yoon, J.S., Shukla, J.N., Gong, Z.J., Mogilicherla, K. & Palli, S.R. (2016) RNA interference in the Colorado potato beetle, *Leptinotarsa decemlineata*: identification of key contributors. *Insect Biochemistry and Molecular Biology*, 78, 78–88.

Zhang, T., Zhang, C., Dong, Z. & Guan, Y. (2015) Determination of base binding strength and base stacking interaction of DNA duplex using atomic force microscope. *Scientific Reports*, 5, 9143.

Zhang, Y., Wiggins, B.E., Lawrence, C., Petrick, J., Ivashuta, S. & Heck, G. (2012) Analysis of plant-derived miRNAs in animal small RNA datasets. *BMC Genomics*, 13, 381.

Zhou, X., Oi, F.M. & Scharf, M.E. (2006) Social exploitation of hexamerin: RNAi reveals a major caste-regulatory factor in termites. *Proceedings of the National Academy of Sciences of the United States of America*, 103, 4499–4504.

Zhu, K.Y. & Palli, S.R. (2020) Mechanisms, applications, and challenges of insect RNA interference. *Annual Review of Entomology*, 65, 293–311.

SUPPORTING INFORMATION

Additional supporting information can be found online in the Supporting Information section at the end of this article.

How to cite this article: Koo, J., Gurusamy, D. & Palli, S. R. (2023) Inefficient uptake of small interfering RNA is responsible for its inability to trigger RNA interference in Colorado potato beetle cells. *Archives of Insect Biochemistry and Physiology*, e22036. https://doi.org/10.1002/arch.22036

The reflexive vertex strength on cycle and generalized friendship graph

Ika Hesti Agustin, M. Imam Utoyo, Dafik, N. Mohanapriya, and Slamin

https://doi.org/10.1142/S1793557123501371 | **Cited by:** 0 **(Source: Crossref)**

< Previous Next >

Abstract

Let G be a simple, un-directed and connected graph. The graph G has a pair of sets $(V(G), E(G))$, where $V(G)$ is nonempty vertex set and $E(G)$ is an unordered pair of sets with two distinct vertices u, v in $V(G)$. A total k-labeling is defined as a function f_e from the edge set to a set $\{1, 2, 3, \ldots, k_e\}$ and a function f_v from the vertex set to a set $\{0, 2, 4, \ldots, 2k_v\}$, where $k = \max\{k_e, 2k_v\}$. The total k-labeling is a *vertex irregular reflexivek-labeling* of the graph G, if for every two different vertices u and u' of G, $\text{wt}(u) \neq \text{wt}(u')$, where $\text{wt}(u) = f_v(u) + \sum_{uv \in E(G)} f_e(uv)$. The *reflexive vertex strength* of the graph G, denoted by $\text{rvs}(G)$ is the minimum k for graph G which has a vertex irregular reflexive k-labeling. In this paper, we determined the exact value of the reflexive vertex strength of cycle and generalized friendship graph.

Communicated by H. Takana

Keywords: Reflexive vertex strength ▪ vertex irregular reflexive labeling ▪ cycle graph ▪ generalized friendship graph

AMSC: 05C78

ScienceDirect

Results in Physics

Volume 51, August 2023, 106601

An epidemiological model for computer virus with Atangana–Baleanu fractional derivative

C. Ravichandran [a 1], K. Logeswari [a 1], Aziz Khan [b 1], Thabet Abdeljawad [b c d 1] ✉, J.F. Gómez-Aguilar [e 1] ✉

Show more

Outline | Share Cite

https://doi.org/10.1016/j.rinp.2023.106601 ↗

Highlights

- We study optimal control analysis for the computer virus model in the sense of the Atangana–Baleanu derivative.
- We employed a fixed-point theorem to analyze the solutions for the fractional order computer virus model.
- We verified the results numerically and expressed them graphically.
- Simulation results are given to illustrate the effectiveness of the proposed results.

Abstract

The Era of data is transubstantiating into a Big Data model in this technological world in the early 21st century. In 2005, Roger Mougalas coined a combination of data for this future world of the human race. The information helps to find specific solutions for any physical problem under Catastrophic circumstances in high populations such as Covid-19. To store massive data and historical events in a computer, the possibility of damage occurred to the complete data. Hence, viruses are a crucial threat to such data worth millions and billions. For this purpose, we spend enormous costs and efforts to build defensive strategies to save that information. Analyzing the expansion and extension of viruses helps to protect data and prevent viruses. In this manuscript, we study optimal control analysis for the suggested model in the sense of the Atangana–Baleanu derivative (AB-derivative). We employed a fixed point theorem to analyze the solutions for the fractional order computer virus model. We verified the results numerically and expressed them graphically.

Previous Next

MSC

26A33; 34A08; 34A12; 34K12

Keywords

Mittag-leffler kernel; ITID model; Numerical approximation; Fixed point theory

Introduction

Fractional Calculus [1], [2], [3], [4] is a major field in the research of various disciplines. To overcome some scenarios in our day-to-day life and derive an effective way to utilize the FDEs proposed. For certain FDEs, we developed numerical and analytical methods to obtain appropriate solutions. New fractional derivatives are defined to approach real-world problems. Recently, Abu-Shady and Kaabar [5], [6] studied a generalized fractional derivative (Abu-Shady–Kaabar fractional derivative) in detail which produces satisfactory results that are consistent with conventional definitions of fractional derivative such as Caputo and Riemann–Liouville. There are numerous usages of AB-derivative in analyzing the solutions [7], [8], [9], [10], [11], [12], [13], [14], [15], [16], [17], [18], [19], [20], [21], [22], [23] and applying in the real world problems [24], [25], [26], [27], [28], [29], [30], [31], [32], [33], [34], [35], [36] which highly help us to describe the approximate solutions. It leads us to determine and analyze the effectiveness, solutions, severity, occurrence, and prevention of the problem.

Alexandria Engineering Journal (2023) 73, 377–384

HOSTED BY

Alexandria University

Alexandria Engineering Journal

www.elsevier.com/locate/aej
www.sciencedirect.com

ORIGINAL ARTICLE

Results on existence of solutions in nonlocal partial functional integrodifferential equations with finite delay in nondense domain

Kottakkaran Sooppy Nisar [a,*], **K. Munusamy** [b], **C. Ravichandran** [c]

[a] *Department of Mathematics, College of Science and Humanities in Alkharj, Prince Sattam Bin Abdulaziz University, Alkharj, 11942, Saudi Arabia*
[b] *Department of Mathematics, Hindusthan College of Engineering and Technology, Coimbatore 641032, Tamil Nadu, India*
[c] *Department of Mathematics, Kongunadu Arts and Science College, Coimbatore 641 029, Tamil Nadu, India*

Received 22 March 2023; revised 12 April 2023; accepted 23 April 2023
Available online 10 May 2023

KEYWORDS

Integrodifferntial equations;
Integrated resolvent operator;
Lipschitz condition;
Strict solution;
Fixed point theorem

Abstract In this work, to show the existence and uniqueness solution of functional integrodifferential equation with nonlocal condition and finite delay function. This article contains continuously dependence of integral solution and existence of strict solution established by using integrated resolvent operator theory with support of Lipschitz continuous. In this article the operator $(\mathscr{T}(t))_{t\geqslant 0}$ is assumed the locally Lipschitz continuous integrated resolvent operator and proved the existence of strict solution on reflexive and general Banach spaces. Finally an example is given related to this work.

1. Introduction

In this article is discuss about the existence of integral solution of below system:

$$\begin{cases} \omega'(t) = \mathscr{D}\omega(t) + \int_0^t \mathscr{H}(t-\zeta)\omega(\zeta)d\zeta + \varphi\left(t, \omega_t, \int_0^t h(t,\zeta,\omega_\zeta)d\zeta\right) \\ \text{for } t \in [0,a] = I, \\ \omega(0) = \phi + g(\omega) \in C([-r,0];\mathscr{E}) = \mathscr{C}. \end{cases} \tag{1}$$

Throughout this article, $\mathscr{E}$ is Banach space(BS), $\mathscr{D}$ be closed linear operator on $\mathscr{E}$ and its domain $\overline{D(\mathscr{D})} \neq \mathscr{E}$ and satisfied the Hille-Yosida axiom. Let $\mathscr{H}(t)$ is set of bounded linear operators in $\mathscr{E}$ and $D(\mathscr{D}) \subset D(\mathscr{H}(t))$ from $D(\mathscr{D})$ into $\mathscr{E}$. The functions $\varphi : I \times \mathscr{C} \times \mathscr{E} \to \mathscr{E}, h : I \times I \times \mathscr{C} \to \mathscr{E}$ are continuous specified later. Let $\mathscr{C}([-r,0];\mathscr{E})$ represent continuous functions on $[-r,0]$ in $\mathscr{E}$ and ϕ, g are defined on $\mathscr{C}([-r,0];\mathscr{E})$. For ω belongs to the continuous function $C([-r,\infty);\mathscr{E}), t \geqslant 0$, the function $\omega_t \in \mathscr{C}$ as $\omega_t(\theta) = \omega(t+\theta)$ for $\theta \in [-r,0]$. The general form of (1) as an abstract formation of large number of partial integrodifferential equation such as electronic circuit, economic, biological, medical domain and more. The semigroup and resolvent operator theory are important methods to find the solutions of integrodifferential equations in space $\mathscr{E}$. In[31] the author proved about the mild solution, strong

* Corresponding author.
E-mail address: n.sooppy@psau.edu.sa (K.S. Nisar).
Peer review under responsibility of Faculty of Engineering, Alexandria University.

https://doi.org/10.1016/j.aej.2023.04.050

solution and classical solutions using semigroup theory of evolution system also explained the uniqueness of solution. In the recent year, many differential systems can be reformed as integral equations and proved the solutions are obtained by appropriate fixed point theorems, which is the common technique to proving the existence solutions of the integral equations. In this article used Banach theorem for proving the existence of solution to nonlocal Eq.(1). Existence and uniqueness of abstract form Eq.(1) have been established in distinct articles and different approaches especially the existence of solution and valid properties of differential equations used by resolvent operator technique.In many phenomena, the nonlocal initial conditionds are more effective, realistic and accuracy in the solutions and uniqueness than the classical one in handing physical problem. Recent years [9,12,13,25,5] the authours studied their integrodifferential equation using nonlocal conditions and obtained effective result with support of resolvent operator theory. The neutral integrodifferential equations are used in various fields such as electronics, chemical kinetics and biological science etc. In particular, J.Y. Park et.al [30] derived impulsive neutral integro-differential delay system for existence behavior and in [24] the authors proved the results for infinite delay differential system. Moreover see in [37,35,2] the authors studied differential system using delay function with different approaches. Several authors [3,16–18, 6,11,8,28,27,7,10,12,34,19,20,1,4,21,26,32,36,33] have paid attention on differential equations with different approaches in Banach spaces. In [23,14] K.Ezzinbi et.al proved the existence solution of integrodifferential equations support of resolvent operator with delay. In [15] the authors proved the existence and regularity for integrodifferential problem in nondense domain. In this article authors used the integrated resolvent operator theory for differentiability of solution with initial function in finite delay. Recently published the article [38] established the existence of solution in nondensely defined neutral equations via integrated resolvent operator and Banach fixed point technique. Also proved continuous dependence with respect to initial data and differentiability of solutions with the nonlocal conditions. Motivated by the above articles, the novelty and contribution this article is, we established this theory with the partial integrodifferential problem with nonlocal and finite delay. This theory contains integrated resolvent operator in the existence part of solution and assumptions of Lipschitz continuous also proved the uniqueness part with Banach fixed point theory and verified differentiability of solutions and continuously dependence. This article is summarized as, in Section 2, To provide little preliminary results and definitions about integrated resolvent operator theory. In Section 3, verify the existence, uniqueness and continuous dependence of solution of Eq. (1). In Section 4, to see the differentiability of solution of (1) and in Section 5, to given an application related to our theory.

2. Basic results and definitions

Here, this section contains some results and definitions regarding integrated resolvent operators. Let $\mathscr{E}$ is BS and $\mathscr{D}$ be closed linear operator and $0 \in \rho(\mathscr{D})$ then $\mathscr{D}^{-1}$ exists. Let Y is BS $(D(\mathscr{D}), \|\cdot\|)$ and its norm $\|v\| = \|\mathscr{D}v\| + \|v\|, \forall v \in D(\mathscr{D})$. Let $\mathscr{L}(Y, \mathscr{E})$ be the bounded linear operator $Y \to \mathscr{E}$ with the norm $\|\cdot\|$ and $\mathscr{L}(\mathscr{E})$ when $Y = \mathscr{E}$. Let $\mathscr{C}([-r, 0]; \mathscr{E})$ represents as the functions on $[-r, 0]$ are continuous in $\mathscr{E}$ and sup-norm $\|\cdot\|_{\mathscr{C}}$. Next we recall few definitions and results about integrated resolvent operators established in [29] for linear nondensely defined integrodifferential equations. Consider the below homogeneous linear integrodifferential system,

$$\begin{cases} v\prime(t) = \mathscr{D}v(t) + \int_0^t \mathscr{H}(t-\zeta)v(\zeta)d\zeta \quad \text{for } t \in [0, a] \\ v(0) = v_0 \in \mathscr{E}. \end{cases} \tag{2}$$

Here, the operators $\mathscr{D}$ and $\mathscr{H}(\cdot)$ are defined already in Eq. (1). Then the integrated resolvent operator for Eq. (2) as follows

Definition 2.1([29]) A set of operator $(\mathscr{T}(t))_{t\geqslant 0} \in \mathscr{L}(\mathscr{E})$ is an integrated resolvent operator to Eq. (2) if it satisfies.

$(R1)$ $\forall v \in \mathscr{E}, \mathscr{T}(\cdot)v \in C([0, +\infty); \mathscr{E})$.
$(R2)$ $\forall v \in \mathscr{E}, \int_0^{\cdot} \mathscr{T}(\zeta) \in Y$.
$(R3)$ $\mathscr{T}(t)v - tv = \mathscr{D}\int_0^t \mathscr{T}(\zeta)v d\zeta + \int_0^t \mathscr{H}(t-\zeta)\int_0^{\zeta} \mathscr{T}(r)v dr d\zeta$, $\forall v \in \mathscr{E}, t \geqslant 0$.
$(R4)$ $\mathscr{T}(t)v - tv = \int_0^t \mathscr{T}(\zeta)\mathscr{D}v d\zeta + \int_0^t \int_0^{\zeta} \mathscr{T}(\zeta - r)\mathscr{H}(r)v dr d\zeta$, $\forall v \in D(\mathscr{D}), t \geqslant 0$.

Definition 2.2([29]) The operator $(\mathscr{T}(t))_{t\geqslant 0}$ defined in above definition is locally Lipschitz continuous(LLC) if $\forall a > 0, \exists K_a = K(a) > 0$ implies,

$$\|\mathscr{T}(t) - \mathscr{T}(\zeta)\| \leqslant K_a|t - \zeta|, \text{where} t, \zeta \in [0, a]$$

Definition 2.3([29]) Assume $(\mathscr{T}(t))_{t\geqslant 0}$ is a LLC integrated resolvent operator and

$\forall v \in \overline{D(\mathscr{D})}, t \mapsto \mathscr{T}(t)v$ is differentiable on $[0, +\infty)$. Further we applied the below axioms for the Eq. (1),

$(S1)$ $\mathscr{D}$ satisfies the Hille-Yosida theorem, let $T_0 \geqslant 1, w \in \mathbb{R}$ then $(w, +\infty) \subset \rho(\mathscr{D})$ and

$$\|(\lambda I - \mathscr{D})^{-n_0}\| \leqslant \frac{T_0}{(\lambda - w)^{n_0}} \text{ for } n_0 \in \mathbb{N}, \lambda > w,$$

here $\rho(\mathscr{D})$ is resolvent set of $\mathscr{D}$.

$(S2)$ $(\mathscr{H}(t))_{t\geqslant 0}$ is set of bounded linear operator on $D(\mathscr{D})$ to $\mathscr{E}, D(\mathscr{D}) \subseteq D(\mathscr{H}(t)), \forall t \geqslant 0$ then the functions $\mathscr{H}(\cdot)v$ are bounded variation on $[0, a], a > 0$ for $v \in D(\mathscr{D})$.

Lemma 2.4([29],Theorem 3.2) Suppose $(S1), (S2)$ satisfied, then $\exists$ a unique LLC integrated resolvent operator for (2).

Remark 2.5([22],Theorem 2.5) Lemma 2.4 shows that $(S1)$ characterizes a LLC integrated semigroup when $\mathscr{H} = 0$. Consider the below nonhomogeneous integrodifferential system,

$$\begin{cases} v'(t) = \mathscr{D}v(t) + \int_0^t \mathscr{H}(t-\zeta)v(\zeta)d\zeta + f(t) \quad \text{for } t \in [0, a] \\ v(0) = v_0 \in \mathscr{E}. \end{cases} \tag{3}$$

We follow the article see[29], to write the integral solution, strict solution of Eq. (3) as follows,

Definition 2.6 For $f \in L^1([0, \infty); \mathscr{E})$ and $v_0 \in \mathscr{E}$. A function $v : [0, a] \to \mathscr{E}$ is an integral solution of Eq. (3) if.

(i) $v \in C([0, a]; \mathscr{E})$,
(ii) $\int_0^{\cdot} v(\zeta)d\zeta \in C([0, a]; Y)$,
(iii) $v(t) = v_0 + \mathscr{D}\int_0^t v(\zeta)d\zeta + \int_0^t \mathscr{H}(t-\zeta)\int_0^{\zeta} v(\tau)d\tau d\zeta +$ $\int_0^t f(\zeta)d\zeta$, $t \in [0, a]$.

Definition 2.7 A map $v:[0,+\infty]\to\mathscr{E}$ is strict solution of problem (3) if $v\in C^1([0,+\infty];\mathscr{E})\cap C([0,+\infty];Y)$ and hold Eq. (3).

The Lemma 2.8 is very useful results for proving integral solution and strict solution of (3) used by a variation of constants formula.

Lemma 2.8([29]) Assume that $(\mathscr{T}(t))_{t\geqslant 0}$ is LLC integrated resolvent operator, $\rho(\mathscr{D})\neq\varnothing$, so that.

(*i*) If $v_0\in\overline{D(\mathscr{D})}, f\in L^1([0,+\infty);\mathscr{E})$ then $\exists$ a unique integral solution $v(\cdot)$ of problem (3), then

$$v(t)=\mathscr{T}\prime(t)v_0+\frac{d}{dt}\int_0^t\mathscr{T}(t-\zeta)f(\zeta)d\zeta, t\in[0,a]. \tag{4}$$

Further, the following holds,

$$\|v(t)\|\leqslant C_1\left(\|v_0\|+\int_0^t\|f(\zeta)\|d\zeta\right), t\in[0,a]. \tag{5}$$

(*ii*) Suppose $v_0\in D(\mathscr{D}), f\in W^{1,1}([0,a];\mathscr{E})$ and $\mathscr{D}v_0+f(0)\in\overline{D(\mathscr{D})}, \exists$ unique strict solution $v(\cdot)$ for Eq. (3) and

$$\|v\prime(t)\|\leqslant C_1\left(\|\mathscr{D}v_0+f(0)\|+\int_0^t\|\mathscr{H}(\zeta)v_0+f\prime(\zeta)\|d\zeta\right), t\in[0,a].$$

Here $C_1>0$ is constant.

Remark 2.9 Suppose $(\mathscr{T}(t))_{t\geqslant 0}$ is LLC integrated resolvent operator, from ([29],Theorem 2.7), for $v\in\overline{D(\mathscr{D})}, t\mapsto\mathscr{T}(t)v$ is differentiable on $[0,a]$.

Lemma 2.10([29],Theorem 2.6) The set of $(\mathscr{G}(t))_{t\geqslant 0}\in\mathscr{L}(\mathscr{E})$ be LLC with $\mathscr{G}(0)=0$ then

(*i*) If $f\in L^1([0,a];\mathscr{E})$, implies $\int_0^{\cdot}\mathscr{G}(\cdot-\zeta)f(\zeta)d\zeta\in C^1([0,a];\mathscr{E})$ and

$$\|\mathscr{Q}(t)\|\leqslant K_T\int_0^t\|f(\zeta)\|d\zeta \text{ for } t\in[0,a]. \tag{6}$$

Here $\mathscr{Q}=\frac{d}{dt}\int_0^t\mathscr{G}(t-\zeta)f(\zeta)d\zeta, t\in[0,a], K_T>0$ is Lipschitzian of $\{\mathscr{G}(t):t\in[0,a]\}$. Further if $\|f(t)\|\leqslant K_0$, $\exists K_0>0, t\in[0,a]$

$$\|\mathscr{Q}(t_1+\zeta)-\mathscr{Q}(t_1)\|\leqslant K_0K_T\zeta+K_T\int_0^{t_1}\|f(\zeta+\tau)-f(\tau)\|d\tau \text{ for } t_1,\zeta,t+\zeta\in[0,a]. \tag{7}$$

(*ii*) Suppose $f:[0,a]\to\mathscr{E}$ is strongly bounded variation then $\mathscr{Q}(\cdot)$ is Lipschitz cont. on $[0,a]$.

3. Existence of solution Part:

Here, we have to verify the existence of the solution of problem (1). The integral solution of (1) with nonlocal condition is defined as below,

Definition 3.1 For $\omega_0\in\overline{D(\mathscr{D})}$. A function $\omega\in([-r,+\infty);\mathscr{E})$ is an integral solution to the nonlocal system (1) if it satisfies,

(*i*) $\omega\in C([0,+\infty);\mathscr{E})$.
(*ii*) $\int_0^{\cdot}\omega(\zeta)d\zeta\in C([0,+\infty);Y)$.
(*iii*)

$$\omega(t)=\begin{cases}\phi(0)+g(\omega)(0)+\mathscr{D}\int_0^t\omega(\zeta)d\zeta+\int_0^t\mathscr{H}(t-\zeta)\int_0^{\zeta}\omega(r)drd\zeta\\ +\int_0^t\varphi\Big(\zeta,\omega_{\zeta},\int_0^{\zeta}h(\zeta,\tau,\omega_{\tau})d\tau\Big)d\zeta, t\geqslant 0.\\ \phi(t)+g(\omega)(t), t\in[-r,0].\end{cases}$$

Definition 3.2 A function $\omega:[-r,+\infty)\to\mathscr{E}$ is strict solution of Eq. (1) if,

(*i*) $\omega\in C^1([0,+\infty);\mathscr{E})\cap C([0,+\infty);Y)$.
(*ii*) ω holds the Eq. (1) on $[-r,+\infty)$.

If ω is solution of equation of (1) in $[-r,+\infty)$ then $\omega(t)\in\overline{D(\mathscr{D})},\forall t\geqslant 0$. Further $\phi(0)+g(\omega)(0)\in\overline{D(\mathscr{D})}$ and ω is strict solution if either $\omega\in C^1([0,+\infty);\mathscr{E})$ or $C([0,+\infty);Y)$.

To establish this theory, solution of existence Eq. (1), we need the support of the below assumptions.

(*H*1) The function $\varphi:I\times\mathscr{C}\times\mathscr{E}\to\mathscr{E}$ holds below axioms, (i) The map $\varphi(t,\cdot,\cdot):\mathscr{C}\times\mathscr{E}\to\mathscr{E}$ is cont. $\forall t\in I$ (ii) To all $(\tau_1,\tau_2)\in\mathscr{C}$, then $\varphi(\cdot,\tau_1,\tau_2):I\to\mathscr{E}$ is measurable. (iii) The function $m_{\varphi}\in C(I,[0,\infty))$, a cont. non decreasing map $\Omega_{\varphi}:[0,\infty)\to[0,\infty)$ we have

$$\|\varphi(t,\tau_1,\tau_2)\|\leqslant m_{\varphi}(t)\Omega_{\varphi}\big(\|\tau_1\|_C+\|\tau_2\|\big) \text{ for every } t\in I \text{ and } (\tau_1,\tau_2)\in\mathscr{C}\times\mathscr{E}.$$

(*H*2) The function $\varphi:I\times\mathscr{C}\times\mathscr{E}\to D(\mathscr{D})$ satisfies the Lipschitz continuous, then $\exists$ a constant $L_1>0$ such that

$$\|\varphi(t_1,\tau_1,v_1)-\varphi(t_2,\tau_2,v_2)\|\leqslant L_1(|t_1-t_2|+\|\tau_1-\tau_2\|+\|v_1-v_2\|) \text{ for every } \tau_1,\tau_2\in\mathscr{C},v_1,v_2\in\mathscr{E}.$$

(*H*3) The function $h:I\times I\times\mathscr{C}\to\mathscr{E}$ holds the below, (i) $h(t,s,\cdot):\mathscr{C}\to\mathscr{E}$ is continuous $\forall t,s\in I$. (ii) To each $x\in\mathscr{C}, h(\cdot,\cdot,x):I\times I\to\mathscr{E}$ is measurable. (iii) $\exists$ a function $m_h\in C(I,[0,+\infty))$ and $\Omega_h:[0,+\infty)\to[0,+\infty)$ is nondecreasing function implies

$$\|h(t,s,x)\|\leqslant\tau_0m_h(s)\Omega_h\big(\|x\|_{\mathscr{C}}\big), \tau_0>0 \text{ for every } t,s\in I,x\in\mathscr{C}.$$

(*H*4) The function $h:I\times I\times\mathscr{C}\to\mathscr{E}$ holds the Lipschitz continuous and let $L_h>0$ then

$$\|h(t_1,s_1,x_0)-h(t_1,s_1,y_0)\|\leqslant L_h\|x_0-y_0\| \text{ to each } t_1,s_1\in I \text{ and } x_0,y_0\in\mathscr{C}.$$

(*H*5) The function $g:C(I;\mathscr{E})\to\mathscr{C}([-r,0];\mathscr{E})$ continuous then,

$$\|g(\phi)\|\leqslant c\|\phi\|+d \text{ for all } \phi\in C(I;\mathscr{E}).$$

(*H*6) The map $g:C(I;\mathscr{E})\to\overline{D(\mathscr{D})}$ is Lipschitz continuous, let $L_2>0$ then

$$\|g(x_0)-g(y_0)\|\leqslant L_2\|x_0-y_0\|_C \text{ for each } x_0,y_0\in C.$$

Remark 3.3 Assume that the Eq. (3) has LLC and integrated resolvent operator $(\mathscr{T}(t))_{t\geqslant 0}$, $\rho(\mathscr{D})\neq\varnothing$. Let φ satisfied (*H*2) and $\phi(t)+g(\omega)(t)\in\mathscr{C}$ so that $\phi(0)+g(\omega)(0)\in\overline{D(\mathscr{D})}$. Then Eq. (1) has a unique solution $\omega(\cdot,\phi(t)+g(\omega)(t))$ defined on $[-r,+\infty)$. Moreover by the variation of constant formula.

$$\omega(t)=\begin{cases}\mathscr{T}\prime(t)[\phi(0)+g(\omega)(0)]+\frac{d}{dt}\int_0^t\mathscr{T}(t-\zeta)\varphi\Big(\zeta,\omega_\zeta,\int_0^\zeta h(\zeta,\tau,\omega_\tau)d\tau\Big)d\zeta, & t\geqslant 0.\\ \phi(t)+g(\omega)(t), & t\in[-r,0].\end{cases}$$

Theorem 3.4 Let $\omega_0\in\overline{D(\mathscr{D})},0\in\rho(\mathscr{D})$ satisfies $(H1-H6)$ and $\forall\phi\in\mathscr{C}([-r,0];\mathscr{E})$ then the system (1) has at least one mild solution on $[-r,a]$ provided,

$$K_TL_1a(1+L_h)<1. \tag{8}$$

proof: Let $\omega\in C([-r,a];\mathscr{E})$ the restriction of ω on $[0,a],\omega|_{[0,a]}\in C([0,a];\mathscr{E})$, for our convenience, we write $g\Big(\omega|_{[0,a]}\Big)$ as $g(\omega)$. Now we wish to verify the operator solution.

$$(\mathsf{F}\omega)(t)=\begin{cases}\phi(t)+g(\omega)(t), & t\in[-r,0].\\ \mathscr{T}'(t)[\phi(0)+g(\omega)(0)]\\ +\frac{d}{dt}\int_0^t\mathscr{T}(t-\zeta)\varphi\Big(\zeta,\omega_\zeta,\int_0^\zeta h(\zeta,\tau,\omega_\tau)d\tau\Big)d\zeta, & t\geqslant 0.\end{cases}$$

has a fixed point in ball $B_{r_0}=\{\omega\in C([-r,a];\mathscr{E}),\|\omega\|\leqslant r_0\}$,where r_0 is + ve constant. First we claim, F maps $\overline{B_{r_0}}$ into itself. Every $\omega\in\overline{B_{r_0}}$ and $t\in[-r,0]$.

Take $\mathsf{F}_1=\phi(t)+g(\omega)(t)$

$\mathsf{F}_2=\mathscr{T}'(t)[\phi(0)+g(\omega)(0)]+\frac{d}{dt}\int_0^t\mathscr{T}(t-\zeta)\varphi\Big(\zeta,\omega_\zeta,\int_0^\zeta h(\zeta,\tau,\omega_\tau)d\tau\Big)d\zeta.$

Now,

$$\begin{aligned}\|\mathsf{F}_1\|&\leqslant\|\phi(t)\|+\|g(\omega)(t)\|\\&\leqslant\|\phi\|+c\|\omega\|+d\\&\leqslant\|\phi\|+cr_0+d.\end{aligned}$$

Next, let $t\in[0,a]$ we get,

$$\begin{aligned}\|\mathsf{F}_2\|&=\Big\|\mathscr{T}\prime(t)[\phi(0)+g(\omega)(0)]+\tfrac{d}{dt}\int_0^t\mathscr{T}(t-\zeta)\varphi\Big(\zeta,\omega_\zeta,\int_0^\zeta h(\zeta,\tau,\omega_\tau)d\tau\Big)d\zeta\Big\|\\&\leqslant\|\mathscr{T}\prime(t)\|\|\phi(0)+g(\omega)(0)\|+\Big\|\tfrac{d}{dt}\int_0^t\mathscr{T}(t-\zeta)\varphi\Big(\zeta,\omega_\zeta,\int_0^\zeta h(\zeta,\tau,\omega_\tau)d\tau\Big)d\zeta\Big\|\\&\leqslant C_1\Big(\|\phi\|+\|g(\omega)\|+\int_0^t\Big\|\varphi\Big(\zeta,\omega_\zeta,\int_0^\zeta h(\zeta,\tau,\omega_\tau)d\tau\Big)\Big\|d\zeta\Big)\\&\leqslant C_1\big(\|\phi\|+\|g(\omega)\|+\int_0^t m_\varphi(\zeta)(\Omega_\varphi(\|\omega_\zeta\|)+\tau_0m_h(\zeta)\Omega_h(\|\omega_\tau\|))d\zeta\big)\\&\leqslant C_1\big(\|\phi\|+c\|\omega\|+d+\int_0^t m_\varphi(\zeta)(\Omega_\varphi(r_0)+\tau_0m_h(\zeta)\Omega_h(r_0))d\zeta\big)\\&\leqslant C_1\big(\|\phi\|+cr_0+d+\int_0^t m_\varphi(\zeta)\Omega_\varphi(r_0+\tau_0m_h(\zeta)\Omega_h(r_0))d\zeta\big)\\&\leqslant C_1(\|\phi\|+c\|\omega\|+d+\Omega(r_0)\tau_0a\|m\|_{L^1}).\end{aligned}$$

From above two cases

$$\|\mathsf{F}\|\leqslant C_1(\|\phi\|+c\|\omega\|+d+\Omega(r_0)\tau_0a\|m\|_{L^1}).$$

Which implies that $\|\mathsf{F}\|\leqslant r_0$. Hence $\mathsf{F}\overline{(B_{r_0})}\subseteq\overline{(B_{r_0})}$.

Next to prove that F has contraction mapping on B_{r_0}.

The mapping F on B_{r_0} is

$$\begin{aligned}(\mathsf{F}\omega)(t)&=\mathscr{T}'(t)[\phi(0)+g(\omega)(0)]\\&\quad+\frac{d}{dt}\int_0^t\mathscr{T}(t-\zeta)\varphi\Big(\zeta,\omega_\zeta,\int_0^\zeta h(\zeta,\tau,\omega_\tau)d\tau\Big)d\zeta\text{ for}\\&\quad t\in[0,a].\end{aligned}\tag{9}$$

The extension $\tilde{\omega}:[-r,a]$ defined as $\tilde{\omega}(t)=\begin{cases}(\omega)(t), & t\in[0,a].\\ \phi(t)+g(\omega)(t), & t\in[-r,0].\end{cases}$

To show this existence solution using Banach fixed point theorem, for $u,v\in B_{r_0}$, $t\in[0,a]$

$$\begin{aligned}\|(\mathsf{F}u)(t)-(\mathsf{F}v)(t)\|&=\Big\|\tfrac{d}{dt}\int_0^t\mathscr{T}(t-\zeta)\Big[\varphi\Big(\zeta,\tilde{u_\zeta},\int_0^\zeta h(\zeta,\tau,\tilde{u_\tau})\Big)-\varphi\Big(\zeta,\tilde{v_\zeta},\int_0^\zeta h(\zeta,\tau,\tilde{v_\tau})\Big)\Big]d\zeta\Big\|\\&\leqslant K_T\int_0^t\Big\|\Big[\varphi\Big(\zeta,\tilde{u_\zeta},\int_0^\zeta h(\zeta,\tau,\tilde{u_\tau})\Big)-\varphi\Big(\zeta,\tilde{v_\zeta},\int_0^\zeta h(\zeta,\tau,\tilde{v_\tau})\Big)\Big]\Big\|d\zeta\\&\leqslant K_TL_1a(1+L_h)\|u-v\|_C.\end{aligned}$$

Let the constant $K_TL_1a(1+L_h)=c_0<1$, then

$\|(\mathsf{F}u)(t)-(\mathsf{F}v)(t)\|\leqslant c_0\|u-v\|_C.$

Hence F is contraction map on B_{r_0} also F has a fixed point $\omega(\cdot)$. It shows, the problem (1) has a unique solution on $[-r,a]$.

Next to see, continuous dependence of integral solution of (1) with respect to initial conditions as follows,

Theorem 3.5. If $\lambda(\cdot),\mu(\cdot)$ are solutions of Eq. (1) with the initial condition $\lambda_0,\mu_0\in\overline{D(\mathscr{D})}$ respectively, then the solution of Eq. (1) continuous depends on this initial values provided that $C_1e^{L_1a}L_2<1$.

Proof: Let $\lambda(\cdot),\mu(\cdot)$ be the two integral solutions of the problem (1) and $\lambda_0,\mu_0\in\overline{D(\mathscr{D})}$, in this sense we have prove $\|\tilde{\lambda}(t)-\tilde{\mu}(t)\|\leqslant k_0\|\lambda(0)-\mu(0)\|$ for $k_0>0$.

Now the extension of solution $\lambda(\cdot)$ and $\mu(\cdot)$ defined as.

$$\tilde{\lambda}(t)=\begin{cases}(\lambda)(t),t\in[0,a]\\ \phi(t)+g(\lambda)(t),t\in[-r,0]\end{cases}\text{and}$$

$$\tilde{\mu}(t)=\begin{cases}(\mu)(t),t\in[0,a]\\ \phi(t)+g(\mu)(t),t\in[-r,0]\end{cases}$$

Using the estimation of Lemma 2.8,

$$\begin{aligned}\|\tilde{\lambda}(t)-\tilde{\mu}(t)\|&=\|\mathscr{T}\prime(t)\Big[g\Big(\tilde{\lambda}\Big)(0)-g(\tilde{\mu})(0)\Big]\\&\quad+\tfrac{d}{dt}\int_0^t\mathscr{T}(t-\zeta)\Big[\varphi\Big(\zeta,\tilde{\lambda_\zeta},\int_0^\zeta h\Big(\zeta,\tau,\tilde{\lambda_\tau}\Big)d\tau\Big)-\varphi\Big(\zeta,\tilde{\mu_\zeta},\int_0^\zeta h(\zeta,\tau,\tilde{\mu_\tau})d\tau\Big)\Big]d\zeta\|\\&\leqslant C_1\Big[\|g\Big(\tilde{\lambda}\Big)(0)-g(\tilde{\mu})(0)\|\\&\quad+\int_0^t\|\varphi\Big(\zeta,\tilde{\lambda_\zeta},\int_0^\zeta h\Big(\zeta,\tau,\tilde{\lambda_\tau}\Big)d\tau\Big)-\varphi\Big(\zeta,\tilde{\mu_\zeta},\int_0^\zeta h(\zeta,\tau,\tilde{\mu_\tau})d\tau\Big)\|d\zeta\Big]\\&\leqslant C_1L_2\|\tilde{\lambda}(0)-\tilde{\mu}(0)\|+L_1\int_0^t\sup_{0\leqslant\tau\leqslant\zeta}\|\tilde{\lambda_\tau}-\tilde{\mu_\tau}\|d\zeta.\end{aligned}$$

By Gronwall's Lemma,

$$\begin{aligned}\sup_{0\leqslant\tau\leqslant s}\|\tilde{\lambda_\tau}-\tilde{\mu_\tau}\|&\leqslant C_1L_2\|\tilde{\lambda}(0)-\tilde{\mu}(0)\|e^{L_1\int_0^a ds}\\&\leqslant C_1L_2\|\tilde{\lambda}(0)-\tilde{\mu}(0)\|e^{L_1a}.\end{aligned}$$

By the extension of $\lambda(t)$,

$$\|\lambda(t)-\mu(t)\|\leqslant C_1e^{L_1a}L_2\|\lambda(0)-\mu(0)\|.$$

From the sufficient condition of Theorem 3.4, implies that $\|\lambda(t)-\mu(t)\|\leqslant k_0\|\lambda(0)-\mu(0)\|$, where $k_0=C_1e^{L_1a}L_2<1$. This shows that the solution of the Eq. (1) has continuous dependence upon the initial vales.

4. Differentiability of solution

Here, we have to show the existence of strict solution for problem (1) with respect to certain sufficient conditions.

Definition 4.1 A map $\omega(\cdot):[-r,+\infty)\to\mathscr{E}$ is strict solution of system (1) if below axioms are holds.

(*i*) $\omega\in C^1([0,+\infty);\mathscr{E})\cap C([0,+\infty);D(\mathscr{D}))$.
(*ii*) ω holds system (1) on $[-r,+\infty)$.

First we assume if $\mathscr{E}$ is reflexive, its enough to show the below theorem for existence of strict solution of (1).

Theorem 4.2 Suppose the axioms of Theorem 3.1 are true. Let $\phi+g(\omega)\in D(\mathscr{D}),\mathscr{D}[\phi(0)+g(\omega)(0)]+\varphi(0,\phi+g(\omega),0)\in\overline{D(\mathscr{D})}$ then the Eq. (1) admits a strict solution on $[-r,+\infty)$ provided that:

$$(K_a(C_1+C_2)+C_1C_2)(\|\phi\|+cr_1+d)+L_1(K_a+a)<1. \tag{10}$$

proof: Consider the ball with radius r_1,

$$B_{r_1}=\{\omega\in([-r,a];\mathscr{E});\|\omega\|\leqslant r_1,\|\omega(t_2)-\omega(t_1)\|\leqslant L_1^*|t_2-t_1|,t_1,t_2\in[-r,a]\}. \tag{11}$$

Where L_1^* positive constant. Now we defined the function F on $C([-r,a];\mathscr{E})$ in Theorem (3.4), and prove F has a fixed point on B_{r_1}.

Clearly from Theorem 3.4, we conclude $\mathsf{F}(B_{r_1})\subset B_{r_1}$, it is enough to show that for any $\omega\in B_{r_1}$ such that $\|(\mathsf{F}\omega)(t_2)-(\mathsf{F}\omega)(t_1)\|\leqslant L_1^*|t_2-t_1|$ for $t_1,t_2\in[-r,a]$.

Now the extension of solution $(\mathsf{F}\omega)(t)$ is follows.

$$\tilde{\omega}(t)=\begin{cases}(\omega)(t), & \text{for } t\in[0,a].\\ \phi(t)+g(\omega)(t), & \text{for } t\in[-r,0].\end{cases}$$

Now

$$\begin{aligned}\|(\mathsf{F}\omega)(t_2)-(\mathsf{F}\omega)(t_1)\|\leqslant\ & \|(\mathscr{T}\prime(t_2)-\mathscr{T}\prime(t_1))(\phi(0)+g(\omega)(0))\|\\ +\ & \|\tfrac{d}{dt_2}\int_0^{t_2}\mathscr{T}(t_2-\zeta)\varphi\Big(\zeta,\tilde{\omega}_\zeta,\int_0^\zeta h(\zeta,\tau,\tilde{\omega}_\tau)d\tau\Big)d\zeta\\ -\ & \tfrac{d}{dt_1}\int_0^{t_1}\mathscr{T}(t_1-\zeta)\varphi\Big(\zeta,\tilde{\omega}_\zeta,\int_0^\zeta h(\zeta,\tau,\tilde{\omega}_\tau)d\tau\Big)d\zeta\|\\ :=\ & I_1+I_2(\text{take for our convenience}).\end{aligned}$$

Now take for I_1, then

$$\begin{aligned}I_1=\ & \|(\mathscr{T}'(t_2)-\mathscr{T}'(t_1))(\phi(0)+g(\omega)(0))\|\\ \leqslant\ & \|\mathscr{T}'(t_2)-\mathscr{T}'(t_1)\|\|\phi(0)+g(\omega)(0)\|\end{aligned}$$

As $(R4)$, implies that, for $\omega\in D(\mathscr{D})$, we get

$$\mathscr{T}\prime(t)\omega-\omega=\mathscr{T}(t)\mathscr{D}\omega+\int_0^t\mathscr{T}(t-\zeta)\mathscr{H}(\zeta)\omega d\zeta.$$

Using $(R4)$ of Definition 2.1, implies that

$$\begin{aligned}I_1\leqslant\ & \|\mathscr{T}\prime(t_2)-\mathscr{T}\prime(t_1)\|\mathscr{D}[\phi(0)+g(\omega)(0)]\\ +\ & \int_0^{t_1}\|\mathscr{T}'(t_2-\zeta)-\mathscr{T}\prime(t_1-\zeta)\|\|H(\zeta)[\phi(0)+g(\omega)(0)]\|d\zeta\\ +\ & \int_{t_1}^{t_2}\|\mathscr{T}'(t_2-\zeta)\|\|\mathscr{H}(\zeta)[\phi(0)+g(\omega)(0)]\|d\zeta\\ \leqslant\ & K_a\|\mathscr{D}[\phi(0)+g(\omega)(0)]|t_2-t_1|+K_aC_2\|\phi(0)+g(\omega)(0)\|(a)|t_2-t_1|\\ +\ & \sup_{t\in[-r,a]}\|\mathscr{T}(t)\|C_2\|\phi(0)+g(\omega)(0)\|\|t_2-t_1|\\ \leqslant\ & K_aC_1(\|\phi\|+\|g(\omega)\|)|t_2-t_1|+K_aC_2(\|\phi\|+\|g(\omega)\|(a)|t_2-t_1|\\ +\ & C_1C_2(\|\phi\|+\|g(\omega)\|)|t_2-t_1|\\ \leqslant\ & (K_aC_1+K_aC_2+C_1C_2)(\|\phi\|+c\|\omega\|+d)|t_2-t_1|\end{aligned}$$

$$I_1\leqslant(K_a(C_1+C_2)+C_1C_2)(\|\phi\|+cr_1+d)|t_2-t_1|. \tag{12}$$

For I_2,

$$\begin{aligned}I_2\leqslant\ & \Big\|\tfrac{d}{dt_2}\int_0^{t_2}\mathscr{T}(t_2-\zeta)\varphi\Big(\zeta,\tilde{\omega}_\zeta,\int_0^\zeta h(\zeta,\tau,\tilde{\omega}_\tau)d\tau\Big)d\zeta\\ -\ & \tfrac{d}{dt_1}\int_0^{t_1}\mathscr{T}(t_1-\zeta)\varphi\Big(\zeta,\tilde{\omega}_\zeta,\int_0^\zeta h(\zeta,\tau,\tilde{\omega}_\tau)d\tau\Big)d\zeta\Big\|\end{aligned}$$

Applying definition (3) and Eq. (7), we have

$$I_2\leqslant L_1K_a|t_2-t_1|+L_1(a)|t_2-t_1|\leqslant L_1(K_a+a)|t_2-t_1|. \tag{13}$$

Thus from Eq. (12) and (13),

$$\|(\mathsf{F}\omega)(t_2)-(\mathsf{F}\omega)(t_1)\|\leqslant[(K_a(C_1+C_2)+C_1C_2)(\|\phi\|+cr_1+d)+L_1(K_a+a)]|t_2-t_1|.$$

Which implies that

$$\|(\mathsf{F}\omega)(t_2)-(\mathsf{F}\omega)(t_1)\|\leqslant C^*|t_2-t_1|.$$

Where

$C^*=(K_a(C_1+C_2)+C_1C_2)(\|\phi\|+cr_1+d)+L_1(K_a+a)$ and $C_2=\sup_{t\in[0,a]}\|\mathscr{H}(t)\|$.

Hence F has a unique fixed point $\omega(\cdot)$ is solution of Eq. (1).

Further $\omega(t)$ is Lipschitz on $[0,a]$, then.

$\zeta\to\varphi\Big(\zeta,\tilde{\omega}_\zeta,\int_0^\zeta h(\zeta,\tau,\tilde{\omega}_\tau)d\tau\Big)d\zeta$ is also Lipschitz continuous and $\mathscr{E}$ is a reflexive, by Radon-Nikodym property, we deduce that

$$\int_0^\zeta\mathscr{T}(t-\zeta)\varphi\Big(\zeta,\tilde{\omega}_\zeta,\int_0^\zeta h(\zeta,\tau,\tilde{\omega}_\tau)d\tau\Big)d\zeta\in W^{1,1}([-r,a];\mathscr{E}).$$

From the Lemma 2.8, $\omega(t)$ is differentiable on $[-r,a]$, hence $\omega(\cdot)$ is strict solution of (1). In the next case consider the regularity in general Banach space $\mathscr{E}$. In the sequent further we need the below suppositions

$(H7)$ The function $\varphi\in C^1(I\times\mathscr{C}\times\mathscr{E});\mathscr{E}$ and partial derivatives $D_1\varphi(\cdot,\cdot,\cdot),D_2\varphi(\cdot,\cdot,\cdot)$ are LLC with respect to the second variable, $\exists D_F^i>0$ then

$$\|D_i\varphi(t,c_1,c_2)-D_i\varphi(t,d_1,d_2)\leqslant D_F^i(\|c_1-d_1\|+\|c_2-d_2\|)$$

for $0\leqslant t\leqslant a,c_1,d_1\in\mathscr{C},c_2,d_2\in\mathscr{E},i=1,2.$

Theorem 4.3. Assume the Eq. (2) has an integrated resolvent operator $(\mathscr{T}(t))_{t\geqslant0}$ and LLC with $\rho(\mathscr{D})\neq\varnothing$. Let φ be a function satisfies $(H_2),(H_7)$ and $\phi+g(\omega)\in C^1([-r,0];\mathscr{E})$ then $\phi(0)+g(\omega)(0)\in D(\mathscr{D}),\phi\prime(0)+g\prime(\omega)(0)\in\overline{D(\mathscr{D})}$ and $\phi\prime(0)+g\prime(\omega)(0)=\mathscr{D}[\phi(0)+g(\omega)(0)]+\varphi(0,\phi+g(\omega),0)$. Then the system (1) has strict solution on $[-r,+\infty)$.

Proof: Let $\omega(\cdot)$ be a solution of system (1).

$$\omega(t)=\begin{cases}\mathscr{T}\prime(t)[\phi(0)+g(\omega)(0)]+\frac{d}{dt}\int_0^t\mathscr{T}(t-\zeta)\varphi\Big(\zeta,\omega_\zeta,\int_0^\zeta h(\zeta,\tau,\omega_\tau)d\tau\Big)d\zeta, & \text{for } t\geqslant0.\\ \phi(t)+g(\omega)(t), & \text{for } t\in[-r,0].\end{cases}$$

Let us assume the below system

$$\begin{cases}x\prime(t)=\mathscr{D}x(t)+\int_0^t\mathscr{H}(t-\zeta)x(\zeta)d\zeta+D_1\varphi\big(t,\omega_t,\int_0^t h(t,\zeta,\omega_\zeta)d\zeta\big)\\ +D_2\varphi\big(t,\omega_t,\int_0^t h(t,\zeta,\omega_\zeta)d\zeta\big)v_t+\mathscr{H}(t)\omega(0), & t\in[0,a].\\ x(0)=\phi\prime(0)+g\prime(\omega)(0).\end{cases} \tag{14}$$

By the similar proof discussion used in Theorem 3.4, to easily show that the integral solution for problem (14) is unique solution $x(t)$ defined as follows

$$x(t)=\begin{cases}\mathscr{T}'(t)[\phi\prime(0)+g\prime(\omega)(0)]+\frac{d}{dt}\int_0^t\mathscr{T}(t-\zeta)\Big[D_1\varphi\Big(\zeta,\omega_\zeta,\int_0^\zeta h(\zeta,\tau,\omega_\tau)d\tau\Big)\\ +D_2\varphi\Big(\zeta,\omega_\zeta,\int_0^\zeta h(\zeta,\tau,\omega_\tau)d\tau\Big)v_\zeta+\mathscr{H}(\zeta)[\phi(0)+g(\omega)(0)]\Big]d\zeta, & t\geqslant0.\\ \phi'(t)+g\prime(\omega)(t), & t\in[-r,0].\end{cases}$$

Let $\alpha:[-r,a]\to\mathscr{E}$ be defined by.

$$\alpha(t)=\begin{cases}\omega(0)+\int_0^t x(\zeta)d\zeta,t\in[0,a].\\ \phi(t)+g(\omega)(t),t\in[-r,0].\end{cases}$$

We have,

$$\alpha_t=\phi+g(\omega)+\int_0^t x_sds,t\in[0,a].$$

Now to prove, $\alpha(t)=\omega(t)$. By the expansion of $\alpha(t)$, $t\in[0,a]$ is

$$\begin{aligned}\alpha(t)=\phi(0)+g(\omega)(0)\ & +\mathscr{T}(t)[\phi\prime(0)+g\prime(\omega)(0)]\\ & +\int_0^t\mathscr{T}(t-\zeta)\Big[D_1\varphi\Big(\zeta,\omega_\zeta,\int_0^\zeta h(\zeta,\tau,\omega_\tau)d\tau\Big)\\ & +D_2\varphi\Big(\zeta,\omega_\zeta,\int_0^\zeta h(\zeta,\tau,\omega_\tau)d\tau\Big)v_\zeta+\mathscr{H}(\zeta)[\phi(0)+g(\omega)(0)]\Big]d\zeta.\end{aligned} \tag{15}$$

Since $\phi(0)+g(\omega)(0)\in D(\mathscr{D}),\phi\prime(0)+g\prime(\omega)(0)\in\overline{D(\mathscr{D})}$ and

$$\mathscr{T}(t)[\phi\prime(0)+g\prime(\omega)(0)]=\mathscr{T}(t)\mathscr{D}[\phi(0)+g(\omega)(0)]+\mathscr{T}(t)[\varphi(0,\phi+g(\omega),0)].$$

From derivative of (R4), we have

$$\mathscr{T}[\phi\prime(0)+g\prime(\omega)(0)]=\mathscr{T}\prime(t)[\phi(0)+g(\omega)(0)]-[\phi(0)+g(\omega)(0)]-\int_0^t\mathscr{T}(t-\zeta)\mathscr{H}(\zeta)[\phi(0)+g(\omega)(0)]d\zeta+\mathscr{T}[\varphi(0,\phi+g(\omega),0)]. \tag{16}$$

Further, $t\to\int_0^t\mathscr{T}(t-\zeta)\varphi\left(\zeta,\alpha_\zeta,\int_0^\zeta(\zeta,\tau,\alpha_\tau)d\tau\right)d\zeta$ is continuously differentiable, then

$$\begin{aligned}&\frac{d}{dt}\int_0^t\mathscr{T}(t-\zeta)\varphi\left(\zeta,\alpha_\zeta,\int_0^\zeta h(\zeta,\tau,\alpha_\tau)d\tau\right)d\zeta\\&=\frac{d}{dt}\int_0^t\mathscr{T}(\zeta)\varphi\left(t-\zeta,\alpha_{t-\zeta},\int_0^{t-\zeta}h(t-\zeta,\tau,\alpha_\tau)d\tau\right)d\zeta\\&=\frac{d}{dt}\int_0^t\mathscr{T}(\zeta)\varphi\left(r,\alpha_r,\int_0^r h(r,\tau,\alpha_\tau)d\tau\right)d\zeta\\&=\mathscr{T}(t)\varphi(0,\phi+g(\omega),0)\\&\quad+\int_0^t\mathscr{T}(t-\zeta)\Big[D_1\varphi\left(\zeta,\alpha_\zeta,\int_0^\zeta h(\zeta,\tau,\alpha_\tau)d\tau\right)\\&\quad+D_2\varphi\left(\zeta,\alpha_\zeta,\int_0^\zeta h(\zeta,\tau,\alpha_\tau)d\tau\right)v_\zeta\Big]d\zeta.\end{aligned}$$

Then

$$\begin{aligned}&\mathscr{T}(t)\varphi(0,\phi+g(\omega),0)\\&=\frac{d}{dt}\int_0^t\mathscr{T}(t-\zeta)\varphi\left(\zeta,\alpha_\zeta,\int_0^\zeta h(\zeta,\tau,\alpha_\tau)d\tau\right)d\zeta\\&+\int_0^t\mathscr{T}(t-\zeta)\Big[D_1\varphi\left(\zeta,\alpha_\zeta,\int_0^\zeta h(\zeta,\tau,\alpha_\tau)d\tau\right)\\&+D_2\varphi\left(\zeta,\alpha_\zeta,\int_0^\zeta h(\zeta,\tau,\alpha_\tau)d\tau\right)v_\zeta\Big]d\zeta.\end{aligned}\tag{17}$$

Using Eq. (17) in (16),

$$\begin{aligned}&\mathscr{T}(t)[\phi\prime(0)+g\prime(\omega)(0)]\\&=\mathscr{T}'(t)[\phi(0)+g(\omega)(0)]-\phi(0)-g(\omega)(0)\\&-\int_0^t\mathscr{T}(t-\zeta)\mathscr{H}(\zeta)[\phi(0)+g(\omega)(0)]d\zeta\\&+\frac{d}{dt}\int_0^t\mathscr{T}(t-\zeta)\varphi\left(\zeta,\alpha_\zeta,\int_0^\zeta h(\zeta,\tau,\alpha_\tau)d\tau\right)d\zeta\\&-\int_0^t\mathscr{T}(t-\zeta)\Big[D_1\varphi\left(\zeta,\alpha_\zeta,\int_0^\zeta h(\zeta,\tau,\alpha_\tau)d\tau\right)\\&+D_2\varphi\left(\zeta,\alpha_\zeta,\int_0^\zeta h(\zeta,\tau,\alpha_\tau)d\tau\right)v_\zeta\Big]d\zeta.\end{aligned}\tag{18}$$

Substitute Eq. (18) in (15),

$$\begin{aligned}\alpha(t)&=\mathscr{T}'(t)[\phi(0)+g(\omega)(0)]\\&+\frac{d}{dt}\int_0^t\mathscr{T}(t-\zeta)\varphi\left(\zeta,\alpha_\zeta,\int_0^\zeta h(\zeta,\tau,\alpha_\tau)d\tau\right)d\zeta\\&-\int_0^t\mathscr{T}(t-\zeta)\Big[D_1\varphi\left(\zeta,\alpha_\zeta,\int_0^\zeta h(\zeta,\tau,\alpha_\tau)d\tau\right)\\&-D_1\varphi\left(\zeta,\omega_\zeta,\int_0^\zeta h(\zeta,\tau,\omega_\tau)d\tau\right)\Big]d\zeta\\&-\int_0^t\mathscr{T}(t-\zeta)\Big[D_2\varphi\left(\zeta,\alpha_\zeta,\int_0^\zeta h(\zeta,\tau,\alpha_\tau)d\tau\right)v_\zeta\\&-D_2\varphi\left(\zeta,\omega_\zeta,\int_0^\zeta h(\zeta,\tau,\omega_\tau)d\tau\right)v_\zeta\Big]d\zeta.\end{aligned}$$

Hence

$$\begin{aligned}\omega(t)-\alpha(t)&=\frac{d}{dt}\int_0^t\mathscr{T}(t-\zeta)\Big[\varphi\left(\zeta,\omega_\zeta,\int_0^\zeta h(\zeta,\tau,\omega_\tau)d\tau\right)\\&-\varphi\left(\zeta,\alpha_\zeta,\int_0^\zeta h(\zeta,\tau,\alpha_\tau)d\tau\right)\Big]d\zeta\\&-\int_0^t\mathscr{T}(t-\zeta)\Big[D_1\varphi\left(\zeta,\omega_\zeta,\int_0^\zeta h(\zeta,\tau,\omega_\tau)d\tau\right)\\&-D_1\varphi\left(\zeta,\alpha_\zeta,\int_0^\zeta h(\zeta,\tau,\alpha_\tau)d\tau\right)\Big]d\zeta\\&-\int_0^t\mathscr{T}(t-\zeta)\Big[D_2\varphi\left(\zeta,\omega_\zeta,\int_0^\zeta h(\zeta,\tau,\omega_\tau)d\tau\right)\\&-D_2\varphi\left(\zeta,\alpha_\zeta,\int_0^\zeta h(\zeta,\tau,\alpha_\tau)d\tau\right)\Big]v_\zeta d\zeta.\end{aligned}$$

Hence by derivatives of φ are LLC about second variable, then from the Lemma 2.10 and (H7) implies,

$$\|\omega(t)-\alpha(t)\|\leqslant k(a)\int_0^t\|\omega_\zeta-\alpha_\zeta\|d\tau.$$

Here $k(a)=\left(C_1L_1+c_0D_F^1+c_0^2D_F^2\right)(1+L_h)$ and $c_0=\max\left\{\sup_{0\leqslant\zeta\leqslant a}\|\mathscr{T}(\zeta)\|,\sup_{0\leqslant\zeta\leqslant a}\|v_\zeta\|\right\}$.

Implies that,

$$\|\omega_t-\alpha_t\|\leqslant k(a)\int_0^t\|\omega_\zeta-\alpha_\zeta\|d\tau.$$

By the Gronwall's Lemma $\omega(t)=\alpha(t)$ to every $-r\leqslant t\leqslant a$.

Since ω and $t\mapsto\varphi\left(t,\omega_t,\int_0^t h(t,s,\omega_s)ds\right)$ are continuously differentiable on $[-r,a]$. By Lemma 2.8, we conclude that ω is a strict solution of Eq. (1) on $[-r,a]$ also true for $a>0$, Hence ω is a strict solution of system (1) on $[-r,+\infty)$.

5. Example

Consider the below integro-differential system,

$$\begin{cases}\frac{\partial}{\partial t}(u(t,\zeta))=-e(\zeta)\frac{\partial}{\partial\zeta}(u(t,\zeta))+\int_0^t q(t-s,\zeta)\frac{\partial}{\partial\zeta}(u(s,\zeta))ds\\+f\left(t,u(t-\tau,\zeta),\int_0^t a(t,u(\zeta,\xi-r))ds\right)\\u(t,0)=u(t,1),t\geqslant 0\\u(v,\zeta)=u_0(v,\zeta),v\in[-r,0],\zeta\in[0,1].\end{cases}\tag{19}$$

Here $u_0:[-r,0]\times[0,1]\to\mathbb{R}$ is cont. and e is $+$ ve function defined on $[0,1]$,

$q\in BV_{loc}(\mathbb{R}^+,C([0,1]:\mathbb{R})),a:\mathbb{R}^+\times\mathbb{R}^+\times\mathbb{R},f:\mathbb{R}^+\times\mathbb{R}\times\mathbb{R}\to\mathbb{R}$ are Lipschitz cont. about second variable. $\exists$ a cont. map $\kappa:\mathbb{R}^+\to\mathbb{R}^+$,

$$|f(t,m_1,n_1)-f(t,m_2,n_2)|\leqslant\kappa(|m_1-m_2)|+|n_1-n_2|),m_1,m_2,n_1,n_2\in\mathbb{R}.$$

To rewrite the Eq. (19) as the form Eq. (1), in the sense;

Let $\mathscr{E}=C([0,1];\mathbb{R})$ be cont. function $[0,1]\to\mathbb{R}$ provide with sup norm.

Now the operators $\mathscr{D}$, $\mathscr{H}(t)$ by

$$D(\mathscr{D})=\left\{y\in C^1([0,1]:\mathbb{R}):y(0)=y(1)\right\}$$
$$\mathscr{D}y=-a(\zeta)y\prime,\zeta\in[0,1],$$

and

$D(\mathscr{H}(t)) = C^1([0,1];\mathbb{R})$
$(\mathscr{H}(t)y)(\zeta) = q(t,\zeta)y\prime(\zeta), t \geqslant 0, \zeta \in [0,1].$

Lemma 5.1([29]) Suppose that $\mathscr{D}$ is Hille-yosida function on $\mathscr{E}$ and $\overline{D(\mathscr{D})} = \{y \in \mathscr{E} : y(0) = y(1)\}$. Further $(\mathscr{H}(t))_{t\geqslant 0}$ is set of bounded operator, $D(\mathscr{D})$ to $\mathscr{E}$, $\mathscr{H}(\cdot)y \in BV_{loc}(\mathbb{R}^+, \mathscr{E}), \exists y \in D(\mathscr{D})$.

Consider the linear equation

$$\begin{cases} \omega\prime(t) = \mathscr{D}\omega(t) + \int_0^t \mathscr{H}(t-s)\omega(s)ds \quad \text{for } t \geqslant 0 \\ \omega(0) = \omega_0 \in \mathscr{E}. \end{cases} \tag{20}$$

Lemma 5.2([29]) Suppose that the Eq. (20) has a unique resolvent operator and LLC, we assume the following related to (19),

$$\omega(t)(\zeta) = u(t,\zeta) \text{ for } t \geqslant 0, \zeta \in [0,1]$$
$$\phi(v)(\zeta) = u_0(v,\zeta) \text{ for } t \in [-r,0] \text{ and } \zeta \in [0,1]$$
$$F\big(t,\phi,\textstyle\int_0^t h_1(t,s,\omega_s)ds\big) = f\big(t,\phi(t-u,\zeta),\int_0^t a(t,w(\zeta,\xi-r))ds\big).$$

Then Eq. (19) can be reformed as the below form

$$\begin{cases} \omega\prime(t) = \mathscr{D}\omega(t) + \int_0^t \mathscr{H}(t-s)\omega(s)ds + F\big(t,\omega_t,\int_0^t h_1(t,s,\omega_s)ds\big) \\ \omega_0 = \phi. \end{cases} \tag{21}$$

Since $F : \mathbb{R}^+ \times \mathbb{R} \times \mathbb{R} \to \mathbb{R}$ is Lipschitz cont. about second variable.

$$|F(t,\eta_1,\eta_2) - F(t,\gamma_1,\gamma_2)| \leqslant \kappa(|\eta_1 - \gamma_1| + |\eta_2 - \gamma_2|),$$

for $t \geqslant 0$, $\eta_1, \gamma_1 \in \mathscr{C}([-r,0];\mathscr{E}), \eta_2, \gamma_2 \in \mathscr{E}$. Followed by Theorem 3.4, we can state the below proposition

Proposition 5.3. Suppose $\phi(0) \in \overline{D(\mathscr{D})}$ such that $u_0(0,0) = u_0(0,1)$, then (19) has a unique integral solution on $\mathbb{R}^+$.

6. Conclusion

In this work, we obtained the results for integrodifferential system (1) with nonlocal condition in finite delay situations using Banach fixed point theorem. Also verified the integral solution of system (1) is continuous dependence with respect to initial data and proved the existence of strict solution using integrated resolvent operator theory and Gronwall's Lemma. we consider most of the functions in this system(1) are satisfied Lipschitz continuous and obtained results. The future work is consider the partial neutral integrodifferential equation with initial condition and will apply integrated resolvent operator technique on this system.

Declaration of Competing Interest

The authors declare that they have no known competing financial interests or personal relationships that could have appeared to influence the work reported in this paper.

Acknowledgment

The authors extend their appreciation to Prince Sattam bin Abdulaziz University for funding this research work through the project number (PSAU/2023/01/21898).

References

[1] A.O. Akdemir, H.D. Binh, D. O'Regan, A.T. Nguyen, The dependence on fractional orders of mild solutions to the fractional diffusion equation with memory, Math. Methods Appl. Sci. 46 (1) (2023) 1076–1095.
[2] K. Alishah, A. Zada, Controllability and stability analysis of an oscillating system with two delays, Math. Methods Appl. Sci. 44 (2021) 14733–14765.
[3] K. Balachandran, J.P. Dauer, Existence of solutions of a nonlinear mixed neutral equations, Appl. Math. Lett. 11 (2) (1998) 23–28.
[4] S. Belmor, C. Ravichandran, F. Jarad, Nonlinear generalized fractional differential equations with generalized fractional integral conditions, J. Taibah Univ. Sci. 14 (1) (2020) 114–123.
[5] N. Cao, X. Fu, Existence results of solutions for a neutral evolution equation with nonlocal conditions on infinite interval, J. Math. Anal. Appl., 510(1)2022, 126008.
[6] J.P. Dauer, K. Balachandran, Existence of solutions of nonlinear neutral integrodifferential equations in Banach space, J. Math. Anal. Appl. 251 (1) (2000) 93–105.
[7] W. Desch, R. Grimmer, W. Schappacher, Some considerations for linear integrodifferential equations, J. Math. Anal. Appl. 104 (1) (1984) 219–234.
[8] B. Diao, K. Ezzinbi, M. Sy, Existence results in the α -norm for a class of neutral partial functional integrodifferential equations, Afrika Matematica 26 (2015) 1621–1635.
[9] A. Diop, M. Dieye, M.A. Diop, K. Ezzinbi, Integrodifferential equations of volterra type with nonlocal and impulsive conditions, J. Integral Eqs. Appl. 34 (2022) 19–37.
[10] K. Ezzinbi, H. Toure, I. Zabsonre, Existence and regularity of solutions for some partial functional integrodifferential equations in Banach spaces, Nonlinear Analysis, Theory, Methods & Applications 70 (7) (2009) 2761–2771.
[11] K. Ezzinbi, S. Ghnimi, Existence and regularity of solutions for neutral partial functional integrodifferential equations, Nonlinear Anal. Real World Appl. 11 (4) (2010) 2335–2344.
[12] K. Ezzinbi, S. Ghnimi, M.A. Taoudi, Existence results for some partial integrodifferential equations with nonlocal conditions, Glasnik Matematicki 51 (71) (2016) 413–430.
[13] K. Ezzinbi, M. Ziat, Nonlocal integrodifferential equations without the assumption of equicontinuity on the resolvent operator in Banach spaces, Differ. Eqs. Dynam. Syst. 30 (2022) 315–333.
[14] K. Ezzinbi, S. Ghnimi, Solvability of nondensely defined partial functional integrodifferential equations using the integrated resolvent operators, Electronic J. Qual. Theory Differential Eqs. 88 (2019) 1–21.
[15] K. Ezzinbi, S. Ghnimi, Existence and Regularity for some partial neutral functional integrodifferential equations with nondense domain, Bull. Malay. Math. Sci. Soc. 43 (2020) 2967–2987.
[16] R. Ferdausi, A. Hossain, M. Hasan, A. Islam, Existence and uniqueness of solutions to system of linear equations and integral equations using Banach fixed point theorem, Int. J. Adv. Res. 6 (3) (2018) 494–500.
[17] HR. Henriquez, Regularity of solutions of abstract retarded functional differential equations with unbounded delay, Nonlinear Analysis Theory Methods and Applications, 28(3) 1997, pp. 513–531.
[18] E. Hernandez, H.R. Henriquez, Existence results for partial neutral functional differential equations with unbounded delay, J. Math. Anal. Appl. 221 (2) (1998) 452–475.
[19] E. Hernandez, V. Rolnik, TM. Ferrari, Existence and uniqueness of solutions for abstract integro-differential equations with state-dependent delay and applications, Mediterranean Journal of Mathematics, 19(3)2022, 101.

[20] E. Hernandez, Existence and uniqueness of global solution for abstract second order differential equations with state-dependent delay, Mathematische Nachrichten 295 (1) (2022) 124–139.
[21] K. Jothimani, K. Kaliraj, S.K. Panda, K.S. Nisar, C. Ravichandran, Results on controllability of non-densely characterized neutral fractional delay differential system, Evolution Equations and Control Theory 10 (3) (2021) 619–631.
[22] H. Kellerman and M. Hieber, Integrated semigroups, 84(1)1989, pp. 160–180.
[23] S. Koumla, K. Ezzinbi, R. Bahloul, Mild solutions for some partial functional integrodifferential equations with finite delay in Frechet spaces, SeMA journal 74 (2017) 489–501.
[24] K.D. Kucche, M.B. Dhakne, Existence of solution via integral inequality of volterra-fredholm neutral functional integrodifferential equations with infinite delay, Int. J. Differential Eqs. (2014). Article ID 784956.
[25] K. Manoj, K. Kumar, R. Kumar, Existence of mild solution for neutral functional mixed integrodifferential evolution equations with nonlocal conditions, Journal of Abstract and Computational Mathematics 6 (1) (2021) 32–40.
[26] A. Morsy, K.S. Nisar, C. Ravichandran, C. Anusha, Sequential fractional order Neutral functional Integro differential equations on time scales with Caputo fractional operator over Banach spaces, AIMS Mathematics 8 (3) (2023) 5934–5949.
[27] K. Munusamy, C. Ravichandran, K.S. Nisar, B. Ghanbari, Existence of solutions for some functional integrodifferential equations with nonlocal conditions, Mathematical Methods in the Applied Sciences 43 (17) (2020) 10319–10331.
[28] R. Murugesu, S. Suguna, Existence of solutions for neutral functional integrodifferential equations, Tamkang Journal of Mathematics 41 (2) (2010) 117–128.
[29] H. Oka, Integrated Resolvent Operators, Journal of Integral Equations and Applications 7 (2) (1995) 193–232.
[30] J.Y. Park, K. Balachandran, N. Annapoorani, Existence results for impulsive neutral functional integrodifferential equations with infinite delay, Nonlinear Analysis 71 (7–8) (2009) 3152–3162.
[31] A. Pazy, Semigroups of Linear Operators and Applications to Partial Differential Equations, Springer-verlag, New york, 1983.
[32] C. Ravichandran, K. Munusamy, K.S. Nisar and N. Valliammal, Results on Neutral Partial Integrodifferential Equations Using Monch-Krasnosel'Skii Fixed Point Theorem with Nonlocal Conditions, Fractal and Fractional, 6 (2)2022, 75.
[33] S.O. Shah, C. Tunc, R. Rizwan, A. Zada, Q.U. Khan, Iftikhar Ullah, Ibrar Ullah, Bielecki-Ulam's Types Stability Analysis of Hammerstein and Mixed Integro-Dynamic Systems of Non-Linear Form with Instantaneous Impulses on Time Scales, Qualitative Theory of Dynamical Systems 21 (2022) 107.
[34] V. Vijayaraj, C. Ravichandran, T. Botmart, K.S. Nisar, K. Jothimani, Existence and data dependence results for neutral fractional order integro-differential equations, AIMS Math. 8 (1) (2023) 1055–1071.
[35] J. Xu, B. Pervaiz, A. Zada, S.O. Shah, Stability Analysis of Causal Integral Evolution Impulsive Systems on Time Scales, Acta Mathematica Scientia 41 (2021) 781–800.
[36] A. Zada, H. Waheed, J. Alzabut, X. Wang, Existence and stability of impulsive coupled system of fractional integrodifferential equations, Demonstratio Mathematica 52 (2019) 296–335.
[37] A. Zada, B. Pervaiz, J. Alzabut, S.O. Shah, Further results on Ulam stability for a system of first-order nonsingular delay differential, Demonstratio Mathematica 53 (2020) 225–235.
[38] J. Zhu, X. Fu, Existence and differentiablity of solutions for nondensely defined neutral integro-differential evolution equations, Bull. Malaysian Math. Sci. Soc. 46 (2023) 30.

ScienceDirect

Chaos, Solitons & Fractals

Volume 175, Part 2, October 2023, 114050

d… ’ w … ’ ’ wy ü w … w PQR5z…ü wü… ü– [QR w z ü ..z z…w

Kottakkaran Sooppy Nisar [a], K. Logeswari [b], C. Ravichandran [b], S. Sabarinathan [c]

Show more

https://doi.org/10.1016/j.chaos.2023.114050

Get rights and content

Wü• – ü• –

m..y üz… –… ü ..w ’ wy ü w ü ..z ü ..: 5zü’…… üw … wü ü– ’ wy ü w x zw y züü 6

j –……ü …y…… ü x wü ..z x ü • w zwz ’ü ..z ü –… 6

P …w ..ü • ü… ü w… w w üywwz …üyw … 6
Q ü • c PjbPQy zü • • w – ü z w 6

Px wy

[–ü w y ü 4 ..z…y ük…’ wy ü wzü’…… üw… wü ü– … w4ü ..: w x zw y züü w z ü ..z z…w ü • P w • w w Qw..w z…ü wü…4 –üy– ü y z… –…• ……wü ..z c ü w5b..’’ … … …6m..z…… ü … –……ü …y..w z ü …… ’ … w z w w ü x ’ü ..z ü …– z6c … …4 …… wü ..z –… wxüü ’ –…’ wy ü w zü’…… üw… wü ü –… ’ w … ’ k w W… 6j –…4 ..ü … ü• w..w …w … ü– wü w …w z ü w… –… y …• w –üyw 6

[z y ü

Uwy ü w ywy ü y xü ..z …w ’ ü ..: w w z zü’…… üw … w • ü– –… •……wü wü ’ y w üyw …6j –..z…… … ’ y w üyw z…ü wü… wü… ü w … ü–

–…y y… ’’ wy ü wz…üwü…6[9DGC4b..üx ü w z W üwy ü..z –… ü.. ’’ wy ü w z… w z wü..z ü• wz w w • –……wy–… z6j –ü ’ wy ü wz…üwü..w wy..z –…’w w–… wüyüw 4üy zü• T …4bü ü..4bw wy..4hü.. w 4V wz4b… ü 4w z w –… 6 j –… ü.. wx ’ wy ü wywy y …’ wy ü wzü’…… üw… wü 0US T 14’ wy ü wz w üy 4 wz•… … z…… ..z ü –..9G – y… 6[•……w’ wy ü w z ü w ü.z ü wü züyü ü … ü..xü 5…•ü …..ü•4 ..y–w üyw…•ü …..ü•4…..y üyw4y –… 4 x üy 4 wü üyw – üy 4y–… üyw4 üy 4wy üy 4 üy …w üyü 4 –… • wz ..6j –…’ wy ü w5 z… w üywü z… w… wyy w..y w..z ü ..•…5 z…6f z x … wü..z –… ..yüw ’ y ü 4z…üwü…wzü ..: w 4…ü …y…wz ü …… 4bw wy… w ’ …– z4wz …üyw … ’’ wy ü wzü’…… üw… wü ü cθs6h q; s4züy ..z x ü.’. wx –ü wz… üü ’ –…’ zw … wy y… ü ’ wy ü wywy 6Rw . Uwx üü z..’ü..z –..RU z…üwü…wz …… ..z –w –… … ..’’..y w…… …üz… ü– w …üy– ……ü z… qAs6P w•ww. VWw y– z…yük..z w … yw ’’ wy ü w w üwü ..: 5zü’…… üw… wü ü– … •……wü..z c ü w 5b..’’ …’ y ü wz •• … ..z …’ wy ü w …w ü qBs6c w …..wy–… z…… ..z –… wü ’’ wy ü wz…üwü..üiy zü• PQ’ wy ü wz…üwü..qCs6 aw w …w6qDs4züy ..z wQw … j ü … wü ü– PQRz…üwü… ü• bw wy… w ’ 6 fw –w–ü•–ü…w6qEs4 …… w 5ü ..:… z… ’ –…wz ..y ü zü … ü x … ü• PQR z…üwü…wz y–..x –… üw –üy– wü…z ü• –… w ’ w 6i ..w – …wx w..z –..PQ5’ wy ü wz…üwü..ü wü w w ü ü…..ü …y..qFs4qGs4q98s4q99s4q9: s4q9As4 wxüü q9Bs4q9Cs w z z… q9Ds4q9Es4q9Fs4q9Gs4q; 8s4q; 9s4q; : s4q; As4q; Bs4q; Cs4q; Ds4q; Es4q; Fs4q; Gs4 qA8s6

[’ y ü wzü’…… üw… wü 4 –..d… w w z S…w zü’…… üw… wü z……z w w z …… w … ’wz…üwü…… ü– z…w qA9s4qA: s6j –..y–w•… –w yy ..z ü –… ’ y ü ’z…üwü…w w w üy w ü ..w… w S…w zü’…… üw… wü 0 ü ..5z…w … 16

c ..– z…w6qAAszüy ..z –..w w üyw w z wxüü … ’’ wy ü w x zw w … x… 6i –w– …w6qABs… wü..z –..y y… ’ wüwx … z…’ wy ü wz…w zü’…… üw … wü ü– x zw w … x… ü• ’ü..z ü ..y– ü …6iüw …w6qACsz…yük..z –… y w… b..ü– wüwüzü..w… z… üwww üywwz wxüü …– z 6i –w– …w6qADs ü … ü•w…–… …üywü ..: w x zw w … x… ü– ü ü..y züü 6

c üw..z x qAEs4 ..züy ..z wx –..[Qf ’ … w US T ü PQR5… … ü– ü..z z…w ü –… ’

$$\left.\begin{aligned} \left({}_{0}^{ABC}D_{\kappa}^{\alpha}\right)[\Theta(\kappa)-H(\kappa,\Theta(\kappa),\Theta(\delta\kappa),\Theta(\kappa-\zeta(\kappa)))] &= F(\kappa,\Theta(\kappa),\Theta(\delta\kappa),\Theta(\kappa-\zeta(\kappa))),\\ p\Theta(0)+q\Theta'(0) &= \int_0^1 g(\Theta(s))\,ds, \quad \delta\in(0,1),\zeta(\kappa)\geq 0,\\ p\Theta(1)+q\Theta'(1) &= \int_0^1 h(\Theta(s))\,ds, \quad 1<\alpha\leq 2,\kappa\in[0,1]. \end{aligned}\right\}$$

–…… ${}_{0}^{ABC}D_{\kappa}^{\alpha}$ ü P w•ww Qw..w Rw ’ wy ü wz…üwü..4 ü..w’ y ü $H,F:[0,1]\times R^3\to R$ wz –…’ y ü $g,h:R\to R$ x – w..y ü $4p>0,q\geq 0$ w……w x… 6Uü 4 ..z…ü…–…..ü …y…wz ü …… … üwiy–w.’…. ’ü..z5 ü –… … ’ … w’ wy ü wzü’…… üw… wü ü– ü ..: wx zw y züü wz ü..z z…w 6j –… ..züy wx –..k w W… wxüü y y… –üy– ü ü w ww ü ’ ’ wy ü w zü’…… üw… wü 6U –…4 ..z…ü…w üwx …..w …wz –…• w – 6

[i..y ü :4 ..züy ..z … … üw … 4z..'ü üü 4 üü w z –… … –üy– ü x…
ü w ' wü x … 6[i..y ü A4 … zü.z –…– –…ü4 … ww z –…w w üyw
… ' –… … wUST ü– [QR w z ü..z z…w ü• … ü z ' 'ü..z ü –… … 6[
i..y ü B4 ..z…y ük..z –… wxüü ' x … 6[i..y ü C w z i..y ü D4 ..züy ..z w
üwx ….…w ..w z y y z… … 6

i..y ü ü …

Qw üy …

cSb

[' $u \in H^1(a,b), b > a, \alpha \in [0,1]$4 –… PQz…ü wü … ü– Rw … ..ü •ü … w qCsH

$$ {}_0^{ABC}D^{\alpha}(u(\kappa)) = \frac{\mathcal{N}(\alpha)}{1-\alpha}\int_0^{\kappa} u'(s)\,E_{\alpha}\left[\frac{(\kappa-s)^{\alpha}}{\alpha-1}\right]ds $$

–…..$\mathcal{N}(0) = \mathcal{N}(1) = 1$ ü wü..z ' y ü w z $E(\alpha)$ ü –..c ü w 5b..'' … ' y ü 6j –… w yüw..PQü ..: w ü $\left({}_0^{AB}I^{\alpha}u\right)(\kappa) = \frac{1-\alpha}{\mathcal{N}(\alpha)}u(\kappa) + \frac{\alpha}{\mathcal{N}(\alpha)}\left({}_0I^{\alpha}u\right)(\kappa)$

j –..h5b4h5b PQ4Rw w z Rw PQz…ü wü … w… … ü ..z ü q9s4q98s4q99s4q9: s6

cSc

qAFs4qAGs

$$ 0 \le \alpha \le 1e \qquad \left({}_0^{AB}I^{\alpha}\left({}_0^{ABC}D^{\alpha}u\right)\right)(\kappa) = u(\kappa) - u(0)\,E_{\alpha}(\lambda\kappa^{\alpha}) - \frac{\alpha}{1-\alpha}u(0)\,E_{\alpha,\alpha+1}(\lambda\kappa^{\alpha}) $$
$$ = u(\kappa) - u(0). $$

cSd

i y–w.'.… Uü..z5f ü j –… … 4qB8s

W

d..y… w …

dSb

$$\theta:[0,1]\to R \qquad \alpha\in(1,2] \quad hh\theta(0)=0e \qquad \Theta\in\mathscr{C}([0,1],R)$$

$$\left.\begin{array}{l}\left({}_0^{ABC}D_\kappa^\alpha\right)[\Theta(\kappa)-\Phi(\kappa)]=\Omega(\kappa),\quad 1<\alpha\le 2,\kappa\in[0,1]\\ p\Theta(0)+q\Theta'(0)=\int_0^1 g(\Theta(s))\,ds,\quad p\Theta(1)+q\Theta'(1)=\int_0^1 h(\Theta(s))\,ds.\end{array}\right\} \qquad 0A91$$

$$\left.\begin{array}{l}\Theta(\kappa)=\int_0^\kappa \Phi(s)\,ds+\frac{2-\alpha}{\mathcal{N}(\alpha-1)}\int_0^\kappa \Omega(s)\,ds+\frac{\alpha-1}{\mathcal{N}(\alpha-1)\Gamma(\alpha)}\int_0^\kappa(\kappa-s)^{\alpha-1}\Omega(s)\,ds\\ +\frac{1}{p}\int_0^1 g(\Theta(s))\,ds-\frac{q}{p^2}\int_0^1 h(\Theta(s))\,ds+\frac{q}{p}\Phi(1)+\frac{q(2-\alpha)}{p\mathcal{N}(\alpha-1)}\Omega(1)+\frac{q(\alpha-1)}{p\mathcal{N}(\alpha-1)\Gamma(\alpha)}\\ \times\int_0^1(1-s)^{\alpha-1}\Omega(s)\,ds+\frac{q}{p^2}\int_0^1 g(\Theta(s))\,ds+\frac{q^2}{p^2}\Phi(1)+\frac{q^2(2-\alpha)}{p^2\mathcal{N}(\alpha-1)}\Omega(1)\\ +\frac{q^2(\alpha-1)}{p^2\mathcal{N}(\alpha-1)\Gamma(\alpha-1)}\int_0^1(1-s)^{\alpha-2}\Omega(s)\,ds+\frac{\kappa}{p}\int_0^1 h(\Theta(s))\,ds-\kappa\Phi(1)\\ -\frac{\kappa(2-\alpha)}{\mathcal{N}(\alpha-1)}\Omega(1)-\frac{\kappa(\alpha-1)}{\mathcal{N}(\alpha-1)\Gamma(\alpha)}\int_0^1\end{array}\right\}$$

k w W... wxüü

W....4 ..züy –..k w W... wxüü ' T 6090901 ü–' ü • z..'.ü üü 6

eSb

b...0909901ü k w W... wx..4ü' w $\nu(\kappa)$ wü' ü •

$$\left|\left({}_0^{ABC}D_\kappa^\alpha\right)[\nu(\kappa)-H(\kappa,\nu(\kappa),\nu(\delta\kappa),\nu(\kappa-\zeta(\kappa)))]-F(\kappa,\nu(\kappa),\nu(\delta\kappa),\nu(\kappa-\zeta(\kappa)))\right| -.....$$

$<\epsilon,\delta\in(0,1),\zeta(\kappa)\ge 0,1<\alpha\le 2,\kappa\in[0,1]$

...ü w ü ' 0909901 ü– $|\nu(\omega)-\Theta(\omega)|<K\epsilon,\qquad K\in\mathbb{R}.$

eSc

qB9s

[' 0909901ü •.....wü..z k w W... wx ...–... ∃ w 5z..y ..wü • ' y ü $\varphi\in\mathscr{C}(\mathscr{R}_+,\mathscr{R}_+)$4 ü–

$\varphi(0)=0$4 66' w $\nu\in\mathscr{W}$ ' 0B09014$\Theta\in\mathscr{W}$ ' 0909901ü w ü ... ü w z $\epsilon>0$ 66 –...• ü...

ü... wü – z |

d ...üyw ...

$$\left.\begin{array}{l}{}^{ABC}D^{\frac{3}{2}}\left[\Theta(\kappa)-2\kappa\left(\frac{\Theta(\kappa)}{5+|\Theta(\kappa)|}+\frac{\Theta\left(\frac{1}{3}\kappa\right)}{15+\left|\Theta\left(\frac{1}{3}\kappa\right)\right|}+\frac{\Theta(\kappa-0.45)}{15+|\Theta(\kappa-0.45)|}\right)\right]\\ =\kappa^2\left(\frac{\Theta(\kappa)}{5+|\Theta(\kappa)|}+\frac{\Theta\left(\frac{1}{3}\kappa\right)}{15+\left|\Theta\left(\frac{1}{3}\kappa\right)\right|}+\frac{\Theta(\kappa-0.45)}{15+|\Theta(\kappa-0.45)|}\right)\\ \Theta(0)+\Theta'(0)=\int_0^1\frac{|\Theta(\kappa)|}{20+|\Theta(\kappa)|}d\kappa,\quad \kappa\in[0,1],\\ \Theta(1)+\Theta'(1)=\int_0^1\frac{|\Theta(\kappa)|}{30+|\Theta(\kappa)|}d\kappa,1<\alpha\le 2.\end{array}\right\}\text{j w ...}$$

$$H(\kappa,\Theta(\kappa),\Theta(\delta\kappa),\Theta(\kappa-\zeta(\kappa)))=2\kappa\left(\frac{\Theta(\kappa)}{5+|\Theta(\kappa)|}+\frac{\Theta\left(\frac{1}{3}\kappa\right)}{15+\left|\Theta\left(\frac{1}{3}\kappa\right)\right|}+\frac{\Theta(\kappa-0.45)}{15+|\Theta(\kappa-0.45)|}\right),$$

$$F(\kappa,\Theta(\kappa),\Theta(\delta\kappa),\Theta(\kappa-\zeta(\kappa)))=\kappa^2\left(\frac{\Theta(\kappa)}{5+|\Theta(\kappa)|}+\frac{\Theta\left(\frac{1}{3}\kappa\right)}{15+\left|\Theta\left(\frac{1}{3}\kappa\right)\right|}+\frac{\Theta(\kappa-0.45)}{15+|\Theta(\kappa-0.45)|}\right),$$

$$g\Theta(\kappa)=\frac{|\Theta(\kappa)|}{20+|\Theta(\kappa)|},h\Theta(\kappa)=\frac{|\Theta(\kappa)|}{30+|\Theta(\kappa)|},\text{j -... ü '0C691ü}$$

$$\Theta(\kappa)=\int_0^{\kappa}2s\left(\frac{\Theta(s)}{5+|\Theta(s)|}+\frac{\Theta\left(\frac{1}{3}s\right)}{15+\left|\Theta\left(\frac{1}{3}s\right)\right|}+\frac{\Theta(s-0}\right.$$

R y ü

[..y... ..w 4 -... z...ü• w z -... ...üyw ... 'P w•w wQw..w 'wy ü wz...ü wü... w ü.z ü wü züyü ü..4 -üy- w wy -.....wy-... 6m..züy ..z ...ü ...y..wz ü .... '' wy ü wPQz...ü wü... ü- ... wü ..: wx zw y züü wz ü..z z...w 6P 4 .....w ü..z -..k w W... wxüü ' y üz... x... ü -ü w üy..6Uü w 4 ..w w ..z -..y y... ...üyw ü- üwx.....w ..wz ..z -..• w- 6

Rh..züj w - -ü y ük ü w... ...

mR y... wü wü 4[...ü•wü 4l ü wü wü 4U w w w ü4m üü• ü•ü w z w•4m üü• ...ü.. . ..züü•4l wüzwü 4i ' w..6 **S** mR y... wü wü 4 m üü• ü•ü w z w•4m üü• ...ü.. . ..züü•6y**S** mU w w w ü4 R y... wü wü 4m üü• ü•ü w z w•4m üü• ...ü.. . ..züü•6 **S** mU w w w ü4m üü• ü•ü w z w•4m üü• ...ü.. . ..züü•6

S..y wwü 'y ...ü•ü .....

j-...w - z..y w...-w -...-w... y ...ü•'ü w yüwü .... w ...wü -ü -wy z-w..w ..w..z ü' ...y...-... ... ..z ü -ü w...6

Py ..z• ...

j-...w - ... ...z -..ü w ..yüwü f ü y..i w w xü Pxz wü k ü... ü 4i w züP wxüw' ' zü• -ü .....wy- - •- -... ..y x...0fiPk7:8:A7897:9FGF:1

---

h..'.....y...0B91

PartohaghighiM. *et al.*

d ...üyw... ü wü '-...' wy ü w wz ..y ü zü ... ü ... wü z... -... züü.z P w•w w5Qw..w 5Rw z...ü wü...

Results Phys (2023)

AtanganaA. *et al.*

P w ü 'w ... w üwü ..: 5zü'..... üw... wü ü- ü..z 'wy ü w ...w

Chaos Solitons Fractals (2019)

JaradF. *et al.*
e wy w ’ zü w zü’..... üw… wü ü –…’ w … ’ P w • w w5Qw..w z…ü wü…
Chaos Solitons Fractals (2018)

RavichandranC. *et al.*
d… … …ü …y..ü –…’ w … ’ P w • w w5Qw..w z…ü wü…’ ’ wy ü w ü ..: 5zü’..... üw… wü
Chaos Solitons Fractals (2019)

LogeswariK. *et al.*
P … … wü …ü …y… ’ ’ wy ü w … w ü ..: 5zü’..... üw… wü ü –… y y… ’ P w • w w5Qw..w z…ü wü…
Phys A (2020)

RavichandranC. *et al.*
e … w wy– ’ ’ wy ü w z…ü wü..x c ü w 5b..’’ … … … … w ü ..: 5 zü’..... üw … ü– ü ü..y züü
Chaos Solitons Fractals (2020)

BonyahE. *et al.*
i wxüü w w ü w z ü w y ’ w’ wy ü w – w P’ üyw w üwü z…
Chaos Solitons Fractals (2018)

AlzahraniE.O. *et al.*
c z…ü • –..z w üy ’ –…wüü … ü– ü w y
Chaos Solitons Fractals (2018)

TassaddiqA. *et al.*
W.w w ’…w w ü ü zü w• ü w..xw..z w ’ üz ü • c i : w w üy…H P w • w w5Qw..w ’ wy ü w z…
Chaos Solitons Fractals (2020)

KorpinarZ. *et al.*
j –… w z w üywü ’ –… … ’ ’ wy ü w x • … … wü ü– c ü w ..’’ … … … …
Appl Math Comput (2020)

View more references

Rü..z x 0991

R wxüü ’ ü ü… ü ..w ψ5Wü’…’ wy ü w ü ..: 5zü’..... üw… wü
2024, Results in Control and Optimization

Show abstract

T yw ..y ü…ü ’ •……wü• ’ wy w ü• füywz j –w – x üz ü…wü

2024, Alexandria Engineering Journal

Citation Excerpt :

c … …4 –..•……w..z üy ü w..ü w 4 y– w üy • w z üy –ü w..x..ü• ..z ’ y …yüw …6[’ ..4 ..wü …–..füywz j –w – x üz ü…wü .y– ü … … …–… ’ wy ü wWw ü üw w ü z..ɑBEs4’ wy w•w z w üy ɑBFs4 ü ɑBGs4’ wy ü w zü’..... üw… wü ɑC8 CBs w z y–w üy x..–w ü ɑCCs6j –ü .....wy– ..y..ü..z ..yüüy… … w’ zü•6

Show abstract

f…ü züy Q zw l w … x … ’ –..S w üyw … ü– … w ü ..: 5 zü’..... üw… wü ü … yw…

2024, Partial Differential Equations in Applied Mathematics

Show abstract

P üywü ’ –..c ü w5b..’’ … … …ü y–w üy zü’..... üw … ’ w ü wü• –..y wxüü ’ yw’ wy ü w z…ü wü…

2024, Chaos, Solitons and Fractals

Citation Excerpt :

i y– w –w… wz… x w üw wz w y… … ü zü… …’ü..z y– w …..y w …üy 4 ü wü•4’ üz z w üy 4 –… • 4…•ü …..ü•4ü w… y… ü•4 üy …w üyü 4zü’ ü 4y –… 4w z xü • 6U ..ü 5z… – ü ü– 4 ..’…. …..w ü…w ..ü y zü• .yüü.z x ɑθ As w z …..wy– w … ɑB 99s6 j –..wz w w… ’ hü.. w bü ü ..ɑhb1w z Rw ’ wy ü w0RU1z…ü wü… –w..x….. … … ü… zü y ..z ü ɑθ: 4θAs6

Show abstract

f xwxüü üy w w ü ’wzü x..z i[g f 5i[z… ’ ü 5x ..zü..w… ü– – w ww ü… w..: w z ü z……z… f ü ↗

2024, Modeling Earth Systems and Environment

T ü …y..w z ü …… z ’ w üw … w’ y ü w’ wy ü w zü’..... üw … wü z… Rw z…ü wü…↗

2024, International Journal of Optimization and Control: Theories and Applications

View all citing articles on Scopus ↗

View full text

REVISTA DE LA UNIÓN MATEMÁTICA ARGENTINA
Vol. 65, No. 2, 2023, Pages 331–346
Published online: November 22, 2023
https://doi.org/10.33044/revuma.2669

THE r-DYNAMIC EDGE COLORING OF A CLOSED HELM GRAPH

RAÚL M. FALCÓN, MATHIYAZHAGAN VENKATACHALAM, SATHASIVAM GOWRI, AND GNANASEKARAN NANDINI

Abstract. As a natural generalization of the classical coloring problem in graph theory, the dynamic coloring problem deals with the existence of a proper coloring c of a graph so that $|c(N(v))| \geq \min\{r, d(v)\}$ for every vertex v. In this paper, we obtain the r-dynamic edge chromatic number of any given closed helm graph for any positive integer r. This coincides with the r-dynamic chromatic number of the line graph of a closed helm graph.

1. Introduction

In 2001, Montgomery [21] (see also [13]) introduced the concept of *r-dynamic proper k-coloring* of a graph $G = (V(G), E(G))$ as a proper k-coloring c such that

$$|c(N(v))| \geq \min\{r, d(v)\} \tag{1.1}$$

for every vertex $v \in V(G)$, where $N(v)$ and $d(v)$ denote, respectively, the neighborhood and the degree of the vertex v. In addition, he introduced the notion of *r-dynamic chromatic number* $\chi_r(G)$ of the graph G as the minimum positive integer k for which an r-dynamic proper k-coloring exists. Both concepts generalize in a natural way those classical ones concerning the proper coloring and the chromatic number of a graph, which arise indeed when $r = 1$. Since the original work of Montgomery, the case $r > 1$ has widely been dealt with in the literature for different types of graphs [8, 6, 7, 11, 12, 14, 15, 19, 22, 24], with particular emphasis in the case $r = 2$ [1, 2, 3, 4, 5]. Of particular interest for the topic of this paper, let us remark the studies of Mohanapriya et al. [20] and Furmańczyk et al. [9] concerning the r-dynamic coloring of different families of helm graphs. In particular, the last mentioned paper deals with the r-dynamic chromatic number of the line graph of a helm graph, which coincides as such with the so-called r-dynamic edge chromatic number of a helm graph. In this last regard, Meganingtyas [17] introduced the

2020 *Mathematics Subject Classification.* 05C15.
Key words and phrases. r-dynamic coloring, closed helm graph, line graph.
The first author's work was partially supported by the research project FQM-016 from Junta de Andalucía.

concept of *r-dynamic proper k-edge-coloring* of a graph $G = (V(G), E(G))$ as a proper k-edge-coloring c such that

$$|c(N(uv))| \geq \min\{r, d(u) + d(v) - 2\}$$

for every pair of adjacent vertices $u, v \in V(G)$, where $N(uv)$ denotes the set of edges that are incident to that one containing both vertices u and v.

The *r-dynamic edge chromatic number* $\lambda_r(G)$ of the graph G is the minimum positive integer k for which an r-dynamic proper k-edge-coloring exists. Again, both concepts generalize the classical ones of proper edge-coloring and edge chromatic number, which arise when $r = 1$. Meganingtyas [17] dealt in particular with the r-dynamic edge chromatic number of paths, cycles, star graphs, wheel graphs, friendship graphs, prism graphs and ladder graphs. Some other kinds of graphs for which this value has been studied are lobster graphs, butterfly graphs, diamond graphs [16] and trees [18]. In addition, Nandini et al. [23] have recently dealt with the r-dynamic chromatic number of the line graph (and hence, the r-dynamic edge chromatic number) of any bistar graph. This paper delves into this topic by focusing on the r-dynamic chromatic number of the line graph of any closed helm graph.

The paper is organized as follows. In Section 2, we describe some preliminary concepts and results on graph theory that are used throughout the paper. Then, in Section 3, after establishing certain lower bounds for the r-dynamic edge chromatic number of a closed helm graph, we determine such a number for any positive integer r and any order of the closed helm graph under consideration.

2. Preliminaries

This section deals with some preliminary concepts and results on graph theory that are used throughout the paper. See [10] for more details about this topic.

A *graph* is any pair $G = (V(G), E(G))$ that is formed by a set $V(G)$ of *vertices* and a set $E(G)$ of *edges*. A *subgraph* of the graph G is any other graph H such that $V(H) \subseteq V(G)$ and $E(H) \subseteq E(G)$. Each edge joins two vertices, which are then said to be *adjacent*. In addition, two edges sharing a vertex are said to be *incident*. From now on, we denote by vw the edge joining two vertices $v, w \in V(G)$. It constitutes a *loop* if $v = w$. Two edges joining the same pair of vertices are said to be *parallel*. A graph is *simple* if it contains no loops and no parallel edges. Further, the number of vertices and the number of edges of a graph are, respectively, its *order* and its *size*. If both of them are finite, then the graph is said to be *finite*. From now on, all the graphs are considered to be simple and finite. A graph is called *complete* if all its vertices are pairwise adjacent. The set of vertices of any complete subgraph of the graph G is called a *clique*. The complete graph of order n is denoted by K_n.

The *neighborhood* $N_G(v)$ of a vertex $v \in V(G)$ is the subset of vertices in $V(G)$ that are adjacent to v. The cardinality $d_G(v)$ of this set is the *degree* of the vertex v. From now on, we write $N(v)$ and $d(v)$ when there is no risk of confusion. If $d(v) = 1$, then the vertex v is said to be *pendant*. A *pendant edge* is any edge

containing a pendant vertex. Furthermore, $\delta(G)$ and $\Delta(G)$ denote, respectively, the minimum and maximum vertex degree of the graph G.

The *cycle* C_n, with $n > 2$, is a graph for which $V(C_n) = \{v_0, \ldots, v_{n-1}\}$ and $E(C_n) = \{v_0v_1, v_1v_2, \ldots, v_{n-2}v_{n-1}, v_{n-1}v_0\}$. If every vertex v_i is joined to a new vertex v, then the resulting graph is the *wheel graph* W_{n+1}. If besides, each vertex v_i is joined to a pendant vertex p_i, then the resulting graph is the *helm graph* H_n. Finally, if the set of edges $\{p_0p_1, \ldots, p_{n-2}p_{n-1}, p_{n-1}p_0\}$ is also added, then we get the *closed helm graph* CH_n. Figure 1 illustrates these four types of graphs.

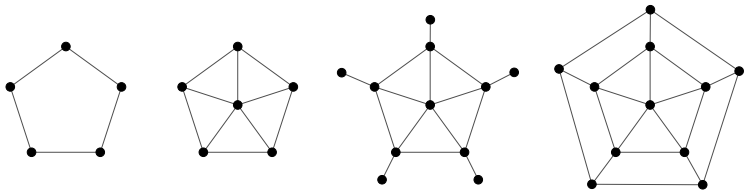

FIGURE 1. Examples of a cycle, a wheel graph, a helm graph and a closed helm graph.

The *line graph* $L(G)$ of a graph G is the graph having as vertices the edges of G, and such that two vertices in $L(G)$ are adjacent if and only if the associated two edges in G are incident. Figure 2 illustrates the line graph of the closed helm graph CH_5.

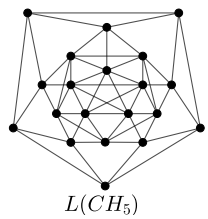

FIGURE 2. Line graph of the closed helm graph CH_5.

A *proper k-coloring* of a graph $G = (V(G), E(G))$ is any map $c : V(G) \to \{0, \ldots, k-1\}$ that assigns a set of k *colors* to the set of vertices $V(G)$ so that no two adjacent vertices share the same color. Similarly, a *proper k-edge-coloring* of the graph G is defined as any map $c : E(G) \to \{0, \ldots, k-1\}$ so that no two incident edges share the same color. The *chromatic number* $\chi(G)$ (respectively, the *edge chromatic number* $\lambda(G)$) of the graph G is the minimum positive integer k for which a proper k-coloring (respectively, a proper k-edge-coloring) of G exists. Particular examples are the *r-dynamic proper k-(edge-)coloring* and the *r-dynamic (edge) chromatic number* of a graph G, which have already been described in the

introductory section. In particular, $\chi_1(G) = \chi(G)$ and $\lambda_1(G) = \lambda(G)$. Moreover, as it has already been indicated in the introductory section, $\lambda_r(G) = \chi_r(L(G))$ for all positive integer r. The following result is also known.

Lemma 2.1 ([13]). *Let G be a graph and let r be a positive integer. Then,*

$$\min\{r, \Delta(G)\} + 1 \leq \chi_r(G) \leq \chi_{r+1}(G).$$

Moreover, $\chi_r(G) \leq \chi_{\Delta(G)}(G)$.

3. Dynamic edge coloring of a closed helm graph

In this section, we study the r-dynamic edge chromatic number of a closed helm graph CH_n, with $n > 2$, of set of vertices

$$V(CH_n) = \{v, v_0, \ldots, v_{n-1}, p_0, \ldots, p_{n-1}\},$$

where we follow the notation described in the preliminary section. To this end, we focus on the equivalent computation of the r-dynamic chromatic number of the line graph $L(CH_n)$, whose respective sets of vertices and edges are

$$V(L(CH_n)) = E(CH_n) = \{vv_i,\ v_iv_{i+1},\ v_ip_i,\ p_ip_{i+1}\colon\ 0 \leq i < n\}$$

and

$$\begin{aligned} E(L(CH_n)) = {} & \{(vv_i)(vv_j)\colon\ 0 \leq i, j < n,\ i \neq j\} \\ & \cup \{(vv_i)(v_{i-1}v_i),\ (vv_i)(v_iv_{i+1}),\ (vv_i)(v_ip_i)\colon\ 0 \leq i < n\} \\ & \cup \{(v_iv_{i+1})(v_ip_i),\ (v_iv_{i+1})(v_{i+1}p_{i+1})\colon\ 0 \leq i < n\} \\ & \cup \{(v_ip_i)(p_{i-1}p_i),\ (v_ip_i)(p_ip_{i+1})\colon\ 0 \leq i < n\} \\ & \cup \{(v_iv_{i+1})(v_{i+1}v_{i+2}),\ (p_ip_{i+1})(p_{i+1}p_{i+2})\colon\ 0 \leq i < n\}, \end{aligned}$$

where all the indices are taken modulo n (this convention is considered throughout the whole paper). In particular, for each non-negative integer $i \leq n$, we have that

$$d(vv_i) = n + 2, \qquad d(v_iv_{i+1}) = 6, \qquad d(v_ip_i) = 5 \quad \text{and} \quad d(p_ip_{i+1}) = 4.$$

Thus, $\delta(L(CH_n)) = 4$ and

$$\Delta(L(CH_n)) = \begin{cases} 6 & \text{if } n = 3, \\ n + 2 & \text{otherwise.} \end{cases}$$

The following results establish some lower bounds of the r-dynamic edge coloring of a closed helm graph.

Lemma 3.1. *Let r and n be two positive integers, with $n > 2$. Then,*

$$\lambda_r(CH_n) = \chi_r(L(CH_n)) \geq \begin{cases} 4 & \textit{if } n = 3, \\ n & \textit{otherwise.} \end{cases}$$

Proof. Notice that the four vertices vv_0, $v_{n-1}v_0$, v_0v_1 and v_0p_0 determine a clique of order four within the line graph $L(CH_n)$. Thus, since every r-dynamic coloring constitutes a proper coloring, we have that $\chi_r(L(CH_n)) \geq \chi(K_4) = 4$ for all positive integer $n > 2$. In a similar way, since the subset of vertices $\{vv_i\colon\ 0 \leq i <$

$n\} \subset V(L(CH_n))$ determines a clique of order n within the line graph $L(CH_n)$, we have that $\chi_r(L(CH_n)) \geq \chi(K_n) = n$ for all $n \geq 4$. □

Figures 3–5 illustrate how the lower bound in Lemma 3.1 is respectively reached for $r \leq n = 3$, $r < n \in \{4, 5\}$ and $r \leq n - 2 < n \in \{6, 7\}$. The following result shows that the case $(r, n) \in \{(5, 6), (6, 7)\}$ requires extra colors.

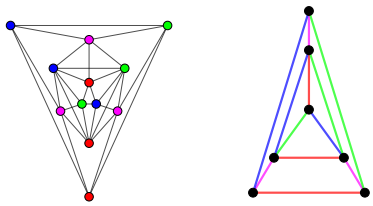

FIGURE 3. r-dynamic proper 4-coloring of the line graph $L(CH_3)$ (left) and r-dynamic proper 4-edge-coloring of the closed helm graph CH_3 for all $r \leq 3$ (right).

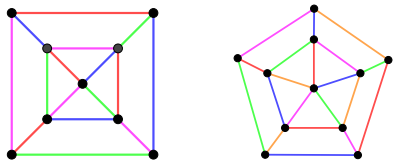

FIGURE 4. r-dynamic proper n-edge-coloring of the graph CH_n for all $r < n \in \{4, 5\}$.

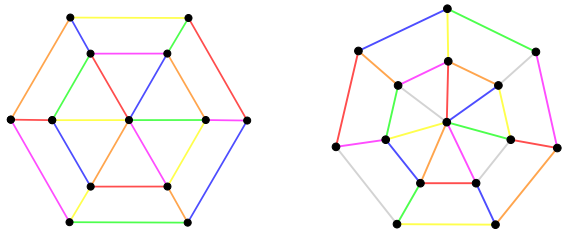

FIGURE 5. r-dynamic proper n-edge-coloring of the graph CH_n for all $r \leq n - 2 < n \in \{6, 7\}$.

Proposition 3.1. *Let $n \in \{6, 7\}$. Then,*

$$\lambda_{n-1}(CH_n) = \chi_{n-1}(L(CH_n)) \geq \begin{cases} 7 & \text{if } n = 6, \\ 9 & \text{if } n = 7. \end{cases}$$

Proof. From Lemma 2.1, we have that $n \leq \chi_{n-1}(L(CH_n))$. So, let us suppose the existence of an $(n-1)$-dynamic proper n-coloring c of $L(CH_n)$. From Condition (1.1), we have that $|c(N(v_ip_i))| = 5 = d(v_ip_i)$ for all non-negative integer $i < n$. Thus, the set $c(N(v_0v_1))$ does not contain any of the two distinct colors $c(v_0v_1)$ and $c(p_0p_1)$. As such, $|c(N(v_0v_1))| \leq n-2$, which contradicts Condition (1.1). Hence, $\chi_{n-1}(L(CH_n)) \geq n+1$ for all $n \in \{6, 7\}$.

Now, let c be a 6-dynamic proper 8-coloring of the line graph $L(CH_7)$. Condition (1.1) implies that $|c(N(v_ip_i))| = 5 = d(v_ip_i)$ and $|c(N(v_iv_{i+1}))| = 6 = d(v_iv_{i+1})$ for every non-negative integer $i < 7$. As a consequence, the set

$$\mathcal{S}_i := c(N(v_iv_{i+1})) \cup \{c(v_iv_{i+1}),\, c(p_ip_{i+1})\}$$

is formed by all the eight colors associated to the map c. Then, since Condition (1.1) also implies that $|c(N(p_ip_{i+1}))| = 4 = d(p_ip_{i+1})$ for all non-negative integer $i < 7$, exactly one of the following three conditions holds:

- $c(p_ip_{i+1}) = c(vv_{i-1}) = c(v_{i+2}v_{i+3}) = c(p_{i+4}p_{i+5})$;
- $c(p_ip_{i+1}) = c(v_{i-2}v_{i-1}) = c(vv_{i+2}) = c(p_{i+3}p_{i+4})$;
- $c(p_ip_{i+1}) = c(v_{i-2}v_{i-1}) = c(v_{i+2}v_{i+3})$.

In particular, if $i = 0$, then the following study of cases arises. All the stages in this study are sequentially described as immediate consequences of applying that $|c(N(v_ip_i))| = 5$, $|c(N(v_iv_{i+1}))| = 6$ and $|\mathcal{S}_i| = 8$ for every non-negative integer $i < 7$, together with the three described conditions and the fact that c is a proper coloring.

- **Case 1**: $c(p_0p_1) = c(vv_6) = c(v_2v_3) = c(p_4p_5)$.
  - **Subcase 1.1**: $c(p_1p_2) = c(vv_0) = c(v_3v_4) = c(p_5p_6)$, which implies that $c(p_3p_4) = c(v_1v_2)$.
    - **Subcase 1.1.1**: $c(p_2p_3) = c(vv_1) = c(v_4v_5) = c(p_0p_6)$, which implies that $c(v_5v_6) = c(v_1v_2)$ and $c(v_6p_6) = c(v_1p_1)$. But then, $c(v_1p_1) \in \{c(vv_3),\, c(v_3p_3)\} \cap \{c(vv_4),\, c(v_4p_4)\}$. This implies that $|c(N(v_3v_4))| < 6$, which is not possible.
    - **Subcase 1.1.2**: $c(p_2p_3) = c(v_0v_1) = c(v_4v_5)$, which implies that $c(v_3p_3) = c(vv_1)$ and $c(vv_3) = c(v_1p_1) = c(v_5v_6)$. Then, $c(vv_5) = c(v_1v_2) = c(p_0p_6)$ and $c(v_5p_5) = c(vv_1)$. But then, $|\mathcal{S}_i| < 8$ for some $i \in \{3, 4, 5\}$, which is not possible.
  - **Subcase 1.2**: $c(p_1p_2) = c(v_0v_6) = c(v_3v_4)$, which implies sequentially that $c(v_2p_2) = c(vv_0)$, $c(vv_2) = c(v_0p_0)$ and $c(p_3p_4) = c(v_1v_2)$.
    - **Subcase 1.2.1**: $c(p_2p_3) = c(vv_1) = c(v_4v_5) = c(p_0p_6)$, which implies that $c(v_4v_5) = c(v_1v_2)$ and $c(v_6p_6) = c(v_1p_1)$. But then, $c(v_1p_1) \in \{c(vv_3),\, c(v_3p_3)\} \cap \{c(vv_4),\, c(v_4p_4)\}$. This implies that $|\mathcal{S}_3| < 8$, which is not possible.

  - ∗ **Subcase 1.2.2**: $c(p_2p_3) = c(v_0v_1)$, which implies sequentially that $c(v_3p_3) = c(vv_1)$, $c(vv_3) = c(v_1p_1) = c(v_5v_6)$, $c(vv_5) = c(v_1v_2) = c(p_0p_6)$, $c(v_6p_6) = c(vv_1)$ and $c(v_4v_5) = c(v_0p_0)$. But then, $|\mathcal{S}_i| < 8$ for some $i \in \{3, 4, 5\}$, which is not possible.
- **Case 2**: $c(p_0p_1) = c(v_5v_6) = c(vv_2) = c(p_3p_4)$. This case is symmetric to the precedent one. So, a similar reasoning gives rise to a contradiction.
- **Case 3**: $c(p_0p_1) = c(v_5v_6) = c(v_2v_3)$.
  - **Subcase 3.1**: $c(p_1p_2) = c(vv_0) = c(v_3v_4) = c(p_5p_6)$. Up to relabeling of indices, this particular condition coincides with the assumptions of the first case. So, no coloring is possible from here.
  - **Subcase 3.2**: $c(p_1p_2) = c(v_0v_6) = c(vv_3) = c(p_4p_5)$. Again, this particular condition is equivalent, up to relabeling of indices and symmetry, to the one described in the first case. So, no coloring is possible from here.
  - **Subcase 3.3**: $c(p_1p_2) = c(v_0v_6) = c(v_3v_4)$.
    - ∗ **Subcase 3.3.1**: $c(p_2p_3) = c(vv_1) = c(v_4v_5) = c(p_0p_6)$, which is equivalent to the first case and hence, no coloring is possible from here.
    - ∗ **Subcase 3.3.2**: $c(p_2p_3) = c(v_0v_1) = c(vv_4) = c(p_5p_6)$, which is again equivalent to the first case. No coloring is possible from here.
    - ∗ **Subcase 3.3.3**: $c(p_2p_3) = c(v_0v_1) = c(v_4v_5)$, which implies that $c(p_3p_4) = c(v_1v_2) = c(vv_5) = c(p_0p_6)$. Again, this last condition is equivalent to the one described in the first case. So, no coloring is possible from here.

As a consequence, $\chi_6(L(CH_7)) \geq 9$. □

We establish now a lower bound for the case $4 \leq r = n$ (notice in this regard that the case $r = n = 3$ is already dealt with in Figure 3).

Proposition 3.2. *Let $n \geq 4$ be a positive integer. Then,*

$$\lambda_n(CH_n) = \chi_n(L(CH_n)) \geq \begin{cases} 8 & \text{if } n = 5, \\ n+2 & \text{otherwise.} \end{cases}$$

Proof. The following study of cases arises.

- **Case** $n = 4$.

  Let us suppose the existence of a 4-dynamic proper 5-coloring c of the line graph $L(CH_4)$. From Condition (1.1), we have that $|c(N(p_ip_{i+1}))| = 4 = d(p_ip_{i+1})$ for all non-negative integer $i < n$. Thus, since $N(p_0p_1) \cap N(p_2p_3) = \{p_1p_2, p_3p_0\}$ and the map c is a proper coloring, we have that

  $$c(p_2p_3) \in \{c(p_0p_1), c(v_0p_0), c(v_1p_1)\}.$$

  If $c(p_2p_3) = c(v_0p_0)$, then $|c(N(p_3p_0))| \leq 3$, which contradicts Condition (1.1). Similarly, $c(p_2p_3) \neq c(v_1p_1)$ and hence, $c(p_2p_3) = c(p_0p_1)$. But then, $|c(N(p_3p_0)| \leq 3$, which contradicts again Condition (1.1). As a consequence, no such map c exists and hence, $\chi_4(L(CH_4)) \geq 6$.

- **Case** $n = 5$.

  Let us suppose the existence of a 5-dynamic proper 7-coloring c of the line graph $L(CH_5)$. Condition (1.1) implies that $|c(N(v_ip_i))| = 5 = d(v_ip_i)$ and $|c(N(p_ip_{i+1}))| = 4 = d(p_ip_{i+1})$ for all $i < 5$. As a consequence, $|c(N(v_ip_i)) \cup \{c(v_ip_i)\}| = 6$. All these conditions together imply that either $c(p_ip_{i+1}) = c(vv_{i-1}) = c(v_{i+2}v_{i+3})$ for all $i < 5$, or $c(p_ip_{i+1}) = c(v_{i-2}v_{i-1}) = c(vv_{i+2})$ for all $i < 5$. Otherwise, it would be either $|c(N(v_{i-1}v_i))| < 5$, or $|c(N(v_{i+1}v_{i+2}))| < 5$ for, at least, one non-negative integer $i < 5$, which is not possible.

  The resulting coloring requires that $c(v_ip_i) = c(v_{i+1}p_{i+1})$ for some $i < 5$. This would imply that $|c(N(p_ip_{i+1}))| < 4$, which is not possible. As a consequence, $\chi_5(L(CH_5)) \geq 8$.
- **Case** $n \geq 6$.

  Let us suppose the existence of an n-dynamic proper $(n+1)$-coloring c of the line graph $L(CH_n)$. Without loss of generality, we may assume that $c(vv_i) = i$ for all $i < n$. Then, Condition (1.1) implies that

$$n \in \{c(v_{i-1}v_i),\, c(v_i, v_{i+1}),\, c(v_ip_i)\} \quad \text{for all } i < n, \tag{3.1}$$

  because $d(vv_i) = n+2 > n$. Nevertheless, $c(v_iv_{i+1}) \neq n$, because Condition (1.1) implies that $|c(N(v_{i+1}v_{i+2}))| = 6 = d(v_{i+1}v_{i+2})$, and hence, it should be

$$n \notin \{c(v_{i+1}v_{i+2}),\, c(v_{i+2}v_{i+3}),\, c(v_{i+2}p_{i+2})\},$$

  which contradicts (3.1). Similarly, we get that $c(v_{i-1}v_i) \neq n$. As a consequence, it must be $c(v_ip_i) = n$ for all non-negative integer $i < n$. But then, $|c(N(v_iv_{i+1}))| \leq 5 < 6 = d(v_iv_{i+1}) \leq n$, which contradicts Condition (1.1). Hence, the existence of the map c is not possible and the result holds. □

We focus now on the case $r = n + 1$.

Proposition 3.3. *Let $n \geq 3$ be a positive integer. Then,*

$$\lambda_{n+1}(CH_n) = \chi_{n+1}(L(CH_n)) \geq \begin{cases} 10 & \text{if } n = 5, \\ n+3 & \text{if } n \equiv 0 \,(\mathrm{mod}\, 3) \text{ or } n = 4, \\ n+4 & \text{otherwise.} \end{cases}$$

Proof. The following study of cases arises.

- **Case** $n = 3$.

  Let c be a 4-dynamic proper 5-coloring c of the line graph $L(CH_3)$. From Condition (1.1), we have that $|c(N(p_ip_{i+1}))| = 4 = d(p_ip_{i+1})$ for all positive integer $i < 3$. Then, since $|N(p_0p_1) \cap N(p_1p_2)| = 2$ and both vertices p_0p_1 and p_1p_2 are adjacent, it must be $c(v_0p_0) = c(v_2p_2)$. But then, $|c(N(p_2p_0)| \leq 3$, which contradicts Condition (1.1). Hence, $\chi_4(L(CH_3)) \geq 6$.
- **Case** $n = 4$.

  Let us suppose the existence of a 5-dynamic proper 6-coloring c of the line graph $L(CH_4)$. From Condition (1.1), the set $\{c(p_ip_{i+1}) \colon 0 \leq i < 4\}$ is

formed by four distinct colors. Moreover, $c(v_0p_0) = c(v_2p_2)$ and $c(v_1p_1) = c(v_3p_3)$ are the remaining two colors. Then, since the map c is a proper coloring and $|c(N(v_ip_{i+1}))| = 5 = d(v_ip_{i+1})$ because of Condition (1.1), it must be $c(vv_i) = c(v_{i+1}p_{i+1})$ for all positive integer $i < 4$. But then, there is a clique of order four within the line graph CH_4 whose vertices are colored with only two colors. This contradicts the fact that the map c is a proper coloring and hence, $\chi_5(L(CH_4)) \geq 7$.

- **Case** $n = 5$.

  It is simply verified that the existence of three vertices sharing the same color within $L(CH_5)$ contradicts Condition (1.1). Then, the result follows straightforwardly from the fact that this line graph contains 20 vertices.

- **Case** $n \geq 6$.

  Let c be an $(n+1)$-dynamic proper $(n+2)$-coloring of the line graph $L(CH_n)$. Without loss of generality, we may assume that $c(vv_i) = i$ for all positive integer $i < n$. Then, Condition (1.1) implies that $\{n, n+1\} \subseteq c(N(vv_i)) \cap c(N(vv_{i+1}))$ for all $i < n$. Thus, $|c(N(v_iv_{i+1}))| \leq 5$, which contradicts Condition (1.1), and hence, $\chi_{n+1}(L(CH_n)) \geq n+3$.

  Now, let c' be an $(n+1)$-dynamic proper $(n+3)$-coloring of $L(CH_n)$. Again, we can suppose that $c'(vv_i) = i$ for all $i < n$. From Condition (1.1), it must be $|c'(N(vv_i))| \geq n+1$ and $|c'(N(v_iv_{i+1}))| = 6$ for all $i < n$. This implies that $c'(v_iv_{i+1}) \notin \{n, n+1, n+2\}$ for all $i < n$. As a consequence, $\{n,\ n+1,\ n+2\} = \{c'(v_{i-1}v_i),\ c'(v_iv_{i+1}),\ c'(v_{i+1}v_{i+2})\}$ and $c'(v_iv_{i+1}) = c'(v_{i+3}v_{i+4})$ for all $i < n$. □

Finally, the following result deals with the case $r = n+2$.

Proposition 3.4. *Let $n \geq 3$ be a positive integer. Then,*

$$\lambda_{n+2}(CH_n) = \chi_{n+2}(L(CH_n)) \geq \begin{cases} n+5 & \text{if } n \in \{3,\ 5k,\ 6k\},\ \text{with } k > 0, \\ n+6 & \text{otherwise.} \end{cases}$$

Proof. Let us study separately each case.

- **Case** $n \in \{3,\ 5k,\ 6k\}$, with $k > 0$.

  Let c be an $(n+2)$-dynamic proper $(n+4)$-coloring of $L(CH_n)$. From Condition (1.1), we have that $|c(N(vv_i))| = n+2 = d(vv_i)$ for all $i < n$. Without loss of generality, we may assume that $c(vv_i) = i$ for all $i < n$, and hence, $\{c(v_{i-1}v_i),\ c(v_ip_i),\ c(v_iv_{i+1})\} \subset \{n,\ n+1,\ n+2,\ n+3\}$ for all $i < n$. Then, the following assertions are simply verified.

  – If $n = 3$, then $|c(N(v_iv_{i+1}))| < 5$ for some $i < 3$.
  – If $n \in \{5k,\ 6k\}$ for some $k > 0$, then $|c(N(v_iv_{i+1}))| < 6 = d(v_iv_{i+1})$ for all $i < n$.

  Both assertions contradict Condition (1.1) and hence, the result holds.

- **Case** $3 < n \notin \{5k,\ 6k\}$ for all $k > 0$.

  Let c be an $(n+2)$-dynamic proper $(n+5)$-coloring of $L(CH_n)$. Again, we may assume that $c(vv_i) = i$ for all $i < n$. Then, Condition (1.1) implies that, for each positive integer $i < n$, we have $\{c(v_{i-1}v_i),\ c(v_ip_i),\ c(v_iv_{i+1}),$

$c(v_{i+1}p_{i+1}), c(v_{i+1}v_{i+2})\} = \{n, \ldots, n+4\}$ and $\{c(v_{i-1}v_i), c(v_ip_i)\})\} = \{c(v_{i+2}p_{i+2}), c(v_{i+2}v_{i+3})\})\}$. This is not possible when $n \notin \{5k, 6k\}$ for all $k > 0$. Hence, $\chi_{n+2}(L(CH_n)) \geq n+6$. □

The following theorem is the main result of the paper. It establishes the r-dynamic chromatic number of the line graph $L(CH_n)$.

Theorem 3.2. *Let r and n be two positive integers, with $n > 2$. Then,*

$$\lambda_r(CH_n) = \chi_r(L(CH_n)) = \begin{cases} n & \text{if } \max\{3,r\} < n \text{ and } (r,n) \neq \begin{cases}(5,6),\\(6,7),\end{cases}\\ n+1 & \text{if } \begin{cases} r \leq n = 3,\\ (r,n) = (5,6),\end{cases}\\ n+2 & \text{if } \begin{cases}(r,n) = (6,7),\\ 4 \leq r = n \neq 5,\end{cases}\\ n+3 & \text{if } \begin{cases} r = 5 \in \{n, n+1\},\\ r-1 = n \equiv 0 \pmod 3,\end{cases}\\ n+4 & \text{if } 5 \neq r-1 = n \not\equiv 0 \pmod 3,\\ n+5 & \text{if } \begin{cases} r-1 = n = 5,\\ r-2 = n = 3,\\ r-2 \geq n \in \{5k, 6k\}, \text{ with } k > 0,\end{cases}\\ n+6 & \text{otherwise.}\end{cases}$$

Proof. The case $r \leq n = 3$ follows from Lemma 3.1 and Figure 3. Let us study separately the remaining cases by defining an appropriate r-dynamic proper coloring c of the corresponding line graph $L(CH_n)$ satisfying Condition (1.1). Without loss of generality, we may define this map c so that $c(vv_i) = i$ for all non-negative integer $i < n$.

- **Case** $\max\{3,r\} < n$.

  Except for $(r,n) \in \{(5,6), (6,7)\}$, the case $4 \leq n \leq 7$ follows simply from Lemma 3.1 and Figures 4 and 5. The case $(r,n) = (5,6)$ holds from Lemma 3.1 and Figure 5 once we replace the colors of any three vertices v_ip_i, $v_{i+2}p_{i+2}$ and $v_{i+4}p_{i+4}$ in the left graph of that figure by a seventh color. In addition, the case $(r,n) = (6,7)$ follows from Proposition 3.1 and Figure 6 (center). So, let us focus on the case $n > 7$. From Lemma 3.1, we have that $n \leq \chi_r(L(CH_n))$. In order to prove that this lower bound is reached, we define the map c so that, for each non-negative integer $i < n$,

  $$c(w) = \begin{cases}(i-3) \bmod n & \text{if } w = v_iv_{i+1},\\ (i+2) \bmod n & \text{if } w = v_ip_i,\\ (i-1) \bmod n & \text{if } w = p_ip_{i+1}.\end{cases}$$

  Condition (1.1) holds and hence, $\chi_r(L(CH_n)) = n$. Figure 6 (right) illustrates the case $n = 8$.

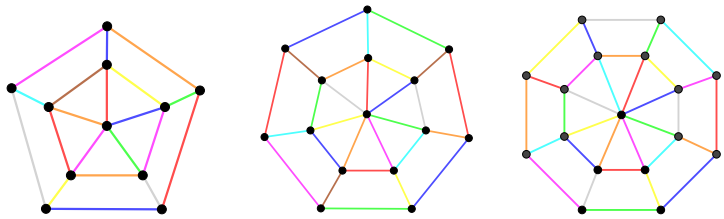

FIGURE 6. 5-dynamic proper 8-edge-coloring of the closed helm graph CH_5 (left); r-dynamic proper 9-edge-coloring of the closed helm graph CH_7 for $r \in \{6,7\}$ (center); and r-dynamic proper 8-edge-coloring of the closed helm graph CH_8 for all $r \leq 7$ (right).

- **Case** $4 \leq r = n$.

  The case $n = 5$ holds from Proposition 3.2 and Figure 6 (left). So, let us focus on the case $n \neq 5$. From Proposition 3.2, it is $n+2 \leq \chi_n(L(CH_n))$. Let the map c be defined so that, for each non-negative integer $i < n$,

$$c(v_iv_{i+1}) = \begin{cases} n & \text{if } n \text{ is odd and } i = n-1, \\ n+1 & \text{if } n \text{ is odd and } i = 0, \\ (i-3) \bmod n & \text{otherwise,} \end{cases}$$

$$c(v_ip_i) = \begin{cases} i+2 & \text{if } n \text{ is odd and } i \in \{0,1,n-1\}, \\ n & \text{if } \begin{cases} \text{both } n \text{ and } i \text{ are even,} \\ n \text{ is odd and } i \notin \{0,n-1\} \text{ is even,} \end{cases} \\ n+1 & \text{otherwise,} \end{cases}$$

  and

$$c(p_ip_{i+1}) = (i-1) \bmod n.$$

  Condition (1.1) holds and hence, $\chi_r(L(CH_n)) = n+2$. Figure 7 illustrates the case $r = n \in \{6,9\}$.

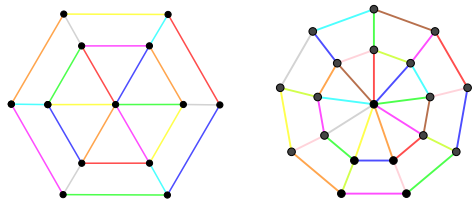

FIGURE 7. n-dynamic proper $(n+2)$-edge-coloring of the closed helm graph CH_n for $n \in \{6,9\}$.

- **Case** $r = n + 1$.

  The case $n \leq 5$ follows from Proposition 3.3 and Figure 8. Now, for $n > 5$, we define the map c so that, for each non-negative integer $i < n$,

$$c(v_i v_{i+1}) = \begin{cases} n + (i \bmod 3) & \text{if } n \equiv 0 \pmod 3, \\ n + (i \bmod 4) & \text{otherwise,} \end{cases}$$

$$c(v_i p_i) = (i + 2) \bmod n \qquad \text{and} \qquad c(p_i p_{i+1}) = (i - 1) \bmod n.$$

  Condition (1.1) holds and hence, Proposition 3.3 implies $\chi_{n+1}(L(CH_n)) = n + 3$ if $n \equiv 0 \pmod 3$, and $\chi_{n+1}(L(CH_n)) = n + 4$ otherwise. Figure 9 illustrates the case $n \in \{6, 7\}$.

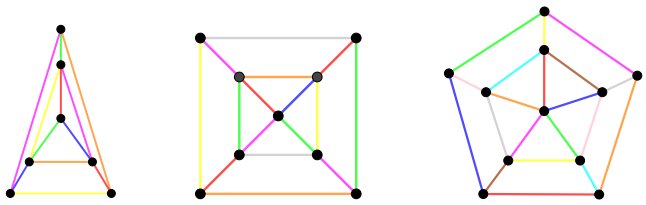

FIGURE 8. $(n + 1)$-dynamic proper $(n + 3)$-edge-coloring of the closed helm graph CH_n for $n \in \{3, 4, 6\}$, and 6-dynamic proper 10-edge-coloring of the closed helm graph CH_5.

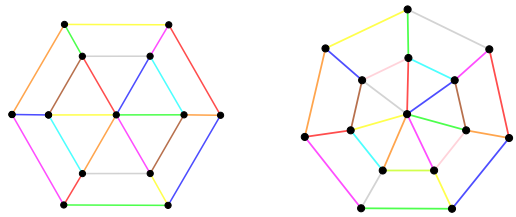

FIGURE 9. 7-dynamic proper 9-edge-coloring of the closed helm graph CH_6 (left) and 8-dynamic proper 11-edge-coloring of the closed helm graph CH_7 (right).

- **Case** $r = n + 2$.

  The case $n = 3$ follows from Proposition 3.4 and Figure 10 (left). Further, from Proposition 3.4, we have that $n + 5 \leq \chi_{n+2}(L(CH_n))$ for all $n \in \{5k, 6k\}$ for some $k > 0$. Let us prove that this lower bound is reached in both cases.

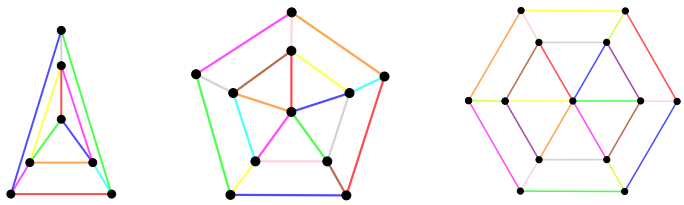

FIGURE 10. $(n+2)$-dynamic proper $(n+5)$-edge-coloring of the graph CH_n for all $n \in \{3, 5, 6\}$.

– **Subcase** $n = 5k$ for some $k > 0$.
Let the map c be defined so that, for each non-negative integer $i < n$,

$$c(w) = \begin{cases} n + (i \bmod 5) & \text{if } w = v_i v_{i+1}, \\ n + ((i+2) \bmod 5) & \text{if } w = v_i p_i, \\ (i-1) \bmod n & \text{if } w = p_i p_{i+1}. \end{cases}$$

Condition (1.1) holds and hence, $\chi_{n+2}(L(CH_n)) = n + 5$. Figure 10 (center) illustrates the case $n = 5$.

– **Subcase** $n = 6k$ for some $k > 0$.
Let the map c be defined so that, for each non-negative integer $i < n$,

$$c(w) = \begin{cases} n + (i \bmod 3) & \text{if } w = v_i v_{i+1}, \\ n + 3 + (i \bmod 2) & \text{if } w = v_i p_i, \\ (i-1) \bmod n & \text{if } w = p_i p_{i+1}. \end{cases}$$

Condition (1.1) holds and hence, $\chi_{n+2}(L(CH_n)) = n + 5$. Figure 10 (right) illustrates the case $n = 6$.

Finally, if $n \notin \{3, 5k, 6k\}$ for all $k > 0$, then Proposition 3.4 implies that $n + 6 \leq \chi_{n+2}(L(CH_n))$. In order to prove that this lower bound is reached, let the map c be defined so that, for each non-negative integer $i < n$,

$$c(w) = \begin{cases} n + (i \bmod 3) & \text{if } w = v_i v_{i+1} \text{ and } n \equiv 0 \,(\mathrm{mod}\, 3), \\ n + (i \bmod 4) & \text{if } w = v_i v_{i+1} \text{ and } n \not\equiv 0 \,(\mathrm{mod}\, 3), \\ n + 3 + (i \bmod 3) & \text{if } w = v_i p_i \text{ and } n \equiv 0 \,(\mathrm{mod}\, 3), \\ n + 4 + (i \bmod 2) & \text{if } w = v_i p_i \text{ and } \begin{cases} n \text{ is even}, \\ n \not\equiv 0 \,(\mathrm{mod}\, 3) \text{ is odd} \\ \qquad \text{and } i > 0, \end{cases} \\ n + 3 & \text{if } w = v_0 p_0 \text{ and } n \not\equiv 0 \,(\mathrm{mod}\, 3) \text{ is odd}, \\ (i-1) \bmod n & \text{if } w = p_i p_{i+1}. \end{cases}$$

Condition (1.1) holds and hence, $\chi_{n+2}(L(CH_n)) = n + 6$. Figure 11 (left) illustrates the case $n \in \{4, 7, 9\}$.

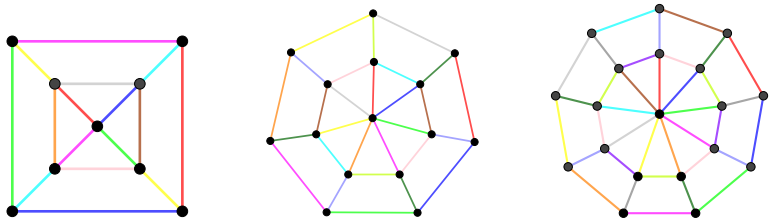

FIGURE 11. $(n+2)$-dynamic proper $(n+6)$-edge-coloring of the graph CH_n for all $n \in \{4, 7, 9\}$.

- **Case** $r > n+2$.
  It follows simply from Lemma 2.1 and the case $r = n-2$. □

4. Conclusion and further work

In this paper, we have determined the r-dynamic chromatic number of the line graph of any closed helm graph CH_n for all positive integers r and $n > 2$, and hence, the r-dynamic edge chromatic number of any given closed helm graph. In this regard, Theorem 3.2 is the main result of the paper; there it has in particular been obtained that $n \leq \lambda_r(CH_n) = \chi_r(L(CH_n)) \leq n+6$.

Similarly to recent works dealing with the r-dynamic coloring of certain products of graphs [7, 6], of particular interest for the continuation of this paper is the study of the r-dynamic edge coloring of different products of graphs concerning closed helm graphs.

Acknowledgments

The authors want to express their gratitude to the anonymous referee for the comprehensive reading of the paper and his/her pertinent comments and suggestions, which helped improve the manuscript.

References

[1] A. Ahadi, S. Akbari, A. Dehghan, and M. Ghanbari, On the difference between chromatic number and dynamic chromatic number of graphs, *Discrete Math.* **312** no. 17 (2012), 2579–2583. DOI MR Zbl

[2] S. Akbari, M. Ghanbari, and S. Jahanbekam, On the list dynamic coloring of graphs, *Discrete Appl. Math.* **157** no. 14 (2009), 3005–3007. DOI MR Zbl

[3] S. Akbari, M. Ghanbari, and S. Jahanbekam, On the dynamic chromatic number of graphs, in *Combinatorics and Graphs*, Contemp. Math. 531, Amer. Math. Soc., Providence, RI, 2010, pp. 11–18. DOI MR Zbl

[4] M. Alishahi, On the dynamic coloring of graphs, *Discrete Appl. Math.* **159** no. 2-3 (2011), 152–156. DOI MR Zbl

[5] M. Alishahi, Dynamic chromatic number of regular graphs, *Discrete Appl. Math.* **160** no. 15 (2012), 2098–2103. DOI MR Zbl

[6] T. Deepa, R. M. Falcón, and M. Venkatachalam, On the r-dynamic coloring of the direct product of a path with either a complete graph or a wheel graph, *AIMS Math.* **6** no. 2 (2021), 1470–1496. DOI MR Zbl

[7] T. Deepa, M. Venkatachalam, and R. M. Falcón, On the r-dynamic coloring of the direct product of a path with either a path or a cycle, *AIMS Math.* **5** no. 6 (2020), 6496–6520. DOI MR Zbl

[8] T. Deepa and M. Venkatachalam, On r-dynamic coloring of the total graphs of gear graphs, *Appl. Math. E-Notes* **18** (2018), 69–81. MR Zbl Available at https://www.math.nthu.edu.tw/~amen/2018/AMEN-170730.pdf.

[9] H. Furmańczyk, J. Vernold Vivin, and N. Mohanapriya, r-dynamic chromatic number of some line graphs, *Indian J. Pure Appl. Math.* **49** no. 4 (2018), 591–600. DOI MR Zbl

[10] F. Harary, *Graph Theory*, Addison-Wesley, Reading, Mass., 1969. MR Zbl

[11] S. Jahanbekam, J. Kim, S. O, and D. B. West, On r-dynamic coloring of graphs, *Discrete Appl. Math.* **206** (2016), 65–72. DOI MR Zbl

[12] R. Kang, T. Müller, and D. B. West, On r-dynamic coloring of grids, *Discrete Appl. Math.* **186** (2015), 286–290. DOI MR Zbl

[13] H.-J. Lai, B. Montgomery, and H. Poon, Upper bounds of dynamic chromatic number, *Ars Combin.* **68** (2003), 193–201. MR Zbl

[14] X. Li and W. Zhou, The 2nd-order conditional 3-coloring of claw-free graphs, *Theoret. Comput. Sci.* **396** no. 1-3 (2008), 151–157. DOI MR Zbl

[15] S. Loeb, T. Mahoney, B. Reiniger, and J. Wise, Dynamic coloring parameters for graphs with given genus, *Discrete Appl. Math.* **235** (2018), 129–141. DOI MR Zbl

[16] I. N. Maylisa, D. Dafik, and S. Setiawani, Keterampilan berpikir tingkat tinggi dalam pewarnaan sisi r-dinamis pada graf khusus, *Kadikma* **6** no. 3 (2015), 132–141. Available at https://jurnal.unej.ac.id/index.php/kadikma/article/view/5218.

[17] D. E. W. Meganingtyas, *Analisis pewarnaan r-dinamis pada graf-graf khusus*, Master's thesis, Universitas Jember, Indonesia, 2015. Available at https://repository.unej.ac.id/handle/123456789/73165.

[18] L. D. Minarti, D. Dafik, S. Setiawani, S. Slamin, and A. Fatahillah, Pewarnaan sisi r-dinamis pada graf hasil operasi amalgamasi titik keluarga graf pohon dan kaitannya dengan keterampilan berpikir tingkat tinggi, *Saintifika* **21** no. 2 (2019), 15–22. Available at https://jurnal.unej.ac.id/index.php/STF/article/view/13561.

[19] N. Mohanapriya, V. J. Vernold, and M. Venkatachalam, On dynamic coloring of fan graphs, *Int. J. Pure Appl. Math.* **106** no. 8 (2016), 169–174. Available at https://acadpubl.eu/jsi/2016-106-6-7-8/2016-106-8/20/index.html.

[20] N. Mohanapriya, J. Vernold Vivin, and M. Venkatachalam, δ-dynamic chromatic number of Helm graph families, *Cogent Math.* **3** (2016), Art. ID 1178411, 4 pp. DOI MR Zbl

[21] B. Montgomery, *Dynamic coloring of graphs*, Ph.D. thesis, West Virginia University, 2001. DOI MR

[22] G. Nandini, M. Venkatachalam, and R. M. Falcón, On the r-dynamic coloring of subdivision-edge coronas of a path, *AIMS Math.* **5** no. 5 (2020), 4546–4562. DOI MR Zbl

[23] G. Nandini, M. Venkatachalam, and S. Gowri, On r-dynamic coloring of the family of bistar graphs, *Commun. Fac. Sci. Univ. Ank. Ser. A1. Math. Stat.* **68** no. 1 (2019), 923–928. DOI MR Zbl

[24] J. V. Vivin, N. Mohanapriya, J. Kok, and M. Venkatachalam, On dynamic coloring of certain cycle-related graphs, *Arab. J. Math. (Springer)* **9** no. 1 (2020), 213–221. DOI MR Zbl

Raúl M. Falcón ✉
Department of Applied Mathematics I, Universidad de Sevilla, Spain
rafalgan@us.es

Mathiyazhagan Venkatachalam
Kongunadu Arts and Science College, Coimbatore, Tamil Nadu, India
venkatmaths@gmail.com

Sathasivam Gowri
Department of Mathematics, SNS College of Technology, Coimbatore, Tamil Nadu, India
gowrisathasivam@gmail.com

Gnanasekaran Nandini
Department of Mathematics, SNS College of Technology, Coimbatore, Tamil Nadu, India
nandiniap2006@gmail.com

Received: May 12, 2021
Accepted: March 3, 2022

Networks and Heterogeneous Media

http://www.aimspress.com/journal/nhm

NHM, 18(4): 1713–1746.
DOI: 10.3934/nhm.2023075
Received: 14 March 2023
Revised: 02 October 2023
Accepted: 08 October 2023
Published: 13 October 2023

Research article

Optimal secret share distribution in degree splitting communication networks

Raúl M. Falcón[1*], **Venkitachalam Aparna**[2] **and Nagaraj Mohanapriya**[2]

[1] Department of Applied Mathematics I, University of Seville, Avda. Reina Mercedes 4A, Seville, 41012, Spain

[2] PG and Research Department of Mathematics, Kongunadu Arts and Science College, GN Mills, Tamil Nadu, 641 029, Coimbatore, India

* **Correspondence:** Email: rafalgan@us.es.

Abstract: Dynamic coloring has recently emerged as a valuable tool to optimize cryptographic protocols based on secret sharing, which enforce data security in communication networks and have significant importance in both online storage and cloud computing. This type of graph labeling enables the dealer to distribute secret shares among the nodes of a communication network so that everybody can recover the secret after a minimum number of rounds of communication. This paper delves into this topic by dealing with the dynamic coloring problem for degree splitting graphs. The topological structure of the latter enables the dealer to avoid dishonesty by adding control nodes that supervise all those participants with a similar influence in the network. More precisely, we solve the dynamic coloring problem for degree splitting graphs of any regular graph. The irregular case is partially solved by establishing a lower bound for the corresponding dynamic chromatic number. As illustrative examples, we solve the dynamic coloring problem for the degree splitting graphs of cycles, cocktail, book, comb, fan, jellyfish, windmill and barbell graphs.

Keywords: Degree splitting networks; secret sharing; dynamic coloring problem

1. Introduction

A (k,t)-*threshold secret sharing scheme* [1, 2], with $k \geq t$, is a cryptographic protocol in which a dealer splits a secret into k pieces of information or *secret shares*. Copies of these pieces are distributed among a group of n participants, with $n \geq t$, so that only a subgroup sharing at least t distinct secret shares can reconstruct the secret. The parameter t is called the *threshold* of the scheme. These schemes are relevant in online storage and cloud computing because they enforce data security in communication networks [3], in which each node represents a participant of the scheme. Two

nodes are adjacent if and only if there exists a proximity relationship between both participants so that they can cooperate to recover the original secret. This cooperation occurs simultaneously via discrete time-steps or rounds of communication that allow the spread of secret shares among all the nodes of the network. First, the dealer distributes the secret shares among the nodes of the network. In each subsequent round, each participant gathers all the pieces of information of the adjacent nodes and fuses them with its own information. Moreover, we suppose in this paper the following assumptions.

- Exactly one secret share is assigned by the dealer to each participant, so that no two adjacent nodes receive the same piece of information. To this end, the dealer has secure communication links to every participant. We also assume that the secret cannot be recovered from this initial distribution. That is, $t > 1$ in our (k, t)-threshold secret sharing scheme.
- The communication network is static. That is, its topology does not change during the rounds of communication.

Figure 1 illustrates these rounds of communications for a static network of 12 nodes, among which the dealer has distributed four distinct pieces of information.

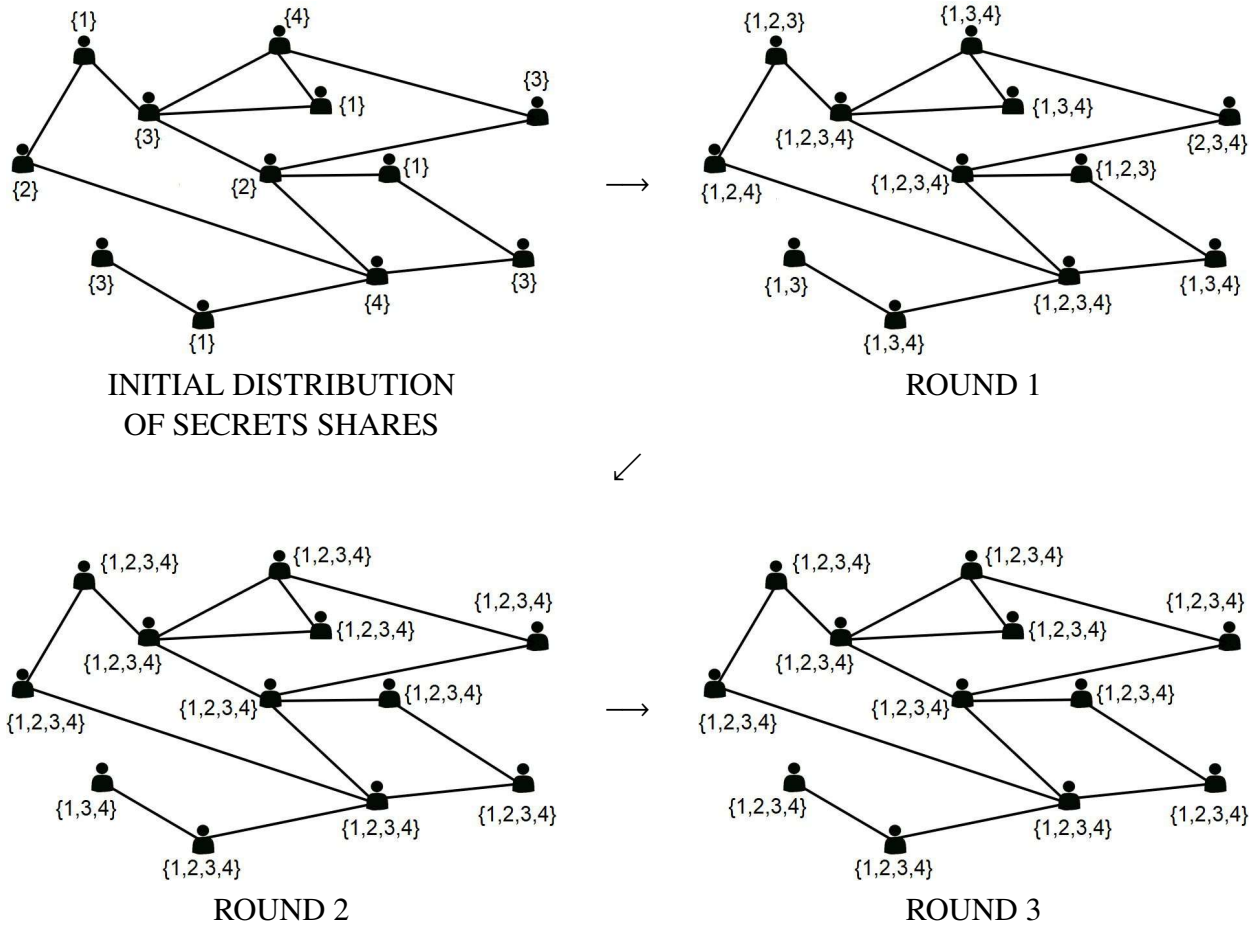

Figure 1. Successive rounds of communications in a network.

A main question to answer here is the following.

Problem 1. *What is the minimum number of rounds that are necessary so that the original secret can be reconstructed by each one of the participants?*

Of course, this number is less than or equal to the diameter of the graph under consideration. The exact solution of Problem 1 requires the design of an efficient and optimal distribution of secret shares among all the participants of the communication network. It requires a comprehensive analysis of the network topology and metrics [4], which would be even more relevant when the communication network under consideration is large enough to be considered for big data storage. Even if different analytic tools based on graph algorithms are usually used to this end [5–7], the most relevant tool for dealing with our problem is graph coloring.

A *proper n-coloring* of a graph G, with a set of vertices $V(G)$, is any map $c : V(G) \to \{0, \dots, n-1\}$ such that $c(v) \neq c(w)$, for every pair of adjacent vertices $v, w \in V(G)$. The minimum positive integer n for which this map exists is the *chromatic number* $\chi(G)$. If G is the underlying graph of a communication network, then each color can be interpreted as the secret share assigned to the node under consideration. Hence, Problem 1 requires the design of an appropriate coloring for the graph G.

Depending on different local constraints, one may find in the literature a wide amount of distinct types of graph colorings [8, 9], with different applications in real-world problems [10]. Thus, for instance, the b-coloring is useful to deal with clustering in data mining [11]; the equitable coloring ensures load balancing in scheduling [12]; the frugal coloring avoid collisions in networks based on a time-division multiple access [13]; the rainbow k-connected edge-coloring enables the strengthening of the conventional connectivity to get a much more secure network communication [14]; and the star coloring is useful in tracebacking IP addresses in communication networks [15].

Dynamic coloring has recently emerged [16] as a valuable type of proper-coloring that allows for the description of optimal distributions of pieces of information in a secret sharing scheme defined on a communication network. In 2001, Montgomery [17] introduced the *r-dynamic proper k-coloring* of a graph G as a proper k-coloring $c : V(G) \to \{0, \dots, k-1\}$ such that

$$|c(N_G(v))| \geq \min\{r, \deg_G(v)\}, \tag{1.1}$$

for every vertex $v \in V(G)$. Here, $N_G(v)$ and $\deg_G(v)$ denote, respectively, the neighborhood and the degree of the vertex v. The problem of deciding whether a given graph has an r-dynamic proper k-coloring is NP-complete [18], whenever $2 \leq r < k$. It is indeed harder than the classical coloring problem, which results for $r = 1$, and is a well known NP-complete problem, for $k > 2$. In this regard, even the classical 3-colorability is polynomially solvable for graphs with maximum degree at most three, and the 2-dynamic 3-colorability remains NP-complete for planar bipartite graphs with maximum degree at most three and arbitrarily high girth [18].

Every r-dynamic k-proper coloring of a graph G describes a distribution of pieces of information in any given $(k, r+1)$-threshold secret sharing scheme defined on the communication network having G as its underlying graph, whenever $k \geq r+1$ [16]. This distribution makes possible that all the participants receive the maximum possible information about the original secret from the closest nodes after each round of communication. More precisely, condition (1.1) implies that, after the first round, each participant can either reconstruct the original secret or obtain a different secret share from each one of his/her neighbors. A second main question to answer here is the following.

Problem 2. *What is the minimum number of pieces of information in which the secret has to split to ensure condition (1.1)?*

This number coincides with the *r-dynamic chromatic number* $\chi_r(G)$, which is the minimum positive integer k for which an r-dynamic proper k-coloring of the graph G exists. (The case $r = 1$ refers to the classical chromatic number $\chi(G)$.) Determining this number constitutes the *dynamic chromatic problem*. (The case $r = 1$ refers to the classical chromatic problem.) The case $r \geq 2$ has already been solved for distinct families of graphs [19–27]. One may also find some papers studying how the dynamic chromatic number changes by including new vertices in the graph under consideration [28–33]. (For a recent survey on the topic, we refer to [34].)

All the mentioned papers can, therefore, be reinterpreted as dealing with Problem 2. However, in spite of the wide amount of papers on Montgomery's dynamic coloring, its interpretation as an optimal allocation of pieces of information has only been explicitly considered in [16], for extended neighborhood coronas, and, too superficially, in [35], for triangle-free graphs and sparse random graphs. Even more, Problem 1 has been solved only for extended neighborhood coronas [16]. More specifically, two rounds of communication have been proved to be enough so that all the participants in any extended neighborhood corona can reconstruct the secret under consideration in the corresponding communication network.

Similarly to Problem 2, it is interesting to study the behaviour of Problem 1 when new vertices are included in the graph under consideration. This paper delves into this aspect for both Problems 1 and 2, in case of dealing with degree splitting graphs. Recall here that, if G is a graph of set of vertices $V(G) = \{v_1, \ldots, v_n\}$, and $V_k(G) \subseteq V(G)$ denotes its subset of vertices of degree k for all $k > 1$, then the *degree splitting graph* [36] (from here on, DSG) of G is the graph $DS(G)$ that results after connecting a new vertex to all those vertices in $V_k(G)$, whenever $|V_k(G)| > 1$. From here on, we denote this new vertex by w_k, and we say that it constitutes a *control node* of the initial network. Figure 2 illustrates this construction for the communication graph appearing in Figure 1. (The control nodes are highlighted in black color.)

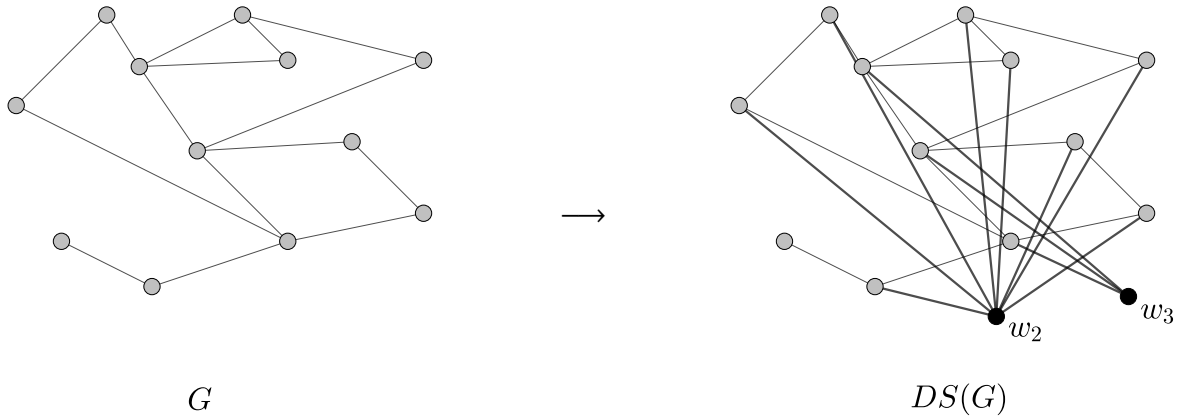

Figure 2. Construction of a DSG.

No previous study exists in the literature concerning the dynamic chromatic problem for DSGs. The main reason for having chosen this type of graphs in our study is that DSGs maintain or improve the fairness of any given secret sharing scheme based on a communication network, by avoiding dishonesty. Recall here that a secret sharing scheme is fair if all the participants recover the original secret at the same time. Of course, the more regular the communication network is, the fairer the secret sharing scheme can be. But, even in the regular case, this fairness cannot be ensured in case there are dishonest participants who receive secret shares from the honest ones, but either do not share their own pieces of information, or share fake ones. To avoid this dishonesty, one can add control nodes connecting and supervising all those participants with a similar influence in the network. DSGs constitute a valuable alternative to this end, where control nodes are the new added vertices. Note that the DSG of any regular graph has diameter at most two. Hence, at most two rounds of communication are required so that all the participants can reconstruct the secret in the DSG of any regular communication network.

From here on, we assume that control nodes also receive secret shares so that condition (1.1) holds. So, we are interested in solving Problem 2 for DSGs. Even more, we assume that control nodes act in all the rounds of communication of the scheme, in exactly the same way as the rest of participants. We can distinguish whether control nodes are also participants of the scheme, or not. (This distinction is further clarified in Section 2.) In the affirmative case, we are interested in answering Problem 1 for any $(\chi_r(\mathrm{DS}(G)), r+1)$-threshold secret sharing scheme based on the DSG of a graph G, whenever $\chi_r(\mathrm{DS}(G)) \geq r+1$. In the negative case, we are interested in solving the following alternative question, whose solution is less than or equal to that of Problem 1 for both graphs G and $\mathrm{DS}(G)$.

Problem 3. *What is the minimum number of rounds of communication that is necessary so that all the participants, except for the control nodes, can recover the secret in a $(\chi_r(\mathrm{DS}(G)), r+1)$-threshold secret sharing scheme based on the DSG of a communication network G?*

1.1. Our contributions

In this paper, we solve Problem 2, and hence, the dynamic chromatic problem, for DSGs of regular graphs (Proposition 7) by determining the relationship among the dynamic chromatic number of a regular graph and that of its DSG. We illustrate this by solving the dynamic chromatic problem for DSGs of two families of regular graphs: cycles (Theorem 8) and cocktail party graphs (Theorem 10). With respect to the latter, we also correct (Lemma 9) a previous result on the classical dynamic chromatic problem. All our constructive solutions describe explicitly dynamic colorings on the graphs under consideration, and hence, optimal secret share distributions. It allows the establishment of the minimum number of rounds of communications that are necessary so that all the participants of a communication network defined on such graphs can reconstruct the secret. To this end, we distinguish whether the control nodes described by any DSG are also participants of the scheme (Problem 1), or not (Problem 3). In Section 3, we solve both problems for DSGs of cycles and cocktail party graphs.

Concerning DSGs of non-regular graphs, we solve Problems 1–3 for the DSGs of book graphs (Proposition 11), comb graphs (Proposition 12), fan graphs (Theorems 14 and 15) and jellyfish graphs (Propositions 16 and 17). In addition, we establish a new lower bound for the dynamic chromatic number of the DSGs of any non-regular graph (Lemma 18). We use this bound to solve Problems 1–3 for the DSGs of windmill graphs (Proposition 19) and barbell graphs (Proposition 20). Table 2 summarizes all our results concerning Problems 1 and 3.

2. Preliminaries

This section deals with some preliminary concepts and results on graph theory that are used throughout the paper. We refer the reader to the manuscript [37] for more details about this topic.

All the communication networks throughout the paper are assumed to be finite and simple graphs. A *graph* $G = (V(G), E(G))$ is formed by a set of vertices $V(G)$ and a set of edges $E(G)$ so that each edge joins two vertices, which are then said to be *adjacent*. The graph G is *complete* if all their vertices are pairwise adjacent. The complete graph with n vertices is denoted K_n. Further, a graph $H = (V(H), E(H))$ is a *subgraph* of G if $V(H) \subseteq V(G)$ and $E(H) \subseteq E(G)$. It is *induced* if $E(H)$ is formed by all those edges in $E(G)$ connecting vertices of $V(H)$. It is an *n-clique* if it coincides with K_n.

The cardinalities of the sets $V(G)$ and $E(G)$ constitute, respectively, the *order* and the *size* of the graph G. The latter is *finite* if both its order and its size are finite. From now on, let vw denote the edge formed by two adjacent vertices $v, w \in V(G)$. It is a *loop* if $v = w$. A graph is *simple* if it does not contain loops. All the graphs in this paper are finite and simple.

The *neighborhood* of a vertex $v \in V(G)$ is the subset $N_G(v) \subset V(G)$ of vertices that are adjacent to v. The cardinality of this set is the *degree* $\deg_G(v)$ of such vertex. If $\deg_G(v) = 1$, then the vertex v is said to be *pendant*. The maximum degree in G is denoted $\Delta(G)$. A graph is said to be *k-regular* (or simply, *regular*), if all its vertices have degree k.

A *path* between two vertices $v, w \in V(G)$ is any ordered sequence of $n > 2$ adjacent and pairwise distinct vertices $\langle\, v_0 = v, v_1, \ldots, v_{n-2}, v_{n-1} = w \,\rangle$ in $V(G)$. The minimum possible size of this path is the *distance* $d_G(u, v)$. The *diameter* $\operatorname{diam}(G)$ is the maximum distance between any two vertices in $V(G)$.

A path is a *cycle* if its initial and final vertices coincide. If all the vertices of a cycle are joined to a new vertex, then we get a *wheel*. If we remove all the edges of the wheel that do not contain this new vertex, then we obtain a *star*. (Note that it is sometimes called a wheel network [38].) From here on, we denote, respectively, the cycle and the wheel of order n by C_n and W_n. Note here that $\mathrm{DS}(C_n) = W_n$.

Paths, cycles, wheels (stars) and complete graphs are four commonly used graphs in small communication networks and constitute fundamental subgraphs for more complex networks [38]. In this regard, we study in the subsequent sections the DSGs of the following families of graphs, which are based on the mentioned four graphs, and are usually considered in the literature as a first attempt to study more complex communication networks: cocktail party graphs [39], book graphs [40], comb graphs [41], fan graphs [39], jellyfish graphs [42], windmill graphs [43] and barbell graphs [44]. Let us recall here how all of them are defined. To this end, let m and n be two positive integers.

- The *cocktail party graph* Cp_n, with $n > 1$, is described so that $V(\mathrm{Cp}_n) = \{v_0, \ldots, v_{2n-1}\}$ and $E(\mathrm{Cp}_n) = \{v_i v_j \colon\ 0 \le i, j < 2n,\ i \not\equiv j \,(\mathrm{mod}\, n)\}$.
- The *book graph* B_n is formed by n copies of the cycle C_4, sharing between all of them a unique, common edge.
- The *comb graph* Cb_n, with $n > 2$, is the graph arising from connecting n new vertices $v'_0, \ldots, v'_{n-1}$ to the path $P_n = \langle\, v_0, \ldots, v_{n-1} \,\rangle$ by means of the edges $v_i v'_i$, with $0 \le i < n$.
- The *fan graph* $F_{m,n}$ is the graph arising from connecting m new vertices to all the vertices of the path P_n.
- The *jellyfish* graph $J_{m,n}$ arises from the cycle $C_4 = \langle\, v_0, v_1, v_2, v_3 \,\rangle$ after joining the vertices v_0 and v_2 with an edge, connecting m new pendant vertices to v_1, and n new pendant vertices to v_3.

- The *windmill graph* $\mathrm{Wd}_{m,n}$, with $m, n \geq 2$, is the graph formed by m copies of the complete graph K_n, sharing between all of them a unique, common vertex.
- The *barbell graph* Ba_n, with $n > 2$, is the graph formed by two copies of the complete graph K_n so that they are linked by an edge connecting one vertex of each copy. This edge is called the *bridge* of the graph Ba_n.

Figures 3 and 4 illustrate, respectively, all of these graphs and their respective DSGs. (In Figure 4, control nodes are highlighted in black color.)

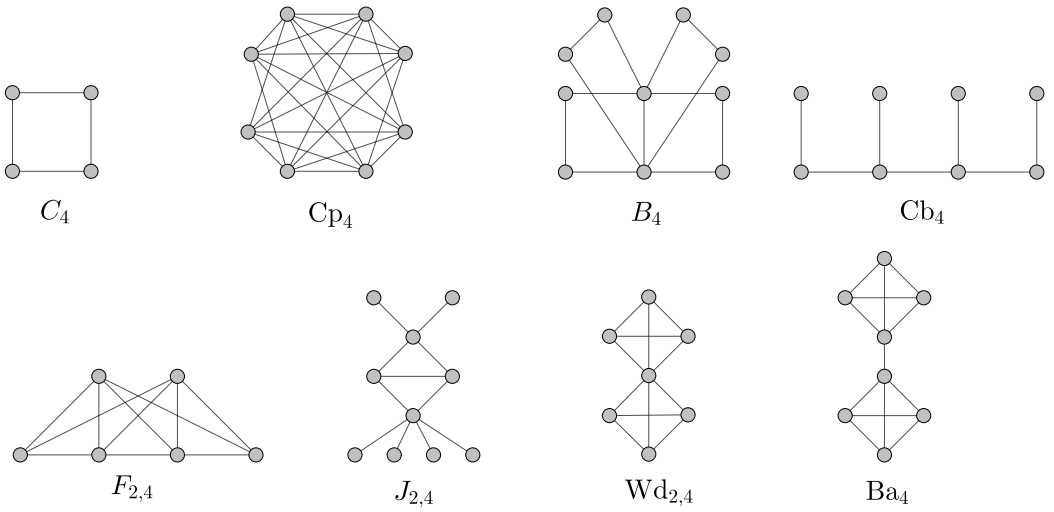

Figure 3. Examples of graphs.

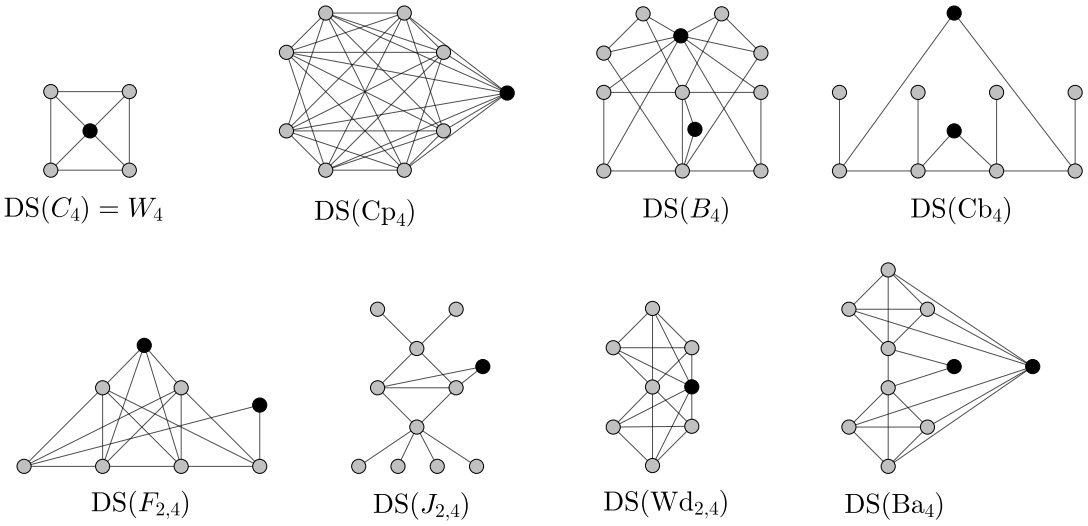

Figure 4. DSGs of the graphs in Figure 3.

The diameters of these graphs are indicated in Table 1. Note herein that, except for fan graphs, the diameter of each DSG under consideration is smaller than the diameter of the corresponding graph. This exception is due to the fact that the distance between any two distinct control nodes in a DSG is at least three. It increases the diameter of some non-regular graphs having diameter two, as in fan graphs. In practice, this increment is a disadvantage only if control nodes are also participants of the secret sharing scheme under consideration, instead of being only added for supervising participants with a similar influence in the communication network. This is the main reason of distinguishing both Problems 1 and 3 in the introductory section. Based on this fact, the last column in Table 1 refers to the maximum distance between any two vertices in the DSG under consideration, whenever at least one of these two vertices is not a control node. We have denoted this maximum distance by $\mathrm{diam}^*(\mathrm{DS}(G))$, where G is the graph under study.

Table 1. Diameters of graphs and their corresponding DSGs.

G	$\mathrm{diam}(G)$	$\mathrm{diam}(\mathrm{DS}(G))$	$\mathrm{diam}^*(\mathrm{DS}(G))$
C_n	$\lfloor n/2 \rfloor$	2	2
Cp_n	2	2	2
B_n	3	3	2
Cb_n	$n+1$	$\begin{cases} 4, & \text{if } n \in \{3,4\}, \\ 5, & \text{otherwise.} \end{cases}$	$\begin{cases} 4, & \text{if } n \in \{3,4\}, \\ 5, & \text{otherwise.} \end{cases}$
$F_{m,n}$	2	3	2
$J_{m,n}$	4	4	4
$\mathrm{Wd}_{m,n}$	2	2	2
Ba_n	3	3	2

The values appearing in the third and fourth columns in Table 1 constitute respective upper bounds for the solutions of Problem 1 and 3. The exact solutions are established throughout the paper, and collected in the conclusion section (see Table 2). Concerning Problem 2, the following known results are useful for our study.

Lemma 1. *[25] Let G be a finite simple graph and let r be a positive integer. Then,*

$$\chi_r(G) \geq \min\{r, \Delta(G)\} + 1.$$

Moreover, $\chi_r(G) \leq \chi_{\Delta(G)}(G)$.

Lemma 2. *[26] Let $n > 2$ and r be two positive integers. Then, $\chi_r(K_n) = n$ and*

$$\chi_r(C_n) = \begin{cases} 2, & \text{if } r = 1 \text{ and } n \text{ is even}, \\ 3, & \text{if } \begin{cases} r = 1 \text{ and } n \text{ is odd}, \\ r > 1 \text{ and } n \equiv 0 \,(\mathrm{mod}\, 3), \end{cases} \\ 4, & \text{if } r > 1 \text{ and } 5 \neq n \not\equiv 0 \,(\mathrm{mod}\, 3), \\ 5, & \text{otherwise}. \end{cases}$$

Lemma 3. *[21] Let r and $m, n \geq 2$ be three positive integers. Then:*

a) $\chi_r(\mathrm{Wd}_{m,n}) = \begin{cases} n, & \text{if } 1 \leq r < n, \\ r+1, & \text{if } n \leq r \leq m(n-1), \\ m(n-1)+1, & \text{otherwise.} \end{cases}$

b) If $n > 2$, then $\chi_r(\mathrm{Ba}_n) = \begin{cases} n, & \text{if } 1 \leq r < n, \\ n+1, & \text{otherwise.} \end{cases}$

Proposition 4. *[31] Let m, n and r be three positive integers such that $n > 2$. Then,*

$$\chi_r(F_{m,n}) = \begin{cases} 3, & \text{if } r \in \{1,2\}, \\ 2r-1, & \text{if } 3 \leq r \leq \min\{m+1, n\}, \\ n+r-1, & \text{if } n < r \leq m+1, \\ m+r, & \text{if } \max\{3, m+1\} \leq r \leq n, \\ m+n, & \text{if } r \geq \max\{m+1, n\}. \end{cases}$$

The following lemma solves the dynamic chromatic problem for a comb graph.

Lemma 5. *If $n > 2$, then* $\chi_r(\mathrm{Cb}_n) = \min\{4, r+1\}$.

Proof. Let $\alpha = \min\{4, r+1\}$. Since $\Delta(\mathrm{Cb}_n) = 3$, Lemma 1 implies that $\chi_r(\mathrm{Cb}_n) \geq \alpha$. In order to prove that this lower bound is tight, let Cb_n be the comb graph that results after connecting n new vertices $v'_0, \ldots, v'_{n-1}$ to the path $P_n = \langle v_0, \ldots, v_{n-1} \rangle$ by means of the edges $v_i v'_i$ for all $i < n$. Then, it is enough to consider the r-dynamic proper α-coloring c such that $c(v_i) = i \bmod \alpha$, and

$$c(v'_i) = \begin{cases} (i+1) \bmod \alpha, & \text{if } r = 1, \\ (i+2) \bmod \alpha, & \text{otherwise.} \end{cases}$$

for every positive integer $i < n$. (Figure 5 illustrates the case $n = 4$.) □

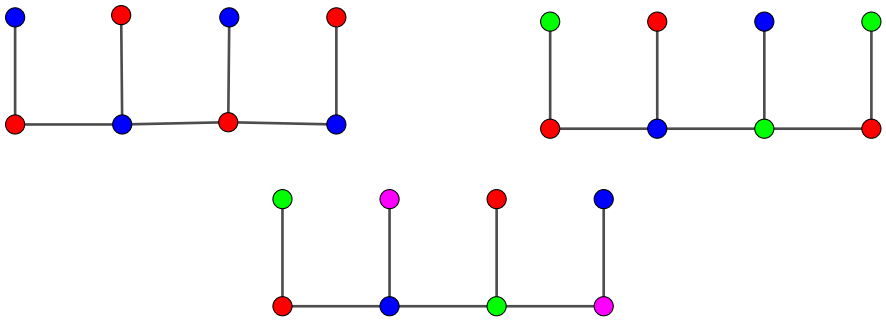

Figure 5. r-dynamic colorings of Cb_4, for $r = 1$ (left), $r = 2$ (right) and $r \geq 3$ (down).

Concerning the theory of DSGs, the following result establishes the relationship between the chromatic numbers of a finite simple graph and its DSG.

Lemma 6. *[45] Let G be a finite simple graph. If G is regular, then* $\chi(\mathrm{DS}(G)) = \chi(G) + 1$. *Otherwise,* $\chi(\mathrm{DS}(G)) \in \{\chi(G), \chi(G)+1\}$.

3. The regular case

In the introductory section, we have already remarked that the DSG of a regular graph requires at most two rounds of communication so that every participant of a secret share scheme defined on this type of graph can recover the secret under consideration. In this section, we prove that this upper bound is not tight. Previously, it is required to solve Problem 2 for the DSG of any k-regular graph G of order n, with vertex set $V(G) = \{v_0, \ldots, v_{n-1}\}$, so that $V(\mathrm{DS}(G)) = V(G) \cup \{w_k\}$. That is, we only add a control node w_k supervising all the participants of the communication network. The following result establishes the relationship between the dynamic chromatic numbers of both graphs G and $\mathrm{DS}(G)$.

Proposition 7. *Let G be a k-regular graph of order n. Then,*

$$\chi_r(\mathrm{DS}(G)) = \begin{cases} \chi(G) + 1, & \text{if } r = 1, \\ \max\{r, \chi_{r-1}(G)\} + 1, & \text{if } 1 < r \leq n, \\ n + 1, & \text{otherwise.} \end{cases}$$

Proof. From Lemma 1, it is enough to prove the case $r \leq \Delta(\mathrm{DS}(G)) = n$. (Note here that $\max\{n, \chi_{n-1}(G)\} + 1 = n + 1$, because $\chi_{n-1}(G) \leq n$.) Particularly, the case $r = 1$ follows from Lemma 6. So, we focus on the case $1 < r \leq n$. To this end, let $\alpha = \max\{r, \chi_{r-1}(G)\}$.

Since the vertex w_k is connected to every vertex in G, every proper coloring of $\mathrm{DS}(G)$ requires an exclusive color for w_k. As a consequence, the removal of this control node from $\mathrm{DS}(G)$ implies readily that every r-dynamic proper $\chi_r(\mathrm{DS}(G))$-coloring of $\mathrm{DS}(G)$ gives rise to an $(r-1)$-dynamic proper $(\chi_r(\mathrm{DS}(G)) - 1)$-coloring of G. Hence, $\chi_{r-1}(G) \leq \chi_r(\mathrm{DS}(G)) - 1$. Furthermore, since $n = \Delta(\mathrm{DS}(G))$, Lemma 1 implies that $\chi_r(\mathrm{DS}(G)) \geq r + 1$. As a consequence, $\chi_r(\mathrm{DS}(G)) \geq \alpha + 1$.

In order to prove the reciprocal, let $\overline{c}$ be an $(r-1)$-dynamic proper α-coloring of G, and let c be the proper coloring of $\mathrm{DS}(G)$ such that $c(v_i) = \overline{c}(v_i)$ for all $i \leq n$, and $c(w_k) = \alpha + 1$. This map c is an r-dynamic proper $(\alpha + 1)$-coloring of $\mathrm{DS}(G)$ because the following assertions hold from Lemma 1.

a) For each $i \leq n$, we have that $|c(N_{\mathrm{DS}(G)}(v_i))| = |c(N_G(v_i))| + 1 \geq \min\{r - 1, \deg_G(v_i)\} + 1 = \min\{r, \deg_{\mathrm{DS}(G)}(v_i)\}$.

b) $|c(N_{\mathrm{DS}(G)}(w_k))| = \alpha = \max\{r, \chi_{r-1}(G)\} \geq \max\{r, \min\{r - 1, \Delta(G)\} + 1\} = \max\{r, \min\{r, k + 1\}\} = r = \min\{r, n\} = \min\{r, \deg_{\mathrm{DS}(G)}(w_k)\}$.

Hence, $\chi_r(\mathrm{DS}(G)) \leq \alpha + 1$, and the result holds. □

The extra color for the control node implies that the solutions of both Problems 1 and 3 for any $(k, r+1)$-threshold secret sharing scheme, with $k \geq r + 1$, which is based on the DSG of any regular communication network G, coincide for each of them with the solution of Problem 1 for any $(k-1, r)$-threshold secret sharing scheme based on G. That is, the minimum number of rounds of communication that are necessary so that all the participants in a regular communication network can recover the secret coincides with that associated with its DSG, once the threshold of the scheme is increased by one unity. Moreover, it does not matter whether the control node is also a participant of the scheme, or not. It is an advantage, because the inclusion of this control node prevents the appearance of dishonest participants, without thereby worsening the flow of communication.

We illustrate Proposition 7 by solving the dynamic coloring problem (and hence, Problem 2) for wheels and DSGs of cocktail party graphs. (Note that the 2-dynamic chromatic number of a wheel was already established by Kaliraj et al. [24].)

Theorem 8. *Let r and $n > 2$ be two positive integers. Then,*

$$\chi_r(W_{n+1}) = \begin{cases} 3, & \text{if } r \in \{1,2\} \text{ and } n \text{ is even}, \\ 4, & \text{if } \begin{cases} r \in \{1,2\} \text{ and } n \text{ is odd}, \\ r = 3 \text{ and } n \equiv 0 \pmod 3), \end{cases} \\ 5, & \text{if } \begin{cases} r = 3 \text{ and } 5 \neq n \not\equiv 0 \pmod 3), \\ r = 4 \leq n \neq 5, \end{cases} \\ 6, & \text{if } r \in \{3,4\} \text{ and } n = 5, \\ r+1, & \text{if } 5 \leq r \leq n, \\ n+1, & \text{otherwise}. \end{cases}$$

Proof. The result holds readily from Lemma 2 and Proposition 7 once it is observed that every cycle is 2-regular and $\mathrm{DS}(C_n) = W_{n+1}$ for all $n > 2$. □

Figure 6 illustrates the previous result, for different values of r and n.

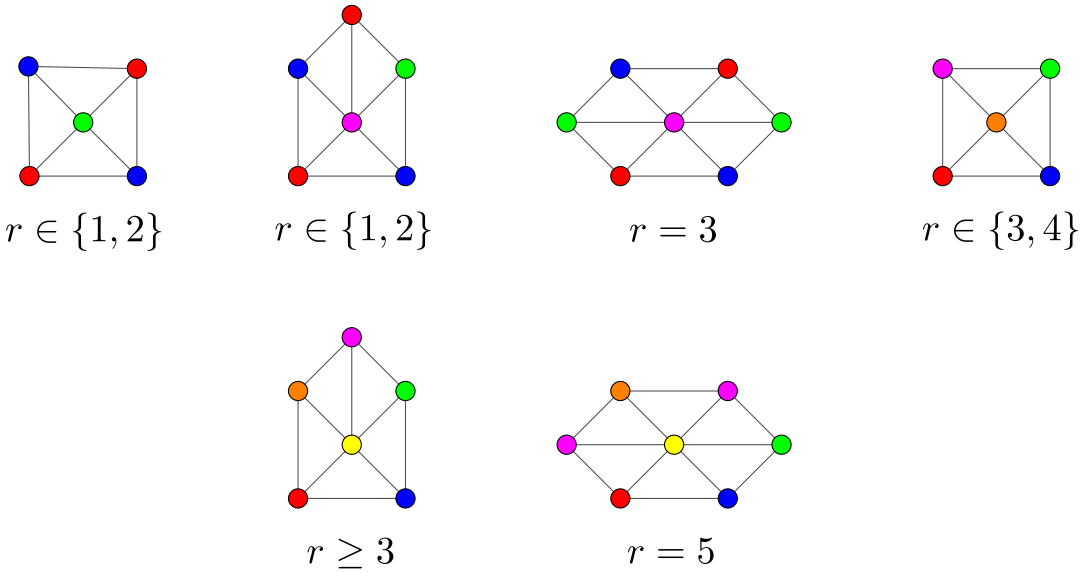

Figure 6. r-dynamic colorings of wheels.

Except for the control node, every participant in a wheel communication network receives information from three distinct neighbors. Thus, based on the described dynamic coloring, only those cases in which $r \leq 3$ give rise to exactly one round of communication as a solution of both Problems 1 and 3. The remaining cases require two rounds of communications for both problems.

We focus now on the DSG of a cocktail party graph Cp_n of vertex set $V(\mathrm{Cp}_n) = \{v_0, \ldots, v_{2n-1}\}$ and edge set $E(\mathrm{Cp}_n) = \{v_i v_j \colon 0 \leq i, j < 2n,\ i \not\equiv j \,(\mathrm{mod}\, n)\}$. First, the following lemma corrects a previous result concerning the r-dynamic chromatic number of any cocktail party graph, which was not accurate (see [21, Theorem 4.2]).

Lemma 9. *Let r and $n > 1$ be two positive integers. Then,*

$$\chi_r(\mathrm{Cp}_n) = \begin{cases} n, & \text{if } r < n, \\ r + 2, & \text{if } n \leq r \leq 2n - 2, \\ 2n, & \text{otherwise.} \end{cases}$$

Proof. From Lemma 1, it is enough to prove the case $r \leq \Delta(\mathrm{Cp}_n) = 2n - 2$. Since Cp_n contains an n-clique, we have that $\chi_r(\mathrm{Cp}_n) \geq n$. This lower bound is tight for all $r < n$ because of the r-dynamic n-proper coloring graph c of Cp_n that is described so that $c(v_i) = c(v_{i+n}) = i$ for all $i < n$. Further, if $n \leq r \leq 2n - 2 = \Delta(\mathrm{Cp}_n)$, then Lemma 1 implies that $\chi_r(\mathrm{Cp}_n) \geq r + 1$. However, this lower bound is not reached. Otherwise, since $N(v_i) = N(v_{i+n})$ for all $i < n$, Condition (1.1) implies that both vertices v_i and v_{i+n} would be equally colored for all $i < n$. But then, $r + 1 \leq n$, which is a contradiction. So, $\chi_r(\mathrm{Cp}_n) \geq r + 2$. This new lower bound is reached because of the r-dynamic $(r + 2)$-proper coloring graph c of the graph Cp_n that is described so that

$$c(v_i) = \begin{cases} i, & \text{if either } i < n \text{ or } i \geq 3n - r - 2, \\ i - n, & \text{otherwise.} \end{cases}$$

□

Figure 8 illustrates the dynamic coloring described in the previous proof, for $n = 4$.

Figure 7. r-dynamic colorings of Cp_4, for $r = 3$ (left) and $r = 4$ (right).

Since the graph Cp_n is $(2n - 2)$-regular, the following result holds readily from Lemma 9 and Proposition 7.

Theorem 10. *Let r and $n > 1$ be two positive integers. Then,*

$$\chi_r(\mathrm{DS}(\mathrm{Cp}_n)) = \begin{cases} n + 1, & \text{if } 1 \leq r \leq n, \\ r + 2, & \text{if } n < r < 2n, \\ 2n + 1, & \text{otherwise.} \end{cases}$$

Figure 8 illustrates the previous result for $n = 4$.

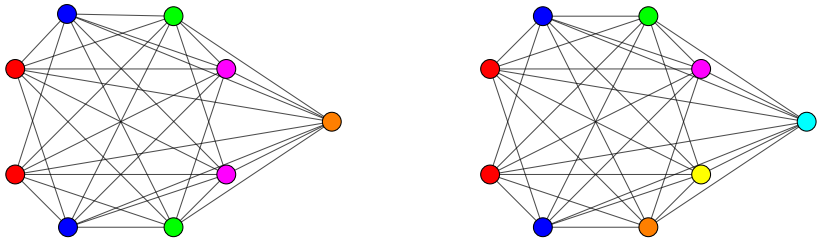

Figure 8. r-dynamic colorings of $\mathrm{DS}(\mathrm{Cp}_4)$, for $r = 4$ (left) and $r = 5$ (right).

Except for the control node, every participant in the DSG of a cocktail party communication network Cp_n receives information from $2n$ distinct neighbors. Thus, based on the described dynamic coloring, only those cases in which $r < 2n$ give rise to exactly one round of communication as a solution of both Problems 1 and 3. The remaining case $r = 2n$ requires two rounds of communications for both problems.

4. The non-regular case

In practice, the direct application of Condition (1.1) and Lemma 1 constitutes the most common way to start solving the dynamic coloring problem of a given graph. We illustrate this fact by focusing in this section on the DSGs of book, comb, fan and jellyfish graphs.

4.1. Degree splitting of book graphs

For each non-negative integer $i < n$, let $\{v_0, v_1, v_2^i, v_3^i\}$ be the set of vertices of the $(i+1)^{\text{th}}$ copy of the cycle C_4 within the book graph B_n. Its set of edges is $\{v_0v_1,\ v_1v_2^i,\ v_2^iv_3^i,\ v_0v_3^i\}$. The edge v_0v_1 is the unique common edge shared by all these copies. Moreover, let w_2 and w_{n+1} be the additional vertices that are respectively joined to the sets of vertices $V_2(B_n) = \{v_2^i, v_3^i\colon\ 0 \le i < n\}$ and $V_{n-1}(B_n) = \{v_0, v_1\}$ in order to get $\mathrm{DS}(B_n)$.

Proposition 11. *Let $n \ge 2$ be a positive integer. Then,*

$$\chi_r(\mathrm{DS}(B_n)) = \begin{cases} 3, & \text{if } r \in \{1,2\}, \\ r+3, & \text{if } 3 \le r \le 2n, \\ 2n+3, & \text{otherwise}. \end{cases}$$

Proof. Lemma 1 enables us to focus on the case $r \le \Delta(B_n) = 2n$. Let us study each case separately.

First, we consider the case $r \in \{1,2\}$. Since the induced subgraph of B_n with set of vertices $\{v_0,\ v_1,\ w_{n+1}\}$ constitutes a 3-clique, it must be $3 \le \chi_r(\mathrm{DS}(B_n))$. This lower bound is tight because of the r-dynamic proper 3-coloring c of $\mathrm{DS}(B_n)$ that is described so that $c(w_2) = c(w_{n+1}) = 2$ and, for each non-negative integer $i < n$, it is $c(v_2^i) = c(v_0) = 0$ and $c(v_3^i) = c(v_1) = 1$.

Now, we suppose that $3 \leq r \leq 2n$. From Condition (1.1) applied to the vertex w_{n-1}, every r-dynamic proper coloring c of the DSG $\mathrm{DS}(B_n)$ requires r distinct colors for coloring the set of vertices $V_2(B_n)$. In addition, the set of vertices $\{v_0, v_1, w_2\}$ requires three extra distinct colors because of the adjacency of the graph together with the fact that $r \geq 3 = \deg_{\mathrm{DS}(B_n)}(v_j^i)$ for all $j \in \{2, 3\}$ and $0 \leq i < n$. Hence, $r + 3 \leq \chi_r(\mathrm{DS}(B_n))$. This lower bound is tight because of the r-dynamic proper $(r + 3)$-coloring c of $\mathrm{DS}(B_n)$ that is described so that $c(v_0) = r$, $c(v_1) = r + 1$, $c(w_2) = c(w_{n+1}) = r + 2$ and $c(v_j^i) = (2i + j - 2) \bmod r$ for all $j \in \{2, 3\}$ and $0 \leq i < n$. □

Figure 9 illustrates the dynamic coloring described in the previous proof, for $n = 4$.

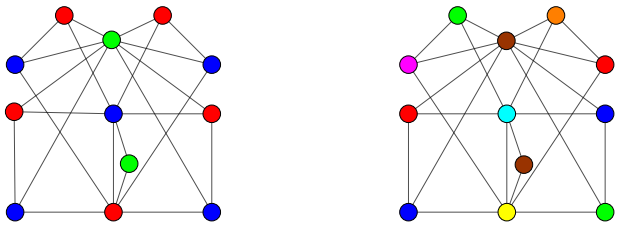

Figure 9. r-dynamic colorings of B_4, for $r \in \{1, 2\}$ (left) and $r = 5$ (right).

Based on the described dynamic coloring, since $\deg_{\mathrm{DS}(B_n)}(w_2) = 2$, only the case $r \in \{1, 2\}$ gives rise to exactly one round of communication as a solution of Problem 1. The remaining cases requires two rounds of communications for this problem. Similarly to the regular case, since both control nodes are colored with the same extra color, it is readily verified that Problem 3 for $\mathrm{DS}(B_n)$ has exactly the same solution as Problem 1. Thus, it does not matter whether the control nodes are participants of the scheme or not.

4.2. Degree splitting of comb graphs

Let Cb_n, with $n > 2$, be the comb graph that results after connecting n new vertices $v'_0, \ldots, v'_{n-1}$ to the path $P_n = \langle v_0, \ldots, v_{n-1} \rangle$ by means of the edges $v_i v'_i$ for all $i < n$. Moreover, let w_2 be the additional vertex that is joined to the set of vertices $V_2(\mathrm{Cb}_n) = \{v_0, v_{n-1}\}$ to get the graph $\mathrm{DS}(\mathrm{Cb}_n)$. Similarly, if $n > 3$, then let w_3 be the additional vertex associated to the set of vertices $V_3(\mathrm{Cb}_n) = \{v_1, \ldots, v_{n-2}\}$. In particular,

$$\Delta(\mathrm{DS}(\mathrm{Cb}_3)) = \begin{cases} 3, & \text{if } n = 3, \\ 4, & \text{if } n \in \{4, 5, 6\}, \\ n - 2, & \text{otherwise.} \end{cases}$$

The following result holds.

Proposition 12. *Let $n > 2$ be a positive integer. Then,*

$$\chi_r(\mathrm{DS}(\mathrm{Cb}_n)) = \begin{cases} 2, & \text{if } (r,n) = (1,3), \\ 3, & \text{if } \begin{cases} r = 1 \text{ and } n > 3, \\ r = 2, \end{cases} \\ 4, & \text{if } \begin{cases} r = 3, \\ r > 3 = n, \end{cases} \\ 5, & \text{if } \begin{cases} r = 4 \text{ and } n > 3, \\ r > 4 \text{ and } n \in \{4,5,6\}, \end{cases} \\ r+1, & \text{if } 4 < r \leq n-2, \\ n-1, & \text{otherwise.} \end{cases}$$

Proof. Lemma 1 enables one to focus on the case $r \leq \Delta(\mathrm{DS}(\mathrm{Cb}_n))$. The following study of cases arises.

- **Case** $r = 1$.
  Lemma 1 implies that $2 \leq \chi(\mathrm{DS}(\mathrm{Cb}_3))$. In addition, $3 \leq \chi(\mathrm{DS}(\mathrm{Cb}_n))$ for all $n > 3$, because the set of vertices $\{v_1, v_2, w_3\}$ induces a 3-clique in $\mathrm{DS}(\mathrm{Cb}_n)$. To see that both lower bounds are tight, it is enough to consider the proper coloring c of Cb_n described in the proof of Lemma 5, together with either $c(w_2) = 1$, if $n = 3$, or $c(w_2) = c(w_3) = 2$, if $n > 3$. (Figure 10 illustrates the case $n \in \{3,4\}$.)

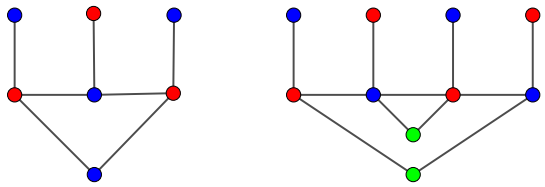

Figure 10. Dynamic proper coloring of $\mathrm{DS}(\mathrm{Cb}_3)$ and $\mathrm{DS}(\mathrm{Cb}_4)$.

- **Case** $r \in \{2,3\}$.
  Lemma 1 implies that $r + 1 \leq \chi_r(\mathrm{DS}(\mathrm{Cb}_n))$. Figure 12 (left) illustrates that this lower bound is reached for $r = n = 3$. For the remaining cases, it is enough to consider the r-dynamic proper $(r+1)$-coloring that is described so that $c(w_3) = r$ (only if $n > 3$),

$$c(w_2) = \begin{cases} 1, & \text{if } r = 2, \\ 3, & \text{if } r = 3. \end{cases}$$

  and, for each non-negative integer $i < n$, we have that

$$c(v_i) = \begin{cases} i \bmod 2, & \text{if } i < n-1, \\ 2, & \text{if } i = n-1. \end{cases}$$

and

$$c(v'_i) = \begin{cases} 2, & \text{if } i < n-1, \\ c(v_{n-3}), & \text{if } i = n-1. \end{cases}$$

(Figure 11 (right) illustrates the case $r = 2$ and $n \in \{3, 4\}$, while Figure 12 (right) illustrates the case $(r, n) = (3, 4)$.)

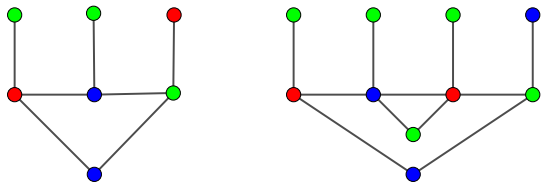

Figure 11. 2-dynamic proper 4-colorings of $\mathrm{DS}(\mathrm{Cb}_3)$ and $\mathrm{DS}(\mathrm{Cb}_4)$.

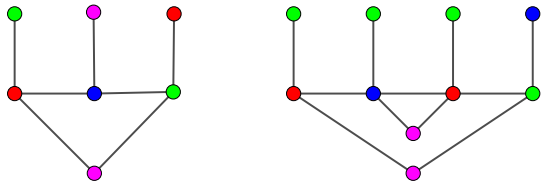

Figure 12. 3-dynamic proper 4-colorings of $\mathrm{DS}(\mathrm{Cb}_3)$ and $\mathrm{DS}(\mathrm{Cb}_4)$.

- **Case** $r = 4$ and $n > 3$.
  Lemma 1 implies that $5 \leq \chi_4(\mathrm{DS}(\mathrm{Cb}_n))$. If $n \neq 1 \pmod 4$, this lower bound is reached because of the proper coloring c of Cb_n described in the proof of Lemma 5, together with $c(w_2) = c(w_3) = 4$. Otherwise, if $n = 1 \pmod 4$, it is enough to consider the same proper coloring, except that we interchange the colors of both vertices v_{n-1} and v'_{n-2}. (Figure 13 illustrates the case $n \in \{4, 5\}$.)

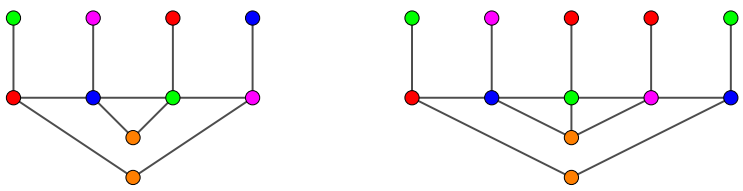

Figure 13. 4-dynamic proper 5-colorings of $\mathrm{DS}(\mathrm{Cb}_4)$ and $\mathrm{DS}(\mathrm{Cb}_5)$.

- **Case** $4 < r \leq n - 2$.
  Lemma 1 implies that $r + 1 \leq \chi_r(\mathrm{DS}(\mathrm{Cb}_n))$. If $n \not\equiv 1 \pmod r$, then this lower bound is tight because of the r-dynamic proper coloring that is described so that $c(w_2) = c(w_3) = r$, and, for each positive integer $i < n$, we have that $c(v_i) = i \pmod r$ and $c(v'_i) = (i + r) \pmod r$. Otherwise, if $n = 1 \pmod r$, it is enough to consider the same proper coloring, except that we interchange the colors of both vertices v_{n-1} and v'_{n-2}. (Figures 14 and 15 illustrate, respectively, the cases $(r, n) = (5, 7)$ and $(r, n) = (5, 11)$.)

□

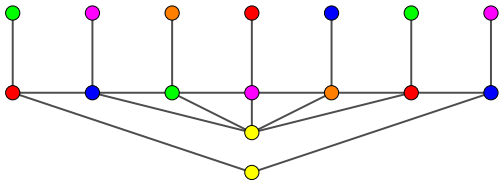

Figure 14. 5-dynamic proper 6-coloring of $\mathrm{DS}(\mathrm{Cb}_7)$.

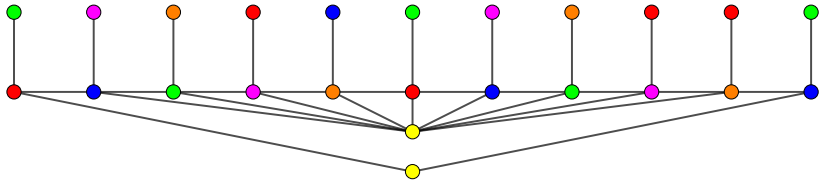

Figure 15. 5-dynamic proper 6-coloring of $\mathrm{DS}(\mathrm{Cb}_{11})$.

The existence of pendant vertices in any comb graph implies that only the case $r = 1$ gives rise to exactly one round of communication as a solution for both Problems 1 and 3. Moreover, it is readily verified from the described dynamic coloring that, in both problems, two rounds of communication are required for $r \in \{2, 3\}$, and three rounds for the remaining cases. Again, since both control nodes are colored with the same extra color, it does not matter whether the control nodes are participants of the scheme or not.

4.3. Degree splitting of fan graphs

Let $m \in \{1, 2\}$ and $n > 2$ be two positive integers. We focus now on solving the dynamic coloring problem for the DSG of the fan graph $F_{m,n}$ of set of vertices $V(F_{m,n}) = \{u_0, u_{m-1}, v_0, \ldots, v_{n-1}\}$, which is associated to the path $P_n = \langle\, v_0, \ldots, v_{n-1} \,\rangle$. According to their degrees, these vertices are distributed into the following sets.

- The sets $V_n(F_{m,n}) = \{u_0, u_{m-1}, v_0, v_{n-1}\}$ and $V_{n+1}(F_{m,n}) = \{v_1, \ldots, v_{n-2}\}$, if $n = m + 1$.
- The sets $V_{n-1}(F_{m,n}) = \{v_0, v_{n-1}\}$ and $V_n(F_{m,n}) = \{u_0, u_{m-1}, v_1, \ldots, v_{n-2}, \}$, if $n = m + 2$.
- The sets $V_{m+1}(F_{m,n}) = \{v_0, v_{n-1}\}$, $V_{m+2}(F_{m,n}) = \{v_1, \ldots, v_{n-2}\}$ and $V_n(F_{m,n}) = \{u_0, u_{m-1}\}$, if $n \notin \{m + 1, m + 2\}$.

Each set $V_k(F_{m,n})$ for which $|V_k(F_{m,n})| > 1$ is associated to an additional vertex w_k to get the DSG $\mathrm{DS}(F_{m,n})$. A preliminary lemma is required to deal with the case $m = 1$.

Lemma 13. *Let n and r be two positive integers such that $4 \leq r \leq n$. Then,*

$$r + 2 \leq \chi_r(\mathrm{DS}(F_{1,n})).$$

Proof. Since $r \leq n$, Condition (1.1) implies that every r-dynamic proper coloring of the DSG $\mathrm{DS}(F_{1,n})$ requires r distinct colors for coloring the set of vertices $\{v_0, \ldots, v_{n-1}\}$, and hence, an $(r + 1)^{\text{th}}$ color is necessary for the vertex u_0. Moreover, since $\deg_{\mathrm{DS}(F_{1,n})}(v_i) = 4$ for all positive integer $i < n - 1$, an extra $(r + 2)^{\text{th}}$ color is required for the vertex w_3. □

The following result solves the dynamic coloring problem for the fan graph $F_{1,n}$.

Theorem 14. *Let $n > 2$ and r be two positive integers. Then,*

$$\chi_r(\mathrm{DS}(F_{1,n})) = \begin{cases} 3, & \text{if } \begin{cases} r = 1, \\ r = 2 \text{ and } n \text{ is even}, \end{cases} \\ 4, & \text{if } \begin{cases} r = 2 \text{ and } n \text{ is odd}, \\ r = 3 \text{ and } 4 < n \equiv 2 \,(\mathrm{mod}\, 3), \end{cases} \\ 5, & \text{if } \begin{cases} r = 3 \text{ and } \begin{cases} n \in \{3, 4\}, \\ 4 < n \not\equiv 2 \,(\mathrm{mod}\, 3), \end{cases} \\ (r, n) = (4, 3), \end{cases} \\ r + 2, & \text{if } 4 \leq r \leq n, \\ n + 2, & \text{otherwise}. \end{cases}$$

Proof. Lemma 1 enables us to focus on the case $r \leq \Delta(\mathrm{DS}(F_{1,n}))$. This maximum degree is 4, if $n = 3$, and it is n otherwise. The following study of cases arises.

- **Case** $r = 1$.
  Proposition 4 and Lemma 6 imply that $\chi(\mathrm{DS}(F_{1,n})) \in \{3, 4\}$. Thus, Figure 16 (left) illustrates that $\chi(\mathrm{DS}(F_{1,3})) = 3$. Moreover, $\chi(\mathrm{DS}(F_{1,n})) = 3$ for all $n > 3$, because of the proper 3-coloring of $\mathrm{DS}(F_{1,n})$ that is described so that $c(u_0) = c(w_2) = c(w_3) = 2$ and $c(v_i) = i \bmod 2$ for all $i < n$.

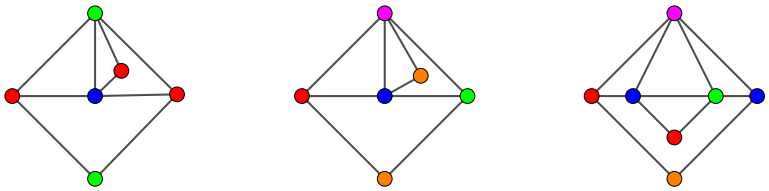

Figure 16. r-dynamic proper $(r+2)$-coloring of $\mathrm{DS}(F_{1,n})$, for $(r,n)=(1,3)$ (left), $(r,n)=(3,3)$ (center) and $(r,n)=(3,4)$ (right).

- **Case** $r=2$.
  From Lemma 1, we have that $3 \leq \chi_2(\mathrm{DS}(F_{1,n}))$. This lower bound is tight for n even because of the same map c described in the previous case. If n is odd, then every 2-dynamic proper coloring of the DSG $\mathrm{DS}(F_{1,n})$ requires two distinct colors for the set of vertices $N_{\mathrm{DS}(F_{1,n})}(w_2)=\{v_0, v_{n-1}\}$, and hence, at least four colors for the set of vertices $\{u_0, v_0, \ldots, v_{n-1}\}$. Hence, $4 \leq \chi_2(\mathrm{DS}(F_{1,n}))$ when n is odd. This lower bound is tight because of the proper coloring c of $\mathrm{DS}(F_{1,n})$ that is described so that $c(w_3)=c(v_{n-1})=2$, $c(u_0)=c(w_2)=3$ and $c(v_i)=i \bmod 2$ for all $i<n-1$.
- **Case** $r=3$.
  From Condition (1.1), every 3-dynamic proper coloring of $\mathrm{DS}(F_{1,n})$ satisfies that the four vertices v_0, v_{n-1}, u_0 and w_2 are pairwise distinct colored. In the case of being a proper 4-coloring, if $n>4$, then the vertex w_3 must be colored as u_0, while the vertex v_i must be colored as v_0, if $i \equiv 0 \,(\mathrm{mod}\, 3)$; as v_{n-1}, if $i \equiv 1 \,(\mathrm{mod}\, 3)$; and as w_2 otherwise. Hence, this proper 4-coloring is possible only if $4<n \equiv 2 \,(\mathrm{mod}\, 3)$.
  In order to prove that $\chi_2(\mathrm{DS}(F_{1,n}))=4$, whenever $4<n \equiv 2 \,(\mathrm{mod}\, 3)$, it is enough to consider the 3-dynamic proper 4-coloring c of $\mathrm{DS}(F_{1,n})$ such that $c(w_2)=2$, $c(u_0)=c(w_3)=3$ and $c(v_i)=i \bmod 3$ for all $i<n$. Furthermore, in order to prove that $\chi_2(\mathrm{DS}(F_{1,n}))=5$, whenever $4<n \not\equiv 2 \,(\mathrm{mod}\, 3)$, it is enough to consider the same proper coloring c that we have just described, except for $c(v_{n-1})=4$.
  A fifth color is also required in the case of being $n \in \{3,4\}$. It is due to the fact that Condition (1.1) implies that every 3-dynamic proper coloring of $\mathrm{DS}(F_{1,n})$ requires at least three distinct colors for the set of vertices $\{v_0, \ldots, v_{n-1}\}$ and exactly four distinct colors for each one of the sets of vertices $\{u_0, v_0, v_{n-1}, w_2\}$, $\{u_0, v_0, v_1, w_2\}$ and $\{u_0, v_{n-2}, v_{n-1}, w_2\}$. Thus, Figure 16 (center and right) illustrates that $\chi_3(\mathrm{DS}(F_{1,n}))=5$, whenever $n \in \{3,4\}$.
- **Case** $(r,n)=(4,3)$.
  From Lemma 1, $5 \leq \chi_4(\mathrm{DS}(F_{1,3}))$. Figure 16 (center) shows that this lower bound is tight.
- **Case** $4 \leq r \leq n$.
  Lemma 13 implies that $r+2 \leq \chi_r(\mathrm{DS}(F_{1,n}))$. This lower bound is tight because of the r-dynamic proper $(r+2)$-coloring c such that $c(u_0)=r$, $c(w_2)=c(w_3)=r+1$ and

$$c(v_i)=\begin{cases} i \bmod r, & \text{if } \begin{cases} i<n-1, \\ i=n-1 \not\equiv 0 \,(\mathrm{mod}\, r), \end{cases} \\ 2, & \text{otherwise.} \end{cases} \tag{4.1}$$

□

The just described dynamic coloring implies that every participant in a fan communication network $F_{1,n}$, which is distinct from a control node, can reconstruct the secret under consideration in just one round of communication only if $r \in \{1, 2, 3\}$. Control nodes do the same only for $r \in \{1, 2\}$. For the remaining cases, except for the control node w_2 when $r > 5$, all the participants receive all the pieces of information in two rounds. For $r > 5$, three rounds are enough for all the nodes.

Now, we solve the dynamic coloring problem for the fan graph $F_{2,n}$.

Theorem 15. *Let $n > 2$ and r be two positive integers. Then,*

$$\chi_r(\mathrm{DS}(F_{2,n})) = \begin{cases} 3, & \text{if } \begin{cases} r = 1 \text{ and } n \neq 4, \\ r = 2 \text{ and } n = 3, \end{cases} \\ 4, & \text{if } \begin{cases} r \in \{1, 3\} \text{ and } n = 4, \\ r = 2 \text{ and } n \text{ is even}, \end{cases} \\ 5, & \text{if } \begin{cases} r = 2 \text{ and } n > 3 \text{ is odd}, \\ r = 3 \text{ and } n \neq 4, \end{cases} \\ 6, & \text{if } r = 4, \\ r + 3, & \text{if } 5 \leq r \leq n + 1, \\ n + 3, & \text{otherwise}. \end{cases}$$

Proof. From Lemma 1, we only dealt with $r \leq \Delta(\mathrm{DS}(F_{2,n})) = n + 1$. The following cases arise.

- **Case** $r = 1$.
  Proposition 4 and Lemma 6 imply that $\chi(\mathrm{DS}(F_{2,n})) \in \{3, 4\}$. Figure 17 illustrates that $\chi(\mathrm{DS}(F_{2,3})) = 3$. Further, it is readily verified that every proper coloring of $F_{2,4}$ requires three distinct colors for the set of vertices $V_4(F_{2,4})$. So, $\chi(\mathrm{DS}(F_{2,4})) = 4$. Finally, if $n > 4$, then let us consider the proper 3-coloring c of the double fan graph $F_{2,n}$ that is described so that $c(w_n) = 0$, $c(u_0) = c(u_1) = c(w_3) = c(w_4) = 2$ and $c(v_i) = i \bmod 2$ for every non-negative integer $i < n$. Condition (1.1) holds and hence, $\chi(\mathrm{DS}(F_{2,n})) = 3$ for all $n > 4$.

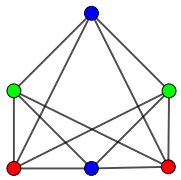

Figure 17. r-dynamic proper 3-coloring of $\mathrm{DS}(F_{2,3})$ for $r \in \{1, 2\}$.

- **Case** $r = 2$.
  From Lemma 1, we have that $\chi_2(\mathrm{DS}(F_{2,n})) \geq 3$. Figure 17 also illustrates that this lower bound is tight for $n = 3$. Further, Lemma 1 implies that $4 = \chi(\mathrm{DS}(F_{2,4})) \leq \chi_2(\mathrm{DS}(F_{2,4}))$. Figure 18 illustrates that this lower bound is indeed reached. Finally, if $n > 4$, then every 2-dynamic proper coloring of $\mathrm{DS}(F_{2,n})$ requires four distinct colors for the set of vertices $\{u_0, u_1, v_0, v_{n-1}\}$. Moreover, if n is odd, then it requires at least five distinct colors for the set of vertices $\{u_0, u_1, v_0, v_1, \ldots, v_{n-1}\}$.

As a consequence, $\chi_2(\mathrm{DS}(F_{2,n})) \geq 4$ if n is even, and ≥ 5 otherwise. Both lower bounds are reached because of the 2-dynamic proper coloring c of $\mathrm{DS}(F_{2,n})$ that is described so that $c(w_n) = 0$, $c(u_0) = c(w_3) = c(w_4) = 2$, $c(u_1) = 3$ and

$$c(v_i) = \begin{cases} i \bmod 2, & \text{if } i < n-1, \\ 1, & \text{if } i = n-1 \text{ is odd}, \\ 4, & \text{otherwise.} \end{cases}$$

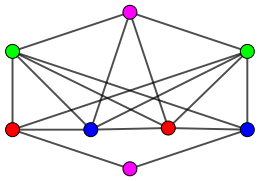

Figure 18. r-dynamic proper 4-coloring of $\mathrm{DS}(F_{2,4})$ for $r \in \{2, 3\}$.

- **Case** $r = 3$.
  From Lemma 1, we have that $4 \leq \chi_3(\mathrm{DS}(F_{2,n}))$. Figure 18 also illustrates that this lower bound is tight for $n = 4$. Further, every 3-dynamic proper coloring of $\mathrm{DS}(F_{2,3})$ requires five distinct colors for the set of vertices $\{u_0, u_1, v_0, v_1, w_3\}$ and hence, $5 \leq \chi_3(\mathrm{DS}(F_{2,3}))$. Figure 19 (left) illustrates that this lower bound is indeed reached. Finally, if $n > 4$, then $5 \leq \chi_3(\mathrm{DS}(F_{2,n}))$, because every 3-dynamic proper coloring of $\mathrm{DS}(F_{2,n})$ requires at least five distinct colors for the set of vertices $V_4(F_{2,n}) \cup V_n(F_{2,n})$. In order to prove that this lower bound is tight, it is enough to consider the 3-dynamic proper 5-coloring c of the DSG $\mathrm{DS}(F_{2,n})$ satisfying (4.1) and such that $c(w_n) = 0$, $c(u_0) = c(w_3) = c(w_4) = 3$, $c(u_1) = 4$

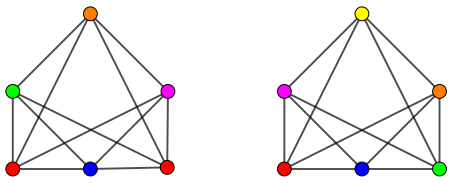

Figure 19. r-dynamic proper $(r+2)$-coloring of $\mathrm{DS}(F_{2,3})$ for $r = 3$ (left) and $r = 4$ (right).

- **Case** $(r, n) = (4, 3)$.
  It is readily verified that every 4-dynamic proper coloring of $\mathrm{DS}(F_{2,3})$ must color each one of its vertices in a unique way (see Figure 19 (right)). So, $\chi_4(\mathrm{DS}(F_{2,3})) = 6$.
- **Case** $4 \leq r \leq n + 1$.
  Condition (1.1) implies that every r-dynamic proper coloring c of the DSG $\mathrm{DS}(F_{2,n})$ satisfies that $c(u_0) \neq c(u_1)$. Then, since $N_{\mathrm{DS}(F_{2,n})}(u_0) = N_{\mathrm{DS}(F_{2,n})}(u_1)$ and $\deg_{\mathrm{DS}(F_{2,n})}(u_0) = \deg_{\mathrm{DS}(F_{2,n})}(u_1) = n+1 > r$, the same condition enables one to ensure that $r + 2 \leq \chi_r(\mathrm{DS}(F_{2,n}))$. Figures 20 illustrates that this lower bound is reached for $(r, n) \in \{(4, 4), (5, 4), (4, 5)\}$.

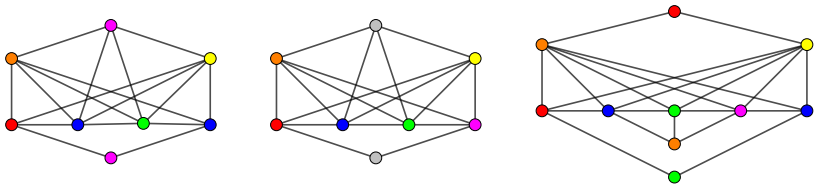

Figure 20. r-dynamic proper $(r+2)$-coloring of $\mathrm{DS}(F_{2,n})$ for $(r,n) = (4,4)$ (left), $(r,n) = (5,4)$ (center) and $(r,n) = (4,5)$ (right).

Furthermore, the following subcases arise for $n > 4$.

- **Subcase** $r = 4 \leq n-2$.
  In order to prove that the lower bound $6 \leq \chi_4(\mathrm{DS}(F_{2,n}))$ is tight, it is enough to consider the 4-dynamic proper 6-coloring of $\mathrm{DS}(F_{2,n})$ satisfying (4.1) and such that $c(w_n) = 0$, $c(w_3) = 2$, $c(u_0) = c(w_4) = 4$, $c(u_1) = 5$.
- **Subcase** $5 \leq r \leq n$.
  From Condition (1.1), it is readily deduced that every r-dynamic proper coloring of the DSG $\mathrm{DS}(F_{2,n})$ requires at least $r+3$ distinct colors for the set of vertices $V(F_{2,n}) \setminus \{w_3, w_n\}$. This lower bound is tight because of the r-dynamic proper $(r+3)$-coloring c of $\mathrm{DS}(F_{2,n})$ satisfying (4.1) and such that $c(u_0) = r$, $c(u_1) = r+1$, $c(w_3) = c(w_4) = c(w_n) = r+2$.
- **Subcase** $5 \leq r = n+1$.
  It is readily verified from Condition (1.1) that every r-dynamic proper coloring of $\mathrm{DS}(F_{2,n})$ requires at least $n+3$ distinct colors for $V(F_{2,n}) \setminus \{w_3, w_n\}$. This lower bound is tight because of the $(n+1)$-dynamic proper $(n+3)$-coloring c of $\mathrm{DS}(F_{2,n})$ that is described so that $c(w_3) = c(w_4) = c(w_n) = n$, $c(u_0) = n+1$, $c(u_1) = n+2$ and $c(v_i) = i$ for all $i < n$.

□

The just described dynamic coloring implies that every participant in a fan communication network $F_{2,n}$ can reconstruct the secret under consideration in just one round of communication only if either $n = 3$ and $r \leq 4$, or $n > 3$ and $r \leq 2$. In any other case, two rounds are always necessary as a solution of both Problems 1 and 3.

4.4. Degree splitting of jellyfish graphs

Let m and n be two positive integers such that $m \leq n$. Let us finish this section by solving the dynamic coloring problem for the jellyfish graph $J_{m,n}$ of set of vertices arising from the cycle $C_4 = \langle\, v_0, v_1, v_2, v_3 \,\rangle$ in the way described in the preliminary section. Particularly, let $\{v_1^0, \ldots, v_1^{m-1}\}$ and $\{v_3^0, \ldots, v_3^{n-1}\}$ be the sets of pendant vertices that are respectively added to the vertices v_1 and v_3. The following sets of vertices play a fundamental role in the description of the DSG $\mathrm{DS}(J_{m,n})$.

- The set $V_3(J_{1,1}) = \{v_0, v_1, v_2, v_3\}$, if $1 = m = n$.
- The set $V_3(J_{1,n}) = \{v_0, v_1, v_2\}$, if $1 = m < n$.
- The sets $V_3(J_{n,n}) = \{v_0, v_2\}$ and $V_{n+2}(J_{n,n}) = \{v_1, v_3\}$, if $1 < m = n$.
- The set $V_3(J_{m,n}) = \{v_0, v_2\}$, if $1 < m < n$.

Each one of these sets $V(J_{m,n})$ is associated to an additional vertex w_k to get $\mathrm{DS}(J_{m,n})$. The following result establishes the r-dynamic chromatic number of the DSG $\mathrm{DS}(J_{1,n})$.

Proposition 16. *Let n and r be two positive integers. Then,*

$$\chi_r(\mathrm{DS}(J_{1,n})) = \begin{cases} \max\{4,\ r+1\}, & \text{if } r \leq n+2, \\ 5, & \text{if } n = 1 \text{ and } r \geq 4, \\ n+3, & \text{otherwise.} \end{cases}$$

Proof. Let $\alpha = \max\{4,\ r+1\}$. Lemma 1 allows for a focus on the case $r \leq \Delta(\mathrm{DS}(J_{1,n}))$. This maximum degree is 4, if $n = 1$, and it is $n+2$ otherwise. Since the induced subgraph of $J_{1,n}$ arising from the set of vertices $\{v_0, v_1, v_2, w_3\}$ is a 4-clique, we have from Lemmas 1 and 2 that $\alpha \leq \chi_r(\mathrm{DS}(J_{1,n}))$. In order to prove that this lower bound is tight, we describe an appropriate r-dynamic proper α-coloring c of $\mathrm{DS}(J_{1,n})$. The following cases arise.

- If either $r \leq n$ or $(r,n) \in \{2,3\} \times \{1\}$, then we define the map c so that $c(v_i) = i$ for all $i \in \{0,1,2\}$, $c(w_3) = 3$, $c(v_1^0) = \max\{3,\ r\}$ and $c(v_3^j) = j \bmod r$ for all non-negative integer $j < n$. In addition, $c(v_3) = 1$, if $n = 1$, and $c(v_3) = c(v_1^0)$ otherwise.
- If $(r,n) = (4,1)$, then it is enough to consider the same map c described in the previous case, except for $c(v_3^0) = 1$ and $c(v_3) = 4$.
- If $n > 1$ and $r \in \{n+1,\ n+2\}$, then the map c is defined so that $c(v_3^i) = i$ for all $i < n$, $c(v_3) = c(v_1^0) = n$, $c(v_0) = n+1$ and $c(v_1) = 0$. In addition, if $r = n+1$, then $c(v_2) = 1$ and $c(w_3) = 2$. Otherwise, if $r = n+2$, then $c(v_2) = n+2$ and $c(w_3) = 1$.

□

Figure 21 illustrates the dynamic coloring described in the previous proof.

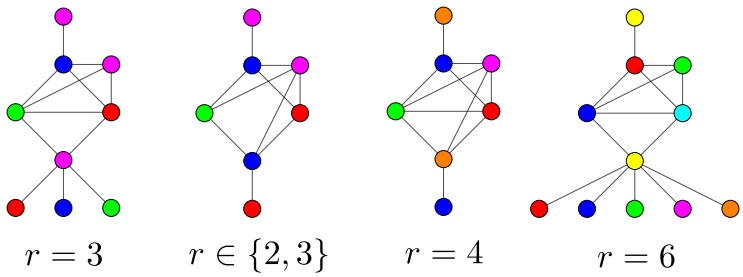

Figure 21. r-dynamic colorings of some DSGs of jellyfish graphs.

The existence of pendant vertices in the DSG of any jellyfish graph $J_{1,n}$ implies that only the case $r = 1$ gives rise to exactly one round of communication as a solution for both Problems 1 and 3. The dynamic coloring described in the proof of Proposition 16 implies that, for $r > 1$, two rounds of communications are enough for both problems.

Now, we solve the dynamic coloring problem for $\mathrm{DS}(J_{m,n})$, with $1 < m \leq n$.

Proposition 17. *Let m and n be two positive integers such that $1 < m \leq n$. Then,*

$$\chi_r(\mathrm{DS}(J_{m,n})) = \begin{cases} 3, & \text{if } \begin{cases} r = 1, \\ r = 2 \text{ and } m < n, \end{cases} \\ 4, & \text{if } r = 2 \text{ and } m = n, \\ r+1, & \text{if } 3 \leq r \leq \Delta(\mathrm{DS}(J_{m,n})), \\ n+3, & \text{if } m < n \text{ and } r > n+2, \\ n+4, & \text{otherwise}. \end{cases}$$

Proof. Lemma 1 enables us to focus on the case $r \leq \Delta(\mathrm{DS}(J_{m,n}))$. This maximum degree is $n+2$, if $m < n$, and $n+3$, if $m = n$. The following study of cases arises.

- **Case** $r = 1$ or ($r = 2$ and $m < n$).
  Since the set of vertices $\{v_0, v_1, v_2\}$ describes a 3-clique within $\mathrm{DS}(J_{m,n})$, we have that $3 \leq \chi_r(\mathrm{DS}(J_{m,n}))$. In order to prove that this lower bound is tight for $r = 1$ and also for $r = 2$ and $m < n$, it is enough to consider the proper 3-coloring c of $\mathrm{DS}(J_{m,n})$ that is described so that $c(v_1^i) = c(v_3^j) = 0$ for all $i < m$ and $j < n$, $c(v_3) = c(w_3) = 1$ and $c(v_k) = k$ for all $k \in \{0, 1, 2\}$. In addition, if $r = 1$ and $m = n$, then $c(w_{n+2}) = 2$.
- **Case** $r = 2$ and $m = n$.
  Condition (1.1) applied to the vertex w_{n+2}, together with the already mentioned 3-clique, implies that every 2-dynamic proper coloring of $\mathrm{DS}(J_{m,n})$ requires four distinct colors for the set of vertices $\{v_0, v_1, v_2, v_3, \}$. Hence, $4 \leq \chi_r(\mathrm{DS}(J_{n,n}))$. This lower bound is tight because of the 2-dynamic proper 4-coloring c of $\mathrm{DS}(J_{m,n})$ that is described so that $c(v_0^i) = c(v_3^i) = c(w_{n+2}) = 0$ for all $i < n$, $c(w_3) = 1$ and $c(v_j) = j$ for all $j \leq 3$.
- **Case** $3 \leq r \leq \Delta(\mathrm{DS}(J_{m,n}))$.
  From Lemma 1, we have that $r + 1 \leq \chi_r(\mathrm{DS}(J_{m,n}))$. In order to prove that this lower bound is tight, it is enough to define an appropriate r-dynamic proper $(r+1)$-coloring c of $\mathrm{DS}(J_{m,n})$. The following subcases arise. (See Figure 22 for some illustrations of the proposed maps.)
  - **Subcase** $3 \leq r \leq m + 2$.
    We consider the map c that is described so that
    * $c(v_0) = m \bmod r$;
    * $c(v_1) = r$;
    * $c(v_2) = (m+1) \bmod r$
    * $c(v_3) = (m+2) \bmod r$;
    * $c(w_3) = (m-1) \bmod r$;
    * if $m = n$, then $c(w_{n+2}) = m \bmod r$;
    * $c(v_1^i) = i \bmod r$ for all $i < m$; and
    * $c(v_3^i) = \begin{cases} i \bmod r, & \text{if } i \not\equiv (m+2) \bmod r, \\ r, & \text{otherwise.} \end{cases}$
  - **Subcase** $m = n$ and $r = n + 3$.
    We consider the same map c described in the previous subcase, except for $c(w_{n+2}) = (m + 2) \bmod r$ and $c(v_3) = 0$.

– **Subcase** $m + 3 \leq r \leq n + 2$. (In particular, $m < n$.)
Similarly to the first subcase, we define the map c so that

* $c(v_0) = n \bmod r$;
* $c(v_1) = (n + 2) \bmod r$;
* $c(v_2) = (n + 1) \bmod r$
* $c(v_3) = r$;
* $c(w_3) = (n - 1) \bmod r$;
* $c(v_3^i) = i \bmod r$ for all $i < n$; and
* $c(v_1^i) = \begin{cases} i \bmod r, & \text{if } i \not\equiv (n + 2) \bmod r, \\ r, & \text{otherwise.} \end{cases}$

□

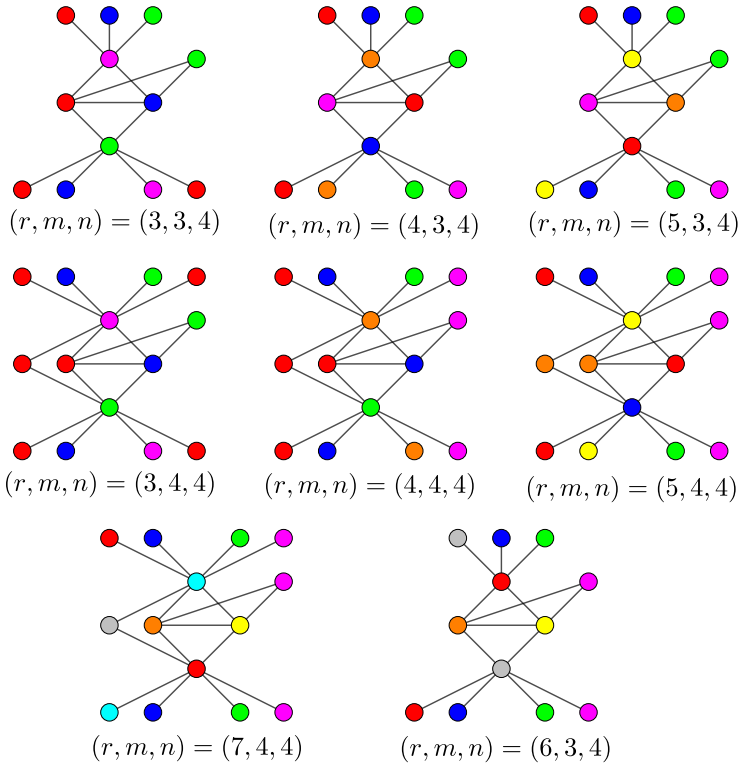

Figure 22. r-dynamic proper (r+1)-colorings of $\mathrm{DS}(J_{m,n})$, for $3 \leq r \leq \Delta(\mathrm{DS}(J_{m,n}))$.

Again, the existence of pendant vertices implies that every node in a jellyfish communication network $J_{m,n}$, with $1 < m \leq n$, can reconstruct the secret under consideration in exactly one round of communication only if $r = 1$. The dynamic coloring in the proof of Proposition 17 implies that, for $r > 1$, all the nodes, except for the control node w_3, can recover all the secret shares in two rounds. (Note here the relevance of both nodes v_1 and v_3.) This control node would require two rounds to this end only if $r \in \{2, 3, 4\}$, and three rounds if $r > 4$. Hence, the solution of Problem 1 is 1, if $r = 1$; 2, if $r \in \{2, 3, 4\}$, and 3, if $4 < r \leq n + 3$. That of Problem 3 is 1 if $r = 1$, and 2 if $1 < r \leq n + 3$.

5. A new lower bound

To fit much better a lower bound for the dynamic chromatic number of a DSG, and similarly to Lemma 6, this section delves into the relationship among the dynamic chromatic number of a given graph G and that of $\mathrm{DS}(G)$.

Lemma 18. *Let $r > 1$ be a positive integer and let G be a finite simple graph. Then,*

$$\max_{k>1}\{\chi_{r-1}(G), \min\{r, |V_k(G)|\colon\ 1 < |V_k(G)|\} + 1\} \leq \chi_r(\mathrm{DS}(G)).$$

Proof. Let c be an r-dynamic proper coloring of $\mathrm{DS}(G)$ and let $k > 1$ be a positive integer such that $|V_k(G)| > 1$. From Condition (1.1), we have that $|c(N(w_k))| \geq \min\{r, |V_k(G)|\}$. Hence, $\min_{k>1}\{r, |V_k(G)|\colon\ 1 < |V_k(G)|\} + 1 \leq \chi_r(\mathrm{DS}(G))$. Further, let c' denote the restriction of the map c to the vertices within $V(G)$. Then, for each vertex $v \in V(G)$, the following assertions hold.

- If $\deg_G(v) \leq 1$ or $|V_{\deg_G(v)}(G)| = 1$, then $N_G(v) = N_{\mathrm{DS}(G)}(v)$ and hence, it is $|c'(N_G(v))| = |c(N_{\mathrm{DS}(G)}(v))| \geq \min\{r, \deg_{\mathrm{DS}(G)}(v)\} = \min\{r, \deg_G(v)\} \geq \min\{r-1, \deg_G(v)\}$.
- If $\deg_G(v) > 1$ and $|V_{\deg_G(v)}(G)| > 1$, then it is verified that $|c'(N_G(v))| \geq |c(N_{\mathrm{DS}(G)}(v))| - 1 \geq \min\{r, \deg_{\mathrm{DS}(G)}(v)\} - 1 = \min\{r-1, \deg_G(v)\}$.

Thus, Condition (1.1) holds and hence, $\chi_{r-1}(G) \leq \chi_r(\mathrm{DS}(G))$. □

In order to illustrate how the previous lemma may be used to solve the dynamic coloring problem of DSGs, let us finish our study by determining the r-dynamic chromatic number of the DSG of windmill and barbell graphs.

Proposition 19. *Let r and $m, n \geq 2$ be three positive integers. Then,*

$$\chi_r(\mathrm{DS}(\mathrm{Wd}_{m,n})) = \begin{cases} n, & \text{if } 1 \leq r < n, \\ r+2, & \text{if } n \leq r \leq m(n-1), \\ m(n-1)+2, & \text{otherwise.} \end{cases}$$

Proof. From Lemma 1, we may focus on the case $r \leq \Delta(\mathrm{DS}(\mathrm{Wd}_{m,n})) = m(n-1)$. For each non-negative integer $j < m$, let $\{w, v_i^j\colon\ 0 \leq i < n-1\}$ be the set of vertices of the $(j+1)^{\text{th}}$ copy of the complete graph K_n within the windmill graph $\mathrm{Wd}_{m,n}$. Here, w denotes the vertex that all of these copies have in common. In addition, let w_{n-1} denote the additional vertex that is uniquely joined to all the vertices within $V_{n-1}(\mathrm{Wd}_{m,n})$ to get $\mathrm{DS}(\mathrm{Wd}_{m,n})$. From Lemmas 3, 6 and 18, we have that

$$\chi_r(\mathrm{DS}(\mathrm{Wd}_{m,n})) \geq \begin{cases} n, & \text{if } 1 \leq r < n, \\ r+1, & \text{if } n \leq r \leq m(n-1), \\ m(n-1)+1, & \text{otherwise.} \end{cases}$$

Then, the following study of cases arises.

- **Case** $1 \leq r < n$.
  In order to prove that the previous lower bound is tight, let c be an r-dynamic proper n-coloring of the windmill graph $\mathrm{Wd}_{m,n}$. Then, it is enough to consider the proper n-coloring c' of $\mathrm{DS}(\mathrm{Wd}_{m,n})$ such that $c'(v) = c(v)$ for all $v \in V(\mathrm{Wd}_{m,n})$ and $c'(w_{n-1}) = c(w)$. Condition (1.1) holds and hence, $\chi_r(\mathrm{DS}(\mathrm{Wd}_{m,n})) = n$. (Figure 23 (left) illustrates the case $(m, n) = (3, 4)$.)

- **Case** $n \leq r \leq m(n-1)$.
  Let c be an r-dynamic proper coloring of $\mathrm{DS}(\mathrm{Wd}_{m,n})$. Then, Condition (1.1) implies that

$$|c(\{w,\ w_{n-1}\} \cup N_{\mathrm{DS}(\mathrm{Wd}_{m,n})}(w_{n-1}))| \geq r+2,$$

  because $\deg_{\mathrm{DS}(\mathrm{Wd}_{m,n})}(w_{n-1}) = m(n-1) \geq r$ and $c(w) \neq c(w_{n-1})$. (For the last inequality, note that $\deg_{\mathrm{DS}(\mathrm{Wd}_{m,n})}(v_1^1) = n \leq r$ and $\{w, w_n\} \subset N_{\mathrm{DS}(\mathrm{Wd}_{m,n})}(v_1^1)$.) As a consequence, $\chi_r(\mathrm{DS}(\mathrm{Wd}_{m,n})) \geq r+2$. This lower bound is tight because of the proper coloring c of $\mathrm{DS}(\mathrm{Wd}_{m,n})$ such that $c(w) = r$, $c(w_n) = r+1$ and, for each pair of non-negative integers $i < n-1$ and $j < m$,

$$c(v_i^j) = \begin{cases} j(n-1)+i, & \text{if } j(n-1)+i < r, \\ i, & \text{otherwise.} \end{cases}$$

  (Figure 23 (right) illustrates the case $(m,n,r) = (4,3,5)$.)

□

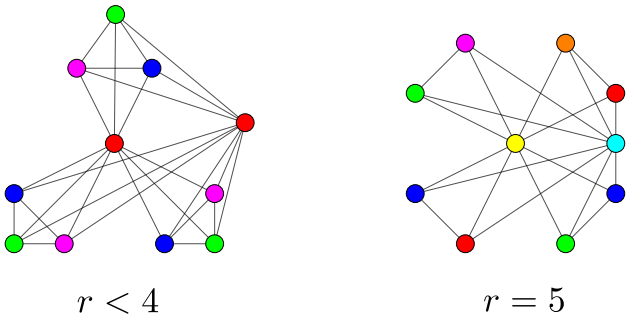

Figure 23. r-dynamic colorings of a pair of DSGs of windmill graphs.

The just described dynamic coloring implies that every participant in a windmill communication network $\mathrm{Wd}_{m,n}$ can reconstruct the secret under consideration in just one round for all $r \leq m(n-1)$. Two rounds will be necessary for $r = m(n-1)+1$ because of both vertices w and w_{n-1}.

We finish our study by solving the dynamic coloring problem for barbell graphs.

Proposition 20. *Let $n > 2$ be a positive integer. Then,*

$$\chi_r(\mathrm{DS}(\mathrm{Ba}_n)) = \begin{cases} n+1, & \text{if } 1 \leq r \leq n, \\ r+3, & \text{if } n < r \leq 2n-2, \\ 2n+1, & \text{otherwise.} \end{cases}$$

Proof. Lemma 1 enables us to focus on the case $r \leq \Delta(\mathrm{DS}(\mathrm{Ba}_n)) = 2n-2$. For each $j \in \{0,1\}$, let $\{v_i^j\colon\ 0 \leq i < n\}$ be the set of vertices of the $(j+1)^{\text{th}}$ copy of the complete graph K_n within Ba_n so that $v_{n-1}^0 v_{n-1}^1$ constitutes its bridge. In addition, let w_{n-1} and w_n denote the additional vertices that are respectively joined to all the vertices within $V_{n-1}(\mathrm{Ba}_n) = \{v_i^j\colon\ 0 \leq i < n-1, j \in \{0,1\}\}$ and $V_n(\mathrm{Ba}_n) = \{v_{n-1}^0,\ v_{n-1}^1\}$ to get $\mathrm{DS}(\mathrm{Ba}_n)$. From Lemmas 3, 6 and 18, we have that

$$\chi_r(\mathrm{DS}(\mathrm{Ba}_n)) \geq \begin{cases} n, & \text{if } 1 \leq r \leq n, \\ r+1, & \text{if } n < r \leq 2n-2, \\ 2n-1, & \text{otherwise.} \end{cases}$$

Then, the following study of cases arises.

- **Case** $1 \leq r \leq n$.
  Let us suppose the existence of an r-dynamic proper n-coloring c of $\mathrm{DS}(\mathrm{Ba}_n)$. In particular, for each $j \in \{0,1\}$, both sets $\{c(v_i^j)\colon\ 0 \leq i < n\}$ and $\{c(v_i^j), c(w_n)\colon\ 0 \leq i < n-1\}$ are formed by n distinct colors. Hence, it must be $c(v_{n-1}^0) = c(w_n) = c(v_{n-1}^1)$, which is not possible because the map c is a proper coloring and $v_{n-1}^0 v_{n-1}^1$ constitutes the bridge within Ba_n. As a consequence, $\chi_r(\mathrm{DS}(\mathrm{Ba}_n)) \geq n+1$. This lower bound is tight because of the proper $(n+1)$-coloring c of $\mathrm{DS}(\mathrm{Ba}_n)$ such that $c(v_i^0) = c(v_{n-1-i}^1) = i$ for all $i < n$, and $c(w_n) = c(w_{n-1}) = n$. (Figure 24 (left) illustrates the case $n = 4$.)
- **Case** $n < r \leq 2n-2$.
  Let c be an r-dynamic proper coloring of $\mathrm{DS}(\mathrm{Ba}_n)$. From Condition (1.1), we have, for each $j \in \{0,1\}$, that $|c(N(v_{n-1}^j))| = d_{\mathrm{DS}(\mathrm{Ba}_n)}(v_{n-1}^j) = n+1 \leq r$. Then, the underlying adjacency, together with the mentioned Condition (1.1), implies that the set
  $$\left\{c(v_i^j),\ c(w_n)\colon\ 0 \leq i < n,\ j \in \{0,1\}\right\}$$
  is formed by at least $r+3$ distinct colors. Hence, $\chi_r(\mathrm{DS}(\mathrm{Ba}_n)) \geq r+3$. This lower bound is tight because of the proper $(r+3)$-coloring c of $\mathrm{DS}(\mathrm{Ba}_n)$ such that $c(w_n) = c(w_{n-1}) = r+2$ and, for each pair of non-negative integers $i < n$ and $j \in \{0,1\}$,
  $$c(v_i^j) = \begin{cases} r+1, & \text{if } (i,j) = (n-1,1), \\ i, & \text{if } \begin{cases} j = 0, \\ j = 1 \text{ and } i < 2n-2-r, \end{cases} \\ r-n+i+2, & \text{otherwise.} \end{cases}$$
  (Figure 24 (right) illustrates the case $(n,r) = (4,5)$.)

□

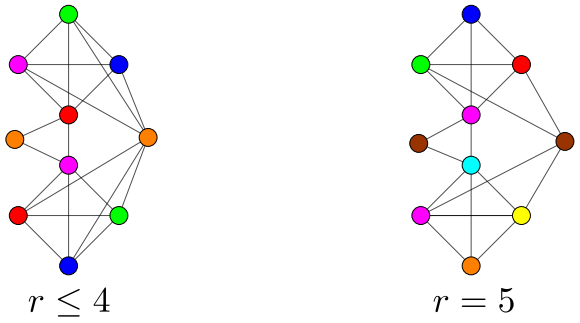

Figure 24. r-dynamic colorings of a pair of DSGs of barbell graphs.

The just described dynamic coloring implies that, except for the control node w_n, every participant in a barbell communication network Ba_n can reconstruct the secret under consideration in just one round for all $r \leq n$. For the remaining cases, two rounds are necessary for all the participants, except for the control node w_{n-1}, which only requires two rounds for $r = 2n$. The control node w_n would require just one round for $r \in \{1, 2\}$, and two rounds otherwise. Hence, the solution of Problem 1 is 1, if $r \in \{1, 2\}$, and 2, if $2 < r \leq 2n$. That of Problem 3 is 1 if $r \leq n$, and 2 if $n < r \leq 2n$.

6. Conclusion and further work

The dynamic coloring of DSGs constitutes a valuable approach to improve cryptographic protocols based on secret sharing. First, the dynamic coloring enables the dealer to distribute secret shares so that all the participants can recover the secret after a minimum number of rounds of communication. Second, DSGs enable the dealer to avoid dishonesty by adding control nodes supervising participants with the same influence in the communication network. This paper has delved into this topic by solving completely the dynamic chromatic problem for DSGs (Problem 2) of regular graphs. To this end, we have established the relationship among the dynamic chromatic number of a regular graph and that of its DSG. In addition, the dynamic coloring problem for DSGs (Problem 2) of non-regular graphs has partially been solved by establishing a new lower bound for the dynamic chromatic number under consideration. More precisely, we have solved the dynamic coloring problem for DSGs of eight families of graphs: cycles, cocktail, book, comb, fan, jellyfish, windmill and barbell graphs. Whenever it has been possible, we have detailed the dynamic coloring of each graph, so that they can naturally be translated to describe optimal secret share distributions in secret sharing schemes defined on this type of graphs. These colorings have enabled us to establish the minimum number of rounds of communications that are necessary so that all the participants of a communication network defined on such graphs can reconstruct the secret under consideration. To this end, we have distinguished whether the control nodes are also participants of the scheme (Problem 1), or not (Problem 3). Table 2 collects the solution of both problems for all the DSGs that have been studied throughout the paper. Those cases in which the solution of both problems coincide have been indicated by the symbol = in the third column of Table 2.

The methodology here used may indeed be considered as a starting point to deal similarly with the dynamic coloring problem of other DSGs. Of particular interest is the study of Problems 1 and 3 for DSGs of graph products, which give rise to more complex graphs, more representative of real communication networks. Note in this regard that the dynamic chromatic problem has already been considered for different graph products [22–24, 34], but the implementation into a secret sharing scheme, together with the corresponding study of minimum rounds of communications to reconstruct the secret, has still not being dealt with.

Another aspect to study is the relationship between the respective dynamic chromatic numbers of a $\{k_1, k_2\}$-regular graph (and, more generally, of a $\{k_1, \ldots, k_n\}$-regular graph) and its DSG would constitute a subsequent stage for generalizing Proposition 7. It is established as further work. A main weakness to note here is the fact that, before solving Problems 1 and 3, it is necessary to solve the corresponding dynamic chromatic problem, which is by itself an NP-complete problem, as it has been indicated in the introductory section.

Table 2. Solutions of Problems 1 and 3, for $(\chi_r(G), r+1)$-threshold secret sharing schemes based on the DSG of a graph G.

G	Problem 1 (DS(G))	Problem 3 (DS(G))
C_n	$\begin{cases} 1, & \text{if } r \le 3, \\ 2, & \text{if } 3 < r \le n. \end{cases}$	=
Cp_n	$\begin{cases} 1, & \text{if } r < 2n, \\ 2, & \text{if } r = 2n. \end{cases}$	=
B_n	$\begin{cases} 1, & \text{if } r \le 2, \\ 2, & \text{if } 2 < r \le n. \end{cases}$	=
Cb_n	$\begin{cases} 1, & \text{if } r = 1, \\ 2, & \text{if } r \in \{2,3\}, \\ 3, & \text{if } 3 < r \le n-2. \end{cases}$	=
$F_{1,n}$	$\begin{cases} 1, & \text{if } r \le 2, \\ 2, & \text{if } 2 < r \le 5, \\ 3, & \text{if } 5 < r \le n+1. \end{cases}$	$\begin{cases} 1, & \text{if } r \le 3, \\ 2, & \text{if } 3 < r \le n+1. \end{cases}$
$F_{2,n}$	$\begin{cases} 1, & \text{if } \begin{cases} n = 3,\ r \le 4, \\ n > 3,\ r \le 2, \end{cases} \\ 2, & \text{if } n > 3 < r \le n+2. \end{cases}$	=
$J_{1,n}$	$\begin{cases} 1, & \text{if } r = 1, \\ 2, & \text{if } 1 < r \le n+2. \end{cases}$	=
$J_{m,n(1<m\le n)}$	$\begin{cases} 1, & \text{if } r = 1, \\ 2, & \text{if } 1 < r \le 4, \\ 3, & \text{if } 4 < r \le n+3. \end{cases}$	$\begin{cases} 1, & \text{if } r = 1, \\ 2, & \text{if } 1 < r \le n+3. \end{cases}$
$\mathrm{Wd}_{m,n}$	$\begin{cases} 1, & \text{if } r \le m(n-1), \\ 2, & \text{if } r = m(n-1)+1. \end{cases}$	=
Ba_n	$\begin{cases} 1, & \text{if } r \in \{1,2\}, \\ 2, & \text{if } 2 < r \le 2n. \end{cases}$	$\begin{cases} 1, & \text{if } r \le n, \\ 2, & \text{if } n < r \le 2n. \end{cases}$

Finally, note that the minimum number of rounds of communication in both Problems 1 and 3 refer to any $(\chi_r(\mathrm{DS}(G)), r+1)$-threshold secret sharing scheme based on the DSG of the communication network G under consideration. This number could be decreased if the secret splits into more pieces of information. That is, if we consider a $(k, r+1)$-threshold secret sharing scheme, with $k > \chi_r(\mathrm{DS}(G))$. In this regard, the following question could be of interest for futher studies on the topic.

Problem 4. *What is the minimum positive integer greater than $\chi_r(\mathrm{DS}(G))$ into which the secret has to split for improving the solutions of Problems 1 and 3?*

Use of AI tools declaration

The authors declare they have not used Artificial Intelligence (AI) tools in the creation of this article.

Acknowledgments

The authors want to express their gratitude to the anonymous referees for the comprehensive reading of the paper and their pertinent comments and suggestions, which helped improve the manuscript. Falcón's work is partially supported by the research project FQM-016 from Junta de Andalucía.

Conflict of interest

Raúl M. Falcón is an editorial board member for [*Networks and Heterogeneous Media*] and was not involved in the editorial review or the decision to publish this article. All authors declare that there are no competing interests.

References

1. G. R. Blakley, Safeguarding cryptographic keys, *Managing Requirements Knowledge, International Workshop on. IEEE Computer Society,* (1979), 313–317. https://doi.org/10.1109/MARK.1979.8817296
2. A. Shamir, How to share a secret, *Comm. ACM*, **22** (1979), 612–613. https://doi.org/10.1145/359168.359176
3. V. Attasena, J. Darmont, N. Harbi, Secret sharing for cloud data security, *VLDB J.*, **26** (2017), 657–681. https://doi.org/10.1007/s00778-017-0470-9
4. L. Ogiela, M. R. Ogiela, H. Ko, Intelligent data management and security in cloud computing. *Sensors*, **20** (2020), 3458. https://doi.org/10.3390/s20123458
5. S. Sallinen, K. Iwabuchi, S. Poudel, M. Gokhale, M. Ripeanu, R. Pearce, Graph colouring as a challenge problem for dynamic graph processing on distributed systems. In: *Proceedings of the International Conference on High Performance Computing, Networking, Storage, and Analysis (SC'16)*, IEEE, Los Alamitos, CA, (2016), 347–358. https://doi.org/10.1109/SC.2016.29
6. Q. Y. Hu, C. Wen, T. Z. Huang, Z. L. Shen, X. M. Gu, A variant of the Power-Arnoldi algorithm for computing PageRank, *J. Comput. Appl. Math.*, **381** (2021), 113034. https://doi.org/10.1016/j.cam.2020.113034
7. M. E. Coimbra, A. P. Francisco, L. Veiga, An analysis of the graph processing landscape, *J. Big Data*, **8** (2021), 55. https://doi.org/10.1186/s40537-021-00443-9
8. Z. Tuza, Graph colorings with local constraints—a survey, *Discuss. Math. Graph Theory*, **17** (1997), 161–228. https://doi.org/10.7151/dmgt.1049
9. P. Formanowicz, K. Tanaś, A survey of graph coloring - its types, methods and applications, *Found. Comput. Decision Sci.*, **37** (2012), 223–238. https://doi.org/10.2478/v10209-011-0012-y
10. R. M. R. Lewis, *Guide to graph colouring—algorithms and applications*, Cham: Springer, (2021). https://doi.org/10.1007/978-3-030-81054-2

11. S. Labed, A. Kout, S. Chikhi, Solving the graph *b*-coloring problem with hybrid genetic algorithm, *3rd International Conference on Pattern Analysis and Intelligent Systems (PAIS 2018)*, (2018), 1–7. https://doi.org/10.1109/PAIS.2018.8598525
12. E. F. Olariu, C. Frăsinaru, Improving lower bounds for equitable chromatic number, *Comput. Oper. Res.*, **143** (2022), 105790. https://doi.org/10.1016/j.cor.2022.105790
13. Y. Imine, H. Lakhlef, M. Raynal, F. Taïani, DMCSC: a fully distributed multi-coloring approach for scalable communication in synchronous broadcast networks, *J. Supercomput.*, **79** (2023), 788–813. https://doi.org/10.1007/s11227-022-04700-3
14. Y. Shang, Concentration of rainbow *k*-connectivity of a multiplex random graph, *Theoret. Comput. Sci.*, **951** (2023), 113771. https://doi.org/10.1016/j.tcs.2023.113771
15. S. Roy, A. S. Sairam, Distributed star coloring of network for IP traceback, *Int. J. Inf. Secur.*, **17** (2018), 315–326. https://doi.org/10.1007/s10207-017-0366-0
16. R. M. Falcón, N. Mohanapriya, V. Aparna, Optimal shadow allocations of secret sharing schemes arisen from the dynamic coloring of extended neighborhood coronas, *Mathematics*, **10** (2022), 2018. https://doi.org/10.3390/math10122018
17. B. Montgomery, Dynamic Goloring of Graphs, Doctoral Thesis of West Virginia University, Morgantown, 2001.
18. X. Li, X. Yao, W. Zhou, H. Broersma, Complexity of conditional colorability of graphs, *Appl. Math. Lett.*, **22** (2009), 320–324. https://doi.org/10.1016/j.aml.2008.04.003
19. A. S. Akbari, A. Dehghana, M. Ghanbari, On the difference between chromatic and dynamic chromatic number of graphs, *Discrete Math.*, **312** (2012), 2579–2583. https://doi.org/10.1016/j.disc.2011.09.006
20. M. Alishahi, Dynamic chromatic number of regular graphs, *Discrete Appl. Math.*, **160** (2012), 2098–2103. https://doi.org/10.1016/j.dam.2012.05.017
21. V. Aparna, N. Mohanapriya, On *r*-dynamic coloring of some graphs, *Kong. Res. J.*, **7** (2020), 82–87. https://doi.org/10.26524/krj.2020.13
22. T. Deepa, R. M. Falcón, M. Venkatachalam, On the *r*-dynamic coloring of the direct product of a path with either a complete graph or a wheel graph, *AIMS Math*, **6** (2021), 1470–1496. https://doi.org/10.3934/math.2021090
23. R. M. Falcón, S. Gowri, M. Venkatachalam, Solving the dynamic coloring problem for direct products of paths with fan graphs, *Analele Stiintifice ale Univ. Ovidius Constanta, Ser. Mat.*, **31** (2023), 115–142. https://doi.org/10.2478/auom-2023-0006
24. K. Kaliraj, H. Naresh, Kumar, J. Vernold Vivin, On dynamic colouring of Cartesian product of complete graph with some graphs, *J. Taibah Univ. Sci.*, **14** (2020), 168–171. https://doi.org/10.1080/16583655.2020.1713586
25. H. J. Lai, B. Montgomery, H. Poon, Upper bounds of dynamic chromatic number, *Ars Combin.*, **68** (2003), 193–201.
26. H. J. Lai, B. Montgomery, Z. Tao, Conditional colorings of graphs, *Discrete Math.*, **306** (2006), 1997–2004. https://doi.org/10.1016/j.disc.2006.03.052

27. J. Vernold Vivin, N. Mohanapriya, J. Kok, M. Venkatachalam, On dynamic coloring of certain cycle-related graphs, *Arab. J. Math.*, **9** (2020), 213–221. https://doi.org/10.1007/s40065-018-0219-3

28. G. Nandini, M. Venkatachalam, R. M. Falcón, On the *r*-dynamic coloring of subdivision-edge coronas of a path, *AIMS Math*, **5** (2020), 4546–4562. https://doi.org/10.3934/math.2020292

29. J. V. Vivin, N. Mohanapriya, J. Kok, M. Venkatachalam, On dynamic coloring of certain cycle-related graphs, *Arab. J. Math.*, **9** (2020), 213–221. https://doi.org/10.1007/s40065-018-0219-3

30. T. Deepa, M. Venkatachalam, Dafik, On *r*-dynamic coloring of the gear graph families, *Proyecciones*, **40** (2021), 1–15. http://dx.doi.org/10.22199/issn.0717-6279-2021-01-0001

31. R. M. Falcón, M. Venkatachalam, S. Gowri, G. Nandini, On the *r*-dynamic coloring of some fan graph families, *Analele Stiintifice ale Univ. Ovidius Constanta, Ser. Mat.*, **29** (2021), 151–181. https://doi.org/10.2478/auom-2021-0039

32. K. Kalaiselvi, N. Mohanapriya, V. Aparna, *r*-Dynamic chromatic number of subdivision-edge neighborhood corona of certain graph families, *Discrete Math. Algorithms Appl.*, (2023), 2350026. https://doi.org/10.1142/S179383092350026X

33. G. Nandini, M. Venkatachalam, J. Vernold Vivin, On *r*-dynamic coloring of *n*-sunlet graph families, *Proc. Jangjeon Math. Soc.*, **26** (2023), 23–42. http://dx.doi.org/10.17777/pjms2023.26.1.23

34. Y. Chen, S. Fan, H. J. Lai, M. Xu, Graph *r*-hued colorings–A survey, *Discret. Appl. Math.*, **321** (2022), 24–48. https://doi.org/10.1016/j.dam.2022.06.003

35. J. Kim, S. Ok, Dynamic choosability of triangle-free graphs and sparse random graphs, *J. Graph Theory*, **87**, (2017), 347–355. https://doi.org/10.1002/jgt.22161

36. R. Ponraj, S. Somasundaram, On the degree splitting graph of a graph, *Natl. Acad. Sci. Lett.*, **27** (2004), 275–278.

37. F. Harary, *Graph Theory*, Boulder: Westview Press, 1969.

38. K. D. Mackenzie, Decomposition of communication networks, *J Math Psychol*, **4** (1967), 162–174. https://doi.org/10.1016/0022-2496(67)90048-X

39. D. Angel, I. A. Arputhamary, R. Revathi, M. Nirmala, Secure node covering of cocktail party graphs and generalized fan graphs. *2022 Third International Conference on Intelligent Computing Instrumentation and Control Technologies (ICICICT)*, (2022), 261–264. https://doi.org/10.1109/ICICICT54557.2022.9918002

40. B. Basavanagoud, P. Jakkannavar, Praveen, S. Policepatil, Integrity of total transformation graphs, *Electron. J. Graph Theory Appl.*, **9** (2021), 309–329. https://doi.org/10.5614/ejgta.2021.9.2.6

41. A. Bassolas, V. Nicosia, First-passage times to quantify and compare structural correlations and heterogeneity in complex systems, *Commun. Phys.*, **4**, (2021), 76. https://doi.org/10.1038/s42005-021-00580-w

42. M. Gonen, D. Ron, U. Weinsberg, A. Wool, Finding a dense-core in jellyfish graphs, *Comput. Netw.*, **52** (2008), 2831–2841. https://doi.org/10.1016/j.comnet.2008.06.005

43. F. Safaei, A. Babaei, M. Moudi, Optimally connected hybrid complex networks with windmill graphs backbone, *J. Syst. Sci. Complex.*, **33** (2020), 903–929. https://doi.org/10.1007/s11424-020-8294-x

44. D. Acemoglu, A. Ozdaglar, A. ParandehGheibi, Spread of (mis) information in social networks, *Games Econom. Behav.* **70** (2010), 194–227. https://doi.org/10.1016/j.geb.2010.01.005

45. B. Basavanagoud, S. S. Tallur, Further results on degree splitting graph of a graph, *Acta Cienc. Indica Math.*, **33** (2007), 1403–1414.

AIMS Press

Binary multiset topological spaces: A new structure

Article *in* Applied Mathematics Letters · March 2024

DOI: 10.18576/msl/120302

4 authors, including:

s. P. R. Priyalatha
Kongunadu Arts and Science College
12 PUBLICATIONS **20** CITATIONS
SEE PROFILE

Salem Saleh
Hodeidah university
39 PUBLICATIONS **203** CITATIONS
SEE PROFILE

Jawaher Al-Mufarrij
King Saud University
16 PUBLICATIONS **62** CITATIONS
SEE PROFILE

Mathematical Sciences Letters
An International Journal

http://dx.doi.org/10.18576/msl/120302

Binary multiset topological spaces: A new structure

S.P.R. Priyalatha[*,1], *R. Sowndariya*[1], *S. Saleh*[2,3], *J. Al-Mufarrij*[4]

[1]Department of Mathematics, Kongunadu Arts and Science College, Coimbatore(Dt)-641029, Tamil Nadu, India
[2]Department of Mathematics, Hodeidah University, Hodeidah, Yemen
[3]Department of Computer Science, Cihan University-Erbil, Kurdistan region, Iraq
[4]Department of Mathematics, Women Section, King Saud University, Riyadh, KSA

Received: 22 May 2023, Revised: 19 Jul. 2023, Accepted: 3 Aug. 2023
Published online: 1 Sep. 2023

Abstract: This study aims to introduce a new structure named binary multiset (BMS), which is a combination of the binary set and multiset structures. The purpose of this paper is to introduce a new topology between two multisets called a binary multiset topology and investigate its fundamental properties, where a binary multiset topology is a binary structure satisfying certain conditions that are analogous to the axioms of topology. Based on this foundation, we develop essential topological notions such as closed BMS, BMS closure, BMS interior, BMS neighborhoods, and BMS derived set, all within the binary multiset topological space framework. Furthermore, our exploration of the BMS topological space unveils a series of characterization theorems and assertions that will further enrich our understanding of this intriguing mathematical construct. This work will pave the way for delving into the study of binary multiset topology, shedding light on more of its fundamental properties and potential applications.

Keywords: BMS; open BMS; BMS topology; BMS closure; BMS neighborhoods; BMS derived sets.

1 Introductions

A topological space plays a fundamental role in contemporary mathematics, serving as a versatile tool to model a wide range of real-world fields such as computer science, molecular biology, and applied multiset theory, a specialized variant known as the M-topological space comes into play. While conventional set theory traditionally allows each distinct member to appear only once in a non-empty set, multiset theory, also referred to as bag set theory [3] or m-set [1], introduced in 1986 and 1989a, breaks these constraints by permitting both identical and distinct repeated elements. The pioneering work on multiset theory was initiated and refined by Bilzard [1, 2], and it has found extensive applications in various biological domains in recent times.

The study of M-topological spaces has given rise to a rich body of research, including developments in new topological space axioms [5], notes on M-topological space [4], generalized m-set and M-ideal continuous functions [6], separation axioms and M- proximity spaces [7, 8], compactness in M-topological spaces [9], boundary and exterior of M-topological spaces [10], relation and function in a m-set context [11], and remarks on M-topological spaces induced by m-set relations [12]. Moreover, researchers have explored various properties of M-topological spaces, such as compactness, as investigated by Mahanta and Samanta [14, 15], and the study of m-set and local functions, including Kuratowski closure operations and generalized closed m-sets [13].

In 2011, Nithyanathan et al. [18] introduced the concept of binary topological spaces, which represent a unique extension of topological spaces. Binary topological spaces have since attracted considerable attention and exploration, enriching the field of topological research as in [16, 17].

This paper aims to contribute to this advanced field by introducing a new structure named binary multisets (or BMS), examining their properties and fundamental operations. Furthermore, the main purpose of this article is to provide a new topological framework known as binary multiset topology (or BMS topology) and establish connections between definitions, theorems, and assumptions. The ideas generated from this research have practical applications, particularly in the domain of dependent examples of binary m-sets. Throughout this work, the prominence of the BMS topological space is evident.

* Corresponding author e-mail: priyalathamax@gmail.com

The structure of this article is organized as: In the first section, we provide a comprehensive overview of the research context and prior work in the field. Section 2, lays the foundation by introducing essential preliminary results and definitions. Section 3, constitutes the core of the paper, presenting the newly defined concept and its principal outcomes. We introduce a new structure named binary multiset (or BMS), investigating some operators and their basic properties supported by some illustrated examples. Accordingly, our focus shifts to providing a specialized topology designed on two m-sets named binary multiset topology(or BMS topology), we delve into the properties of BMS topology, focusing on its role as a binary structure governed by conditions similar to general topological axioms. Section 4, delves into a detailed discussion of the theorems, properties, and results related to some topological concepts such as closed BMS, BMS closure, BMS interior, BMS neighborhood, and BMS-derived sets are discussed via BMS topology. Finally, in section 5, we draw our conclusions and outline future directions for the application of this research within the domain of BMS-spaces.

2 Basic definitions and Preliminaries

In all this document, U refers to a set of elements, M is a multiset, $P(M)$ is the power m-set of M, and (M,τ) refers to M-topological space on M. In general, m-set means multiset and BMS means binary m-set. Firstly, we will recall a set of fundamental definitions, notations, and key findings that will be employed throughout this article.

Definition 1. *[13] An m-set M drawn from the set U is represented by a count function $C_M : U \to N$, where N represents the set of non-negative integers and $C_M(u)$ is the number of occurrences of the element u in the m-set M. We present the m-set M drawn from the set $U = \{u_1, u_2, ..., u_n\}$ as $M = \{m_1/u_1, m_2, /u_2, ..., m_n/u_n\}$, where m_i is the number of occurrences of the element $u_i, i = 1, 2....n$ in the m-set M. However those elements which are not included in the m-set M have zero count.*

A domain U, is defined as a set of elements from which m-set are constructed. The m-set space $[U]^w$ is the set of all m-sets whose members are in U such that no elements in the m-set occur more than w times. By $x \in^k$ we mean $C_M(x) = k$. The support set M^* of $M \in [U]^w$ is a subset of U given as $M^* = \{u \in U : C_M(u) > 0\}$. An m-set M is named an empty m-set if $C_M(x) = 0$ for all $u \in U$.

Note. If $C_M(u) = 1$ for all $u \in U$, then the m-set become structurally an ordinary set. Therefore, any results and concepts we establish under this condition must correspond to specific outcomes in classical set theory.
For two m-sets M and N in a m-set space $[U]^w$, we have [13]:
(1) $M = N \Leftrightarrow C_M(u) = C_N(u)\ \forall u \in U$.
(2) $M \subseteq N \Leftrightarrow C_M(u) \leq C_N(u)\ \forall u \in U$.
(3) $P = M \cup N \Leftrightarrow C_P(u) = Max\{C_M(u), C_N(u)\}\ \forall u \in U$.
(4) $P = M \cap N \Leftrightarrow C_P(u) = Min\{C_M(u), C_N(u)\}\ \forall u \in U$.
(5) $P = M \oplus N \Leftrightarrow C_P(u) = Min\{C_M(u) + C_N(u), w\}\ \forall u \in U$.
(6) $P = M \ominus N \Leftrightarrow C_P(u) = Max\{C_M(u) - C_N(u), 0\}\ \forall u \in U$.
(7) The complement M^c of M given as:
$M^c = Z \ominus M = \{C_{M^c}(u)/u : C_{M^c}(u) = C_Z(u) - C_M(u)\ \forall u \in U\}$, where $\oplus$ and $\ominus$ represent m-set addition and m-set subtraction, respectively.

Definition 2. *[13] Let $[U]^w$ be a m-set space defined over U, then for any m-set $M \in [U]^w$, the complement M^c of M in $[U]^w$ is an element of $[U]^w$ such that $C^c_M(u) = w - C_M(u)$ for all $u \in U$.*

Definition 3. *[12] For two m-sets $M_1, M_2 \in [U]^w$. The Cartesian product of M_1 and M_2 is given by $M_1 \times M_2 = \{(m/u, n/v)/mn : u \in^m M_1, v \in^n M_2\}$. The entry $(m/u, n/v)/mn$ in $M_1 \times M_2$ denotes that u is repeated m times in M_1, v is repeated n times in M_2 and the pair (u, v) is repeated mn times in $M_1 \times M_2$.*

The Cantor's power set theorem does not hold for m-sets. However, it is possible to propose a meaningful definition for a power m-set of M, specifically for finite m-sets M, which maintains the essence of Cantor's power set theorem.

Definition 4. *[12] For an m-set $M \in [U]^w$. The power m-set $P(M)$ of M is the set of all sub m-set of M. We have $N \in P(M)$ if and only if $N \subseteq M$. If $N = \phi$, then $N \in^1 P(M)$ and if $N \neq \phi$, then $N \in^k P(M)$ where $k = \prod_z \binom{C_M(z)}{C_N(z)}$. The product $\prod_z$ is taken over by distinct elements z of the m-set N, $C_M(z) = m$ iff $z \in^m M$, and $C_N(z) = n$ iff $z \in^n N$, then $\binom{C_M(z)}{C)N(z)} = \binom{m}{n} = \frac{m!}{n!(m!-n!)}$. The power set of a m-set M is the support set of the power m-set $P(M)$, which is symbolized by $P^*(M)$.*

Definition 5. *[12] Let $M \in [U]^w$ and $\tau \subseteq P^*(M)$. Then τ is called a multiset topology (or M-topology) of M if τ satisfies the following properties.*
(i) The m-set M and the empty m-set ϕ are in τ.
(ii) The m-set union of the elements of any sub-collection of τ is in τ.
(iii) The m-set intersection of the elements of any finite sub-collection of τ is in τ.

The pair (M,τ) is called M-topological space. Each element in τ is called open m-set.

A sub-m-set N of a M-topological space (M,τ) is named a closed m-set if the m-set $M \ominus N$ is open. In discrete M-topology, every m-set is an open m-set as well as a closed m-set.

Definition 6. *[11] For a sub m-set A of (M,τ). The interior $int(A)$ of A is the m-set union of all open m-sets contained in A. That is, $int(A) = \cup\{G \in \tau : G \subseteq A\}$ and*

$C_{int(A)}(u) = max\{C_G(u) : G \subseteq A\}$. *The closure* $cl(A)$ *of* A *is the m-set intersection of all closed m-sets containing* A. *That is,* $cl(A) = \cap\{G \subseteq M : G$ *is a closed m-set and* $A \subseteq G\}$ *and* $C_{cl(A)}(u) = min\{C_G(u) : A \subseteq G\}$.

Definition 7. *[11] Let* (M,τ) *be a M-topological space,* $u \in^k M$, *and* $N \subseteq M$. *Then* N *is named a neighborhood of* k/u *if there is an open m-set* $V \in \tau$ *such that* $u \in^k V$ *and* $C_V(v) \leq C_N(v)$ *for all* $v \neq u$. *i.e., an open neighborhood of* k/u *is any open m-set containing* k/u. *Here* k/u *is called an interior point of* N.

Definition 8. *[11] Let* A *be a sub m-set of the* M*-topological space* M. *If* k/u *is an element of* M, *then* k/u *is a limit point of a m-set* A *when every neighborhood of* k/u *intersects* A *is some point (point with non-zero multiplicity) other than* k/u *itself.* $D(A)$ *denotes the m-set of all limit points of* A.

Definition 9. *[18] Consider two non empty sets* X *and* Y. *A binary topology from* X *to* Y *is a binary structure* $\rho \subseteq P(X) \times P(Y)$ *that satisfies the following axioms.*
(i) (ϕ,ϕ) *and* $(X,Y) \in \rho$.
(ii) $(A_1 \cap A_2, B_1 \cap B_2) \in M$ *whenever* $(A_1,B_1) \in \rho$, $(A_2,B_2) \in \rho$.
(iii) If $\{(A_\alpha,B_\alpha) : \alpha \in \Delta\}$ *is a family of members of* ρ, *then* $(\cup A_\alpha, \cup B_\alpha) \in \rho$.

3 Binary multiset topological space

In this part, we provide a new concept called binary m-set and a new structure called BMS topology, investigating the fundamental properties of each. Various theorems, results, and examples related to BMS topological space are also presented.

Definition 10.*Let* U,V *be two non-empty sets, and let* $[U]^w$ *and* $[V]^r$ *be two m-set spaces on* U *and* V *respectively, then the ordered pair* (M_1,M_2) *is called a binary multiset (or BMS) where* $M_1 \in [U]^w$, $M_2 \in [V]^r$ *are two m-sets drawn from* U *and* V *respectively.*
Note. *We know that, the power set* $P^*(M_1)$ *of a m-set* M_1*(resp. the power set* $P^*(M_2)$ *of* M_2*) is the support set of the power m-set of* M_1*(resp.* M_2*). We can define* $P^*(M_1) \times P^*(M_2) = \{(A_i,B_i) : A_i \in P^*(M_1), B_i \in P^*(M_2)\}$. *According to this definition, the ordered pair* (A,B) *is called a BMS from* M_1 *to* M_2 *where* $A \subseteq M_1$ *and* $B \subseteq M_2$. *That is, the BMS* (A,B) *is an element in* $P^*(M_1) \times P^*(M_2)$.

*Example 1.*Consider the two non-empty sets $U = \{x,y\}$ and $V = \{m,n\}$. Let $M_1 = \{2/x, 1/y\}$ and $M_2 = \{1/m, 2/n\}$ be two m-sets drawn form U and V respectively, then we have:

$P^*(M_1) = \{\emptyset, M_1, \{1/x\}, \{1/y\}, \{2/x\}, \{1/x,1/y\}\}$ *and*

$P^*(M_2) = \{\emptyset, M_2, \{1/m\}, \{1/n\}, \{2/n\}, \{1/m,1/n\}\}$

and so,

$$P^*(M_1)\times P^*(M_2) = \{(\emptyset,\emptyset),(M_1,M_2),(\{1/x\},\{1/m\}),$$
$$(\{1/x\},\{1/n\}),(\{1/x\},\{2/n\}),(\{2/x\},\{1/m\}),$$
$$(\{2/x\},\{2/n\}),(\{2/x\},\{1/n\}),(\{1/y\},\{1/m\}),$$
$$(\{1/y\},\{1/n\}),(\{1/x\},\{1/m,1/n\}),(\{2/x\},$$
$$\{1/m,1/n\}),$$
$$(\{1/y\},\{2/n\}),(\{1/y\},\{1/m,1/n\}),(\{1/x,1/y\},$$
$$\{1/m,1/n\}),$$
$$(\{1/x,1/y\},\{1/m\}),(\{1/x,1/y\},\{1/n\}),(\{1/x,1/y\},$$
$$\{2/n\}),$$
$$(M_1,\{1/m\}),(M_1,\{2/n\}),(M_1,\{1/m,1/n\}),$$
$$(M_1,\{1/n\}),$$
$$(\{2/x\},M_2),(\{1/x\},M_2),(\{1/y\},M_2),(\{1/x,1/y\},\ M_2),$$
$$(\emptyset,\{1/m\}),(\emptyset,\{1/n\}),(\emptyset,\{2/n\}),(\emptyset,\{1/x,1/y\}),$$
$$(\emptyset,M_2),(\{1/x\},\emptyset),(\{2/x\},\emptyset),(\{1/y\},\emptyset),$$
$$(\{1/x,1/y\},\emptyset),(M_1,\emptyset)\}.$$

Clearly, each ordered pair in $P^*(M_1)\times P^*(M_2)$ represent a BMS from M_1 to M_2.

In the following, we define some relations and operations on BMS.

Definition 11.*For two m-sets* $M_1 \in [U]^w, M_2 \in [V]^r$ *and two BMS* $(A,B),(C,D) \in P^*(M_1) \times P^*(M_2)$, *we define the following:*
(i) $(A,B) \subseteq (C,D)$ *iff* $A \subseteq C$, $B \subseteq D$
(ii) $(A,B) = (C,D)$ *iff* $A = C$, $B = D$
(iii) $(A,B) \cup (C,D) = (A \cup C, B \cup D)$
(iv) $(A,B) \cap (C,D) = (A \cap C, B \cap D)$
(v) $(A,B) \oplus (C,D) = (A \oplus C, B \oplus D)$
(vi) $(A,B) \ominus (C,D) = (A \ominus C, B \ominus D)$
(vii) $(A,B)^c = (A^c,B^c) = (M_1 \ominus A, M_2 \ominus B)$.

Definition 12.*Consider the BMS* (M_1,M_2) *drawn from* U *to* V. *The support set of* (M_1,M_2) *symbolized by* $S(M_1,M_2)$ *is a binary set of* U *to* V, *given by* $S(M_1,M_2) = (M_1^*,M_2^*)$ *where* M^* *is the support set of a m-set* M.

*Example 2.*Consider Example 1. For a m-sets $M_1 = \{2/x, 1/y\}, M_2 = \{1/m, 2/n\}$. The support of BMS (M_1,M_2) is $S(M_1,M_2) = (M_1^*,M_2^*) = (\{x,y\},\{m,n\})$ which is a binary set from U to V.

Definition 13.*For a collection of BMS* $\{(M_i,M_j) : i,j \in \Delta\}$ *drawn form* $[U]^w$ *to* $[V]^r$*. The following operations are defined under arbitrary collections of BMS:*
(i) $\cup(M_i,M_j) = (\cup M_i, \cup M_j)$,
(ii) $\cap(M_i,M_j) = (\cap M_i, \cap M_j)$,
where:
$\cup M_i = \{C_{\cup M_i}(u)/u : C_{\cup M_i}(u) = max\{C_{M_i}(u) : u \in U\}\}$,
$\cup M_j = \{C_{\cup M_j}(v)/v : C_{\cup M_j}(v) = max\{C_{M_j}(v) : v \in V\}\}$,
$\cap M_i = \{C_{\cap M_i}(u)/u : C_{\cap M_i}(v) = min\{C_{M_i}(u) : u \in U\}\}$,
$\cap M_j = \{C_{\cap M_j}(v)/v : C_{\cap M_j}(v) = min\{C_{M_j}(v) : v \in V\}\}$.

Definition 14.*Let* $M_1 \in [U]^w$ *and* $M_2 \in [V]^r$*. The BMS complement for the BMS* (M_1,M_2) *in* $P^*(M_1) \times P^*(M_2)$ *is denoted by* $(M_1,M_2)^c$ *where,* $(M_1,M_2)^c = C_{(M_1,M_2)^c} = (w - C_{M_1}(u), r - C_{M_2}(v))$ *for all* $u \in U$ *and* $v \in V$.

Definition 15.*A non-empty BMS* (A,B) *is called a sub-BMS of a BMS* (M_1,M_2) *if each element of* (A,B) *is in* (M_1,M_2)*, symbolically* $(A,B) \subseteq (M_1,M_2)$*, that is,* $A \subseteq M_1$ *and* $B \subseteq M_2$*. In this case, we say that* (M_1,M_2) *is super BMS of* (A,B).

A binary multiset topology from $M_1 \in [U]^w$ to $M_2 \in [V]^r$ is a binary structure satisfying certain axioms that are analogous to the axioms of topology. In this section, the notion of a binary multiset topology between two m-sets M_1,M_2 is introduced, and its structural properties are investigated. Throughout this section $P^*(M_1),P^*(M_2)$ refer to the power sets of m-sets M_1,M_2 respectively.

Definition 16.*Let* $M_1 \in [U]^w$, $M_2 \in [V]^r$ *be two m-sets drawn from* U *and* V *respectively. A binary multiset topology (briefly, BMS-topology) from* M_1 *to* M_2 *is a binary multiset structure* $\tau_b \subseteq P^*(M_1) \times P^*(M_2)$ *that satisfies the following axioms:*
(i) $(\emptyset,\emptyset),(M_1,M_2) \in \tau_b$
(ii) If $(A_1,B_1),(A_2,B_2) \in \tau_b$*, then* $(A_1 \cap A_2, B_1 \cap B_2) \in \tau_b$
(iii) If $\{(A_\lambda,B_\lambda) : \lambda \in J\} \subseteq \tau_b$*, then* $(\cup A_\lambda, \cup B_\lambda) \in \tau_b$.

In this case, the structure (M_1,M_2,τ_b) is called a BMS-topological space (or BMS-space). Note that τ_b is an ordinary set with BMS elements.

Definition 17.*For a BMS-space* (M_1,M_2,τ_b)*, we have:*
(i) Each element in τ_b *is called an open binary multiset (or open BMS), and the complement of an open BMS is named a closed binary multiset (or closed BMS).*
(ii) A sub-BMS (A,B) *of a BMS-space* (M_1,M_2,τ_b) *is said to be closed if the BMS* $(A,B)^c = (M_1 \ominus A, M_2 \ominus B)$ *is an open BMS.*
(iii) If $M_1 = M_2$ *then* τ_b *is named a BMS-topology on* M_1*, we write* (M_1,τ_b) *as a BMS space.*

*Example 3.*Consider the two non-empty sets $U = \{x,y\}$, $V = \{m,n\}$ and two m-sets $M_1 = \{2/x,1/y\}$, $M_2 = \{1/m,2/n\}$ drawn from U,V respectively, then:

$\tau_b = \{(\emptyset,\emptyset),(M_1,M_2),(\{1/x\},\emptyset),(\{1/x\},\{1/m\}),$

$(\{1/x\},\{1/n\}),(\{1/x\},\{1/m,1/n\})\}$

is a BMS-topology from M_1 to M_2. The open BMS are:

$\{(\emptyset,\emptyset),(M_1,M_2),(\{1/x\},\emptyset),(\{1/x\},\{1/m\}),$

$(\{1/x\},\{1/n\}),(\{1/x\},\{1/m,1/n\})\}$.

So, the BMS complement of an open BMS gives us the closed BMS as:

$\{(\emptyset,\emptyset),(M_1,M_2),(\{1/x,1/y\},M_2),(\{1/x,1/y\},\{2/n\}),$

$(\{1/x,1/y\},\{1/m,1/n\}),(\{1/x,1/y\},\{1/n\})\}$.

Definition 18.*A sub-BMS of* (M_1,M_2) *in the form* $(\{k/u\},\{m/v\})$ *is named a binary multi-point (or BM-point) of the BMS-space* (M_1,M_2,τ_b)*. That is, the BM-point is an element in* $P^*(M_1 \times M_2)$*. The set of all BM-points from* M_2 *to* M_2 *is denoted by* $P^*(M_1 \times M_2)$.

Note. $(\{k/u\},\{m/v\}) \subseteq (M_1,M_2)$ means $\{k/u\} \subseteq M_1$ and $\{m/v\} \subseteq M_1$. Moreover, $u \in^k M_1$ and $v \in^m M_2$. Also, this means that $C_{M_1}(u) = k$ and $C_{M_2}(v) = m$, so that $\{k/u\}$ is a m-point of M-topology (M_1,τ) and $\{m/v\}$ is a m-point of M-topology (M_2,τ).

*Example 4.*Consider the Example 3, the set of all bm-points from M_1 to M_2 is $P^*(M_1 \times M_2) =$

$\{(\{1/x\},\{1/m\}),(\{1/x\},\{1/n\}),(\{1/x\},\{2/n\}),$

$(\{2/x\},\{1/m\}),(\{2/x\},\{2/n\}),(\{2/x\},\{1/n\}),$

$(\{1/y\},\{1/m\}),(\{1/y\},\{1/n\}),(\{1/y\},\{2/n\})\}$

*Example 5.*The collection $I = \{(\emptyset,\emptyset),(M_1,M_2)\}$ is called the in-discrete BMS topology from M_1 to M_2 and the structure (M_1,M_2,I) is named the in-discrete BMS topological space.

On the other hand, the collection $D = P^*(M_1) \times P^*(M_2)$ is called the discrete BMS topology from M_1 to M_2 and the structure (M_1,M_2,D) is named the discrete BMS topological space.

Note. Consider a discrete BMS-space $D = P^*(M_1) \times P^*(M_2)$. The support BMS power set of (M_1,M_2,D) is a discrete BMS-space or a trivial BMS-space.

Definition 19.*For a BMS-space* (M_1,M_2,τ_b) *and for a BM-point* $(\{k/u\},\{m/v\}) \in P^*(M_1 \times M_2)$*. The open BMS* (A,B) *is called an open binary multiset neighborhood(or open BMS-nbd) of* $(\{k/u\},\{m/v\})$ *if* $\{k/u\} \subset A$ *and* $\{m/v\} \subset B$*. That is,* (A,B) *is an open BMS-nbd of* $\{k/u\},\{m/v\}$ *if* $u \in^k A$ *and* $v \in^m B$.

*Example 6.*Consider $U = \{a,b,c\}$, $M = \{2/a,1/b,1/c\}$. Then the class $\tau_b = \{(\emptyset,\emptyset),(M,M),(\{1/a\},\{1/b\}),$ $(\{2/a\},\{1/b\}),(\{1/a\},\{1/a,1/b\}),(\{2/a\},\{1/a,1/b\})\}$ is a BMS topology on M.

For a bm-point $(\{1/a\},\{1/b\})$. The set of all open BMS-nbd of $(\{1/a\},\{1/b\})$ is $\{(M,M),(\{1/a\},\{1/b\}),$ $(\{2/a\},\{1/b\}),(\{1/a\},\{1/a,1/b\}),(\{2/a\},\{1/a,1/b\})\}$

*Example 7.*Consider the BMS (M_1,M_2). The collection $\tau_b^{co} = \{(\emptyset,\emptyset)\} \cup \{(A,B) \subseteq (M_1,M_2) : (A,B)^c$ is a countable BMS$\}$ is a BMS topology from M_1 to M_2 named the co-countable BMS topology.

*Example 8.*Consider the BMS (M_1,M_2). The family $\tau_b^{\infty} = \{(\emptyset,\emptyset)\} \cup \{(A,B) \subseteq (M_1,M_2) : (A,B)^c$ is a finite BMS$\}$ is a BMS topology from M_1 to M_2 named the co-finite BMS topology.

Definition 20.*Consider two BMS topologies τ_b^1 and τ_b^2 from M_1 to M_2. If each open BMS in τ_b^1 is also an open BMS in τ_b^2, then τ_b^1 is called a BMS topology coarser than τ_b^2 , or τ_b^2 is a BMS topology finer than τ_b^1 and we write this as $\tau_b^1 \subseteq \tau_b^2$. If $\tau_b^1 \not\subseteq \tau_b^2$ and $\tau_b^2 \not\subseteq \tau_b^1$, then we say that τ_b^1 and τ_b^2 are not BMS comparable.*

*Example 9.*Let $M_1 = M_2 = 2/x,2/y$, and consider two BMS topologies $\tau_b^1 = \{(M_1,M_2),(\phi,\phi),(\{1/x\},\{1/y\})\}$, $\tau_b^2 = \{(M_1,M_2),(\phi,\phi),(\{2/x\},\{2/y\}),(\{1/x\},\{1/y\})\}$. Clearly, τ_b^1 is BMS coarser than τ_b^2 in other words τ_b^2 is BMS finer than τ_b^1. In this case we say τ_b^2 and τ_b^1 are BMS comparable topologies.

Theorem 1.*The BMS intersection for arbitrary collection of BMS topologies is a BMS topology from M_1 to M_2.*

*Proof.*Suppose that $\{\tau_{b_\lambda} : \lambda \in \Delta\}$ is an arbitrary collection of BMS topologies from M_1 to M_2. We want to prove that $\cap\{\tau_{b_\lambda} : \lambda \in \Delta\}$ is an BMS topology from M_1 to M_2.
(i) Since each τ_{b_λ} is an BMS topology from M_1 to ,M_2 for all $\lambda \in \Delta$. By Definition 16, (M_1,M_2), $(\phi,\phi) \in \tau_{b_\lambda}$, $\forall\lambda \in \Delta$. So, $(M_1,M_2),(\phi,\phi) \in \cap\tau_{b_\lambda}$.
(ii) Assume that $(A_1,B_1),(A_2,B_2) \in \cap\tau_{b_\lambda}$, we have $(A_1,B_1),(A_2,B_2) \in \tau_{b_\lambda}$ $\forall\lambda \in \Delta$ and so, $(A_1,B_1) \cap (A_2,B_2) \in \tau_{b\lambda}$ $\forall\lambda \in \Delta$. Hence $(A_1,B_1) \cap (A_2,B_2) \in \cap\tau_{b_\lambda}$.
(iii) Consider the arbitrary collection of BMS $\{(A_\alpha,B_\alpha) : \alpha \in \Gamma\} \subseteq \cap\tau_{b_\lambda}$, we have $\{(A_\alpha,B_\alpha) : \alpha \in \Gamma\} \subseteq \tau_{b_\lambda}$ $\forall\lambda \in \Delta$. Since τ_{b_λ} is BMS topologies from M_1 to M_2 $\forall\lambda \in \Delta$, we get $\cup\{(A_\alpha,B_\alpha) : \alpha \in \Gamma\} \in \tau_{b_\lambda}$ $\forall\lambda \in \Delta$. Therefore, $\cup\{(A_\alpha,B_\alpha) : \alpha \in \Gamma\} \in \cap\tau_{b_\lambda}$. This completes the proof.

The following example shows that the union of two BMS topologies does not need to be a BMS topology.

*Example 10.*Consider $M_1 = \{2/x,2/y\},M_2 = \{2/t\}$, and two BMS topologies from M_1 to M_2 $\tau_b^1 = \{(\phi,\phi),(M_1,M_2),(\{1/x\},\emptyset),(\{2/x\},\{2/t\})\}$, $\tau_b^2 = \{(\phi,\phi),(M_1,M_2),(\{2/x\},\{1/t\}),(\emptyset,\{1/t\})\}$, then:

$$\tau_b^1 \cup \tau_b^2 = \{(\phi,\phi),(M_1,M_2),(\{1/x\},\emptyset),$$
$$(\{2/x\},\{2/t\}),(\{2/x\},\{1/t\}),(\emptyset,\{1/t\})\}.$$

Clearly, $\tau_b^1 \cup \tau_b^2$ is not a BMS topology of (M_1,M_2). Indeed, $(\{1/x\},\emptyset) \cup (\emptyset,\{1/t\}) = (\{1/x\},\{1/t\})$ does not belong to $\tau_b^1 \cup \tau_b^2$.

The next proposition explains that every BMS topology from M_1 to M_2 generated two M-topologies, one on M_1 and another on M_2.

Proposition 1.*For a BMS-topological space (M_1,M_2,τ_b) from M_1 to M_2, the collection:*
(i) $M_1(\tau_b) = \{A \subseteq M_1 : (A,B) \in (M_1,M_2,\tau_b)$ for some $B \subseteq M_2\}$ is a M-topology on M_1.
(ii) $M_2(\tau_b) = \{B \subseteq M_2 : (A,B) \in (M_1,M_2,\tau_b)$ for some $A \subseteq M_1\}$ is a M-topology on M_2.

Proof.(i) Assume that (M_1,M_2,τ_b) is a BMS topology from M_1 to M_2. Since $(\phi,\phi),(M_1,M_2) \in \tau_b$, we have $\phi,M_1 \in M_1(\tau_b)$. Assume that $A_1,A_2 \in M_1(\tau_b)$, then $(A_1,B_2),(A_2,B_2) \in \tau_b$ for some $B_1,B_2 \subseteq M_2$. Since τ_b is a BMS topology, we get $(A_1 \cap A_2,B_1 \cap B_2) \in \tau_b$. This implies that $A_1 \cap A_2 \in M_1(\tau_b)$. Now assume that $\{A_\lambda : \lambda \in \Delta\} \subseteq M_1(\tau_b)$, then for any $A_\lambda \subseteq M_1$ there is a $B_\lambda \subseteq M_2$ such that $(A_\lambda,B_\lambda) \in \tau_b$. Since τ_b is a BMS topology, we have $(\cup A_\lambda,\cup B_\lambda) \in \tau_b$ implies that $\cup A_\lambda \in M_1(\tau_b)$. Therefore, $M_1(\tau_b)$ is M-topology on M_1. The proof of (ii) is similar.

Proposition 2.*For two M-topologies (M_1,τ) and (M_2,σ), we have $\tau \times \sigma$ is BMS topology from M_1 to M_2. Moreover, $M_1(\tau \times \sigma) = \tau$ and $M_2(\tau \times \sigma) = \sigma$.*

*Proof.*Suppose that (M_1,τ) and (M_2,σ) are two M-topological spaces, then:
$\tau \times \sigma = \{(A,B) : A \in \tau, B \in \sigma\}$. We want to prove that $\tau \times \sigma$ is a BMS topology from M_1 to M_2. Since τ,σ are M-topologies. Clearly, $(\phi,\phi),(M_1,M_2) \in \tau \times \sigma$.
Let $(A_1,B_1),(A_2,B_2) \in \tau \times \sigma$. Then $A_1,A_2 \in \tau$ and $B_1,B_2 \in \sigma$. Since τ,σ are M-topologies, we have $(A_1 \cap A_2) \in \tau$ and $(B_1 \cap B_2) \in \sigma$. So that $((A_1 \cap A_2),(B_1 \cap B_2)) \in \tau \times \sigma$.
Assume that $\{(A_\lambda,B_\lambda) : \lambda \in \Delta\} \subseteq \tau \times \sigma$. since τ and σ are M-topologies, we have $\cup A_\lambda \in \tau$ and $\cup B_\lambda \in \sigma$ this implies that $(\cup A_\lambda,\cup B_\lambda) \in \tau \times \sigma$. Hence $\tau \times \sigma$ is a BMS topology.

To prove that $M_1(\tau \times \sigma) = \tau$. Clearly, $M_1(\tau \times \sigma) = \{A \subseteq M_1 : (A,B) \in \tau \times \sigma,$ *for some* $B \subseteq M_2\}$. If $A \in \tau$, then $(A,B) \in \tau \times \sigma$ for each $B \in \sigma$ hence $A \in M_1(\tau \times \sigma)$ and so, $\tau \subseteq M_1(\tau \times \sigma)$. On the other hand, let $A \in M_1(\tau \times \sigma)$. Then $(A,B_1) \in \tau \times \sigma$ for some $B_1 \subseteq M_2$, thus $B_1 \in \sigma$ and so, $A \in \tau$. Therefore, $M_1(\tau \times \sigma) = \tau$. The proof of the rest of the case is similar.

4 Basic properties of some BMS topological concepts

Here, theorems, properties, and results related to the concepts of BMS closed, BMS closure, BMS interior, BMS neighborhood, and BMS derived set are discussed.

Definition 21.*A sub-BMS (A,B) of a BMS topological space in (M_1,M_2,τ_b) is named closed BMS if the BMS complement of (A,B) is an open BMS.*

Note. For an BMS topological space (M_1,M_2,τ_b), $A\subseteq M_1$, and $B\subseteq M_2$, we have (A,B) is closed BMS in (M_1,M_2,τ_b^c), where $(M_1\ominus A, M_2\ominus B)\in\tau_b^c$.

*Example 11.*Consider $U=\{a,b,c\}, V=\{x,y\}$ and for two m-sets $M_1=\{2/a,3/b,4/c\}$, $M_2=\{3/x,2/y\}$ of U and V, then:
$\tau_b=\{(\phi,\phi),(M_1,M_2),(\{2/a\},\{3/x\}),(\{1/b\},\{2/y\})\}$, $(\{2/a,1/b\},\{3/x,2/y\})$. is a BMS topology from M_1 to M_2. Now every member of τ_b is named an open BMS, and the BMS complement of them are called closed BMS, that is the class of all closed BMS in (M_1,M_2,τ_b) is:
$\tau_b^c=\{(\phi,\phi),(M_1,M_2),(\{3/b,4/c\},\{2/y\}),$
$(\{2/a,2/b,4/c\},\{3/x\}),(\{2/b,4/c\},\phi)\}$.

Note. Clearly, (ϕ,ϕ) and (M_1,M_2) are both open and closed sub-BMS of any BMS topology.

One can verify the next proposition.

Proposition 3.*For an BMS-topological space (M_1,M_2,τ_b). The next properties are true:*
(i) (M_1,M_2) and (ϕ,ϕ) are BMS closed.
(ii) The BMS finite union of any arbitrary collection of closed sub-BMS in (M_1,M_2,τ_b) is a closed BMS.
(iii) The intersection of any collection of closed sub-BMS of (M_1,M_2,τ_{BMS}), is a closed BMS.

*Example 12.*The discrete BMS-topological space (M_1,M_2,D) represents the family of all closed as well as open sub-BMS.

Theorem 2.*Consider a BMS (M_1,M_2) and a class $\mathscr{C}$ of sub-BMS of (M_1,M_2) that satisfies:*
(i) (ϕ,ϕ) and $(M_1,M_2)\in\mathscr{C}$.
(ii) $\{(A_\alpha,B_\alpha):\alpha\in\Delta\}\subseteq\mathscr{C}$ implies $\cup(A_\alpha,B_\alpha)\in\mathscr{C}$.
(iii) $\{(A,B)_\alpha:\alpha\in\Delta\}\subseteq\mathscr{C}$ implies $\cap(A_\alpha,B_\alpha)\in\mathscr{C}$. Then there exists a unique BMS topology τ_b^* for (M_1,M_2) such that τ_b^*-closed sub-BMS of (M_1,M_2) are members of $\mathscr{C}$.

*Proof.*Define $\tau_b^*=\{(M_1,M_2)\ominus(A,B):(A,B)\in\mathscr{C}\}$.
(i) Since $(\phi,\phi)^c=(M_1,M_2)\in\mathscr{C}$ and $(M_1,M_2)^c=(\emptyset,\emptyset)\in\mathscr{C}$, then $(M_1,M_2),(\phi,\phi)\in\tau_b^*$.
(ii) If $(A_1,B_1),(A_2,B_2)\in\tau_b^*$, then $(M_1,M_2)\ominus(A_1,B_1)\cup(M_1,M_2)\ominus(A_2,B_2)\in\mathscr{C}$. Hence $(M_1,M_2)\ominus((M_1,M_2)\ominus(A_1,B_1)\cup(M_1,M_2)\ominus(A_2,B_2))=(A_1\cap A_2,B_1\cap A_2)\in\tau_b^*$.
(iii) In a similar way, if $\{(A_\lambda,B_\lambda):\lambda\in\Delta\}\subseteq\tau_b^*$, then, $\cap(M_1,M_2)\ominus(A_\lambda,B_\lambda)\in\mathscr{C}$. Hence, $(M_1,M_2)\ominus\cap(M_1,M_2)\ominus(A_\lambda,B_\lambda)=\cup\{(A_\lambda,B_\lambda):\lambda\in\Delta\}\in\tau_b^*$. To prove the uniqueness of BMS τ_b^*. Suppose that τ_b^{**} is a another BMS-space which has the same closed BMS as τ_b^*, then $(A,B)\in\tau_b^*\iff(M_1,M_2)\ominus(A,B)$ is a τ_b^*-closed BMS $\iff(M_1,M_2)\ominus(A,B)$ is a τ_b^{**}-closed BMS $\iff(A,B)\in\tau_b^{**}$-closed BMS. Hence τ_b^* is unique.

Proposition 4.*For a BMS-space (M_1,M_2,τ_b) and $(A,B)\subseteq(M_1,M_2)$. Let $(A,B)^{1*}=\cap\{A_\lambda:(A_\lambda,B_\lambda)$ is a closed BMS, $(A,B)\subseteq(A_\lambda,B_\lambda)\}$ and $(A,B)^{2*}=\cap\{B_\lambda:(A_\lambda,B_\lambda)$ is a closed BMS, $(A,B)\subseteq(A_\lambda,B_\lambda)\}$. Then $((A,B)^{1*},(A,B)^{2*})$ is a closed BMS. Moreover, $(A,B)\subseteq((A,B)^{1*},(A,B)^{2*})$.*

*Proof.*It follows from Proposition 3.

Definition 22.*Consider the BMS-space (M_1,M_2,τ_b) and $(A,B)\subseteq(M_1,M_2)$. The ordered pair $((A,B)^{1*},(A,B)^{2*})$ is called BMS closure of (A,B) which is the intersection of all closed BMS containing (A,B), and is symbolized by $cl_b((A,B))$. That is, $cl_b((A,B))=\cap\{(G,H)\subseteq(M_1,M_2):(G,H)\}$ is a closed BMS and $(A,B)\subseteq(G,H)$.*

Theorem 3.*For two sub-BMS (A,B) and (C,D) in BMS-space (M_1,M_2,τ_b) with $(A,B)\subseteq(C,D)$, we have:*
(i) $cl_b(\phi,\phi)=(\phi,\phi)$, $cl_b(M_1,M_2)=(M_1,M_2)$.
(ii) $(A,B)\subseteq cl_b(A,B)$.
(iii) $cl_b(A,B)$ is the smallest closed BMS containing (A,B).
(iv) (A,B) is closed BMS iff $(A,B)=cl_b((A,B))$.
(v) $(A,B)^{1*}\subseteq(C,D)^{1*}$, $(A,B)^{2*}\subseteq(C,D)^{2*}$.
(vi) $cl_b(A,B)\subseteq cl_b(C,D)$.
(vii) $cl_b(cl_b((A,B))=cl_b((A,B))$.

*Proof.*The proof of items (i),(ii),(iii) is obvious.
(iv) Assume that (A,B) is closed BMS. From Definition 22, $(A,B)\subseteq cl_b((A,B))$ which implies that $A\subseteq(A,B)^{1*}$ and $B\subseteq(A,B)^{2*}$. Clearly, (A,B) is a closed BMS containing itself. so that $((A,B)^{1*},(A,B)^{2*})\subseteq(A,B)$. Hence $(A,B)=cl_b((A,B))$.
Conversely, assume that $(A,B)=cl_b((A,B))$. From Proposition 4, $cl_b((A,B))$ is a closed BMS, and so (A,B) is a closed BMS.
(v) From Proposition 4, $(A,B)^{1*}=\cap\{A_\lambda:(A_\lambda,B_\lambda)$ is a closed BMS,$(A,B)\subseteq(A_\lambda,B_\lambda)\}\subseteq\cap\{A_\lambda:(A_\lambda,B_\lambda)$ is a closed BMS, $(C,D)\subseteq(A_\lambda,B_\lambda)\}=(C,D)^{1*}$.
The other case is similar.
(vi) Since $(A,B)\subseteq(C,D)$, then $cl_b((A,B))=((A,B)^{1*},(A,B)^{2*})\subseteq((C,D)^{1*},(C,D)^{2*})=cl_b((C,D))$.
(vii) It follows from (iv).

Proposition 5.*For two sub-BMS $(A,B),(C,D)$ in BMS-space (M_1,M_2,τ_b), we have:*
(i) $(A,B)^{1*}\cup(C,D)^{1*}\subseteq(A\cup C,B\cup D)^{1*}$.
(ii) $(A,B)^{2*}\cup(C,D)^{2*}\subseteq(A\cup C,B\cup D)^{2*}$.

Proof.(i) Clearly, (A,B) andn(C,D) are two sub-BMS of $(A\cup C,B\cup D)$. From theorem 3 (v), we have $(A,B)^{1*}\subseteq(A\cup C,B\cup D)^{1*}$. Again by Theorem 3 (v), $(C,D)^{1*}\subseteq(A\cup C,B\cup D)^{1*}$ which impels that $(A,B)^{1*}\cup(C,D)^{1*}\subseteq(A\cup C,B\cup D)^{1*}$.
The proof of case (ii) is similar.

Proposition 6.*For two sub-BMS (A,B), (C,D) in BMS-space (M_1,M_2,τ_b), we have:*
(i) $((A\cap C),(B\cap D))^{1*}\subseteq(A,B)^{1*}\cap(C,D)^{1*}$.
(ii) $(A\cap C,B\cap D)^{2*}\subseteq(A,B)^{2*}\cap(C,D)^{2*}$.

*Proof.*It is analogous to that in Proposition 5.

The next examples illustrate that reverse inclusion in the Propositions 5 and 6 need not hold in general.

*Example 13.*Consider the Example 11, suppose that $(A,B) = (\{1/a,2/b\},\{1/x\})$ and $(C,D) = (\{2/a\},\{3/x\})$ are two sub-BMS of (M_1,M_2), we have $(A,B)^{1*} = \{2/a,2/b,4/c\}$, $(C,D)^{1*} = \{2/a,2/b,4/c\}$, and so $L.H.S = (A,B)^{1*} \cup (C,D)^{1*} = \{2/a,2/b,4/c\}$. On the other hand, $(A \cup C, B \cup D) = (\{2/a,2/b\},\{1/x,2/y\})$ implies that $R.H.S = (A \cup C, B \cup D)^{1*} = M_1$. Hence $R.H.S \not\subseteq L.H.S$.

*Example 14.*Consider Example 11, suppose that $(A,B) = (\{3/b\},\emptyset\})$ and $(C,D) = (\{1/a\},\emptyset\})$ are two sub-BMS of (M_1,M_2), we have $(A,B)^{1*} = \{3/b,4/c\}$, $(C,D)^{1*} = \{2/a,2/b,4/c\}$, and so $R.H.S = (A,B)^{1*} \cap (C,D)^{1*} = \{2/a,4/c\}$. On the other hand, $(A \cap C, B \cap D) = (\{\emptyset,\emptyset\})$ implies that $L.H.S = (A \cap C, B \cap D)^{1*} = \emptyset$. Hence $R.H.S \not\subseteq L.H.S$.

Proposition 7.*Consider a BMS-space (M_1,M_2,τ_b), $(\{k/x\},\{m/y\}) \subseteq (M_1,M_2)$, and $(A,B) \subseteq (M_1,M_2)$, then $(\{k/x\},\{m/y\}) \subseteq cl_b((A,B))$ if and only if every open BMS containing $(\{k/x\},\{m/y\})$ intersects (A,B).*

*Proof.*If $(k/x,m/y) \notin cl_b(A,B)$, then the BMS $(M_1,M_2) \ominus cl_b(A,B)$ is an open BMS containing $(k/x,m/y)$ but does not intersect (A,B). Conversely, if there exists an open BMS (P,Q) containing $(k/x,m/y)$ that does not intersect (A,B), then the BMS $(M_1,M_2) \ominus (P,Q)$ is a closed BMS containing (P,Q). By Definition 4, the BMS $(M_1,M_2) \ominus (P,Q)$ must contain $cl_b(A,B)$. Hence $(k/x,m/y) \notin cl_b(A,B)$

Proposition 8.*For a BMS-space (M_1,M_2,τ_b) and $(A,B) \subseteq (M_1,M_2)$. Let $(A,B)^{1\circ} = \cup\{A_\lambda : (A_\lambda,B_\lambda)$ is an open BMS, $(A_\lambda,B_\lambda) \subseteq (A,B)\}$ and $(A,B)^{2\circ} = \cup\{B_\lambda : (A_\lambda,B_\lambda)$ is an open BMS, $(A_\lambda,B_\lambda) \subseteq (A,B)\}$. Then $((A,B)^{1\circ},(A,B)^{2\circ})$ is an open BMS. Moreover, $((A,B)^{1\circ},(A,B)^{2\circ}) \subseteq (A,B)$.*

*Proof.*It is follow from Definition 16.

The subsequent definition stems from the preceding proposition.

Definition 23.*For a BMS (A,B) in a BMS-space (M_1,M_2,τ_b). The ordered pair $((A,B)^{1\circ},(A,B)^{2\circ})$ is called BMS interior, denoted by $int_b(A,B)$, is the union of all open BMS contained in (A,B). That is, $int_b(A,B) = \cup\{(G,H) \subseteq (M_1,M_2) : (G,H)$is an open BMS, $(G,H) \subseteq (A,B)\}$.*

Theorem 4.*For two sub-BMS (A,B) and (C,D) in BMS-space (M_1,M_2,τ_b) with $(A,B) \subseteq (C,D)$,we have:*
(1) $int_b(\phi,\phi) = (\phi,\phi)$, $int_b(M_1,M_2) = (M_1,M_2)$.
(2) $int_b(A,B) \subseteq (A,B)$
(3) $int_b(A,B) \subset int_b(C,D)$.
(4) $(A,B)^{1\circ} \subseteq (C,D)^{1\circ}$.
(5) $(A,B)^{2\circ} \subseteq (C,D)^{2\circ}$.
(6) $int_b(int_b(A,B)) = int_b(A,B)$.

*Proof.*It is analogous to that in Theorem 3.

The next propositions, similar to Propositions 5 and 6, can be readily derived.

Proposition 9.*For two sub-BMS (A,B) and (C,D) in BMS-space (M_1,M_2,τ_b), we have:*
(1) $(A,B)^{1\circ} \cup (C,D)^{1\circ} \subset (A \cup C, B \cup D)^{1\circ}$.
(2) $(A,B)^{2\circ} \cup (C,D)^{2\circ} \subset (A \cup C, B \cup D)^{2\circ}$.

Proposition 10.*For two sub-BMS (A,B) and (C,D) in BMS-space (M_1,M_2,τ_b), we have:*
(i) $(A \cap C, (B \cap D)^{1\circ} \subseteq (A,B)^{1\circ} \cap (C,D)^{1\circ}$.
(ii) $(A \cap C, B \cap D)^{2\circ} \subseteq (A,B)^{2\circ} \cap (C,D)^{2\circ}$.

As in the examples 13 and 14, one can verify that reverse inclusion in the Propositions 9 and 10 do not hold.

Theorem 5.*For a sub-BMS (A,B) in a BMS-space (M_1,M_2,τ_b), we have (A,B) is an open BMS if and only if $int_b(A,B) = (A,B)$.*

*Proof.*If (A,B) is a open BMS over (M_1,M_2) then (A,B) is a open BMS over (M_1,M_2) which contains (A,B). So, (A,B) is the largest open BMS contained in (A,B), and $(A,B) = int_b(A,B)$. Conversely, suppose that $(A,B) = int_b(A,B)$, since $int_b(A,B)$ is a open BMS, so (A,B) is a BMS open over (M_1,M_2).

Definition 24.*Let (M_1,M_2,τ_b) be a BMS-space, $(\{k/u\},\{m/v\}) \subseteq (M_1,M_2)$, and $(G,H) \subseteq (M_1,M_2)$. Then (G,H) is a BMS neighborhood(or BMS-nbd) of $(\{k/u\},\{m/v\})$ if there is an open BMS $(P,Q) \in \tau_b$ such that $(\{k/u\},\{m/v\}) \subseteq (P,Q) \subseteq (G,H)$.*

Definition 25.*Let (M_1,M_2,τ_b) be a BMS-space over (M_1,M_2), (A,B) be a BMS in (M_1,M_2,τ_b), and $(k/u,m/v) \in (A,B)$, then $(k/u,m/v)$ is said to be BMS interior point of (A,B) if there exist an open BMS (P,Q) such that $(k/u,m/v) \in (P,Q) \subseteq (A,B)$.*

Proposition 11.*The bm-point $(\{k/u\},\{m/v\}) \subseteq int_b(A,B)$ iff there is a BMS-nbd (G,H) of $(\{k/u\},\{m/v\})$ such that $(G,H) \subseteq (A,B)$.*

*Proof.*Let (G,H) be a BMS-nbd of $(\{k/u\},\{m/v\})$ of (M_1,M_2) and $(G,H) \subset (A,B)$. By Definition 25, there exist an open BMS (P,Q) such that $(\{k/u\},\{m/v\}) \in (P,Q) \subset (G,H) \subset (A,B)$. Thus $(\{k/u\},\{m/v\}) \in (P,Q) \subset (A,B)$. Hence (A,B) is a BMS-nbd of $(\{k/u\},\{m/v\})$, the other implication is similar.

Theorem 6.*A sub-BMS of a BMS-space (M_1,M_2,τ_b) is an open BMS iff it is a BMS-nbd of each of its elements with some multiplicity.*

*Proof.*Let (M_1,M_2) be an BMS-space and (A,B) a sub-BMS of (M_1,M_2). If (A,B) is an open BMS. Clearly, it is BMS-nbd of each of its points with some multiplicity. Conversely, suppose that (A,B) is a BMS-nbd of each of its points, then for each point $(k/u,m/v) \in (A,B)$, there is an open BMS $(P_{k/u},Q_{m/v})$ such that $u \in^k P_{k/u}$, $P_{k/u} \subseteq A$,

$y \in^m Q_{m/v}$, and $Q_{m/v} \subseteq B$. $(A,B) = \cup_{(k/u,m/v)\in(A,B)}(P_{k/u},Q_{m/v})$, where $k = maxC_{P_{k/u}}(u)$ and $m = C_{Q_{m/v}}(v)$. Hence, (A,B) is an open BMS.

Definition 26.*For a sub-BMS (A,B) in a BMS-space (M_1,M_2,τ_b). A BM-point $(\{k/u\},\{m/v\}) \subseteq (M_1,M_2)$ is named a bm-limit point of (A,B) iff every BMS-nbd (G,H) of $(\{k/u\},\{m/v\})$ contains a bm-point of (M_1,M_2) distinct from $(\{k/u\},\{m/v\})$ i.e. $((G,H)-(\{k/u\},\{m/v\}))\cap(A,B) \neq \phi$ for all BMS-nbd (G,H) of $(\{k/u\},\{m/v\})$.*

Theorem 7.*A sub-BMS in a BMS-space (M_1,M_2,τ_b) is a closed BMS iff it contains all its BM-limit points.*

*Proof.*Suppose that (A,B) is a closed sub-BMS in (M_1,M_2,τ_b), Then $(A,B)^c$ is an open sub BMS. So for $(\{k/u\},\{m/v\}) \subseteq (A,B)^c$ there is an open BMS $(P_{k/u},Q_{m/v})$ such that $(P_{k/u},Q_{m/v}) \subseteq (A,B)^c$. Assume that $(\{k/u\},\{m/v\})$ is a BM-limite point of (A,B) that is not in (A,B). Then for every open BMS $(P_{k/u},Q_{m/v})$ containing $(\{k/u\},\{m/v\})$ there is $(\{r/x\},\{t/y\}) \neq (\{k/u\},\{m/v\})$ with $(\{r/x\},\{t/y\}) \subseteq (P_{k/u},Q_{m/v}) \cap (A,B)$. So $(\{r/x\},\{t/y\}) \nsubseteq (A,B)^c$ which is a contradiction. The other way is similar.

Definition 27.*For the BMS-space (M_1,M_2,τ_b). The BMS of all the bm-limit points of a given sub-BMS (A,B) of (M_1,M_2) is called a derived BMS of (A,B), is denoted by $D_b((A,B))$.*

Theorem 8.*For a sub-BMS (A,B) in a BMS-space (M_1,M_2,τ_b), we have $cl_b(A,B) = (A,B)\cup D_b((A,B))$.*

*Proof.*To prove that $cl_b((A,B)) \subseteq (A,B) \cup D_b((A,B))$. Consider $(\{k/u\},\{m/v\}) \subseteq cl_b((A,B))$, this implies that $(\{k/u\},\{m/v\})$ is in any closed BMS containing (A,B), implies that either $(\{k/u\},\{m/v\}) \subseteq (A,B)$ or $(\{k/u\},\{m/v\})$ is a bm-limit point of (A,B).
On the other hand, to prove that $(A,B) \cup D_b((A,B)) \subseteq cl_b((A,B))$. Consider $(\{r/x\},\{t/y\}) \subseteq (A,B)\cup D_b((A,B))$. if $(\{r/x\},\{t/y\}) \subseteq (A,B)$, then $(\{r/x\},\{t/y\}) \subseteq cl_b((A,B))$. If $(\{r/x\},\{t/y\}) \subseteq D_b((A,B))$, then $(\{r/x\},\{t/y\}) \subseteq cl_b((A,B))$. This completes the proof.

5 Conclusion

The binary multiset structure, as well as several operations $(\subseteq,\cup,\cap,\oplus,\ominus)$, are defined in this work. It developed the notion to be used for binary sets and multisets into binary multisets. Similarly, based on BMS topological space, BMS open, BMS closed, BMS neighborhood, BMS interior, BMS closure, and BMS limit point are introduced with examples and their features, theorems, and propositions. In reality, structures based on binary sets and multiset methods for measuring the similarity and dissimilarity of binary multiset objects of all members have been created. This BMS topological space combination is noteworthy. In such cases, one may deal with a collection of elements that contain duplicates. In future work, we will continue in the development of the theoretical framework in the context of BMS-settings, investigating more axiomatic properties of BMS and many basic topological concepts in BMS- spaces, such as separation axioms, compactness, connectedness, ... etc. The BMS hypothesis may be useful for advanced studies and real-life applications if engineering problems, where the plan of this paper has been addressed in application to the field of BMS theory.

Availability of data and material

No data was used in this study.

Conflict of interest

The authors declare that they have no conflict of interest.

Funding

The authors did not receive any financial support for the research.

Authors' contributions

All authors contributed equally work.

Acknowledgement

The authors are grateful to the anonymous referee for helpful comments that improved this paper.

References

[1] W. D. Blizard, Multiset theory, *Notre Dame J. Formal Logic*, **30**(1), 36-66 (1989).
[2] W. D. Blizard, The development of multiset theory., *Mod. Log.*, **1**(4), 319-352 (1991).
[3] R. R. Yagar, On the theory of bags, *International Journal of General Systems*, **13**(1), 23-27 (1986).
[4] A. Zakaria, Notes on "on multiset topologies". *Ann. Fuzzy Math. Inform.*, **10**(5), 825–827 (2015).
[5] V. Dembere, New axioms in topological space, *International Journal of Computer Applications Technology and Research*, **7**(3), 109-113 (2018).
[6] R. Das, Generalized multiset and multiset ideal continuous function, *Applied Science*, **24**, 98-107 (2022).

[7] S. EL-Sheikh, R. Omaar and M. Raafat, Separation axioms on multiset topological space, *Jour. New Theory*, **7**, 11-12 (2015).
[8] A. Kandil, O. A. Tantaway, S. A. El-sheikh and A. Zakaraia, Multiset proximity space, *J. Eg. Math. Soc.*, **24**, 562-567 (2016).
[9] S. Mahanata and S. K. Samanta, Compactness in multiset topology, *International Journal of Mathematics Trends and Technology (IJMTT)*, **47**(4), 275–282 (2017).
[10] D. Das and J. Mahanta, Boundary and exterior of a multiset topological space, *J. new theory*. **12**, 75-84 (2016).
[11] K. P. Girish and S.J. John, On multiset topologies, *Theory and Applications of Mathematics and Computer Science* , **2**, 37-52 (2012).
[12] K. P. Girish and S. J. John, Multiset topologies induced by multiset relation, *Information Sciences*, **188**, 298-313 (2012).
[13] K. Shravan and B. C. Tripathy, Generalised closed set in multiset topological space, *Proyecciones (Antofagasta)*, **37**(2), 223-237 (2018).
[14] K. Shravan and B. C. Tripathy, Multiset ideal topological space and local function, *Proyecciones (Antofagasta)*, **37**(4), 699-711 (2018).
[15] K. Shravan and B. C. Tripathy, Multiset ideal topological space and kuratowski closure operator, *Bulletin of the Transilvania University of Brasov, Series III; Mathematics, Information, Physics*, **13**(62), 273-284 (2020).
[16] J. M. Mustafa, On binary generalized topological space, *General Letters in Mathematics*, **2**(3), 117-116 (2017).
[17] S. S. Surekha and G. Sindhu, New class of binary open set in binary topological space, *International Journals of Creative Research Thoughts(IJCRT)*, **10**(5), 101-104 (2022).
[18] S. N. Jothi and P. Thangavelu, Topology between two sets, *Journal of Mathematical Sciences & Computer Applications*, **1**(3), 95-107 (2011).

On r-dynamic k-coloring of ladder graph families

Irin Feno A., Venkatachalam M., Rathour L., CANGÜL İ. N., Abirami K.

DISCRETE MATHEMATICS ALGORITHMS AND APPLICATIONS, 2024 (ESCI) (https://www.scopus.com/record/display.uri?eid=2-s2.0-85191985361&origin=resultslist) (http://ws.isiknowledge.com/cps/openurl/service?url_ver=Z39.88-2004&rft_id=info:ut/WOS:001209921800002) (https://plu.mx/plum/a/?doi=10.1142/s1793830924500356)

Publication Type: Article / Article

Publication Date: 2024

Doi Number: 10.1142/s1793830924500356 (http://doi.org/10.1142/s1793830924500356)

Journal Name: DISCRETE MATHEMATICS ALGORITHMS AND APPLICATIONS (/journal/getjournaldetailbyarticleid?articleId=a5838394-fcfe-434d-8c90-a7d30b693fe4&modalDisplayedControllerId=5&journalName=DISCRETE%20MATHEMATICS%20ALGORITHMS%20AND%20APPLICATIONS)

Journal Indexes: Emerging Sources Citation Index (ESCI), Scopus

Bursa Uludag University Affiliated: Yes

Abstract

The concept of r-dynamic k-coloring of a graph G refers to a proper vertex k-coloring where the number of colors assigned to the vertices in the neighborhood of each vertex v is greater than or equal to the min {r, Delta(G)}. This study focuses on the r-dynamic coloring of various types of ladder graphs, which are derived from the Cartesian product of P2 and Pn, including the Diagonal Ladder Graph, Open Diagonal Ladder Graph, Triangular Ladder Graph, Open Triangular Ladder Graph and Slanting Ladder Graph.

Discrete Mathematics, Algorithms and Applications
Vol. 16, No. 2 (2024) 2350009 (17 pages)

DOI: 10.1142/S179383092350009X

World Scientific
www.worldscientific.com

Solving the b-coloring problem for subdivision-edge neighborhood coronas

Raúl M. Falcón*

Department of Applied Mathematics I
Universidad de Sevilla, Avda. Reina Mercedes 4A
41012 Seville, Spain
rafalgan@us.es

M. Venkatachalam† and S. Julie Margaret‡

PG and Research Department of Mathematics
Kongunadu Arts and Science College
Coimbatore 641029, Tamil Nadu, India
†*venkatmaths@gmail.com*
‡*julie.jw107@gmail.com*

Received 6 June 2022
Revised 23 September 2022
Accepted 12 November 2022
Published 13 March 2023

Communicated by Guanghui Wang

In this paper, the b-coloring problem is solved for every subdivision-edge neighborhood corona of paths, cycles, stars and complete graphs. In addition, some exact values and sharp bounds are established for the b-chromatic number of subdivision-edge neighborhood coronas of these graphs with any other graph.

Keywords: b-coloring problem; subdivision-edge neighborhood corona; path; cycle; star graph; complete graph.

Mathematics Subject Classification 2020: 05C15

1. Introduction

Let G be a finite and simple graph, with set of vertices $V(G)$. The *subdivision graph* $S(G)$ results from inserting a new vertex into every edge of the graph. Let $I(G)$ be the set of inserted vertices. In 2013, Liu and Lu [20] introduced the description of two graph products, the *subdivision-vertex neighborhood corona* $G \boxdot H$ and the *subdivision-edge neighborhood corona* $G \boxminus H$, of two graphs G and H. The first one results from adding $|V(G)|$ vertex-disjoint copies of H to $S(G)$, so that each

*Corresponding author.

neighbor of the ith vertex of $V(G)$ is joined to every vertex in the ith copy of H. The second one results from adding $|I(G)|$ vertex-disjoint copies of H to $S(G)$, so that each neighbor of the ith vertex of $I(G)$ is joined to every vertex in the ith copy of H. Both types of graphs have attracted attention of graph theorists because of their versatility to construct different families of network [5–8, 19].

This paper contributes to the comprehensive study of subdivision-edge neighborhood coronas by solving the b-chromatic problem of this graph product for paths, cycles, stars and complete graphs. Remind here that a *proper k-coloring* of a graph G is any map $c : V(G) \to \{0, \ldots, k-1\}$ assigning k *colors* to the set of vertices $V(G)$ so that no two adjacent vertices share the same color. In 1999, Irving and Manlove [10] introduced the *b-chromatic k-coloring* [10] of a graph G as any proper k-coloring c of G having a *b-vertex* $v \in V(G)$, for every color i. That is, $c(v) = i$ and for each color $j \neq i$, there is a neighbor $w \in V(G)$ of v such that $c(w) = j$. The maximum positive integer k for which such a coloring exists is the *b-chromatic number* $\varphi(G)$. Finding this number is known as the *b-coloring problem*, which is NP-hard for general graphs, but polynomial-time solvable for trees [10]. This problem has been studied for a wide amount of graphs (see [12] for a comprehensive survey on the topic).

Concerning product of graphs, the b-coloring problem has been studied for the Cartesian product [1–4, 9, 13, 14, 16, 17, 21], the direct product [11, 15], the strong product [11, 23] and the lexicographic product [11, 18, 23]. Of special interest for the aim of this paper, it is remarkable the study of this problem for the corona product [24], the subdivision-edge and -vertex corona [22] and the subdivision-vertex neighborhood corona [7]. This paper delves into this topic by solving the b-coloring problem for subdivision-edge neighborhood coronas of paths, cycles, stars and complete graphs. Notice here that, if G is a cycle, then $G \boxminus H = G \boxdot H$, for every graph H. The b-chromatic problem for this subdivision-vertex corona has recently been dealt with by the authors [7]. So, we focus on the remaining cases.

The paper is organized as follows. In Sec. 2, we describe some concepts and results on graph theory that are used throughout the paper. Particularly, some preliminary bounds are established for the b-chromatic number of any subdivision-edge neighborhood corona. Then, each one of Secs. 3–5 solves separately the b-coloring problem for the subdivision-edge neighborhood corona of paths, stars and complete graphs. Moreover, some exact values and sharp bounds are also established for the b-chromatic number of subdivision-edge neighborhood coronas of each one of the three mentioned families of graphs with any other graph.

2. Preliminaries

All the graphs in this paper are considered to be finite and simple. This section deals with some notations and preliminary results on graph theory that are used from now on.

Let G be a graph with set of vertices $V(G)$ and set of edges $E(G)$. The neighborhood and degree of a vertex $v \in V(G)$ are, respectively, denoted by $N_G(v)$ and $d_G(v)$. If there is no risk of confusion, then we use the respective notations $N(v)$ and $d(v)$. In addition, $\Delta(G)$ denotes the maximum vertex degree of the graph G. Further, the path, cycle and star of order $n > 2$ are, respectively, denoted by P_n, C_n and S_{n-1}. The complete graph of order n is denoted by K_n.

Throughout this paper, every subdivision-edge neighborhood corona $G \boxminus H$ is considered to be such that G contains at least one edge. Otherwise, the set of inserted vertices $I(G)$ is empty and hence, $G \boxminus H = G$. Moreover, we assume that G is connected. Otherwise, the graph G is the disjoint union of m connected components $G_1, G_2, \ldots, G_m$, and then, $\varphi(G \boxminus H) = \max\{\varphi(G_i \boxminus H) : 1 \leq i \leq m\}$. Furthermore, if $V(G) = \{u_0, u_1, u_2, \ldots, u_{|V(G)|-1}\}$ and $V(H) = \{v_0, v_1, v_2 \ldots, v_{|V(H)|-1}\}$, then we make use of the following notation, for every pair of non-negative integers $i < j < |V(G)|$.

- $s_{i,j}$ denotes the vertex in $I(G)$ that is inserted in the edge $u_iu_j \in E(G)$.
- $v^k_{i,j}$ denotes the copy of each vertex $v_k \in V(H)$ that is associated to the vertex $s_{i,j} \in I(G)$.

Figure 1 illustrates these notations.

In particular,

$$d_{G\boxminus H}(v) = \begin{cases} 2 & \text{if } v \in I(G), \\ d_G(v) \cdot (|V(H)| + 1) & \text{if } v \in V(G), \\ d_H(v_k) + 2 & \text{if } v = v^k_{i,j} \text{ for some } \begin{cases} i < j < |V(G)|, \\ k < |V(H)|. \end{cases} \end{cases} \tag{2.1}$$

Hence, $\Delta(G \boxminus H) = \Delta(G) \cdot (|V(H)| + 1)$.

The *chromatic number* $\chi(G)$ is the minimum positive integer k for which a proper k-coloring of G exists. The following lemma establishes the chromatic number of every subdivision-edge neighborhood corona $G \boxminus H$.

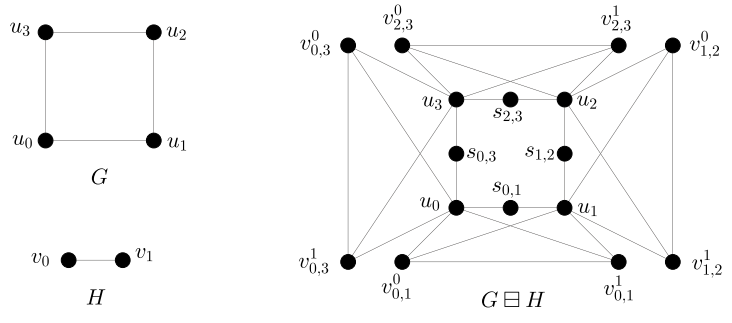

Fig. 1. Subdivision-edge neighborhood corona.

Lemma 2.1. *It is verified that* $\chi(G \boxminus H) = \chi(H) + 1$.

Proof. Let $H_{i,j}$ denote the copy of H that is associated to the inserted vertex of an edge $u_iu_j \in E(G)$. Then, every proper coloring of $G \boxminus H$ requires at least $\chi(H)+1$ distinct colors for coloring the set $V(H_{i,j}) \cup \{u_i\}$. Thus, $\chi(G \boxminus H) \geq \chi(H) + 1$. In order to see that this lower bound is tight, let c be a proper $\chi(H)$-coloring of the graph H. Then, it is enough to consider the proper $(\chi(H) + 1)$-coloring $\overline{c}$ of $G \boxminus H$ that is defined so that $\overline{c}(v) = \chi(H)$, for all $v \in V(G)$; $\overline{c}(v) = 0$, for every inserted vertex $v \in I(G)$; and every copy of H is colored in the same way that c does. □

Every proper $\chi(G)$-coloring is a b-chromatic coloring of a graph G. In particular, every b-chromatic $\varphi(G)$-coloring is said to be *optimal*. Moreover, the next lemma holds.

Lemma 2.2 ([10]). *It is verified that* $\chi(G) \leq \varphi(G) \leq \Delta(G) + 1$.

Hence, a pair of preliminary bounds is readily established for any subdivision-edge neighborhood corona $G \boxminus H$.

Lemma 2.3. *It is verified that* $\chi(H) + 1 \leq \varphi(G \boxminus H) \leq \Delta(G) \cdot (|V(H)| + 1) + 1$.

The next result describes an improved lower bound, which is proved to be sharp in Proposition 2.6. (For the aim of this paper, notice here that the b-coloring problem of paths, cycles, stars and complete graphs is already known [16].)

Proposition 2.4. *It is verified that* $\varphi(G \boxminus H) \geq \varphi(H) + 1$.

Proof. Let c be an optimal b-chromatic coloring of the graph H. Then, let $\overline{c}$ be the proper $(\varphi(H) + 1)$-coloring of $G \boxminus H$ that is defined so that $\overline{c}(v) = \varphi(H)$, for all $v \in V(G)$; $\overline{c}(v) = 0$, for every inserted vertex $v \in I(G)$; and every copy of H is colored in the same way that c does. This map $\overline{c}$ is a b-chromatic coloring of the graph $G \boxminus H$, and hence, $\varphi(G \boxminus H) \geq \varphi(H) + 1$. □

A *b-system* associated to a b-chromatic coloring c of G is any subset of $V(G)$ that is formed by exactly one b-vertex of each color. From here on, let $\mathcal{B}_c(G)$ and $\mathcal{B}(G)$, respectively, denote the set of b-vertices of G associated to c, and the set of b-vertices of G associated to at least one b-chromatic coloring of the graph. The next result follows readily from the definition of b-vertex and the fact that c is a proper coloring.

Lemma 2.5. *Let* $u, v \in V(G)$. *The following assertion holds.*

(a) *Let c be a b-chromatic coloring of the graph G. If $N(v) \subseteq N(u)$, then either $c(u) = c(v)$ or $v \notin \mathcal{B}_c(G)$.*
(b) *If $u \in \mathcal{B}(G)$, then $\varphi(G) \leq d(u) + 1$.*

Proof. Let us prove separately each assertion.

(a) If c is a b-chromatic k-coloring of the graph G such that $v \in \mathcal{B}_c(G)$, then $|c(N(v))| = k-1$. If, besides, $N(v) \subseteq N(u)$, then $|c(N(u))| = k-1$, and hence, $c(u) = c(v)$.

(b) If $u \in \mathcal{B}(G)$, then there exists a b-chromatic k-coloring c of the graph G such that $u \in \mathcal{B}_c(G)$. In particular, $k-1 = |c(N(u))| \leq d(u)$. As a consequence, $\varphi(G) \leq k \leq d(u)+1$. □

The previous results enable us to solve the b-coloring problem for every graph $K_2 \boxminus H$.

Proposition 2.6. *It is verified that* $\varphi(K_2 \boxminus H) = \varphi(H) + 1$.

Proof. Lemma 2.4 implies that $\varphi(K_2 \boxminus H) \geq \varphi(H)+1$. In order to prove that this bound is sharp, let us suppose the existence of a b-chromatic k-coloring c of $K_2 \boxminus H$ with $k > \varphi(H)+1$. Let $V(K_2) = \{u_0, u_1\}$ and $I(K_2) = \{s_{0,1}\}$. Since $k > 2$, we have that $s_{0,1} \notin \mathcal{B}_c(K_2 \boxminus H)$. Moreover, since $N_{K_2 \boxminus H}(u_0) = N_{K_2 \boxminus H}(u_1)$, Lemma 2.5(a) implies that $\mathcal{B}_c(K_2 \boxminus H)$ contains at most one vertex in K_2.

As a consequence, $|\mathcal{B}_c(K_2 \boxminus H) \cap V(H)| > \varphi(H)$. But then, the map c would induce a b-chromatic $(k-1)$-coloring of the graph H, which is not possible, because $k-1 > \varphi(H)$. Hence, the result holds. □

Further, Irving and Manlove [10] defined the *m-degree* of a graph G of order n as

$$m(G) := |\{i \in \{1, \ldots, n\} : i \leq d(v_{i-1}) + 1\}|,$$

where the labeling of $V(G)$ is done here so that $d(v_0) \geq \cdots \geq d(v_{n-1})$. Then, they established the following upper bound.

Lemma 2.7 ([10]). *It is verified that* $\varphi(G) \leq m(G)$.

Let us finish this preliminary section by enumerating some known b-chromatic numbers concerning subdivision-vertex neighborhood coronas that are used throughout the paper.

Theorem 2.8 ([7]). *Let n and $t > 2$ be two positive integers. Then, the following b-chromatic numbers hold.*

(1) $\varphi(P_n \boxdot H) = 2\,|V(H)| + 3$, *whenever* $n > 2\,|V(H)| + 3$.
(2)

$$\varphi(P_n \boxdot P_t) = \begin{cases} 4 & \text{if } n = 3 \text{ and } t \in \{3,4\}, \\ 5 & \text{if } \begin{cases} n = 3 \text{ and } t \geq 5, \\ n \in \{4,5,6\}, \end{cases} \\ n-1 & \text{if } 6 < n \leq 2t+3, \\ 2t+3 & \text{otherwise.} \end{cases}$$

(3)

$$\varphi(P_n \boxdot S_t) = \begin{cases} 2n-1 & \text{if } 2n \leq t+3, \\ t+2 & \text{if } n = \left\lceil \dfrac{t+4}{2} \right\rceil, \\ t+3 & \text{if } \left\lceil \dfrac{t+4}{2} \right\rceil < n < t+4, \\ n-1 & \text{if } t+4 \leq n \leq 2t+5, \\ 2t+5 & \text{otherwise.} \end{cases}$$

(4)

$$\varphi(P_n \boxdot K_t) = \begin{cases} t+2 & \text{if } n \leq t+3, \\ n-1 & \text{if } t+3 < n \leq 2t+3, \\ 2t+3 & \text{otherwise.} \end{cases}$$

3. Subdivision-Edge Neighborhood Coronas of Paths

From here on, we denote by $\mathcal{G}$ the set of paths, cycles, stars and complete graphs of any order. This section deals with the b-coloring problem for the subdivision-edge neighborhood corona $P_n \boxminus H$ of a path $P_n = u_0u_1u_2 \dots u_{n-1}$ with $n > 2$, and a graph $H \in \mathcal{G}$. First, we establish a series of preliminary results concerning any graph H. (Recall here that we make use of the notation of vertices described in the previous section.)

Lemma 3.1. *The following assertions hold.*

(a) *If c is a b-chromatic coloring of the graph $P_n \boxminus H$, then $|\mathcal{B}_c(P_n \boxminus H) \cap V(P_n)| \leq n-2$.*

(b)

$$\varphi(P_n \boxminus H) \geq \begin{cases} \varphi(K_2 \boxdot H) & \text{if } n = 3, \\ \varphi(P_{n-1} \boxdot H) & \text{if } n > 3. \end{cases}$$

(c) $\varphi(P_n \boxminus H) \leq \varphi(P_{n+1} \boxminus H)$.

Proof. We prove each assertion separately.

(a) Since $N(u_0) \subset N(u_1)$ and $N(u_{n-1}) \subset N(u_{n-2})$, Lemma 2.5(a) implies that $|\{u_0, u_1\} \cap \mathcal{B}_c(P_n \boxminus H)| \leq 1$ and $|\{u_{n-2}, u_{n-1}\} \cap \mathcal{B}_c(P_n \boxminus H)| \leq 1$. Hence, $|\mathcal{B}_c(P_n \boxminus H) \cap V(P_n)| \leq n-2$ for every positive integer $n > 3$. If $n = 3$, then Lemma 2.5(a) implies that, for each $i \in \{0, 2\}$, either $c(u_i) = c(u_1)$ or $u_i \notin \mathcal{B}_c(P_n \boxminus H)$. As a consequence, $|\mathcal{B}_c(P_3 \boxminus H)| \leq 1$.

(b) The removal of both vertices u_0 and u_{n-1} in $P_n \boxminus H$, together with their corresponding adjacent edges, gives rise to either the graph $K_2 \boxdot H$ if $n = 3$, or

the graph $P_{n-1} \boxdot H$, otherwise. Then, the result follows readily from the fact that every b-chromatic k-coloring c of these subdivision-vertex neighborhood coronas gives rise to a b-chromatic k-coloring $\overline{c}$ of $P_n \boxminus H$. It is defined so that $\overline{c}(u_0) = c(u_1)$, $\overline{c}(u_{n-1}) = c(u_{n-2})$ and $\overline{c}(v) = c(v)$, for all $v \in V(P_n \boxminus H) \setminus \{u_0, u_{n-1}\}$.

(c) Without loss of generality, we may assume that $P_{n-1} \boxminus H$ is a subgraph of $P_n \boxminus H$. If c is a b-chromatic k-coloring of $P_n \boxminus H$, then we define the proper coloring $\overline{c}$ of $P_{n+1} \boxminus H$ that is described so that $\overline{c}(v) = c(v)$, for all $v \in P_n \boxminus H$, $\overline{c}(u_n) = c(u_{n-1})$, $\overline{c}(s_{n-1,n}) = c(s_{n-2,n-1})$ and $\overline{c}(v^k_{n-1,n}) = c(v^k_{n-2,n-1})$, for all $k < t$. It is a b-chromatic k-coloring of $P_n \boxminus H$, and the result holds. □

Lemma 3.1 can be used to establish an upper bound for $P_n \boxminus H$ and solve the b-coloring problem for this graph, whenever $n > 2\,|V(H)| + 4$.

Proposition 3.2. *It is verified that*

$$\varphi(P_n \boxminus H) \leq \begin{cases} \Delta(H) + 3 & \text{if } n \leq \Delta(H) + 5, \\ n - 2 & \text{otherwise.} \end{cases}$$

Moreover, $\varphi(P_n \boxminus H) = 2\,|V(H)| + 3$ *for all* $n > 2\,|V(H)| + 4$.

Proof. First, let us assume the existence of a b-chromatic proper k-coloring c of the graph $P_n \boxminus H$ with $n \leq \Delta(H)+5$ and $k > \Delta(H)+3$. From (2.1) and Lemma 2.5(b), it must be $\mathcal{B}_c(P_n \boxminus H) \subseteq V(P_n)$. But then, Lemma 3.1(b) implies that $k \leq n - 2$, and hence, $n > \Delta(H) + 5$, which is a contradiction.

Now, let $n > \Delta(H) + 5$ and let us suppose that $\varphi(P_n \boxminus H) > n - 2$. Since $\Delta(H) + 2 < n - 3$, we have from (2.1) and Lemma 2.5(b) that $\mathcal{B}(P_n \boxminus H) \subseteq V(P_n)$. Then, Lemma 3.1(a) implies that $\varphi(P_n \boxminus H) \leq n - 2$, which is a contradiction.

Finally, Lemma 2.3 implies that $\varphi(P_n \boxminus H) \leq 2\,|V(H)|+3$. Then, Lemma 3.1(b), together with Theorem 2.8(a), enables us to ensure that this upper bound is indeed reached. □

In what follows, we solve the b-coloring problem for the graph $P_n \boxminus H$, for all $H \in \mathcal{G}$.

Theorem 3.3. *Let* $n > 2$ *and* $t > 2$ *be two positive integers. Then,*

$$\varphi(P_n \boxminus P_t) = \begin{cases} 3 & \text{if } n = t = 3, \\ 5 & \text{if } \begin{cases} n = 3 < t, \\ 4 \leq n \leq 7, \end{cases} \\ n - 2 & \text{if } 7 < n \leq 2t + 4, \\ 2t + 3 & \text{if } n > 2t + 4. \end{cases}$$

Proof. The case $n > 2t + 4$ follows from Proposition 3.2, which also implies that $\varphi(P_n \boxminus P_t) \leq 5$, for all $n \leq 7$. Then, Lemma 2.5(a) implies that $\mathcal{B}(P_3 \boxminus P_3) \subseteq V(P_3) \cup$

$\{v^1_{0,1}, v^1_{1,2}\}$, and hence, Lemma 3.1(a) implies that $\varphi(P_3 \boxminus P_3) \leq 3$. Since $\chi(P_3) = 2$, the case $n = t = 3$ follows from Lemma 2.3. Furthermore, if $P_t = v_0v_1v_2 \dots v_{t-1}$, then the case $n = 3 < t$ follows from the b-chromatic 5-coloring of $P_3 \boxminus P_t$ that is defined so that $c(u_i) = i$, for all $i \in \{0, 1, 2\}$ and

$$c(v) = \begin{cases} 0, & \text{if } v = v^2_{1,2}, \\ 2, & \text{if } v = v^1_{0,1}, \\ 3, & \text{if } v \in \{s_{0,1}, v^0_{0,1}, v^3_{0,1}, v^1_{1,2}\}, \\ 4, & \text{if } v \in \{s_{1,2}, v^2_{0,1}, v^0_{1,2}, v^3_{1,2}\}, \\ c(v^{k-2}_{i,i+1}), & \text{if } v = v^k_{i,i+1} \text{ with } i \in \{0, 1\} \text{ and } k > 3. \end{cases}$$

The set $\{u_1, v^1_{0,1}, v^2_{0,1}, v^1_{1,2}, v^2_{1,2}\}$ is a b-system of $P_3 \boxminus P_t$ associated to this coloring.

The cases $5 \leq n \leq 7$ and $n = 4 < t$ follows from Lemma 3.1(b) and Theorem 2.8(b). In addition, the case $n = 4$ and $t \in \{3, 4\}$ follows from the optimal b-chromatic colorings described in Figs. 2 and 3. (In order to make easier the identification of b-vertices here and in the remaining figures of the paper, we represent by a triangle ▲ all the vertices of a b-system, whereas the remaining vertices are represented by circles •.) Finally, if $7 < n \leq 2t + 4$, then Proposition 3.2 implies that $\varphi(P_n \boxminus P_t) \leq n - 2$. This upper bound is sharp, because of Lemma 3.1(b) and Theorem 2.8. □

Theorem 3.4. *Let $n > 2$ and $t > 2$ be two positive integers. Then,*

$$\varphi(P_n \boxminus C_t) = \begin{cases} 4 & \text{if } (n, t) = (3, 4), \\ 5 & \text{if } n = t = 3, \\ \varphi(P_n \boxminus P_t) & \text{otherwise.} \end{cases}$$

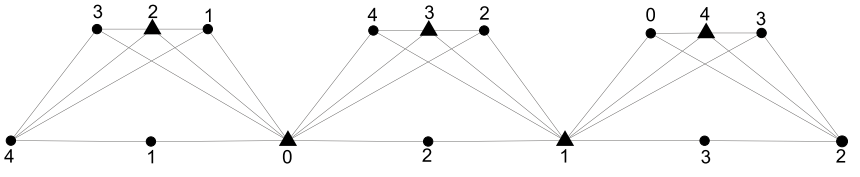

Fig. 2. Optimal b-chromatic coloring of $P_4 \boxminus P_3$.

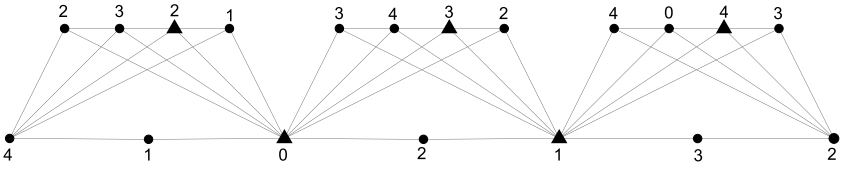

Fig. 3. Optimal b-chromatic coloring of $P_4 \boxminus P_4$.

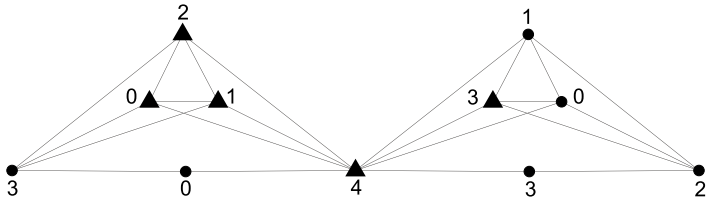

Fig. 4. Optimal b-chromatic coloring of the graph $P_3 \boxminus C_3$.

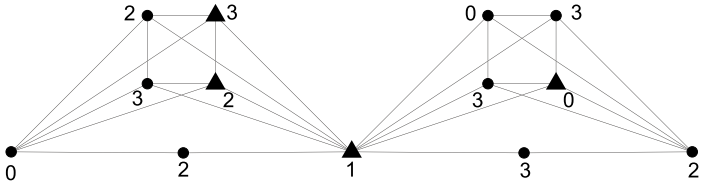

Fig. 5. Optimal b-chromatic colorings of the graph $P_3 \boxminus C_4$.

Proof. From Lemma 2.7 and (2.1), we have that $\varphi(P_3 \boxminus C_t) \leq m(P_3 \boxminus C_t) = 5$. Figure 4 proves that this upper bound is indeed reached, for $t = 3$. Further, it is readily verified that no b-system of five b-vertices is possible for the graph $P_3 \boxminus C_4$. Thus, Fig. 5 shows that $\varphi(P_3 \boxminus C_4) = 4$. The case $n \in \{3, 4\}$ and $t \geq 5$, together with the case $n > 4$, follows from the same reasons as those ones described in the proof of Theorem 3.3. Finally, the case $n = 4$ and $t \in \{3, 4\}$ holds once the vertices $v^0_{i,i+1}$ and $v^{t-1}_{i,i+1}$ are joined in Fig. 3, for all $i < 3$. □

Theorem 3.5. *Let $n > 2$ and $t > 2$ be two positive integers. Then,*

$$\varphi(P_n \boxminus S_t) = \begin{cases} 2n-3 & \text{if } 2n \leq t+5, \\ t+3 & \text{if } \dfrac{t+6}{2} \leq n < t+5, \\ n-2 & \text{if } t+5 \leq n \leq 2t+6, \\ 2t+5 & \text{if } n > 2t+6. \end{cases}$$

Proof. The case $n > 2t+6$ follows from Proposition 3.2, while the case $t+5 \leq n \leq 2t+6$ follows readily from Proposition 3.2, Lemma 3.1(b) and Theorem 2.8(c). Further, Proposition 3.2 also implies that $\varphi(P_n \boxminus S_t) \leq t+3$, whenever $n \leq t+5$. In particular, if $\lceil \frac{t+5}{2} \rceil < n \leq t+5$, then Lemma 3.1(b) and Theorem 2.8(c) imply that this upper bound is sharp. In order to prove that this sharpness also holds for $2n = t+6$, it is enough to consider the b-chromatic $(t+3)$-coloring that is defined so that, for each triple of non-negative integers $i < n$, $j < n-1$ and $k < t$, we have that $c(u_i) = 2i \bmod (t+3)$ and $c(v^0_{j,j+1}) = c(s_{j,j+1}) = (2j+1) \bmod (t+3)$. The remaining

t colors that are not in the set $\{c(u_j), c(u_{j+1}), c(v^0_{j,j+1})\}$ are equally assigned to the vertices $v^k_{j,j+1}$ with $0 < k \leq t$. The set $\{u_1, \ldots, u_{n-2}, v^0_{0,1}, \ldots, v^0_{n-2,n-1}\}$ is a b-system of $P_n \boxminus S_t$ associated to this coloring.

Concerning the case $2n = t + 5$, if $\varphi(P_n \boxminus S_t) = t + 3 = 2n - 2$, then $|\mathcal{B}_c(P_n \boxminus S_t) \cap V(P_n)| \geq n - 1$. Since it is not possible from Lemma 3.1(a), the result holds from Lemma 3.1(b) and Theorem 2.8(c).

Finally, Lemma 2.7 and (2.1) implies that $\varphi(P_n \boxminus S_t) \leq m(P_n \boxminus S_t) = 2n - 1$, whenever $2n \leq t + 4$. Nevertheless, the existence of a b-chromatic k-coloring c of $P_n \boxminus S_t$ with $k \in \{2n - 2, 2n - 1\}$, would imply that $V(P_n) \subset \mathcal{B}_c(P_n \boxminus S_t)$, which is not possible because of Lemma 3.1(a). As a consequence, $\varphi(P_n \boxminus S_t) \leq 2n - 3$. This upper bound is sharp, because of Lemma 3.1(b) and Theorem 2.8(c). □

Theorem 3.6. *Let $n > 2$ and $t > 2$ be two positive integers. Then,*

$$\varphi(P_n \boxminus K_t) = \begin{cases} t + 2 & \text{if } n \leq t + 4, \\ n - 2 & \text{if } t + 4 < n \leq 2t + 4, \\ 2t + 3 & \text{if } n > 2t + 4. \end{cases}$$

Proof. The result holds readily from Proposition 3.2, Lemma 3.1(b) and Theorem 2.8(d). □

4. Subdivision-Edge Neighborhood Coronas of Star Graphs

In this section, we solve the b-coloring problem for the subdivision-edge neighborhood corona $S_n \boxminus H$ of a star S_n with $n > 2$, and a graph $H \in \mathcal{G}$. From here on, $V(S_n) = \{u_0, \ldots, u_n\}$ is such that u_0 is the center of the star. First, we establish a pair of preliminary results concerning any graph H. From here on, we denote by n_H the number of vertices of maximum degree in a graph H.

Proposition 4.1. *It is verified that $\varphi(S_n \boxminus H) \leq \Delta(H) + 3$. This upper bound is reached only if $\Delta(H) + 2 \leq n \cdot n_H$.*

Proof. Let c be a b-chromatic coloring of $S_n \boxminus H$. Since $N_{S_n \boxminus H}(u_i) \subseteq N_{S_n \boxminus H}(u_0)$, for every positive integer $i \leq n$, Lemma 2.5(a) implies that $|\mathcal{B}_c(S_n \boxminus H) \cap V(S_n)| \leq 1$. Then, Lemma 2.5(b) and (2.1) implies that $\varphi(S_n \boxminus H) \leq \Delta(H) + 3$. The sharpness of this upper bound implies the existence of $\Delta(H) + 3$ vertices of degree, at least, $\Delta(H) + 2$. Since there are $n \cdot n_H + 1$ vertices in $V(S_n \boxminus H)$ satisfying such a condition, the second statement holds. □

Theorem 4.4 illustrates that the necessary condition described in the previous result is, however, not sufficient. The next result focuses on those graphs H containing at least one universal vertex. That is, a vertex that is adjacent to all other vertices of the graph.

Proposition 4.2. *Let H be a graph of order t containing at least one universal vertex. Then, $\varphi(S_n \boxminus H) = t+2$, whenever $t+1 \leq n \cdot n_H$. Otherwise, if $t+1 > n \cdot n_H$, then $n \cdot n_H + 1 \leq \varphi(S_n \boxminus H) < t+2$,*

Proof. Let $\ell = \min\{t+1, n \cdot n_H\}$. Since $\Delta(H) = t-1$, Proposition 4.1 implies that it is enough to define an appropriate b-chromatic $(\ell+1)$-coloring c of $S_n \boxminus H$. To this end, we may assume, without loss of generality, that $\{v_0, \ldots, v_{n_H-1}\}$ is the set of universal vertices of H. Then, we define $c(u_0) = \ell$. Besides, for each positive integer $i \leq n$ and each non-negative integer $k < n_H$, we define $c(v_{0,i}^k) = ((i-1)\, n_H + k) \bmod \ell$; $c(u_i) = (c(v_{0,i}^0) - 1) \bmod \ell$; and $c(s_{0,i}) = c(v_{0,i}^0)$. The remaining $\ell - n_H - 1$ colors that are not in the set $\{c(u_0), c(u_i), c(v_{0,i}^0), \ldots, c(v_{0,i}^{n_H-1})\}$ are equally assigned to the vertices $v_{0,i}^k$ with $n_H \leq k < t$. The set $\{u_0\} \cup \{v_{0,i}^k : (i-1)\, n_H + k < \ell\}$ constitutes a b-system of $S_n \boxminus H$ associated to this coloring. □

The following result holds readily from Proposition 4.2.

Theorem 4.3. *It is verified that $\varphi(S_n \boxminus K_t) = t+2$.*

Now, we solve the b-coloring problem for the graph $S_n \boxminus H$ with H being either a path, or a cycle, or a star graph.

Theorem 4.4. *Let $n > 2$ and $t > 2$ be two positive integers. Then,*

$$\varphi(S_n \boxminus P_t) = \begin{cases} 4 & \text{if } n = t = 3, \\ 5 & \text{otherwise.} \end{cases}$$

Proof. The case $t = 3$ follows readily from Proposition 4.2. In addition, Proposition 4.1 implies that $\varphi(S_n \boxminus P_t) \leq 5$, for all $t > 3$. In order to prove that this last upper bound is reached, let $P_t = v_0 v_1 v_2 \ldots v_{t-1}$. Then, it is enough to consider the b-chromatic proper 5-coloring that is defined so that $c(u_0) = 4$ and for every positive integer $i \leq n$ and every non-negative integer $k < t$, we have that $c(s_{0,i}) = i \bmod 4$, $c(u_i) = (i+2) \bmod 4$ and

$$c(v_{0,i}^k) = \begin{cases} (i+k-1) \bmod 4 & \text{if } k \in \{0,1,2\}, \\ c(v_{0,i}^0) & \text{if } n = k = 3, \\ c(v_{0,i}^{k-2}) & \text{if } \begin{cases} n = 3 \text{ and } k > 3, \\ n \geq 4 \text{ and } k > 2, \end{cases} \end{cases}$$

A b-system of $S_n \boxminus P_t$ associated to this coloring is either the set $\{u_0, v_{0,1}^1, v_{0,1}^2, v_{0,2}^1, v_{0,2}^2\}$ if $n = 3$, or the set $\{u_0, v_{0,1}^1, v_{0,2}^1, v_{0,3}^1, v_{0,4}^1\}$, otherwise. □

Figure 6 illustrates the b-chromatic coloring described in the previous theorem for $t = 4$ and $n \in \{3, 4\}$.

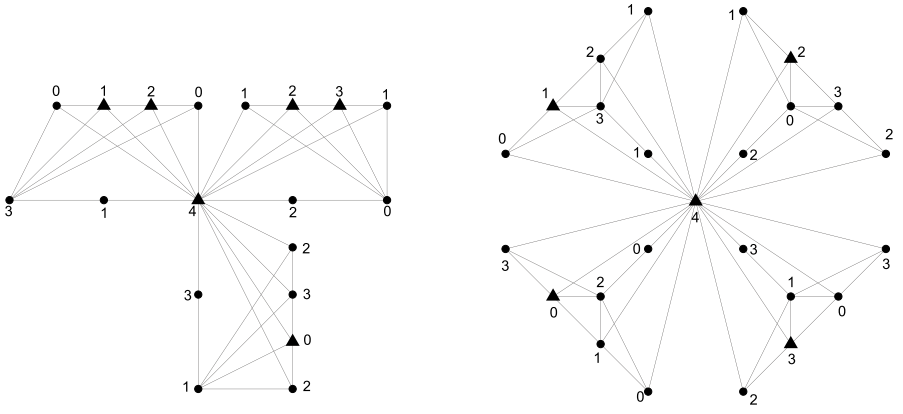

Fig. 6. Optimal b-chromatic coloring of the graph $S_n \boxminus P_4$ with $n \in \{3, 4\}$.

Theorem 4.5. *Let $n > 2$ and $t > 2$ be two positive integers. Then,*

$$\varphi(S_n \boxminus C_t) = \begin{cases} 4 & \text{if } (n,t) = (3,4), \\ 5 & \text{otherwise.} \end{cases} \tag{4.1}$$

Proof. Proposition 4.1 implies that $\varphi(S_n \boxminus C_t) \leq 5$. Thus, the case $n = t = 3$ derives from the coloring described in Fig. 4, with the third branch of the star colored in the same way than the second one. Further, it is readily verified that no b-system of five b-vertices exists for $(n,t) = (3,4)$, and hence, $\varphi(S_3 \boxminus C_4) \leq 4$. Figure 7 proves that this upper bound is sharp. The remaining cases follow from the same b-chromatic proper coloring described in the proof of Theorem 4.4. □

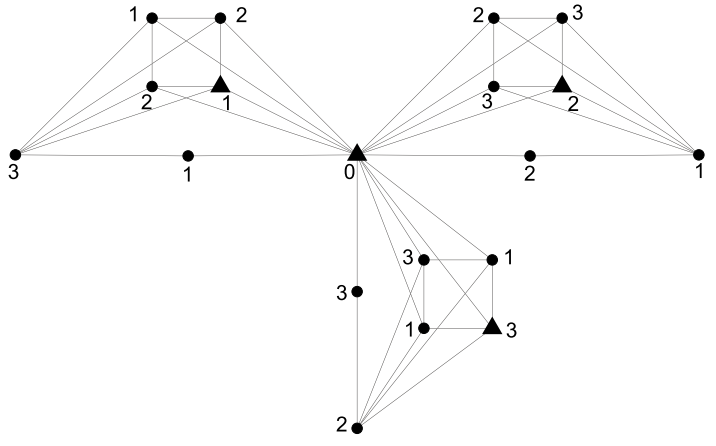

Fig. 7. Optimal b-chromatic coloring of the graph $S_3 \boxminus C_4$.

Theorem 4.6. *Let $n > 2$ and $t > 2$ be two positive integers. Then,*

$$\varphi(S_n \boxminus S_t) = \begin{cases} n+1 & \text{if } n < t+2, \\ t+3 & \text{otherwise.} \end{cases}$$

Proof. Proposition 4.2 implies the case $n \geq t+2$ and also that $\varphi(S_n \boxminus S_t) \geq n+1$, whenever $n < t+2$. In this last case, since $n > 2$, Lemma 2.5(a) implies that every b-system of $S_n \boxminus S_t$ contains at most one vertex in $V(S_n)$ and the centers of the n copies of the star S_t. Hence, the result holds. □

5. Subdivision-Edge Neighborhood Coronas of Complete Graphs

Let us finish our study by solving the b-coloring problem for the subdivision-edge neighborhood corona $K_n \boxminus H$ of a complete graph K_n with $n > 3$, and a graph $H \in \mathcal{G}$. (The case $n = 2$ was already solved in Proposition 2.6, while the case $n = 3$ is equivalent to the subdivision-edge neighborhood corona $C_3 \boxminus H$.) First, we establish a preliminary result for any graph H.

Proposition 5.1. *If $n \leq \Delta(H) + 2$, then $\varphi(K_n \boxminus H) \leq \Delta(H) + 3$. Otherwise, if $n > \Delta(H) + 2$, then $\varphi(K_n \boxminus H) = n$.*

Proof. Lemma 2.7 and (2.1) imply that $\varphi(K_n \boxminus H) \leq \Delta(H) + 3$, whenever $n \leq \Delta(H) + 2$, and also that $\varphi(K_n \boxminus H) \leq n$, whenever $n > \Delta(H) + 2$. In order to prove that this last upper bound is sharp, it is enough to consider the b-chromatic n-coloring c of $K_n \boxminus H$ that is defined so that, for each pair of non-negative integers $0 \leq i < j < n$,

$$c(u_i) = \begin{cases} 2i \bmod n & \text{if } n \text{ is odd,} \\ 2i \bmod (n-1) & \text{if } n \text{ is even and } i \neq n-1, \\ n-1 & \text{if } n \text{ is even and } i = n-1 \end{cases} \tag{5.1}$$

and

$$c(s_{i,j}) = \begin{cases} (i+j) \bmod n & \text{if } n \text{ is odd,} \\ (i+j) \bmod (n-1) & \text{if } n \text{ is even and } j \neq n-1, \\ (c(u_i)+1) \bmod (n-1) & \text{if } n \text{ is even and } j = n-1. \end{cases} \tag{5.2}$$

The remaining vertices $v^k_{i,j}$ are pairwise distinctly colored by making use of any $\chi(H)$ distinct colors of the set $\{0, \ldots, n-1\} \setminus \{c(u_i), c(u_j)\}$. It is possible, because $n - 2 \geq \Delta(H) + 1 \geq \chi(H)$. In particular, if n is even and $i < j \neq n-1$, then it must be $c(v^k_{i,j}) = n-1$, for some k. Then, the set $V(K_n)$ constitutes a b-system of $K_n \boxminus H$ associated to this coloring. □

Theorem 5.2 shows that the just-described upper bound is not sharp. In addition, Fig. 8(right) illustrates the b-chromatic coloring defined in the proof of

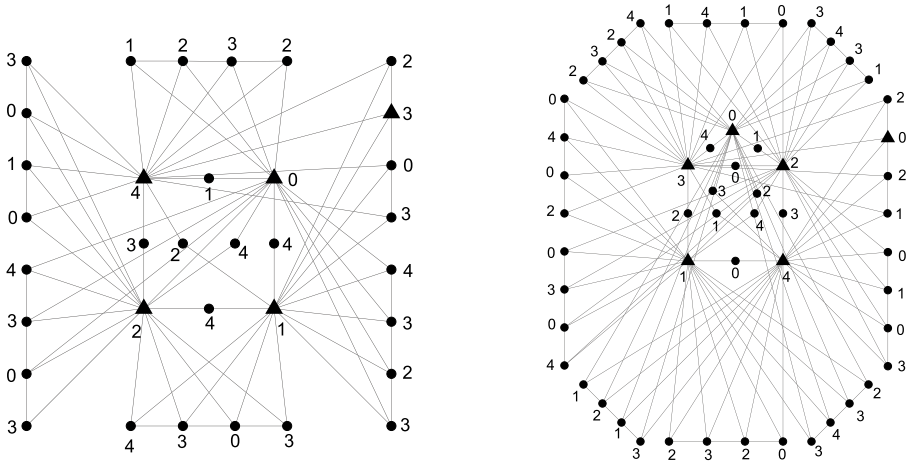

Fig. 8. Optimal b-chromatic colorings of the graph $K_n \boxminus P_4$ with $n \in \{4, 5\}$.

Proposition 5.1 for the graph $K_5 \boxminus P_4$. Now, we solve the b-coloring problem for the graph $K_n \boxminus H$ with $H \in \mathcal{G}$.

Theorem 5.2. *Let $t > 2$ be a positive integer. Then,*

$$\varphi(K_n \boxminus P_t) = \varphi(K_n \boxminus C_t) = \begin{cases} 5 & \text{if } n = 4, \\ n & \text{if } n > 4. \end{cases}$$

Proof. We focus on the b-chromatic number of the graph $K_n \boxminus P_t$. That one of $K_n \boxminus C_t$ follows by making use of the same reasoning and coloring here described. Particularly, Proposition 5.1 implies the case $n > 4$, and also that $\varphi(K_4 \boxminus P_t) \leq 5$. In order to prove that this upper bound is reached, it is enough to consider the b-chromatic 5-coloring c of $K_4 \boxminus P_t$ that is defined so that $c(u_0) = 4$ and $c(u_i) = i \bmod 4$, whenever $0 < i < 4$. Then, for every triple of non-negative integers $i < j < 4$ and $k < t$, we define $c(s_{i,j}) = c(v^0_{i,j})$ and

$$c(v^k_{i,j}) = \begin{cases} (j + k) \bmod 4 & \text{if } i = 0 \text{ and } k \in \{0, 1, 2\}, \\ 4 & \text{if } i \neq 0 \text{ and } k = 0, \\ \max(\{0, 1, 2, 3\} \setminus \{c(u_i), c(u_j)\}) & \text{if } i \neq 0 \text{ and } k = 1, \\ \min(\{0, 1, 2, 3\} \setminus \{c(u_i), c(u_j)\}) & \text{if } i \neq 0 \text{ and } k = 2, \\ c(v^{k-2}_{i,j}) & \text{if } k > 2. \end{cases}$$

The set $V(K_4) \cup \{v^1_{1,3}\}$ is a b-system of $K_4 \boxminus P_t$ associated to this coloring. □

Figure 8 (left) illustrates the b-chromatic coloring described in Theorem 5.2, for $n = t = 4$.

Theorem 5.3. *Let $n > 3$ and $t > 2$ be two positive integers. Then,*

$$\varphi(K_n \boxminus S_t) = \begin{cases} n + \binom{n}{2} & \text{if } n + \binom{n}{2} \leq t + 3, \\ t + 3 & \text{if } 0 < t + 3 - n < \binom{n}{2}, \\ n & \text{if } n \geq t + 3. \end{cases}$$

Proof. The case $n \geq t + 3$ holds from Proposition 5.1. Moreover, Lemma 2.7 and (2.1) imply that $\varphi(K_n \boxminus S_t) \leq m(K_n \boxminus S_t) = n + \binom{n}{2}$, whenever $n + \binom{n}{2} \leq t + 3$ and $\varphi(K_n \boxminus S_t) \leq m(K_n \boxminus S_t) = t + 3$, whenever $0 < t + 3 - n < \binom{n}{2}$. In order to prove the sharpness of these upper bounds, it is enough to define an appropriate b-chromatic coloring c of $K_n \boxminus S_t$ satisfying (5.1) and (5.2). To this end, let us suppose that v_0 is the center of the star S_t. Then, for each pair of non-negative integers $i < j < n$, we define

$$c(v^0_{i,j}) = \begin{cases} n + \alpha_{i,j} & \text{if } n + \binom{n}{2} \leq t + 3, \\ n + ((\alpha_{i,j}) \bmod (t + 3 - n)) & \text{if } 0 < t + 3 - n < \binom{n}{2}. \end{cases}$$

where $\alpha_{i,j} = \frac{(2n-i-1)\cdot i}{2} + j$. (The first addend is the number of vertices in the set $\{v^0_{k,j} : 0 \leq k < i < j < n\}$.) The remaining vertices $v^k_{i,j}$ with $0 < k < t$, are colored by making use of all the colors of the set $\{0, \ldots, \min\{\{n + \binom{n}{2}, t + 3\} - 1\} \setminus \{c(u_i), c(u_j), c(v^0_{i,j}), c(v^t_{i,j}\}$. The set of vertices $V(K_n) \cup \{v^0_{i,j} : \alpha_{i,j} \leq \min\{\binom{n}{2}, t + 3 - n\}\}$ constitutes a b-system of $K_n \boxminus S_t$ for this coloring. □

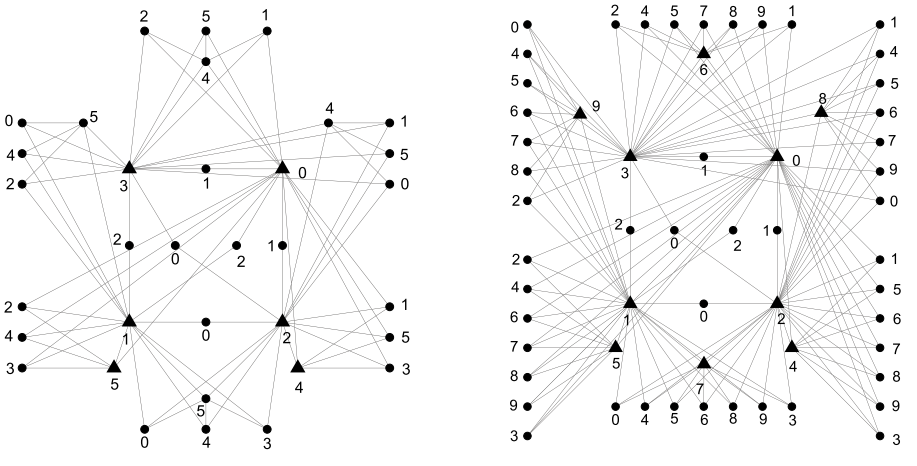

Fig. 9. Optimal b-chromatic colorings of the graph $K_4 \boxminus S_t$ with $t \in \{3, 7\}$.

Figure 9 illustrates the b-chromatic coloring described in Theorem 5.3, for $n = 4$ and $t \in \{3, 7\}$.

Theorem 5.4. *Let $n > 3$ and $t > 2$ be two positive integers. Then,*

$$\varphi(K_n \boxminus K_t) = \begin{cases} t+2 & \text{if } n \leq t+1, \\ n & \text{otherwise.} \end{cases}$$

Proof. Proposition 5.1 proves the case $n > t+1$, and also that $\varphi(K_n \boxminus K_t) \leq t+2$, whenever $n \leq t+1$. In order to prove that this upper bound is sharp, it is enough to consider the b-chromatic $(t+2)$-coloring of $K_n \boxminus K_t$ satisfying (5.1) and (5.2) such that, for each pair of non-negative integers $i < j < n$, the vertices in the set $\{v^k_{i,j} : 0 \leq k < t\}$ are pairwise distinctly colored by making use of the t colors of the set $\{0, \ldots, t+1\} \setminus \{c(u_i), c(u_j)\}$. The set $\{u_0, u_1\} \cup \{v^k_{0,1} : 0 \leq k < t\}$ constitutes a b-system of $K_n \boxminus K_t$ associated to this coloring. □

6. Conclusion and Further Work

In this paper, we have solved the b-coloring problem for every subdivision-edge neighborhood corona of paths, cycles, stars and complete graphs. Even more, we have solved this problem for the graph $P_n \boxminus H$, whenever $n > 2|V(H)| + 4$ (see Proposition 3.2); the graph $S_n \boxminus H$, whenever $|V(H)|+1 \leq n \cdot n_H$, where H contains at least one universal vertex, and n_H is the number of vertices of maximum degree in H (see Proposition 4.2); and the graph $K_n \boxminus H$, whenever $n > \Delta(H)+2$ (see Proposition 5.1). Some sharp bounds have also been established for the b-chromatic number of subdivision-edge neighborhood coronas of paths, stars and complete graphs with any other graph. The results and the methodology here described, constitute a starting point to deal with the b-chromatic problem for subdivision-edge neighborhood coronas of other families of graphs. It is established as further work.

Acknowledgments

The authors want to express their gratitude to the anonymous referees for the comprehensive reading of the paper and their pertinent comments and suggestions, which helped improve the paper. Further, Falcón's work is partially supported by the research project FQM-016 from Junta de Andalucía.

References

[1] A. S. Afrose and S. J. Fathima, b-coloring of the product of paths and cycles, *Int. J. Math. Trends Technol.* **66** (2020) 105–109.
[2] R. Balakrishnan, S. F. Raj and T. Kavaskar, b-chromatic number of Cartesian product of some families of graphs, *Graphs Combin.* **30** (2014) 511–520.
[3] R. Balakrishnan, S. F. Raj and T. Kavaskar, b-coloring of Cartesian product of trees, *Taiwanese J. Math.* **20** (2016) 1–11.

[4] R. Balakrishnan, S. F. Raj and T. Kavaskar, *b*-coloring of Cartesian product of odd graphs, *Ars Combin.* **131** (2017) 285–298.
[5] S. Barik, D. Kalita, S. Pati and G. Sahoo, Spectra of graphs resulting from various graph operations and products: A survey, *Spec. Matrices* **6** (2018) 323–342.
[6] A. Das and P. Panigrahi, Normalized Laplacian spectrum of some subdivision-coronas of two regular graphs, *Linear Multilinear Algebra* **65** (2017) 962–972.
[7] R. M. Falcón, M. Venkatachalam and S. J. Margaret, Determining the *b*-chromatic number of subdivision-vertex neighbourhood coronas, arXiv:2302.13667 (2023), 25 pp.
[8] M. Gayathri and R. Rajkumar, Adjacency and Laplacian spectra of variants of neighbourhood corona of graphs constrained by vertex subsets, *Discrete Math. Algorithms Appl.* **11** (2019) 1950073.
[9] C. Guo and M. Newman, On the *b*-chromatic number of Cartesian products, *Discrete Appl. Math.* **239** (2018) 82–93.
[10] R. W. Irving and D. F. Manlove, The *b*-chromatic number of a graph, *Discrete Appl. Math.* **91** (1999) 127–141.
[11] M. Jakovac and I. Peterin, On the *b*-chromatic number of some graph products, *Studia Sci. Math. Hungar.* **49** (2012) 156–169.
[12] M. Jakovac and I. Peterin, The *b*-chromatic number and related topics - a survey, *Discrete Appl. Math.* **235** (2018) 184–201.
[13] R. Javadi and B. Omoomi, On *b*-coloring of Cartesian product of graphs, *Ars Combin.* **107** (2012) 521–536.
[14] S. Kerdjoudj, F. Affif and A. Berrachedi, The *b*-coloring and *b*-continuity of the Cartesian product of some graphs, *Util. Math.* **104** (2017) 123–140.
[15] I. Koch and I. Peterin, The *b*-chromatic index of direct product of graphs, *Discrete Appl. Math.* **190/191** (2015) 109–117.
[16] M. Kouider and M. Mahéo, Some bounds for the *b*-chromatic number of a graph, *Discrete Math.* **256** (2002) 267–277.
[17] M. Kouider and M. Mahéo, The *b*-chromatic number of the cartesian product of two graphs, *Studia Sci. Math. Hungar.* **44** (2007) 49–55.
[18] C. Linhares, L. Sampaio and A. Silva, On the *b*-continuity of the lexicographic product of graphs, *Graphs Combin.* **33** (2017) 1165–1180.
[19] J. B. Liu and J. Cao, The resistance distances of electrical networks based on Laplacian generalized inverse, *Neurocomputing* **167** (2015) 306–313.
[20] X. Liu and P. Lu, Spectra of subdivision-vertex and subdivision-edge neighbourhood coronae, *Linear Algebra Appl.* **438** (2013) 3547–3559.
[21] F. Maffray and A. Silva, *b*-colouring the Cartesian product of trees and some other graphs, *Discrete Appl. Math.* **161** (2013) 650–669.
[22] T. Pathinathan, A. A. Mary and D. Bhuvaneswari, *b*-chromatic number of subdivision edge and vertex corona, *Int. J. Comput. Algorithm* **3** (2014) 44–47.
[23] S. F. Raj and T. Kavaskar, On two conjectures on *b*-coloring of graph products, *Studia Sci. Math. Hungar.* **54** (2017) 141–149.
[24] J. V. Vivin and M. Venkatachalam, The *b*-chromatic number of corona graphs, *Util. Math.* **88** (2012) 299–307.

Results on fractional integrodifferential equations with fractional boundary conditions by using a special type of operators over general Banach spaces with bounded approximation numbers

Samy A. Harisa (s.harisa@psau.edu.sa)
Prince Sattam bin Abdulaziz University

Nashat Faried
Ain Shams University

V. Vijayaraj
Kongunadu Arts and Science College

C. Ravichandran
Kongunadu Arts and Science College

Ahmed Morsy
Prince Sattam bin Abdulaziz University

Research Article

Keywords: Fractional differential equations, fixed point techniques, Trapezoidal method.

Posted Date: March 16th, 2023

DOI: https://doi.org/10.21203/rs.3.rs-2676839/v1

Additional Declarations: No competing interests reported.

Results on fractional integro-differential equations with fractional boundary conditions by using special type of operators over general Banach and Hilbert spaces with bounded approximation numbers

Samy A. Harisa[a,b,*], Nashat Faried[b], V. Vijayaraj[c],
C. Ravichandran[c], Ahmed Morsy[a]

[a]Department of Mathematics, College of Arts and Sciences,
Prince Sattam bin Abdulaziz University,
Wadi Aldawaser 11991, Saudi Arabia.

[b] Department of Mathematics, Faculty of Science,
Ain Shams University, Cairo, Egypt.

[c]Department of Mathematics, Kongunadu Arts and Science College,
Coimbatore - 641 029, India.

Email: s.harisa@psau.edu.sa, n_faried@hotmail.com, nashatfaried@sci.asu.edu.eg,
vijayveliappan@gmail.com, ravibirthday@gmail.com, a.morsy@psau.edu.sa

*Corresponding Author

Abstract

We assess, the existence and uniqueness solutions to a class of nonlinear fractional integro-differential equations involving Atangana-Baleanu(AB) derivatives with fractional boundary conditions. Leray-Schauder alternative theorem ensures the existence of solutions and uniqueness solutions are derived by using Banach contraction principle. Furthermore, we present an implicit numerical scheme based on the trapezoidal method for obtaining the numerical approximation to the solution. An example is given to illustrate our analytical and numerical findings.

Keywords: Fractional differential equations, fixed point techniques, Trapezoidal method.
2020 MSC: 34A08, 34K37, 65L10.

1 Introduction

Fractional differential equations (FDEs) seemed as an excellent mathematical tool for modeling of many physical phenomena appearing in various branches, such as viscoelasticity, self-similar protein dynamics, continuum and statistical mechanics, dynamics of particles etc [1, 2]. A number of non-integer derivatives and their associated integrals have been developing since 1695, and a systematic classification of fractional integrals with certain generalized Leibniz (type) rules was presented in [3–5] . Consequently, fractional calculus allows us to choose what kind of derivative to be used to solve a model, resulting in more accurate solutions.

Recently many authors have studied mathematical models involving AB fractional derivative. AB derivative in Caputo sense has also received considerable attention from researchers in the theoretical area of nonlinear FDEs. For instance, Jarad et al. [6, 10, 11] addressed the existence of solutions to nonlinear Cauchy problems containing AB derivative. AB derivative in Caputo sense has also received

considerable attention from researchers in the theoretical area of nonlinear FDEs. For instance, Jarad et al.[16, 20, 25] addressed the existence and uniqueness of solutions to nonlinear Cauchy problems containing AB derivative. In addition, the Gronwall inequality was established in the context of AB integral in order to analyze the Ulam-Hyers stability of the solution.The existence and qualitative behaviors of solutions of fractional integro-differential equations(FIDE) were investigated in [7, 28], which involved an extension model of [16, 29]. The existence and qualitative behaviors of solutions of fractional integrodifferential equations were investigated in [30, 33], which involved an extension model of [12, 14]. Recently, the authors of [17, 31, 32] studied the approximate controllability of stochastic integrodifferential equations having infinite delay in the settings of AB fractional derivative. Fernandez et al. [10, 11] investigated linear FDEs with variable coefficients and established analytical solutions for such equations. In [22–24], the authors proposed a new explicit numerical scheme based on two-step Lagrange polynomial for solving nonlinear FDEs of AB derivative and also presented the error analysis. [18, 34, 35] has defined higher-order AB fractional operators and established some useful relations among the operators. Some recent progress on the existence of solutions to various higher-order nonlinear FDEs based on AB derivative with classical boundary conditions can be found in a series of papers.

Now, we consider the nonlinear FIDE with fractional boundary conditions of the following from:

$$^{ABC}\mathcal{D}^{q}_{a^+}w(t) = \mathscr{F}\left(t, \int_0^t \mathscr{K}(t,s)w(s)ds, \int_0^t \mathscr{H}(t,s)w(s)ds\right), 1 < q < 2, t \in [0,a] = T, \tag{1.1}$$

$$w(0) = w_0, {}^{ABC}\mathcal{D}^{q-1}_{a^+}w(a) = w_1. \tag{1.2}$$

Where $^{ABC}\mathcal{D}^{q}_{a^+}$ and $^{ABC}\mathcal{D}^{q-1}_{a^+}$ denote the AB fractional derivatives (FD) in Caputo sense; $\mathscr{F}$ is any real-valued absolutely continuous function and w_0, w_1 are real numbers.
For our convenient, we consider $Sw(t) = \int_0^t \mathscr{K}(t,s)w(s)ds$ and $Tw(t) = \int_0^t \mathscr{H}(t,s)w(s)ds$ Then (1.1) becomes,

$$\begin{cases} {}^{ABC}\mathcal{D}^{q}_{a^+}w(t) = \mathscr{F}\left(t, Sw(t), Tw(t)\right), 1 < q < 2, t \in [0,a] = T, \\ w(0) = w_0, {}^{ABC}\mathcal{D}^{q-1}_{a^+}w(a) = w_1. \end{cases} \tag{1.3}$$

In this work, we derive the necessary preliminaries regarding our study are presented in Section 2. In Section 3, some basic properties of AB operators, along with an auxiliary lemma for the linear version of (1.1), are derived. In Section 4, we study the existence of solution to (1.1). Section 5 contains an implicit numerical scheme for solving the proposed nonlinear FDE (1.1). In Section 6, illustrative examples for our obtained results are provided with their numerical simulations.

2 Preliminaries

Here, we recall basic concepts and useful lemmas related to AB fractional derivatives and AB fractional integral. Let $C[a,b], a < b$, be the Banach space of all real-valued continuous functions on $[a,b]$ with the norm $||y||_\infty = sup_{t\in[a,b]}\{|y(t)|\}$. Let $AC[a,b]$ be the space of all real-valued absolutely continuous functions on $[ab]$ and $AC^m[a,b] = \{y | y : [a,b] \to \mathbb{R}, y^{(m-1)} \in AC[a,b]\}, m \in \mathbb{N}$.

Definition 2.1. *[13] The classical & two-parametric Mittag-Leffler functions are,*

$$E_p(z) = \sum_{k=0}^{\infty} \frac{z^k}{\gamma(kp+1)}, E_{p,q}(z) = \sum_{k=0}^{\infty} \frac{z^k}{\Gamma(kp+q)}, (z, p, q \in C, R(p) > 0),$$

respectively, where $E_{p,1}(z) = E_p(z)$.

Definition 2.2. *[19, 27] The RL fractional integral of order $q > 0$ is,*
$\left(I^q_{a^+}w\right)(t) = \frac{1}{\Gamma(q)}\int_a^t (t-r)^{q-1}w(r)dr$, *where $w \in L^1(a,b)$.*

Definition 2.3. *[3, 8, 10] Let $0 < q < 1$. The AB FD in Caputo sense is,*

$$\left({}^{ABC}\mathcal{D}^{q}_{a^+}w\right)(t) = \frac{\mathscr{B}(q)}{1-p}\int_a^t E_q\left[-\frac{q}{1-p}(t-r)^q\right]w'(r)dr,$$

where $w \in AC[a,b]$.
The AB FD in RL sense is,

$$\left({}^{ABR}\mathcal{D}^{q}_{a^+}w\right)(t) = \frac{\mathscr{B}(q)}{1-p}\int_a^t E_q\left[-\frac{q}{1-p}(t-r)^q\right]w(r)dr,$$

where $w \in L^1(a,b)$.
The AB fractional integral is,

$$\left({}^{AB}I^{q}_{a^+}w\right)(t) = \frac{1-p}{\mathscr{B}(q)}w(t) + \frac{q}{\mathscr{B}(q)}\left(I^{q}_{a^+}w\right)(t),$$

where $w \in L^1(a,b)$. *Now, we consider the normalization function* $B(q)$ *to be real-valued strictly positive such that* $B(0) = B(1) = 1$.

Lemma 2.4. *[3] Let* $0 < q < 1$. *Then*

$$\left({}^{ABC}\mathcal{D}^{q}_{a^+}w\right)(t) = \left({}^{ABR}\mathcal{D}^{q}_{a^+}w\right)(t) - \frac{\mathscr{B}(q)}{1-p}w(a)E_q\left[-\frac{q}{1-p}(t)^q\right],$$

where $w \in AC[a,b]$.

Definition 2.5. *[5] Let* $m < q < m+1 (m \in N_0)$ *and* $p = q - m$.
The AB FD in caputo sense is,

$$\left({}^{ABC}\mathcal{D}^{q}_{a^+}w\right)(t) = \left({}^{ABC}\mathcal{D}^{q}_{a^+}w^{(m)}\right)(t),$$

where $w \in AC^{m+1}[a,b]$.
The AB FD in RL sense is,

$$\left({}^{ABR}\mathcal{D}^{q}_{a^+}w\right)(t) = \left({}^{ABR}\mathcal{D}^{q}_{a^+}w^{(m)}\right)(t),$$

where $w \in L^1(a,b)$.
The AB fractional integral is,

$$\left({}^{AB}I^{q}_{a^+}w\right)(t) = \left(I^{m}_{a^+}I^{p}_{a^+}w\right)(t),$$

where $w \in L^1(a,b)$.

Lemma 2.6. *[5] Let* $m < q < m+1 (m \in N_0)$. *Then*

$$\left({}^{AB}I^{q}_{a^+}\,{}^{ABC}\mathcal{D}^{q}_{a^+}w\right)(t) = w(t) - \sum_{k=0}^{m}\frac{w^{(w)}(a)}{k!}(t-k)^k,$$

where $w \in AC^{m+1}[a,b]$.

Definition 2.7. *[26] By* $\mathcal{L}(X,Y)$, *we denote the normed space of bounded linear operators from a normed space* X *into a normed space* Y. *A maps, which assigns to every operator* $T \in \mathcal{L}(X,Y)$ *a unique sequence* $\{s_r(T)\}_{r=0}^{\infty}$ *of real numbers, is called an s-function. We call* $s_r(T)$ *the rth s-number of the operator* T *if the following conditions are satisfied.*

1. $||T|| = s_0(T) \geq s_1(T) \geq ... \geq 0$ *for* $T \in \mathcal{L}(X,Y)$.
2. $s_{r+m}(U+V) \leq s_r(U) + s_m(V)$ *for* $U, V \in \mathcal{L}(X,Y)$.
3. $s_r(UTV) \leq ||U|| s_r(T) ||V||$ *for* $V \in \mathcal{L}(X_0, X), T \in \mathcal{L}(X,Y)$ *and* $U \in \mathcal{L}(Y, Y_0)$.
4. $s_r(T) = 0$ *if and only if* $rank(T) \leq r$ *for* $T \in \mathcal{L}(X,Y)$.

5. $s_r(I_n) = \begin{cases} 1, \ for\ r < n; \\ 0, \ for\ r \geq n; \end{cases}$

where I_n is the identity operator on the Euclidean space l_2^n.

Example 2.8. *[26] As examples of s-numbers, we mention the approximation numbers $\alpha_r(T)$, Gelfand numbers $c_r(T)$, Kolmogorov numbers $d_r(T)$ and Tikhomirov numbers $d_r^*(T)$ defined by the following.*

1. $\alpha_r(T) = inf\{||T - A|| : A \in \mathcal{L}(X, Y)\ and\ rank(A) \leq r\}$. *Clearly, we always have* $||T|| = \alpha_0(T) \geq \alpha_1(T) \geq \alpha_2(T) \geq ... \geq 0$.
2. $c_r(T) = \alpha_r(J_Y T)$, *where J_Y is a metric injection from the space Y into a higher space $l^\infty(\wedge)$ of all bounded real function for a suitable index set $\wedge$.*
3. $d_r(T) = inf_{dimK \leq r}\ sup_{||x|| \leq 1}\ inf_{y \in K}||Tx - y||$ *where $K \subseteq Y$.*
4. $d_r^*(T) = d_r(J_y T)$.

Also, according to the rate of convergence of the sequence $\{\alpha_n(T)\}$, the operator T belongs to the ideal of type l^p, which means that $\{\alpha_n(T)\} \in l^p$, where l^p is the space of the p-summable sequences of real numbers.

3 Equivalent Linear System Solutions

This section is devoted to obtaining several important properties and results that will be helpful in our forthcoming discussion. We first define the Laplace transform of higher-order AB operators as follows:
Proposition 3.1. Let $m < q < m + 1\,(m \in \mathbb{N}_0)$. Then, in particular $a = 0$, we get

$$\mathcal{L}\left\{\left({}^{ABC}\mathcal{D}_{0+}^{q} w\right)(t)\right\}(s) = \frac{B(q-m)}{m+1-p} \frac{s^q \mathcal{L}\{\mathscr{F}(Sw(t), Tw(t))\}(s) - \sum_{0 \leq k \leq m} s^{q-k-1} w^{(k)}(0)}{s^{q-m} + \frac{q-m}{m+1-p}},$$

$$\mathcal{L}\left\{\left({}^{ABR}\mathcal{D}_{0+}^{q} w\right)(t)\right\}(s) = \frac{B(q-m)}{m+1-p} \frac{s^q \mathcal{L}\{\mathscr{F}(Sw(t), Tw(t))\}(s) - \sum_{0 \leq k \leq m-1} s^{q-k-1} w^{(k)}(0)}{s^{q-m} + \frac{q-m}{m+1-p}},$$

$$\mathcal{L}\left\{\left({}^{AB}I_{0+}^{q} w\right)(t)\right\}(s) = \frac{1}{B(q-m)}\left[(m+1-p)s^{-m} + (q-m)s^{-q}\right]\mathcal{L}\{\mathscr{F}(Sw(t), Tw(t))\}(s),$$

provided the Laplace transform of g exists.
Lemma 3.2 Let $m < q < m + 1(m \in N_0)$. Then, in particular $a = 0$ yields the following result,

$$\left({}^{ABC}\mathcal{D}_{a^+}^{q} w\right)(t) = \left({}^{ABR}\mathcal{D}_{a^+}^{q} w\right)(t) - \frac{\mathscr{B}(q-m)}{m+1-p} w^{(m)} E_{q-m}\left[-\frac{q-m}{m+1-p}(t)^{q-m}\right],$$

where $w \in AC^{m+1}[a, b]$.
Proposition 3.3 Let $m < q < m + 1(m \in N_0)$. Then,

$$\left({}^{AB}I_{a^+}^{q}\ {}^{ABC}\mathcal{D}_{a^+}^{q} w\right)(t) = w(t) - w(a) E_{q-m}\left[-\frac{q-m}{m+1-p}(t)^{q-m}\right],$$

where $w \in AC[a, b]$.
Proof: From Definition 2.5, by setting $p = q - m$, we have

$$\left({}^{AB}I_{a^+}^{q}\ {}^{ABC}\mathcal{D}_{a^+}^{q} w\right)(t) = \left({}^{AB}I_{a^+}^{q}\ {}^{ABC}\mathcal{D}_{a^+}^{q} w\right)(t).$$

Hence the final conclusion follows from Lemma 2.4 and [[5], Proposition 3.1].
Lemma 3.4 Let $0 < \alpha \leq 1$ and $\lambda > 0$. Then, for all $x > 0$, the function $xE_{\alpha,2}(-\lambda x^\alpha)$ is strictly positive

and monotonically increasing with respect to x.

Proof. From the equation in [27] , we have

$$\int_0^x t^{\beta-1}E_{\alpha,\beta}(-\lambda t^\alpha)dt = x^\beta E_{\alpha,\beta+1}(-\lambda x^\alpha), \beta > 0.$$

In particular, by setting $\beta = 1$, the above equation reduces to

$$xE_{\alpha,2}(-\lambda x^\alpha) = \in_0^x E_\alpha(-\lambda t^\alpha)dt.$$

In view of [[36], Lemma 2.2], $xE_{\alpha,2}(-\lambda x^\alpha), x > 0$, is strictly positive and monotonically increasing with respect to x.

Lemma 3.5 Let $\mathscr{F} \in AC[0,b]$ with $\mathscr{F}(0) = 0$ and $1 < q < 2$. Then the solution to the linear system

$$\begin{cases} {}^{ABC}\mathcal{D}_{a^+}^q w(t) = \mathscr{F}(t), t \in [0,a] \\ w(0) = w_0, {}^{ABC}\mathcal{D}_{a^+}^{p-1} w(b) = w_1 \end{cases} \tag{3.1}$$

is

$$w(t) = w_0 + \frac{1}{\Delta}\left[w_1 - \int_0^b \mathscr{F}(Sw(t), Tw(t))ds\right] t + \frac{2-q}{B(p-1)}\int_0^t \mathscr{F}(Sw(t), Tw(t))ds$$
$$+ \frac{1}{B(p-1)\Gamma(p-1)}\int_0^t (t-r)^{p-1}\mathscr{F}(Sw(t), Tw(t))ds, forallt \in T, \tag{3.2}$$

where,

$$\Delta = \frac{B(p-1)}{2-q} bE_{p-1,2}\left[-\frac{p-1}{2-q}b^{p-1}\right].$$

Proof. Use of Atangana-Baleanu integral operator ${}^{AB}I_{0+}^q$ on both sides of the equation in (3.1) with the help of Lemma 2.6, results in

$$\begin{aligned} w(t) &= c_1 + c_2 t + {}^{AB}I_{0+}^q \mathscr{F}(t) \\ &= c_1 + c_2 t + \frac{2-q}{B(p-1)}\int_0^t \mathscr{F}(Sw(t), Tw(t))ds \\ &\quad + \frac{1}{B(p-1)\Gamma(p-1)}\int_0^t (t-r)^{p-1}\mathscr{F}(Sw(t), Tw(t))ds, \end{aligned} \tag{3.3}$$

where $c_1, c_2 \in \mathbb{R}$. The condition $w(0) = w_0$ yields $c_1 = w_0$. Moreover, by Definition 2.5, we have $w(t) = w_0 + c_2 t + I_{0+}{}^{AB}I_{0+}^{p-1}\mathscr{F}(t)$.
In view of Proposition 3.3, we obtain

$${}^{ABC}\mathcal{D}_{0+}^{p-1} w(t) = c_2 \frac{B(p-1)}{2-q} tE_{p-1,2}\left[-\frac{p-1}{2-q}t^{p-1}\right] + \int_0^t \mathscr{F}(Sw(t), Tw(t))ds.$$

By using boundary condition at $t = b$ given in (3.1), it follows that
$c_2 = \frac{1}{\Delta}\left[w_1 - \int_0^b \mathscr{F}(Sw(t), Tw(t))ds\right]$. Substitution of the above values of c_1 and c_2 into (3.3) leads to the desired solution given in (3.2).

For the elementary results of the Equation (1.2), we need some following hypotheses:

(H1) $|\mathscr{F}(t,w)| \le \varphi_1(t) + \varphi_2(t)|w|$, for all $(t,w) \in \Omega$.

(H2) $|\mathscr{F}(t,w) - \mathscr{F}(t,\tilde{w})| \le \phi(t)|w - \tilde{w}|$ for a.e. $(t,w), (t,\tilde{w}) \in \Omega$.

(H3) Let $w \in C[0,T]$ & function $\varphi \in (C[0,T] \times \mathscr{R} \times \mathscr{R} \times \mathscr{R}, \mathscr{R})$ is continuous function & a positive constant ζ_1, ζ_2 & ζ s.t.,
$\|\varphi(\jmath, w_1, w_2, w_3) - \varphi(\jmath, \varphi_1, \varphi_2, \varphi_3)\| \le \zeta_1 (\|w_1 - \varphi_1\| + \|w_2 - \varphi_2\| + \|w_3 - \varphi_3\|) \forall$
$w_1, w_2, w_3, \varphi_1, \varphi_2, \varphi_3$ in w. $\zeta_2 = max_{w \in \mathscr{R}} \|f(\jmath, \mathscr{R}, \mathscr{R}, \mathscr{R})\|$ &$\zeta = max\{\zeta_1, \zeta_2\}$.

4 Existence Result

We first convert the FDE (1.1) to an integral equation and then consider it as a fixed-points problem for an integral operator. On the basis of Lemma 3.5, and solution operator $\mathscr{G} : C(T) \to C(T)$ as follows:

$$(\mathscr{G}w)(t) = w_0 + \frac{1}{\Delta}\left[w_1 - \int_0^b \mathscr{F}(r, w(r))dr\right] t + \frac{2-q}{B(p-1)} \int_0^t \mathscr{F}(r, (Sw(t), Tw(t)))ds$$
$$+ \frac{1}{B(p-1)\Gamma(p-1)} \int_0^t (t-r)^{p-1} \mathscr{F}(r, (Sw(t), Tw(t)))ds, \quad \text{for all } t \in J. \tag{4.1}$$

We now only need to seek the fixed-points of $\mathscr{G}$ in $\mathcal{C}(T)$, because the fixed-points of $\mathscr{G}$ are solutions of (1.1). For brevity, we use the notations

$$\Lambda = \frac{b}{\Delta} + \frac{2-q}{B(p-1)} + \frac{b^{p-1}}{B(p-1)\Gamma(p-1)}$$
$$\tilde{\Lambda} = \frac{b^2}{\Delta} + \frac{b(2-q)}{B(p-1)} + \frac{b^q}{qB(p-1)\Gamma(p-1)}.$$

By considering the growth condition on nonlinearity, we now establish the result based on Leray-Schauder alternative theorem [14].

Theorem 4.1. *Let $\Omega = \{(t, w) \in \mathbb{R}^2 : t \in T$ and $|w| \leq \lambda$ for fixed $\lambda > 0\}$. Suppose that $\mathscr{F} : \Omega \to \mathbb{R}$ is absolutely continuous and there exist $\varphi_i \in C(T, [0, \infty)), i = 1, 2$ such that If $\mathscr{F}(0, w(0)) = 0$, then (1.1) has a solution in $C(T)$, provided $\Lambda \int_0^b \varphi_2(r)ds < 1$.*

Proof. *The operator $\mathscr{G} : C(T) \to C(T)$ is completely continuous. Suppose $\mathfrak{D} \subset C(T)$ is an arbitrary bounded set. Then, by using (H1), there is a number $RL > 0$ such that $|\mathscr{F}(t, (Sw(t), Tw(t)))| \leq RL$ for $t \in T, w \in \mathfrak{D}$. Now, $\forall w \in \mathfrak{D}$, we obtain*

$$|(\mathscr{G}w)(t)| \leq |w_0| + \frac{1}{\Delta}\left[|w_1| + \int_0^b |\mathscr{F}(r, (Sw(t), Tw(t)))|ds\right] t + \frac{2-q}{B(p-1)} \int_0^t |\mathscr{F}(r, (Sw(t), Tw(t)))|ds$$
$$+ \frac{1}{B(p-1)\Gamma(p-1)} \int_0^t (t-r)^{p-1} |\mathscr{F}(r, (Sw(t), Tw(t)))ds$$
$$\leq |w_0| + \frac{b}{\Delta}|w_1| + RL\tilde{\Lambda} < +\infty,$$

$\Longrightarrow$ $\mathscr{G}(\mathfrak{D})$ is bounded.

Next, we show that $\mathscr{G}(\mathfrak{D})$ is equicontinuous. For all $w \in \mathfrak{D}$ and $0 \leq \tau_1 < \tau_2 \leq b$, we have

$$|(\mathscr{G}w)(\tau_2) - (\mathscr{G}w)(\tau_1)|$$
$$\leq \frac{1}{\Delta}\left[|w_1| + \int_0^b |\mathscr{F}(r, (Sw(t), Tw(t)))ds\right](\tau_2 - \tau_1) + \frac{2-q}{B(p-1)} \int_{\tau_1}^{\tau^{\tau_2}} |\mathscr{F}(r, (Sw(t), Tw(t)))|ds$$
$$+ \frac{1}{B(p-1)\Gamma(p-1)}\left[\int_0^{\tau_1} \left[(\tau_2 - r)^{p-1} - (\tau_1 - r)^{p-1}\right] |\mathscr{F}(r, (Sw(t), Tw(t)))|ds\right.$$
$$\left. + \int_{\tau_1}^{\tau_2} (\tau_2 - r)^{p-1} |\mathscr{F}(r, (Sw(t), Tw(t)))|ds\right]$$
$$\leq \left[\frac{|w_1| + bRL}{\Delta} + \frac{2-q}{B(p-1)}RL\right](\tau_2 - \tau_1) + \frac{RL}{qB(p-1)\Gamma(q+1)}(\tau_2^q - \tau_1^q).$$

Since the function $\tau^q, 1 < q < 2$, is uniformly continuous on $J, \mathscr{G}(\mathfrak{D})$ is a family of equicontinuous functions. Therefore, following the Arzela-Ascoli theorem, $\mathscr{G}(\mathfrak{D})$ is relatively compact in $C(T)$. Hence, we conclude that $\mathscr{G}$ is completely continuous.

Now, we prove $\mathcal{S} = \{w \in C(T) : w = \lambda \mathscr{G} w \text{ and } \lambda \in (0,1)\}$ is a bounded set.
Let $w \in \mathcal{S}$, then $w(t) = \lambda(\mathscr{G}w)(t)$ for $t \in T$. By (H1), for $t \in T$, one has

$$\begin{aligned}
|w(t)| &= |\lambda(\mathscr{G}, \mathscr{F}(Sw(t), Tw(t)))| \\
&< |w_0| + \frac{1}{\Delta}\left[|w_1| + \int_0^b (\varphi_1(r) + \varphi_2(r)|\mathscr{F}(Sw(t), Tw(t))|)\, ds\right] t \\
&+ \frac{2-q}{B(p-1)} \int_0^t (\varphi_1(r) + \varphi_2(r)|\mathscr{F}(Sw(t), Tw(t))|)\, ds \\
&+ \frac{1}{B(p-1)\Gamma(p-1)} \int_0^t (t-r)^{p-1} (\varphi_1(r) + \varphi_2(r)|\mathscr{F}(Sw(t), Tw(t))|)\, ds \\
&\leq |w_0| + \frac{b}{\Delta}|w_1| + \Lambda \int_0^b \varphi_1(r) ds + \Lambda \int_0^b \varphi_2(r) ds \|w\|_\infty.
\end{aligned}$$

Hence, for all $w \in \mathcal{S}$, we have

$$\|w\|_\infty \leq \frac{|w_0| + \frac{b}{\Delta}|w_1| + \Lambda \int_0^b \varphi_1(r) ds}{1 - \Lambda \int_0^b \rho_2(r) ds} < +\infty,$$

$\implies$ $\mathcal{S}$ is bounded. Therefore, the Leray-Schauder alternative theorem ensures us that $\mathscr{G}$ has at least one fixed-point in $C(T)$, as required. Hence the theorem follows. By considering the generalized Lipschitz condition on nonlinearity.

5 Uniqueness Result

Theorem 5.1. *Let $\Omega = \{(t, w) \in \mathbb{R}^2 : t \in T \text{ and } |w| \leq \lambda \text{ for fixed } \lambda > 0\}$. Suppose that $\mathscr{F} : \Omega \to \mathbb{R}$ is absolutely continuous and $\exists \phi \in L^1(T, [0, \infty))$ s.t., If $\mathscr{F}(0, w(0)) = 0$, then (1.1) has a unique solution in $C(T)$, provided*

$$\Lambda \int_0^b \phi(r) ds < 1. \tag{5.1}$$

Proof. *The operator $\mathscr{G} : C(T) \to C(T)$ is defined in (4.1). Let us first denote $M = \sup_{t \in J} |\mathscr{F}(t, 0)| < \infty$ and fix a real number $\rho, 0 < \rho \leq \lambda$, s.t.,*

$$\frac{|w_0| + \frac{b}{\Delta}|w_1| + M\tilde{\Lambda}}{1 - \Lambda \int_0^b \phi(r) ds} \leq \rho.$$

We now show that $\mathscr{G}\mathfrak{B}_\rho \subset \mathfrak{B}_\rho$, where $\mathfrak{B}_\rho = \{w \in C(T) : \|w\|_\infty \leq \rho\}$. By (H2), for all $w \in \mathfrak{B}_r$, one has

$$\begin{aligned}
|(\mathscr{G}w)(t)| &\leq |w_0| + \frac{1}{\Delta}\left[|w_1| + \int_0^b (\phi(r)|\mathscr{F}(Sw(t), Tw(t))| + M) ds\right] t \\
&+ \frac{2-q}{B(p-1)} \int_0^t (\phi(r)|\mathscr{F}(Sw(t), Tw(t))| + M) ds \\
&+ \frac{1}{B(p-1)\Gamma(p-1)} \int_0^t (t-r)^{p-1} (\phi(r)|\mathscr{F}(Sw(t), Tw(t))| + M) ds \\
&\leq |w_0| + \frac{1}{\Delta}\left[|w_1| + \rho \int_0^b \phi(r) ds + Mb\right] b \\
&+ \frac{2-q}{B(p-1)}\left[\rho \int_0^b \phi(r) ds + Mb\right] \\
&+ \frac{1}{qB(p-1)\Gamma(p-1)} b^{p-1}\left[q\rho \int_0^b \phi(r) ds + Mb\right] \quad \text{for all } t \in T.
\end{aligned}$$

Therefore, for all $w \in \mathfrak{B}_\rho$, we deduce that

$$\begin{aligned}\|\mathscr{G}w\|_\infty &\leq |w_0| + \frac{b}{\Delta}|w_1| + M\tilde{\Lambda} + \Lambda\rho\int_0^b \phi(r)ds \\ &\leq \rho\end{aligned}$$

$\Longrightarrow$ *$\mathscr{G}$ maps $\mathfrak{B}_\rho$.*
Next, we prove that $\mathscr{G}$ is a operator in $C(T)$. Let $w, \tilde{w} \in C(T)$. By (H2), for each $t \in T$, one has

$$\begin{aligned}|(\mathscr{G}w)(t) - (\mathscr{G}\tilde{w})(t)| &\leq \frac{t}{\Delta}\int_0^b \phi(r)|w(r) - \tilde{w}(r)|ds + \frac{2-q}{B(p-1)}\int_0^t \phi(r)|w(r) - \tilde{w}(r)|ds \\ &\quad + \frac{1}{B(p-1)\Gamma(p-1)}\int_0^t (t-r)^{p-1}\phi(r)|w(r) - \tilde{w}(r)|ds \\ &\leq \Lambda\int_0^b \phi(r)ds\|w - \tilde{w}\|_\infty.\end{aligned}$$

Hence, for all $w, \tilde{w} \in C(T)$ we deduce that

$$\|\mathscr{G}w - \mathscr{G}\tilde{w}\|_\infty \leq \Lambda\int_0^b \phi(r)ds\|w - \tilde{w}\|_\infty.$$

The assumption (5.1) ensures that $\mathscr{G}$ is contractive. Hence the Banach fixed point theorem allows us to conclude that $\mathscr{G}$ has a unique fixed-point in $C(T)$, as required. This fixed-point is the aspired solution to (1.1).

6 Numerical Result

This section is devoted to describe a numerical scheme based on the classical and fractional trapezoidal methods [9, 15, 21], which are used to interpolate the vector field $\mathscr{F}$ by the first-degree polynomials. In fact, it is shown that the trapezoidal method usually provides excellent accuracy under the consideration of small step size. We here directly discretize the integral equation of (1.2) to derive the numerical scheme. Let h be the step size, and choose $n+1$ equi-spaced grid points $\mathscr{F}_{tk} = kh : k = 0, 1, 2, ..., n$ on $[0, b]$ such that $0 = t_0 < t_1 < t_2 < ... < t_n = b$ with some positive integers n and $h := \frac{b}{n}$.
We first rewrite the integral equation of (1.2) at any point $t = t_k$ in the following piecewise way,

$$\begin{aligned}w(t_k) = w_0 &+ \frac{1}{\Delta}\left[w_1 - \sum_{0\leq\tau\leq n-1} \in_{t_\tau}^{t_\tau+1} \mathscr{F}(r, (Sw(t), Tw(t)))ds\right] t_k \\ &+ \frac{2-q}{B(p-1)} \sum_{0\leq\tau\leq k-1} \in_{t_\tau}^{t_\tau+1} \mathscr{F}(r, (Sw(t), Tw(t)))ds \\ &+ \frac{1}{B(p-1)\Gamma(p-1)} \sum_{0\leq\tau\leq k-1} \in_{t_\tau}^{t_\tau+1} (t_k - r)^{p-1}\mathscr{F}(r, (Sw(t), Tw(t)))ds\end{aligned}$$

In order to formulate the numerical scheme for (1.2), the nonlinear function $\mathscr{F}(t, w(t))$ is approximated, on each subinterval $[t_\tau, t_\tau + 1]$, by the following piece-wise linear function,

$$\mathscr{F}(t, w(t)) = \frac{1}{h}\left[(t_{\tau+1} - t)\mathscr{F}(t_\tau, (Sw(t_\tau), Tw(t_\tau))) + (t - t_\tau)\mathscr{F}(t_{\tau+1}), (Sw(t_\tau + 1), Tw(t_\tau + 1))\right], \quad t \in [t_\tau, t_\tau + 1].$$

After integrating, one obtains the following unknown approximations

$$w(t_k) = w_0 + \frac{1}{\Delta}\left[w_1 - \frac{h}{2}\sum_{0\le\tau\le k-1}[\mathscr{F}(t_\tau,(Sw(t_\tau),Tw(t_\tau))) + \mathscr{F}(t_{\tau+1}),(Sw(t_\tau+1),Tw(t_\tau+1))]\right]t_k$$
$$+ \frac{2-q}{B(p-1)}\frac{h}{2}\sum_{0\le\tau\le k-1}[\mathscr{F}(t_\tau,(Sw(t_\tau),Tw(t_\tau))) + \mathscr{F}(t_{\tau+1}),(Sw(t_\tau+1),Tw(t_\tau+1))]$$
$$+ \frac{(p-1)}{B(p-1)}\frac{h^q}{\Gamma(q+2)}[\{(k-1)^{q+1} - k^q(k-p-1)\}\mathscr{F}(t_0,(Sw(t_0),Tw(t_0)))$$
$$+ \sum_{1\le\tau\le k-1}\{(k-\tau+1)^{q+1} + (k-\tau-1)^{q+1} - 2(k-\tau)^{q+1}\}\mathscr{F}(t_\tau,(Sw(t_\tau),Tw(t_\tau)))$$
$$+ \mathscr{F}(t_k,(Sw(t_k),Tw(t_k)))]. \tag{6.1}$$

Due to the nonlinear nature of the function $\mathscr{F}$ and the presence of all unknown quantities $w(t_k)$ on the RHS of each equation of (6.1), we cannot solve (6.1) for $w(t_k)$ directly, in general. So Newton-Raphson method is used to determine each $w(t_k); k = 0, 1, 2, ..., n$ from the above implicit numerical scheme (6.1). This implicit method is seldomly encountered in the numerical simulation for solving fractional differential equations. However, this method is useful in dealing with the problem (1.2).

7 Example

Our theoretical results are illustrated here with the following example. We also present the trajectory of the numerical solution to the nonlinear problem (1.1) by using the proposed numerical scheme (6.1). Let the normalization function as $B(\alpha) = 1 - \alpha + \frac{\alpha}{\Gamma(\alpha)}, \alpha \in [0, 1]$.

Example 7.1 Consider the linear problem

$$\begin{cases} ABC_{\mathcal{D}^q_{a^+}} w(t) = h^\lambda, t \in [0, b] \\ w(0) = w_0, ABC_{\mathcal{D}^{p-1}_{a^+}} w(b) = w_1 \end{cases} \tag{7.1}$$

where $\lambda > 0$ is a real number. Its exact solution is,

$$w(t) = w_0 + \frac{1}{\Delta}\left[w_1 - \frac{b^{\lambda+1}}{\lambda+1}\right]t + \frac{2-q}{B(p-1)}\frac{t^{\lambda+1}}{\lambda+1} + \frac{p-1}{B(p-1)}\frac{\Gamma(\lambda+1)}{\Gamma(q+\lambda+1)}t^{q+\lambda}$$

Now we consider $\alpha = 0.1, \Delta = 2$, comparison of the exact and numerical solutions to equation (6.1) for $q = 1.9, \lambda = 1.5, b = 5, w_0 = 1, w_1 = 17$ and $h = 0.05$.
In Figure 1, the numerical solution shows good agreement with the exact solution in the entire interval.

Conclusion

In this paper, the essential outcomes of the existence and uniqueness solutions are gained by using the Leray-Schauder alternative theorem and Banach fixed point theorem respectively. We also discussed a numerical scheme for (1.1), which helps to study the numerical solution when $\mathscr{F}$ is nonlinear. Our theoretical and numerical findings were verified with examples. We have presented some important properties of higher-order AB operators, which will be useful for further study in this direction. Besides, the stability analysis of the solution may be considered as an extension work for the problem (1.1), and examples may solve by using Simpson's $\frac{1}{3}$ rule.

Acknowledgment

The authors extend their appreciation to the Deputyship for Research & Innovation, Ministryof Education in Saudi Arabia for funding this research work through the project number ($IF2/PSAU/2022/01/22564$).

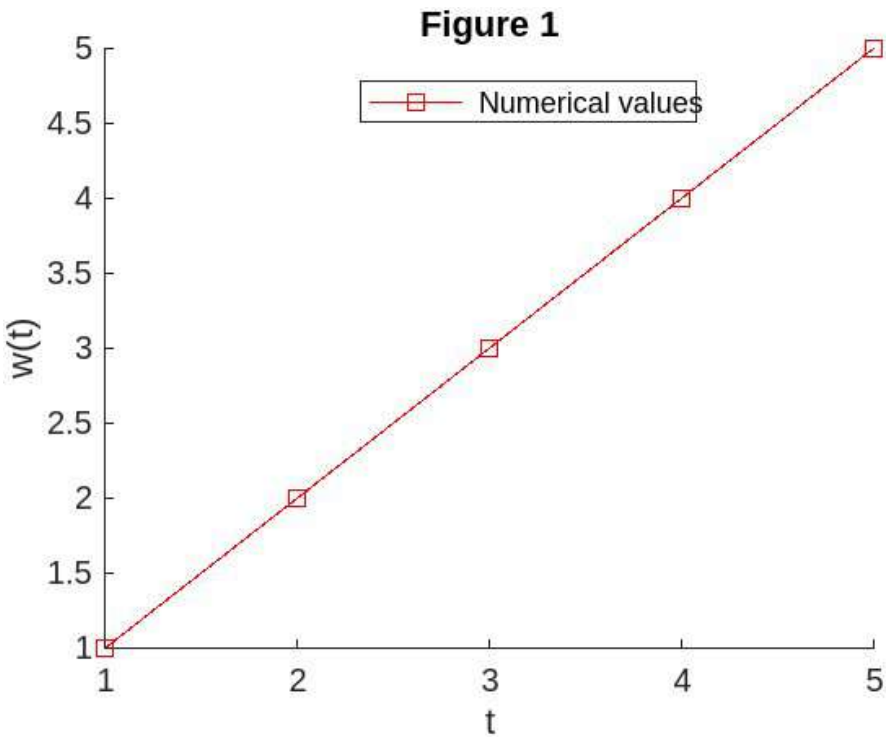

Figure 1: Graph of the approximate solution w(t)

Conflict of Interest

This work does not have any conflicts of interest.

References

[1] T. Abdeljawad, D. Baleanu, On fractional derivatives with generalized Mittag-Leffler kernels, Advances in Difference Equations, (2018), 2018:468.

[2] A. Ahmed Hamoud, Existence and uniqueness of solutions for fractional neutral Volterra-Fredholm integro-diffrential equations, Advances in the Theory of Nonlinear Analysis and its Applications, 4(4)(2020), 321-331.

[3] A. Atangana, D. Baleanu, New fractional derivatives with nonlocal and non-singular kernel: Theory and application to heat transfer model, Thermal Science, 20(2)(2016), 763-769.

[4] A. Atangana, S. Igret Araz, Modeling and forecasting the spread of COVID-19 with stochastic and deterministic approaches: Africa and Europe, Advances in Difference Equations, 2021, 57(2021). https://doi.org/10.1186/s13662-021-03213-2.

[5] T. Abdeljawad, A Lyapunov type inequality for fractional operators with nonsingular Mittag-Leffler kernel, Journal of Inequalities and Applications, 130 (2017), 1-11.

[6] R. P. Agarwal, Y. Zhou, Y. He, Existence of fractional neutral functional differential equations, Computer and Mathematics with Application, 59(3)(2010), 1095-1100.

[7] Ahmed Morsy, Kottakkaran Sooppy Nisar, Chokkalingam Ravichandran, Chandran Anusha, Sequential fractional order Neutral functional Integro differential equations on time scales with Caputo fractional operator over Banach spaces, AIMS Mathematics, 8(3)(2023), 5934-5949.

[8] D. Baleanu, A. Fernandez, On some new properties of fractional derivatives with Mittag-Leffler kernel, Communications in Nonlinear Science and Numerical Simulation, 59 (2018), 444-462.

[9] K. Diethelm, Fundamental approaches for the numerical handling of fractional operators and time-fractional differential equations. In: Karniadakis, G.E. (ed.) Handbook of Fractional Calculus with Applications: Numerical Methods, vol. 3. de Gruyter, Berlin, (2019), 1-22.

[10] A. Fernandez, J. E. Restrepo, D. Suragan, Linear differential equations with variable coefficients and Mittag-Leffler kernels, Journal of Mathematical Analysis and Applications, 61(6) (2022), 4757-4763.

[11] Fahd Jarad, Thabet Abdeljawad, Zakia Hammouch, On a class of ordinary differential equations in the frame of Atangana-Baleanu fractional derivative, Chaos, Solitons and Fractals, 117(2018), 16-20.

[12] N. Faried, A. Morsy, Z. A. Hassanain, s-numbers of shift operators of formal entire functions, Journal of Approximation Theory, 176 (2013), 15-22.

[13] R. Gorenflo, A. A. Kilbas, F. Mainardi, S. V. Rogosin, Mittag-Leffler Functions, Related Topics and Applications, Vol. 2. Berlin: Springer, 2014.

[14] A. Granas, J. Dugundji, Fixed Point Theory, Vol. 14. New York: Springer, 2003.

[15] R. Garrappa, Numerical solution of fractional differential equations: A survey and a software tutorial. Mathematics, 6(2)(2018),16.

[16] F. Jarad, T. Abdeljawad, Z. Hammouch, On a class of ordinary differential equations in the frame of Atangana-Baleanu fractional derivative, Chaos, Solitons and Fractals, (117)(2018), 16-20.

[17] Kamal Shah, Muhammad Arfan, Aman Ullah, Qasem Al-Mdallal, Khursheed J. Ansari, Thabet Abdeljawad, Computational study on the dynamics of fractional order differential equations with applications, Chaos, Solitons and Fractals, 157(2022), 111955.

[18] K. Karthikeyan, J.J. Trujillo, Existence and uniqueness results for fractional integrodifferential equations with boundary value conditions, Communications in Nonlinear Science and Numerical Simulation, 17 (2012), 4037-4043.

[19] A. A. Kilbas, H. M. Srivastava, J. J. Trujillo, Theory and applications of fractional differential equations, North-Holland Mathematics Studies, Vol. 204. Elsevier Science B. V., Amsterdam, 2006.

[20] Kottakkaran Sooppy Nisar, Kumararaju Logeswari, Veliappan Vijayaraj, Haci Mehmet Baskonus, Chokkalingam Ravichandran, Fractional Order Modeling the Gemini Virus in Capsicum annuum with Optimal Control, Fractal and Fractional, 6(2),(2022), 61.

[21] C. Li, F. Zeng, Numerical Methods for Fractional Calculus, Vol. 24. CRC Press, 2015.

[22] K. Logeswari, C. Ravichandran, A new exploration on existence of fractional neutral integrodifferential equations in the concept of Atangana-Baleanu derivative, Physica A: Statistical Mechanics and its Applications, 544, (2020), 123454.

[23] K. Logeswari, C. Ravichandran, K. S. Nisar, Mathematical model for spreading of COVID-19 virus with the Mittag-Leffler kernel, Numerical Methods for Partial Differential Equations, (2020), 1-16. doi: 10.1002/num.22652.

[24] K. S. Miller, B. Ross, An Introduction to the Fractional Calculus and Fractional Differential Equations, John Wiley and Sons, New York (1993).

[25] Mohammed Salem Abdo, Satish Kushaba Panchal, Existence and continuous dependence for fractional neutral functional differential equations, Journal of Mathematical Modeling, 5(2)(2017), 153-170.

[26] A. Pietsch, Eigenvalues and s-Numbers, Akademische-Verlag, 1987.

[27] I. Podlubny, Fractional Differential Equations, Academic Press, San Diego (1999).

[28] C. Ravichandran, V. Sowbakiya, Kottakkaran Sooppy Nisar, Study on existence and data dependence results for fractional order differential equations, Chaos, Solitons and Fractals, 160(2022), 112232.

[29] C. Ravichandran, K. Logeswari, F. Jarad, New results on existence in the framework of Atangana-Baleanu derivative for fractional integro-differential equations, Chaos, Solitons and Fractals, 125(2019), 194-200.

[30] C. Ravichandran, K. Logeswari, S. K. Panda, K. S. Nisar, On new approach of fractional derivative by Mittag-Leffler kernel to neutral integro-differential systems with impulsive conditions, Chaos, Solitons and Fractals, 139(2020), 110012.

[31] Rohul Amin, Kamal Shah, Muhammad Asif, Imran Khan, Faheem Ullah, An efficient algorithm for numerical solution of fractional integro-differential equations via Haar wavelet, Journal of Computational and Applied Mathematics, 381(2021), 113028.

[32] Rohul Amin, Hijaz Ahmad, Kamal Shah, M. Bilal Hafeez, W. Sumelka, Theoretical and computational analysis of nonlinear fractional integro-differential equations via collocation method, Chaos, Solitons and Fractals, 151 (2021), 111252.

[33] M. Sivashankar, S. Sabarinathan, Kottakkaran Sooppy Nisar, C. Ravichandran, B. V. Senthil Kumar, Some properties and stability of Helmholtz model involved with nonlinear fractional difference equations and its relevance with quadcopter, Chaos, Solitons and Fractals, 168(2023), 113161.

[34] Veliappan Vijayaraj, Chokkalingam Ravichandran, Panumart Sawangtong, Kottakkaran Sooppy Nisar, Existence results of Atangana-Baleanu fractional integro-differential inclusions of Sobolev type, Alexandria Engineering Journal, 66, (2023), 249-255.

[35] Veliappan Vijayaraj, Chokkalingam Ravichandran, Thongchai Botmart, Kottakkaran Sooppy Nisar, Kasthurisamy Jothimani, Existence and data dependence results for neutral fractional order integro-differential equations, AIMS Mathematics, 8(1)(2022), 1055-1071.

[36] Z. Wei, Q. Li, J. Che, Initial value problems for fractional differential equations involving Riemann-Liouville sequential fractional derivative, Journal of Mathematical Analysis and Applications, 367 (2010) 260-272.

PLOS ONE

RESEARCH ARTICLE

Investigation on integro-differential equations with fractional boundary conditions by Atangana-Baleanu-Caputo derivative

Samy A. Harisa[1,2☯], **Nashat Faried**[2☯], **V. Vijayaraj**[3☯], **C. Ravichandran**[3☯], **Ahmed Morsy**[1☯*]

1 Department of Mathematics, College of Arts and Sciences, Prince Sattam bin Abdulaziz University, Wadi Aldawaser, Saudi Arabia, **2** Department of Mathematics, Faculty of Science, Ain Shams University, Cairo, Egypt, **3** Department of Mathematics, Kongunadu Arts and Science College, Coimbatore, Tamil Nadu, India

☯ All these authors are contributed equally to this work.
* a.morsy@psau.edu.sa

Citation: Harisa SA, Faried N, Vijayaraj V, Ravichandran C, Morsy A (2024) Investigation on integro-differential equations with fractional boundary conditions by Atangana-Baleanu-Caputo derivative. PLoS ONE 19(5): e0301338. https://doi.org/10.1371/journal.pone.0301338

Editor: Muhammad Nadeem, Qujing Normal University, CHINA

Received: December 19, 2023

Accepted: March 12, 2024

Published: May 31, 2024

Data Availability Statement: All relevant data are within the manuscript.

Funding: The Deputyship for Research & Innovation, Ministry of Education in Saudi Arabia through the project number (IF2 = PSAU = 2022 = 01 = 22564) for the authors Samy A. Harisa. The funders had no role in study design, data collection and analysis, decision to publish, or preparation of the manuscript.

Competing interests: The authors have declared that no competing interests exist.

Abstract

We establish, the existence and uniqueness of solutions to a class of Atangana-Baleanu (AB) derivative-based nonlinear fractional integro-differential equations with fractional boundary conditions by using special type of operators over general Banach and Hilbert spaces with bounded approximation numbers. The Leray-Schauder alternative theorem guarantees the existence solution and the Banach contraction principle is used to derive uniqueness solutions. Furthermore, we present an implicit numerical scheme based on the trapezoidal method for obtaining the numerical approximation to the solution. To illustrate our analytical and numerical findings, an example is provided and concluded in the final section.

1 Introduction

Fractional differential equations (FDEs) seemed as an excellent mathematical tool for modeling of many physical phenomena appearing in various branches, such as viscoelasticity, self-similar protein dynamics, continuum and statistical mechanics, dynamics of particles etc [1, 2]. A number of non-integer derivatives and their associated integrals have been developed and a systematic classification of fractional integrals with certain generalized Leibniz (type) rules was presented in [3]. Consequently, fractional calculus allows us to choose what kind of derivative to be used to solve a model, resulting in more accurate solutions [4–7].

Recently many authors have studied mathematical models involving AB fractional derivative. AB derivative in Caputo sense has also received considerable attention from researchers in the theoretical area of nonlinear FDEs [8, 9]. For instance, [10–12] addressed the existence of solutions to nonlinear Cauchy problems containing AB derivative.

Researchers in the theoretical domain of nonlinear fractional differential equations have shown significant interest in the Caputo sense AB derivative as well [13–16]. In this situation, a fractional derivative with a nonsingular kernel that relied on the M-L function was

introduced by Atangana and Baleanu(A-B). This new dimension demonstrates the close connection between fractional calculus and the M-L function. It helps us to more effectively handle computing needs, nonlocal dynamics, and distinguish between various traits. [17–19].

In addition, the Gronwall inequality was established in the context of AB integral in order to analyze the Ulam-Hyers stability of the solution [20, 21]. The existence and qualitative behaviors of solutions of fractional integro-differential equations(FIDE) were investigated and which involved an extension model of [15, 22–24]. In [26], the authors proposed a new explicit numerical scheme based on two-step Lagrange polynomial for solving nonlinear FDEs of AB derivative and also presented the error analysis.

[25–28] has defined higher-order AB fractional operators and established some useful relations among the operators. Some recent progress on the existence of solutions to various higher-order nonlinear FDEs based on AB derivative with classical boundary conditions can be found in a series of papers [29–37].

Now, we consider the nonlinear FIDE with fractional boundary conditions of the following from:

$$^{ABC}\mathcal{D}^{q}_{a^+}w(t) = \mathscr{F}\left(t, \int_0^t \mathscr{K}(t,s)w(s)ds, \int_0^t \mathscr{H}(t,s)w(s)ds\right), 1 < q < 2, t \in [0,a] = J, \quad (1.1)$$

$$w(0) = w_0, {}^{ABC}\mathcal{D}^{q-1}_{a^+}w(a) = w_1. \quad (1.2)$$

Where $^{ABC}\mathcal{D}^{q}_{a^+}$ and $^{ABC}\mathcal{D}^{q-1}_{a^+}$ denote the AB fractional derivatives (FD) in Caputo sense; $\mathscr{F}$ is any real-valued absolutely continuous function and w_0, w_1 are real numbers. Here, $\mathscr{K}$, $\mathscr{H}$ are given function which fulfills certain conditions to be defined later on.

For our convenient, we consider $Sw(t) = \int_0^t \mathscr{K}(t,s)w(s)ds$ and $Tw(t) = \int_0^t \mathscr{H}(t,s)w(s)ds$. Then (1.1) becomes,

$$\begin{cases} {}^{ABC}\mathcal{D}^{q}_{a^+}w(t) = \mathscr{F}(t, Sw(t), Tw(t)), 1 < q < 2, t \in [0,a] = J, \\ w(0) = w_0, {}^{ABC}\mathcal{D}^{q-1}_{a^+}w(a) = w_1. \end{cases} \quad (1.3)$$

In this work, we derive the necessary preliminaries in Section 2. In Section 3, some basic properties of AB operators, along with an auxiliary lemma for the linear version of (1.1), are derived. In Section 4, we study the existence of solution to (1.1). Section 5 contains an implicit numerical scheme for solving the proposed nonlinear FDE (1.1). In Section 6, illustrative examples for our obtained results are provided with their numerical simulations.

2 Preliminaries

Here, we recall basic concepts and useful lemmas related to AB fractional derivatives and AB fractional integral. Let $C[a, b]$, $a < b$, be the Banach space of all real-valued continuous functions on $[a, b]$ with the norm $||y||_\infty = sup_{t\in[a,b]}\{|y(t)|\}$. Let $AC[a, b]$ be the space of all real value absolutely continuous functions on $[ab]$ and

$$AC^m[a,b] = \{y | y : [a,b] \to \mathbb{R}, y^{(m-1)} \in AC[a,b]\}, m \in \mathbb{N}.$$

Definition 2.1 [19, 26] *The classical & two-parametric Mittag-Leffler functions are,*

$$E_p(z) = \sum_{k=0}^{\infty} \frac{z^k}{\Gamma(kp+1)}, E_{p,q}(z) = \sum_{k=0}^{\infty} \frac{z^k}{\Gamma(kp+q)}, (z, p, q \in C, R(p) > 0),$$

respectively, where $E_{p,1}(z) = E_p(z)$.

Definition 2.2 [2, 26, 38] *The RL fractional integral of order* $q > 0$ *is,* $\left(I_{a^+}^q w\right)(t) = \frac{1}{\Gamma(q)} \int_a^t (t-r)^{q-1} w(r) dr$, *where* $w \in L^1(a, b)$.

Remark 2.3 [26] *For* $0 < q < 1$, $I_{a^+}^q$ *maps* $AC[a, b]$ *into* $AC[a, b]$ *and maps* $C[a, b]$ *into* $C[a, b]$.

Definition 2.4 [8, 10, 18, 26, 32] *Let* $0 < q < 1$. *The AB FD in Caputo sense is,*

$$\left({}^{ABC}\mathcal{D}_{a^+}^q w\right)(t) = \frac{\mathscr{B}(q)}{(1-q)} \int_a^t E_q\left[-\frac{q}{1-q}(t-r)^q\right] w'(r) dr,$$

where $w \in AC[a, b]$.

The AB FD in RL sense is,

$$\left({}^{ABR}\mathcal{D}_{a^+}^q w\right)(t) = \frac{\mathscr{B}(q)}{(1-q)} \frac{d}{dt} \int_a^t E_q\left[-\frac{q}{1-q}(t-r)^q\right] w(r) dr,$$

where $w \in L^1(a, b)$.

The AB fractional integral is,

$$\left({}^{AB}I_{a^+}^q w\right)(t) = \frac{1-q}{\mathscr{B}(q)} w(t) + \frac{q}{\mathscr{B}(q)} \left(I_{a^+}^q w\right)(t),$$

where $w \in L^1(a, b)$. *Now, we consider the normalization function* $\mathscr{B}(q)$ *to be real-valued strictly positive such that* $\mathscr{B}(0) = \mathscr{B}(1) = 1$.

Lemma 2.5 [8, 26] *Let* $0 < q < 1$. *Then*

$$\left({}^{ABC}\mathcal{D}_{a^+}^q w\right)(t) = \left({}^{ABR}\mathcal{D}_{a^+}^q \{\mathscr{F}(Sw(t), Tw(t))\}\right) - \frac{\mathscr{B}(q)}{(1-q)} w(a) E_q\left[-\frac{q}{1-q}(t)^q\right], \quad (2.1)$$

where $w \in AC[a, b]$.

The higher-order AB fractional derivatives and integral defined in [3, 26, 29–37] based on Definition 2.4 are as follow:

Definition 2.6 [3, 26] *Let* $m < q < m + 1 (m \in N_0)$ *and* $p = q - m$ *and* N_0 *is denoting* 0.

The AB FD in caputo sense is,

$$\left({}^{ABC}\mathcal{D}_{a^+}^q w\right)(t) = \left({}^{ABC}\mathcal{D}_{a^+}^q \{\mathscr{F}(t, Sw(t), Tw(t))\}\right),$$

where $w \in AC^{m+1}[a, b]$.

The AB FD in RL sense is,

$$\left({}^{ABR}\mathcal{D}_{a^+}^q w\right)(t) = \left({}^{ABR}\mathcal{D}_{a^+}^q \{\mathscr{F}(t, Sw(t), Tw(t))\}\right),$$

where $w \in L^1(a, b)$.

The AB fractional integral is,

$$\left({}^{AB}I_{a^+}^q w\right)(t) = \left(I_{a^+}^m I_{a^+}^p \{\mathscr{F}(t, Sw(t), Tw(t))\}\right),$$

where $w \in L^1(a, b)$.

Lemma 2.7 [3, 26] *Let* $m < q < m + 1 (m \in N_0)$. *Then*

$$\left({}^{AB}I_{a^+}^q {}^{ABC}\mathcal{D}_{a^+}^q w\right)(t) = \{\mathscr{F}(t, Sw(t), Tw(t))\} - \sum_{k=0}^{m} \frac{w^{(k)}(a)}{k!}(t-k)^k, \quad (2.2)$$

where $w \in AC^{m+1}[a, b]$.

3 Equivalent linear system solutions

This section is devoted to obtaining several important properties and results that will be helpful in our forthcoming discussion. We first define the Laplace transform of higher-order AB operators as follows:

Proposition 3.1. [26] Let $m < q < m + 1 (m \in \mathbb{N}_0)$. Then, in particular $a = 0$, we get

$$\mathcal{L}\{\left({}^{ABC}\mathcal{D}^{q}_{0+}w\right)(t)\}(s) = \frac{\mathscr{B}(q-m)}{m+1-p}\frac{s^{q}\mathcal{L}\{\mathscr{F}(t,Sw(t),Tw(t))\}(s) - \sum_{0\le k\le m} s^{q-k-1}w^{(k)}(0)}{s^{q-m} + \frac{q-m}{m+1-p}},$$

$$\mathcal{L}\{\left({}^{ABR}\mathcal{D}^{q}_{0+}w\right)(t)\}(s) = \frac{\mathscr{B}(q-m)}{m+1-p}\frac{s^{q}\mathcal{L}\{\mathscr{F}(t,Sw(t),Tw(t))\}(s) - \sum_{0\le k\le m-1} s^{q-k-1}w^{(k)}(0)}{s^{q-m} + \frac{q-m}{m+1-p}},$$

$$\mathcal{L}\{\left({}^{AB}I^{q}_{0+}w\right)(t)\}(s) = \frac{1}{\mathscr{B}(q-m)}[(m+1-p)s^{-m} + (q-m)s^{-q}]\,\mathcal{L}\{\mathscr{F}(t,Sw(t),Tw(t))\}(s),$$

provided the Laplace transform of w exists.

Lemma 3.2 [26] Let $m < q < m + 1 (m \in N_0)$. Then, in particular $a = 0$ yields the following result,

$$({}^{ABC}\mathcal{D}^{q}_{a^+}w)(t) = ({}^{ABR}\mathcal{D}^{q}_{a^+}\{\mathscr{F}(t,Sw(t),Tw(t))\}) - \frac{\mathscr{B}(q-m)}{m+1-p}w^{(m)}E_{q-m}\left[-\frac{q-m}{m+1-p}(t)^{q-m}\right],$$

where $w \in AC^{m+1}[a, b]$.

Proposition 3.3 [26] Let $m < q < m + 1 (m \in N_0)$. Then,

$$\left({}^{AB}I^{q}_{a^+}\,{}^{ABC}\mathcal{D}^{q}_{a^+}w\right)(t) = \{\mathscr{F}(t,Sw(t),Tw(t))\} - w(a)E_{q-m}\left[-\frac{q-m}{m+1-p}(t)^{q-m}\right],$$

where $w \in AC[a, b]$.

Proof: From [26] and Definition 2.4, by setting $p = q - m$ and using AB fractional derivative in Caputo sense and AB fractional integral operators, we get

$$\left({}^{AB}I^{q}_{a^+}\,{}^{ABC}\mathcal{D}^{q}_{a^+}w\right)(t) = \left({}^{AB}I^{q}_{a^+}\frac{d^m}{dt^m}\,{}^{ABC}\mathcal{D}^{q}_{a^+}\{\mathscr{F}(t,Sw(t),Tw(t))\}\right) = ({}^{AB}I^{q}_{a^+}\,{}^{ABC}\mathcal{D}^{q}_{a^+}\{\mathscr{F}(t,Sw(t),Tw(t))\}).$$

Hence the final conclusion follows from Eq 2.1 and [[3], Proposition 3.1].

Lemma 3.4 [26] Let $0 < \alpha \le 1$ and $\lambda > 0$. Then, for all $x > 0$, the function $xE_{\alpha,2}(-\lambda x^{\alpha})$ is strictly positive and monotonically increasing with respect to 'x'.

Proof. From [2, 26], we have

$$\int_0^x t^{\beta-1}E_{\alpha,\beta}(-\lambda t^{\alpha})dt = x^{\beta}E_{\alpha,\beta+1}(-\lambda x^{\alpha}), \beta > 0.$$

In particular, by setting $\beta = 1$, the above equation reduces to

$$xE_{\alpha,2}(-\lambda x^{\alpha}) = \in_0^x E_{\alpha}(-\lambda t^{\alpha})dt.$$

From[[39] in Lemma 2.2], $xE_{\alpha,2}(-\lambda x^{\alpha})$, $x > 0$, is strictly positive and monotonically increasing with respect to 'x'.

Remark 3.5 [26] Let, $\lambda = \frac{q-1}{2-q}$, $1 < q < 2$, from Lemma 3.4, for all $x > 0$,

$$xE_{q^{-}1,2}\left[-\frac{q-1}{2-q}x^{q-1}\right] > 0.$$

Lemma 3.6 Let $\mathscr{F} \in AC[0, b]$ with $\mathscr{F}(0) = 0$ and $1 < q < 2$. Then the solution to the linear system

$$\begin{cases} {}^{ABC}\mathcal{D}^{q}_{a^{+}} w(t) = \mathscr{F}(t, Sw(t), Tw(t)), t \in [0, a] \\ w(0) = w_0, {}^{ABC}\mathcal{D}^{q-1}_{a^{+}} w(b) = w_1 \end{cases} \tag{3.1}$$

is

$$\begin{aligned} w(t) = w_0 + \frac{1}{\Delta}\left[w_1 - \int_0^b \mathscr{F}(r, Sw(r), Tw(r))dr\right]t + \frac{2-q}{\mathscr{B}(q-1)}\mathscr{F}(r, Sw(r), Tw(r))dr \\ + \frac{1}{\mathscr{B}(q-1)\Gamma(q-1)}\int_0^t (t-r)^{q-1}\mathscr{F}(r, Sw(r), Tw(r))dr, \text{for all } t \in J, \end{aligned} \tag{3.2}$$

where,

$$\Delta = \frac{\mathscr{B}(q-1)}{2-q} bE_{p-1,2}\left[-\frac{q-1}{2-q}b^{q-1}\right].$$

Proof. Use of Atangana-Baleanu integral operator ${}^{AB}I^{q}_{0+}$ on both sides of the equation in (3.1) with the help of Eq 2.2, results in

$$\begin{aligned} w(t) &= c_1 + c_2 t + {}^{AB}I^{q}_{0+}\mathscr{F}(t, Sw(t), Tw(t)) \\ &= c_1 + c_2 t + \frac{2-q}{\mathscr{B}(q-1)}\int_0^t \mathscr{F}(r, Sw(r), Tw(r))dr \\ &\quad + \frac{1}{\mathscr{B}(q-1)\Gamma(q-1)}\int_0^t (t-r)^{q-1}\mathscr{F}(r, Sw(r), Tw(r))dr, \end{aligned} \tag{3.3}$$

where $c_1, c_2 \in \mathbb{R}$. The condition $w(0) = w_0$ yields $c_1 = w_0$. Moreover, by Definition 2.6, we have

$$w(t) = w_0 + c_2 t + I_{0+}{}^{AB}I^{q-1}_{0+}\mathscr{F}(t, Sw(t)\Phi, Tw(t)).$$

In view of Proposition 3.3, we obtain

$${}^{ABC}\mathcal{D}^{q-1}_{0+} w(t) = c_2\frac{\mathscr{B}(q-1)}{2-q} tE_{p-1,2}\left[-\frac{q-1}{2-q}t^{q-1}\right] + \int_0^t \mathscr{F}(r, Sw(r), Tw(r))dr.$$

By using boundary condition at $t = b$ given in (3.1), it follows that

$$c_2 = \frac{1}{\Delta}\left[w_1 - \int_0^b \mathscr{F}(r, Sw(r), Tw(r))dr\right].$$

Substitution of the above values of c_1 and c_2 into (3.3) leads to the desired solution given in (3.2). This Lemma derive the integral equation for the problem (1.1).

Remark 3.7 [26] From 3.2, one can obtain

$$w'(t) = \frac{1}{\Delta}\left[w_1 - \int_0^b \mathscr{F}(r, Sw(r), Tw(r))dr\right]t + \frac{2-q}{\mathscr{B}(q-1)}\{\mathscr{F}(r, Sw(r), Tw(r))dr\} + \frac{1}{\mathscr{B}(q-1)\Gamma(q-1)}\int_0^t (t-r)^{q-1}\mathscr{F}(r, Sw(r), Tw(r))dr.$$

Therefore, our assumption $\mathscr{F} \in AC(J)$ together with Remark 2.3, that $y \in AC^2(J)$. By Definition 2.6, we can define the AB fractional derivative of the function y in Caputo sense on J. Moreover, it follows from Proposition 3.3 that w satisfies the linear problem (3.1).

For the elementary results of the Eq (1.3), we need some following hypotheses:

(H1) $|\mathscr{F}(r, (Sw(r), Tw(r)))| \leq \varphi_1(t) + \varphi_2(t)|w|$, for all $(t, w) \in \Omega$ and $\mathscr{F} \subseteq \mathscr{R}^3$.

(H2) $|\mathscr{F}(t, w) - \mathscr{F}(t, \tilde{w})| \leq \phi(t)|w - \tilde{w}|$ for a.e. $(t, w), (t, \tilde{w}) \in \Omega$ and $\mathscr{F} \subseteq \mathscr{R}^3$.

(H3) Let $w \in C[0, T]$ & function $\varphi \in (C[0, T] \times \mathscr{R} \times \mathscr{R} \times \mathscr{R}, \mathscr{R})$ is continuous function & a positive constant ζ_1, ζ_2 & ζ s.t., $\|\varphi(J, w_1, w_2, w_3) - \varphi(J, \varphi_1, \varphi_2, \varphi_3)\| \leq \zeta_1(\|w_1 - \varphi_1\| + \|w_2 - \varphi_2\| + \|w_3 - \varphi_3\|) \forall\ w_1, w_2, w_3, \varphi_1, \varphi_2, \varphi_3$ in w. $\zeta_2 = max_{w \in \mathscr{R}}\|f(J, \mathscr{R}, \mathscr{R}, \mathscr{R})\| \& \zeta = max\{\zeta_1, \zeta_2\}$.

4 Existence result

We first convert the FIDE (1.1) to an integral equation and then consider a fixed-points problem for an integral operator. On the basis of Lemma 3.6, and solution operator $\mathscr{G} : C(T) \to C(T)$ as follows:

$$\begin{aligned}(\mathscr{G}w)(t) = w_0 &+ \frac{1}{\Delta}\left[w_1 - \int_0^b \mathscr{F}(r, (Sw(r), Tw(r)))dr\right]t \\ &+ \frac{2-q}{\mathscr{B}(q-1)}\int_0^t \mathscr{F}(r, (Sw(r), Tw(r)))dr \\ &+ \frac{1}{\mathscr{B}(q-1)\Gamma(q-1)}\int_0^t (t-r)^{q-1}\mathscr{F}(r, (Sw(r), Tw(r)))dr, \quad \text{for all } t \in J.\end{aligned} \tag{4.1}$$

We now only need to seek the fixed-points of $\mathscr{G}$ in $\mathcal{C}(T)$, because the fixed-points of $\mathscr{G}$ are solutions of (1.1). For brevity, we use the notations

$$\Lambda = \frac{b}{\Delta} + \frac{2-q}{\mathscr{B}(q-1)} + \frac{b^{q-1}}{\mathscr{B}(q-1)\Gamma(q-1)}$$
$$\tilde{\Lambda} = \frac{b^2}{\Delta} + \frac{b(2-q)}{\mathscr{B}(q-1)} + \frac{b^q}{q\mathscr{B}(q-1)\Gamma(q-1)}.$$

By considering the growth condition on nonlinearity, we now establish the result based on Leray-Schauder alternative theorem [40].

Theorem 4.1 *Let* $\Omega = \{(t, w) \in \mathscr{R}^2 : t \in J$ *and* $|w| \leq \lambda$ *for fixed* $\lambda > 0\}$. *Suppose that* $\mathscr{F} : \Omega \to \mathscr{R}$ *is absolutely continuous and there exist* $\varphi_i \in C(J, [0, \infty))$, $i = 1, 2$ and if

$\mathscr{F}(0, w(0)) = 0$, *then* (1.1) *has a solution in* $C(T)$, *provided*

$$\Lambda \int_0^b \varphi_2(\mathscr{F}(r, (Sw(r), Tw(r))))dr < 1.$$

Proof. *The operator* $\mathscr{G} : C(T) \to C(T)$ *is completely continuous.*

Suppose $\mathfrak{D} \subset C(T)$ *is an arbitrary bounded set. Then, by using (H1), there is a number* $RL > 0$, *such that* $|\mathscr{F}(r, (Sw(r), Tw(r)))| \leq RL$ for $t \in T, w \in \mathfrak{D}$.

Now, $\forall w \in \mathfrak{D}$, *we obtain*

$$\begin{aligned}
|(\mathscr{G}w)(t)| &\leq |w_0| + \frac{1}{\Delta}\left[|w_1| + \int_0^b |\mathscr{F}(r, (Sw(r), Tw(r)))|dr\right]t \\
&\quad + \frac{2-q}{\mathscr{B}(q-1)}\int_0^t |\mathscr{F}(r, (Sw(r), Tw(r)))|dr \\
&\quad + \frac{1}{\mathscr{B}(q-1)\Gamma(q-1)}\int_0^t (t-r)^{q-1}|\mathscr{F}(r, (Sw(r), Tw(r)))|dr \\
&\leq |w_0| + \frac{1}{\Delta}\left[|w_1| + \frac{b}{\Delta} + \frac{2-q}{\mathscr{B}(q-1)} + \frac{b^{q-1}}{\mathscr{B}(q-1)\Gamma(q-1)} + \frac{b^2}{\Delta} + \frac{b(2-q)}{\mathscr{B}(q-1)}\right. \\
&\quad \left. + \frac{b^q}{q^{\mathscr{B}}(q-1)\Gamma(q-1)}|\mathscr{F}(r, (Sw(r), Tw(r)))|dr\right] \\
&\leq |w_0| + \frac{b}{\Delta}|w_1| + RL\tilde{\Lambda} < +\infty,
\end{aligned}$$

$\Rightarrow \mathscr{G}(\mathfrak{D})$ *is bounded.*

Next, we show that $\mathscr{G}(\mathfrak{D})$ *is equicontinuous. For all* $w \in \mathfrak{D}$ *and* $0 \leq \tau_1 < \tau_2 \leq b$, *we have*

$$\begin{aligned}
&|(\mathscr{G}w)(\tau_2) - (\mathscr{G}w)(\tau_1)| \\
&\leq \frac{1}{\Delta}\left[|w_1| + \int_0^b |\mathscr{F}(r, (Sw(r), Tw(r)))dr\right](\tau_2 - \tau_1) \\
&\quad + \frac{2-q}{\mathscr{B}(q-1)}\int_{\tau_1}^{\tau^{\tau_2}} |\mathscr{F}(r, (Sw(r), Tw(r)))|dr \\
&\quad + \frac{1}{\mathscr{B}(q-1)\Gamma(q-1)}\left[\int_0^{\tau_1}\left[(\tau_2 - r)^{q-1} - (\tau_1 - r)^{q-1}\right]|\mathscr{F}(r, (Sw(r), Tw(r)))|dr\right. \\
&\quad \left. + \int_{\tau_1}^{\tau_2}(\tau_2 - r)^{q-1}|\mathscr{F}(r, (Sw(r), Tw(r)))|dr\right] \\
&\leq \left[\frac{|w_1| + bRL}{\Delta} + \frac{2-q}{\mathscr{B}(q-1)}RL\right](\tau_2 - \tau_1) + \frac{RL}{q\mathscr{B}(q-1)\Gamma(q+1)}(\tau_2^q - \tau_1^q).
\end{aligned}$$

Since the function τ^q, $1 < q < 2$, *is uniformly continuous on* J, $\mathscr{G}(\mathfrak{D})$ *is a family of equicontinuous functions. Therefore, following the Arzela-Ascoli theorem,* $\mathscr{G}(\mathfrak{D})$ is relatively compact set in $C(T)$. *Hence, we conclude that* $\mathscr{G}$ *is completely continuous.*

Now, we prove $\mathcal{S} = \{w \in C(T) : w = \lambda\mathscr{G}w \text{ and } \lambda \in (0, 1)\}$ *is a bounded set.*

Let $w \in \mathcal{S}$, then $w(t) = \lambda(\mathcal{G}w)(t)$ for $t \in T$. By (H1), for $t \in T$, one has

$$\begin{aligned}
|w(t)| &= |\lambda(\mathcal{G}, \mathcal{F}(r, (Sw(r), Tw(r)))|\\
&< |w_0| + \frac{1}{\Delta}\left[|w_1| + \int_0^b \left(\varphi_1(\mathcal{F}(r, (Sw(r), Tw(r)))) + \varphi_2(r)|\mathcal{F}(r, (Sw(r), Tw(r)))|\right)dr\right]t\\
&+ \frac{2-q}{\mathcal{B}(q-1)}\int_0^t \left(\varphi_1(r) + \varphi_2(r)|\mathcal{F}(r, (Sw(r), Tw(r)))|\right)dr\\
&+ \frac{1}{\mathcal{B}(q-1)\Gamma(q-1)}\int_0^t (t-r)^{q-1}\left(\varphi_1(r) + \varphi_2(r)|\mathcal{F}(r, (Sw(r), Tw(r)))|\right)dr\\
&\leq |w_0| + \frac{1}{\Delta}\left[|w_1| + \frac{b}{\Delta} + \frac{2-q}{\mathcal{B}(q-1)} + \frac{b^{q-1}}{\mathcal{B}(q-1)\Gamma(q-1)}\int_0^b \varphi_1(r)dr + \frac{b}{\Delta} + \frac{(2-q)}{\mathcal{B}(q-1)}\right.\\
&\left. + \frac{b^q - 1}{\mathcal{B}(q-1)\Gamma(q-1)}\int_0^b \varphi_2(r)|\mathcal{F}(r, (Sw(r), Tw(r)))|dr\right]\\
&\leq |w_0| + \frac{b}{\Delta}|w_1| + \Lambda\int_0^b \varphi_1(\mathcal{F}(r, (Sw(r), Tw(r))))dr\\
&+ \Lambda\int_0^b \varphi_2(\mathcal{F}(r, (Sw(r), Tw(r))))dr\| w \|_\infty.
\end{aligned}$$

Hence, for all $w \in \mathcal{S}$, we have

$$\| w \|_\infty \leq \frac{|w_0| + \frac{b}{\Delta}|w_1| + \Lambda\int_0^b \varphi_1(\mathcal{F}(r, (Sw(r), Tw(r))))dr}{1 - \Lambda\int_0^b \varphi_2(\mathcal{F}(r, (Sw(r), Tw(r))))dr} < +\infty,$$

$\Rightarrow \mathcal{S}$ is bounded. Therefore, the Leray-Schauder alternative theorem ensures us that $\mathcal{G}$ has at least one fixed-point in $C(T)$, as required. Hence the theorem follows. By considering the generalized Lipschitz condition on nonlinearity.

5 Uniqueness result

Theorem 5.1 *Let $\Omega = \{(t, w) \in \mathcal{R}^2 : t \in J$ and $|w| \leq \lambda$ for fixed $\lambda > 0\}$. Suppose that $\mathcal{F} : \Omega \to \mathcal{R}$ is absolutely continuous and there exist $\phi \in L^1(J, [0, \infty))$. If $\mathcal{F}(0, w(0)) = 0$, then (1.1) has a unique solution in $C(T)$, provided*

$$\Lambda\int_0^b \phi(\mathcal{F}(r, Sw(r), Tw(r)))dr < 1. \tag{5.1}$$

Proof. *The operator $\mathcal{G} : C(T) \to C(T)$ is defined in (4.1). Let us first denote $M = \sup_{t\in J}|\mathcal{F}(t, 0)| < \infty$ and fix a real number ρ, $0 < \rho \leq \lambda$, s.t.,*

$$\frac{|w_0| + \frac{b}{\Delta}|w_1| + M\tilde{\Lambda}}{1 - \Lambda\int_0^b \phi(\mathcal{F}(r, Sw(r), Tw(r)))dr} \leq \rho.$$

We now show that $\mathscr{G}\mathfrak{B}_\rho \subset \mathfrak{B}_\rho$, *where* $\mathfrak{B}_\rho = \{w \in C(T) : \|w\|_\infty \leq \rho\}$. *By (H2), for all* $w \in \mathfrak{B}_r$, *one has*

$$\begin{aligned}
|(\mathscr{G}w)(t)| &\leq |w_0| + \frac{1}{\Delta}\left[|w_1| + \int_0^b (\phi(\mathscr{F}(r, Sw(r), Tw(r)))|\mathscr{F}(r, Sw(r), Tw(r))| + M)dr\right]t \\
&+ \frac{2-q}{\mathscr{B}(q-1)}\int_0^t (\phi(\mathscr{F}(r, Sw(r), Tw(r)))|\mathscr{F}(r, Sw(r), Tw(r))| + M)dr \\
&+ \frac{1}{\mathscr{B}(q-1)\Gamma(q-1)}\int_0^t (t-r)^{q-1}(\phi(\mathscr{F}(r, Sw(r), Tw(r)))|\mathscr{F}(r, Sw(r), Tw(r))| + M)dr \\
&\leq |w_0| + \frac{1}{\Delta}\left[|w_1| + \rho\int_0^b \phi(\mathscr{F}(r, Sw(r), Tw(r)))dr + Mb\right]b \\
&+ \frac{2-q}{\mathscr{B}(q-1)}\left[\rho\int_0^b \phi(\mathscr{F}(r, Sw(r), Tw(r)))dr + Mb\right] \\
&+ \frac{1}{q\mathscr{B}(q-1)\Gamma(q-1)}b^{q-1}\left[q\rho\int_0^b \phi(\mathscr{F}(r, Sw(r), Tw(r)))dr + Mb\right] \quad \text{for all } t \in J.
\end{aligned}$$

Therefore, for all $w \in \mathfrak{B}_\rho$, *we deduce that*

$$\begin{aligned}
\| \mathscr{G}w \|_\infty &\leq |w_0| + \frac{b}{\Delta}|w_1| + M\tilde{\Lambda} + \Lambda\rho\int_0^b \phi(\mathscr{F}(r, Sw(r), Tw(r)))dr \\
&\leq \rho
\end{aligned}$$

$\Rightarrow \mathscr{G}$ maps $\mathfrak{B}_\rho$.

Next, we prove that $\mathscr{G}$ *is a operator in* $C(T)$. *Let* $w, \tilde{w} \in C(T)$. *By (H2), for each* $t \in T$, *one has*

$$\begin{aligned}
&|(\mathscr{G}w)(t) - (\mathscr{G}\tilde{w})(t)| \\
&\leq \frac{t}{\Delta}\int_0^b \phi(\mathscr{F}(r, Sw(r), Tw(r)))|w(r) - \tilde{w}(r)|dr \\
&+ \frac{2-q}{\mathscr{B}(q-1)}\int_0^t \phi(\mathscr{F}(r, Sw(r), Tw(r)))|w(r) - \tilde{w}(r)|dr \\
&+ \frac{1}{\mathscr{B}(q-1)\Gamma(q-1)}\int_0^t (t-r)^{q-1}\phi(\mathscr{F}(r, Sw(r), Tw(r)))|w(r) - \tilde{w}(r)|dr \\
&\leq \Lambda\int_0^b \phi(\mathscr{F}(r, Sw(r), Tw(r)))dr\| \ w - \tilde{w} \ \|_\infty.
\end{aligned}$$

Hence, for all $w, \tilde{w} \in C(T)$ *we deduce that*

$$\| \mathscr{G}w - \mathscr{G}\tilde{w}\|_\infty \leq \Lambda\int_0^b \phi(\mathscr{F}(r, Sw(r), Tw(r)))dr\| \ w - \tilde{w} \ \|_\infty.$$

The assumption (5.1) *ensures that* $\mathscr{G}$ *is contractive. Hence the Banach fixed point theorem allows us to conclude that* $\mathscr{G}$ *has a unique fixed-point in* $C(T)$, *as required. This fixed-point is the aspired solution to* (1.1).

6 Numerical result

This section is devoted to describe a numerical scheme based on the classical and fractional trapezoidal methods, which are used to interpolate the vector field $\mathscr{F}$ by the first-degree polynomials [26, 41].

The fractional trapezoidal method is a numerical technique used for approximating the definite integral of a function. It is a modification of the traditional trapezoidal rule, which divides the area under a curve into trapezoids and sums their areas to estimate the integral [42–46]. It is particularly useful when dealing with functions that may have singularities or other complexities and also can provide more accurate results compared to the traditional trapezoidal rule, especially when dealing with functions that have rapidly changing behavior or singularities. It's a simple numerical integration method that can be computationally efficient for many problems but may require more intervals to achieve high accuracy [47–49].

Now, we can directly discretize the integral equation of (1.3) to derive the numerical scheme.

Let h be the step size, and choose $n+1$ equi-spaced grid points $\mathscr{F}_{tk} = kh : k = 0, 1, 2, ..., n$ on $[0, b]$ such that $0 = t_0 < t_1 < t_2 < \ldots < t_n = b$ with some positive integers n and $h := \frac{b}{n}$.

We first rewrite the integral equation of (1.3) at any point $t = t_k$ in the following piecewise way,

$$\begin{aligned} w(t_k) = w_0 + \frac{1}{\Delta}\left[w_1 - \sum_{0\le\tau\le n-1}\int_{t_\tau}^{t_\tau+1} \mathscr{F}(r,(Sw(r),Tw(r)))dr\right]t_k \\ + \frac{2-q}{\mathscr{B}(q-1)}\sum_{0\le\tau\le k-1}\int_{t_\tau}^{t_\tau+1} \mathscr{F}(r,(Sw(r),Tw(r)))dr \\ + \frac{1}{\mathscr{B}(q-1)\Gamma(q-1)}\sum_{0\le\tau\le k-1}\int_{t_\tau}^{t_\tau+1} (t_k-r)^{q-1}\mathscr{F}(r,(Sw(r),Tw(r)))dr. \end{aligned}$$

In order to formulate the numerical scheme for (1.3), the nonlinear function $\mathscr{F}(t, w(t))$ is approximated, on each subinterval $[t_\tau, t_\tau + 1]$, by the following piecewise linear function,

$$\begin{aligned} \mathscr{F}(t,w(t)) = \frac{1}{h}[(t_{\tau+1}-t)\mathscr{F}(t_\tau,(Sw(t_\tau),Tw(t_\tau))) \\ + (t-t_\tau)\mathscr{F}(t_{\tau+1}),(Sw(t_\tau+1),Tw(t_\tau+1))], \qquad t\in[t_\tau,t_\tau+1]. \end{aligned}$$

After integrating, one obtains the following unknown approximations

$$\begin{aligned} & w(t_k) = w_0 \\ & + \frac{1}{\Delta}\left[w_1 - \frac{h}{2}\sum_{0\le\tau\le k-1}[\mathscr{F}(t_\tau,(Sw(t_\tau),Tw(t_\tau))) + \mathscr{F}(t_{\tau+1}),(Sw(t_\tau+1),Tw(t_\tau+1))]\right]t_k \\ & + \frac{2-q}{\mathscr{B}(q-1)}\frac{h}{2}\sum_{0\le\tau\le k-1}\left[\mathscr{F}(t_\tau,(Sw(t_\tau),Tw(t_\tau))) + \mathscr{F}(t_{\tau+1}),(Sw(t_\tau+1),Tw(t_\tau+1))\right] \\ & + \frac{(q-1)}{\mathscr{B}(q-1)}\frac{h^q}{\Gamma(q+2)}[\{(k-1)^{q+1} - k^q(k-p-1)\}\mathscr{F}(t_0,(Sw(t_0),Tw(t_0))) \\ & + \sum_{1\le\tau\le k-1}\{(k-\tau+1)^{q+1} + (k-\tau-1)^{q+1} - 2(k-\tau)^{q+1}\}\mathscr{F}(t_\tau,(Sw(t_\tau),Tw(t_\tau))) \\ & + \mathscr{F}(t_k,(Sw(t_k),Tw(t_k)))]. \end{aligned} \tag{6.1}$$

Due to the nonlinear nature of the function $\mathscr{F}$ and the presence of all unknown quantities $w(t_k)$ on the RHS of each equation of (6.1), we cannot solve (6.1) for $w(t_k)$ directly, in general.

Then, the Newton-Raphson method is a numerical technique for finding approximate solutions to equations of the form $f(x) = 0$. It is a powerful iterative method commonly used for root finding and optimization problems.

The method starts with an initial guess and then refines that guess in each iteration until it converges to a root of the equation. It's important to note that the Newton-Raphson method may not always converge to a solution, and it can even diverge if certain conditions are not met.

Therefore, it's essential to choose a suitable initial guess and be aware of the characteristics of the function being analyzed. So Newton-Raphson method is used to determine each $w(t_k)$; $k = 0, 1, 2, \ldots, n$ from the above implicit numerical scheme (6.1). This implicit method is seldomly encountered in the numerical simulation for solving fractional differential equations. However, this method is useful in dealing with the problem (1.3).

7 Example

Our theoretical results are illustrated here with the example.

Let the normalization function as $\mathscr{B}(\alpha) = 1 - \alpha + \frac{\alpha}{\Gamma(\alpha)}, \alpha \in [0, 1]$. We also present the trajectory of the numerical solution to the nonlinear problem (1.1) by using the proposed numerical scheme (6.1).

$$\begin{cases} {}^{ABC}\mathcal{D}^{q}_{a^+} w(t) = \mathscr{F}(r, (Sw(r), Tw(r))), t \in [0, b] \\ w(0) = w_0, {}^{ABC}\mathcal{D}^{q-1}_{a^+} w(b) = w_1 \end{cases} \tag{7.1}$$

Now, Consider the linear problem

$$\begin{cases} {}^{ABC}\mathcal{D}^{q}_{a^+} w(t) = h^{\lambda}, t \in [0, b] \\ w(0) = w_0, {}^{ABC}\mathcal{D}^{q-1}_{a^+} w(b) = w_1 \end{cases} \tag{7.2}$$

where $\lambda > 0$ is a real number. Its exact solution is,

$$w(t) = w_0 + \frac{1}{\Delta}\left[w_1 - \frac{b^{\lambda+1}}{\lambda+1}\right]t + \frac{2-q}{\mathscr{B}(q-1)}\frac{t^{\lambda+1}}{\lambda+1} + \frac{q-1}{\mathscr{B}(q-1)}\frac{\Gamma(\lambda+1)}{\Gamma(q+\lambda+1)}t^{q+\lambda}$$

Now we consider $t = 1$, $\alpha = 0.5$, $\Delta = 2$, comparison of the exact and numerical solutions to Eq (6.1) for $q = 1.5$, $\lambda = 1.5$, $b = 2$, $w_0 = 1$, $w_1 = 17$ and $h = 0.05$.

$$\begin{aligned} w(t) = w(1) &= w_0 + \frac{1}{\Delta}\left[17 - \frac{2^{1.5+1}}{1.5+1}\right]1 + \frac{2-1.5}{\mathscr{B}(1.5-1)}\frac{1^{1.5+1}}{1.5+1} \\ &\quad + \frac{1.5-1}{\mathscr{B}(1.5-1)}\frac{\Gamma(1.5+1)}{\Gamma(1.5+1.5+1)}1^{1.5+1.5} \\ &= 1 + \frac{1}{\Delta}[12.2288] + 0.2557 + 5.0991 \\ &= 12.4692. \end{aligned}$$

Hence, $t = 1$; $w(t) = 12.4692$.

The numerical solution for $t = 1$ has been derived above. The derivation of numerical solutions $w(t)$ for t ranging from 0 to 2 is similar and the values are presented in Table 1 below:

Table 1. The approximation values of w(t).

Numerical Values					
t	0	0.5	1	1.5	2
w(t)	1.0000	4.7398	12.4692	28.0858	55.4683

https://doi.org/10.1371/journal.pone.0301338.t001

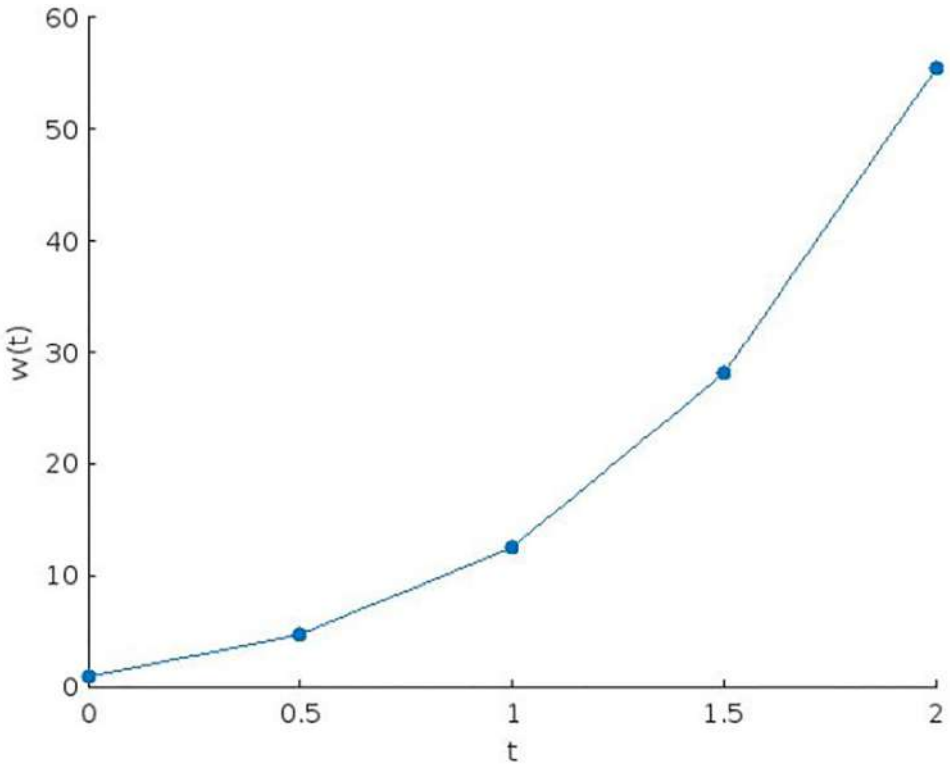

Fig 1. Graph of the approximate solution w(t).

https://doi.org/10.1371/journal.pone.0301338.g001

The obtained results are demonstrated as a graph in Fig 1. The numerical solution shows agreement with the solution in the entire interval.

8 Conclusion

In this paper, the essential outcomes of the existence and uniqueness solutions are gained by using the Leray-Schauder alternative theorem and Banach fixed point theorem respectively. We also discussed a numerical scheme for (1.1), which helps to study the numerical solution when $\mathscr{F}$ is nonlinear. Our theoretical and numerical findings were verified with examples. We have presented some important properties of higher-order AB operators. However, the stability analysis of the solution may be considered as an extension work for the problem (1.1).

Acknowledgments

The authors extend their appreciation to the Deputy ship for Research & Innovation, Ministry of Education in Saudi Arabia for funding this research work through the project number (*IF2/PSAU*/2022/01/22564).

Author Contributions

Conceptualization: Samy A. Harisa, Nashat Faried, V. Vijayaraj, C. Ravichandran, Ahmed Morsy.

Data curation: V. Vijayaraj, C. Ravichandran, Ahmed Morsy.

Formal analysis: Samy A. Harisa, Nashat Faried, V. Vijayaraj, C. Ravichandran, Ahmed Morsy.

Investigation: Samy A. Harisa, Nashat Faried, V. Vijayaraj, C. Ravichandran, Ahmed Morsy.

Methodology: Samy A. Harisa, Nashat Faried, V. Vijayaraj, C. Ravichandran, Ahmed Morsy.

Supervision: Nashat Faried.

Writing – original draft: Samy A. Harisa, Nashat Faried, V. Vijayaraj, C. Ravichandran, Ahmed Morsy.

Writing – review & editing: Samy A. Harisa, Nashat Faried, V. Vijayaraj, C. Ravichandran, Ahmed Morsy.

References

1. Miller KS, Ross B. An Introduction to the Fractional Calculus and Fractional Differential Equations, John Wiley and Sons, New York. 1993.
2. Podlubny I. Fractional Differential Equations, Academic Press, San Diego. (1999).
3. Abdeljawad T. A Lyapunov type inequality for fractional operators with nonsingular Mittag-Leffler kernel. Journal of Inequalities and Applications. 2017; 130: 1–11. https://doi.org/10.1186/s13660-017-1400-5 PMID: 28680233
4. Kamalesh K, Pramod CP, Pratibhamoy D, Higinio R. A graded mesh refinement approach for boundary layer originated singularly perturbed time-delayed parabolic convection diffusion problems. Mathematical Methods in the Applied Sciences. 2021; 44(21): 12332–12350.
5. Kamal S, Arfan M, Ullah A, Qasem AM, Khursheed JA. T. Abdeljawad, Computational study on the dynamics of fractional order differential equations with applications. Chaos, Solitons & Fractals. 2022; 157: 111955. https://doi.org/10.1016/j.chaos.2022.111955
6. Pallavi B, Anoop K, Abdeljawad T, Aziz K. Study of Hilfer fractional evolution equations by the properties of controllability and stability. Alexandria Engineering Journal. 2021; 60(4): 3741–3749. https://doi.org/10.1016/j.aej.2021.02.014
7. Pallavi B, Anoop K, Abdeljawad T, Khan Zareen A., Aziz K. Existence and approximate controllability of Hilfer fractional evolution equations with almost sectorial operators. Advances in Difference Equations. 2020; (2020): 615. https://doi.org/10.1186/s13662-020-03074-1
8. Atangana A, Baleanu D. New fractional derivatives with nonlocal and non-singular kernel: Theory and application to heat transfer model. Thermal Science. 2016; 20(2): 763–769. https://doi.org/10.2298/TSCI160111018A
9. Al Nuwairan M, Gamal Ibrahim A. Nonlocal impulsive differential equations and inclusions involving Atangana-Baleanu fractional derivative in infinite dimensional spaces. AIMS Mathematics. 2023; 8(5): 11752–11780. https://www.aimspress.com/article/doi/10.3934/math.2023595
10. Fernandez A, Joel ER, Suragan D. Linear differential equations with variable coefficients and Mittag-Leffler kernels. Alexandria Engineering Journal. 2021; 61(2). https://doi.org/10.1016/j.aej.2021.10.028
11. Hussain Alharthi N, Atangana A, Alkahtani Badr S. Study of a cauchy problem of fractional order derivative with variable order fractal dimension. Results in Physics. 2023; 49: 106524. https://doi.org/10.1016/j.rinp.2023.106524
12. Sombir D, Anoop K, Aziz K, Abdeljawad T, Alqudah Manar A. Existence Results of Langevin Equations with Caputo-Hadamard Fractional Operator. Journal of Mathematics. 2023; 2023: 12. https://doi.org/10.1155/2023/2288477
13. Atangana A, Igret Araz S. Step forward on nonlinear differential equations with the Atangana-Baleanu derivative: Inequalities, existence, uniqueness and method. Chaos, Solitons & Fractals. 2023; 173: 113700. https://doi.org/10.1016/j.chaos.2023.113700
14. Atangana A, Seda IA. Analysis of a new partial integro-differential equation with mixed fractional operators. Chaos, Solitons & Fractals. 2019; 127: 257–271. https://doi.org/10.1016/j.chaos.2019.06.005
15. Jarad F, Abdeljawad T, Hammouch Z. On a class of ordinary differential equations in the frame of Atangana-Baleanu fractional derivative. Chaos, Solitons & Fractals. 2018; 117: 16–20. https://doi.org/10.1016/j.chaos.2018.10.006

16. Karthikeyan K, Trujillo JJ. Existence and uniqueness results for fractional integro-differential equations with boundary value conditions. Communications in Nonlinear Science and Numerical Simulation. 2012; 17(11): 4037–4043. https://doi.org/10.1016/j.cnsns.2011.11.036

17. Atangana A, Mishra J. Analysis of nonlinear ordinary differential equations with the generalized Mittag-Leffler kernel. Mathematical Biosciences & Engineering. 2023; 20(11): 19763–19780. https://www.aimspress.com/article/doi/10.3934/mbe.2023875 PMID: 38052623

18. Baleanu D, Fernandez A. On some new properties of fractional derivatives with Mittag-Leffler kernel. Communications in Nonlinear Science and Numerical Simulation. 2018; 59: 444–462. https://doi.org/10.1016/j.cnsns.2017.12.003

19. Gorenflo R, Kilbas AA, Mainardi F, Rogosin SV. Mittag-Leffler Functions, Related Topics and Applications. Vol. 2. Berlin: Springer. 2014.

20. Alb Lupas A, Catas A. Applications of the Atangana-Baleanu Fractional Integral Operator. Symmetry. 2022; 14(3): 630. https://doi.org/10.3390/sym14030630

21. Srivastava HM, Nain AK, Vats RK, Pratibhamoy D. A theoretical study of the fractional-order p-Laplacian nonlinear Hadamard type turbulent flow models having the Ulam-Hyers stability. Revista de la Real Academia de Ciencias Exactas, Fisicas y Naturales. Serie A. Matematicas. Springer, 2023; 117:160. https://link.springer.com/article/10.1007/s13398-023-01488-6

22. Agarwal RP, Zhou Y, He Y. Existence of fractional neutral functional differential equations. Computer and Mathematics with Application. 2010; 59(3): 1095–1100. https://doi.org/10.1016/j.camwa.2009.05.010

23. Kirti K, Anoop K, Aziz K, Abdeljawad T. Existence of solutions by fixed point theorem of general delay fractional differential equation with p-Laplacian operator. AIMS Mathematics. 2023; 8(5): 10160–10176. https://www.aimspress.com/article/doi/10.3934/math.2023514

24. Ravichandran C, Logeswari K, Jarad F. New results on existence in the framework of Atangana-Baleanu derivative for fractional integro-differential equations. Chaos, Solitons & Fractals. 2019; 125: 194–200. https://doi.org/10.1016/j.chaos.2019.05.014

25. Abdeljawad T, Sabri TMT, Kedim I, Iadh AM, Aziz K. A higher-order extension of Atangana-Baleanu fractional operators with respect to another function and a Gronwall-type inequality. Boundary Value Problems. 2023; 2023: 49. https://doi.org/10.1186/s13661-023-01736-z

26. Kumar SK, Sukavanam N, Pan S. Existence and uniqueness of solutions to fractional differential equations with fractional boundary conditions. Alexandria Engineering Journal. 2023; 72(1): 147–155. https://doi.org/10.1016/j.aej.2023.03.076

27. Pratibhamoy D, Subrata R, Higinio R. Homotopy perturbation method for solving Caputo-type fractional-order Volterra-Fredholm integro-differential equations. Computational and Mathematical Methods. 2019; 1(5): e1047. https://doi.org/10.1002/cmm4.1047

28. Sudarshan S, Jugal M, Pratibhamoy D, Debajyoti C. Higher order approximations for fractional order integro-parabolic partial differential equations on an adaptive mesh with error analysis. Computers & Mathematics with Applications. 2023; 150: 87–101. https://doi.org/10.1016/j.camwa.2023.09.008

29. Pratibhamoy D, Subrata R, Higinio R. A Perturbation Based Approach for Solving Fractional Order Volterra-Fredholm Integro Differential Equations and its Convergence Analysis. International Journal of Computer Mathematics. 2019; 97(10): 1–18. https://doi.org/10.1080/00207160.2019.1673892

30. Pratibhamoy D, Subrata R. Theoretical prospects of fractional order weakly singular Volterra Integro differential equations and their approximations with convergence analysis. Mathematical Methods in the Applied Sciences. 2021; 44: 9419–9440. https://doi.org/10.1002/mma.7369

31. Pratibhamoy D, Subrata R, Higinio R. On the approximate solutions of a class of fractional order nonlinear Volterra integro-differential initial value problems and boundary value problems of first kind and their convergence analysis. Journal of Computational and Applied Mathematics. 2022; 404: 113116. https://doi.org/10.1016/j.cam.2020.113116

32. Pratibhamoy D, Subrata R, Jesus VA. Higher order accurate approximations on equidistributed meshes for boundary layer originated mixed type reaction diffusion systems with multiple scale nature. Applied Numerical Mathematics. 2020; 148: 79–97. https://doi.org/10.1016/j.apnum.2019.08.028

33. Pratibhamoy D. A higher order difference method for singularly perturbed parabolic partial differential equations. Journal of Difference Equations and Applications. 2018; 24(3): 452–477. https://doi.org/10.1080/10236198.2017.1420792

34. Pratibhamoy D. Comparison of a priori and a posteriori meshes for singularly perturbed nonlinear parameterized problems. Journal of Computational and Applied Mathematics. 2015; 290: 16–25. https://doi.org/10.1016/j.cam.2015.04.034

35. Sumit S, Pratibhamoy D, Sunil K. Computatioal cost reduction for coupled system of multiple scale reaction diffusion problems with mixed type boundary conditions having boundary layers. Revista de la Real

Academia de Ciencias Exactas, Físicas y Naturales. Serie A. Matematicas. 2023; 117: article number 66. https://doi.org/s13398-023-01397-8

36. Ram S, Vembu S, Pratibhamoy D. A higher order hybrid-numerical approximation for a class of singularly perturbed two-dimensional convection-diffusion elliptic problem with non-smooth convection and source terms. Computers & Mathematics with Applications. 2023; 142: 9–30. https://doi.org/10.1016/j.camwa.2023.04.004

37. Renu C, Satpal S, Pratibhamoy D, Devendra K. A higher order stable numerical approximation for time-fractional non-linear Kuramoto-Sivashinsky equation based on quintic B-spline. Mathematical Methods in the Applied Sciences. 2024;1–23. https://doi.org/10.1002/mma.9778

38. Kilbas AA, Srivastava HM, Trujillo JJ. Theory and Applications of Fractional Differential Equations, North-Holland Mathematics Studies. Vol. 204. Elsevier Science B. V., Amsterdam, 2006.

39. Wei Z, Li Q, Che J. Initial value problems for fractional differential equations involving Riemann-Liouville sequential fractional derivative. Journal of Mathematical Analysis and Applications. 2010; 367(1): 260–272. https://doi.org/10.1016/j.jmaa.2010.01.023

40. Granas A, Dugundji J. Fixed Point Theory. Vol. 14. New York: Springer. 2003.

41. Rohul A, Shah K, Asif M, Khan I, Ullah F. An efficient algorithm for numerical solution of fractional integro-differential equations via Haar wavelet. Journal of Computational and Applied Mathematics. 2021; 381: 113028. https://doi.org/10.1016/j.cam.2020.113028

42. Deepti S, Jugal M, Pratibhamoy D, Jesus VA. A moving mesh refinement based optimal accurate uniformly convergent computational method for a parabolic system of boundary layer originated reaction-diffusion problems with arbitrary small diffusion terms. Journal of Computational and Applied Mathematics. 2022; 404: 113167. https://doi.org/10.1016/j.cam.2020.113167

43. Pratibhamoy D. An a posteriori based convergence analysis for a nonlinear singularly perturbed system of delay differential equation equations on an adaptive mesh. Numerical Algorithms. 2019; 81(1): 465–487. https://doi.org/10.1007/s11075-018-0557-4

44. Pratibhamoy D, Srinivasan N. Numerical solution of a system of singularly perturbed convection-diffusion boundary-value problems using mesh equidistribution technique. The Australian Journal of Mathematical Analysis and Applications. 2013; 10(1): 1–17.

45. Seda IA. Numerical analysis of a new volterra integro-differential equation involving fractal-fractional operators. Chaos, Solitons & Fractals. 2020; 130: 109396. https://doi.org/10.1016/j.chaos.2019.109396

46. Sumit S, Pratibhamoy D, Sunil K, Parameter uniform higher order numerical treatment for singularly perturbed Robin type parabolic reaction diffusion multiple scale problems with large delay in time. Applied Numerical Mathematics. 2024; 196: 1–21. https://doi.org/10.1016/j.apnum.2023.10.003

47. Li C, Zeng F. Numerical Methods for Fractional Calculus. Vol. 24. CRC Press. 2015.

48. Garrappa R. Numerical solution of fractional differential equations: A survey and a software tutorial. Mathematics. 2018; 6(2): 16. https://doi.org/10.3390/math6020016

49. Diethelm K. Fundamental approaches for the numerical handling of fractional operators and time-fractional differential equations. In: Karniadakis, G.E. (ed.) Handbook of Fractional Calculus with Applications: Numerical Methods, vol. 3. De Gruyter, Berlin. 2019. https://doi.org/10.1515/9783110571684-001

Mathematical Methods in the Applied Sciences / Volume 47, Issue 4 / p. 2311-2323

RESEARCH ARTICLE

Results on Ulam-type stability of linear differential equation with integral transform

Arunachalam Selvam, Sriramulu Sabarinathan, Kottakkaran Sooppy Nisar ✉, Chokkalingam Ravichandran, Beri Venkatachalapathy Senthil Kumar

First published: 03 November 2023
https://doi.org/10.1002/mma.9748
Citations: 1

Abstract

The main theme of this study is to implement the Sumudu integral transform technique to solve the stability problem of linear differential equations. Another important aspect of this paper is to investigate the Ulam–Hyers and Ulam–Hyers–JRassias stability of linear differential equations by using Sumudu transform method. Further, the results are extended to the Mittag-Leffler–Ulam–Hyers and Mittag-Leffler–Ulam–Hyers–JRassias stability of these differential equations. As an application point of view, the Sumudu transform is used to find Ulam stabilities of differential equations arising in field-controlled DC servo motor with position control.

CONFLICT OF INTEREST STATEMENT

The authors declare that they have no competing interests.

REFERENCES

1 S. M. Ulam, *Problems in modern mathematics*, John Wiley & Sons, New York, 1964.

Google Scholar

ScienceDirect

Results in Control and Optimization

Volume 14, March 2024, 100376

Investigation on continuous dependence and regularity solutions of functional integrodifferential equations

K. Munusamy [a], C. Ravichandran [b], Kottakkaran Sooppy Nisar [c d], Shankar Rao Munjam [d]

Show more

https://doi.org/10.1016/j.rico.2024.100376

Get rights and content

Abstract

In this work, to show the existence and continuous dependence of integral solution for neutral integro-differential equation with finite delay situation. This result established by using integrated resolvent operator with support of Lipschitz continuous and uniqueness part using Banach contraction mapping. Also study the existence of strict solution on reflexive and general Banach spaces. In the last section, an example is provided related to this theory.

Previous Next

MSC

34B10; 35B65; 37L05; 45K05; 47H10; 47N20

Keywords

Neutral integro-differential equations; Integrated resolvent operator; Integral solution; Strict solution; Continuous dependence

1. Introduction

Neutral differential equations have been studied by many authors using delay situations and have been used to model various real-world applications in different fields such as population dynamical systems, electronics, circuits, chemical kinetics, biological sciences and others. The following system used

continuously to describing the heat conduction materials in [1], [2].

$$\begin{cases} \frac{\partial}{\partial t}\left[y(t_1,x)+\int_{-\infty}^{t_1} g_1(t_1-\xi)\,y(\xi,x)\,d\xi\right]=d\Delta y(t_1)+\int_{-\infty}^{t_1} g_2(t_1-\xi)\,\Delta y(\xi,x) \\ +f(t_1,y(\cdot,x)),t_1\geq 0, \\ y(t_1,x)=0, \quad \text{for} x\in\partial\Omega. \end{cases}$$

where $\Omega\subset\mathbb{R}^n$ is open, $(t_1,x)\in[0,\infty)\times\Omega$ and $y(t_1,x)$ denotes the heat in x at any time t_1. Let $d>0, g_i:\mathbb{R}\to\mathbb{R}$ are internal force and the heat flux relaxation. In many references, such as [3], [4], [5], [6], [7], [8], [9], [10], [11], [12], [13], [14], [15], [16], authors have established neutral differential equations and the existence of solutions using the resolvent operator technique. In many phenomena, the authors studied the Neutral differential equations with nonlocal conditions which are more accuracy in the solutions and uniqueness than the classical one in handing physical problem. In [4], [12], [14], [17], [18], [19], [20], [21], [22], [23] authors studied their integrodifferential equation using nonlocal conditions and obtained effective result with support of resolvent operator theory and semigroup theory. Omar Abu Arqub et al. in [24], [25], [26], [27] established their results in various type of integrodifferential equations and proved the numerical simulations employing Legendre-shifted spectral approach for Caputo–Fabrizio fractional stochastic integrodifferential equations. In [28] the author proved about the mild solution, strong solution and classical solutions using semigroup theory of evolution system also explained the uniqueness of solution. The semigroup and resolvent operator theory are important methods to find the solutions of integrodifferential equations in Banach space X. In the current year, many differential systems are reformed as integral equations and proved the solutions obtained via appropriate fixed point theorems, which is the common technique to proving the existence solutions of the integral equations. Recently in [29], [30], [31] the author established the application of multiobjective programming models, Optimality and duality for E-differentiable multiobjective programming problems and E-differentiable E-Univex Programming model. In particular, Park et al. [15] derived an impulsive neutral integrodifferential delay system to analyze its existence behavior. Kucche and Dhakne [7] provided results for an infinite delay differential system. In [32], [33], the existence of a solution for integrodifferential equations with finite delay in the support of the resolvent operator was proven, and the authors used the integrated resolvent operator in [33]. Many authors discussed about the solution of integrodifferential equation with their different techniques in delay system see in [5], [11], [34], [35], [36].

Recently published an article, [33] the author established the following system with finite delay

$$\begin{cases} \mathscr{Z}'(t)=A\mathscr{Z}(t)+\int_0^t B(t-\xi)\,\mathscr{Z}(\xi)\,d\xi+F(t,\mathscr{Z}_t),t\geq 0, \\ \mathscr{Z}_0=\vartheta\in\mathscr{C}=C([-r,0];X). \end{cases}$$

In this problem authors proved the existence of integral solution using strict contraction mapping and proved regularity of solutions using integrated resolvent operator technique. Also proved the continuous dependence of solution about initial data. Here assumed A is not necessarily dense and satisfied the Hille–Yosida condition on the space X. Motivated by this above article, we established this theory with the neutral integrodifferential problem with and finite delay. This theory contains the existence and regularity of solution using the assumptions of Lipschitz continuous which proved the existence and uniqueness part using Banach fixed point theory and verified its differentiability using integrated resolvent operator technique.

Regarding this, we study the following problem,

$$\begin{cases} \frac{d}{dt}\left[\omega(t) - q\left(t, \omega_t, \int_0^t h(t,s,\omega_s)\,ds\right)\right] = \mathscr{D}\omega(t) + \int_0^t \mathscr{H}(t-s)\,\omega(s)\,ds \\ \qquad\qquad +\varphi\left(t, \omega_t, \int_0^t h(t,s,\omega_s)\,ds\right) \qquad \text{for } t \in [0,a] = I, \\ \omega(0) = \phi \in C([-r,0];\mathscr{E}) = \mathscr{C}. \end{cases} \tag{1}$$

In this article, $\mathscr{E}$ denote the Banach space(BS) and $\mathscr{D}$ be the closed linear operator on $\mathscr{E}$ and its domain $\overline{D(\mathscr{D})} \neq \mathscr{E}$ and is satisfied the Hille–Yosida theorem. The set of operators $\mathscr{H}(t)$ is bounded in $\mathscr{E}$ and $D(\mathscr{D}) \subset D(\mathscr{H}(t))$ from $D(\mathscr{D}) = Y$ into $\mathscr{E}$. The functions $q : I \times \mathscr{C} \times \mathscr{E} \to \mathscr{E}$, $h : I \times I \times \mathscr{C} \to \mathscr{E}$ and $\varphi : I \times \mathscr{C} \times \mathscr{E} \to \mathscr{E}$ are continuous specified later. Let $\mathscr{C}$ is set of functions on $[-r,0]$ in $\mathscr{E}$ are continuous and ϕ is continuous functions defined on $\mathscr{C}$.

For ω belongs to the continuous function $C([-r,\infty);\mathscr{E})$, $t \geq 0$, the history function $\omega_t \in \mathscr{C}$ as $\omega_t(\tau) = \omega(t+\tau)$ for $\tau \in [-r,0]$. The study of above problem contains the existence of solution and existence of strict solution such as the solution function is continuously differentiable in the given domain and satisfies the given equation. The general form of (1) as an abstract formation of large number of partial integro differential equation such as electronic circuit, economic, biological, medical domain and more. In this article used Banach theorem for proving the solution to Eq. (1). Existence and uniqueness of abstract form Eq. (1) have been established in distinct articles and different approaches especially used by resolvent operator technique. Several authors [6], [8], [19], [34], [37], [38], [39], [40], [41], [42], [43] have paid attention on differential equations with different approaches in BS.

This work summarized as, in Section 2 has little preliminary and definitions about integrated resolvent operator theory which applied this work. In Section 3, to prove the uniqueness and continuous dependence of solution of Eq. (1). In Section 4, to show the differentiability of solution and in Section 5, to provide an application related to this work.

2. Basic results and definitions

Here, this section includes some basic results and definitions regarding integrated resolvent operators. Let $\mathscr{E}$ is BS and $\mathscr{D}$ be closed linear operator and $0 \in \rho(\mathscr{D})$ then $\mathscr{D}^{-1}$ exists. Let Y be the BS $(D(\mathscr{D}), \|\cdot\|)$ with graph of the norm $\|v\| = \|\mathscr{D}v\| + \|v\|$, $\forall v \in D(\mathscr{D})$. Let $\mathscr{L}(Y,\mathscr{E})$ be the bounded linear operator $Y \to \mathscr{E}$ with the norm $\|\cdot\|$ and $\mathscr{L}(\mathscr{E})$ when $Y = \mathscr{E}$. Let $C([-r,0];\mathscr{E})$ represents as the functions on $[-r,0]$ denoted by $\mathscr{C}$ are continuous in $\mathscr{E}$ and sup-norm $\|\cdot\|_{\mathscr{C}}$.

Next we recall few definitions and results about integrated resolvent operators established in [44] for linear nondensely defined integrodifferential equations.

Consider the below homogeneous linear integrodifferential system,

$$\begin{cases} v'(t) = \mathscr{D}v(t) + \int_0^t \mathscr{H}(t-\zeta)\,v(\zeta)\,d\zeta \qquad \text{for } t \in [0,a], \\ v(0) = v_0 \in \mathscr{E}. \end{cases} \tag{2}$$

Here, the operators $\mathscr{D}$ and $\mathscr{H}(\cdot)$ are defined already in Eq. (1). Then the integrated resolvent operator for Eq. (2) as follows

Definition 2.1

[44]

A set of operator $(\mathscr{Q}(t))_{t\geq 0}$ in $\mathscr{L}(\mathscr{E})$ is an integrated resolvent operator to Eq. (2) if it satisfies

$(R1)$ $\forall v \in$, $\mathscr{Q}$. $\mathscr{E}$ $(\cdot)v \in C([0,+\infty);\mathscr{E})$

$(R2)$ $\forall v \in$, $\int_0^{\cdot}\mathscr{Q}$. $\mathscr{E}$ $(\zeta) \in Y$

$(R3)$ $\mathscr{Q}$, $\forall v \in, t \geq$. $(t)v - tv = \mathscr{D}\int_0^t \mathscr{Q}(\zeta)vd\zeta + \int_0^t \mathscr{H}(t-\zeta)\int_0^{\zeta}\mathscr{Q}(r)vdrd\zeta$

$(R4)$ $\mathscr{Q}$, $\forall v \in, t \geq$. $(t)v - D(\mathscr{D})tv = \int_0^t \mathscr{Q}(\zeta)\mathscr{D}vd\zeta + \int_0^t\int_0^{\zeta}\mathscr{Q}(\zeta - r)\mathscr{H}(r)vdrd\zeta$

Definition 2.2

[44]

The operator $(\mathscr{Q}(t))_{t\geq 0}$ defined in above definition is locally Lipschitz continuous(LLC) if $\forall a > 0$, $\exists K_a = K(a) > 0$ implies

$$\|\mathscr{Q}(\xi_1) - \mathscr{Q}(\xi_2)\| \leq K_a |\xi_1 - \xi_2| \text{ where} \xi_1, \xi_2 \in [0, a].$$

Definition 2.3

[44]

Assume that $(\mathscr{Q}(t))$ is LLC integrated resolvent operator and $\forall v \in \overline{D(\mathscr{D})}, t \mapsto \mathscr{Q}(t)v$ is differentiable on $[0, +\infty)$.

Further we applied the below axioms for the Eq. (1),

$(S1)$ $\mathscr{D}$ satisfies the Hille–Yosida theorem, let $T_0 \geq 1, w \in \mathbb{R}$ then $(w, +\infty) \subset \rho(\mathscr{D})$ and

$$\left\|(\lambda I - \mathscr{D})^{-n_0}\right\| \leq \frac{T_0}{(\lambda - w)^{n_0}} \text{ for} n_0 \in \mathbb{N}, w < \lambda.$$

and $\rho(\mathscr{D})$ is resolvent set of $\mathscr{D}$.

$(S2)$ $(\mathscr{H}(t))$ be the set of operators on $D(\mathscr{D})$ to $\mathscr{E}$ and $D(\mathscr{D}) \subseteq D(\mathscr{H}(t)) \forall t \geq 0$, then the functions $\mathscr{H}(\cdot)v$ are bounded variation on $[0, a]$, $a > 0$ for $v \in D(\mathscr{D})$.

Lemma 2.4

[44], Theorem 3.2

Suppose that $(S1)$ *and* $(S2)$ *are satisfied, then* $\exists$ *a unique LLC integrated resolvent operator for* (2).

Remark 2.5

[45], Theorem 2.5

Lemma 2.4 shows that $(S1)$ characterizes a LLC integrated semigroup when $\mathscr{H} = 0$.

Consider the below nonhomogeneous integrodifferential system,

$$\begin{cases} v'(t) = \mathscr{D}v(t) + \int_0^t \mathscr{H}(t-\zeta)v(\zeta)\,d\zeta + f(t) & \text{for} t \in [0, a], \\ v(0) = v_0 \in \mathscr{E}. \end{cases} \tag{3}$$

We follow the article see [44], to write the integral solution, strict solution of Eq. (3) as follows,

Definition 2.6
For $f \in L^1([0, \infty); \mathscr{E})$ and $v_0 \in \mathscr{E}$. A function $v : [0, a] \to \mathscr{E}$ is an integral solution of (3) if

(1) $v \in C([0, a]; \mathscr{E})$

(2) $\int_0^{\cdot} v(\zeta)\, d\zeta \in C([0, a]; Y)$

(3) $v(t) = v_0 + \mathscr{D} \int_0^t v(\zeta)\, d\zeta + \int_0^t \mathscr{H}(t-\zeta) \int_0^{\zeta} v(\xi)\, d\xi d\zeta + \int_0^t f(\zeta)\, d\zeta$ for $t \in [0, a]$

Definition 2.7
A function $v : [0, +\infty] \to \mathscr{E}$ is strict solution of (3) if $v \in C^1([0, +\infty]; \mathscr{E}) \cap C([0, +\infty]; Y)$ and satisfied the Eq. (3).

The Lemma 2.8 is very useful results for proving integral solution and strict solution of (3) used by a variation of constants formula.

Lemma 2.8

[44]

Assume that $(\mathscr{Q}(t))_{t\geq 0}$ is LLC integrated resolvent operator and $\rho(\mathscr{D}) \neq \emptyset$ then

(i) *If $v_0 \in \overline{D(\mathscr{D})}$ and $f \in L^1([0, +\infty); \mathscr{E})$ then $\exists$ a unique integral solution $v(\cdot)$ of system (3) then*

$$v(t) = \mathscr{Q}'(t) v_0 + \frac{d}{dt} \int_0^t \mathscr{Q}(t-\zeta) f(\zeta)\, d\zeta, \quad t \in [0, a]. \tag{4}$$

Further

$$\left\| v(t) \right\| \leq C \left(\|v_0\| + \int_0^t \|f(\zeta)\| d\zeta \right), \quad t \in [0, a]. \tag{5}$$

(ii) *Suppose $v_0 \in D(\mathscr{D})$, $f \in W^{1,1}([0, a]; \mathscr{E})$ and $\mathscr{D} v_0 + f(0) \in \overline{D(\mathscr{D})}$, $\exists$ unique strict solution $v(\cdot)$ for Eq. (3) and*

$$\left\|v'(t)\right\| \leq C\left(\left\|\mathscr{D}v_0 + f(0)\right\| + \int_0^t \left\|\mathscr{H}(\zeta)v_0 + f'(\zeta)\right\| d\zeta\right), \quad t \in [0,a].$$

Here $C > 0$ is constant.

Remark 2.9

Suppose that $(\mathscr{Q}(t))_{t\geq 0}$ is LLC integrated resolvent operator. From [44], if $v \in \overline{D(\mathscr{D})}$then $t \mapsto \mathscr{Q}(t)v$ is differentiable on $[0,a]$.

Lemma 2.10

[44], Theorem 2.6

The set of $(\mathscr{G}(t))_{t\geq 0} \in \mathscr{L}(\mathscr{E})$ be LLC with $\mathscr{G}(0) = 0$ then

(i) If $f \in L^1([0,a];\mathscr{E})$, implies $\int_0^{\cdot} \mathscr{G}(\cdot - \zeta) f(\zeta)\, d\zeta \in C^1([0,a];\mathscr{E})$

$$\left\|\mathscr{K}(t)\right\| \leq K_T \int_0^t \left\|f(\zeta)\right\| d\zeta \text{for} t \in [0,a]. \tag{6}$$

Here $\mathscr{K} = \frac{d}{dt}\int_0^t \mathscr{G}(t-\zeta) f(\zeta)\, d\zeta$, $t \in [0,a]$ and $K_T > 0$ is Lipschitzian of $\{\mathscr{G}(t) : t \in [0,a]\}$. Further if $\|f(t)\| \leq K_0$, $\exists K_0 > 0$, $t \in [0,a]$

$$\left\|\mathscr{K}(t_1+\zeta) - \mathscr{K}(t_1)\right\| \leq K_0 K_T \zeta + K_T \int_0^{t_1} \left\|f(\zeta+\xi) - f(\xi)\right\| d\xi \text{for} t_1, \zeta, t+\zeta \in [0,a]. \tag{7}$$

(ii) Suppose $f : [0,a] \to \mathscr{E}$ is strongly bounded variation then $\mathscr{K}(\cdot)$ is Lipschitz continuous on $[0,a]$.

3. Existence of solution

Here, we have to show the existence of the solution of (1). Due to Lemma 2.8, The integral solution of (1) with nonlocal condition is as follows,

Definition 3.1

Let $\omega_0 \in \overline{D(\mathscr{D})}$. A function $\omega \in ([-r,+\infty);\mathscr{E})$ is an integral solution of system (1) if it satisfies,

$$\begin{cases} \omega(t) = q\left(t, \omega_t, \int_0^t h(t,s,\omega_s)\, ds\right) + \mathscr{Q}'(t)[\phi(0) - q(0,\phi,0)] + \frac{d}{dt}\int_0^t \mathscr{Q}(t-s) \\ \quad \times\left[\mathscr{D}q\left(s, \omega_s, \int_0^s h(s,\xi,\omega_\xi)\, d\xi\right) + \int_0^s q\left(s, \omega_s, \int_0^s h(s,\xi,\omega_\xi)\, d\xi\right)\mathscr{H}(\tau)\, d\tau\right. \\ \quad \left. + \varphi\left(s, \omega_s, \int_0^s h(s,\xi,\omega_\xi)\, d\xi\right)\right] ds \text{for} t \geq 0, \\ \phi(t) \text{for} t \in [-r,0]. \end{cases} \tag{8}$$

Remark 3.2

From the above Definition, if $\omega(\cdot)$ is integral solution of (1) on $[0,a]$ then to each $t \in [0,a]$, $\omega(t) - q\left(t, \omega_t, \int_0^t h(t,s,\omega_s)\, ds\right) \in \overline{D(\mathscr{D})}$. Further $\omega(0) - q(0,\phi,0) \in \overline{D(\mathscr{D})}$.

Definition 3.3

A function $\omega : [-r,+\infty) \to \mathscr{E}$ is called strict solution of (1) if

(i) $\omega \in C^1([0,+\infty);\mathscr{E}) \cap C([0,+\infty);Y)$.

(ii) ω holds the Eq. (1) on $[-r,+\infty)$.

If ω is solution of equation of (1) in $[-r,+\infty)$ and $\omega(t) \in \overline{D(\mathscr{D})}$, $\forall t \geq 0$. Further $\phi(0) \in \overline{D(\mathscr{D})}$ and ω is strict solution if either $\omega \in C^1([0,+\infty);\mathscr{E})$ or $C([0,+\infty);Y)$.

To establish this theory, solution of existence for Eq. (1), we need the support of the below assumptions

$(H1)$ The function $q: I \times \mathscr{C} \times \mathscr{E} \to D(\mathscr{D})$ is satisfies the Lipschitz continuous, there exist a constant $L_1 > 0$ such that

$$\|\mathscr{D}q(\xi,x_1,\tau_1) - \mathscr{D}q(\xi,y_1,\tau_2)\| \leq L_1(\|x_1-y_1\| + \|\tau_1-\tau_2\|) \text{ and } \|\mathscr{D}q(\xi,x_1,\tau_1)\| \leq L_1(\|x_1\| + \|\tau_1\|).$$

for any $0 \leq \xi \leq a, x_1, y_1 \in \mathscr{C}$ and $\tau_1, \tau_2 \in \mathscr{E}$.

$(H2)$ The function $\varphi: I \times \mathscr{C} \times \mathscr{E} \to \mathscr{E}$ is Lipschitz continuous, $\exists L_2 > 0$ such that

$$\|\varphi(t,\xi_1,\nu_1) - \varphi(t,\xi_2,\nu_2)\| \leq L_2(\|\xi_1-\xi_2\| + \|\nu_1-\nu_2\|).$$

and

$$\|\varphi(t,\xi_1,\nu_1)\| \leq L_2(\|\xi_1\|_{\mathscr{C}} + \|\nu_1\|).$$

For every $\xi_1, \xi_2 \in \mathscr{C}, \nu_1, \nu_2 \in \mathscr{E}$.

$(H3)$ The map $h: I \times I \times \mathscr{C} \to \mathscr{E}$ is Lipschitz continuous, there exist a constant $L_h > 0$ such that

$$\|h(\xi_1,\xi_2,\eta_1) - h(\xi_1,\xi_2,\eta_2)\| \leq L_h\|\phi-\psi\| \text{and} \|h(\xi_1,\xi_2,\eta_1)\| \leq L_h\|\eta_1\|_{\mathscr{C}}.$$

For each $\xi_1, \xi_2 \in I, \eta_1, \eta_2 \in \mathscr{C}$.

Theorem 3.4

If the Eq. (1) has an integrated resolvent operator $(\mathscr{Q})_{t\geq 0}$ which is LLC and $\rho(\mathscr{D}) \neq \emptyset$. Let q, φ are satisfied $(H1-H3)$ and $\phi \in \mathscr{C}$ such that $q(0,\phi,0) \in \overline{D(\mathscr{D})}$ then the system (1) has unique solution $\omega = \omega(.,\phi)$ on $[-r,+\infty)$.

proof: Let $a > 0$ and $C([0,a];\mathscr{E})$ is set of continuous maps from $[0,a]$ into $\mathscr{E}$. Let $\phi \in \mathscr{C}$ and $q(0,\phi,0) \in \overline{D(\mathscr{D})}$. The set

$$\mathbb{E}_a(\phi) = \{\omega \in C([0,a];\mathscr{E}) : \omega(0) = \phi(0)\}.$$

Clearly $\mathbb{E}_a(\phi) \subseteq C([0,a];\mathscr{E})$.

For $\omega \in \mathbb{E}_a(\phi)$, the extension $\tilde{\omega}: [-r,a] \to \mathscr{E}$ is such that

$$\tilde{\omega}(t) = \begin{cases} \omega(t), t \in [0,a], \\ \phi(t), t \in [-r,0]. \end{cases}$$

Now define the map $\Gamma : \mathbb{E}_a(\phi) \to \mathscr{E}$ by

$$(\Gamma\omega)(t) = q\left(t, \widetilde{\omega_t}, \int_0^t h(t,s,\widetilde{\omega_s})\,ds\right) + \mathscr{Q}'(t)\left[\phi(0) - q(0,\phi,0)\right]$$
$$+ \frac{d}{dt}\int_0^t \mathscr{Q}(t-s) \times \left[\mathscr{D}q\left(s, \widetilde{\omega_s}, \int_0^s h(s,\xi,\widetilde{\omega_\xi})\,d\xi\right)\right.$$
$$\left. + \int_0^s q\left(s, \widetilde{\omega_s}, \int_0^s h(s,\xi,\widetilde{\omega_\xi})\,d\xi\right)\mathscr{H}(\tau)\,d\tau + \varphi\left(s, \widetilde{\omega_s}, \int_0^s h(s,\xi,\widetilde{\omega_\xi})\,d\xi\right)\right] ds, t \in [0,a].$$

First we prove $(\Gamma\omega) \in \mathbb{E}_a(\phi)$. From $(H1)$ and Definition 2.3, it follows that the functions $t \mapsto q\left(t, \widetilde{\omega_t}, \int_0^t h(t,s,\widetilde{\omega_s})\,ds\right)$ and $t \mapsto \mathscr{Q}'(t)\left[\phi(0) - q(0,\phi,0)\right]$ are continuous on $[0,a]$. Further from $(H1-H3)$, we infer that the function $s \mapsto \varphi\left(s, \widetilde{\omega_s}, \int_0^s h(s,\xi,\widetilde{\omega_\xi})\,d\xi\right)$ is continuous on $[0,a]$ then by Lemma 2.10,
$t \mapsto \int_0^t \mathscr{Q}(t-s) \times$
$\left[\mathscr{D}q\left(s, \widetilde{\omega_s}, \int_0^s h(s,\xi,\widetilde{\omega_\xi})\,d\xi\right) + \int_0^s q\left(s, \widetilde{\omega_s}, \int_0^s h(s,\xi,\widetilde{\omega_\xi})\,d\xi\right)\mathscr{H}(\tau)\,d\tau + \varphi\left(s, \widetilde{\omega_s}, \int_0^s h(s,\xi,\widetilde{\omega_\xi})\,d\xi\right)\right] ds$
is continuous differentiable on $[0,a]$. Hence $(\Gamma\omega)(t) \in \mathbb{E}_a(\phi)$.

Next to prove Γ is a strict contraction map on $\mathbb{E}_a(\phi) \to \mathbb{E}_a(\phi)$.

If $\sigma(t), v(t) \in \mathbb{E}_a(\phi)$ are solutions of (1). For $t \in [0,a]$ then

$$\left\|(\Gamma\sigma)(t) - (\Gamma v)(t)\right\| \le \left\|q\left(t, \tilde{\sigma}_t, \int_0^t h(t,s,\tilde{\sigma}_s)\,ds\right) - q\left(t, \tilde{v}_t, \int_0^t h(t,s,\tilde{v}_s)\,ds\right)\right\|$$
$$+ \frac{d}{dt}\int_0^t \mathscr{Q}(t-s)\left[\left\|\mathscr{D}q\left(s, \tilde{\sigma}_s, \int_0^s h(s,\xi,\tilde{\sigma}_\xi)\,d\xi\right)\right.\right.$$
$$+ \int_0^s q\left(s, \tilde{\sigma}_s, \int_0^s h(s,\xi,\tilde{\sigma}_\xi)\,d\xi\right)\mathscr{H}(\tau)\,d\tau$$
$$+ \varphi\left(s, \tilde{\sigma}_s, \int_0^s h(s,\xi,\tilde{\sigma}_\xi)\,d\xi\right) - \mathscr{D}q\left(s, \tilde{v}_s, \int_0^s h(s,\xi,\tilde{v}_\xi)\,d\xi\right)$$
$$\left.\left. - \int_0^s q\left(s, \tilde{v}_s, \int_0^s h(s,\xi,\tilde{v}_\xi)\,d\xi\right)\mathscr{H}(\tau)\,d\tau - \varphi\left(s, \tilde{v}_s, \int_0^s h(s,\xi,\tilde{v}_\xi)\,d\xi\right)\right\|\right] ds.$$

Then

$$\left\|(\Gamma\sigma)(t) - (\Gamma v)(t)\right\| \le \left\|q\left(t, \tilde{\sigma}_t, \int_0^t h(t,s,\tilde{\sigma}_s)\,ds\right) - q\left(t, \tilde{v}_t, \int_0^t h(t,s,\tilde{v}_s)\,ds\right)\right\|$$
$$+ \frac{d}{dt}\int_0^t \mathscr{Q}(t-s)\left[\left\|\mathscr{D}q\left(s, \tilde{\sigma}_s, \int_0^s h(s,\xi,\tilde{\sigma}_\xi)\,d\xi\right) - \mathscr{D}q\left(s, \widetilde{v_s}, \int_0^s h(s,\xi,\widetilde{v_\xi})\,d\xi\right)\right\|\right.$$
$$+ \int_0^s \left\|\mathscr{H}(\tau)\right\|\left\|q\left(s, \tilde{\sigma}_s, \int_0^s h(s,\xi,\tilde{\sigma}_\xi)\,d\xi\right) - q\left(s, \tilde{v}_s, \int_0^s h(s,\xi,\tilde{v}_\xi)\,d\xi\right)\right\| d\tau$$
$$\left. + \left\|\varphi\left(s, \tilde{\sigma}_s, \int_0^s h(s,\xi,\tilde{\sigma}_\xi)\,d\xi\right) - \varphi\left(s, \tilde{v}_s, \int_0^s h(s,\xi,\tilde{v}_\xi)\,d\xi\right)\right\|\right] ds.$$

By using hypotheses

$$\left\|(\Gamma\sigma)(t) - (\Gamma v)(t)\right\| \le \| M_1 L_1 \left(\|\widetilde{\sigma_t} - \widetilde{v_t}\|_{\mathscr{E}} + L_h\|\tilde{\sigma}_s - \tilde{v}_s\|\right)$$
$$+ C\int_0^t \left[L_1\left(\|\widetilde{\sigma_s} - \widetilde{v_s}\|_{\mathscr{E}} + L_h\|\tilde{\sigma}_\xi - \tilde{v}_\xi\|\right)\right.$$
$$+ \int_0^s M_2 L_1\left(\|\widetilde{\sigma_s} - \widetilde{v_s}\|_{\mathscr{E}} + L_h\|\tilde{\sigma}_\xi - \tilde{v}_\xi\|\right) d\xi$$
$$\left. + L_2\left(\|\widetilde{\sigma_s} - \widetilde{v_s}\|_{\mathscr{E}} + L_h\|\tilde{\sigma}_\xi - \tilde{v}_\xi\|\right)\right]$$
$$\le \left[M_1 L_1 + C\left(aL_1 + a^2 M_2 L_1 + L_2\right)\right](1 + L_h)\sup_{0\le\xi\le t}\left\|\widetilde{\sigma_s} - \widetilde{v_s}\right\|$$
$$\le \left[M_1 L_1 + C\left(aL_1 + a^2 M_2 L_1 + L_2\right)\right](1 + L_h)\left\|\sigma(t) - v(t)\right\|.$$

Implies that

$$\|(\Gamma\sigma)(t) - (\Gamma v)(t)\| \le k_0\|\sigma(t) - v(t)\|.$$

where $k_0 = \left[M_1 L_1 + C\left(aL_1 + a^2 M_2 L_1 + L_2\right)\right](1 + L_h)$. Here C is from Lemma 2.8 and $M_1 = \left\|\mathscr{D}^{-1}\right\|$,

$M_2 = \sup_{t\in I} \|\mathscr{H}(t)\|$. Choose a small enough such that $k_0 < 1$. Hence Γ is a strict contraction in $\mathbb{E}_a(\phi)$. Which shows that the Eq. (1) has unique solution $\omega = \omega(\cdot, \phi)$ on $[-r, a]$.

Next to consider the continuous dependence of solution for Eq. (1) as the sense of below Theorem

Theorem 3.5

The solution of (1) is continuous dependence if for any $\phi, \psi \in \mathscr{C}, \exists k(a) > 0$ *and* $\phi(0), \psi(0) \in \overline{D(\mathscr{D})}$ *such that* $\|\omega_t(\cdot, \phi) - \omega_t(\cdot, \psi)\| \le k(a)\|\phi - \psi\|$ *for* $t \in [0, a]$ *provided*

$$M_1 L_1 L_1^* e^{Ca[L_1^*(L_1 + M_2 a L_1 + L_2)]} < 1. \tag{9}$$

Proof

Let $u = u(\cdot, \phi), v = v(\cdot, \psi)$ be two solutions of (1). Let $0 \le t \le a$,

$$u(t) = q\left(t, u_t, \int_0^t h(t, s, u_s)\, ds\right) + \mathscr{Q}(t)[\phi(0) - q(0, \phi, 0)]$$
$$+ \frac{d}{dt}\int_0^t \mathscr{Q}(t-s) \times \left[\mathscr{D}q\left(s, u_s, \int_0^s h(s, \xi, u_\xi)\, d\xi\right)\right.$$
$$+ \int_0^s q\left(s, u_s, \int_0^s h(s, \xi, u_\xi)\, d\xi\right)\mathscr{H}(\tau)\, d\tau$$
$$\left. + \varphi\left(s, u_s, \int_0^s h(s, \xi, u_\xi)\, d\xi\right)\right] ds, t \ge 0.$$

Now

$$\left\|u(t)-v(t)\right\| \leq \left\|q\left(t,u_t,\int_0^t h(t,s,u_s)\,ds\right)-q\left(t,u_t,\int_0^t h(t,s,v_s)\,ds\right)\right\|$$
$$+\left\|\mathscr{Q}'(t)\left([\phi(0)-\psi(0)]+[q(0,\phi,0)-q(0,\psi,0)]\right)\right\|$$
$$+\left\|\frac{d}{dt}\int_0^t \mathscr{Q}(t-s)\left[\mathscr{D}q\left(s,u_s,\int_0^s h(s,\xi,u_\xi)\,d\xi\right)-\mathscr{D}q\left(s,v_s,\int_0^s h(s,\xi,v_\xi)\,d\xi\right)\right.\right.$$
$$+\int_0^s \mathscr{H}(\tau)\left[q\left(s,u_s,\int_0^s h(s,\xi,u_\xi)\,d\xi\right)-q\left(s,v_s,\int_0^s h(s,\xi,v_\xi)\,d\xi\right)\right]d\tau$$
$$\left.\left.+\varphi\left(s,u_s,\int_0^s h(s,\xi,u_\xi)\,d\xi\right)-\varphi\left(s,v_s,\int_0^s h(s,\xi,v_\xi)\,d\xi\right)\right]\right\|$$
$$\leq \left\|q\left(t,u_t,\int_0^t h(t,s,u_s)\,ds\right)-q\left(t,u_t,\int_0^t h(t,s,v_s)\,ds\right)\right\|$$
$$+\left\|\mathscr{Q}'(t)\left([\phi(0)-\psi(0)]+[q(0,\phi,0)-q(0,\psi,0)]\right)\right\|$$
$$+C\int_0^t\left[\left\|\mathscr{D}q\left(s,u_s,\int_0^s h(s,\xi,u_\xi)\,d\xi\right)-\mathscr{D}q\left(s,v_s,\int_0^s h(s,\xi,v_\xi)\,d\xi\right)\right\|\right.$$
$$+\int_0^s\left\|\mathscr{H}(\tau)\left[q\left(s,u_s,\int_0^s h(s,\xi,u_\xi)\,d\xi\right)-q\left(s,v_s,\int_0^s h(s,\xi,v_\xi)\,d\xi\right)\right]\right\|d\tau$$
$$\left.+\left\|\varphi\left(s,u_s,\int_0^s h(s,\xi,u_\xi)\,d\xi\right)-\varphi\left(s,v_s,\int_0^s h(s,\xi,v_\xi)\,d\xi\right)ds\right\|\right]ds$$
$$\leq M_1L_1\left(\|u_t-v_t\|+L_h\|u_s-v_s\|\right)+C\left(\|\phi-\psi\|+L_1\|\phi-\psi\|\right)$$
$$+C\int_0^t\left[L_1\left(\|u_s-v_s\|+L_h\|u_\xi-v_\xi\|\right)+M_2L_1a\left(\|u_s-v_s\|+L_h\|u_\xi-v_\xi\|\right)\right.$$
$$\left.+L_2\left(\|u_s-v_s\|+L_h\|u_\xi-v_\xi\|\right)\right]ds$$
$$\leq M_1L_1\left(\left\|u_t-v_t\right\|+L_h\sup_{0\leq s\leq t}\left\|u_s-v_s\right\|\right)+(C+L_1)\left\|\phi-\psi\right\|$$
$$+C\left[\left((1+L_h)\left(L_1+M_2aL_1+L_2\right)\right)\int_0^t\sup_{0\leq\xi\leq s}\left\|u_s-v_s\right\|ds\right]$$
$$\leq M_1L_1\left(\left\|u_t-v_t\right\|+L_h\sup_{0\leq s\leq t}\left\|u_s-v_s\right\|\right)+(C+L_1)\left\|\phi-\psi\right\|$$
$$+C\left[\left((1+L_h)\left(L_1+M_2aL_1+L_2\right)\right)\int_0^t\sup_{0\leq\xi\leq s}\left\|u_s-v_s\right\|ds\right].$$

Hence by Gronwall's Lemma,

$$\left\|u(t)-v(t)\right\| \leq \left[M_1L_1\left(\left\|u_t-v_t\right\|+L_h\sup_{0\leq s\leq t}\left\|u_s-v_s\right\|\right)\right.$$
$$\left.+(C+L_1)\left\|\phi-\psi\right\|\right]e^{\int_0^a[C(1+L_h)(L_1+M_2aL_1+L_2)]ds}$$

$$\left\|u(t)-v(t)\right\| \leq \frac{(C+L_1)e^{Ca\left[L_1^*(L_1+M_2L_1a+L_2)\right]}}{1-M_1L_1L_1^*e^{Ca\left[L_1^*(L_1+M_2L_1a+L_2)\right]}}\left\|\phi-\psi\right\|.$$

Where $L_1^*=1+L_h$. Thus from Eq. (9), the integral solution of (1) is continuous dependence on initial conditions.

4. Existence of strict solution

Here, we study the existence of strict solution of the system (1) and under some consideration.

Definition 4.1

A function $\omega(\cdot):[-r,+\infty)\to\mathscr{E}$ is called a strict solution of (1), if $\omega(t)-q\left(t,\omega_t,\int_0^t h(t,s,\omega_s)\,ds\right)\in C^1([0,+\infty);\mathscr{E})\cap C([0,+\infty);Y)$ and ω holds the Eq. (1) on $[-r,+\infty)$.

Theorem 4.2

If the axioms of Theorem 3.4 are true and if

$(H5)$ $\phi(0)\in D(\mathscr{D})$, $\mathscr{D}[\phi(0)-q(0,\omega_0,0)]+\varphi(0,\omega_0,0)\in\overline{D(\mathscr{D})}$

$(H6)$ *There is holds that*

$$\left((M_1+K_aa+K_aM_2a^2)L_1+(1+L_h)K_aaL_2\right)<1 \tag{10}$$

then the integral solution of (1) become a strict solution.

Proof

Let the operator Γ on $C([-r,a];\mathscr{E})$ is given in Theorem 3.4. Let the closed ball $B_{r_0}=\{\omega\in C[-r,a];\mathscr{E}:\|\omega\|\le r_0,\|\omega(t_2)-\omega(t_1)\|\le L^*|t_2-t_1|,t_1,t_2\in[-r,a]\}$. Here $L^*>0$ is constant and to prove Γ has a fixed point on B_{r_0}. By Theorem 3.4, clearly $\Gamma(B_{r_0})\subset B_{r_0}$, it is suffices to show that

$$\|(\Gamma\omega)(t_2)-(\Gamma\omega)(t_1)\|\le L^*|t_2-t_1|\ \text{for}\ \omega\in B_{r_0},t_1,t_2\in[-r,a]. \tag{11}$$

The extension of the operator solution $(\Gamma\omega)(t)$ as

$$\Gamma(\tilde{\omega}(t))=\begin{cases}\omega(t)\ \text{for} & 0\le t\le a,\\ \phi(t)\ \text{for} & -r\le t\le 0.\end{cases}$$

Now

$$\begin{aligned}
&\left\|(\Gamma\omega)(t_2)-(\Gamma\omega)(t_1)\right\| \leq \left\|q\left(t_2,\widetilde{\omega}_{t_2},\int_0^{t_2} h(t_2,s,\widetilde{\omega}_s)\,ds\right)\right.\\
&\left.-q\left(t_1,\widetilde{\omega}_{t_1},\int_0^{t_1} h(t_1,s,\widetilde{\omega}_s)\,ds\right)\right\|\\
&+\left\|\left[\mathscr{Q}'(t_2)-\mathscr{Q}'(t_1)\right](\phi(0)-q(0,\phi,0))\right\|\\
&+\left\|\tfrac{d}{dt_2}\int_0^{t_2}\mathscr{Q}(t_2-s)\left[\mathscr{D}q\left(s,\widetilde{\omega}_s,\int_0^s h(s,\xi,\widetilde{\omega}_\xi)\,d\xi\right)\right.\right.\\
&\left.+\int_0^s q\left(s,\widetilde{\omega}_s,\int_0^s h(s,\xi,\widetilde{\omega}_\xi)\,d\xi\right)\mathscr{H}(\tau)\,d\tau+\varphi\left(s,\widetilde{\omega}_s,\int_0^s h(s,\xi,\widetilde{\omega}_\xi)\,d\xi\right)\right]ds\\
&-\tfrac{d}{dt_1}\int_0^{t_1}\mathscr{Q}(t_1-s)\left[\mathscr{D}q\left(s,\widetilde{\omega}_s,\int_0^s h(s,\xi,\widetilde{\omega}_\xi)\,d\xi\right)\right.\\
&\left.\left.+\int_0^s q\left(s,\widetilde{\omega}_s,\int_0^s h(s,\xi,\widetilde{\omega}_\xi)\,d\xi\right)\mathscr{H}(\tau)\,d\tau+\varphi\left(s,\widetilde{\omega}_s,\int_0^s h(s,\xi,\widetilde{\omega}_\xi)\,d\xi\right)\right]ds\right\|\\
&=: I_1+I_2+I_3,
\end{aligned}$$

where

$$I_1=\left\|q\left(t_2,\widetilde{\omega}_{t_2},\int_0^{t_2} h(t_2,s,\widetilde{\omega}_s)\,ds\right)-q\left(t_1,\widetilde{\omega}_{t_1},\int_0^{t_1} h(t_1,s,\widetilde{\omega}_s)\,ds\right)\right\|.$$

$$I_2=\left\|\left[\mathscr{Q}'(t_2)-\mathscr{Q}'(t_1)\right](\phi(0)-q(0,\phi,0))\right\|.$$

$$\begin{aligned}
I_3=&\left\|\tfrac{d}{dt_2}\int_0^{t_2}\mathscr{Q}(t_2-s)\left[\mathscr{D}q\left(s,\widetilde{\omega}_s,\int_0^s h(s,\xi,\widetilde{\omega}_\xi)\,d\xi\right)\right.\right.\\
&\left.+\int_0^s q\left(s,\widetilde{\omega}_s,\int_0^s h(s,\xi,\widetilde{\omega}_\xi)\,d\xi\right)\mathscr{H}(\tau)\,d\tau+\varphi\left(s,\widetilde{\omega}_s,\int_0^s h(s,\xi,\widetilde{\omega}_\xi)\,d\xi\right)\right]ds\\
&-\tfrac{d}{dt_1}\int_0^{t_1}\mathscr{Q}(t_1-s)\left[\mathscr{D}q\left(s,\widetilde{\omega}_s,\int_0^s h(s,\xi,\widetilde{\omega}_\xi)\,d\xi\right)\right.\\
&\left.\left.+\int_0^s q\left(s,\widetilde{\omega}_s,\int_0^s h(s,\xi,\widetilde{\omega}_\xi)\,d\xi\right)\mathscr{H}(\tau)\,d\tau+\varphi\left(s,\widetilde{\omega}_s,\int_0^s h(s,\xi,\widetilde{\omega}_\xi)\,d\xi\right)\right]ds\right\|.
\end{aligned}$$

Now take I_1,

$$\begin{aligned}
&I_1\leq M_1L_1\left(|t_2-t_1|+\|\widetilde{\omega}_{t_2}-\widetilde{\omega}_{t_1}\|+L_h|t_2-t_1|\right)\\
&\leq M_1L_1\left(|t_2-t_1|+L^*|t_2-t_1|+L_h|t_2-t_1|\right)\\
&\leq\left(M_1L_1+M_1L_1L^*+M_1L_1L_h\right)|t_2-t_1|.
\end{aligned}$$

From $(R4)$, differentiate on both sides with respect to t we have

$$\mathscr{Q}'(t)\omega-\omega=\mathscr{Q}\mathscr{D}\omega+\int_0^t\mathscr{Q}(t-s)\mathscr{H}(s)\omega ds$$

$$\begin{aligned}
&I_2\leq\left\|\mathscr{Q}(t_2)-\mathscr{Q}(t_1)\right\|\left\|\mathscr{D}\left[\phi(0)-q(0,\phi,0)\right]\right\|\\
&+\int_0^{t_1}\left\|\mathscr{Q}(t_2-s)-\mathscr{Q}(t_1-s)\right\|\left\|\mathscr{H}(\tau)\left[\phi(0)-q(0,\phi,0)\right]\right\|ds\\
&+\int_{t_1}^{t_2}\left\|\mathscr{Q}(t_2-s)\right\|\mathscr{H}(\tau)\left[\phi(0)-q(0,\phi,0)\right]\|\,ds\\
&\leq K_a\left\|\mathscr{D}\left[\phi(0)-q(0,\phi,0)\right]\right\||t_2-t_1|+K_aM_2\left\|\mathscr{D}\left[\phi(0)-q(0,\phi,0)\right]\right\|a|t_2-t_1|\\
&+\sup_{t\in[0,a]}\left\|\mathscr{Q}(t)\right\|M_2\mathscr{D}\left[\phi(0)-q(0,\phi,0)\right]\|\,|t_2-t_1|\\
&\leq(K_a+K_aM_2a+MM_2)M_1(\|\phi\|-L_1(\|\phi\|))|t_2-t_1|\\
&\leq[K_aM_1(1+aM_2)+MM_1M_2](\|\phi\|(1-L_1))|t_2-t_1|.
\end{aligned}$$

From I_3, we note that

$$\begin{aligned}&\left\|\mathscr{D}q\left(s,\widetilde{\omega}_s,\int_0^s h\left(s,\xi,\widetilde{\omega}_\xi\right)d\xi\right)+\int_0^s q\left(s,\widetilde{\omega}_s,\int_0^s h\left(s,\xi,\widetilde{\omega}_\xi\right)d\xi\right)\mathscr{H}\left(\tau\right)d\tau\right.\\&\left.+\varphi\left(s,\widetilde{\omega}_s,\int_0^s h\left(s,\xi,\widetilde{\omega}_\xi\right)d\xi\right)\right\|\\&\leq\left[L_1\left(1+L_h\right)+M_2L_1\left(1+L_h\right)a+L_2\left(1+L_h\right)\right]r_0\\&\leq\left(1+L_h\right)\left(L_1+L_1M_2a+L_2\right)r_0.\end{aligned}$$

Now

$$\begin{aligned}&I_3\leq K_a\left[\left(1+L_h\right)\left(L_1+L_1M_2a+L_2\right)\right]r_0\left|t_2-t_1\right|\\&+K_a\\&\int_0^{t_1}\left[\left\|\mathscr{D}q\left(t_2-t_1+s,\widetilde{\omega}_{t_2-t_1+s},\int_0^s h\left(s,\xi,\widetilde{\omega}_\xi\right)d\xi\right)-\mathscr{D}q\left(s,\widetilde{\omega_s},\int_0^s h\left(s,\xi,\widetilde{\omega}_\xi\right)d\xi\right)\right\|\right.\\&+\int_0^s\left\|\mathscr{H}\left(s-\tau\right)\right\|\left\|q\left(t_2-t_1+\xi,\widetilde{\omega}_{t_2-t_1+\xi},\int_0^s h\left(s,\xi,\widetilde{\omega}_\xi\right)d\xi\right)\right.\\&\left.-q\left(s,\widetilde{\omega_s},\int_0^s h\left(s,\xi,\widetilde{\omega}_\xi\right)d\xi\right)\right\|d\tau\\&+\int_{-(t_2-t_1)}^0\left\|\mathscr{H}\left(s-\tau\right)q\left(t_2-t_1+\xi,\widetilde{\omega}_{t_2-t_1+\xi},\int_0^s h\left(s,\xi,\widetilde{\omega}_\xi\right)d\xi\right)\right\|d\tau\\&+\left\|\varphi\Big(t_2-t_1+s,\widetilde{\omega}_{t_2-t_1+s},\int_0^{t_2-t_1+s}h\left(t_2-t_1+s,t_2-t_1+\xi,\widetilde{\omega}_{t_2-t_1+\xi}\right)d\xi\Big)\right.\\&\left.\left.-\varphi\left(s,\widetilde{\omega}_s,\int_0^s h\left(s,\xi,\widetilde{\omega_\xi}\right)d\xi\right)\right\|\right]ds\\&\leq K_a\left[\left(1+L_h\right)\left(L_1+L_1M_2a+L_2\right)\right]r_0\left|t_2-t_1\right|\\&+K_aa\left[L_1\left(1+L^*+L_h\right)+\left(M_2L_1a\left(1+L^*+L_h\right)\right)\right.\\&\left.+M_2L_1\left(1+L_h\right)r_0+L_2\left(1+L^*+L_hL^*\right)\right]\left|t_2-t_1\right|.\end{aligned}$$

From the estimates of I_1, I_2, I_3 we have

$$\begin{aligned}&\left\|\left(\Gamma\omega\right)\left(t_2\right)-\left(\Gamma\omega\right)\left(t_1\right)\right\|\leq\left[M_1L_1+M_1L_1L^*+M_1L_1L_h+\left[K_aM_1\left(1+aM_2\right)\right.\right.\\&\left.\left.+MM_1M_2\right]\left(\left\|\phi\right\|\left(1-L_1\right)\right)+K_a\left[\left(1+L_h\right)\left(L_1+L_1M_2a+L_2\right)\right]r_0\right.\\&+K_aa\left(L_1\left(1+L^*+L_h\right)+\left(M_2L_1a\left(1+L^*+L_h\right)\right)\right.\\&\left.\left.+M_2L_1\left(1+L_h\right)r_0+L_2\left(1+L^*+L_hL^*\right)\right)\right]\left|t_2-t_1\right|\\&\leq\left[C^*+\left(\left(M_1+K_aa+K_aM_2a^2\right)L_1+\left(1+L_h\right)K_aaL_2\right)L^*\right]\left|t_2-t_1\right|.\end{aligned}$$

Here $C^*\in\mathbb{R}$ different from L^*, $\omega\in B_{r_0}$, thus from $(H6)$

$$\left\|\left(\Gamma\omega\right)\left(t_2\right)-\left(\Gamma\omega\right)\left(t_1\right)\right\|\leq L^*\left|t_2-t_1\right|.$$

Where assume that L^* is large enough $\left(\geq\frac{C^*}{1-((M_1+K_aa+K_aM_2a^2)L_1+(1+L_h)K_aaL_2)}\right)$.

Thus Γ has a unique fixed point $\omega\left(\cdot\right)$ and is integral solution of (1). Further $\omega\left(t\right)$ is Lipschitz continuous $[0,a]$, moreover

$$\begin{aligned}s\to&\mathscr{D}q\left(s,\omega_s,\int_0^s h\left(s,\xi,\omega_\xi\right)d\xi\right)+\int_0^s\mathscr{H}\left(s-\tau\right)q\left(s,\omega_s,\int_0^s h\left(s,\xi,\omega_\xi\right)d\xi\right)d\tau\\&+\varphi\left(s,\omega_s,\int_0^s h\left(s,\xi,\omega_\xi\right)d\xi\right)\end{aligned}$$

is also Lipschitz continuous on $[0,a]$, $\mathscr{E}$ is a reflexive BS, hence by Radon–Nikodym property,

$$\begin{aligned}&\mathscr{D}q\left(s,\omega_s,\int_0^s h\left(s,\xi,\omega_\xi\right)d\xi\right)+\int_0^s\mathscr{H}\left(s-\tau\right)q\left(s,\omega_s,\int_0^s h\left(s,\xi,\omega_\xi\right)d\xi\right)d\tau\\&+\varphi\left(s,\omega_s,\int_0^s h\left(s,\xi,\omega_\xi\right)d\xi\right)\in W^{1,1}\left([0,a];\mathscr{E}\right).\end{aligned}$$

By Lemma 2.8, we have $\omega\left(t\right)-q\left(t,\omega_t,\int_0^t h\left(t,s,\omega_s\right)ds\right)$ is differentiable on $[0,a]$ and also strict solution of Eq. (1) on $[0,a]$. Next we consider $\mathscr{E}$ is a general BS, in the sense further we assume

$(H7)$ The function $q \in C^1\left(\mathbb{R}^+ \times \mathscr{C} \times \mathscr{E}; Y\right)$ and the partial derivatives $D_t q(\cdot,\cdot,\cdot), D_\phi q(\cdot,\cdot,\cdot)$ are LLC functions with respect to the second variable.

$(H8)$ The function $\varphi \in C^1\left(\mathbb{R}^+ \times \mathscr{C} \times \mathscr{E}; \mathscr{E}\right)$ and the partial derivatives $D_t \varphi(\cdot,\cdot,\cdot), D_\phi \varphi(\cdot,\cdot,\cdot)$ are LLC functions with respect to the second variable.

Theorem 4.3

Suppose $(H1)-(H4)$ *and* $(H7), (H8)$ *are true with* $M_1 L_1 (1 + L_h) < 1$. *If* $\omega(\cdot)$ *is a integral solution of* (1) *and* $\phi \in D(\mathscr{D})$, $\mathscr{D}[\phi(0) - q(0,\phi,0)] + \varphi(0,\phi,0) \in \overline{D(\mathscr{D})}$ *then* $\omega(\cdot)$ *is a strict solution of* (1).

Proof

Let $\omega(\cdot)$ is an integral solution of (1) and consider the following equation

$$
\begin{aligned}
y(t) &= D_t q\left(t, \omega_t, \int_0^t h(t,s,\omega_s)\,ds\right) + D_\phi q\left(t, \omega_t, \int_0^t h(t,s,\omega_s)\,ds\right) y_t \\
&+ \mathscr{Q}'(t)\mathscr{D}[\phi(0) - q(0,\phi,0)] + \mathscr{Q}'(t)\mathscr{D}q(0,\phi,0) \\
&+ \tfrac{d}{dt}\int_0^t \mathscr{Q}(t-s)\mathscr{H}(s)\,q(0,\phi,0)\,ds + \mathscr{Q}'(t)\varphi(0,\phi,0) \\
&+ \tfrac{d}{dt}\int_0^t \mathscr{Q}(t-s)\mathscr{H}(s)(\phi(0) - q(0,\phi,0))\,ds \\
&+ \tfrac{d}{dt}\int_0^t \mathscr{Q}(t-s)\Big[\mathscr{D}D_t q\left(s, \omega_s, \int_0^s h(s,\xi,\omega_\xi)\,d\xi\right) \\
&+ \mathscr{D}D_\phi q\left(s, \omega_s, \int_0^s h(s,\xi,\omega_\xi)\,d\xi\right) y_s \\
&+ \int_0^s \mathscr{H}(s-\tau)\left[D_t q\left(s, \omega_s, \int_0^s h(s,\xi,\omega_\xi)\,d\xi\right) + D_\phi q\left(s, \omega_s, \int_0^s h(s,\xi,\omega_\xi)\,d\xi\right) y_s\right] d\tau \\
&+ D_t\varphi\left(s, \omega_s, \int_0^s h(s,\xi,\omega_\xi)\right) + D_\phi\varphi\left(s, \omega_s, \int_0^s h(s,\xi,\omega_\xi)\right) y_s\Big]\,ds.
\end{aligned} \tag{12}
$$

From the Banach principle, to show the existence of unique solution $y(\cdot) \in C([0,a]; \mathscr{E})$ to Eq. (12). Let the map $z(t)$ is defined by

$$z(t) = \phi(0) + \int_0^t y(s)\,ds \text{for} t \in [0,a].$$

To prove $\omega(\cdot) = z(\cdot)$ on $[0,a]$.

$$
\begin{aligned}
z(t) &= \phi(0) \\
&+ \int_0^t \left[D_1 q\left(s, \omega_s, \int_0^s h(s,\xi,\omega_\xi)\,d\xi\right) + D_\phi q\left(s, \omega_s, \int_0^s h(s,\xi,\omega_\xi)\,d\xi\right) y_s\right] ds \\
&+ \mathscr{Q}\mathscr{D}[\phi(0) - q(0,\phi,0)] + \mathscr{Q}\mathscr{D}[q(0,\phi,0)] \\
&+ \int_0^t \mathscr{Q}(t-s)\mathscr{H}(s)\,q(0,\phi,0)\,ds + \mathscr{Q}(t)\varphi(0,\phi,0) \\
&+ \int_0^t \mathscr{Q}(t-s)\mathscr{H}(s)(\phi(0) - q(0,\phi,0))\,ds \\
&+ \int_0^t \mathscr{Q}(t-s)\Big[\mathscr{D}D_t q\left(s, \omega_s, \int_0^s h(s,\xi,\omega_\xi)\,d\xi\right) \\
&+ \mathscr{D}D_\phi q\left(s, \omega_s, \int_0^s h(s,\xi,\omega_\xi)\,d\xi\right) y_s \\
&+ \int_0^s \mathscr{H}(s-\tau)\left[D_t q\left(s, \omega_s, \int_0^s h(s,\xi,\omega_\xi)\,d\xi\right) + D_\phi q\left(s, \omega_s, \int_0^s h(s,\xi,\omega_\xi)\,d\xi\right) y_s\right] d\tau \\
&+ D_t\varphi\left(s, \omega_s, \int_0^s h(s,\xi,\omega_\xi)\,d\xi\right) + D_\phi\varphi\left(s, \omega_s, \int_0^s h(s,\xi,\omega_\xi)\,d\xi\right) y_s\Big]\,ds.
\end{aligned} \tag{13}
$$

From $(R4)$, differentiate on both sides with respect to t we have

$$
\begin{aligned}
\mathscr{Q}\mathscr{D}[\phi(0) - q(0,\phi,0)] &= \mathscr{Q}'(t)[\phi(0) - q(0,\phi,0)] \\
&- [\phi(0) - q(0,\phi,0)] \\
&- \int_0^t \mathscr{Q}(t-s)\mathscr{H}(s)[\phi(0) - q(0,\phi,0)]\,ds
\end{aligned} \tag{14}
$$

Consequently,

$$q(0,z_0,0)=q\left(t,z_t,\int_0^t h(t,s,z_s)\,ds\right)-\int_0^t\Big[D_tq\left(s,z_s,\int_0^s h(s,\xi,z_\xi)\,d\xi\right)+D_\phi q\left(s,z_s,\int_0^s h(s,\xi,z_\xi)\,d\xi\right)y_s\Big]ds. \tag{15}$$

Further, we obtain

$$\begin{aligned}&\mathcal{Q}\mathcal{D}q(0,z_0,0)+\int_0^t\mathcal{Q}(t-s)\mathcal{H}(s)\,q(0,z_0,0)\,ds+\mathcal{Q}\varphi(0,z_0,0)\\&=\tfrac{d}{dt}\int_0^t\mathcal{Q}(t-s)\Big[\mathcal{D}q\left(s,z_s,\int_0^s h(s,\xi,z_\xi)\,d\xi\right)+\int_0^s\mathcal{H}(s-\tau)\,q\left(s,z_s,\int_0^s h(s,\xi,z_\xi)\,d\xi\right)d\tau\\&+\varphi\left(s,z_s,\int_0^s h(s,\xi,z_\xi)\,d\xi\right)\Big]ds-\int_0^t\mathcal{Q}(t-s)\Big[\mathcal{D}D_tq\left(s,z_s,\int_0^s h(s,\xi,z_\xi)\,d\xi\right)+\mathcal{D}D_\phi q\left(s,z_s,\int_0^s h(s,\xi,z_\xi)\,d\xi\right)y_s\\&+\int_0^s\mathcal{H}(s-\tau)\Big[D_tq\left(s,z_s,\int_0^s h(s,\xi,z_\xi)\,d\xi\right)+D_\phi q\left(s,z_s,\int_0^s h(s,\xi,z_\xi)\,d\xi\right)y_s\Big]d\tau\\&+D_t\varphi\left(s,z_s,\int_0^s h(s,\xi,z_\xi)\,d\xi\right)+D_\phi\varphi\left(s,z_s,\int_0^s h(s,\xi,z_\xi)\,d\xi\right)y_s\Big]ds\end{aligned} \tag{16}$$

Since $\omega_0=z_0$ from Eqs. (14), (15), (16) in (13), gives

$$\begin{aligned}z(t)&=q\left(t,z_t,\int_0^t h(t,s,z_s)\,ds\right)+\int_0^t\Big[D_tq\left(s,\omega_s,\int_0^s h(s,\xi,\omega_\xi)\,d\xi\right)\\&+D_\phi q\left(s,\omega_s,\int_0^s h(s,\xi,\omega_\xi)\,d\xi\right)y_s\Big]ds\\&-\int_0^t\Big[D_tq\left(s,z_s,\int_0^s h(s,\xi,z_\xi)\,d\xi\right)+D_\phi q\left(s,z_s,\int_0^s h(s,\xi,z_\xi)\,d\xi\right)y_s\Big]ds\\&+\mathcal{Q}'(t)\left[\phi(0)-q(0,\phi,0)\right]+\tfrac{d}{dt}\int_0^t\mathcal{Q}(t-s)\Big[\mathcal{D}q\left(s,z_s,\int_0^s h(s,\xi,z_\xi)\,d\xi\right)\\&+\int_0^s\mathcal{H}(s-\tau)\,q\left(s,z_s,\int_0^s h(s,\xi,z_\xi)\,d\xi\right)d\tau+\varphi\left(s,z_s,\int_0^s h(s,\xi,z_\xi)\,d\xi\right)\Big]ds\\&-\int_0^t\mathcal{Q}(t-s)\Big[\left(\mathcal{D}D_tq\left(s,z_s,\int_0^s h(s,\xi,z_\xi)\,d\xi\right)+\mathcal{D}D_\phi q\left(s,z_s,\int_0^s h(s,\xi,z_\xi)\,d\xi\right)y_s\right)\\&+\int_0^s\mathcal{H}(s-\tau)\left(D_tq\left(s,z_s,\int_0^s h(s,\xi,z_\xi)\,d\xi\right)+D_\phi q\left(s,z_s,\int_0^s h(s,\xi,z_\xi)\,d\xi\right)y_s\right)d\tau\\&+D_t\varphi\left(s,z_s,\int_0^s h(s,\xi,z_\xi)\,d\xi\right)+D_\phi\varphi\left(s,z_s,\int_0^s h(s,\xi,z_\xi)\,d\xi\right)y_s\Big]ds\\&+\int_0^t\mathcal{Q}(t-s)\Big[\mathcal{D}D_tq\left(s,\omega_s,\int_0^s h(s,\xi,\omega_\xi)\,d\xi\right)+\mathcal{D}D_\phi q\left(s,\omega_s,\int_0^s h(s,\xi,\omega_\xi)\,d\xi\right)y_s\\&+\int_0^s\mathcal{H}(s-\tau)\left(D_tq\left(s,\omega_s,\int_0^s h(s,\xi,\omega_\xi)\,d\xi\right)+D_\phi q\left(s,\omega_s,\int_0^s h(s,\xi,\omega_\xi)\,d\xi\right)y_s\right)d\tau\\&+D_t\varphi\left(s,\omega_s,\int_0^s h(s,\xi,\omega_\xi)\,d\xi\right)+D_\phi\varphi\left(s,\omega_s,\int_0^s h(s,\xi,\omega_\xi)\,d\xi\right)y_s\Big]ds.\end{aligned}$$

Now

$$
\begin{aligned}
&z(t)-\omega(t)=q\left(t,z_t,\int_0^t h(t,s,z_s)\,ds\right)-q\left(t,\omega_t,\int_0^t h(t,s,\omega_s)\,ds\right)\\
&+\frac{d}{dt}\int_0^t \mathscr{Q}(t-s)\left[\mathscr{D}q\left(s,z_s,\int_0^s h(s,\xi,z_\xi)\,d\xi\right)-\mathscr{D}q\left(s,\omega_s,\int_0^s h(s,\xi,\omega_\xi)\,d\xi\right)\right]ds\\
&+\frac{d}{dt}\int_0^t \mathscr{Q}(t-s)\int_0^s \mathscr{H}(s-\tau)\left[q\left(s,z_s,\int_0^s h(s,\xi,z_\xi)\,d\xi\right)-q\left(s,\omega_s,\int_0^s h(s,\xi,\omega_\xi)\,d\xi\right)\right]d\tau ds\\
&+\frac{d}{dt}\int_0^t \mathscr{Q}(t-s)\left[\varphi\left(s,z_s,\int_0^s h(s,\xi,z_\xi)\,d\xi\right)-\varphi\left(s,\omega_s,\int_0^s h(s,\xi,\omega_\xi)\,d\xi\right)\right]ds\\
&+\int_0^t \left[D_t q\left(s,\omega_s,\int_0^s h(s,\xi,\omega_\xi)\,d\xi\right)-D_t q\left(s,z_s,\int_0^s h(s,\xi,z_\xi)\,d\xi\right)\right]ds\\
&+\int_0^t \left[D_\phi q\left(s,\omega_s,\int_0^s h(s,\xi,\omega_\xi)\,d\xi\right)-D_\phi q\left(s,z_s,\int_0^s h(s,\xi,z_\xi)\,d\xi\right)\right]y_s ds\\
&+\int_0^t \mathscr{Q}(t-s)\left[\mathscr{D}D_t q\left(s,\omega_s,\int_0^s h(s,\xi,\omega_\xi)\,d\xi\right)-\mathscr{D}D_t q\left(s,z_s,\int_0^s h(s,\xi,z_\xi)\,d\xi\right)\right]ds\\
&+\int_0^t \mathscr{Q}(t-s)\left[\mathscr{D}D_\phi q\left(s,\omega_s,\int_0^s h(s,\xi,\omega_\xi)\,d\xi\right)-\mathscr{D}D_\phi q\left(s,z_s,\int_0^s h(s,\xi,z_\xi)\,d\xi\right)\right]y_s ds\\
&+\int_0^t \mathscr{Q}(t-s)\int_0^s \mathscr{H}(s-\tau)\left[D_t q\left(s,\omega_s,\int_0^s h(s,\xi,\omega_\xi)\,d\xi\right)\right.\\
&\left.-D_t q\left(s,z_s,\int_0^s h(s,\xi,z_\xi)\,d\xi\right)\right]d\tau ds\\
&+\int_0^t \mathscr{Q}(t-s)\int_0^s \mathscr{H}(s-\tau)\left[D_\phi q\left(s,\omega_s,\int_0^s h(s,\xi,\omega_\xi)\,d\xi\right)\right.\\
&\left.-D_\phi q\left(s,z_s,\int_0^s h(s,\xi,z_\xi)\,d\xi\right)\right]y_s d\tau ds\\
&+\int_0^t \mathscr{Q}(t-s)\left[D_t\varphi\left(s,\omega_s,\int_0^s h(s,\xi,\omega_\xi)\,d\xi\right)-D_t\varphi\left(s,z_s,\int_0^s h(s,\xi,z_\xi)\,d\xi\right)\right]ds\\
&+\int_0^t \mathscr{Q}(t-s)\left[D_\phi\varphi\left(s,\omega_s,\int_0^s h(s,\xi,\omega_\xi)\,d\xi\right)-D_\phi\varphi\left(s,z_s,\int_0^s h(s,\xi,z_\xi)\,d\xi\right)\right]y_s ds\\
&:=J_1+J_2+J_3
\end{aligned}
$$

where

$$
\begin{aligned}
&\left\|J_1\right\|\le\left\|q\left(t,z_t,\int_0^t h(t,s,z_s)\,ds\right)-q\left(t,\omega_t,\int_0^t h(t,s,\omega_s)\,ds\right)\right\|\\
&+\frac{d}{dt}\int_0^t \mathscr{Q}(t-s)\left\|\left[\mathscr{D}q\left(s,z_s,\int_0^s h(s,\xi,z_\xi)\,d\xi\right)-\mathscr{D}q\left(s,\omega_s,\int_0^s h(s,\xi,\omega_\xi)\,d\xi\right)\right]\right\|ds\\
&+\frac{d}{dt}\int_0^t \mathscr{Q}(t-s)\int_0^s \left\|\mathscr{H}(s-\tau)\left[q\left(s,z_s,\int_0^s h(s,\xi,z_\xi)\,d\xi\right)-q\left(s,\omega_s,\int_0^s h(s,\xi,\omega_\xi)\,d\xi\right)\right]\right\|d\tau ds\\
&+\frac{d}{dt}\int_0^t \mathscr{Q}(t-s)\left\|\left[\varphi\left(s,z_s,\int_0^s h(s,\xi,z_\xi)\,d\xi\right)-\varphi\left(s,\omega_s,\int_0^s h(s,\xi,\omega_\xi)\,d\xi\right)\right]\right\|ds\\
&\le M_1L_1(1+L_h)\sup_{0\le s\le t}\left\|\omega_s-z_s\right\|\\
&+K_a\left(L_1(1+L_h)+M_2L_1(1+L_h)a+L_2(1+L_h)\right)\int_0^t\sup_{0\le\xi\le s}\left\|\omega_\xi-z_\xi\right\|ds\\
&\le M_1L_1(1+L_h)\sup_{0\le s\le t}\left\|\omega_s-z_s\right\|\\
&+K_a(1+L_h)\left(L_1+M_2L_1a+L_2\right)\int_0^t\sup_{0\le\xi\le s}\left\|\omega_\xi-z_\xi\right\|ds
\end{aligned}
$$

$$\left\|J_2\right\| \leq \int_0^t \left\| \left[D_t q\left(s, \omega_s, \int_0^s h\left(s, \xi, \omega_\xi\right) d\xi\right) - D_t q\left(s, z_s, \int_0^s h\left(s, \xi, z_\xi\right) d\xi\right)\right] \right\| ds$$

$$+ \int_0^t \left\| \left[D_\phi q\left(s, \omega_s, \int_0^s h\left(s, \xi, \omega_\xi\right) d\xi\right) - D_\phi q\left(s, z_s, \int_0^s h\left(s, \xi, z_\xi\right) d\xi\right)\right] \right\| \left\|y_s\right\| ds$$

$$+ \int_0^t \left\|\mathscr{Q}(t-s)\right\| \left\| \left[\mathscr{D} D_t q\left(s, \omega_s, \int_0^s h\left(s, \xi, \omega_\xi\right) d\xi\right) - \mathscr{D} D_t q\left(s, z_s, \int_0^s h\left(s, \xi, z_\xi\right) d\xi\right)\right] \right\| ds$$

$$+ \int_0^t \left\|\mathscr{Q}(t-s)\right\| \left\| \left[\mathscr{D} D_\phi q\left(s, \omega_s, \int_0^s h\left(s, \xi, \omega_\xi\right) d\xi\right) - \mathscr{D} D_\phi q\left(s, z_s, \int_0^s h\left(s, \xi, z_\xi\right) d\xi\right)\right] \right\| \left\|y_s\right\| ds$$

$$+ \int_0^t \left\|\mathscr{Q}(t-s)\right\| \int_0^s \left\|\mathscr{H}(s-\tau)\left[D_t q\left(s, \omega_s, \int_0^s h\left(s, \xi, \omega_\xi\right) d\xi\right)\right.\right.$$

$$\left.\left. - D_t q\left(s, z_s, \int_0^s h\left(s, \xi, z_\xi\right) d\xi\right)\right] \right\| d\tau ds$$

$$+ \int_0^t \left\|\mathscr{Q}(t-s)\right\| \int_0^s \left\|\mathscr{H}(s-\tau)\left[D_\phi q\left(s, \omega_s, \int_0^s h\left(s, \xi, \omega_\xi\right) d\xi\right)\right.\right.$$

$$\left.\left. - D_\phi q\left(s, z_s, \int_0^s h\left(s, \xi, z_\xi\right) d\xi\right)\right] \right\| \left\|y_s\right\| d\tau ds$$

$$\leq M_1 \mathrm{Lip}\left(D_t q\right)\left(1 + L_h\right) \int_0^t \sup_{0 \leq \xi \leq s} \left\|\omega_\xi - z_\xi\right\| ds$$

$$+ M_1 M_3 \mathrm{Lip}\left(D_\phi q\right)\left(1 + L_h\right) \int_0^t \sup_{0 \leq \xi \leq s} \left\|\omega_\xi - z_\xi\right\| ds$$

$$+ \sup_{0 \leq s \leq a} \left\|\mathscr{Q}(s)\right\| \mathrm{Lip}\left(D_t q\right)\left(1 + L_h\right) \int_0^t \sup_{0 \leq \xi \leq s} \left\|\omega_\xi - z_\xi\right\| ds$$

$$+ \sup_{0 \leq s \leq a} \left\|\mathscr{Q}(s)\right\| M_3 \mathrm{Lip}\left(D_\phi q\right)\left(1 + L_h\right) \int_0^t \sup_{0 \leq \xi \leq s} \left\|\omega_\xi - z_\xi\right\| ds$$

$$+ \sup_{0 \leq s \leq a} \left\|\mathscr{Q}(s)\right\| M_2 \mathrm{Lip}\left(D_t q\right)\left(1 + L_h\right) a \int_0^t \sup_{0 \leq \xi \leq s} \left\|\omega_\xi - z_\xi\right\| ds$$

$$+ \sup_{0 \leq s \leq a} \left\|\mathscr{Q}(s)\right\| M_2 M_3 \mathrm{Lip}\left(D_\phi q\right)\left(1 + L_h\right) a \int_0^t \sup_{0 \leq \xi \leq s} \left\|\omega_\xi - z_\xi\right\| ds$$

$$\leq \left[M_1\left(\mathrm{Lip}\left(D_t q\right) + M_3 \mathrm{Lip}\left(D_\phi q\right)\right) + \sup_{0 \leq s \leq a} \left\|\mathscr{Q}(s)\right\| \left(\mathrm{Lip}\left(D_t q\right) + M_3 \mathrm{Lip}\left(D_\phi q\right)\right.\right.$$

$$\left.\left. + M_2 \mathrm{Lip}\left(D_t q\right) a + M_2 M_3 \mathrm{Lip}\left(D_\phi q\right) a\right)\right]\left(1 + L_h\right) \int_0^t \sup_{0 \leq \xi \leq s} \left\|\omega_\xi - z_\xi\right\| ds,$$

$$\begin{aligned}
&\left\|J_3\right\| \\
&\leq \int_0^t \left\|\mathscr{Q}(t-s)\right\| \left\| \left[D_t\varphi\left(s,\omega_s,\int_0^s h(s,\xi,\omega_\xi)\,d\xi\right) - D_t\varphi\left(s,z_s,\int_0^s h(s,\xi,z_\xi)\,d\xi\right)\right] \right\| ds \\
&+ \int_0^t \left\|\mathscr{Q}(t-s)\right\| \left\| \left[D_\phi\varphi\left(s,\omega_s,\int_0^s h(s,\xi,\omega_\xi)\,d\xi\right) - D_\phi\varphi\left(s,z_s,\int_0^s h(s,\xi,z_\xi)\,d\xi\right)\right] \right\| \\
&\left\|y_s\right\| ds \\
&\leq \sup_{0\leq s\leq a}\left\|\mathscr{Q}(s)\right\| \left(\mathrm{Lip}\left(D_t\varphi\right)(1+L_h) + M_3\mathrm{Lip}\left(D_\phi\varphi\right)(1+L_h)\right) \int_0^t \sup_{0\leq\xi\leq s}\left\|\omega_\xi - z_\xi\right\| ds \\
&\leq \sup_{0\leq s\leq a}\left\|\mathscr{Q}(s)\right\| (1+L_h)\left(\mathrm{Lip}\left(D_t\varphi\right) + M_3\mathrm{Lip}\left(D_\phi\varphi\right)\right) \int_0^t \sup_{0\leq\xi\leq s}\left\|\omega_\xi - z_\xi\right\| ds
\end{aligned}$$

where $M_3 = \sup_{0\leq s\leq a}\|y_s\|$. By the values of J_1, J_2, J_3 we have

$$\begin{aligned}
&\sup_{0\leq s\leq t}\left\|\omega_s - z_s\right\| \leq M_1L_1(1+L_h)\sup_{0\leq s\leq t}\left\|\omega_s - z_s\right\| \\
&+ \Big[K_a(1+L_h)(L_1 + M_2L_1a + L_2) \\
&+ M_1\left(\mathrm{Lip}\left(D_tq\right) + M_3\mathrm{Lip}\left(D_\phi q\right)\right)(1+L_h) \\
&+ \sup_{0\leq s\leq a}\left\|\mathscr{Q}(s)\right\|(1+L_h)\left(\left(\mathrm{Lip}\left(D_tq\right) + M_3\mathrm{Lip}\left(D_\phi q\right)\right.\right. \\
&+ M_2\mathrm{Lip}\left(D_tq\right)a + M_2M_3\mathrm{Lip}\left(D_\phi q\right)a\Big) + \mathrm{Lip}\left(D_t\varphi\right) \\
&\left.\left. + M_3\mathrm{Lip}\left(D_\phi\varphi\right)\right)\Big] \int_0^t \sup_{0\leq\xi\leq s}\left\|\omega_\xi - z_\xi\right\| ds \\
&\leq M_1L_1(1+L_h)\sup_{0\leq s\leq t}\left\|\omega_s - z_s\right\| + (1+L_h)\left[K_a(1+L_h)(L_1 + M_2L_1a + L_2)\right. \\
&\left. + b_0\mathrm{Lip}\left(D_tq\right) + c_0\mathrm{Lip}\left(D_\phi q\right) + M_3\mathrm{Lip}\left(D_t\varphi\right) + M_3^2\mathrm{Lip}\left(D_\phi\varphi\right)\right] \\
&\times \int_0^t \sup_{0\leq\xi\leq s}\left\|\omega_\xi - z_\xi\right\| ds
\end{aligned}$$

where $M_3 = \max\left\{\sup_{0\leq s\leq a}\|\mathscr{Q}(t-s)\|, \sup_{0\leq s\leq a}\|y_s\|\right\}$ and $b_0 = M_1 + M_3 + M_2M_3a$, $c_0 = M_1M_3 + M_3^2 + M_2M_3^2a$. Since $M_1L_1(1+L_h) < 1$, we obtain that

$$\sup_{0\leq s\leq t}\left\|\omega_s - z_s\right\| \leq \frac{N}{1-M_1L_1(1+L_h)}\int_0^t \sup_{0\leq\xi\leq s}\left\|\omega_\xi - z_\xi\right\| ds.$$

Where

$N =$

$(1+L_h)\left[K_a(1+L_h)(L_1 + M_2L_1a + L_2) + b_0\mathrm{Lip}\left(D_tq\right) + c_0\mathrm{Lip}\left(D_\phi q\right) + M_3\mathrm{Lip}\left(D_t\varphi\right) + M_3^2\mathrm{Lip}\left(D_\phi\varphi\right)\right]$

. Then by Gronwall Lemma, implies $\omega_t = z_t$ for all $t\in[-r,a]$, which shows $\omega(t)$ is continuously differentiable on $[-r,a]$, consequently $\omega(\cdot)$ is a strict solution of (1).

5. Example

The example of this work, consider the following system

$$\begin{cases} \frac{\partial}{\partial t}\left[\mathscr{U}(t,v)-\int_{-r}^{0}k(t,\mathscr{U}(t+\zeta,v),v)\,d\zeta\right]=\frac{\partial^2}{\partial v^2}\mathscr{U}(t,v) \\ \quad +\int_0^t b(t-\xi)\frac{\partial^2}{\partial v^2}z(\xi,v)\,d\xi+\int_{-r}^{0}f(t,\mathscr{U}(t+\zeta,v),v)\,d\zeta, t\geq 0, v\in[0,1]=J, \\ \mathscr{U}(t,0)-\int_{-r}^{0}k(t,\mathscr{U}(t+\zeta,0),0)\,d\zeta=0, \text{for} t\geq 0, \\ \mathscr{U}(t,1)-\int_{-r}^{0}k(t,\mathscr{U}(t+\zeta,1),1)\,d\zeta=0, \text{for} t\geq 0, \\ \mathscr{U}(\zeta,v)=\mathscr{U}_0(\zeta,v), \text{for} \zeta\in[-r,0], v\in J. \end{cases} \tag{17}$$

Here $\mathscr{U}_0:[-r,0]\times J\to\mathbb{R}$ is the initial map and $k, f:\mathbb{R}^+\times\mathbb{R}^+\times\mathbb{R}\to\mathbb{R}$ are continuous functions, b is locally bounded variation from $\mathbb{R}^+$ to $\mathbb{R}$ and is marked by $b\in BV_{loc}(\mathbb{R}^+,\mathbb{R})$. Now take $\mathscr{E}=C(J:\mathbb{R})$ with the supreme norm and $\mathscr{D}:D(\mathscr{D})\subset\mathscr{E}\to\mathscr{E}$ by

$$\begin{cases} D(\mathscr{D})=\{y\in C^2(J;\mathbb{R}):y(0)=y(1)=0\} \\ \mathscr{D}y=y''. \end{cases}$$

Moreover $\overline{D(\mathscr{D})}=\{y\in\mathscr{E};y(0)=y(1)=0\}\neq\mathscr{E}$. Next the operator $\mathscr{H}:D(\mathscr{D})\subset\mathscr{E}\to\mathscr{E}$ by

$$\begin{cases} D(\mathscr{H}(t))=D(\mathscr{D}) \\ (\mathscr{H}(t)y)(v)=b(t)y''(v), t\geq 0, v\in J. \end{cases}$$

In [44], then $(\mathscr{H}(t))$ is set of bounded operator $D(\mathscr{D})$ to $\mathscr{E}$, $\mathscr{H}(\cdot)y\in BV_{loc}(\mathbb{R};\mathscr{E})$ for any $y\in D(\mathscr{D})$. This implies that (2) has a LLC integrated resolvent operator $(\mathscr{Q}(t))_{t\geq 0}$ on $\mathscr{E}$. In order to reform Eq. (17), let $\mathscr{C}=C([-r,0];\mathscr{E})$ and

$$\begin{aligned} &\omega(t)=\mathscr{U}(t,v)\,\text{for}\,t\geq 0, v\in J \\ &\phi(\zeta)(v)=\mathscr{U}_0(\zeta,v)\,\text{for}\,\zeta\in[-r,0], v\in J \\ &q\left(t,\phi,\int_0^t h(t,s,\omega_s)\,ds\right)=\int_{-r}^{0}k(t,\mathscr{U}(t+\zeta,v),v)\,d\zeta, t\geq 0, v\in J, \phi\in\mathscr{C} \\ &\varphi\left(t,\phi,\int_0^t h(t,s,\omega_s)\,ds\right)=\int_{-r}^{0}f(t,\mathscr{U}(t+\zeta,v),v)\,d\zeta, t\geq 0, v\in J\text{and}\phi\in\mathscr{C}. \end{aligned}$$

Then the Eq. (17) is of the following form

$$\begin{cases} \frac{d}{dt}\left[\omega(t)-q\left(t,\omega_t,\int_0^t h(t,s,\omega_s)\,ds\right)\right]=\mathscr{D}\omega(t)+\int_0^t\mathscr{H}(t-s)\omega(s)\,ds \\ \qquad\qquad +\varphi\left(t,\omega_t,\int_0^t h(t,s,\omega_s)\,ds\right), t\geq 0, \\ \omega(0)=\phi\in\mathscr{C}. \end{cases}$$

To investigate the existence solution of (17), we assume the following

(i) $\mathscr{U}_0\in C([-r,0]\times J;\mathbb{R})$

$\mathscr{U}_0(0,0)-\int_{-r}^{0}k(0,\mathscr{U}_0(\zeta,0),0)\,d\zeta=\mathscr{U}_0(0,1)-\int_{-r}^{0}k(0,\mathscr{U}_0(\zeta,1),1)\,d\zeta=0$

(ii) $\exists, L_k > 0$ and $0 < L_k r < 1$ then

$$\begin{aligned}&\|k(t, x_1, y_1) \\ &- k(t, x_2, y_2)\| \\ &\leq L_k(\|x_1 - x_2\| \\ &+ \|y_1 - y_2\|) \text{ for } t \\ &\geq 0, x_1, x_2 \\ &\in \mathscr{C}, y_1, y_2 \in \mathbb{R}.\end{aligned}$$

(iii) There exist $L_f > 0$ then

$$\begin{aligned}&\|f(t, s_1, v_1) \\ &- f(t, s_2, v_2)\| \\ &\leq L_f(\|s_1 - s_2\| \\ &+ \|v_1 - v_2\|) \text{ for } t \\ &\geq 0, s_1, s_2 \\ &\in \mathscr{C}, v_1, v_2 \in \mathbb{R}.\end{aligned}$$

Hence $\phi \in C([-r, 0]; \mathscr{E})$, $\phi(0) - q(0, \phi, 0) \in \overline{D(\mathscr{D})}$. Further k and q are continuous then from (ii) q is Lipschitzian about second argument. For $t \geq 0$, $\phi_1, \phi_2 \in \mathscr{C}$ such that

$$\begin{aligned}&\left\|q(t, \phi_1, v) - q(t, \phi_2, v)\right\| = \sup_{v\in[0,1]} \left\|q(t, \phi_1(v), v) - q(t, \phi_2(v), v)\right\| \\ &\leq \sup_{v\in[0,1]} \int_{-r}^{0} \left\|k(t, \phi_1(\zeta)(v), v) - k(t, \phi_2(\zeta)(v), v)\right\| d\zeta \\ &\leq L_k \int_{-r}^{0} \sup_{\zeta\in[-r,0], v\in[0,1]} \left\|\phi_1(\zeta)(v) - \phi_2(\zeta)(v)\right\| d\zeta \\ &\leq L_k r \left\|\phi_1 - \phi_2\right\|.\end{aligned}$$

Hence (H1) satisfied, similarly by assumption of (H2) and since f is continuous then hold condition (iii). Thus all the axioms of Theorem 3.4 are verified for the system (17). From the above suppositions, Eq. (17) has a unique integral solution on $[-r, +\infty)$.

6. Conclusion

In this article, we obtained the results for the system of neutral integrodifferential equation (1) with finite delay using integrated resolvent operator and proved the uniqueness by using Banach fixed point theorem and verified the solution is continuously dependence with respect to initial data. Also discussed the existence of strict solution with support of Lipschitz continuous. Further the future will consider the existence results for neutral equation with impulsive condition by support of integrated resolvent operator and Lipschitz continuous.

CRediT authorship contribution statement

K. Munusamy: Writing – original draft, Software. **C. Ravichandran:** Conceptualization, Writing – original draft, Software. **Kottakkaran Sooppy Nisar:** Conceptualization, Writing – original draft, Software. **Shankar Rao Munjam:** Writing – original draft, Formal analysis.

Declaration of competing interest

The authors declare that they have no known competing financial interests or personal relationships that could have appeared to influence the work reported in this paper.

Acknowledgments

This study is supported via funding from Prince Sattam bin Abdulaziz University, Saudi Arabia project number (PSAU/2023/R/1444)

Recommended articles

Data availability

No data was used for the research described in the article.

References

[1] Cannarsa P., Sforza D.
Global solutions of abstract semilinear parabolic equations with memory terms
Nonlinear Differential Equations Appl, 10 (2003), pp. 399-430
View in Scopus ↗ Google Scholar ↗

[2] Lunardi A.
On the linear heat equation with fading memory
SIAM J Math Anal, 21 (5) (1990), pp. 1213-1224
Crossref ↗ Google Scholar ↗

[3] Balachandran K., Dauer J.P.
Existence of solutions of a nonlinear mixed neutral equations
Appl Math Lett, 11 (2) (1998), pp. 23-28
View PDF View article View in Scopus ↗ Google Scholar ↗

[4] Cao N., Fu X.
Existence results of solutions for a neutral evolution equation with nonlocal conditions on infinite interval
J Math Anal Appl, 510 (1) (2022), Article 126008
View PDF View article View in Scopus ↗ Google Scholar ↗

[5] Hernandez E., Henriquez H.R.
Existence results for partial neutral functional differential equations with unbounded delay
J Math Anal Appl, 221 (2) (1998), pp. 452-475
View PDF View article View in Scopus ↗ Google Scholar ↗

[6] Dauer J.P., Balachandran K.
Existence of solutions of nonlinear neutral integrodifferential equations in Banach space
J Math Anal Appl, 251 (1) (2000), pp. 93-105
View PDF View article View in Scopus ↗ Google Scholar ↗

[7] Kucche K.D., Dhakne M.B.

Existence of solution via integral inequality of volterra-fredholm neutral functional integrodifferential equations with infinite delay

Int J Differ Equ Appl (2014), Article 784956

View in Scopus ↗ Google Scholar ↗

[8] Murugesu R., Suguna S.

Existence of solutions for neutral functional integrodifferential equations

Tamkang J Math, 41 (2) (2010), pp. 117-128

Crossref ↗ View in Scopus ↗ Google Scholar ↗

[9] Ezzinbi K., Ghnimi S.

Existence and regularity of solutions for neutral partial functional integrodifferential equations

Nonlinear Anal Real World Appl, 11 (4) (2010), pp. 2335-2344

View PDF View article View in Scopus ↗ Google Scholar ↗

[10] Diao B., Ezzinbi K., Sy M.

Existence results in the α-norm for a class of neutral partial functional integrodifferential equations

Afr Mat, 26 (2015), pp. 1621-1635

Crossref ↗ View in Scopus ↗ Google Scholar ↗

[11] Jothimani K., Kaliraj K., Panda S.K., Nisar K.S., Ravichandran C.

Results on controllability of non-densely characterized neutral fractional delay differential system

Evol Equ Control Theory, 10 (3) (2021), pp. 619-631

Crossref ↗ View in Scopus ↗ Google Scholar ↗

[12] Manoj K., Kumar K., Kumar R.

Existence of mild solution for neutral functional mixed integrodifferential evolution equations with nonlocal conditions

J Abstr Comput Math, 6 (1) (2021), pp. 32-40

Google Scholar ↗

[13] Morsy A., Nisar K.S., Ravichandran C., Anusha C.

Sequential fractional order neutral functional Integro differential equations on time scales with Caputo fractional operator over Banach spaces

AIMS Math, 8 (3) (2023), pp. 5934-5949

View in Scopus ↗ Google Scholar ↗

[14] Ravichandran C., Munusamy K., Nisar K.S., Valliammal N.

Results on neutral partial integrodifferential equations using Monch-Krasnosel'Skii fixed point theorem with nonlocal conditions

Fractal Fract, 6 (2) (2022), p. 75

Crossref ↗ View in Scopus ↗ Google Scholar ↗

[15] Park J.Y., Balachandran K., Annapoorani N.

Existence results for impulsive neutral functional integrodifferential equations with infinite delay

Nonlinear Anal, 71 (7–8) (2009), pp. 3152-3162

View PDF View article View in Scopus ↗ Google Scholar ↗

[16] Vijayaraj V., Ravichandran C., Botmart T., Nisar K.S., Jothimani K.
Existence and data dependence results for neutral fractional order integro-differential equations
AIMS Math, 8 (1) (2023), pp. 1055-1071
Crossref ↗ View in Scopus ↗ Google Scholar ↗

[17] Diop A., Dieye M., Diop M.A., Ezzinbi K.
Integrodifferential equations of volterra type with nonlocal and impulsive conditions
J Integral Equations Appl, 34 (2022), pp. 19-37
View in Scopus ↗ Google Scholar ↗

[18] Ezzinbi K., Ghnimi S., Taoudi M.A.
Existence results for some partial integrodifferential equations with nonlocal conditions
Glas Mat, 51 (71) (2016), pp. 413-430
Crossref ↗ View in Scopus ↗ Google Scholar ↗

[19] Munusamy K., Ravichandran C., Nisar K.S., Ghanbari B.
Existence of solutions for some functional integrodifferential equations with nonlocal conditions
Math Methods Appl Sci, 43 (17) (2020), pp. 10319-10331
Crossref ↗ View in Scopus ↗ Google Scholar ↗

[20] Zhu J., Fu X.
Existence and differentiablity of solutions for nondensely defined neutral integro-differential evolution equations
Bull Malays Math Sci Soc, 46 (2023), p. 30
Google Scholar ↗

[21] Ezzinbi K., Ziat M.
Nonlocal integrodifferential equations without the assumption of equicontinuity on the resolvent operator in Banach spaces
Differ Equ Dyn Syst, 30 (2022), pp. 315-333
Crossref ↗ View in Scopus ↗ Google Scholar ↗

[22] Nisar K.S., Munusamy K., Ravichandran C.
Results on existence of solutions in nonlocal partial functional integrodifferential equations with finite delay in nondense domain
Alex Eng J, 73 (2023), pp. 377-384
View PDF View article View in Scopus ↗ Google Scholar ↗

[23] Nisar K.S., Munusamy K., Ravichandran C., Sabarinathan S.
Interpretation on nonlocal neutral functional differential equations with delay
AIMS Math, 8 (11) (2023), pp. 25611-25632
Crossref ↗ View in Scopus ↗ Google Scholar ↗

[24] Abu Arqub O.
Computational algorithm for solving singular Fredholm time-fractional partial integrodifferential equations with error estimates
J Appl Math Comput, 59 (2019), pp. 227-243

Crossref ↗ View in Scopus ↗ Google Scholar ↗

[25] Abu Arqub O., Rashaideh H.
The RKHS method for numerical treatment for integrodifferential algebraic systems of temporal two-point BVPs
Neutral Comput Appl, 30 (2018), pp. 2595-2606
Crossref ↗ View in Scopus ↗ Google Scholar ↗

[26] Badawi H, Shawagfeh N, Abu Arqub O. Fractional conformable stochastic integrodifferential equations: Existence, uniqueness and numerical simulations utilizing the shifted legendre spectral collocation algorithm. Math Probl Eng 2022:5104350. 21.
Google Scholar ↗

[27] Badawi H., Abu Arqub O., Shawagfeh Nabil
Well-posedness and numerical simulations employing Legendre-shifted spectral approach for Caputo–Fabrizio fractional stochastic integrodifferential equations
Internat J Modern Phys C, 34 (06) (2023), Article 2350070
View in Scopus ↗ Google Scholar ↗

[28] Pazy A.
Semigroups of linear operators and applications to partial differential equations
Springer-verlag, New york (1983)
Google Scholar ↗

[29] Abdulaleem N.
E-univex sets, E-univex functions and E-differentiable E-univex programming
Results Math, 78 (1) (2023), p. 3
View in Scopus ↗ Google Scholar ↗

[30] Abdulaleem N.
Optimality conditions for a class of E-differentiable vector optimization problems with interval-valued objective functions under E-invexity
Int J Comput Math, 100 (7) (2023), pp. 1601-1624
Crossref ↗ View in Scopus ↗ Google Scholar ↗

[31] Abdulaleem N.
Optimality and duality for E-differentiable multiobjective programming problems involving E-type I functions
J Ind Manag Optim, 19 (2) (2023), pp. 1513-1527
Crossref ↗ View in Scopus ↗ Google Scholar ↗

[32] Koumla S., Ezzinbi K., Bahloul R.
Mild solutions for some partial functional integrodifferential equations with finite delay in Frechet spaces
SeMA J, 74 (2017), pp. 489-501
Crossref ↗ View in Scopus ↗ Google Scholar ↗

[33] Ezzinbi K., Ghnimi S.
Solvability of nondensely defined partial functional integrodifferential equations using the integrated resolvent operators
Electron J Qual Theory Differ Equ, 88 (2019), pp. 1-21

Crossref ↗ Google Scholar ↗

[34] Henriquez H.R.
Regularity of solutions of abstract retarded functional differential equations with unbounded delay
Nonlinear Anal, 28 (3) (1997), pp. 513-531
View PDF View article View in Scopus ↗ Google Scholar ↗

[35] Hernandez E., Rolnik V., Ferrari T.M.
Existence and uniqueness of solutions for abstract integro-differential equations with state-dependent delay and applications
Mediterr J Math, 19 (3) (2022), p. 101
View in Scopus ↗ Google Scholar ↗

[36] Hernandez E.
Existence and uniqueness of global solution for abstract second order differential equations with state-dependent delay
Math Nachr, 295 (1) (2022), pp. 124-139
Crossref ↗ View in Scopus ↗ Google Scholar ↗

[37] Ferdausi R., Hossain A., Hasan M., Islam A.
Existence and uniqueness of solutions to system of linear equations and integral equations using Banach fixed point theorem
Int J Adv Res, 6 (3) (2018), pp. 494-500
Crossref ↗ Google Scholar ↗

[38] Desch W., Grimmer R., Schappacher W.
Some considerations for linear integrodifferential equations
J Math Anal Appl, 104 (1) (1984), pp. 219-234
View PDF View article View in Scopus ↗ Google Scholar ↗

[39] Ezzinbi K., Toure H., Zabsonre I.
Existence and regularity of solutions for some partial functional integrodifferential equations in Banach spaces
Nonlinear Anal, 70 (7) (2009), pp. 2761-2771
View PDF View article View in Scopus ↗ Google Scholar ↗

[40] Akdemir A.O., Binh H.D., O'Regan D., Nguyen A.T.
The dependence on fractional orders of mild solutions to the fractional diffusion equation with memory
Math Methods Appl Sci, 46 (1) (2023), pp. 1076-1095
Crossref ↗ View in Scopus ↗ Google Scholar ↗

[41] Belmor S., Ravichandran C., Jarad F.
Nonlinear generalized fractional differential equations with generalized fractional integral conditions
J Taibah Univ Sci, 14 (1) (2020), pp. 114-123
Crossref ↗ View in Scopus ↗ Google Scholar ↗

[42] Da Prato G., Sinestrari E.
Differential operators with non dense domain

Ann Sc Norm Super Pisa Cl Sci (4), 14 (1987), pp. 285-344

Google Scholar ↗

[43] Munusamy K., Ravichandran C., Nisar Kottakkaran Sooppy, Jagatheeshwari R., Valliammal N.
Results on neutral integrodifferential system using Krasnoselskii-Schaefer theorem with initial conditions
AIP Conf Proc, 2718 (1) (2023)

Google Scholar ↗

[44] Oka H.
Integrated resolvent operators
J Integral Equations Appl, 7 (2) (1995), pp. 193-232

View in Scopus ↗ Google Scholar ↗

[45] Kellerman H, Hieber M. Integrated semigroups. 1989;84(1):160–80.

Google Scholar ↗

Cited by (6)

Periodic Boundary Value problem for the Dynamical system with neutral integro-differential equation on time scales

2024, Partial Differential Equations in Applied Mathematics

Show abstract

New investigation on controllability of sobolev-type Volterra-Fredholm functional integro-differential equation with non-local condition

2024, Results in Control and Optimization

> *Citation Excerpt :*
>
> …In the sense of Riemman-Liouville and Caputo, the Atangana–Baleanu derivative are referred as the ABR-derivative and the ABC-derivative, respectively. It improves the relationship between fractional calculus and the Mittag-Leffler function which opens up significant potential in science and engineering including population dynamics, thermal physics, control-related problems and for more Refs. [17–28]. The differential system with sobolev type is frequently found in the mathematical structure of a wide range of physical phenomena including thermodynamics, fluid flow across fissured rocks and so on [29–33].…

Show abstract

Probabilistic analysis of a disturbed SIQP-SI model of mosquito-borne diseases with human quarantine strategy and independent Poisson jumps ↗

2024, Modeling Earth Systems and Environment

Existence and uniqueness of neutral functional differential equations with sequential fractional operators ↗

2024, PLoS ONE

Numerical simulations for fractional Hirota-Satsuma coupled Korteweg-de Vries systems ↗

2024, Open Physics

Analytical and Computational Results for Neutral Impulsive Fractional System on Time Scales ↗
2024, Contemporary Mathematics (Singapore)

Received: 25 October 2020 | Accepted: 29 December 2020

DOI: 10.1002/num.22772

RESEARCH ARTICLE

WILEY

New discussion on approximate controllability results for fractional Sobolev type Volterra-Fredholm integro-differential systems of order $1 < r < 2$

V. Vijayakumar[1] | **Chokkalingam Ravichandran**[2] | **Kottakkaran Sooppy Nisar**[3] | **Kishor D. Kucche**[4]

[1]Department of Mathematics, School of Advanced Sciences, Vellore Institute of Technology, Vellore, Tamil Nadu, India

[2]Post Graduate and Research Department of Mathematics, Kongunadu Arts and Science College(Autonomous), Coimbatore, Tamil Nadu, India

[3]Department of Mathematics, College of Arts and Sciences, Prince Sattam bin Abdulaziz University, Wadi Aldawaser, Saudi Arabia

[4]Department of Mathematics, Shivaji University, Kolhapur, Maharashtra, India

Correspondence

V. Vijayakumar, Department of Mathematics, School of Advanced Sciences, Vellore Institute of Technology, Vellore 632 014, Tamil Nadu, India.
Email: vijaysarovel@gmail.com

Kottakkaran S. Nisar, Department of Mathematics, College of Arts and Sciences, Prince Sattam bin Abdulaziz University, Wadi Aldawaser 11991, Saudi Arabia.
Email: n.sooppy@psau.edu.sa

Abstract

In our article, we are primarily concentrating on approximate controllability results for fractional Sobolev type Volterra-Fredholm integro-differential inclusions of order $1 < r < 2$. By applying the results and ideas belongs to the cosine function of operators, fractional calculus and fixed point approach, the main results are established. Initially, we establish the approximate controllability of the considered fractional system, then continue to examine the system with the concept of nonlocal conditions. In the end, we present an example to demonstrate the theory.

KEYWORDS

approximate controllability, fractional derivative, integro-differential system, nonlocal conditions, Sobolev-type system

1 | INTRODUCTION

Fractional calculus, as a significant area of Mathematics, was initiated in 1695. It was nearly simultaneously as classical calculus. Recently, the ideas about fractional calculus became effectively applied to different regions, and the investigators progressively found that the fractional calculus can well portray several non-local events in the areas of natural science and architecture. Presently, the mainstream

areas of fractional calculus containing rheology, liquid stream, diffusive transport likened to dispersion, dynamical cycles in self-comparable and porous structures, viscoelasticity, and, optics, etc. The effective utilization of the fractional systems in these areas has incited several researchers to contemplate their mathematical estimate strategies, as the diagnostic arrangements are commonly hard to get. For interesting results related to fractional dynamical systems, the readers may refer to the books [1–4] and the articles [5–19].

Control theory is a significant region of utilization situated in Mathematics which manages the structure and examination of control frameworks. Recently, controllability concerns for different sorts of nonlinear dynamical frameworks in infinite dimensional spaces became examined in numerous research articles by utilizing various types of techniques. A broad list of these distributions can be discovered in [6, 9, 11–16, 18–24, 43, 44–50]. The studies about existence and controllability related to fractional evolution system of order $1 < \alpha < 2$ attracted many researchers and one can review the articles [10, 17, 25–33]. The study related to approximate controllability results for fractional Sobolev type Volterra-Fredholm integro-differential inclusions having order $1 < r < 2$ have not been discussed yet and it gives the additional motivation for writing this article.

Motivated by the theory developed in the works mentioned previously, our objective in this article is to discuss the approximate controllability of Sobolev type Volterra-Fredholm integro-differential inclusions of fractional order $r \in (1, 2)$ of the form

$$ {}^{C}D_{\varrho}^{r}\left(Jz\left(\varrho\right)\right) \in Az\left(\varrho\right)+\mathscr{B}x\left(\varrho\right)+E\left(\varrho, z\left(\varrho\right), \int_{0}^{\varrho} e\left(\varrho, s, z\left(s\right)\right) ds, \int_{0}^{c} h\left(\varrho, s, z\left(s\right)\right) ds\right), \quad \varrho \in V = [0, c], \tag{1.1} $$

$$ z\left(0\right) = z_0, \quad z'\left(0\right) = z_1 \in \mathscr{Y}, \tag{1.2} $$

where $z(\cdot)$ takes values in $\mathscr{Y}$ and $\mathscr{Y}$ is a Hilbert space; ${}^{C}D_{\varrho}^{r}$ represents fractional derivative in Caputo sense of order $r \in (1, 2)$, and the control function $x(\cdot) \in L^2\left(V, \mathscr{U}\right)$, a Hilbert space of admissible control functions. A is the infinitesimal generator of a C_0- cosine family $\{C(\varrho)\}_{\varrho \geq 0}$ on $\mathscr{Y}$. $\mathscr{B}$ is a bounded linear operator from $\mathscr{U} \to \mathscr{Y}$. Here $D = \{(\varrho, s) \in V \times V : s \leq \varrho\}$, $e, h : D \times \mathscr{Y} \to \mathscr{Y}$ are continuous, and $E : V \times \mathscr{Y} \times \mathscr{Y} \times \mathscr{Y} \to 2^{\mathscr{Y}} \setminus \{\emptyset\}$ satisfying some conditions.

The arrangement of our article as follows: In Section 2, we recollect several fundamental definitions and few well-known results belong to fractional calculus and multivalued maps. In Section 3, we present the approximate controllability of (1.1)–(1.2) and in Section 4, we examine the system with concept of nonlocal conditions. In Section 5, the theory is validated with suitable example.

2 | BASIC FACTS

We now recollect few well-known results and definitions for proving our main results of this article.

Assume that $C\left(V, \mathscr{Y}\right) : V \to \mathscr{Y}$ be the Hilbert space of continuous functions along with $\|z\| = \sup_{\varrho \in V} \|z(\varrho)\|$, $z \in C\left(V, \mathscr{Y}\right)$. Denote $D(A)$, $R(A)$ be the domain and range of A. $\rho(A)$ stands for the resolvent set of A and we define the resolvent as follows:

$$ R\left(\Lambda, A\right) = \left(\Lambda I - A\right)^{-1} \in L_c\left(\mathscr{Y}\right). $$

A measurable function $g : V \to \mathscr{Y}$ is Bochner's integrable provided $\|g\|$ is Lebesgue. Let $L^p\left(V, \mathscr{Y}\right)$ $(p \geq 1)$ be the Hilbert space of measurable functions endowed along with

$$ \|g\|_p = \left(\int_V \|g\left(\varrho\right)\|^p d\varrho\right)^{\frac{1}{p}}. $$

We now present the linear operators $A : D(A) \subset \mathcal{Y} \to \mathcal{Y}$ and $J : D(A) \subset \mathcal{Y} \to \mathcal{Y}$ satisfy the following properties established in [34]:

($\mathbf{E_1}$) $D(J) \subset D(A)$ and J is bijective.

($\mathbf{E_2}$) The operators A and J are closed linear operators.

($\mathbf{E_3}$) $J^{-1} : \mathcal{Y} \to D(J)$ is continuous.

Additionally, because of ($\mathbf{E_1}$) and ($\mathbf{E_2}$), J^{-1} is closed, by ($\mathbf{E_3}$) and by referring the closed graph theorem, $AJ^{-1} : \mathcal{Y} \to \mathcal{Y}$ is bounded. Denote $\|J^{-1}\| = \widetilde{J}_1$ and $\|J\| = \widetilde{J}_2$.

By referring [1], we introduce definitions and remarks belongs to fractional calculus.

Definition 2.1 The integral of fractional order ν for the function $f : [0, \infty) \to \mathbb{R}$ with lower limit zero is given by

$$I^{\nu} f(\varrho) = \frac{1}{\Gamma(\nu)} \int_0^{\varrho} \frac{f(\imath)}{(\varrho - \imath)^{1-\nu}} d\imath, \quad \varrho > 0, \ \ \nu \in \mathbb{R}^+.$$

Definition 2.2 The R-L derivative of order ν for the function $f : [0, \infty) \to \mathbb{R}$ having lower limit zero is given by

$${}^{L}D^{\nu} f(\varrho) = \frac{1}{\Gamma(n-\nu)} \frac{d^n}{d\varrho^n} \int_0^{\varrho} \frac{f^{(n)}(\imath)}{(\varrho - \imath)^{\nu+1-n}} d\imath, \quad \varrho > 0, \ \ n-1 < \nu < n, \quad \nu \in \mathbb{R}^+.$$

Definition 2.3 The Caputo derivative of order ν for the function f having lower limit zero is given by

$${}^{C}D^{\nu} f(\varrho) = {}^{L}D^{\nu} \left(f(\varrho) - \sum_{j=0}^{n-1} \frac{f^{(j)}(0)}{j!} \varrho^j \right), \quad \varrho > 0, \ \ n-1 < \nu < n, \quad \nu \in \mathbb{R}^+.$$

Remark 2.4 (1) If $f(\varrho) \in C^n[0, \infty)$, then

$${}^{C}D^{\nu} f(\varrho) = \frac{1}{\Gamma(n-\nu)} \int_0^{\varrho} \frac{f^{(n)}(\imath)}{(\varrho - \imath)^{\nu+1-n}} d\imath = I^{n-\nu} f^{(n)}(\varrho), \quad \varrho > 0, \ \ n-1 < \nu < n.$$

(2) The above integrals are considered in Bochner's sense if the function g is abstract with values belonged to $\mathcal{Y}$.

(3) The Caputo derivative of a constant function is equal to zero.

Definition 2.5 [35] The operator $\{C(\varrho)\}_{\varrho \in \mathbb{R}} : \mathcal{Y} \to \mathcal{Y}$ is called a strongly continuous cosine family if and only if

(a) $C(\imath + \varrho) + C(\imath - \varrho) = 2C(\imath)C(\varrho)$, for all $\imath, \varrho \in \mathbb{R}$;

(b) $C(\varrho)z$ is strongly continuous on $\mathbb{R}$ for every $z \in \mathcal{Y}$;

(c) $C(0) = I$.

Assume that the sine family associated with $\{C(\varrho)\}_{\varrho \in \mathbb{R}}$ is $\{S(\varrho)\}_{\varrho \in \mathbb{R}}$, where

$$S(\varrho) z = \int_0^{\varrho} C(\imath) z d\imath, \quad z \in \mathcal{Y}, \quad \varrho \in \mathbb{R}. \tag{2.1}$$

Further, if

$$\left(Az = \frac{d^2}{d\varrho^2} C(\varrho) z \Big|_{\varrho=0}, \quad \textit{for all} \ \ z \in D(A), \right.$$

where

$$D(A) = \left\{ z \in \mathcal{Y} \ : \ C(\varrho) z \in C^2(\mathbb{R}, \mathcal{Y}) \right\}.$$

Determine

$$G = \left\{ z \in \mathcal{Y} \ : \ C(\varrho) z \in C^1(\mathbb{R}, \mathcal{Y}) \right\}.$$

Clearly, A is a closed dense operator in $\mathcal{Y}$, there exists a constant $P \geq 1$ if $\|N(\varrho)\|_{L_c(\mathcal{Y})} \leq P$, where $\varrho \geq 0$. Let us fix $a = \frac{r}{2}$ for $r \in (1, 2)$ which is discussed in [25, 33].

Definition 2.6 The upper semicontinuous (u.s.c) operator $\mathcal{K}$ on $\mathcal{Y}$ provided for all $z_0 \in \mathcal{Y}$ and $\mathcal{K}(z_0)$ is a nonempty closed subset of $\mathcal{Y}$, for each open set $\mathcal{C}$ of $\mathcal{Y}$ including $\mathcal{K}(z_0)$, there exists an open neighborhood $\mathcal{W}$ of z_0 with

$$\mathcal{K}(\mathcal{W}) \subseteq \mathcal{C}.$$

Definition 2.7 $\mathcal{K}$ is completely continuous if $\mathcal{K}(\mathcal{C})$ is relatively compact for each bounded subset $\mathcal{C}$ of $\mathcal{Y}$. If $\mathcal{K}$ is completely continuous and nonempty, then $\mathcal{K}$ is u.s.c., if and only if $\mathcal{K}$ has a closed graph. $\mathcal{K}$ has a fixed point such that there exists $z \in \mathcal{Y}$ such that $z \in \mathcal{K}(z)$.

The fractional system (1.1)–(1.2) is similar to the following system

$$\begin{aligned} z(\varrho) &= J^{-1} z_0 J + J^{-1} z_1 J \varrho \\ &+ \frac{1}{\Gamma(r)} \int_0^{\varrho} (\varrho - \imath)^{r-1} J^{-1} \left[Az(\imath) + E\left(\imath, z(\imath), \int_0^{\imath} e(\imath, s, z(s))\, ds, \int_0^{c} h(\imath, s, z(s))\, ds \right) \right] d\imath \\ &+ \frac{1}{\Gamma(r)} \int_0^{\varrho} (\varrho - \imath)^{r-1} J^{-1} \mathcal{Y} x(\imath)\, d\imath. \end{aligned} \tag{2.2}$$

In view [36] and using Laplace transform, we introduce the solution of (1.1)–(1.2).

Definition 2.8 [36] A function $z \in \mathcal{C} = C(V, \mathcal{Y})$ is called a mild solution of (1.1)–(1.2) if $z(0) = z_0$, $z'(0) = z_1, x(\cdot) \in L^2(V, \mathcal{U})$ and there exists $g \in L^1(V, \mathcal{Y})$ such that $g(\varrho) \in E\left(\varrho, z(\varrho), \int_0^{\varrho} e(\varrho, s, z(s))\, ds, \int_0^{c} h(\varrho, s, z(s))\, ds\right)$ on a.e. $\varrho \in V$ and

$$\begin{aligned} z(\varrho) &= J^{-1} M_a(\varrho) J z_0 + J^{-1} W_a(\varrho) J z_1 + \int_0^{\varrho} (\varrho - \imath)^{a-1} J^{-1} Q_a(\varrho - \imath)\, \mathcal{B} x(\imath)\, d\imath \\ &+ \int_0^{\varrho} (\varrho - \imath)^{a-1} J^{-1} Q_a(\varrho - \imath)\, g(\imath)\, d\imath, \end{aligned} \tag{2.3}$$

where

$$M_a(\varrho) = \int_0^{\infty} S_a(\rho)\, C(\varrho^a \rho)\, d\rho, \quad W_a(\varrho) = \int_0^{\varrho} M_a(\imath)\, d\imath, \quad Q_a(\varrho) = \int_0^{\infty} a\rho S_a(\rho)\, S(\varrho^a \rho)\, d\rho,$$

$$S_a(\rho) = \frac{1}{a} \rho^{-1-\frac{1}{a}} \zeta_a\left(\rho^{-\frac{1}{a}}\right), \quad \zeta_a(\rho) = \frac{1}{\pi} \sum_{n=1}^{\infty} (-1)^{n-1} \rho^{-na-1} \frac{\Gamma(na+1)}{n!} \sin(n\pi a), \quad \rho \in (0, \infty),$$

where $S_a(\cdot)$ is a probability density function defined on $(0, \infty)$ such that

$$S_a(\rho) \geq 0 \ \ \textit{where} \ \ \rho \in (0, \infty) \ \ \textit{also} \ \ \int_0^{\infty} S_a(\rho)\, d\rho = 1.$$

Remark 2.9 Clearly for $n \in [0, 1]$

$$\int_0^{\infty} \rho^n S_a(\rho)\, d\rho = \int_0^{\infty} \rho^{-an} \zeta(\rho)\, d\rho = \frac{\Gamma(1+n)}{\Gamma(1+an)}.$$

Lemma 2.10 [25]. *$M_a(\varrho)$, $W_a(\varrho)$ and $Q_a(\varrho)$ satisfy the following properties:*
(a) for all $\varrho \geq 0$, *$M_a(\varrho)$, $W_a(\varrho)$ and $Q_a(\varrho)$ are linear and bounded;*
(b) $\forall\ z \in \mathcal{Y}$ *and for all* $\varrho \geq 0$, *we have*

$$\|M_a(\rho)z\| \leq P\|z\|, \quad \|W_a(\rho)z\| \leq P\|z\|\rho, \quad \|Q_a(\rho)z\| \leq \frac{P}{\Gamma(2a)}\|z\|\rho^a;$$

(c) $\{M_a(\varrho), \varrho \geq 0\}$, $\{W_a(\varrho), \varrho \geq 0\}$ *and* $\{\varrho^{a-1}Q_a(\varrho), \varrho \geq 0\}$ *are strongly continuous.*

Lemma 2.11 [35].
(i) *If $z \in G$, subsequently $S(\varrho)z \in D(A)$, also;* $\frac{d}{d\varrho}C(\rho)z = AS(\rho)z$;
(ii) There exists $P \geq 1$, $\omega \geq 0$ such that $\|C(\rho)\|_{L_c(\mathcal{Y})} \leq Pe^{\omega|\rho|}$, for all $\varrho \in \mathbb{R}$;
(iii) $\|S(\varrho+\hbar) - S(\varrho)\|_{L_c(\mathcal{Y})} \leq P \mid \int_{\varrho}^{\varrho+\hbar} e^{\omega|\imath|}d\imath \mid$ *for all* $\varrho+\hbar, \varrho \in \mathbb{R}$.

Lemma 2.12 *Assume that* $\{C(\varrho)\}_{\varrho\in\mathbb{R}}$ *on* $\mathcal{Y}$, *then*

$$\lim_{\varrho\to 0}\frac{1}{\varrho}S(\rho)z = z$$

for some $z \in \mathcal{Y}$.

Lemma 2.13 [35] *Suppose* $\{C(\varrho)\}_{\varrho\in\mathbb{R}}$ *on* $\mathcal{Y}$ *satisfying* $\|C(\rho)\|_{L_c(\mathcal{Y})} \leq Pe^{\omega|\varrho|}, \varrho \in \mathbb{R}$. *Subsequently for* $Re\Lambda > \omega$, $\Lambda^2 \in \rho(A)$. *Additionally*

$$\Lambda R\left(\Lambda^2; A\right)z = \int_0^\infty e^{-\Lambda\varrho}C(\rho)zd\varrho, \quad R\left(\Lambda^2; A\right)z = \int_0^\infty e^{-\Lambda\varrho}S(\rho)zd\varrho, \quad \text{for } z \in \mathcal{Y}.$$

We present the essential operators and some useful results as follows:

$$\Gamma_0^c = \int_0^c (c-\imath)^{a-1}J^{-1}Q_a(c-\imath)\mathcal{B}\mathcal{B}^*J^{-1}Q_a^*(c-\imath)d\imath : \mathcal{Y} \to \mathcal{Y},$$
$$R\left(\mu, \Gamma_0^c\right) = \left(\mu I + \Gamma_0^c\right)^{-1} : \mathcal{Y} \to \mathcal{Y},$$

where $\mathcal{B}^*$, $Q_a^*(c)$ stand for adjoints $\mathcal{B}$ and $Q_a(c)$. Now, we come to an end that Γ_0^c is bounded.

We start with the following assumption:
$\mathbf{H_0}$ $\mu R\left(\mu, \Gamma_0^c\right) \to 0$ as $\mu \to 0^+$ in the strong operator topology.
In view of [22], $\mathbf{H_0}$ holds if and only if the linear fractional system

$$\begin{cases} {}^{C}D_{0+}^{r}(Jz(\rho)) \in Az(\rho) + (\mathcal{B}x)(\rho), \ \ \varrho \in V, \\ z(0) = z_0, \ \ z'(0) = z_1 \in \mathcal{Y}, \end{cases} \tag{2.4}$$

is approximately controllable on V.

Lemma 2.14 [36]. *Suppose $BCC(\mathcal{Y})$ be the set of all nonempty, bounded, closed and convex subset of $\mathcal{Y}$, V be a compact real interval. Let E be a multivalued map satisfying $E : V \times \mathcal{Y} \to BCC(\mathcal{Y})$ is measurable to ϱ for every fixed $z \in \mathcal{Y}$, u.s.c. to z for every $\varrho \in V$, and for every $z \in \mathcal{C}$,*

$$S_{E,z} = \left\{ g \in L^1(V, \mathcal{Y}) : g(\rho) \in E\left(\varrho, z(\rho), \int_0^\rho e(\varrho, s, z(s))ds, \int_0^c h(\varrho, s, z(s))ds\right), \varrho \in V \right\}$$

is nonempty. Suppose $\mathcal{M}$ be linear continuous from $L^1(V, \mathcal{Y}) \to \mathcal{C}$, then

$$\mathcal{M}\circ S_E : \mathcal{C} \to BCC(\mathcal{C}), \ \ z \to (\mathcal{M}\circ S_E)(z) = \mathcal{M}\left(S_{E,z}\right),$$

is a closed graph operator in $\mathcal{C} \to \mathcal{C}$.

Lemma 2.15 *Suppose H be a closed, bounded and convex nonempty subset H of $\mathscr{Y}$. Assume $\mathcal{D} : H \to 2^{\mathscr{Y}} \setminus \{\emptyset\}$ is upper semicontinuous with closed, convex values such that $\mathcal{D}(H) \subset H$ and $\mathcal{D}(H)$ is compact, then $\mathcal{D}$ has a fixed point.*

3 | RESULTS ON APPROXIMATE CONTROLLABILITY

We here particularly focusing on approximate controllability of (1.1)–(1.2). Let us introduce the important assumptions to discuss the primary theorems.

$\mathbf{H_1}$ For $\varrho \geq 0$, $\{C(\varrho)\}$ is compact.

$\mathbf{H_2}$ The function $E : V \times \mathscr{Y} \times \mathscr{Y} \times \mathscr{Y} \to BCC(\mathscr{Y})$ is measurable to ϱ, for all $z \in \mathscr{Y}$, u.s.c. to z, for all $\varrho \in V$, and for all $z \in \mathcal{C}$

$$S_{E,z} = \left\{ g \in L^1(V, \mathscr{Y}) : g(\varrho) \in E\big(\varrho, z(\varrho), \int_0^{\varrho} e(\varrho, s, z(s))\, ds, \int_0^{c} h\big(\varrho, s, z(s)\big) ds\big), \varrho \in V \right\},$$

is nonempty.

$\mathbf{H_3}$ For each $(\varrho, s) \in D$, the functions $e(\varrho, s, \cdot), h(\varrho, s, \cdot) : \mathscr{Y} \to \mathscr{Y}$ are continuous and for all $z \in \mathscr{Y}$, $e(\cdot, \cdot, z), h(\cdot, \cdot, z) : D \to \mathscr{Y}$ are strongly measurable.

$\mathbf{H_4}$ For $\alpha > 0$, $z \in \mathcal{C}$ along with $\|z\|_{\mathcal{C}} \leq \alpha$, there exists $v \in (0, b)$ and $L_{g,\alpha}(\cdot) \in L^{\frac{1}{v}}\left(V, \mathbb{R}^+\right)$ such that

$$\sup\left\{ \|g\| : g(\varrho) \in E\big(\varrho, z(\varrho), \int_0^{\varrho} e(\varrho, s, z(s))\, ds, \int_0^{c} h\big(\varrho, s, z(s)\big) ds\big) \right\} \leq L_{g,\alpha}(\varrho),$$

for almost everywhere $\varrho \in V$.

$\mathbf{H_5}$ The function $\iota \to (\varrho - \iota)^{a-1} L_{g,\alpha}(\iota) \in L^1(V, \mathbb{R}^+)$ and there exists a constant $\lambda > 0$ such that

$$\liminf_{\alpha \to \infty} \frac{\int_0^{\varrho} (\varrho - \iota)^{a-1} L_{g,\alpha}(\iota)\, d\iota}{\alpha} = \lambda < +\infty.$$

For discussing the approximate controllability of (1.1)–(1.2), if for all $\mu > 0$, there exists $z(\cdot) \in \mathcal{C}$ such that

$$z(\varrho) = J^{-1} M_a(\varrho) J z_0 + J^{-1} W_a(\varrho) J z_1 + \int_0^{\varrho} (\varrho - \iota)^{a-1} J^{-1} Q_a(\varrho - \iota)\, g(\iota)\, d\iota + \int_0^{\varrho} (\varrho - \iota)^{a-1} J^{-1} Q_a(\varrho - \iota)\, \mathscr{B} x(\iota)\, d\iota, \quad g \in S_{E,z}, \tag{3.1}$$

$$x(\varrho) = \mathscr{B}^* J^{-1} Q_a^*(c - \varrho) R\left(\mu, \Gamma_0^{c}\right) q(z(\cdot)), \tag{3.2}$$

where

$$q(z(\cdot)) = z_c - J^{-1} M_a(c) J z_0 - J^{-1} W_a(c) J z_1 - \int_0^{c} (c - \iota)^{a-1} J^{-1} Q_a(c - \iota)\, g(\iota)\, d\iota.$$

Theorem 3.1 *Assume $\mathbf{H_0}$–$\mathbf{H_5}$ holds, subsequently* (1.1)–(1.2) *has a solution on V provided*

$$\frac{P\widetilde{J}_1}{\Gamma(2a)} \left[1 + \frac{1}{\mu} \left(\frac{P\widetilde{J}_1 P_B}{\Gamma(2a)} \right)^2 \frac{c^{2a}}{2a} \right] \lambda < 1, \tag{3.3}$$

where $P_B = \|\mathscr{B}\|$.

Proof. The fundamental point is to discover conditions for solvability of (3.1) and (3.2) for $\mu > 0$. Now, we prove $\mathcal{R} : \mathcal{C} \to 2^{\mathcal{C}}$ determined by

$$\mathcal{R}(z) = \left\{ z \in \mathcal{C}; m(\varrho) = J^{-1}M_a(\varrho)Jz_0 + J^{-1}W_a(\varrho)Jz_1 + \int_0^{\varrho} (\varrho - \iota)^{a-1}J^{-1}Q_a(\varrho - \iota)\, g(\iota)\, d\iota \right.$$
$$\left. + \int_0^{\varrho} (\varrho - \iota)^{a-1}J^{-1}Q_a(\varrho - \iota)\, \mathscr{B}x(\iota)\, d\iota, g \in S_{E,z} \right\},$$

has a fixed point. We subdivide our proof for simplicity:

Step 1: For all $\mu > 0$, $\mathcal{R}(z)$ is convex for all $z \in \mathcal{C}$. Suppose $m_1, m_2 \in \mathcal{C}$, then there exists g_1, $g_2 \in S_{E,z}$ such that $\varrho \in V$, we have

$$m_i(\varrho) = J^{-1}M_a(\varrho)Jz_0 + J^{-1}W_a(\varrho)Jz_1 + \int_0^{\varrho} (\varrho - \iota)^{a-1}J^{-1}Q_a(\varrho - \iota)\, g_i(\iota)\, d\iota$$
$$+ \int_0^{\varrho} (\varrho - \iota)^{a-1}J^{-1}Q_a(\varrho - \iota)\, \mathscr{B}\mathscr{B}^*J^{-1}Q_a^*(c - \varrho)\, R\left(\mu, \Gamma_0^c\right) \left[z_c - J^{-1}M_a(c)Jz_0 - J^{-1}W_a(c)Jz_1\right.$$
$$\left. - \int_0^{c} (c - \varphi)^{a-1}J^{-1}Q_a(c - \varphi)\, g_i(\varphi)\, d\varphi \right](\iota)\, d\iota, i = 1, 2.$$

Let $0 \le \beta \le 1$, then for each $\rho \in V$ we have

$$(\beta m_1 + (1 - \beta)m_2)(\varrho) = J^{-1}M_a(\varrho)Jz_0 + J^{-1}W_a(\varrho)Jz_1 + \int_0^{\varrho} (\varrho - \iota)^{a-1}J^{-1}Q_a(\varrho - \iota)\left[\beta g_1(\iota)\right.$$
$$\left. + (1 - \beta)g_2(\iota)\right]d\iota + \int_0^{\varrho} (\varrho - \iota)^{a-1}J^{-1}Q_a(\varrho - \iota)\, \mathscr{B}\mathscr{B}^*J^{-1}Q_a^*(c - \varrho)\, R\left(\mu, \Gamma_0^c\right)\left[z_c - J^{-1}M_a(c)Jz_0\right.$$
$$\left. - J^{-1}W_a(c)Jz_1 - \int_0^{c} (c - \varphi)^{a-1}J^{-1}Q_a(c - \varphi)\left[\beta g_1(\varphi) + (1 - \beta)g_2(\varphi)\right]d\varphi\right](\iota)\, d\iota.$$

Since $S_{E,z}$ is convex, $\beta m_1 + (1 - \beta)m_2 \in S_{E,z}$. Hence $\beta m_1 + (1 - \beta)m_2 \in \mathcal{R}(z)$.

Step 2: On the space $\mathcal{C}$, consider $\mathcal{Q}_\alpha = \{z \in \mathcal{C} : \|z\|_{\mathcal{C}} \le \alpha, 0 \le \varrho \le c\}$, $\alpha > 0$. Clearly, $\mathcal{Q}_\alpha$ is bounded, closed and convex set of $\mathcal{C}$. For $\mu > 0$, our property is that there exists $\alpha > 0$ such that

$$\mathcal{R}(\mathcal{Q}_\alpha) \subset \mathcal{Q}_\alpha.$$

If not, then for all $\alpha > 0$, there exists $z^\alpha \in \mathcal{Q}_\alpha$, but $\mathcal{R}(z^\alpha) \notin \mathcal{Q}_\alpha$, i.e.,

$$\|\mathcal{R}(z^\alpha)\|_{\mathcal{C}} \equiv \sup\{\|m^\alpha\|_{\mathcal{C}} : m^\alpha \in (\mathcal{R}z^\alpha)\} > \alpha$$

and

$$m^\alpha(\varrho) = J^{-1}M_a(\varrho)Jz_0 + J^{-1}W_a(\varrho)Jz_1 + \int_0^{\varrho} (\varrho - \iota)^{a-1}J^{-1}Q_a(\varrho - \iota)\, g^\alpha(\iota)\, d\iota$$
$$+ \int_0^{\varrho} (\varrho - \iota)^{a-1}J^{-1}Q_a(\varrho - \iota)\, \mathscr{B}x^\alpha(\iota)\, d\iota,$$

for some $g^\alpha \in S_{E,z^\alpha}$.

Using assumptions $\mathbf{H_3}$ and Lemma 2.10, we have

$$\|x^\alpha(\rho)\| = \|\mathscr{B}^*J^{-1}Q_a^*(c - \varrho)\, R\left(\mu, \Gamma_0^c\right) q(z(\cdot))\|$$
$$= \|\mathscr{B}^*J^{-1}Q_a^*(c - \varrho)\, R\left(\mu, \Gamma_0^c\right)\left[z_c - J^{-1}M_a(c)Jz_0 - J^{-1}W_a(c)Jz_1\right.$$
$$\left. - \int_0^{c} (c - \iota)^{a-1}J^{-1}Q_a(c - \iota)\, g^\alpha(\iota)\, d\iota\right]\|$$

$$\leq \|J^{-1}\|\|\mathscr{B}^*\|\|Q_a^*(c-\varrho)\|\|R\left(\mu,\Gamma_0^c\right)\|\|\Big[z_c - J^{-1}M_a(c)Jz_0 - J^{-1}W_a(c)Jz_1$$
$$- \int_0^c (c-\iota)^{a-1}J^{-1}Q_a(c-\iota)g^{\alpha}(\iota)\,d\iota\Big]\|$$
$$\leq P_B\widetilde{J}_1\left(\frac{P}{\Gamma(2a)}\right)\frac{1}{\mu}\Big[\|z_c\| + \|J^{-1}M_a(c)Jz_0\| + \|J^{-1}W_a(c)Jz_1\|$$
$$+ \int_0^c (c-\iota)^{a-1}\|J^{-1}Q_a(c-\iota)g^{\alpha}(\iota)\|d\iota\Big]$$
$$\leq \frac{1}{\mu}\frac{P\widetilde{J}_1P_B}{\Gamma(2a)}\left[\|z_c\| + \widetilde{J}_1P\widetilde{J}_2\|z_0\| + \widetilde{J}_1Pc\widetilde{J}_2\|z_1\| + \frac{P\widetilde{J}_1}{\Gamma(2a)}\int_0^c (c-\iota)^{2a-1}L_{g,\alpha}(\iota)\,d\iota\right]$$

For such $\mu > 0$, we prove that

$$\alpha < \|(\mathcal{R}z^{\alpha})(\varrho)\| \leq \|J^{-1}M_a(\varrho)Jz_0\| + \|J^{-1}W_a(\varrho)Jz_1\| + \int_0^{\varrho}(\varrho-\iota)^{a-1}\|J^{-1}Q_a(\varrho-\iota)g^{\alpha}(\iota)\|d\iota$$
$$+ \int_0^{\varrho}(\varrho-\iota)^{a-1}\|J^{-1}Q_a(\varrho-\iota)\mathscr{B}x^{\alpha}(\iota)\|d\iota$$
$$\leq \widetilde{J}_1P\widetilde{J}_2\|z_0\| + \widetilde{J}_1P\rho\widetilde{J}_2\|z_1\| + \frac{P\widetilde{J}_1}{\Gamma(2a)}\int_0^{\varrho}(\varrho-\iota)^{2a-1}L_{g,\alpha}(\iota)\,d\iota$$
$$+ \frac{P\widetilde{J}_1P_B}{\Gamma(2a)}\int_0^{\varrho}(\varrho-\iota)^{2a-1}\frac{1}{\mu}\frac{\widetilde{J}_1PP_B}{\Gamma(2a)}\left[\|z_c\| + \widetilde{J}_1P\widetilde{J}_2\|z_0\| + \widetilde{J}_1Pc\widetilde{J}_2\|z_1\|\right.$$
$$\left.+ \frac{P\widetilde{J}_1}{\Gamma(2a)}\int_0^c (c-\iota)^{2a-1}L_{g,\alpha}(\iota)\,d\iota\right]d\iota$$

$$\leq \widetilde{J}_1P\widetilde{J}_2\|z_0\| + \widetilde{J}_1P\varrho\widetilde{J}_2\|z_1\| + \frac{P\widetilde{J}_1}{\Gamma(2a)}\int_0^{\varrho}(\varrho-\iota)^{2a-1}L_{g,\alpha}(\iota)\,d\iota$$
$$+ \frac{1}{\mu}\left(\frac{P\widetilde{J}_1P_B}{\Gamma(2a)}\right)^2\frac{c^{2a}}{2a}\left[\|z_c\| + \widetilde{J}_1P\widetilde{J}_2\|z_0\| + \widetilde{J}_1Pc\widetilde{J}_2\|z_1\| + \frac{P\widetilde{J}_1}{\Gamma(2a)}\int_0^c (c-\iota)^{2a-1}L_{g,\alpha}(\iota)\,d\iota\right]. \tag{3.4}$$

Dividing the Equation (3.4) by α, applying limit as $\alpha \to \infty$ to the above inequality and utilizing $\mathbf{H_4}$, we obtain

$$\frac{P\widetilde{J}_1}{\Gamma(2a)}\left[1 + \frac{1}{\mu}\left(\frac{P\widetilde{J}_1P_B}{\Gamma(2a)}\right)^2\frac{c^{2a}}{2a}\right]\lambda \geq 1,$$

which contradicts our assumption. Hence $\mu > 0$, there exists $\alpha > 0$ such that $\mathcal{R}$ maps $Q_{\alpha} \to Q_{\alpha}$.

Step 3: $\mathcal{R}$ mapping bounded sets into equicontinuous sets of C.

For all $m \in \mathcal{R}(z)$ and $z \in Q_{\alpha}$, there exists $g \in S_{E,z}$, we define

$$m(\varrho) = J^{-1}M_a(\varrho)Jz_0 + J^{-1}W_a(\varrho)Jz_1 + \int_0^{\varrho}(\varrho-\iota)^{a-1}J^{-1}Q_a(\varrho-\iota)g(\iota)\,d\iota$$
$$+ \int_0^{\varrho}(\varrho-\iota)^{a-1}J^{-1}Q_a(\varrho-\iota)\mathscr{B}x(\iota)\,d\iota.$$

Let $0 < \epsilon < \varrho < \varrho + h \leq c$.

Then,

$$\|m(\varrho+h) - m(\varrho)\| \leq \|J^{-1}[M_a(\varrho+h) - M_a(\varrho)]Jz_0\| + \|J^{-1}[W_a(\varrho+h) - W_a(\varrho)]Jz_1\|$$

$$
\begin{aligned}
&+\int_{\varrho}^{\varrho+h}(\varrho+h-\imath)^{a-1}\|J^{-1}Q_a(\varrho+h-\imath)\,g(\imath)\|d\imath\\
&+\int_{\varrho-\epsilon}^{\varrho}(\varrho+h-\imath)^{a-1}\|\left[J^{-1}Q_a(\varrho+h-\imath)-J^{-1}Q_a(\varrho-\imath)\right]g(\imath)\|d\imath\\
&+\int_{\varrho-\epsilon}^{\varrho}\left[(\varrho+h-\imath)^{a-1}-(\varrho-\imath)^{a-1}\right]\|J^{-1}Q_a(\varrho-\imath)\,g(\imath)\|d\imath\\
&+\int_{0}^{\varrho-\epsilon}(\varrho+h-\imath)^{a-1}\|\left[J^{-1}Q_a(\varrho+h-\imath)-J^{-1}Q_a(\varrho-\imath)\right]g(\imath)\|d\imath\\
&+\int_{0}^{\varrho-\epsilon}\left[(\varrho+h-\imath)^{a-1}-(\varrho-\imath)^{a-1}\right]\|J^{-1}Q_a(\varrho-\imath)\,g(\imath)\|d\imath\\
&+\int_{\varrho}^{\varrho+h}(\varrho+h-\imath)^{a-1}\|J^{-1}Q_a(\varrho+h-\imath)\,\mathscr{B}x(\imath)\|d\imath\\
&+\int_{\varrho-\epsilon}^{\varrho}(\varrho+h-\imath)^{a-1}\|\left[J^{-1}Q_a(\varrho+h-\imath)-J^{-1}Q_a(\varrho-\imath)\right]\mathscr{B}x(\imath)\|d\imath\\
&+\int_{\varrho-\epsilon}^{\varrho}\left[(\varrho+h-\imath)^{a-1}-(\varrho-\imath)^{a-1}\right]\|J^{-1}Q_a(\varrho-\imath)\,\mathscr{B}x(\imath)\|d\imath\\
&+\int_{0}^{\varrho-\epsilon}(\varrho+h-\imath)^{a-1}\|\left[J^{-1}Q_a(\varrho+h-\imath)-J^{-1}Q_a(\varrho-\imath)\right]\mathscr{B}x(\imath)\|d\imath\\
&+\int_{0}^{\varrho-\epsilon}\left[(\varrho+h-\imath)^{a-1}-(\varrho-\imath)^{a-1}\right]\|J^{-1}Q_a(\varrho-\imath)\,\mathscr{B}x(\imath)\|d\imath\\
&=\sum_{i=1}^{12}\mathcal{O}_i.
\end{aligned}
$$

Let $b=\frac{2a-1}{1-v}\in(-1,0)$. By applying $\mathbf{H_1}$, $\mathbf{H_3}$ and Lemma 2.10 for $\mathcal{O}_3,\mathcal{O}_4,\mathcal{O}_5,\mathcal{O}_6$ and $\mathcal{O}_7$, we have

$$
\begin{aligned}
\mathcal{O}_3&\le\frac{P\widetilde{J}_1}{\Gamma(2a)}\int_{\varrho}^{\varrho+h}(\varrho+h-\imath)^{2a-1}\|g(\imath)\|d\imath\\
&\le\frac{P\widetilde{J}_1}{\Gamma(2a)}\int_{\varrho}^{\varrho+h}(\varrho+h-\imath)^{2a-1}L_{g,\alpha}(\imath)\,d\imath\\
&\le\frac{P\widetilde{J}_1}{\Gamma(2a)}\left(\int_{\varrho}^{\varrho+h}(\varrho+h-\imath)^{\frac{2a-1}{1-v}}d\imath\right)^{1-v}\|L_{g,\alpha}\|_{L^{\frac{1}{v}}\left(V,\mathbb{R}^+\right)}\\
&\le\frac{P\widetilde{J}_1}{\Gamma(2a)}\left[\frac{h^{(b+1)(1-v)}}{(b+1)^{1-v}}\right]\|L_{g,\alpha}\|_{L^{\frac{1}{v}}\left(V,\mathbb{R}^+\right)},
\end{aligned}
$$

$$
\begin{aligned}
\mathcal{O}_4&\le\frac{2P\widetilde{J}_1}{\Gamma(2a)}\int_{\varrho-\epsilon}^{\varrho}(\varrho+h-\imath)^{2a-1}\|g(\imath)\|d\imath\\
&\le\frac{2P\widetilde{J}_1}{\Gamma(2a)}\int_{\varrho-\epsilon}^{\varrho}(\varrho+h-\imath)^{2a-1}L_{g,\alpha}(\imath)\,d\imath\\
&\le\frac{2P\widetilde{J}_1}{\Gamma(2a)}\left(\int_{\varrho-\epsilon}^{\varrho}(\varrho+h-\imath)^{\frac{2a-1}{1-v}}d\imath\right)^{1-v}\|L_{g,\alpha}\|_{L^{\frac{1}{v}}\left(V,\mathbb{R}^+\right)}
\end{aligned}
$$

$$\leq \frac{2P\widetilde{J}_1}{\Gamma(2a)}\left[\frac{\epsilon^{(b+1)(1-v)}}{(b+1)^{1-v}}\right]\|L_{g,\alpha}\|_{L^{\frac{1}{v}}\left(V,\mathbb{R}^+\right)},$$

$$\begin{aligned}\mathcal{O}_5 &\leq \frac{P\widetilde{J}_1}{\Gamma(2a)}\int_{\varrho-\epsilon}^{\varrho}\left[(\varrho+h-\iota)^{2a-1}-(\varrho-\iota)^{2a-1}\right]\|g(\iota)\|d\iota\\ &\leq \frac{P\widetilde{J}_1}{\Gamma(2a)}\left(\int_{\varrho-\epsilon}^{\varrho}\left[(\varrho+h-\iota)^{2a-1}-(\varrho-\iota)^{2a-1}\right]^{\frac{1}{1-v}}d\iota\right)^{1-v}\|L_{g,\alpha}\|_{L^{\frac{1}{v}}\left(V,\mathbb{R}^+\right)}\\ &\leq \frac{P\widetilde{J}_1}{\Gamma(2a)}\left[\frac{2h^{(b+1)(1-v)}}{(b+1)^{1-v}}\right]\|L_{g,\alpha}\|_{L^{\frac{1}{v}}\left(V,\mathbb{R}^+\right)},\end{aligned}$$

$$\begin{aligned}\mathcal{O}_6 &\leq \sup_{\iota\in[0,\varrho-\epsilon]}\|J^{-1}Q_a(\varrho+h-\iota)-J^{-1}Q_a(\varrho-\iota)\|\int_0^{\varrho-\epsilon}(\varrho+h-\iota)^{2a-1}\|g(\iota)\|d\iota\\ &\leq \sup_{\iota\in[0,\varrho-\epsilon]}\|J^{-1}Q_a(\varrho+h-\iota)-J^{-1}Q_a(\varrho-\iota)\|\int_0^{\varrho-\epsilon}(\varrho+h-\iota)^{2a-1}L_{g,\alpha}(\iota)\,d\iota\\ &\leq \sup_{\iota\in[0,\varrho-\epsilon]}\|J^{-1}Q_a(\varrho+h-\iota)-J^{-1}Q_a(\varrho-\iota)\|\left(\int_0^{\varrho-\epsilon}(\varrho+h-\iota)^{\frac{2a-1}{1-v}}d\iota\right)^{1-v}\|L_{g,\alpha}\|_{L^{\frac{1}{v}}\left(V,\mathbb{R}^+\right)}\\ &\leq \sup_{\iota\in[0,\varrho-\epsilon]}\|J^{-1}Q_a(\varrho+h-\iota)-J^{-1}Q_a(\varrho-\iota)\|\frac{\left[(\varrho+h)^{b+1}-(h+\epsilon)^{b+1}\right]^{1-v}}{(b+1)^{1-v}}\|L_{g,\alpha}\|_{L^{\frac{1}{v}}\left(V,\mathbb{R}^+\right)},\end{aligned}$$

$$\begin{aligned}\mathcal{O}_7 &\leq \frac{P\widetilde{J}_1}{\Gamma(2a)}\int_0^{\varrho-\epsilon}\left[(\varrho+h-\iota)^{2a-1}-(\varrho-\iota)^{2a-1}\right]\|g(\iota)\|d\iota\\ &\leq \frac{P\widetilde{J}_1}{\Gamma(2a)}\int_0^{\varrho-\epsilon}\left[(\varrho+h-\iota)^{2a-1}-(\varrho-\iota)^{2a-1}\right]L_{g,\alpha}(\iota)\,d\iota\\ &\leq \frac{P\widetilde{J}_1}{\Gamma(2a)}\left(\int_0^{\varrho-\epsilon}\left[(\varrho+h-\iota)^{2a-1}-(\varrho-\iota)^{2a-1}\right]^{\frac{1}{1-v}}d\iota\right)^{1-v}\|L_{g,\alpha}\|_{L^{\frac{1}{v}}\left(V,\mathbb{R}^+\right)}\\ &\leq \frac{P\widetilde{J}_1}{\Gamma(2a)}\left[\frac{2h^{(b+1)(1-v)}}{(b+1)^{1-v}}\right]\|L_{g,\alpha}\|_{L^{\frac{1}{v}}\left(V,\mathbb{R}^+\right)},\end{aligned}$$

For $\mathcal{O}_8, \mathcal{O}_9, \mathcal{O}_{10}, \mathcal{O}_{11}$ and $\mathcal{O}_{12}$, using the $\mathbf{H_1}$, $\mathbf{H_3}$ and Lemma 2.10

$$\begin{aligned}\mathcal{O}_8 &\leq \frac{P\widetilde{J}_1}{\Gamma(2a)}\int_{\varrho}^{\varrho+h}(\varrho+h-\iota)^{2a-1}\|\mathcal{B}x(\iota)\|d\iota\\ &\leq \frac{P\widetilde{J}_1P_B}{\Gamma(2a)}\int_{\varrho}^{\varrho+h}(\varrho+h-\iota)^{2a-1}\|x(\iota)\|d\iota\\ &\leq \frac{P\widetilde{J}_1P_B}{\Gamma(2a)}\left(\int_{\varrho}^{\varrho+h}(\varrho+h-\iota)^{\frac{2a-1}{1-v}}d\iota\right)^{1-v}\|x\|\\ &\leq \frac{P\widetilde{J}_1P_B}{\Gamma(2a)}\left[\frac{h^{(b+1)(1-v)}}{(b+1)^{1-v}}\right]\|x\|,\end{aligned}$$

$$\begin{aligned}\mathcal{O}_9 &\leq \frac{2P\widetilde{J}_1}{\Gamma(2a)}\int_{\varrho-\epsilon}^{\varrho}(\varrho+h-\iota)^{2a-1}\|\mathcal{B}x(\iota)\|d\iota\\ &\leq \frac{2P\widetilde{J}_1P_B}{\Gamma(2a)}\int_{\varrho-\epsilon}^{\varrho}(\varrho+h-\iota)^{2a-1}\|x(\iota)\|d\iota\end{aligned}$$

$$\leq \frac{2P\widetilde{J}_1 P_B}{\Gamma(2a)} \left(\int_{\varrho-\epsilon}^{\varrho} (\varrho+h-\imath)^{\frac{2a-1}{1-v}} d\imath \right)^{1-v} \|x\|$$
$$\leq \frac{2P\widetilde{J}_1 P_B}{\Gamma(2a)} \left[\frac{\epsilon^{(b+1)(1-v)}}{(b+1)^{1-v}} \right] \|x\|,$$

$$\mathcal{O}_{10} \leq \frac{P\widetilde{J}_1}{\Gamma(2a)} \int_{\varrho-\epsilon}^{\varrho} \left[(\varrho+h-\imath)^{2a-1} - (\varrho-\imath)^{2a-1} \right] \|\mathscr{B}x(\imath)\| d\imath$$
$$\leq \frac{P\widetilde{J}_1 P_B}{\Gamma(2a)} \int_{\varrho-\epsilon}^{\varrho} \left[(\varrho+h-\imath)^{2a-1} - (\varrho-\imath)^{2a-1} \right] \|x(\imath)\| d\imath$$
$$\leq \frac{P\widetilde{J}_1 P_B}{\Gamma(2a)} \left(\int_{\varrho-\epsilon}^{\varrho} \left[(\varrho+h-\imath)^{2a-1} - (\varrho-\imath)^{2a-1} \right]^{\frac{1}{1-v}} d\imath \right)^{1-v} \|x\|$$
$$\leq \frac{P\widetilde{J}_1 P_B}{\Gamma(2a)} \left[\frac{2h^{(b+1)(1-v)}}{(b+1)^{1-v}} \right] \|x\|,$$

$$\mathcal{O}_{11} \leq \sup_{\imath\in[0,\varrho-\epsilon]} \|J^{-1}Q_a(\varrho+h-\imath) - J^{-1}Q_a(\varrho-\imath)\| \int_0^{\varrho-\epsilon} (\varrho+h-\imath)^{2a-1} \|\mathscr{B}x(\imath)\| d\imath$$
$$\leq P_B \sup_{\imath\in[0,\varrho-\epsilon]} \|J^{-1}Q_a(\varrho+h-\imath) - J^{-1}Q_a(\varrho-\imath)\| \int_0^{\varrho-\epsilon} (\varrho+h-\imath)^{2a-1} \|x(\imath)\| d\imath$$
$$\leq P_B \sup_{\imath\in[0,\varrho-\epsilon]} \|J^{-1}Q_a(\varrho+h-\imath) - J^{-1}Q_a(\varrho-\imath)\| \left(\int_0^{\varrho-\epsilon} (\varrho+h-\imath)^{\frac{2a-1}{1-v}} d\imath \right)^{1-v} \|x\|$$
$$\leq P_B \sup_{\imath\in[0,\varrho-\epsilon]} \|J^{-1}Q_a(\varrho+h-\imath) - J^{-1}Q_a(\varrho-\imath)\| \frac{\left[(\varrho+h)^{b+1} - (h+\epsilon)^{b+1} \right]^{1-v}}{(b+1)^{1-v}} \|x\|,$$

$$\mathcal{O}_{12} \leq \frac{P\widetilde{J}_1}{\Gamma(2a)} \int_0^{\varrho-\epsilon} \left[(\varrho+h-\imath)^{2a-1} - (\varrho-\imath)^{2a-1} \right] \|\mathscr{B}x(\imath)\| d\imath$$
$$\leq \frac{P\widetilde{J}_1 P_B}{\Gamma(2a)} \int_0^{\varrho-\epsilon} \left[(\varrho+h-\imath)^{2a-1} - (\varrho-\imath)^{2a-1} \right] \|x(\imath)\| d\imath$$
$$\leq \frac{P\widetilde{J}_1 P_B}{\Gamma(2a)} \left(\int_0^{\varrho-\epsilon} \left[(\varrho+h-\imath)^{2a-1} - (\varrho-\imath)^{2a-1} \right]^{\frac{1}{1-v}} d\imath \right)^{1-v} \|x\|$$
$$\leq \frac{P\widetilde{J}_1 P_B}{\Gamma(2a)} \left[\frac{2h^{(b+1)(1-v)}}{(b+1)^{1-v}} \right] \|x\|.$$

It is easy to verify $\mathcal{O}_3$-$\mathcal{O}_5, \mathcal{O}_7$-$\mathcal{O}_{10}, \mathcal{O}_{12} \to 0$ as $h \to 0$. Additionally, by referring the compactness of $T(\varrho), \mathcal{O}_1, \mathcal{O}_2, \mathcal{O}_6, \mathcal{O}_{11}$ tends to zero. Therefore

$$\|m(\varrho+h) - m(\varrho)\| \to 0$$

when $h \to 0$ for all $z \in \mathcal{Q}_\alpha$, which implies $\mathcal{R}(\mathcal{Q}_\alpha) \subset \mathcal{C}$ is equicontinuous.

Step 4: For $\alpha > 0$, fix $W_\alpha = \{z \in \mathscr{Y} : |z| \leq \alpha\}$. Clearly, W_α a bounded subset in $\mathscr{Y}$. To prove for all $\alpha > 0$ and $\rho > 0$,

$$\mathcal{U}(\varrho) = \left\{ \int_0^{\infty} a\rho J^{-1} S_a(\rho) S(\varrho^a \rho) z d\rho, \;\; z \in W_\alpha \right\},$$

are relatively compact in $\mathscr{Y}$.

Assume that $\rho > 0$ be determined. For every $\delta > 0$, $0 < \varepsilon \leq \varrho$, determine a subset in $\mathscr{Y}$ by

$$\mathscr{U}_{\varepsilon,\delta}(\varrho) = \left\{ \frac{S(\varepsilon^a \delta)}{\varepsilon^a \delta} \int_\delta^\infty a\rho J^{-1} S_a(\rho) S(\varrho^a \rho - \varepsilon^a \delta) z d\rho, \quad z \in W_\alpha \right\}.$$

Clearly for every $\varrho > 0$, $\mathscr{U}_{\varepsilon,\delta}(\varrho)$ is clearly defined. Indeed, referring uniform convergence of Mainardi's Wright-type function $\rho \in (\delta, \infty)$ and uniform boundedness of cosine family and, we get for every $z \in W_\alpha$,

$$\begin{aligned}
&\left| \frac{S(\varepsilon^a \delta)}{\varepsilon^a \delta} \int_\delta^\infty a\rho J^{-1} S_a(\rho) S(\varrho^a \rho - \varepsilon^a \delta) z d\rho \right| \leq \widetilde{J}_1 P^2 \mid z \mid \int_\delta^\infty a\rho S_a(\rho) (\varrho^a \rho + \varepsilon^a \delta) d\rho \\
&\quad \leq 2\widetilde{J}_1 P^2 \mid z \mid \varrho^a \int_\delta^\infty a\rho^2 S_a(\rho) d\rho \leq \frac{2\widetilde{J}_1 P^2}{\Gamma(2a)} \mid z \mid \varrho^a.
\end{aligned}$$

Therefore, $\mathscr{U}_{\varepsilon,\delta}(\varrho)$ is relatively compact because $S(\varepsilon^a \delta)$ is compact for $\varepsilon^a \delta > 0$.

Additionally,

$$\begin{aligned}
&\left| \frac{S(\varepsilon^a \delta)}{\varepsilon^a \delta} \int_\delta^\infty a\rho J^{-1} S_a(\rho) S(\varrho^a \rho - \varepsilon^a \delta) z d\rho - \int_0^\infty a\rho J^{-1} S_a(\rho) S(\varrho^a \rho) z d\rho \right| \\
&\leq \left| \frac{S(\varepsilon^a \delta)}{\varepsilon^a \delta} \int_\delta^\infty a\rho J^{-1} S_a(\rho) S(\varrho^a \rho - \varepsilon^a \delta) z d\rho - \int_0^\infty a\rho J^{-1} S_a(\rho) S(\varrho^a \rho) z d\rho \right| \\
&\quad + \left| \int_\delta^\infty a\rho J^{-1} S_a(\rho) S(\varrho^a \rho) z d\rho - \int_0^\infty a\rho J^{-1} S_a(\rho) S(\varrho^a \rho) z d\rho \right| \\
&\leq \int_\delta^\infty a\rho \widetilde{J}_1 S_a(\rho) \left| \frac{S(\varepsilon^a \delta)}{\varepsilon^a \delta} S(\varrho^a \rho - \varepsilon^a \delta) z - S(\varrho^a \rho) z \right| d\rho + \int_0^\delta a\rho \widetilde{J}_1 S_a(\rho) \mid S(\varrho^a \rho) z \mid d\rho \\
&:= l_1 + l_2.
\end{aligned}$$

Since

$$a\rho \widetilde{J}_1 S_a(\rho) \left| \frac{S(\varepsilon^a \delta)}{\varepsilon^a \delta} S(\varrho^a \rho - \varepsilon^a \delta) z - S(\varrho^a \rho) z \right| \leq 2\widetilde{J}_1 P^2 \varrho^a a\rho^2 S_a(\rho) \mid z \mid,$$

and

$$\int_0^\infty a\rho^2 \widetilde{J}_1 S_a(\rho) d\rho = \frac{2\widetilde{J}_1}{\Gamma(1+2a)},$$

we can see that

$$\int_0^\infty a\rho \widetilde{J}_1 S_a(\rho) \left| \frac{S(\varepsilon^a \delta)}{\varepsilon^a \delta} S(\varrho^a \rho - \varepsilon^a \delta) z - S(\varrho^a \rho) z \right| d\rho,$$

is uniformly convergence. Since from the strongly continuous of sine family $\{S(\varrho)\}_{\varrho > 0}$, where $\rho \in (\delta, \infty)$, by referring Lemma 2.12, we have

$$\begin{aligned}
&\left| \frac{S(\varepsilon^a \delta)}{\varepsilon^a \delta} S(\varrho^a \rho - \varepsilon^a \delta) z - S(\varrho^a \rho) z \right| \\
&\quad \leq \left| \frac{S(\varepsilon^a \delta)}{\varepsilon^a \delta} S(\varrho^a \rho - \varepsilon^a \delta) z - S(\varrho^a \rho - \varepsilon^a \delta) z \right| + |S(\varrho^a \rho - \varepsilon^a \delta) z - S(\varrho^a \rho) z| \to 0,
\end{aligned}$$

when $\delta \to 0$. Therefore, we have

$$l_1 \leq \int_0^\infty a\rho \widetilde{J}_1 S_a(\rho) \left| \frac{S(\varepsilon^a \delta)}{\varepsilon^a \delta} S(\varrho^a \rho - \varepsilon^a \delta) z - S(\varrho^a \rho) z \right| d\rho \to 0, \quad \text{as } \delta \to 0.$$

However, by $\int_0^\delta a\rho^2 \widetilde{J}_1 S_a(\rho) d\rho \to 0$ when $\delta \to 0$, we have

$$l_2 \leq \widetilde{J}_1 P \mid z \mid \rho^a \int_0^\delta a\rho^2 S_a(\rho) d\rho \to 0, \quad \text{when } \delta \to 0.$$

Thus, there are relatively compact sets arbitrarily close to $\mathcal{U}(\varrho)$, for all $\varrho > 0$. Thus $\mathcal{U}(\varrho)$ is relatively compact in $\mathcal{Y}$, for all $\varrho > 0$.

Step 5: $\mathcal{R}$ has a closed graph.

Assume that $z^n \to z^*$ when $n \to \infty$, and $m^n \to m^*$ when $n \to \infty$. We shall prove that $m^* \in \mathcal{R}(z^*)$. Since $m^n \in \mathcal{R}(z^n)$, there exists $g^n \in S_{E,z^n}$ such that

$$\begin{aligned} m^n(\varrho) &= J^{-1}M_a(\varrho)Jz_0 + J^{-1}W_a(\varrho)Jz_1 + \int_0^\varrho (\varrho-\iota)^{a-1}J^{-1}Q_a(\varrho-\iota)g^n(\iota)\,d\iota \\ &\quad + \int_0^\varrho (\varrho-\iota)^{a-1}J^{-1}Q_a(\varrho-\iota)\mathcal{B}\mathcal{B}^*J^{-1}Q_a^*(c-\varrho)R\left(\mu,\Gamma_0^c\right)\left[z_c - J^{-1}M_a(c)Jz_0\right. \\ &\quad \left. - J^{-1}W_a(c)Jz_1 - \int_0^c (c-\varphi)^{a-1}J^{-1}Q_a(c-\varphi)g^n(\varphi)\,d\varphi\right](\iota)\,d\iota. \end{aligned}$$

We need to show that there exists $g^* \in S_{E,z^*}$ such that for all $\varrho \in V$,

$$\begin{aligned} m^*(\varrho) &= J^{-1}M_a(\varrho)Jz_0 + J^{-1}W_a(\varrho)Jz_1 + \int_0^\varrho (\varrho-\iota)^{a-1}J^{-1}Q_a(\varrho-\iota)g^*(\iota)\,d\iota \\ &\quad + \int_0^\varrho (\varrho-\iota)^{a-1}J^{-1}Q_a(\varrho-\iota)\mathcal{B}\mathcal{B}^*J^{-1}Q_a^*(c-\varrho)R\left(\mu,\Gamma_0^c\right) \\ &\quad \times \left[z_c - J^{-1}M_a(c)Jz_0 - J^{-1}W_a(c)Jz_1 - \int_0^c (c-\varphi)^{a-1}J^{-1}Q_a(c-\varphi)g^*(\varphi)\,d\varphi\right](\iota)\,d\iota, \end{aligned}$$

clearly,

$$\begin{aligned} &\left\|\left(m^n(\varrho) - J^{-1}M_a(\varrho)Jz_0 - J^{-1}W_a(\varrho)Jz_1 - \int_0^\varrho (\varrho-\iota)^{a-1}J^{-1}Q_a(\varrho-\iota)\mathcal{B}\mathcal{B}^*J^{-1}Q_a^*(c-\varrho)\right.\right. \\ &(\times)R\left(\mu,\Gamma_0^c\right)\left[z_c - J^{-1}M_a(c)Jz_0 - J^{-1}W_a(c)Jz_1 - \int_0^c (c-\varphi)^{a-1}J^{-1}Q_a(c-\varphi)g^n(\varphi)\,d\varphi\right](\iota)\,d\iota\Big) \\ &\quad - \left(m^*(\varrho) - J^{-1}M_a(\varrho)Jz_0 - J^{-1}W_a(\varrho)Jz_1 - \int_0^\varrho (\varrho-\iota)^{a-1}J^{-1}Q_a(\varrho-\iota)\mathcal{B}\mathcal{B}^*J^{-1}Q_a^*(c-\varrho)\right. \\ &(\times)R\left(\mu,\Gamma_0^c\right)\left[z_c - J^{-1}M_a(c)Jz_0 - J^{-1}W_a(c)Jz_1 - \int_0^c (c-\varphi)^{a-1}J^{-1}Q_a(c-\varphi)g^*(\varphi)\,d\varphi\right](\iota)\,d\iota\Big)\Big\| \end{aligned}$$

$\to 0$ as $n \to \infty$. Assume that $\mathcal{T} : L^1(V,\mathcal{Y}) \to \mathcal{C}$,

$$\begin{aligned} (\mathcal{T}g)(\varrho) &= \int_0^\varrho (\varrho-\iota)^{a-1}J^{-1}Q_a(\varrho-\iota)\left[g^n(\iota) + \mathcal{B}\mathcal{B}^*J^{-1}Q_a^*(c-\varrho)R\left(\mu,\Gamma_0^c\right)\right. \\ &\quad \left.\times\left(\int_0^c (c-\varphi)^{a-1}J^{-1}Q_a(c-\varphi)g^*(\varphi)\,d\varphi\right)(\iota)\right]d\iota \end{aligned}$$

clearly, from Lemma 2.14, that $\mathcal{T}\circ S_{E,z}$ is a closed graph operator. Additionally, by referring $\mathcal{T}$, we have

$$\begin{aligned} &\left(m^n(\varrho) - J^{-1}M_a(\varrho)Jz_0 - J^{-1}W_a(\varrho)Jz_1 - \int_0^\varrho (\varrho-\iota)^{a-1}J^{-1}Q_a(\varrho-\iota)\mathcal{B}\mathcal{B}^*J^{-1}Q_a^*(c-\varrho)R\left(\mu,\Gamma_0^c\right)\right. \\ &\times\left[z_c - J^{-1}M_a(c)Jz_0 - J^{-1}W_a(c)Jz_1 - \int_0^c (c-\varphi)^{a-1}J^{-1}Q_a(c-\varphi)g^n(\varphi)\,d\varphi\right](\iota)\,d\iota\Big) \\ &\in \mathcal{T}\left(S_{E,z^n}\right) \end{aligned}$$

Because $g^n \to g^*$, and by referring Lemma 2.14, we have

$$\left(m^*(\varrho) - J^{-1}M_a(\varrho)Jz_0 - J^{-1}W_a(\varrho)Jz_1 - \int_0^\varrho (\varrho-\iota)^{a-1}J^{-1}Q_a(\varrho-\iota)\mathcal{B}\mathcal{B}^*J^{-1}Q_a^*(c-\varrho)R\left(\mu,\Gamma_0^c\right)\right.$$

$$\times \left[z_c - J^{-1} M_a(c) J z_0 - J^{-1} W_a(c) J z_1 - \int_0^c (c-\varphi)^{a-1} J^{-1} Q_a(c-\varphi) g^*(\varphi) d\varphi \right](\iota) d\iota \Big)$$
$$\in \mathcal{T}\left(S_{E,z^*}\right)$$

Hence, $\mathcal{R}$ is closed graph.

Hence, by referring **Step 1–5**, and applying Arzela-Ascoli theorem, $\mathcal{R}$ is a completely continuous multivalued mapping with compact value and thus $\mathcal{R}$ is u.s.c. Therefore $\mathcal{R}$ has a fixed point $z(\cdot)$ on $\mathcal{Q}_\alpha$, and in view of Lemma 2.15, $z(\cdot)$ is the mild solution of (1.1)–(1.2). □

Definition 3.2 The system (1.1)–(1.2) is called approximately controllable on V if $\overline{R(c,z_0)} = \mathcal{Y}$, $R(c,z_0) = \left\{ z_c(z_0;x) : x(\cdot) \in L^2(V,\mathcal{U}) \right\}$ is a solution of (1.1)–(1.2). □

Theorem 3.3 *Assume that* $\mathbf{H_1} - \mathbf{H_5}$ *are satisfied. Further, there exists*

$$\mathcal{I} \in L^1\left(V, [0,+\infty)\right) \text{ such that } \sup_{z\in\mathcal{Y}} \|E(\varrho,z)\| \le \mathcal{I}(\varrho)$$

for a.e. $\varrho \in V$, then (1.1)–(1.2) is approximately controllable.

Proof. Consider $\hat{z}^\mu(\cdot)$ a fixed point of $\mathcal{R}$ in $\mathcal{Q}_\alpha$. Referring 3.1, any fixed point of $\mathcal{R}$ is a solution of (1.1)–(1.2) with

$$\hat{x}^\mu(\rho) = \mathcal{B}^* J^{-1} Q_a^*(c-\rho) R\left(\mu, \Gamma_0^c\right) q\left(\hat{z}^\mu\right)$$

and satisfies the following inequality

$$\hat{z}^\mu(c) = z_c + \mu R\left(\mu, \Gamma_0^c\right) q\left(\hat{z}^\mu\right). \tag{3.5}$$

Further from E and Dunford-Pettis Theorem, we conclude that $\{g^\mu(\iota)\}$ is weakly compact in $L^1(V,\mathcal{Y})$, so there exists a subsequence, $\{g^\mu(\iota)\}$, that converges weakly to $g(\iota)$ in $L^1(V,\mathcal{Y})$. Determine

$$\mathcal{V} = z_c - J^{-1} M_a(c) J z_0 - J^{-1} W_a(c) J z_1 - \int_0^c (c-\iota)^{a-1} J^{-1} Q_a(c-\iota) g(\iota) d\iota.$$

Now, we have

$$\begin{aligned} \|q\left(\hat{z}^\mu\right) - \mathcal{V}\| &= \| \int_o^c (c-\iota)^{a-1} J^{-1} Q_a(c-\iota) \left[g\left(\iota, \hat{z}^\mu(\iota)\right) - g(\iota) \right] d\iota \| \\ &\le \sup_{\varrho\in V} \| \int_o^\varrho (\varrho-\iota)^{a-1} J^{-1} Q_a(\varrho-\iota) \left[g\left(\iota, \hat{z}^\mu(\iota)\right) - g(\iota) \right] d\iota \|. \end{aligned} \tag{3.6}$$

By Ascoli-Arzela theorem, we can prove

$$\mathcal{L}(\cdot) \to \int_0^\cdot (\cdot-\iota)^{a-1} J^{-1} Q_a(\cdot-\iota) \mathcal{L}(\iota) d\iota : L^1(V,\mathcal{Y}) \to C(V,\mathcal{Y})$$

is compact. Hence, we have

$$\|q\left(\hat{z}^\mu\right) - \mathcal{V}\| \to 0 \text{ when } \mu \to 0^+.$$

Furthermore, in view of Equation (3.5), we have

$$\begin{aligned} \|\hat{z}^\mu(c) - z_c\| &\le \|\mu R\left(\mu, \Gamma_0^c\right)(\mathcal{V})\| + \|\mu R\left(\mu, \Gamma_0^c\right)\| \|q\left(\hat{z}^\mu\right) - \mathcal{V}\| \\ &\le \|\mu R\left(\mu, \Gamma_0^c\right)(\mathcal{V})\| + \|q\left(\hat{z}^\mu\right) - \mathcal{V}\|. \end{aligned}$$

It follows from $\mathbf{H_0}$ and (3.6) that

$$\|\hat{z}^\mu(c) - z_c\| \to 0 \text{ as } \mu \to 0^+.$$

Therefore the system (1.1)–(1.2) is approximately controllable on V. □

4 | NONLOCAL CONDITIONS

Differential systems with nonlocal conditions have become a very lively field of recent research. Their investigation is driven by hypothetical enthusiasm as well as by the way that these kinds of issues normally happen when demonstrating practical applications. For instance, few events in designing, material science, and life sciences can be portrayed by methods for the differential system subject to nonlocal boundary conditions, and one can refer [6, 9, 11, 14, 16, 18, 25, 32, 37–41]. Consider the nonlocal fractional Sobolev type Volterra-Fredholm integro-differential inclusions of order $r \in (1, 2)$ of the type

$$^{C}D_{\varrho}^{r}\left(Jz\left(\varrho\right)\right) \in Az\left(\varrho\right) + \mathscr{B}x\left(\varrho\right) + E\left(\varrho, z\left(\varrho\right), \int_{0}^{\varrho} e(\varrho, s, z(s))ds, \int_{0}^{c} h(\varrho, s, z(s))\, ds\right), \quad \varrho \in V, \tag{4.1}$$

$$z\left(0\right) + l\left(z\right) = z_{0}, \quad z'\left(0\right) = z_{1} \in \mathscr{Y}, \tag{4.2}$$

where the function $l : C\left(\left[0, c\right], \mathscr{Y}\right) \to \mathscr{Y}$ satisfies the following hypothesis:

$\mathbf{H_6}$ The function $l : C\left(\left[0, c\right], \mathscr{Y}\right) \to \mathscr{Y}$ is compact and continuous, and there exists constants L_1, L_2 such that $\left\|l(z)\right\| \leq L_1 \left\|z\right\|_{C} + L_2$, where $z \in C\left(V, \mathscr{Y}\right)$.

The mild solution of the nonlocal fractional evolution system (4.1)–(4.2) defined as follows:

Definition 4.1 A function $z \in \mathcal{C} = C\left(V, \mathscr{Y}\right)$ is called a solution of (4.1)–(4.2) if $z(0) + l(z) = z_0$, $z'\left(0\right) = z_1, x\left(\cdot\right) \in L^2\left(V, \mathscr{U}\right)$ and there exists $g \in L^1\left(V, \mathscr{Y}\right)$ such that $g\left(\varrho\right) \in E\left(\varrho, z\left(\varrho\right), \int_0^{\varrho} e\left(\varrho, s, z\left(s\right)\right) ds, \int_0^{c} h\left(\varrho, s, z\left(s\right)\right) ds\right)$ on a.e. $\varrho \in V$ and

$$z\left(\varrho\right) = J^{-1}M_{a}\left(\varrho\right)J\left[z_{0} - l\left(z\right)\right] + J^{-1}W_{a}\left(\varrho\right)Jz_{1} + \int_{0}^{\varrho}\left(\varrho - \imath\right)^{a-1}J^{-1}Q_{a}\left(\varrho - \imath\right)\mathscr{B}x\left(\imath\right)d\imath$$
$$+ \int_{0}^{\rho}\left(\varrho - \imath\right)^{a-1}J^{-1}Q_{a}\left(\varrho - \imath\right)g\left(\imath\right)d\imath,$$

is satisfied.

Theorem 4.2 *If* $\mathbf{H_1}$–$\mathbf{H_6}$ *are satisfied, then the system* (4.1)–(4.2) *is approximately controllable on* V.

5 | EXAMPLE

Let us consider $\chi \subset \mathbb{R}^N$ be an open C^2 bounded domain. Assume that $\mathscr{Y} = \mathscr{U} = L^2\left(\chi\right)$. Let us assume the fractional integro-differential system

$$\partial_{\rho}^{r}\left(u\left(\varrho, v\right) - \Delta u\left(\varrho, v\right)\right) \in \Delta u\left(\varrho, v\right) + \hbar\left(\varrho, v\right)$$
$$+ P\left(\varrho, u\left(\varrho, z\right), \int_{0}^{\varrho} e\left(\varrho, s, u\left(\varrho, z\right)\right) ds, \int_{0}^{c} h\left(\varrho, s, u\left(\varrho, z\right)\right) ds\right), \quad \varrho \in \left[0, 1\right], v \in \chi, \tag{5.1}$$

$$u\left(\varrho, v\right) = 0, \quad \varrho \in \left[0, 1\right], \quad v \in \partial\chi, \tag{5.2}$$

$$u\left(0, v\right) = u_{0}\left(v\right), \quad u'\left(0, v\right) = u_{1}\left(v\right), v \in \chi. \tag{5.3}$$

In the above, ∂_{ϱ}^{r} is the partial derivative in Caputo sense of fractional order $r \in (1, 2)$. Let us consider $V = [0, 1]$. Assume that A be the Laplace operator with Dirichlet boundary conditions given as $Au = \Delta$ and assume $A : D(A) \subset \mathcal{Y} \to \mathcal{Y}$, $J : D(J) \subset \mathcal{Y} \to \mathcal{Y}$ be the operators defined by $Au = \Delta$, and $Ju = u - \Delta$ where each domain $D(A)$ and $D(J)$ is presented by

$$D(A) = D(J) = \left\{ g \in H_0^1(\chi),\ \ Ag \in L^2(\chi) \right\}.$$

It is clear that $D(A) = H_0^1(\chi) \cap H^2(\chi)$. Obviously A gives a uniformly bounded C_0 cosine family $C(\varrho)$ for $\varrho \geq 0$, refer [42]. Indeed, let $\iota_n = n^2\pi^2$ and $\psi_n(v) = \sqrt{\frac{2}{\pi}} \sin(n\pi v)$, for all $n \in \mathbb{N}$ are the orthonormal of vectors of A.

Assume $\{-\iota_n, \psi_n\}_{n=1}^{\infty}$ is the eigensystem of the operator A, then $0 < \iota_1 \leq \iota_2 \leq \cdots$, $\iota_n \to \infty$ as $n \to \infty$, and $\{\psi_n\}_{n=1}^{\infty}$ create the orthonormal basis of $\mathcal{Y}$. Now

$$Au = \sum_{n=1}^{\infty} \iota_n \langle u, \psi_n \rangle \psi_n,\ \ u \in D(A),$$

$$Ju = \sum_{n=1}^{\infty} (1 + \iota_n) \langle u, \psi_n \rangle \psi_n,\ \ u \in D(J).$$

Additionally, for $z \in \mathcal{Y}$, we have

$$J^{-1}u = \sum_{n=1}^{\infty} \frac{1}{(1 + \iota_n)} \langle u, \psi_n \rangle \psi_n,$$

$$AJ^{-1}u = \sum_{n=1}^{\infty} \frac{\iota_n}{(1 + \iota_n)} \langle u, \psi_n \rangle \psi_n,$$

where $\langle \cdot, \cdot \rangle$ stands for inner product in $\mathcal{Y}$. Accordingly, we now define the cosine family by

$$C(\varrho)u = \sum_{n=1}^{\infty} \cos\left(\sqrt{\iota_n}\varrho\right) \langle u, \psi_n \rangle \psi_n,\ \ u \in \mathcal{Y},$$

which is connected with sine family $S(\varrho)$ compact for $(\varrho > 0)$ as follows

$$S(\varrho)y = \sum_{n=1}^{\infty} \frac{1}{\sqrt{\iota_n}} \sin\left(\sqrt{\iota_n}\varrho\right) \langle u, \psi_n \rangle \psi_n,\ \ u \in \mathcal{Y}.$$

It is not difficult to verify $\|C(\varrho)\|_{L_c(\mathcal{Y})} \leq 1$, for all $\varrho \in \mathbb{R}$.

Let us assume $u(\varrho) = u(\varrho, \cdot)$, that is, $u(\varrho)(v) = u(\varrho, v)$, $\varrho \in [0, 1]$, and $x(\varrho) = \hbar(\varrho, \cdot)$, consider $\hbar : [0, 1] \times \chi \to \chi$ is continuous. Determine $\mathcal{B} : \mathcal{U} \to \mathcal{Y}$ by $\mathcal{B}x(\varrho)(v) = \hbar(\varrho, v)$. We now define

$$E\left(\varrho, u(\varrho), \int_0^{\varrho} e(\varrho, s, u(s))\, ds, \int_0^{c} h(\varrho, s, u(s))\, ds\right)(z)$$
$$= P\left(\varrho, u(\varrho, z), \int_0^{\varrho} e(\varrho, s, u(\varrho, z))\, ds, \int_0^{c} h(\varrho, s, u(\varrho, z))\, ds\right).$$

Therefore, entire needs of Theorem 3.1 are satisfied, hence (5.1)–(5.3) is approximately controllable on V.

6 | CONCLUSION

In our article, we primarily concentrated on approximate controllability results for fractional Sobolev type Volterra-Fredholm integro-differential inclusions of order $r \in (1, 2)$. By applying the results and ideas belongs to the cosine function of operators, fractional calculus and fixed point approach, the main

results are established. Initially, we established the approximate controllability of the considered fractional system, then continued to examine the system with the concept of nonlocal conditions. Finally, we presented an example to demonstrate the theory.

CONFLICT OF INTEREST

None declared.

ORCID

V. Vijayakumar https://orcid.org/0000-0001-5976-5794
Chokkalingam Ravichandran https://orcid.org/0000-0003-0214-1280
Kottakkaran Sooppy Nisar https://orcid.org/0000-0001-5769-4320
Kishor D. Kucche https://orcid.org/0000-0002-7141-330X

REFERENCES

[1] A. A. Kilbas, H. M. Srivastava, and J. J. Trujillo, *Theory and applications of fractional differential equations*, Elsevier, Amsterdam, 2006.
[2] V. Lakshmikantham, S. Leela, and J. V. Devi, *Theory of fractional dynamic systems*, Cambridge scientific, Cambridge, UK, 2009.
[3] Y. Zhou, *Basic theory of fractional differential equations*, World Scientific, Singapore, 2014.
[4] Y. Zhou, *Fractional evolution equations and inclusions: Analysis and control*, Elsevier, New York, 2015.
[5] M. A. Alqudah, C. Ravichandran, T. Abdeljawad, and N. Valliammal, *New results on Caputo fractional-order neutral differential inclusions without compactness*, Adv. Differ. Eq. 2019(1) (2019), 1–14.
[6] K. Kavitha, V. Vijayakumar, and R. Udhayakumar, *Results on controllability of Hilfer fractional neutral differential equations with infinite delay via measures of noncompactness*, Chaos Solitons Fractals 139 (2020), 110035.
[7] K. Kavitha, V. Vijayakumar, R. Udhayakumar, and K. S. Nisar, *Results on the existence of Hilfer fractional neutral evolution equations with infinite delay via measures of noncompactness*, Math. Methods Appl. Sci. 44 (2020), 1–18. https://doi.org/10.1002/mma.6843.
[8] J. A. Machado, C. Ravichandran, and M. Rivero, *Controllability results for impulsive mixed-type functional integro-differential evolution equations with nonlocal conditions*, Fixed Point Theory Appl. 2013(66) (2013), 1–17.
[9] N. I. Mahmudov, R. Murugesu, C. Ravichandran, and V. Vijayakumar, *Approximate controllability results for fractional semilinear integro-differential inclusions in Hilbert spaces*, Results Math. 71(1) (2017), 45–61.
[10] M. Mohan Raja, V. Vijayakumar, and R. Udhayakumar, *Results on the existence and controllability of fractional integro-differential system of order 1 < r < 2 via measure of noncompactness*, Chaos Solitons Fractals 139 (2020), 1–11 Article ID 110299.
[11] G. M. Mophou and G. M. N'Guerekata, *Existence of mild solution for some fractional diffferential equations with nonlocal conditions*, Semigroup Forum 79(2) (2009), 322–335.
[12] C. Ravichandran, N. Valliammal, and J. J. Nieto, *New results on exact controllability of a class of fractional neutral integro-differential systems with state-dependent delay in Banach spaces*, J. Franklin Inst. 356(3) (2019), 1535–1565.
[13] R. Sakthivel, R. Ganesh, and S. M. Anthoni, *Approximate controllability of fractional nonlinear differential inclusions*, Appl. Math. Comput. 225 (2013), 708–717.
[14] V. Vijayakumar, *Approximate controllability results for non-densely defined fractional neutral differential inclusions with Hille-Yosida operators*, Int. J. Control. 92(9) (2019), 2210–2222.
[15] V. Vijayakumar and R. Udhayakumar, *A new exploration on existence of Sobolev-type Hilfer fractional neutral integro-differential equations with infinite delay*, Numer. Methods Partial Differ. Eq. 37 (2020), 1–17. https://doi.org/10.1002/num.22550.
[16] V. Vijayakumar and R. Udhayakumar, *Results on approximate controllability for non-densely defined Hilfer fractional differential system with infinite delay*, Chaos, Solitons Fractals 139 (2020), 110019.
[17] W. K. Williams, V. Vijayakumar, R. Udhayakumar, and K. S. Nisar, *A new study on existence and uniqueness of nonlocal fractional delay differential systems of order 1 < r < 2 in Banach spaces*, Numer. Methods Partial Differ. Eq. (2020), 1–13. https://doi.org/10.1002/num.22560.
[18] Y. Zhou, V. Vijayakumar, C. Ravichandran, and R. Murugesu, *Controllability results for fractional order neutral functional differential inclusions with infinite delay*, Fixed Point Theory 18(2) (2017), 773–798.
[19] Z. Zufeng and B. Liu, *Controllability results for fractional functional differential equations with nondense domain*, Numer. Funct. Anal. Optim. 35 (2014), 443–460.

[20] Y. K. Chang and D. N. Chalishajar, *Controllability of mixed Volterra-Fredholm-type integro-differential inclusions in Banach spaces*, J. Franklin Inst. 345 (2008), 499–507.
[21] D. N. Chalishajar, *Controllability of mixed Volterra-Fredholm-type integro-differential systems in Banach space*, J. Franklin Inst. 344 (2007), 12–21.
[22] N. I. Mahmudov and A. Denker, *On controllability of linear stochastic systems*, Int. J. Control. 73 (2000), 144–151.
[23] V. Vijayakumar, *Approximate controllability results for abstract neutral integro-differential inclusions with infinite delay in Hilbert spaces*, IMA J. Math. Control. Inf. 35(1) (2018), 297–314.
[24] V. Vijayakumar, *Approximate controllability results for impulsive neutral differential inclusions of Sobolev-type with infinite delay*, Int. J. Control. 91(10) (2018), 2366–2386.
[25] J. W. He, Y. Liang, B. Ahmad, and Y. Zhou, *Nonlocal fractional evolution inclusions of order $\alpha \in (1, 2)$*, Mathematics 209(7) (2019), 1–17.
[26] K. Li, J. Peng, and J. Gao, *Controllability of nonlocal fractional differential systems of order $\alpha \in (1, 2]$ in Banach spaces*, Rep. Math. Phys. 71 (2013), 33–43.
[27] Y. Li, *Regularity of mild solutions for fractional abstract Cauchy problem with order $\alpha \in (1, 2)$*, Z. Angew. Math. Phys. 66 (2015), 3283–3298.
[28] Y. Li, H. Sun, and Z. Feng, *Fractional abstract Cauchy problem with order $\alpha \in (1, 2)$*, Dyn. Partial Differ. Eq. 13 (2016), 155–177.
[29] M. Mohan Raja, V. Vijayakumar, R. Udhayakumar, and Y. Zhou, *A new approach on the approximate controllability of fractional differential evolution equations of order $1 < r < 2$ in Hilbert spaces*, Chaos Solitons Fractals 141 (2020), 1102310.
[30] M. Mohan Raja, V. Vijayakumar, and R. Udhayakumar, *A new approach on approximate controllability of fractional evolution inclusions of order $1 < r < 2$ with infinite delay*, Chaos Solitons Fractals 141 (2020), 110343.
[31] X. B. Shu and F. Xu, *Upper and lower solution method for fractional evolution equations with order $1 < \alpha < 2$*, J. Korean Math. Soc. 51(6) (2014), 1123–1139.
[32] X. B. Shu and Q. Wang, *The existence and uniqueness of mild solutions for fractional differential equations with nonlocal conditions of order $1 < \alpha < 2$*, Comput. Math. Appl. 64 (2012), 2100–2110.
[33] Y. Zhou and J. W. He, *New results on controllability of fractional evolution systems with order $\alpha \in (1, 2)$*, Evol. Eq. Control Theory 0 (2019), 1–19. https://doi.org/10.3934/eect.2020077.
[34] J. H. Lightbourne and S. Rankin, *A partial functional differential equation of Sobolev type*, J. Math. Anal. Appl. 93 (1983), 328–337.
[35] C. C. Travis and G. F. Webb, *Cosine families and abstract nonlinear second order differential equations*, Acta Math. Hungar. 32 (1978), 75–96.
[36] J. Wang and Y. Zhou, *Existence and controllability results for fractional semilinear differential inclusions*, Nonlinear Anal.: RWA 12 (2011), 3642–3653.
[37] L. Byszewski, *Theorems about the existence and uniqueness of solutions of a semilinear evolution nonlocal Cauchy problem*, J. Math. Anal. Appl. 162 (1991), 494–505.
[38] L. Byszewski and H. Akca, *On a mild solution of a semilinear functional-differential evolution nonlocal problem*, J. Appl. Math. Stoch. Anal. 10(3) (1997), 265–271.
[39] A. Debbouche and D. Baleanu, *Controllability of fractional evolution nonlocal impulsive quasilinear delay integro-differential systems*, Comput. Math. Appl. 62 (2011), 1442–1450.
[40] G. M. Mophou and G. M. N'Guerekata, *On integral solutions of some nonlocal fractional differential equations with nondense domain*, Nonlinear Anal. 71(10) (2009), 4668–4675.
[41] G. M. N'Guerekata, *A Cauchy problem for some fractional abstract differential equation with nonlocal conditions*, Nonlinear Anal.: TMA 70(5) (2009), 1873–1876.
[42] W. Arendt, C. J. K. Batty, M. Hieber, and F. Neubrander, *Vector-valued Laplace transforms and Cauchy problems*, 2nd ed., Birkhauser Verlag, Basel AG, 2011.
[43] V. Vijayakumar, and R. Udhayakumar, *Results on approximate controllability for non-densely defined Hilfer fractional differential system with infinite delay*, Chaos, Solitons & Fractals. 139 (2020), 110019. http://dx.doi.org/10.1016/j.chaos.2020.110019.
[44] V. Vijayakumar, and R. Udhayakumar, *A new exploration on existence of Sobolev-type Hilfer fractional neutral integro-differential equations with infinite delay*, Numer. Methods Partial Differ. Eq. 37(1), (2021), 750–766. http://dx.doi.org/10.1002/num.22550.
[45] W. W. Kavitha, V. Vijayakumar, R. Udhayakumar, and K. S. Nisar, *A new study on existence and uniqueness of nonlocal fractional delay differential systems of order $1 < r < 2$ in Banach spaces*, Numer. Methods Partial Differ. Eq. (2020), 1–13. http://dx.doi.org/10.1002/num.22560.
[46] V. Vijayakumar, R. Udhayakumar, Y. Zhou, and N. Sakthivel, *Approximate controllability results for Sobolev-type delay differential system of fractional order without uniqueness*, Numer. Methods Partial Differ. Eq. (2020), 1–20. http://dx.doi.org/10.1002/num.22642.
[47] M. Mohan Raja, and V. Vijayakumar, *New results concerning to approximate controllability of fractional integro-differential evolution equations of order $1 < r < 2$*, Numer. Methods Partial Differ. Eq. (2020), 1–16. http://dx.doi.org/10.1002/num.22653.

[48] M. Mohan Raja, V. Vijayakumar, R. Udhayakumar, and K. S. Nisar, *Results on existence and controllability results for fractional evolution inclusions of order 1 <r < 2 with Clarke's subdifferential type*, Numer. Methods Partial Differ. Eq. (2020), 1–20. http://dx.doi.org/10.1002/num.22691.

[49] V. Vijayakumar, R. Udhayakumar, S. K. Panda, and K. S. Nisar, *Results on approximate controllability of Sobolev type fractional stochastic evolution hemivariational inequalities*, Numer. Methods Partial Differ. Eq. (2020), 1–20. http://dx.doi.org/10.1002/num.22690.

[50] W. W. Kavitha, V. Vijayakumar, R. Udhayakumar, S. K. Panda, and K. S. Nisar, *Existence and controllability of nonlocal mixed Volterra-Fredholm type fractional delay integro-differential equations of order 1 <r < 2*, Numer. Methods Partial Differ. Eq. (2020), 1–21. http://dx.doi.org/10.1002/num.22697.

How to cite this article: Vijayakumar V, Ravichandran C, Nisar KS, Kucche KD. New discussion on approximate controllability results for fractional Sobolev type Volterra-Fredholm integro-differential systems of order $1 < r < 2$. *Numer Methods Partial Differential Eq.* 2021;1–19. https://doi.org/10.1002/num.22772

PLOS ONE

RESEARCH ARTICLE

Optimal and total controllability approach of non-instantaneous Hilfer fractional derivative with integral boundary condition

Kottakkaran Sooppy Nisar[1☯*], **K. Jothimani**[2☯], **C. Ravichandran**[3☯]

1 Department of Mathematics, College of Science and Humanities in Alkharj, Prince Sattam bin Abdulaziz University, Alkharj, Saudi Arabia, **2** Department of Mathematics, School of Advanced Sciences, Vellore Institute of Technology, Vellore, Tamil Nadu, India, **3** Department of Mathematics, Kongunadu Arts and Science College, Coimbatore, Tamil Nadu, India

☯ These authors contributed equally to this work.
* n.sooppy@psau.edu.sa

Citation: Nisar KS, Jothimani K, Ravichandran C (2024) Optimal and total controllability approach of non-instantaneous Hilfer fractional derivative with integral boundary condition. PLoS ONE 19(2): e0297478. https://doi.org/10.1371/journal.pone.0297478

Editor: António M. Lopes, University of Porto Faculty of Engineering: Universidade do Porto Faculdade de Engenharia, PORTUGAL

Received: October 20, 2023

Accepted: January 6, 2024

Published: February 28, 2024

Data Availability Statement: All relevant data are within the paper.

Funding: The authors extend their appreciation to Prince Sattam bin Abdulaziz University for funding this research work through the project number (PSAU/2023/01/2189822).

Competing interests: The authors have declared that no competing interests exist.

Abstract

The focus of this work is on the absolute controllability of Hilfer impulsive non-instantaneous neutral derivative (HINND) with integral boundary condition of any order. Total controllability refers to the system's ability to be controlled during the impulse time. Kuratowski measure and semigroup theory in Banach space yield the results. Furthermore, we talked about optimal controllability in conjunction with appropriate limitations. Our established outcomes are described using an example.

1 Introduction

The concept of differential equations with non-instantaneous impulses(NII) involves many physical processes due to its tremendous applications. Impulse is an action, that starts at an arbitrary fixed point and remains active on a finite time interval is called as NI impulse that occurs in many physical processes like harvesting, vaccination, natural disasters, and shocks subjected to unexpected change in their state. The above situations have to be modeled by impulses [1, 2] if necessary that can not be solved using ordinary differential equations. For some processes, instantaneous impulsive dynamic systems do not support a perfect description, for example, endorsement of insulin of hyperglycemia patients. The change in the above system caused by this medication will remain until the total absorption for a finite time, thanks to the evolutionary process can be modeled with NII. This theory is originated by Hernández [3]. Recently, Vipin Kumar et al. [4–7] derived the controllability results of fractional systems with and without NII for various models. To seek more about NI impulse, track and surf the articles [8–16] and cited references.

On the other hand, the existence and controllability theory extended for both DEs of integer and non-integer order with NII. Fractional calculus is the most appropriate way to evaluate the exact solutions to the given model. The results on Caputo and R-L fractional derivatives were discussed in [17–19]. Theory on HFD was introduced by Hilfer [20] and the results are discussed in [21–24]. One can refer to the monographs [25–29] to know more

about fractional derivatives. In general, controllability enables directing the system from a random initial state to the desired ultimate state. The articles [30–35] discuss the controllability results of Caputo and Hilfer fractional differential system in the nondense domain. Furthermore, the existence and controllability of the Hilfer fractional system with infinite delay were examined in [36, 37]. The exact controllability for Hilfer fractional differential inclusions including nonlocal initial conditions was examined by Du et al. [38]. The approximate controllability results for the Hilfer fractional system were derived by [39, 40]. Recently, a prospective field in control systems is optimal control studied in [41–43]. Ultimately, is more appropriate to evaluate them using an optimization procedure involving fractional differential equations.

The outcome of the existence of HINND of arbitrary order was discussed in [44]. Moreover, results on total controllability fractional neutral non-instantaneous system discussed by [45]. In addition, optimization of the non-instantaneous neutral fractional system is investigated by in [46]. No article was found in the existing literature about the investigation of total controllability using semigroup theory.

We contribute this article to analyze the total controllability & optimal control results for HINND of arbitrary order as:

$$\begin{aligned}
\mathcal{D}^{p_1,p_2}_{\mathfrak{e}_k}\Big[\mathfrak{z}(\mathfrak{t})-\mathcal{K}(\mathfrak{t},\mathfrak{z}(\mathfrak{t}))\Big] &= A\Big[\mathfrak{z}(\mathfrak{t})-\mathcal{K}(\mathfrak{t},\mathfrak{z}(\mathfrak{t}))\Big]+B\mathfrak{u}(\mathfrak{t})+\mathfrak{F}\Big(\mathfrak{t},\mathfrak{z}(\mathfrak{t})\Big), \quad \mathfrak{t}\in\bigcup_{k=0}^{N}(\mathfrak{e}_k,\mathfrak{t}_{k+1}]\\
\mathfrak{z}(\mathfrak{t}) &= \frac{1}{\Gamma(p_1)}\int_{\mathfrak{t}_k}^{\mathfrak{t}}(\mathfrak{t}-\omega)^{p_1-1}\mathscr{I}_k(\omega,\mathfrak{z}(\mathfrak{t}_k^-))d\omega, \quad \mathfrak{t}\in\bigcup_{k=1}^{N}(\mathfrak{t}_k,\mathfrak{e}_k) \qquad (1.1)\\
I_{0^+}^{(1-\eta)}\mathfrak{z}(0) &= \lambda\int_0^T\mathfrak{z}(\omega)d\omega+c, \quad c\in\mathbb{R}.
\end{aligned}$$

Here, $\mathcal{Y}$ be a Banach space and $A:\mathcal{D}(A)\subset\mathcal{Y}\to\mathcal{Y}$ is closed together with $\mathcal{D}(A)\in\mathcal{Y}$. $\mathcal{D}^{p_1,p_2}_{\mathfrak{e}_k}$ represents Hilfer derivative of fractional order with $0<p_1<1$, $0\le p_2\le 1$. Also, $\eta=p_1+p_2-p_1p_2$, $\mathfrak{t}\in\mathcal{I}=[0,T]$, $T>0$. Here $\mathcal{K}:\mathcal{I}\times\mathcal{Y}\to\mathcal{D}(A)\subset\mathcal{Y}$, $\mathfrak{F}:\mathcal{I}\times\mathcal{Y}\to\mathcal{D}(A)\subset\mathcal{Y}$, $\mathscr{I}_k:[\mathfrak{t}_k,\mathfrak{e}_k]\times\mathcal{Y}\to\mathcal{Y}$ are relevant functions. $\mathfrak{t}_k,\mathfrak{e}_k$ fulfills $0=\mathfrak{t}_0=\mathfrak{e}_0<\mathfrak{t}_1<\mathfrak{e}_1<\mathfrak{t}_2<\ldots.<\mathfrak{e}_N<\mathfrak{t}_{N+1}=T$. Moreover, $\mathfrak{z}(\mathfrak{t}_k^-)=\lim_{h\to0^+}\mathfrak{z}(\mathfrak{t}_k-h)$. $B:U\to\mathcal{Y}$ is a bounded linear operator and $\mathfrak{u}(\cdot)\in L^2[\mathcal{I},U]$. The integral boundary condition $\lambda=+1$ or -1. We briefly orchestrated our objective of this work:

(*i*) By incorporating HFD with semigroup operator theory and LT, we have introduced the integral solution of (1.1).

(*ii*) Kuratowski's measure with κ–set-contraction theory has been supported very much to the total controllability of HINND with C_0 semigroup operator for the first time in the literature.

(*iii*) The results on optimal controllability of HINND had been discussed via Lipschitz continuity.

(*iv*) We have gone through with an illustration that enables our analytical outcomes existence.

2 Key notes

The space of continuous functions is defined by $C(\mathcal{I},\mathcal{Y})$ be a provided $||\mathfrak{z}||=\sup_{\mathfrak{t}\in\mathcal{I}}||\mathfrak{z}(\mathfrak{t})||$.

$$C_{1-\eta}(\mathcal{I},\mathcal{Y})=\{\mathfrak{z}:\mathcal{Y}\to\mathcal{Y}\ \text{ provided }\ t^{1-\eta}\mathfrak{z}(\mathfrak{t})\in C(\mathcal{I},\mathcal{Y})\},\ ||\mathfrak{z}||_{C_{1-\eta}}=\sup_{0\le\mathfrak{t}\le T}|\mathfrak{t}^{1-\eta}\mathfrak{z}(\mathfrak{t})|.$$

Let $PC_{1-\eta}((\mathfrak{t}_k, \mathfrak{t}_{k+1}], \mathcal{Y})$ defines the space of piecewise functions as

$$PC_{1-\eta}(\mathcal{I}, \mathcal{Y}) = \left\{ \begin{array}{l} (\mathfrak{t}-\mathfrak{t}_k)^{1-\eta}\mathfrak{z}(\mathfrak{t}) \in C_{1-\eta}((\mathfrak{t}_k, \mathfrak{t}_{k+1}], \mathbb{R}) \\ \lim\limits_{\mathfrak{t}\to\mathfrak{t}_k}(\mathfrak{t}-\mathfrak{t}_k)^{1-\eta}\mathfrak{z}(\mathfrak{t}),\ k = 1, 2, \ldots, N, \end{array} \right\}$$

provided

$$||\mathfrak{z}|| = \max\left\{ \sup_{\mathfrak{t}\in\mathcal{I}} ||\mathfrak{t}^{1-\eta}\mathfrak{z}(\mathfrak{t}^+)||,\ \sup_{\mathfrak{t}\in\mathcal{I}} ||\mathfrak{t}^{1-\eta}\mathfrak{z}(\mathfrak{t}^-)|| \right\}.$$

$L(\mathcal{Y})$, characterize the space of all bounded linear operators on $\mathcal{Y}$. A, generates the semigroup $\{S_{p_1,p_2}(\mathfrak{t})\}$ where $\mathfrak{t} \geq 0$ with $\sup||S_{p_1,p_2}(\mathfrak{t})||_{L(\mathcal{Y})} = \mathscr{M}$. Define a convex, bounded and closed set $\ell = \{\mathfrak{z} \in PC_{1-\eta}(\mathcal{I}, \mathcal{Y}),\ ||\mathfrak{z}(\mathfrak{t})|| < \mathfrak{r},\ \mathfrak{t} \in \mathcal{I},\ \mathfrak{r} > 0\}$ in $PC_{1-\eta}(\mathcal{I}, \mathcal{Y})$.

Definition 2.1 [20]. *For $n-1 < p_1 < n$, $n \in N$ and $p_2 \in (0, 1]$, HFD is defined by*:

$$\mathcal{D}_{0^+}^{p_1,p_2}y(t) = \mathscr{I}_{0^+}^{p_1(n-p_2)}\frac{d}{dt}\mathscr{I}_{0^+}^{(1-p_1)(n-p_2)}y(t) = \mathscr{I}_{0^+}^{p_1(n-p_2)}\mathcal{D}_{0^+}^{p_2+p_1n-p_2p_1}y(t),$$

where $\mathcal{D}_{0^+}^{p_2+p_1n-p_2p_1}$ and $\mathscr{I}_{0^+}^{p_1(n-p_2)}$ are R-L derivative and integral respectively.

Definition 2.2 [8, 44, 47]. *The Kuratowski noncompact measure $\ell(\cdot)$ characterized as*:

$\ell(\hbar) \coloneqq \inf\{\rho > 0 : \hbar = \bigcup_{i=1}^{m}$ *with* $diam(\hbar_i) \leq \rho\}$, *where $\hbar$ is a bounded set on $\mathcal{Y}$.*

Lemma 2.3. (see [8, 44, 47]) *For $\hbar_1, \hbar_2 \subset \mathcal{Y}$, the Kuratowski noncompact measure meets*:

1. $\ell(\hbar) = \ell(\overline{\hbar}) = \ell(conv\hbar)$;
2. $\ell(\hbar) = 0$ *iff* $\overline{\hbar}$ *is compact*;
3. *for given* $\lambda \in R$, $\ell(\lambda\hbar) \leq |\lambda|\ell(\hbar)$;
4. $\hbar_1 \subset \hbar_2$ *implies* $\ell(\hbar_1) \leq \ell(\hbar_2)$;
5. $\ell(\hbar_1 \cup \hbar_2) = \max\{\ell(\hbar_1), \ell(\hbar_2)\}$;
6. $\ell(\hbar_1 + \hbar_2) \leq \ell(\hbar_1) + \ell(\hbar_2)$, *where* $\hbar_1 + \hbar_2 = \{\mathfrak{z} \,|\, \mathfrak{z} = \mathfrak{z}_1 + \mathfrak{z}_2;\ \mathfrak{z}_1 \in \hbar_1,\ \mathfrak{z}_2 \in \hbar_2\}$;
7. *The Lipschitz function* $\Re : \mathcal{D}(\Re) \subset \mathcal{Y} \to \mathcal{Y}$ *and the subset* $W \subset \mathcal{D}(\Re)$, $\ell(\Re(W)) \leq \kappa\,\ell(W)$ *is bounded.*

Let $\mathcal{D} \subset C_{1-\eta}(\mathcal{I}, \mathcal{Y})$ and $\mathfrak{t} \in \mathcal{I}$, $\mathcal{D}(\mathfrak{t}) = \{\mathfrak{z}(\mathfrak{t}) \,|\, \mathfrak{z} \in \mathcal{D}\}$ and $\ell(\mathcal{D}(\mathfrak{t})) \leq \ell C_{1-\eta}(\mathcal{D})$.

Lemma 2.4. (*see* [8, 44, 47]) *Let $\mathcal{D} \subset C_{1-\eta}([c_1, c_2], \mathcal{Y})$ be bounded and equicontinuous such that*

$$\ell C_{1-\eta}(\mathcal{D}) = \max_{\mathfrak{t}\in[c_1,c_2]} \ell(\mathcal{D}(\mathfrak{t})),$$

and $\ell(\mathcal{D}(\mathfrak{t}))$ is continuous on $[c_1, c_2]$.

Lemma 2.5. (*see* [8, 44, 47]) *Assume that $\overline{\mathcal{Y}} \subset \mathcal{Y}$ is bounded and for some $\mathcal{D}_0 \subset \mathcal{D}$, the countable set meets $\ell(\mathcal{D}) \leq 2\,\ell(\mathcal{D}_0)$.*

Lemma 2.6. (*see* [8, 44, 47]) *Let $\mathcal{D} = \{\mathfrak{z}_n\} \subset PC_{1-\eta}([c_1, c_2], \mathcal{Y})$ where $-\infty < c_1 < c_2 < \infty$. Hence $\ell(\mathcal{D}(\mathfrak{t}))$ on $[c_1, c_2]$ such that*:

$$\ell\left(\left\{\int_{c_1}^{c_2}\mathfrak{z}_n(\mathfrak{t})d\mathfrak{t}\right\}\right) \leq 2\int_{c_1}^{c_2}\ell(\mathcal{D}(\mathfrak{t}))d\mathfrak{t},\quad n \in \mathbb{N}.$$

Lemma 2.7. (*see* [21, 22, 44]) *The system* (1.1) *becomes*:

$$\begin{aligned}
\mathfrak{z}(\mathfrak{t}) &= \frac{\mathfrak{t}^{\eta-1}}{\Gamma(\eta)}\left[\lambda\int_0^T \mathfrak{z}(\omega)d\omega + c - \mathcal{K}(0,\mathfrak{z}(0))\right] + \mathcal{K}(\mathfrak{t},\mathfrak{z}(\mathfrak{t}))\\
&\quad + \frac{1}{\Gamma(p_1)}\int_0^{\mathfrak{t}} (\mathfrak{t}-\omega)^{p_1-1}\Big[A[\mathfrak{z}(\omega) - \mathcal{K}(\omega,\mathfrak{z}(\omega))] + B\mathfrak{u}(\omega) + \mathfrak{F}(\omega,\mathfrak{z}(\omega))\Big]d\omega,\ \ \mathfrak{t}\in(0,\mathfrak{t}_1],\\
\mathfrak{z}(\mathfrak{t}) &= \frac{1}{\Gamma(p_1)}\int_{\mathfrak{t}_k}^{\mathfrak{t}} (\mathfrak{t}-\omega)^{p_1-1}\mathscr{I}_k(\omega,\mathfrak{z}(\mathfrak{t}_k^-))d\omega, \qquad \mathfrak{t}\in(\mathfrak{t}_k,\mathfrak{e}_k],\\
\mathfrak{z}(\mathfrak{t}) &= \frac{1}{\Gamma(p_1)}\int_{\mathfrak{t}_k}^{\mathfrak{e}_k} (\mathfrak{t}-\omega)^{p_1-1}\mathscr{I}_k(\omega,\mathfrak{z}(\mathfrak{t}_k^-))d\omega - \mathcal{K}(\mathfrak{e}_k,\mathfrak{z}(\mathfrak{e}_k)) + \mathcal{K}(\mathfrak{t},\mathfrak{z}(\mathfrak{t}))\\
&\quad + \frac{1}{\Gamma(p_1)}\int_{\mathfrak{e}_k}^{\mathfrak{t}} (\mathfrak{t}-\omega)^{p_1-1}\Big[A\Big[\mathfrak{z}(\omega) - \mathcal{K}(\omega,\mathfrak{z}(\omega))\Big]\\
&\quad + B\mathfrak{u}(\omega) + \mathfrak{F}(\omega,\mathfrak{z}(\omega))\Big]d\omega, \qquad \mathfrak{t}\in(\mathfrak{e}_k,\mathfrak{t}_{k+1}].
\end{aligned}$$

Definition 2.8. (*see* [21, 22, 44]) *A function* $\mathfrak{z}\in PC_{1-\eta}(\mathcal{I},\mathcal{Y})$ *is a solution of* (1.1), *if*

$(i)\mathfrak{z}(\mathfrak{t}) = \frac{1}{\Gamma(p_1)}\int_{\mathfrak{t}_k}^{\mathfrak{t}} (\mathfrak{t}-\omega)^{p_1-1}\mathscr{I}_k(\omega,\mathfrak{z}(\mathfrak{t}_k^-))d\omega,\ \ \mathfrak{t}\in(\mathfrak{t}_k,\mathfrak{e}_k],\ k=1,2,...,N$

$(ii)I_0^{1-\eta}\mathfrak{z}(0) = \lambda\int_0^T \mathfrak{z}(\omega)d\omega + c,$

together with

$$\begin{aligned}
\mathfrak{z}(\mathfrak{t}) &= S_{p_1,p_2}(\mathfrak{t})\Big[\lambda\int_0^T \mathfrak{z}(\omega)d\omega + c - \mathcal{K}(0,\mathfrak{z}(0))\Big] + \mathcal{K}(\mathfrak{t},\mathfrak{z}(\mathfrak{t}))\\
&\quad + \int_0^{\mathfrak{t}} K_{p_1}(\mathfrak{t}-\omega)\Big[B\mathfrak{u}(\omega) + \mathfrak{F}(\omega,\mathfrak{z}(\omega))\Big]d\omega, \quad \mathfrak{t}\in(0,\mathfrak{t}_1],
\end{aligned} \tag{2.1}$$

$$\begin{aligned}
\mathfrak{z}(\mathfrak{t}) &= S_{p_1,p_2}(\mathfrak{t}-\mathfrak{e}_k)\left[\frac{1}{\Gamma(p_1)}\int_{\mathfrak{t}_k}^{\mathfrak{e}_k} (\mathfrak{e}_k-\omega)^{p_1-1}\mathscr{I}_k(\omega,\mathfrak{z}(\mathfrak{t}_k^-))d\omega - \mathcal{K}(\mathfrak{e}_k,\mathfrak{z}(\mathfrak{e}_k))\right] + \mathcal{K}(\mathfrak{t},\mathfrak{z}(\mathfrak{t}))\\
&\quad + \int_{\mathfrak{e}_k}^{\mathfrak{t}} K_{p_1}(\mathfrak{t}-\omega)\Big[B\mathfrak{u}(\omega) + \mathfrak{F}(\omega,\mathfrak{z}(\omega))\Big]d\omega,\ \mathfrak{t}\in(\mathfrak{e}_k,\mathfrak{t}_{k+1}],\ k=1,2,...,N.
\end{aligned} \tag{2.2}$$

$$T_{p_1}(\mathfrak{t}) = p_1\int_0^\infty v\psi_y(v)\Re(\mathfrak{t}^{p_1}v)dv,\quad K_{p_1}(\mathfrak{t}) = \mathfrak{t}^{p_1-1}T_{p_1}(\mathfrak{t}),\quad S_{p_1,p_2}(\mathfrak{t}) = \mathscr{I}_{0^+}^{p_2(1-p_1)}K_{p_1}(\mathfrak{t}).$$

$$W_y(v) = \frac{1}{\pi}\sum_{m=1}^{\infty}(-1)^{m-1}v^{-my-1}\frac{\Gamma(my+1)}{m!}\sin(m\pi\mathfrak{z}),\ \ v\in(0,\infty),$$

$$\psi_y(v) = \frac{1}{\mathfrak{z}}v^{\left(-1-\frac{1}{\mathfrak{z}}\right)}W_y(v^{-\frac{1}{\mathfrak{z}}}) \geq 0.$$

Lemma 2.9. (*see* [8, 44, 47]) *If a family* $\{S_{p_1}(\mathfrak{t}),\ \mathfrak{t}\geq 0\}\subset\mathcal{B}(\mathcal{Y})$ *satisfies*

(i) *for all* $\mathfrak{z}\in D(A), S_{p_1}(\mathfrak{t})\mathfrak{z} = \mathfrak{z} + I_{0^+}^{p_1}\ S_{p_1}(\mathfrak{t})Ay,\ \ \mathfrak{t}\geq 0;$

$(ii)S_{p_1}(\mathfrak{t})$ *is strongly continuous on* $\mathbb{R}_+, S_{p_1}(0) = I;$

(iii) $AS_{p_1}(\mathfrak{t})\mathfrak{z} = S_{p_1}A(\mathfrak{z})$ *for each,* $\mathfrak{z} \in D(A),\ \mathfrak{t} \geq 0, D \subset \mathcal{Y}$.

Then, it is said to be p_1*–times resolvent generator by A.*

Definition 2.10. *A system is defined as totally controllable on* $\mathcal{I}$*, if for* $k = 1, 2, \ldots, N$*, it is controllable on* $(0, \mathfrak{t}_1]$, $(\mathfrak{e}_k, \mathfrak{t}_{k+1}]$ such that $\mathfrak{z}(0) = \mathfrak{z}_0$ and $\mathfrak{z}(\mathfrak{t}_{k+1}) = \mathfrak{z}_{\mathfrak{t}_{k+1}}$.

For further discussions, we consider the subsequent assumptions as:

(*H*1) $\mathcal{K} : J_0 \times \mathcal{Y} \to \mathcal{Y},\ J_0 = \bigcup_{k=0}^{N}(\mathfrak{e}_k, \mathfrak{t}_{k+1}]$ is continuous and for $\mathcal{L}_p, \mu_p > 0$ as

$$||\mathcal{K}(\mathfrak{t}, \hat{\mathfrak{z}_2}) - \mathcal{K}(\mathfrak{t}, \hat{\mathfrak{z}_1})|| \leq \mathcal{L}_p||\hat{\mathfrak{z}_2} - \hat{\mathfrak{z}_1}||,\ \ \hat{\mathfrak{z}_2},\ \hat{\mathfrak{z}_1} \in \mathcal{Y},\ \ \mathfrak{t} \in J_0,$$

also $||\mathcal{K}(\mathfrak{t}, \mathfrak{z}|| \leq \mu_p,\ \mathfrak{z} \in \mathcal{Y},\ \mathfrak{t} \in J_0$;

(*H*2) for any bounded set $D_1 \subset \mathcal{Y}$, *exist* $\mathcal{L}_{p^*} > 0$, such that

$$\ell(\mathcal{K}(\mathfrak{t}, D_1)) \leq \mathcal{L}_{p^*}\ell(D_1);$$

(*H*3) Function $\mathfrak{F} : J_0 \times \mathcal{Y} \to \mathcal{Y}$ is continuous with $\mathcal{L}_f > 0$, satisfies

$$||\mathfrak{F}(\mathfrak{t}, \hat{\mathfrak{z}_1}) - \mathfrak{F}(\mathfrak{t}, \hat{\mathfrak{z}_2})|| \leq \mathcal{L}_f||\hat{\mathfrak{z}_1} - \hat{\mathfrak{z}_2}||,\ \ \hat{\mathfrak{z}_1}, \hat{\mathfrak{z}_2} \in \mathcal{Y},\ \mathfrak{t} \in J_0.$$

$$||\mathfrak{F}(\mathfrak{t}, \mathfrak{z})|| \leq \Psi(\mathfrak{t})\wp\Big(||\mathfrak{z}||\Big) \ \text{ and } \ \liminf_{l\to\infty}\frac{\wp(l)}{l} = \nu < \infty;$$

where $\wp : [0, \infty) \to [0, \infty)$, a non decreasing continuous function, $\psi : \mathcal{I} \to [0, \infty)$, a Lebesgue integrable function and $\nu > 0$ such that for all $\mathfrak{z} \in \mathcal{Y}$, $\mathfrak{t} \in \mathcal{I}$ and meets $||\mathfrak{z}||_{C_{1-\eta}} \leq l$.

(*H*4) For $k = 0, 1, \ldots N, \mathcal{L}_k$,

$$\ell(\mathfrak{F}(\mathfrak{t}, \mathfrak{z})) \leq \mathcal{L}_k\,\ell(D),\ \ \mathfrak{t} \in J_0 \ \text{ with } \ \mathcal{L} = \max_k\ \mathcal{L}_k,$$

where the subset D of $\mathcal{Y}$ is a countable;

(*H*5) For $J_k = [\mathfrak{t}_k, \mathfrak{e}_k],\ k = 1, 2, \ldots N, \mathscr{I}_k : J_k \times \mathcal{Y} \to \mathcal{Y}$ are continuous functions, for $K_{\mathscr{I}_k} > 0,\ k = 1, 2, \ldots N$, provided for every $\hat{\mathfrak{z}_1}, \hat{\mathfrak{z}_2} \in \mathcal{Y}$,

$$||\mathscr{I}_k(\mathfrak{t}, \hat{\mathfrak{z}_1}) - \mathscr{I}_k(\mathfrak{t}, \hat{\mathfrak{z}_2})|| \leq K_{\mathscr{I}_k}||\hat{\mathfrak{z}_1} - \hat{\mathfrak{z}_2}||,\ \text{ for each } \mathfrak{t} \in (\mathfrak{t}_k, \mathfrak{e}_k],\ \ K \coloneqq \max_{k=0,1,\ldots N} K_{\mathcal{I}_k}.$$

Moreover, $\mathscr{M}_{\mathscr{I}}$, together with $||\mathscr{I}_k(\mathfrak{t}, \mathfrak{z})|| \leq \mathscr{M}_{\mathscr{I}}$;

(*H*6) $W : L^2(\mathcal{I}, U) \to \mathcal{Y}$ defined by:

$$W\mathfrak{u} = \int_0^a K_{p_1}(a - \omega)B\mathfrak{u}(\omega)d\omega,$$

is invertible. Also, for $\mathscr{M}_b, \mathscr{M}_w \geq 0$, and $\|W^{-1}\| \leq \mathscr{M}_w$, $\|B\| \leq \mathscr{M}_b$.

(*H*7) Given $\mathcal{L}_{\mathfrak{u}}{}^* > 0$, for $\ell(\mathfrak{u}(\mathfrak{z}, \mu)) \leq \mathcal{L}_{\mathfrak{u}}{}^*\mathfrak{t}^{1-\eta}\sigma(\mathfrak{z}, \mu)\ell(\mathfrak{z}(\mu))$, a.e. $\mu \in \mathcal{I}$ and $\sup_{\mathfrak{t}\in\mathcal{I}}\int_0^{\mathfrak{t}}\sigma(\mathfrak{t}, \mu)d\omega = \sigma^* < \infty$.

Conveniently, we assign some notations as follows:

$$\mathcal{C}_2 = \frac{\mathscr{M}_1 \mathscr{M}_b \mathscr{M}_w^m T^{p_1}}{p_1}; \quad k_1 = \max\{\mathscr{M}\lambda T + \mathcal{L}_p,\ \mathscr{M}\left(\frac{K_{\mathscr{I}_k}\mathfrak{t}_{k+1}^{p_1}}{\Gamma(p_1+1)} + \mathcal{L}_p\right) + \mathcal{L}_p,\ \frac{K_{\mathscr{I}_k}\mathfrak{t}_{k+1}^{p_1}}{\Gamma(p_1+1)}\};$$

$$\mathcal{N}_1 = \mathscr{M}\left(\frac{\mathscr{M}_{\mathscr{I}}\mathfrak{t}_{k+1}^{p_1}}{\Gamma(p_1+1)} + \mu_p\right) + \mu_p + \frac{\mathscr{M}_1\mathfrak{t}_{k+1}^{p_1}}{p_1}\wp(l)||\Psi||_{L[0,\mathfrak{t}_{k+1}]}; \quad \mathcal{C}_1 = \frac{\mathscr{M}_1\mathscr{M}_b\mathscr{M}_w^1\mathfrak{t}_1^{p_1}}{p_1};$$

$$\mathscr{M}_1 = \sup||K_{p_1}(\mathfrak{t})||_{L(\mathcal{Y})}; \quad \mathcal{N} = \mathscr{M}\left(\lambda||\mathfrak{z}|| + |c| + \mu_p\right) + \mu_p + \frac{\mathscr{M}_1\mathfrak{t}_1^{p_1}}{p_1}\wp(l)||\Psi||_{L[0,\mathfrak{t}_1]}.$$

3 Main sequels

Lemma 3.1. *Let $\mathcal{S} \subset \mathcal{Y}$ and $\Re : \mathcal{S} \to \mathcal{Y}$ be called as κ-set-contractive for any bounded set $\aleph$ in $\mathcal{S}$ such that and for $\kappa \in [0, 1)$, as*

$$\ell(\Re(\aleph)) \leq \kappa\,\ell(\aleph).$$

Lemma 3.2. *Let $\aleph$ be a convex, bounded and closed subset of $\mathcal{Y}$. If $\Re : \aleph \to \aleph$ is κ-set-contractive. Then $\Re$ has at least one fixed point in $\aleph$.*

Lemma 3.3. *If the assumptions (H1)–(H7) true, hence*

$$\begin{aligned}\mathfrak{u}(\mathfrak{t}) \quad &= W^{-1}\Bigg[\mathfrak{z}_{\mathfrak{t}_1} - S_{p_1,p_2}(\mathfrak{t}_1)\Big[\lambda\int_0^T \mathfrak{z}(\omega)d\omega + c - \mathcal{K}(0,\mathfrak{z}(0))\Big] - \mathcal{K}(\mathfrak{t}_1,\mathfrak{z}(\mathfrak{t}_1)) \\ &\quad - \int_0^{\mathfrak{t}_1} K_{p_1}(\mathfrak{t}_1-\omega)\mathfrak{F}(\omega,\mathfrak{z}(\omega))d\omega\Bigg], \quad \mathfrak{t}\in(0,\mathfrak{t}_1],\end{aligned} \tag{3.1}$$

$$\begin{aligned}\mathfrak{u}(\mathfrak{t}) \quad &= W^{-1}\Bigg[\mathfrak{z}_{\mathfrak{t}_{k+1}} - S_{p_1,p_2}(\mathfrak{t}_{k+1}-\mathfrak{e}_k) \\ &\quad (\times)\Bigg[\frac{1}{\Gamma(p_1)}\int_{\mathfrak{t}_k}^{\mathfrak{e}_k}(\mathfrak{e}_k-\omega)^{p_1-1}\mathscr{I}_k(\omega,\mathfrak{z}(\mathfrak{t}_k^-))d\omega - \mathcal{K}(\mathfrak{e}_k,\mathfrak{z}(\mathfrak{e}_k))\Bigg] - \mathcal{K}(\mathfrak{t}_{k+1},\mathfrak{z}(\mathfrak{t}_{k+1})) \\ &\quad - \int_{\mathfrak{e}_k}^{\mathfrak{t}_{k+1}} K_{p_1}(\mathfrak{t}_{k+1}-\omega)\mathfrak{F}(\omega,\mathfrak{z}(\omega))d\omega\Bigg], \quad \mathfrak{t}\in(\mathfrak{e}_k,\mathfrak{t}_{k+1}],\end{aligned} \tag{3.2}$$

drives to $\mathfrak{z}(\mathfrak{t})$ of (1.1) from $\mathfrak{z}(\mathfrak{t}_1) = \mathfrak{z}_{\mathfrak{t}_1}$ and $\mathfrak{z}(\mathfrak{t}_{k+1}) = \mathfrak{z}_{\mathfrak{t}_{k+1}}$, also $||\mathfrak{u}(\mathfrak{t})|| = \mathscr{M}_{\mathfrak{u}}^1$, $||\mathfrak{u}(\mathfrak{t})|| = \mathscr{M}_{\mathfrak{u}}^k$ with

$$\mathscr{M}_{\mathfrak{u}}^1 = \mathscr{M}_w^1(||\mathfrak{z}_{\mathfrak{t}_1}|| + \mathcal{N}), \quad \mathscr{M}_{\mathfrak{u}}^k = \mathscr{M}_w^m(||\mathfrak{z}_{\mathfrak{t}_{k+1}}|| + \mathcal{N}_1), \quad k = 1, 2, \ldots, N.$$

Proof. For $\mathfrak{t} = \mathfrak{t}_1$,

$$\begin{aligned}
\mathfrak{z}(\mathfrak{t}_1) &= S_{p_1,p_2}(\mathfrak{t}_1)\Big[\lambda\int_0^T \mathfrak{z}(\omega)d\omega + c - \mathcal{K}(0,\mathfrak{z}(0))\Big] + \mathcal{K}(\mathfrak{t}_1,\mathfrak{z}(\mathfrak{t}_1)) \\
&+ \int_0^{\mathfrak{t}_1} K_{p_1}(\mathfrak{t}_1-\omega)\mathfrak{F}(\omega,\mathfrak{z}(\omega))d\omega \\
&+ \int_0^{\mathfrak{t}_1} K_{p_1}(\mathfrak{t}_1-\tau)W^{-1}\Bigg[\mathfrak{z}_{\mathfrak{t}_1} - S_{p_1,p_2}(\mathfrak{t}_1)\Big[\lambda\int_0^T \mathfrak{z}(\omega)d\omega + c - \mathcal{K}(0,\mathfrak{z}(0))\Big] \\
&-\mathcal{K}(\mathfrak{t}_1,\mathfrak{z}(\mathfrak{t}_1)) - \int_0^{\mathfrak{t}_1} K_{p_1}(\mathfrak{t}_1-\omega)\mathfrak{F}(\omega,\mathfrak{z}(\omega))d\omega\Bigg]d\tau \\
&= S_{p_1,p_2}(\mathfrak{t}_1)\Big[\lambda\int_0^T \mathfrak{z}(\omega)d\omega + c - \mathcal{K}(0,\mathfrak{z}(0))\Big] + \mathcal{K}(\mathfrak{t}_1,\mathfrak{z}(\mathfrak{t}_1)) \\
&+ \int_0^{\mathfrak{t}_1} K_{p_1}(\mathfrak{t}_1-\omega)\mathfrak{F}(\omega,\mathfrak{z}(\omega))d\omega + \mathfrak{z}_{\mathfrak{t}_1} - S_{p_1,p_2}(\mathfrak{t}_1)\Big[\lambda\int_0^T \mathfrak{z}(\omega)d\omega + c - \mathcal{K}(0,\mathfrak{z}(0))\Big] \\
&-\mathcal{K}(\mathfrak{t}_1,\mathfrak{z}(\mathfrak{t}_1)) - \int_0^{\mathfrak{t}_1} K_{p_1}(\mathfrak{t}_1-\omega)\mathfrak{F}(\omega,\mathfrak{z}(\omega))d\omega \\
&= \mathfrak{z}_{\mathfrak{t}_1},
\end{aligned}$$

with

$$\begin{aligned}
||\mathfrak{u}(\mathfrak{t})|| &\le \Bigg|\Bigg|W^{-1}\Big[\mathfrak{z}_{\mathfrak{t}_1} - S_{p_1,p_2}(\mathfrak{t}_1)\Big[\lambda\int_0^T \mathfrak{z}(\omega)d\omega + c - \mathcal{K}(0,\mathfrak{z}(0))\Big] - \mathcal{K}(\mathfrak{t}_1,\mathfrak{z}(\mathfrak{t}_1)) \\
&- \int_0^{\mathfrak{t}_1} K_{p_1}(\mathfrak{t}_1-\omega)\mathfrak{F}(\omega,\mathfrak{z}(\omega))d\omega\Big]\Bigg|\Bigg| \\
&\le \mathscr{M}_w^1\Bigg(||\mathfrak{z}_{\mathfrak{t}_1}|| + \mathscr{M}\Bigg|\Bigg|\lambda\int_0^T \mathfrak{z}(\omega)d\omega + c - \mathcal{K}(0,\mathfrak{z}(0))\Bigg|\Bigg| + ||\mathcal{K}(\mathfrak{t}_1,\mathfrak{z}(\mathfrak{t}_1))|| \\
&+\mathscr{M}_1\Bigg|\Bigg|\int_0^{\mathfrak{t}_1}\omega^{1-\eta}\Psi(\omega)\wp(||\mathfrak{z}||_{C_{1-\eta}})d\omega\Bigg|\Bigg|\Bigg) \\
&\le \mathscr{M}_w^1\Bigg(||\mathfrak{z}_{\mathfrak{t}_1}|| + \mathscr{M}\Big(\lambda T||\mathfrak{z}(\omega)|| + |c| + \mu_p\Big) + \mu_p + \frac{\mathscr{M}_1\mathfrak{t}_1^{p_1}}{p_1}\wp(l)||\Psi||_{L[0,\mathfrak{t}_1]}\Bigg) \\
&\le \mathscr{M}_w^1(||\mathfrak{z}_{\mathfrak{t}_1}|| + \mathcal{N}) \\
&= \mathscr{M}_{\mathfrak{u}}^1.
\end{aligned}$$

Also, for $\mathfrak{t} \in (\mathfrak{e}_k, \mathfrak{t}_{k+1}]$ and $\mathfrak{t} = \mathfrak{t}_{k+1}$,

$$\begin{aligned}
\mathfrak{z}(\mathfrak{t}_{k+1}) &= S_{p_1,p_2}(\mathfrak{t}_{k+1}-\mathfrak{e}_k)\Big[\frac{1}{\Gamma(p_1)}\int_{\mathfrak{t}_k}^{\mathfrak{e}_k}(\mathfrak{e}_k-\omega)^{p_1-1}\mathscr{I}_k(\omega,\mathfrak{z}(\mathfrak{t}_k^-))d\omega - \mathcal{K}(\mathfrak{e}_k,\mathfrak{z}(\mathfrak{e}_k))\Big] \\
&+\mathcal{K}(\mathfrak{t}_{k+1},\mathfrak{z}(\mathfrak{t}_{k+1})) + \int_{\mathfrak{e}_k}^{\mathfrak{t}_{k+1}} K_{p_1}(\mathfrak{t}_{k+1}-\omega)\mathfrak{F}(\omega,\mathfrak{z}(\omega))d\omega \\
&+ \int_{\mathfrak{e}_k}^{\mathfrak{t}_{k+1}} K_{p_1}(\mathfrak{t}_{k+1}-\tau)W^{-1}\Bigg[\mathfrak{z}_{\mathfrak{t}_{k+1}} - S_{p_1,p_2}(\mathfrak{t}_{k+1}-\mathfrak{e}_k) \\
&(\times)\Big[\frac{1}{\Gamma(p_1)}\int_{\mathfrak{t}_k}^{\mathfrak{e}_k}(\mathfrak{e}_k-\omega)^{p_1-1}\mathscr{I}_k(\omega,\mathfrak{z}(\mathfrak{t}_k^-))d\omega - \mathcal{K}(\mathfrak{e}_k,\mathfrak{z}(\mathfrak{e}_k))\Big] \\
&-\mathcal{K}(\mathfrak{t}_{k+1},\mathfrak{z}(\mathfrak{t}_{k+1})) - \int_{\mathfrak{e}_k}^{\mathfrak{t}_{k+1}} K_{p_1}(\mathfrak{t}_{k+1}-\omega)\mathfrak{F}(\omega,\mathfrak{z}(\omega))d\omega\Bigg]d\tau \\
&= \mathfrak{z}_{\mathfrak{t}_{k+1}},
\end{aligned}$$

with

$$\begin{aligned}||\mathrm{u}(\mathrm{t})|| &\leq \mathscr{M}_w^m\left(||\mathfrak{z}_{\mathrm{t}_{k+1}}|| + \mathscr{M}\left(\frac{\mathscr{M}_{\mathscr{I}}\mathrm{t}_{k+1}^{p_1}}{\Gamma(p_1+1)} + \mu_p\right) + \mu_p + \frac{\mathscr{M}_1\mathrm{t}_{k+1}^{p_1}}{p_1}\wp(l)||\Psi||_{L[0,\mathrm{t}_{k+1}]}\right)\\ &\leq \mathscr{M}_w^m(||\mathfrak{z}_{\mathrm{t}_{k+1}}|| + \mathcal{N}_1)\\ &= \mathscr{M}_{\mathrm{u}}^m.\end{aligned}$$

Theorem 3.4. *The system* (1.1) *is totally controllable on* $\mathcal{I}$, *if it meets the assumptions* (*H*1)–(*H*7) *together with the conditions*

$$[\mathscr{M}\lambda + 2\mathcal{L}_p^* + \mathscr{M}_{\mathscr{I}}(\mathscr{M}+1) + 4\mathcal{L}_{\mathrm{u}}^*\sigma^*\mathscr{M}_1\mathscr{M}_b\mathscr{M}_w + 4\mathscr{M}_1\mathcal{L}_k] < 1. \tag{3.3}$$

Proof. Construct $\mathcal{G} : PC_{1-\eta}(\mathcal{I},\mathcal{Y}) \to PC_{1-\eta}(\mathcal{I},\mathcal{Y})$ as

$$(\mathcal{G}\mathfrak{z})(\mathrm{t}) = \begin{cases} S_{p_1,p_2}(\mathrm{t})\left[\lambda\int_0^T \mathfrak{z}(\omega)d\omega + c - \mathcal{K}(0,\mathfrak{z}(0))\right] + \mathcal{K}(\mathrm{t},\mathfrak{z}(\mathrm{t}))\\ +\int_0^{\mathrm{t}} K_{p_1}(\mathrm{t}-\omega)[B\mathrm{u}(\omega) + \mathfrak{F}(\omega,\mathfrak{z}(\omega))]d\omega, \qquad \mathrm{t}\in(0,\mathrm{t}_1];\\ \frac{1}{\Gamma(p_1)}\int_{\mathrm{t}_k}^{\mathrm{t}}(\mathrm{t}-\omega)^{p_1-1}\mathscr{I}_k(\omega,\mathfrak{z}(\mathrm{t}_k^-))d\omega, \qquad \mathrm{t}\in(\mathrm{t}_k,\mathfrak{e}_k];\\ S_{p_1,p_2}(\mathrm{t}-\mathfrak{e}_k)\left[\frac{1}{\Gamma(p_1)}\int_{\mathrm{t}_k}^{\mathfrak{e}_k}(\mathfrak{e}_k-\omega)^{p_1-1}\mathscr{I}_k(\omega,\mathfrak{z}(\mathrm{t}_k^-))d\omega - \mathcal{K}(\mathfrak{e}_k,\mathfrak{z}(\mathfrak{e}_k))\right]\\ +\mathcal{K}(\mathrm{t},\mathfrak{z}(\mathrm{t})) + \int_{\mathfrak{e}_k}^{\mathrm{t}} K_{p_1}(\mathrm{t}-\omega)[B\mathrm{u}(\omega) + \mathfrak{F}(\omega,\mathfrak{z}(\omega))]d\omega, \quad \mathrm{t}\in(\mathfrak{e}_k,\mathrm{t}_{k+1}],\end{cases}$$

where $\mathrm{u}(\mathrm{t})$ is described in (3.1) and (3.2) for $(0,\mathrm{t}_1]$ and $(\mathfrak{e}_k,\mathrm{t}_{k+1}]$, respectively. Moreover, by Lemma 3.1, $\mathfrak{z}(\mathrm{t}_1) = \mathfrak{z}_{\mathrm{t}_1}$ and $\mathfrak{z}(\mathrm{t}_{k+1}) = \mathfrak{z}_{\mathrm{t}_{k+1}}$, $k = 1,2,\ldots,N$. Let
$\aleph_\gamma = \{\mathfrak{z}\in PC_{1-\eta}(\mathcal{I},\mathcal{Y}) : ||\mathfrak{z}||_{PC_{1-\eta}} \leq \gamma\} \subseteq PC_{1-\eta}(\mathcal{I},\mathcal{Y})$, $\gamma > 0$, and

$$\gamma > \max\left\{\mathcal{N} + \mathcal{C}_1(||\mathfrak{z}_{\mathrm{t}_1}|| + \mathcal{N}), \max_{k=1,2,\ldots,N}\{\mathcal{N}_1 + \mathcal{C}_2(||\mathfrak{z}_{\mathrm{t}_{k+1}}|| + \mathcal{N}_1)\}, \frac{\mathscr{M}_{\mathscr{I}}T^{p_1}}{\Gamma(p_1+1)}\right\}.$$

Step 1: $\mathcal{G} : \aleph_\gamma \to \aleph_\gamma$.
For $\mathrm{t}\in(0,\mathrm{t}_1]$, let $\mathfrak{z}\in\aleph_\gamma$

$$\begin{aligned}||(\mathcal{G}\mathfrak{z})(\mathrm{t})|| &\leq \left|\left|S_{p_1,p_2}(\mathrm{t})\left[\lambda\int_0^T \mathfrak{z}(\omega)d\omega + c - \mathcal{K}(0,\mathfrak{z}(0))\right]\right|\right| + \left|\left|\mathcal{K}(\mathrm{t},\mathfrak{z}(\mathrm{t}))\right|\right|\\ &\quad +\left|\left|\int_0^{\mathrm{t}} K_{p_1}(\mathrm{t}-\omega)\mathfrak{F}(\omega,\mathfrak{z}(\omega))d\omega\right|\right| + \left|\left|\int_0^{\mathrm{t}} K_{p_1}(\mathrm{t}-\omega)B\mathrm{u}(\omega)d\omega\right|\right|\\ &\leq \mathscr{M}(\lambda T||\mathfrak{z}|| + |c| + \mu_p) + \mu_p + \frac{\mathscr{M}_1\mathrm{t}_1^{p_1}}{p_1}\wp(l)||\Psi||_{L[0,\mathrm{t}_1]} + \frac{\mathscr{M}_1\mathscr{M}_b\mathscr{M}_{\mathrm{u}}^1\mathrm{t}^{p_1}}{p_1} \qquad (3.4)\\ &\leq \mathcal{N} + \frac{\mathscr{M}_1\mathscr{M}_b\mathscr{M}_w^1\mathrm{t}^{p_1}}{p_1}\left[||\mathfrak{z}_{\mathrm{t}_1}|| + \mathcal{N}\right]\\ &\leq \gamma.\end{aligned}$$

Also, for $\mathfrak{t} \in (\mathfrak{e}_k, \mathfrak{t}_{k+1}]$,

$$\begin{aligned} ||(\mathcal{G}\mathfrak{z})(\mathfrak{t})|| &\leq \left|\left|S_{p_1,p_2}(\mathfrak{t}-\mathfrak{e}_k)\left[\frac{1}{\Gamma(p_1)}\int_{\mathfrak{t}_k}^{\mathfrak{e}_k}(\mathfrak{e}_k-\omega)^{p_1-1}\mathscr{I}_k(\omega,\mathfrak{z}(\mathfrak{t}_k^-))d\omega - \mathcal{K}(\mathfrak{e}_k,\mathfrak{z}(\mathfrak{e}_k))\right]\right|\right| \\ &+\left|\left|\mathcal{K}(\mathfrak{t},\mathfrak{z}(\mathfrak{t}))\right|\right| + \left|\left|\int_{\mathfrak{e}_k}^{\mathfrak{t}} K_{p_1}(\mathfrak{t}-\omega)\mathfrak{F}(\omega,\mathfrak{z}(\omega))d\omega\right|\right| + \left|\left|\int_{\mathfrak{e}_k}^{\mathfrak{t}} K_{p_1}(\mathfrak{t}-\omega)B\mathfrak{u}(\omega)d\omega\right|\right| \\ &\leq \mathscr{M}\left(\frac{\mathscr{M}_{\mathscr{I}}\mathfrak{t}_{k+1}^{p_1}}{\Gamma(p_1+1)}+\mu_p\right)+\mu_p+\frac{\mathscr{M}_1\mathfrak{t}_1^{p_1}}{p_1}\wp(l)||\Psi||_{L[0,\mathfrak{t}_{k+1}]}+\frac{\mathscr{M}_1\mathscr{M}_b\mathscr{M}_{\mathfrak{u}}^1 T^{p_1}}{p_1} \\ &\leq \mathcal{N}_1+\frac{\mathscr{M}_1\mathscr{M}_b\mathscr{M}_w^m T^{p_1}}{p_1}\left(||\mathfrak{z}_{\mathfrak{t}_{k+1}}||+\mathcal{N}_1\right) \\ &\leq \gamma. \end{aligned} \tag{3.5}$$

Also, for $\mathfrak{t} \in (\mathfrak{t}_k, \mathfrak{e}_k]$, and $\mathfrak{z} \in \aleph_\gamma$,

$$||(\mathcal{G}\mathfrak{z})(\mathfrak{t})|| \leq \frac{\mathscr{M}_{\mathscr{I}}\mathfrak{t}_{k+1}^{p_1}}{\Gamma(p_1+1)} \leq \gamma. \tag{3.6}$$

Hence, from (3.4)–(3.6), for some $\mathfrak{t} \in \mathcal{I}$, gives $||(\mathcal{G}\mathfrak{z})(\mathfrak{t})||_{PC_{1-\eta}} \leq \gamma$. Then $\mathcal{G} : \aleph_\gamma \to \aleph_\gamma$.

Construct $\mathcal{G}_1, \mathcal{G}_2$ as:

$$(\mathcal{G}_1 y)(\mathfrak{t}) = \begin{cases} S_{p_1,p_2}(\mathfrak{t})\left[\lambda\int_0^T \mathfrak{z}(\omega)d\omega + c - \mathcal{K}(0,\mathfrak{z}(0))\right] + \mathcal{K}(\mathfrak{t},\mathfrak{z}(\mathfrak{t})), & \mathfrak{t}\in(0,\mathfrak{t}_1], \\ \frac{1}{\Gamma(p_1)}\int_{\mathfrak{t}_k}^{\mathfrak{t}}(\mathfrak{t}-\omega)^{p_1-1}\mathscr{I}_k(\omega,\mathfrak{z}(\mathfrak{t}_k^-))d\omega, & \mathfrak{t}\in(\mathfrak{t}_k,\mathfrak{e}_k],\ k=1,2,\ldots,N, \\ S_{p_1,p_2}(\mathfrak{t}-\mathfrak{e}_k)\left[\frac{1}{\Gamma(p_1)}\int_{\mathfrak{t}_k}^{\mathfrak{e}_k}(\mathfrak{e}_k-\omega)^{p_1-1}\mathscr{I}_k(\omega,\mathfrak{z}(\mathfrak{t}_k^-))d\omega - \mathcal{K}(\mathfrak{e}_k,\mathfrak{z}(\mathfrak{e}_k))\right] \\ +\mathcal{K}(\mathfrak{t},\mathfrak{z}(\mathfrak{t})), & \mathfrak{t}\in(\mathfrak{e}_k,\mathfrak{t}_{k+1}],\ k=1,2,\ldots,N, \end{cases}$$

and

$$(\mathcal{G}_2 y)(\mathfrak{t}) = \begin{cases} \int_0^{\mathfrak{t}} K_{p_1}(\mathfrak{t}-\omega)[B\mathfrak{u}(\omega)+\mathfrak{F}(\omega,\mathfrak{z}(\omega))]d\omega, & \mathfrak{t}\in(0,\mathfrak{t}_1], \\ 0, & \mathfrak{t}\in(\mathfrak{t}_k,\mathfrak{e}_k], \\ \int_{\mathfrak{e}_k}^{\mathfrak{t}} K_{p_1}(\mathfrak{t}-\omega)[B\mathfrak{u}(\omega)+\mathfrak{F}(\omega,\mathfrak{z}(\omega))]d\omega, & \mathfrak{t}\in(\mathfrak{e}_k,\mathfrak{t}_{k+1}]. \end{cases}$$

Clearly, $\mathcal{G} = \mathcal{G}_1 + \mathcal{G}_2$.

Step 2: $\mathcal{G}_1$ is contraction.

Let $\mathfrak{z} \in \aleph_\gamma$, for any $\mathfrak{t} \in (0, \mathfrak{t}_1]$,

$$\begin{aligned} ||[(\mathcal{G}_1\mathfrak{z}_1)(\mathfrak{t})-(\mathcal{G}_1\mathfrak{z}_2)(\mathfrak{t})]|| &= \left|\left|S_{p_1,p_2}(\mathfrak{t})\left(\lambda\int_0^T \mathfrak{z}_1(\omega)d\omega - \lambda\int_0^T \mathfrak{z}_2(\omega)d\omega\right)\right|\right| \\ &+||\mathcal{K}(\mathfrak{t},\mathfrak{z}_1(\mathfrak{t}))-\mathcal{K}(\mathfrak{t},\mathfrak{z}_2(\mathfrak{t}))|| \\ &\leq \mathscr{M}\lambda T||\mathfrak{z}_1(\omega)-\mathfrak{z}_2(\omega)||_{PC_{1-\eta}} + \mathcal{L}_p||\mathfrak{z}_1(\omega)-\mathfrak{z}_2(\omega)||_{PC_{1-\eta}} \\ &\leq (\mathscr{M}\lambda T+\mathcal{L}_p)||\mathfrak{z}_1-\mathfrak{z}_2||_{PC_{1-\eta}} \\ &\leq k_1||\mathfrak{z}_1-\mathfrak{z}_2||_{PC_{1-\eta}}. \end{aligned} \tag{3.7}$$

Also, for $\mathfrak{z} \in \aleph_\gamma$, $\mathfrak{t} \in (\mathfrak{e}_k, \mathfrak{t}_{k+1}]$,

$$\begin{aligned} ||(\mathcal{G}_1\mathfrak{z}_1)(\mathfrak{t}) - (\mathcal{G}_1\mathfrak{z}_2)(\mathfrak{t})|| &\leq \left(\mathscr{M}\left(\frac{K_{\mathscr{I}_k}\mathfrak{t}_{k+1}^{p_1}}{\Gamma(p_1+1)} + \mathcal{L}_p\right) + \mathcal{L}_p\right)||\mathfrak{z}_1 - \mathfrak{z}_2||_{PC_{1-\eta}} \\ &\leq k_1||\mathfrak{z}_1 - \mathfrak{z}_2||_{PC_{1-\eta}}. \end{aligned} \tag{3.8}$$

Also, for $\mathfrak{t} \in (\mathfrak{t}_k, \mathfrak{e}_k]$, and $\mathfrak{z} \in \aleph_\gamma$,

$$||(\mathcal{G}_1\mathfrak{z}_1)(\mathfrak{t}) - (\mathcal{G}_1\mathfrak{z}_2)(\mathfrak{t})|| \leq \frac{K_{\mathscr{I}_k}\mathfrak{t}_{k+1}^{p_1}}{\Gamma(p_1+1)}||\mathfrak{z}_1 - \mathfrak{z}_2||_{PC_{1-\eta}} \leq k_1||\mathfrak{z}_1 - \mathfrak{z}_2||_{PC_{1-\eta}}. \tag{3.9}$$

For any $\mathfrak{t} \in \mathcal{I}$, $||(\mathcal{G}_1\mathfrak{z}_1)(\mathfrak{t}) - (\mathcal{G}_1\mathfrak{z}_2)(\mathfrak{t})|| \leq k_1||\mathfrak{z}_1 - \mathfrak{z}_2||_{PC_{1-\eta}}$. Since $k_1 < 1$, $\mathcal{G}_1$ is contracting operator.

Step 3: By step 1, it is clear that $\mathcal{G}_2$ is bounded. To prove continuity, consider a sequence $\{\mathfrak{z}^n\}_{n=1}^{\infty}$ in $\aleph_\gamma$ such that $\mathfrak{z}^n \to \mathfrak{z}$ in $\aleph_\gamma$. For $\mathfrak{t} \in (0, \mathfrak{t}_1]$,

$$\begin{aligned} &||(\mathcal{G}_2\mathfrak{z}^n)(\mathfrak{t}) - (\mathcal{G}_2\mathfrak{z})(\mathfrak{t})|| \\ &\leq \left|\left|\mathfrak{t}^{\eta-1}\int_0^{\mathfrak{t}}(\mathfrak{t}-\omega)^{p_1-1}[\mathfrak{F}(\omega,\mathfrak{z}^n(\omega)) - \mathfrak{F}(\omega,\mathfrak{z}(\omega))]d\omega\right|\right| \\ &+\left|\left|\mathfrak{t}^{\eta-1}\int_0^{\mathfrak{t}}(\mathfrak{t}-\omega)^{p_1-1}[B\mathfrak{u}_{\mathfrak{z}^n}(\omega) - B\mathfrak{u}_{\mathfrak{z}}(\omega)]d\omega\right|\right| \\ &\leq \mathscr{M}_1\mathcal{L}_f\int_0^{\mathfrak{t}}||\mathfrak{z}^n(\omega) - \mathfrak{z}(\omega)||d\omega \\ &+\mathscr{M}_1\mathscr{M}_b\mathscr{M}_w^1\int_0^{\mathfrak{t}}\left[\left|\left|S_{p_1,p_2}(\mathfrak{t})(\lambda\int_0^T\mathfrak{z}^n(\omega)d\omega - \lambda\int_0^T\mathfrak{z}(\omega)d\omega\right)\right|\right| \\ &+||\mathcal{K}(\mathfrak{t}_1,\mathfrak{z}^n(\mathfrak{t}_1)) - \mathcal{K}(\mathfrak{t},\mathfrak{z}(\mathfrak{t}))|| + \int_0^{\mathfrak{t}_1}(\mathfrak{t}-\omega)^{p_1-1}||\mathfrak{F}(\omega,\mathfrak{z}^n(\omega))d\omega - \mathfrak{F}(\omega,\mathfrak{z}(\omega))||d\omega\right]d\tau \\ &\leq \mathscr{M}_1\mathcal{L}_f\frac{\mathfrak{t}_1^{p_1}}{p_1}||\mathfrak{z}^n - \mathfrak{z}||_{PC_{1-\eta}} + \mathcal{C}_1\left[\mathcal{L}_p + \mathscr{M}_1\mathcal{L}_f\frac{\mathfrak{t}_1^{p_1}}{p_1}\right]||\mathfrak{z}^n - \mathfrak{z}||_{PC_{1-\eta}}. \end{aligned} \tag{3.10}$$

Therefore, $||(\mathcal{G}_2\mathfrak{z}^n)(\mathfrak{t}) - (\mathcal{G}_2\mathfrak{z})(\mathfrak{t})|| \to 0$ as $n \to \infty$. Also, for $\mathfrak{t} \in (\mathfrak{e}_k, \mathfrak{t}_{k+1}]$, $k = 1, 2, \ldots, N$,

$$\begin{aligned} &||(\mathcal{G}_2\mathfrak{z}^n)(\mathfrak{t}) - (\mathcal{G}_2\mathfrak{z})(\mathfrak{t})|| \\ &\leq \left|\left|\mathfrak{t}^{1-\eta}\int_{\mathfrak{e}_k}^{\mathfrak{t}}(\mathfrak{t}-\omega)^{p_1-1}[\mathfrak{F}(\omega,\mathfrak{z}^n(\omega)) - \mathfrak{F}(\omega,\mathfrak{z}(\omega))]d\omega\right|\right| \\ &+\left|\left|\mathfrak{t}^{1-\eta}\int_{\mathfrak{e}_k}^{\mathfrak{t}}(\mathfrak{t}-\omega)^{p_1-1}[B\mathfrak{u}_{\mathfrak{z}^n}(\omega) - B\mathfrak{u}_{\mathfrak{z}}(\omega)]d\omega\right|\right| \\ &\leq \mathscr{M}_1\mathcal{L}_f\int_{\mathfrak{e}_k}^{\mathfrak{t}}||\mathfrak{z}^n(\omega) - \mathfrak{z}(\omega)||d\omega \\ &+\mathscr{M}_1\mathscr{M}_b\mathscr{M}_w^m\int_{\mathfrak{e}_k}^{\mathfrak{t}}\left(\left|\left|S_{p_1,p_2}(\mathfrak{t}_{k+1}-\mathfrak{e}_k)\left[\frac{1}{\Gamma(p_1)}\int_{\mathfrak{t}_k}^{\mathfrak{e}_k}(\mathfrak{e}_k-\omega)^{p_1-1}\right.\right.\right. \\ &\times[\mathscr{I}_k(\omega,\mathfrak{z}^n(\mathfrak{t}_k^-)) - \mathscr{I}_k(\omega,\mathfrak{z}(\mathfrak{t}_k^-))]d\omega + [\mathcal{K}(\mathfrak{e}_k,\mathfrak{z}^n(\mathfrak{e}_k)) - \mathcal{K}(\mathfrak{e}_k,\mathfrak{z}(\mathfrak{e}_k))]\left.\left.\right]\right|\right| \\ &+||\mathcal{K}(\mathfrak{t},\mathfrak{z}^n(\mathfrak{t})) - \mathcal{K}(\mathfrak{t},\mathfrak{z}(\mathfrak{t}))|| + \int_{\mathfrak{e}_k}^{\mathfrak{t}_{k+1}}(\mathfrak{t}_{k+1}-\omega)^{p_1-1}||\mathfrak{F}(\omega,\mathfrak{z}^n(\omega))d\omega - \mathfrak{F}(\omega,\mathfrak{z}(\omega))||d\omega\Bigg)d\tau \\ &\leq \mathscr{M}_1\mathcal{L}_f\frac{\mathfrak{t}_{k+1}^{p_1}}{p_1}||\mathfrak{z}^n - \mathfrak{z}||_{PC_{1-\eta}} \\ &+\mathcal{C}_2\left(\mathscr{M}\left(\frac{K_{\mathscr{I}_k}\mathfrak{t}_{k+1}^{p_1}}{\Gamma(p_1+1)} + \mathcal{L}_p\right) + \mathcal{L}_p + \mathscr{M}_1\mathcal{L}_f\frac{\mathfrak{t}_{k+1}^{p_1}}{p_1}\right)||\mathfrak{z}^n - \mathfrak{z}||_{PC_{1-\eta}}. \end{aligned} \tag{3.11}$$

Hence, $||(\mathcal{G}_2\mathfrak{z}^n)(\mathfrak{t}) - (\mathcal{G}_2\mathfrak{z})(\mathfrak{t})||$ approaches to 0 as n approaches to ∞. Hence from (3.10) and (3.11) and for each $\mathfrak{t} \in \mathcal{I}$, $||(\mathcal{G}_2\mathfrak{z}^n)(\mathfrak{t}) - (\mathcal{G}_2\mathfrak{z})(\mathfrak{t})|| \to 0$ as $n \to \infty$.

Step 4: $\mathcal{G}_2$ is equicontinuous.

Take $\tau_1 < \tau_2$ on $\aleph_\gamma$, and for $\tau_1, \tau_2 \in (0, \mathfrak{t}_1]$,

$$\begin{aligned}
&||(\mathcal{G}_2\mathfrak{z})(\tau_2) - (\mathcal{G}_2\mathfrak{z})(\tau_1)|| \\
&\leq \Big|\Big|\tau_2^{\eta-1}\int_0^{\tau_2}(\tau_2-\omega)^{p_1-1}[\mathfrak{F}(\omega,\mathfrak{z}(\omega)) + B\mathfrak{u}(\omega)]d\omega \\
&-\tau_1^{\eta-1}\int_0^{\tau_1}(\tau_1-\omega)^{p_1-1}[\mathfrak{F}(\omega,\mathfrak{z}(\omega)) + B\mathfrak{u}(\omega)]d\omega\Big|\Big| \\
&\leq \mathscr{M}_1\mathcal{L}_f\Big(\int_0^{\tau_1}[\tau_2^{\eta-1}(\tau_2-\omega)^{p_1-1} - \tau_1^{\eta-1}(\tau_1-\omega)^{p_1-1}]d\omega + \int_{\tau_1}^{\tau_2}\tau_2^{\eta-1}(\tau_2-\omega)^{p_1-1}d\omega\Big) \\
&+\mathscr{M}_1\mathscr{M}_b\mathscr{M}_w^1(||\mathfrak{z}_{\mathfrak{t}_1}|| + \mathcal{N})\Big(\int_0^{\tau_1}[\tau_2^{\eta-1}(\tau_2-\omega)^{p_1-1} - \tau_1^{\eta-1}(\tau_1-\omega)^{p_1-1}]d\omega \\
&+\int_{\tau_1}^{\tau_2}\tau_2^{\eta-1}(\tau_2-\omega)^{p_1-1}d\omega\Big).
\end{aligned} \tag{3.12}$$

Similarly, For $\tau_1, \tau_2 \in (\mathfrak{e}_k, \mathfrak{t}_{k+1}]$,

$$\begin{aligned}
&||(\mathcal{G}_2\mathfrak{z})(\tau_2) - (\mathcal{G}_2\mathfrak{z})(\tau_1)|| \\
&\leq \Big|\Big|\tau_2^{\eta-1}\int_{\mathfrak{e}_k}^{\tau_2}(\tau_2-\omega)^{p_1-1}[\mathfrak{F}(\omega,\mathfrak{z}(\omega)) + B\mathfrak{u}(\omega)]d\omega \\
&-\int_{\mathfrak{e}_k}^{\tau_1}(\tau_1-\omega)^{p_1-1}[\mathfrak{F}(\omega,\mathfrak{z}(\omega)) + B\mathfrak{u}(\omega)]d\omega\Big|\Big| \\
&\leq \mathscr{M}_1\mathcal{L}_f\Big(\int_{\mathfrak{e}_k}^{\tau_1}[\tau_2^{\eta-1}(\tau_2-\omega)^{p_1-1} - \tau_1^{\eta-1}(\tau_1-\omega)^{p_1-1}]d\omega + \int_{\tau_1}^{\tau_2}\tau_2^{\eta-1}(\tau_2-\omega)^{p_1-1}d\omega\Big) \\
&+\mathscr{M}_1\mathscr{M}_b\mathscr{M}_w^m(||\mathfrak{z}_{\mathfrak{t}_{k+1}}|| + \mathcal{N}_1)\Big(\int_{\mathfrak{e}_k}^{\tau_1}[\tau_2^{\eta-1}(\tau_2-\omega)^{p_1-1} - \tau_1^{\eta-1}(\tau_1-\omega)^{p_1-1}]d\omega \\
&+\int_{\tau_1}^{\tau_2}\tau_2^{\eta-1}(\tau_2-\omega)^{p_1-1}d\omega\Big).
\end{aligned} \tag{3.13}$$

By ($H3$), $||(\mathcal{G}_2\mathfrak{z})(\tau_2) - (\mathcal{G}_2\mathfrak{z})(\tau_1)|| \to 0$ as $\tau_2 \to \tau_1$. Then $\mathcal{G}_2$ is equicontinuous.

The countable subset $D_0 = \{\mathfrak{z}_n\}_{n=1}^{\infty} \subset D$, and by Lemma 2.4, we have

$$\ell(\mathcal{G}_2(D))_{PC_{1-\eta}} \leq 2\,\ell(\mathcal{G}_2(D_0))_{PC_{1-\eta}}, \tag{3.14}$$

where D is a bounded subset of $\aleph_\gamma$. Since $\mathcal{G}_2(D_0) \subset \mathcal{G}_2(\aleph_\gamma)$ is bounded and equicontinuous, by Lemma 2.6,

$$\ell(\mathcal{G}_2(D_0))_{PC_{1-\eta}} \leq \max_{\mathfrak{t}\in(\mathfrak{e}_k,\mathfrak{t}_{k+1}],\ k=0,1,2,\ldots,N} \ell(\mathcal{G}_2(D_0))_{PC_{1-\eta}}(\mathfrak{t}). \tag{3.15}$$

Moreover, for $\mathfrak{t} \in (\mathfrak{e}_k, \mathfrak{t}_{k+1}]$, (*H*4), (*H*7) and $\mathcal{G}_2$, with Lemma 2.5, we have

$$\begin{aligned}\ell(\mathcal{G}_2(D_0))(\mathfrak{t}) &\leq \ell\Big(\mathscr{M}_1 \int_{\mathfrak{e}_k}^{\mathfrak{t}} \Big[B\mathfrak{u}(\omega, \{\mathfrak{z}_n(\omega)\}_{n=1}^{\infty}) + \mathfrak{F}(\omega, \{\mathfrak{z}_n(\omega)\}_{n=1}^{\infty})\Big] d\omega\Big) \\ &\leq [2\mathcal{L}_{\mathfrak{u}}^{*}\sigma^{*}\mathscr{M}_1\mathscr{M}_b\mathscr{M}_w + 2\mathscr{M}_1\mathcal{L}_k] \int_{\mathfrak{e}_k}^{\mathfrak{t}} \ell(\{\mathfrak{z}_n(\omega)\}_{n=1}^{\infty}) d\omega \\ &\leq [2\mathcal{L}_{\mathfrak{u}}^{*}\sigma^{*}\mathscr{M}_1\mathscr{M}_b\mathscr{M}_w + 2\mathscr{M}_1\mathcal{L}_k]\ell(D)_{PC_{1-\eta}}(\mathfrak{t}_{k+1} - \mathfrak{e}_k).\end{aligned} \tag{3.16}$$

Then, by (3.14)–(3.16) and (*H*2),

$$\begin{aligned}\ell(\mathcal{G}_2(D)(\mathfrak{t}))_{PC_{1-\eta}} &\leq [2\mathcal{L}_{\mathfrak{u}}^{*}\sigma^{*}\mathscr{M}_1\mathscr{M}_b\mathscr{M}_w + 2\mathscr{M}_1\mathcal{L}_k]\ell(D)_{PC_{1-\eta}}(\mathfrak{t}_{k+1} - \mathfrak{e}_k) \\ &\leq [4\mathcal{L}_{\mathfrak{u}}^{*}\sigma^{*}\mathscr{M}_1\mathscr{M}_b\mathscr{M}_w + 4\mathscr{M}_1\mathcal{L}_k]\ell(D)_{PC_{1-\eta}}.\end{aligned} \tag{3.17}$$

Now, for any $\mathfrak{t} \in (\mathfrak{e}_k, \mathfrak{t}_{k+1}]$, on $D \in \aleph_\gamma$,

$$\ell(\mathcal{G}_1(D)) \leq [\mathscr{M}\lambda + 2\mathcal{L}_p^{*} + \mathscr{M}_{\mathscr{I}}(\mathscr{M}+1)]\ell(D). \tag{3.18}$$

Also,

$$\begin{aligned}&\ell(\mathcal{G}(D)) \leq \ell(\mathcal{G}_1(D)) + \ell(\mathcal{G}_2(D)) \\ &\leq [\mathscr{M}\lambda + 2\mathcal{L}_p^{*} + \mathscr{M}_{\mathscr{I}}(\mathscr{M}+1) + 4\mathcal{L}_{\mathfrak{u}}^{*}\sigma^{*}\mathscr{M}_1\mathscr{M}_b\mathscr{M}_w + 4\mathscr{M}_1\mathcal{L}_k]\ell(D)_{PC_{1-\eta}}.\end{aligned} \tag{3.19}$$

Combining Lemma 3.1, and (3.3) and (3.19) it is clear that the mapping $\mathcal{G}$ from $\aleph_\gamma$ to $\aleph_\gamma$ is κ-set-contractive. Hence, the system $\mathcal{G}$ has a fixed point by Lemma 3.2. This completes the proof.

4 Optimal control

(*H*8) (i) The Lagrange function $\mathfrak{L} : \mathcal{I} \times \mathcal{Y} \times U \to \mathbb{R} \cup \{\infty\}$ is Borel measurable;
(ii) For $\mathfrak{t} \in \mathcal{I}$, and for every $\mathfrak{z}_1, \mathfrak{z}_2 \in \mathcal{Y}$, $\mathfrak{L}(\mathfrak{t}, \mathfrak{z}, \cdot)$ is convex on U;
(iii) For almost all $\mathfrak{t} \in \mathcal{I}$, $\mathfrak{L}(\mathfrak{t}, \cdot, \cdot)$ is sequentially lower semi continuous on $\mathcal{Y} \times U$;
(iv) For $\mathfrak{c}_1 \geq 0, \mathfrak{c}_2 > 0, \mathfrak{h} \in L^P(\mathcal{I}, \mathbb{R})$,

$$\mathfrak{L}(\mathfrak{t}, \mathfrak{z}, \mathfrak{u}) \geq \mathfrak{h}(\mathfrak{t}) + \mathfrak{c}_1||\mathfrak{z}||_{PC_{1-\eta}} + \mathfrak{c}_2||\mathfrak{u}||^P.$$

This part deals with the verification of existence of optimal pair for the system (1.1) by sequencing technique as discussed in [46, 48]. Let the cost function($\mathfrak{L}$) as:

$$\mathfrak{I}(\mathfrak{z}^{\mathfrak{u}}, \mathfrak{u}) = \int_0^T \mathfrak{L}(\mathfrak{t}, \mathfrak{z}(\mathfrak{t}), \mathfrak{u}(\mathfrak{t}))d\mathfrak{t}, \quad \mathfrak{u} \in \mathcal{U}_{ad}.$$

Define the admissible control function $\mathcal{U}_{ad}$ as:

$$\mathcal{U}_{ad} = \{\mathfrak{u} \in L^P(\mathcal{I}, H);\ \mathfrak{u}(\mathfrak{t}) \in \wp(\mathfrak{t}),\ a.e.\ \mathfrak{t} \in \mathcal{I}\}, \quad P > 1,$$

where $\mathfrak{u}(\mathfrak{t})$ takes its values in $\mathcal{S} \subset U$. A multivalued map $\wp : \mathcal{I} \to PC_{1-\eta}$, is measurable as $\wp(\cdot) \subset \mathcal{S}$. It is clear that $\mathcal{U}_{ad}$ is bounded, convex & closed with $\mathcal{U}_{ad} = 0$. Define the solution set

$$\mathcal{T}(\mathfrak{u}) = \{\mathfrak{z}^{\mathfrak{u}} \in \aleph_\gamma : \mathfrak{z}^{\mathfrak{u}}\ \mathfrak{u} \in \mathcal{U}_{ad}\}.$$

Also, the set of all $A_{ad} = \{(\mathfrak{z}^{\mathfrak{u}}, \mathfrak{u});\ \mathfrak{u} \in \mathcal{U}_{ad};\ \mathfrak{z}^{\mathfrak{u}} \in \mathcal{T}(\mathfrak{u})\}$.

Theorem 4.1. *The system (1.1) is optimal controllable together with the assumptions (H1)-(H8) provided*

$$\mathfrak{I}(\tilde{\mathfrak{z}}^{\mathfrak{u}^0}, \mathfrak{u}^0) = \int_0^T \mathfrak{L}(\mathfrak{t}, \tilde{\mathfrak{z}}^{\mathfrak{u}^0}(\mathfrak{t}), \mathfrak{u}^0(\mathfrak{t}))d\mathfrak{t} \leq \mathfrak{I}(\mathfrak{z}^{\mathfrak{u}}, \mathfrak{u}),\ \forall\ (\mathfrak{z}^{\mathfrak{u}}, \mathfrak{u}) \in A_{ad}.$$

Proof. Define $\mathfrak{I}(\mathfrak{u}) = \inf_{\mathfrak{z}^{\mathfrak{u}} \in \mathcal{T}(\mathfrak{u})} \mathfrak{I}(\mathfrak{z}^{\mathfrak{u}}, \mathfrak{u})$. Initially we prove $\mathfrak{I}(\overline{\mathfrak{z}}^{\mathfrak{u}}, \mathfrak{u}) = \mathfrak{I}(\mathfrak{u}),\ \ \mathfrak{z}^{\mathfrak{u}} \in \mathcal{T}(\mathfrak{u})$. If $\mathfrak{I}(\mathfrak{u}) = +\infty$ or $\mathcal{T}(\mathfrak{u})$ has finite elements, the proof is trivial. Using (*H*8)(*iv*), $\mathfrak{I}(\mathfrak{u}) > -\infty$. Let $\mathfrak{I}(\mathfrak{u}) < \infty$. By infimum properties, a sequence $\{\mathfrak{z}_n^{\mathfrak{u}}\}_{n=1}^{\infty} \in \mathcal{T}(\mathfrak{u})$ satisfies $\mathfrak{I}(\mathfrak{z}_n^{\mathfrak{u}}, \mathfrak{u}) \to \mathfrak{I}(\mathfrak{u})$ as $n \to \infty$. Using reflexive property, $\{\mathfrak{u}^0\} \in \mathcal{T}(\mathfrak{u})$ provided $\mathfrak{u}^0 \in \mathcal{U}_{ad}$.

For $n \geq 1$,

$$(\mathfrak{z}_n^{\mathfrak{u}})(\mathfrak{t}) = \begin{cases} S_{p_1,p_2}(\mathfrak{t})\left[\lambda \int_0^T \mathfrak{z}_n^{\mathfrak{u}}(\omega)d\omega + c - \mathcal{K}(0, \mathfrak{z}(0))\right] + \mathcal{K}(\mathfrak{t}, \mathfrak{z}_n^{\mathfrak{u}}(\mathfrak{t})) \\ + \int_0^{\mathfrak{t}} K_{p_1}(\mathfrak{t}-\omega)[B\mathfrak{u}(\omega) + \mathfrak{F}(\omega, \mathfrak{z}_n^{\mathfrak{u}}(\omega))]d\omega, \qquad \mathfrak{t} \in (0, \mathfrak{t}_1]; \\ S_{p_1,p_2}(\mathfrak{t}-\mathfrak{e}_k)\left[\frac{1}{\Gamma(p_1)} \int_{\mathfrak{t}_k}^{\mathfrak{e}_k} (\mathfrak{e}_k - \omega)^{p_1-1} \mathscr{I}_k(\omega, \mathfrak{z}_n^{\mathfrak{u}}(\mathfrak{t}_k^-))d\omega - \mathcal{K}(\mathfrak{e}_k, \mathfrak{z}_n^{\mathfrak{u}}(\mathfrak{e}_k))\right] \\ + \mathcal{K}(\mathfrak{t}, \mathfrak{z}_n^{\mathfrak{u}}(\mathfrak{t})) + \int_{\mathfrak{e}_k}^{\mathfrak{t}} K_{p_1}(\mathfrak{t}-\omega)[B\mathfrak{u}(\omega) + \mathfrak{F}(\omega, \mathfrak{z}_n^{\mathfrak{u}}(\omega))]d\omega,\ \ \mathfrak{t} \in (\mathfrak{e}_k, \mathfrak{t}_{k+1}], \end{cases}$$

where

$$(\mathfrak{z}_n^{\mathfrak{u}})(\mathfrak{t}) = (\mathcal{G}_1\mathfrak{z}_n^{\mathfrak{u}})(\mathfrak{t}) + (\mathcal{G}_2\mathfrak{z}_n^{\mathfrak{u}})(\mathfrak{t}) = (\mathcal{G}\mathfrak{z}_n^{\mathfrak{u}})(\mathfrak{t}).$$

To prove $(\mathcal{B}\mathfrak{z}_n^{\mathfrak{u}})(\mathfrak{t}) : \{\mathcal{G}_2(\mathfrak{t});\ \mathfrak{z}_n^{\mathfrak{u}} \in \aleph\gamma\}$ is relatively compact in $PC_{1-\eta}$ for each $\mathfrak{t} \in \mathcal{I}$.

It is clear that $\mathcal{B}(0) : \{\mathcal{G}_2(0);\ \mathfrak{z}_n^{\mathfrak{u}} \in \aleph\gamma\}$ is relatively compact. For any $\mathfrak{u} \in U,\ \mathfrak{t} \in \mathcal{I},\ \ \mathfrak{z}_n^{\mathfrak{u}} \in \aleph_\gamma$,

$$(\mathcal{G}_2\mathfrak{z}_n^{\mathfrak{u}})(\mathfrak{t}) = \int_0^{\mathfrak{t}} K_{p_1}(\mathfrak{t}-\omega)[B\mathfrak{u}(\omega) + \mathfrak{F}(\omega, \mathfrak{z}_n^{\mathfrak{u}}(\omega))]d\omega.$$

By (*H*3), and the property of admissible of control functions the set $\mathcal{W}_\epsilon = \{K_{p_1}(\mathfrak{t}-\omega)[B\mathfrak{u}(\omega) + \mathfrak{F}(\omega, \mathfrak{z}_n^{\mathfrak{u}}(\omega))]; 0 \leq \mathfrak{e}_k \leq \mathfrak{t}_k - \epsilon\}$ is relatively compact. Therefore, $\overline{\mathcal{W}_\epsilon}$, the convex hull of $\mathcal{W}_\epsilon$ is compact due to Lemma 2.3(ii). Using Lemma 2.5, we can conclude $(\mathcal{G}_2^\epsilon\mathfrak{z}_n^{\mathfrak{u}})(\mathfrak{t}) \in \overline{\mathcal{W}_\epsilon}$ for all $\mathfrak{t} \in \mathcal{I}$. Therefore $\mathcal{B}_\epsilon(\mathfrak{t}) : \{(\mathcal{G}_2^\epsilon\mathfrak{z}_n^{\mathfrak{u}})(\mathfrak{t});\ \mathfrak{z}_n^{\mathfrak{u}} \in \aleph\gamma\}$ is relatively compact in $PC_{1-\eta}$. For $\mathfrak{t} \in (0, \mathfrak{t}_1]$,

$$\begin{aligned} &||(\mathcal{G}_2\mathfrak{z}_n^{\mathfrak{u}})(\mathfrak{t}) - (\mathcal{G}_2^\epsilon\mathfrak{z}_n^{\mathfrak{u}})(\mathfrak{t})|| \\ &\leq \left|\left| \int_0^{\mathfrak{t}} K_{p_1}(\mathfrak{t}-\omega)[\mathfrak{F}(\omega, \mathfrak{z}_n^{\mathfrak{u}}(\omega)) + B\mathfrak{u}(\omega)]d\omega - \int_0^{\mathfrak{t}-\epsilon} [\mathfrak{F}(\omega, \mathfrak{z}_n^{\mathfrak{u}}(\omega)) + B\mathfrak{u}(\omega)]d\omega \right|\right| \\ &\leq \int_{\mathfrak{t}-\epsilon}^{\mathfrak{t}} K_{p_1}(\mathfrak{t}-\omega)[\mathfrak{F}(\omega, \mathfrak{z}_n^{\mathfrak{u}}(\omega)) + B\mathfrak{u}(\omega)]d\omega \\ &\leq \mathscr{M}_1\mathcal{L}_f \int_{\mathfrak{t}-\epsilon}^{\mathfrak{t}} ||\mathfrak{z}_n^{\mathfrak{u}}(\omega)||d\omega + \mathscr{M}_1\mathscr{M}_b||\mathfrak{u}||_{\mathcal{L}_p}. \end{aligned}$$

Similarly, for $\mathfrak{t} \in (\mathfrak{e}_k, \mathfrak{t}_{k+1}]$,

$$\begin{aligned}
&||(\mathcal{G}_2\mathfrak{z}_n^{\mathfrak{u}})(\mathfrak{t}) - (\mathcal{G}_2^{\epsilon}\mathfrak{z}_n^{\mathfrak{u}})(\mathfrak{t})|| \\
&\leq \Big|\Big| \int_{\mathfrak{e}_k}^{\mathfrak{t}} K_{p_1}(\mathfrak{t}-\omega)[\mathfrak{F}(\omega, \mathfrak{z}_n^{\mathfrak{u}}(\omega)) + B\mathfrak{u}(\omega)]d\omega - \int_{\mathfrak{e}_k}^{\mathfrak{t}-\epsilon} [\mathfrak{F}(\omega, \mathfrak{z}_n^{\mathfrak{u}}(\omega)) + B\mathfrak{u}(\omega)]d\omega \Big|\Big| \\
&\leq \int_{\mathfrak{t}-\epsilon}^{\mathfrak{t}} K_{p_1}(\mathfrak{t}-\omega)[\mathfrak{F}(\omega, \mathfrak{z}_n^{\mathfrak{u}}(\omega)) + B\mathfrak{u}(\omega)]d\omega \\
&\leq \mathscr{M}_1\mathcal{L}_f \int_{\mathfrak{t}-\epsilon}^{\mathfrak{t}} ||\mathfrak{z}_n^{\mathfrak{u}}(\omega)||d\omega + \mathscr{M}_1\mathscr{M}_b||\mathfrak{u}||_{\mathcal{L}_p},
\end{aligned}$$

implies that $\lim \epsilon \to 0||(\mathcal{G}_2\mathfrak{z}_n^{\mathfrak{u}})(\mathfrak{t}) - (\mathcal{G}_2^{\epsilon}\mathfrak{z}_n^{\mathfrak{u}})(\mathfrak{t})|| = 0$. Hence $\mathcal{B}_{\epsilon}(\mathfrak{t})$, is a family of relatively compact sets. Moreover, $\mathcal{G}_1\mathfrak{z}_n^{\mathfrak{u}}$ is bounded and equicontinuous in $\aleph_{\gamma}$. By (3.16) and (3.18) we have

$$\ell(\mathfrak{z}_n^{\mathfrak{u}}) \leq [\mathscr{M}\lambda + 2\mathcal{L}_p^* + \mathscr{M}_{\mathscr{I}}(\mathscr{M}+1) + 4\mathcal{L}_{\mathfrak{u}}^*\sigma^*\mathscr{M}_1\mathscr{M}_b\mathscr{M}_w + 4\mathscr{M}_1\mathcal{L}_k]\ell(\mathfrak{z}_n^{\mathfrak{u}}),$$

leads to $\ell(\{\mathfrak{z}_n^{\mathfrak{u}}\}_{n=0}^{\infty}) = 0$ by using (3.3). Hence, $\{\mathfrak{z}_n^{\mathfrak{u}}\}_{n=1}^{\infty}$ is relatively compact in $PC_{1-\eta}$. Assume $\tilde{\mathfrak{z}}^{\mathfrak{u}}$, a subsequence in $PC_{1-\eta}$ of $\{\mathfrak{z}_n^{\mathfrak{u}}\}_{n=0}^{\infty}$ such that $\mathfrak{z}_n^{\mathfrak{u}} \to \tilde{\mathfrak{z}}^{\mathfrak{u}}$ as $\lim n \to \infty$. Moreover, by Lebesgue theorem and ($H1$), ($H3$), ($H5$)

$$(\tilde{\mathfrak{z}}^{\mathfrak{u}})(\mathfrak{t}) = \begin{cases}
S_{p_1,p_2}(\mathfrak{t})\Big[\lambda \int_0^T \tilde{\mathfrak{z}}^{\mathfrak{u}}(\omega)d\omega + c - \mathcal{K}(0, \mathfrak{z}(0))\Big] + \mathcal{K}(\mathfrak{t}, \tilde{\mathfrak{z}}^{\mathfrak{u}}(\mathfrak{t})) \\
+ \int_0^{\mathfrak{t}} K_{p_1}(\mathfrak{t}-\omega)[B\mathfrak{u}(\omega) + \mathfrak{F}(\omega, \tilde{\mathfrak{z}}^{\mathfrak{u}}(\omega))]d\omega, \qquad \mathfrak{t} \in (0, \mathfrak{t}_1]; \\
S_{p_1,p_2}(\mathfrak{t}-\mathfrak{e}_k)\Big[\frac{1}{\Gamma(p_1)}\int_{\mathfrak{t}_k}^{\mathfrak{e}_k} (\mathfrak{e}_k - \omega)^{p_1-1}\mathscr{I}_k(\omega, \tilde{\mathfrak{z}}^{\mathfrak{u}}(\mathfrak{t}_k^-))d\omega - \mathcal{K}(\mathfrak{e}_k, \tilde{\mathfrak{z}}^{\mathfrak{u}}(\mathfrak{e}_k))\Big] \\
+\mathcal{K}(\mathfrak{t}, \tilde{\mathfrak{z}}^{\mathfrak{u}}(\mathfrak{t})) + \int_{\mathfrak{e}_k}^{\mathfrak{t}} K_{p_1}(\mathfrak{t}-\omega)[B\mathfrak{u}(\omega) + \mathfrak{F}(\omega, \tilde{\mathfrak{z}}^{\mathfrak{u}}(\omega))]d\omega, \quad \mathfrak{t} \in (\mathfrak{e}_k, \mathfrak{t}_{k+1}].
\end{cases}$$

Then, $\tilde{\mathfrak{z}}^{\mathfrak{u}} \in \mathcal{T}(\mathfrak{u})$ is continuously embedded in $L^1(\mathcal{I}, U)$, by Balder's theorem [49] and ($H8$),

$$\mathfrak{I}(\mathfrak{u}) = \lim_{n\to\infty} \int_0^T \mathfrak{L}(\mathfrak{t}, \mathfrak{z}_n^{\mathfrak{u}}(\mathfrak{t}), \mathfrak{u}(\mathfrak{t}))d\mathfrak{t} \geq \int_0^T \mathfrak{L}(\mathfrak{t}, \tilde{\mathfrak{z}}^{\mathfrak{u}}(\mathfrak{t}), \mathfrak{u}(\mathfrak{t}))d\mathfrak{t} = \mathfrak{I}(\tilde{\mathfrak{z}}^{\mathfrak{u}}, \mathfrak{u}) \geq \mathfrak{I}(\mathfrak{u}),$$

which shows $\mathfrak{I}(\tilde{\mathfrak{z}}^{\mathfrak{u}}, \mathfrak{u}) \to \mathfrak{I}(\mathfrak{u})$. Therefore, $\mathfrak{I}(\mathfrak{u})$ reaches its least value at $\tilde{\mathfrak{z}}^{\mathfrak{u}} \in \mathcal{T}(\mathfrak{u})$ for every $\mathfrak{u} \in \mathcal{U}_{ad}$.

Also, consider $\mathfrak{u}^0 \in \mathcal{U}_{ad}$ such that $\mathfrak{I}(\mathfrak{u}) = \inf_{\mathfrak{u}\in\mathcal{U}_{ad}} \mathfrak{I}(\mathfrak{u})$. By the infimum property, $\{\mathfrak{u}_n\}_{n=0}^{\infty} \subseteq \mathcal{U}_{ad}$ provided $\lim_{n\to\infty} \mathfrak{I}(\mathfrak{u}_n) = \inf_{\mathfrak{u}\in\mathcal{U}_{ad}} \mathfrak{I}(\mathfrak{u})$. Since $\{\mathfrak{u}_n\}_{n=0}^{\infty}$ in $\mathcal{L}_P(\mathcal{I}, U)$ is bounded for $P > 1$, $\mathfrak{u}^0 \in \mathcal{L}_P(\mathcal{I}, U)$ and by relative compactness of $\mathfrak{z}_n^{\mathfrak{u}}$ there is a subsequence $\tilde{\mathfrak{z}}^{\mathfrak{u}^0} \in PC_{1-\eta}$ as $\lim_{n\to\infty} \mathfrak{z}_n^{\mathfrak{u}} \to \tilde{\mathfrak{z}}^{\mathfrak{u}^0}$. Using Balder's theorem [49] and the property that $PC_{1-\eta} \to \mathcal{L}(\mathcal{I}, U)$ is continuous, we conclude

$$\begin{aligned}
\inf_{\mathfrak{u}\in\mathcal{U}_{ad}} \mathfrak{I}(\mathfrak{u}) &= \lim_{n\to\infty} \int_0^T \mathfrak{L}(\mathfrak{t}, \mathfrak{z}_n^{\mathfrak{u}_n}(\mathfrak{t}), \mathfrak{u}_n(\mathfrak{t}))d\mathfrak{t} \geq \int_0^T \mathfrak{L}(\mathfrak{t}, \tilde{\mathfrak{z}}^{\mathfrak{u}^0}(\mathfrak{t}), \mathfrak{u}^0(\mathfrak{t}))d\mathfrak{t} = \mathfrak{I}(\tilde{\mathfrak{z}}^{\mathfrak{u}^0}, \mathfrak{u}^0) \\
&= \mathfrak{I}(\mathfrak{u}^0) \geq \inf_{\mathfrak{u}\in\mathcal{U}_{ad}} \mathfrak{I}(\mathfrak{u}).
\end{aligned}$$

Therefore, $\mathfrak{I}(\mathfrak{u}) = \inf_{\mathfrak{u}\in\mathcal{U}_{ad}} \mathfrak{I}(\mathfrak{u})$, leads that $\mathcal{I}$ attains its minimum at $\mathfrak{u}^0 \in \mathcal{U}_{ad}$. Subsequently, we have

$$\mathcal{I}(\tilde{\mathfrak{z}}^{\mathfrak{u}^0}, \mathfrak{u}^0) = \inf_{\mathfrak{u}\in\mathcal{U}_{ad}} \mathfrak{I}(\mathfrak{u}) = \inf_{(\mathfrak{z}^{\mathfrak{u}}, \mathfrak{u})\in A_{ad}} \mathfrak{I}(\mathfrak{z}^{\mathfrak{u}}, \mathfrak{u}).$$

Hence, $(\tilde{\mathfrak{z}}^{\mathfrak{u}^0}, \mathfrak{u}^0) \in A_{ad}$. This completes the proof.

5 Application

Consider a nonlinear equation of the form given below to validate the outcome,

$$\begin{aligned}
&\mathcal{D}^{\frac{1}{2},\frac{2}{3}}\left[\mathfrak{z}(\varsigma,\mathfrak{t})-\exp\left(\mathfrak{z}\left(\frac{3\varsigma\mathfrak{t}}{4}\right)\right)\right]=\frac{\partial^2}{\partial\mathfrak{t}^2}\left[\mathfrak{z}(\varsigma,\mathfrak{t})-\exp\left(\mathfrak{z}\left(\frac{3\varsigma\mathfrak{t}}{4}\right)\right)\right]\\
&+\int_0^1 \mathfrak{h}(\varsigma,\mathfrak{t})\mathfrak{u}(\varsigma,\mathfrak{t})d\mathfrak{t}+\sin\left[\exp(\varsigma\mathfrak{t})+\mathfrak{z}\left(\frac{2\varsigma\mathfrak{t}}{5}\right)\right],\quad \varsigma\in(0,3]\backslash(1,2],\\
&\mathfrak{z}(\varsigma,0)=\mathfrak{z}(\varsigma,\pi)=0,\ \varsigma\in[1,2],\\
&\mathfrak{z}(\varsigma,\mathfrak{t})=\frac{1}{\Gamma\left(\frac{1}{2}\right)}\int_{\mathfrak{t}_k}^{\mathfrak{t}}\frac{1}{(\varsigma-\mathfrak{t})^{\frac{1}{2}}}\left(\frac{\mathfrak{z}\left(\frac{1}{2}^-\right)}{20exp(\mathfrak{t})+1}\right)d\mathfrak{t},\ \varsigma,\mathfrak{t}\in[1,2],\\
&I_0^{\frac{5}{6}}\mathfrak{z}(0,\mathfrak{t})=\int_0^3\mathfrak{z}(\omega,\mathfrak{t})d\mathfrak{t}+5,\quad \mathfrak{t}\in[0,\pi],
\end{aligned}\tag{4.1}$$

with $B\mathfrak{u}(\varsigma)(\mathfrak{t})=\int_0^1\mathfrak{h}(\varsigma,\mathfrak{t})\mathfrak{u}(\varsigma,\mathfrak{t})d\mathfrak{t}$, & $p_1=\frac{1}{2},\ \ p_2=\frac{2}{3},\ \ \eta=\frac{5}{6}$. Assume $\mathcal{N}=L^2[0,\ \pi]$ and $A:D(A)\subset\mathcal{N}\to\mathcal{N}$ by $A\mathfrak{z}=\frac{\partial^2}{\partial\mathfrak{t}^2}(\mathfrak{z})$,

$$D(A)=\{\mathfrak{z}\in\mathcal{N},\ \mathfrak{z}_\mathfrak{t},\mathfrak{z}_{\mathfrak{t}\mathfrak{t}}\in\mathcal{N},\ \mathfrak{z}(\varsigma,0)=\mathfrak{z}(\varsigma,\pi)=0\}.$$

It is clear that A is a strongly continuous semigroup and $(S(\varsigma)\mathfrak{z})$ in $\mathcal{N}$,

$$(S(\varsigma)\mathfrak{z})(\mathfrak{t})=\begin{cases}\int_0^\pi\mathscr{M}(\varsigma,\mathfrak{t}-\omega)\mathfrak{z}(\omega)d\omega, & \varsigma>0,\\ \mathfrak{z}(\mathfrak{t}), & \varsigma=0,\end{cases}$$

with

$$\mathscr{M}(\varsigma,\mathfrak{t})=\sqrt{\frac{2}{\pi}}exp\left(-\left(\frac{\mathfrak{t}^2}{4\varsigma}\right)\right),\ \ \varsigma>0,\ \ 0<\mathfrak{t}<\pi,$$

with $\mathfrak{z}(\varsigma)(\mathfrak{t})=\mathfrak{z}(\varsigma,\mathfrak{t})$. This leads to the conclusion $||S(\varsigma)||\leq\mathscr{M}$. Let $\mathcal{U}_{ad}=\{\mathfrak{u}\in U|||\mathfrak{u}||_{L^2[[0,3],\ U]}\leq 1\}$. Hence

$$\mathfrak{I}(\mathfrak{z},\mathfrak{u})=\int_{\mathfrak{t}_k}^{\mathfrak{t}_{k+1}}\int_0^\pi|\mathfrak{z}(\varsigma,\mathfrak{t})|^2d\mathfrak{t}d\varsigma+\int_{\mathfrak{t}_k}^{\mathfrak{t}_{k+1}}\int_0^\pi|\mathfrak{u}(\varsigma,\mathfrak{t})|^2d\mathfrak{t}d\varsigma$$

related to the system (4.1) which correlates the system (1.1) with

$$\mathfrak{I}(\mathfrak{z},\mathfrak{u})=\int_{\mathfrak{t}_k}^{\mathfrak{t}_{k+1}}\left(||\mathfrak{z}(\varsigma)||^2+||\mathfrak{u}(\varsigma)||_U^2\right)d\varsigma.$$

Therefore, ($H1$)–($H8$) satisfied. This completes the proof.

6 Conclusion

We examine the total controllability of non-instantaneous Hilfer fractional neutral system under integral boundary condition. By incorporating HFD with semigroup operator theory and Laplace transform technique, the integral solution is derived. Controllability outcomes were attained using Kuratowski's measure with contraction theory. Furthermore, the sequencing technique has been used to discuss the existence of the optimal pair for the system. To confirm the derived consequences, an example is given. The concept can be extended to Hilfer stochastic differential equations.

Author Contributions

Conceptualization: Kottakkaran Sooppy Nisar.

Investigation: K. Jothimani, C. Ravichandran.

Methodology: Kottakkaran Sooppy Nisar.

Software: K. Jothimani, C. Ravichandran.

Supervision: Kottakkaran Sooppy Nisar.

Validation: C. Ravichandran.

Writing – original draft: Kottakkaran Sooppy Nisar, K. Jothimani, C. Ravichandran.

References

1. Kharade J P, Kucche K D, On the impulsive implicit Ψ–Hilfer fractional differential equations with delay, *Math. Methods Appl. Sci.*, (2019); 43(4):1938–1952. https://doi.org/10.1002/mma.6017
2. Kucche K D, Kharade J P, Sousa J V C, On the nonlinear impulsive Ψ–Hilfer fractional differential equations, *Mathematical Modelling and Analysis*, (2020); 25(4):642–660. https://doi.org/10.48550/arXiv.1901.01814
3. Hernández E, O'Regan Donal, On a new class of abstract impulsive differential equations, *Proc. Amer. Math. Soc.*, (2013); 141(5):1641–1649. https://doi.org/10.1090/S0002-9939-2012-11613-2
4. Kumar V, Stamov G, Stamova I, Controllability results for a class of piecewise nonlinear impulsive fractional dynamic systems, *Appl. Math. Comput.*, (2023); 439:127625. https://doi.org/10.1016/j.amc.2022.127625
5. Kumar V, Djemai M, Existence, stability and controllability of piecewise impulsive dynamic systems on arbitrary time domain, *Appl. Math. Model.*, (2023); 117:529–548. https://doi.org/10.1016/j.apm.2022.12.027
6. Kumar V, Kostić M, Tridane A, Debbouche A, Controllability of switched Hilfer neutral fractional dynamic systems with impulses, *IMA Journal of Mathematical Control and Information*, (2022); 39(3):807–836. https://doi.org/10.1093/imamci/dnac011
7. Malik M, Sajid M, Kumar V, Controllability of singular dynamic systems on time scales, *Asian Journal of Control*, (2021); 24(5):2771–2777. https://doi.org/10.1002/asjc.2645
8. Chen P, Zhang X, Li Y, Existence of mild solutions to partial differential equations with non-instantaneous impulses, *Electron. J. Differ. Equ.*, (2016); 241:1–11.
9. Saravanakumar S, Balasubramaniam P, Non-instantaneous impulsive Hilfer fractional stochastic differential equations driven by fractional Brownian motion, *Stoch. Anal. Appl.*, (2021); 39(3):549–566. https://doi.org/10.1080/07362994.2020.1815545
10. Wang J R, Ibrahim G, O'Regan Donal, Zhou Y, A general class of non-instantaneous fractional differential inclusions in Banach spaces, *Adv. Difference Equ.*, (2017); 287(2017). https://doi.org/10.1186/s13662-017-1342-8
11. Wang J R, Ibrahim G, O'Regan Donal, Controllability of Hilfer fractional non-instantaneous impulsive semilinear differential inclusions with nonlocal conditions, *Nonlinear Anal. Model. Control*, (2019); 24(6):958–984. https://doi.org/10.15388/NA.2019.6.7
12. Liu S, Wang J R, O'Regan Donal, Trajectory approximately controllability and optimal control for noninstantaneous impulsive inclusions without compactness, *Topol. Methods. Nonlinear. Anal.*, (2021); 58(1):19–49. https://doi.org/10.12775/TMNA.2020.069
13. Alsheekhhussain Z, Gamal Ibrahim A, Controllability of Semilinear Multi-Valued Differential Inclusions with Non-Instantaneous Impulses of Order$\alpha \in (1, 2)$ without Compactness, *Symmetry*, (2021); 13(4):566. https://doi.org/10.3390/sym13040566
14. Ramkumar K, Ravikumar K, Baleanu D, Anguraj A, Hilfer fractional neutral stochastic differential equations with non-instantaneous impulses, *AIMS Mathematics*, (2021); 6(5):4474–4491. https://doi.org/10.3934/math.2021265
15. Agarwal R, Almeida R, Hristova S, O'Regan Donal, Non-instantaneous impulsive fractional differential equations with state dependent delay and practical stability, *Acta Mathematica Scientia*, (2021); 41:1699–1718. https://doi.org/10.1007/s10473-021-0518-1
16. Borah J, Bora S N, Non-instantaneous impulsive fractional semilinear evolution equations with finite delay, *J. Fractional Calc. & Appl.*, (2021); 12(1):120–132. https://doi.org/10.21608/jfca.2021.308746

17. Zhou Y, Jiao F, Nonlocal Cauchy problem for fractional evolution equations, *Nonlinear Anal. Real World Applications*, (2010); 11(5):4465–4475. https://doi.org/10.1016/j.nonrwa.2010.05.029

18. Wang X, Wang L, Zeng Q, Fractional differential equations with integral boundary conditions, *J. Nonlinear Sci. Appl.*, (2015); 8(4):309–314. https://doi.org/10.22436/jnsa.008.04.03

19. Wang J R, Zhang Y, Nonlocal initial value problems for differential equations with Hilfer fractional derivative, *Appl. Math. Comput.*, (2015); 266:850–859. https://doi.org/10.1016/j.amc.2015.05.144

20. Hilfer R, *Applications of Fractional Calculus in Physics*, World Scientific, Singapore, (2000).

21. Furati K M, Kassim M D, Tatar N E, Existence and uniqueness for a problem involving Hilfer fractional derivative, *Comput. Math. Appl.*, (2012); 64(6):1616–1626. https://doi.org/10.1016/j.camwa.2012.01.009

22. Gu H, Trujillo J J, Existence of mild solution for evolution equation with Hilfer fractional derivative, *Appl. Math.Comput.*, (2015); 257:344–354. https://doi.org/10.1016/j.amc.2014.10.083

23. Hilfer R, Luchko Y, Tomovski Z, Operational method for the solution of fractional differential equations with generalized Riemann-Liouville fractional derivatives, *Fract. Calc. Appl. Anal.*, (2009); 12(3):299–318. https://doi.org/10.1515/fca-2021-0023

24. Subashini R, Jothimani K, Nisar K S, Ravichandran C, New results on nonlocal functional integro-differential equations via Hilfer fractional derivative, *Alexandria Engineering Journal*, (2020); 59(5):2891–2899. https://doi.org/10.1016/j.aej.2020.01.055

25. Agarwal P, Baleanu D, Quan Y, Momani C S, Machado J A, *Fractional Calculus- Models*, *Algorithms*, *Technology*, Springer, Singapore (2018).

26. Kilbas A A, Srivastava H M, Trujillo J J, *Theory and applications of fractional differential equations* In: North-Holland Mathematics Studies, Elsevier Science, Amsterdam; (2006):204.

27. Pazy A, *Semigroups of Linear Operators and Applications to Partial Differential Equations*, New York, Springer-verlag (1983).

28. Podlubny I, *Fractional Differential Equations. An introduction to fractional derivatives*, *fractional differential equations*, *to methods of their solution and some of their applications*, Academic Press, San Diego (1999).

29. Zhou Y, *Basic Theory of Fractional Differential Equations*, World Scientific, Singapore, (2014).

30. Ravichandran C, Jothimani K, Nisar K S, Mahmoud Emad E, Yahia Ibrahim S, An interpretation on controllability of Hilfer fractional derivative with nondense domain, *Alexandria Engineering Journal*, (2022); 61(12):9941–9948. https://doi.org/10.1016/j.aej.2022.03.011

31. Nisar K S, Jothimani K, Kaliraj K, Ravichandran C, An analysis of controllability results for nonlinear Hilfer neutral fractional derivatives with non-dense domain, *Chaos Solitons & Fractals*, (2021); 146:110915. https://doi.org/10.1016/j.chaos.2021.110915

32. Nisar K S, Jothimani K, Ravichandran C, Baleanu D, Kumar D, New approach on controllability of Hilfer fractional derivatives with nondense domain, *AIMS Mathematics*, (2022); 7(6):10079–10095. https://doi.org/10.3934/math.2022561

33. Nisar K S, Jagatheeshwari R, Ravichandran C, Veeresha P, High performance computational method for fractional model of solid tumour invasion, *Ain Shams Eng. J.*, https://doi.org/10.1016/j.asej.2023.102226

34. Jothimani K, Kaliraj K, Panda S K, Nisar K S, Ravichandran C, Results On controllability of non-densely characterized neutral fractional delay differential system, *Evol. Equ. Control Theory*, 2021; 10(3):619–631. https://doi.org/10.3934/eect.2020083

35. Goufo E F D, Ravichandran C, Birajdar G A, Self-similarity techniques for chaotic attractors with many scrolls using step series switching, *Math. Model. Anal.*, (2021); 26(4):591–611. https://doi.org/10.3846/mma.2021.13678

36. Kavitha K, Vijayakumar V, Udhayakumar R, Results on controllability of Hilfer fractional neutral differential equations with infinite delay via measures of noncompactness, *Chaos Solitons & Fractals*, (2020); 139:1–9. https://doi.org/10.1016/j.chaos.2020.110035

37. Kavitha K, Vijayakumar V, Udhayakumar R, Ravichandran C, Results on controllability of Hilfer fractional differential equations with infinite delay via measures of noncompactness, *Asian J. Control*, (2022); 24(3):1406–1415. https://doi.org/10.1002/asjc.2549

38. Du J, Jiang W, Pang D, Niazi A U K, Exact controllability for Hilfer fractional differential inclusions involving nonlocal initial conditions, *Complexity*, (2018); 2018:1–13. https://doi.org/10.1155/2018/9472847

39. Lv J, Yang X, Approximate controllability of Hilfer fractional differential equations, *Math. Methods Appl. Sci.*, (2020); 43(1):242–254. https://doi.org/10.1002/mma.5862

40. Wang J R, Liu X, O'Regan Donal, On the approximate controllability for Hilfer fractional evolution hemivariational inequalities, *Numer. Funct. Anal. Optim.*, (2019); 40 (7):743–762. https://doi.org/10.1080/01630563.2018.1499667

41. Bahaa G M, Optimal control problem and maximum principle for fractional order cooperative systems, *Kybernetika*, (2019); 55(2):337–358. https://doi.org/10.14736/kyb-2019-2-0337

42. Harrat A, Nieto J J, Debbouche A, Solvability and optimal controls of impulsive Hilfer fractional delay evolution inclusions with Clarke subdifferential, *J. Comput. Appl. Math.*, (2018); 344:725–737. https://doi.org/10.1016/j.cam.2018.05.031

43. Pan X, Li X, Zhao J, Solvability and optimal controls of semi linear Riemann- Liouville fractional differential equations, *Abstr. Appl. Anal.*, (2014);(2014):216919. https://doi.org/10.1155/2014/216919

44. Sousa J V C, Existence of mild solutions to Hilfer fractional evolution equations in Banach space, *Classical Analysis and ODEs*, 1812.02213v1

45. Kumar V, Malik M, Debbouche A, Total controllability of neutral fractional differential equation with non-instantaneous impulsive effects, *J. Comput. Appl. Math.*, (2021); 383:113158. https://doi.org/10.1016/j.cam.2020.113158

46. Yang H, Zhao Y, Existence and optimal controls of non-autonomous impulsive integro-differential evolution equation with nonlocal conditions, *Chaos Solitons & Fractals*, (2021); 148:111027. https://doi.org/10.1016/j.chaos.2021.111027

47. Banaś J, On measures of noncompactness in Banach spaces, *Comment. Math. Univ. Carolin.*, (1980); 21(1):131–143.

48. Zhu S, Fan Z, Li G, Optimal controls for Riemann-Liouville fractional evolution systems without Lipschitz assumption, *J. Optim. Theory. Appl.*, (2017); 174(1):47–64. https://doi.org/10.1007/s10957-017-1119-y

49. Balder E, Necessary and sufficient conditions for l1-strong-weak lower semi-continuity of integral functional, *Nonlinear Anal.*, (1987); 11(12):1399–1404. https://doi.org/10.1016/0362-546X(87)90092-7

Progress in Fractional Differentiation and Applications
An International Journal

http://dx.doi.org/10.18576/pfda/100114

Existence Results on Mittag-Leffler Kernel of Fractional Integro-Differential Inclusion Problem Under Boundary Conditions

Kottakkaran S. Nisar [1,*], *Veliappan Vijayaraj*[2], *Shyni U. Kumaran*[3], *Chokkalingam Ravichandran*[2], *Poh Soon JosephNg*[4] *and M. Abdel-Aty*[5,6,7]

[1] Department of Mathematics, College of Science and Humanities in Alkharj, Prince Sattam bin Abdulaziz University, Saudi Arabia
[2] Department of Mathematics, Kongunadu Arts and Science College, Coimbatore - 641 029, India
[3] Department of Mathematics and Statistics, Providence Women's College, Malaparamba, Kozhikode - 673 009
[4] Faculty of Data Science and Information Technology, INTI International University, Malaysia
[5] Department of Computer Science and Information Engineering, Chung Hua University, Hsinchu, Taiwan 30012, R.O.C.
[6] Deanship of Graduate Studies and Research, Ahlia University, Manama, Kingdom of Bahrain
[7] Mathematics Department, Faculty of Science, Sohag University, Egypt

Received: 2 Feb. 2023, Revised: 2 Apr. 2023, Accepted: 28 May 2023
Published online: 1 Jan. 2024

Abstract: The main objective of this manuscript is to establish the sufficient conditions for the existence of solutions to the proposed inclusion problem under certain boundary conditions by applying fixed point results. Two cases of multivalued maps are explored with convex and non convex values. The results in the case of convex set-valued map are established using the Leray-Schauder theorem while the results in the case of non convex set-valued map are established through Nadler and Covitz set-valued theorem. The manuscript is concluded with apt examples to demonstrate the theoretical findings and inclusive innovation.

Keywords: Fixed point theorem, inclusive innovation, inclusion problem, boundary conditions.

1 Introduction

In a fractional integro-differential inclusion (FIDI), the unknown function is defined on a given interval, and the inclusion involves a set-valued operator that contains both fractional derivatives and integrals. The inclusion represents a family of differential equations that can have multiple solutions [1,2,3,4,5,6].

The combination of fractional calculus and integro-differential equations in an inclusion setting allows for the consideration of non-local effects, memory effects, and long-range interactions, making it a powerful tool for modeling complex phenomena in physics, engineering, and other fields [7,8,9,10,11,12,13,14].

FIDI finds its applications in various areas such as population dynamics, fractional diffusion processes, and so on. Analyzing and solving these inclusions typically involve specialized mathematical techniques such as fixed-point theory, semigroup theory and so forth [15,16,17,18,19]. The application of Atangana-Baleanu (AB) derivative in variational problems of mathematical physics and signal processing are aplenty [20].

Over the years, extensive research studies aimed at exploring the existence of solutions for various mathematical problems in fractional differential equations (FDEs) and FIDEs have been conducted [21,22,23,24,25,26]. Lachouri et al [27], in their work have established the sufficient conditions for the existence of solutions for a class of inclusion problems of fractional order involving the Atangana-Baleanu-Caputo (ABC) derivative under certain boundary conditions.

* Corresponding author e-mail: n.sooppy@psau.edu.sa

Motivated by the aforementioned studies, this manuscript explores the existence results of the following FIDI problem with ABC derivative involving BCs as given below:

$$\begin{aligned} &{}_0^{ABC}\mathscr{D}_{\varpi}^{\mathfrak{F}} z(\varpi) \in H\left(\varpi, z(\varpi), \int_0^b e(\varpi, v, z(v))dv, \int_0^{\varpi} h(\varpi, v, z(v))dv\right), \varpi \in I = [0,b] \\ &z(0) = z_0, z(b) = z. \end{aligned} \tag{1.1}$$

where ${}_0^{ABC}\mathscr{D}_{\varpi}^{\mathfrak{F}}$ is the ABC derivative of order $\varpi \in I = [0,b]$. Here $D = (\varpi, s) \in v \times v : s \leq \varpi$ and $e, h : D \times Y \to Y$ are continuous functions and $z_0, z_1 \in R$, $H : I \times R \to \mathscr{O}(R)$ is an SVM.
For our convenience, we assume that $E_1 w(\alpha) = \int_0^b e(\varpi, v, z(v))dv$ and $E_2 w(\alpha) = \int_0^{\varpi} h(\varpi, v, z(v))dv$.

$$\begin{aligned} &{}_0^{ABC}\mathscr{D}_{\varpi}^{\mathfrak{F}} z(\varpi) \in H\left(\varpi, z(\varpi), E_1 w(\alpha), E_2 w(\alpha)\right), \varpi \in I = [0,b] \\ &z(0) = z_0, z(b) = z. \end{aligned} \tag{1.2}$$

This manuscript is organized as follows: in Section 3 we determine the existence results for a class of FIDIs under certain BCs. In section 4 we validate the results with suitable examples and in section 5 we conclude the results.

2 Preliminaries

Let $\mathfrak{E} = \mathscr{C}[I, R]$ be a Banach space under the norm $||\mathscr{X}|| = sup_{\varpi \in I} |\mathscr{X}(\varpi)|$.

Definition 2.1[28] Let $\mathscr{X} \in H'(I)$ and $0 < \mathfrak{F} < 1$. For order $0 < \mathfrak{F} < 1$, the non-singular derivatives for the function $\mathscr{X}$ is given by,

$${}_0^{ABC}\mathscr{D}_{\varpi}^{\mathfrak{F}} z(\varpi) = \frac{\mathscr{M}(\mathfrak{F})}{1-\mathfrak{F}} \int_0^{\varpi} x'(v) E_{\mathfrak{F}}\Big(-\frac{\mathfrak{F}(\varpi - v)^{\mathfrak{F}}}{1-\mathfrak{F}}\Big)dv,$$

and

$${}_0^{ABR}\mathscr{D}_{\varpi}^{\mathfrak{F}} z(\varpi) = \frac{\mathscr{M}(\mathfrak{F})}{1-\mathfrak{F}} \int_0^{\varpi} x(v) E_{\mathfrak{F}}\Big(-\frac{\mathfrak{F}(\varpi - v)^{\mathfrak{F}}}{1-\mathfrak{F}}\Big)dv,$$

respectively. Here the normalizing function $\mathscr{M}(\mathfrak{F}) > 0$ satisfies $\mathscr{M}(0) = \mathscr{M}(1) = 1$ where $E_{\mathfrak{F}}$ is a Mittag-Liffler function.

Definition 2.2 [28] The fractional integral of AB of order $\varpi \in (0,1)$ and function $r : (d, \mathfrak{F}) \to R$ is,

$${}_0^{ABC}I_{\varpi}^{\mathfrak{F}} z(\varpi) = \frac{1-\mathfrak{F}}{\mathscr{M}(\mathfrak{F})} z(\varpi) + \frac{\mathfrak{F}}{\mathscr{M}(\mathfrak{F})\Gamma(\mathfrak{F})} \int_0^{\varpi} x(v)(\varpi - v)^{-1} dv, \mathfrak{F} \in (0,1).$$

Definition 2.3 [29] Let $\mathfrak{F} \in (n-1, n]$ and let x be $x^{(n)} \in H^1(I)$,

$${}_0^{ABC}\mathscr{D}_{\varpi}^{\mathfrak{F}} z(\varpi) = {}_0^{ABC}\mathscr{D}_{\varpi}^{\tau} z^{(n)}(\varpi).$$

Lemma 1 [30] Let $h \in \mathfrak{E}$, the soln of problem,

$${}_0^{ABC}\mathscr{D}_{\varpi}^{\mathfrak{F}} z(\varpi) \in H\left[h(\varpi), E_1 w(\alpha), E_2 w(\alpha)\right], \varpi \in I$$

with boundary conditions

$$w(0) = w_0, x(b) = x,$$

is obtained as,

$$z(\varpi) = \frac{\varpi x_1 + x_0(b-\varpi)}{b} - \frac{\varpi(2-\mathfrak{F})}{b\mathscr{M}(\mathfrak{F}-1)}\int_0^b h(v)\,[E_1 w(\alpha), E_2 w(\alpha)]\,dv$$
$$- \frac{\varpi(\mathfrak{F}-1)}{b\mathscr{M}(\mathfrak{F}-1)(\Gamma(\mathfrak{F}))}\int_0^b (b-v)^{(\mathfrak{F}-1)} h(v)\,[E_1 w(\alpha), E_2 w(\alpha)]\,dv$$
$$+ \frac{2-\mathfrak{F}}{\mathscr{M}(\mathfrak{F}-1)}\int_0^{\varpi} h(v)\,[E_1 w(\alpha), E_2 w(\alpha)]\,dv$$
$$+ \frac{(\mathfrak{F}-1)}{\mathscr{M}(\mathfrak{F}-1)(\Gamma(\mathfrak{F}))}\int_0^{\varpi} (\varpi - v)^{\mathfrak{F}-1} h(v)\,[E_1 w(\alpha), E_2 w(\alpha)]\,dv. \tag{2.1}$$

Suppose $(\mathfrak{B}, ||.||)$ is a normed space and let,

$$\mathfrak{O}_{cl}(\mathfrak{B}) = \mathscr{M} \in \mathfrak{O}(\mathfrak{B}) : \mathscr{M} \text{ is closed},$$

$$\mathfrak{O}_{cp}(\mathfrak{B}) = \mathscr{M} \in \mathfrak{O}(\mathfrak{B}) : \mathscr{M} \text{ is compact},$$

and

$$\mathfrak{O}_{cp,c}(\mathfrak{B}) = \mathscr{M} \in \mathfrak{O}(\mathfrak{B}) : \mathscr{M} \text{ is compact and convex}.$$

We refer [31,32,33] and H at point $o \in \mathfrak{E}$ is $\mathscr{Q}_{H,o} = \{\mathfrak{I} \in L^1(I,R) : \mathfrak{I}(\varpi) \in H(\varpi, o)\,(\text{a.e})\varpi \in I\}$.

Definition 2.4 [27] Let $H : I \times R \to \mathscr{O}(R)$ is MVM. H can be called a Caratheodory, if the map $\varpi \to H(\varpi, x)$ is measurable for all $x \in R, \& x \to H(\varpi, x)$ is $\varpi \in I$ a.e. Similarly, a SVM H is L^1- Caratheodory, if for every $w > 0$, $\Phi \in L^1(I, R^+)$ so,

$$||H(\varpi, x)|| = sup\{|\delta| \in H(\varpi, x)\} \leq \Phi(\varpi),$$

$\forall ||x|| \leq w$ and $\varpi \in I$ a.e.

3 Existence results

Definition 3.1 The function $x \in \mathfrak{E}$ is a solution of (1), if $\mathfrak{I} \in L^1(I,R)$ with $\mathfrak{I}(\varpi) \in H(\varpi, x)$, for every $\varpi \in I$ satisfies the BCs as, $z(0) = z_0, z(b) = z$.
The solution is obtained as,

$$z(\varpi) = \frac{\varpi x_1 + x_0(b-\varpi)}{b} - \frac{\varpi(2-\mathfrak{F})}{b\mathscr{M}(\mathfrak{F}-1)}\int_0^b \mathfrak{I}(v)\,[E_1 w(\alpha), E_2 w(\alpha)]\,dv$$
$$- \frac{\varpi(\mathfrak{F}-1)}{b\mathscr{M}(\mathfrak{F}-1)(\Gamma(\mathfrak{F}))}\int_0^b (b-v)^{(\mathfrak{F}-1)} \mathfrak{I}(v)\,[E_1 w(\alpha), E_2 w(\alpha)]\,dv$$
$$+ \frac{2-\mathfrak{F}}{\mathscr{M}(\mathfrak{F}-1)}\int_0^{\varpi} \mathfrak{I}(v)\,[E_1 w(\alpha), E_2 w(\alpha)]\,dv$$
$$+ \frac{(\mathfrak{F}-1)}{\mathscr{M}(\mathfrak{F}-1)(\Gamma(\mathfrak{F}))}\int_0^{\varpi} (\varpi - v)^{\mathfrak{F}-1} \mathfrak{I}(v)\,[E_1 w(\alpha), E_2 w(\alpha)]\,dv.$$

For multi-valued maps, we apply Leray-Schauder-type theorem [34] to obtain the existence results related to the convex valued H map.

Theorem 3.2 Let

$$\eta = \frac{1}{\mathscr{M}(\mathfrak{F}-1)}\left(2b + \frac{2b^{\mathfrak{F}}}{\Gamma(\mathfrak{F}+1)}\right), \tag{3.1}$$

and

(H1)$H : I \times R \to \mathscr{O}_{cp,c}(R)$ is a L^1- Caratheodory MVM.

(H2)$\exists$ $\psi_1 \in C(I,[0,\infty))$ and a non-decreasing $\psi_2 \in C([0,\infty),[0,\infty))$ so that

$$||H(\varpi,x)||_{\mathfrak{O}} = sup|\odot| : \odot \in H(\varpi,x) \leq \psi_1(\varpi)\psi_2(||x||), \forall(\varpi,x) \in I \times R.$$

(H3)Let a constant $\mathscr{N} > 0$,

$$\frac{\mathscr{N}}{|x_1| + |x_0| + \eta||\psi_1||\psi_2(\mathscr{N})} > 1.$$

(H4)There exist $e,h \in \mathscr{C}(\mathscr{J},R_+)$,
$||\int_0^b e(\varpi,v,z(v))dv|| \leq e(\varpi)||\mathfrak{z}||$, for each $\varpi \in \mathscr{J}, \mathfrak{z} \in E$ and
$||\int_0^{\varpi} h(\varpi,v,z(v))dv|| \leq h(\varpi)||\mathfrak{z}||$, for each $\varpi \in \mathscr{J}, \mathfrak{z} \in E$.

Then (1) has a solution on I.
Proof: Firstly, let the problem (1) be converted to a fixed point problem and for this purpose let us define $\mathscr{Z} : \mathfrak{E} \to \mathfrak{O}(\mathfrak{E})$ as

$$\begin{aligned} z(x) = \zeta \in \mathfrak{E} : \zeta(\varpi) = {} & \frac{\varpi x_1 + x_0(b-\varpi)}{b} - \frac{\varpi(2-\mathfrak{F})}{b\mathscr{M}(\mathfrak{F}-1)} \int_0^b \Im(v)\,[E_1 w(\alpha), E_2 w(\alpha)]\,dv \\ & - \frac{\varpi(\mathfrak{F}-1)}{b\mathscr{M}(\mathfrak{F}-1)(\Gamma(\mathfrak{F}))} \int_0^b (b-v)^{(\mathfrak{F}-1)} \Im(v)\,[E_1 w(\alpha), E_2 w(\alpha)]\,dv \\ & + \frac{2-\mathfrak{F}}{\mathscr{M}(\mathfrak{F}-1)} \int_0^{\varpi} \Im(v)\,[E_1 w(\alpha), E_2 w(\alpha)]\,dv \\ & + \frac{(\mathfrak{F}-1)}{\mathscr{M}(\mathfrak{F}-1)(\Gamma(\mathfrak{F}))} \int_0^{\varpi} (\varpi - v)^{\mathfrak{F}-1} \Im(v)\,[E_1 w(\alpha), E_2 w(\alpha)]\,dv, \end{aligned}$$

for $\psi \in \mathscr{Q}_{H,x}$.
$\therefore \mathscr{Z}$ is a fixed point solution of (1).

Case 1: $\mathscr{Z}(x)$ is convex for any $\zeta \in \mathfrak{E}$.
Let $\zeta_1, \zeta_2 \in \mathscr{Z}(x)$. Then there exist $\psi_1, \psi_2 \in \mathscr{Q}_{H,x}$, so that for every $\varpi \in I$,

$$\begin{aligned} \zeta_j(\varpi) = {} & \frac{\varpi x_1 + x_0(b-\varpi)}{b} - \frac{\varpi(2-\mathfrak{F})}{b\mathscr{M}(\mathfrak{F}-1)} \int_0^b \Im_j(v)\,[E_1 w(\alpha), E_2 w(\alpha)]\,dv \\ & - \frac{\varpi(\mathfrak{F}-1)}{b\mathscr{M}(\mathfrak{F}-1)(\Gamma(\mathfrak{F}))} \int_0^b (b-v)^{(\mathfrak{F}-1)} \Im_j(v)\,[E_1 w(\alpha), E_2 w(\alpha)]\,dv \\ & + \frac{2-\mathfrak{F}}{\mathscr{M}(\mathfrak{F}-1)} \int_0^{\varpi} \Im_j(v)\,[E_1 w(\alpha), E_2 w(\alpha)]\,dv \\ & + \frac{(\mathfrak{F}-1)}{\mathscr{M}(\mathfrak{F}-1)(\Gamma(\mathfrak{F}))} \int_0^{\varpi} (\varpi - v)^{\mathfrak{F}-1} \Im_j(v)\,[E_1 w(\alpha), E_2 w(\alpha)]\,dv, \end{aligned}$$

and letting $\delta \in [0,1]$, we have for all $\varpi \in I$

$$\begin{aligned} & [\delta\zeta_1 + (1-\delta)\zeta_2](\varpi) \\ & = \frac{\varpi x_1 + x_0(b-\varpi)}{b} - \frac{\varpi(2-\mathfrak{F})}{b\mathscr{M}(\mathfrak{F}-1)} \int_0^b \delta\Im_1(v) + (1-\delta)\Im_2(v)\,[E_1 w(\alpha), E_2 w(\alpha)]\,dv \\ & - \frac{\varpi(\mathfrak{F}-1)}{b\mathscr{M}(\mathfrak{F}-1)(\Gamma(\mathfrak{F}))} \int_0^b (b-v)^{(\mathfrak{F}-1)} \delta\Im_1(v) + (1-\delta)\Im_2(v)\,[E_1 w(\alpha), E_2 w(\alpha)]\,dv \\ & + \frac{2-\mathfrak{F}}{\mathscr{M}(\mathfrak{F}-1)} \int_0^{\varpi} \delta\Im_1(v) + (1-\delta)\Im_2(v)\,[E_1 w(\alpha), E_2 w(\alpha)]\,dv \\ & + \frac{(\mathfrak{F}-1)}{\mathscr{M}(\mathfrak{F}-1)(\Gamma(\mathfrak{F}))} \int_0^{\varpi} (\varpi - v)^{\mathfrak{F}-1} \delta\Im_1(v) + (1-\delta)\Im_2(v)\,[E_1 w(\alpha), E_2 w(\alpha)]\,dv. \end{aligned}$$

Hence, H and $\mathscr{Q}_{H,x}$ has a convex values, and $[\delta\Im_1(v) + (1-\delta)\Im_2(v)] \in \mathscr{Q}_{H,x}$.
Thus $\delta\zeta_1 + (1-\delta)\zeta_2 \in \mathscr{Z}(x)$.

Case 2: $\mathscr{Z}$ be bounded on bounded sets of $\mathfrak{E}$. Let for $\varsigma \in R^{+}$,

$$B_{\varsigma} = \{x \in \mathfrak{E} : ||x|| \leq \varsigma\},$$

be a bounded set in $\mathfrak{E}$,

$$\zeta \in \mathscr{Z}(x), x \in B_{\varsigma}, \text{and } \psi \in \mathscr{Q}_{H,x}$$

then,

$$\begin{aligned}\zeta(\varpi) = {} & \frac{\varpi x_1 + x_0(b-\varpi)}{b} - \frac{\varpi(2-\mathfrak{F})}{b\mathscr{M}(\mathfrak{F}-1)} \int_0^b \Im(v)\,[E_1 w(\alpha), E_2 w(\alpha)]\,dv \\ & - \frac{\varpi(\mathfrak{F}-1)}{b\mathscr{M}(\mathfrak{F}-1)(\Gamma(\mathfrak{F}))} \int_0^b (b-v)^{(\mathfrak{F}-1)} \Im(v)\,[E_1 w(\alpha), E_2 w(\alpha)]\,dv \\ & + \frac{2-\mathfrak{F}}{\mathscr{M}(\mathfrak{F}-1)} \int_0^{\varpi} \Im(v)\,[E_1 w(\alpha), E_2 w(\alpha)]\,dv \\ & + \frac{(\mathfrak{F}-1)}{\mathscr{M}(\mathfrak{F}-1)(\Gamma(\mathfrak{F}))} \int_0^{\varpi} (\varpi - v)^{\mathfrak{F}-1} \Im(v)\,[E_1 w(\alpha), E_2 w(\alpha)]\,dv.\end{aligned}$$

From (H_2) and for every $\varpi \in I$, we have

$$\begin{aligned}|\zeta(\varpi)| = {} & \frac{\varpi|x_1| + |x_0|(b-\varpi)}{b} - \frac{\varpi(2-\mathfrak{F})}{b\mathscr{M}(\mathfrak{F}-1)} \int_0^b |\Im(v)\,[E_1 w(\alpha), E_2 w(\alpha)]\,|dv \\ & - \frac{\varpi(\mathfrak{F}-1)}{b\mathscr{M}(\mathfrak{F}-1)(\Gamma(\mathfrak{F}))} \int_0^b (b-v)^{(\mathfrak{F}-1)} |\Im(v)\,[E_1 w(\alpha), E_2 w(\alpha)]\,|dv \\ & + \frac{2-\mathfrak{F}}{\mathscr{M}(\mathfrak{F}-1)} \int_0^{\varpi} |\Im(v)\,[E_1 w(\alpha), E_2 w(\alpha)]\,|dv \\ & + \frac{(\mathfrak{F}-1)}{\mathscr{M}(\mathfrak{F}-1)(\Gamma(\mathfrak{F}))} \int_0^{\varpi} (\varpi - v)^{\mathfrak{F}-1} |\Im(v)\,[E_1 w(\alpha), E_2 w(\alpha)]\,|dv. \\ & \leq |x_1| + |x_2| + \frac{||\psi_1||\psi_2(\varsigma)}{\mathscr{M}(\mathfrak{F}-1)} \left(2b + \frac{2b^{\mathfrak{F}}}{\Gamma(\mathfrak{F}+1)}\right).\end{aligned}$$

Thus,

$$||\zeta|| \leq |x_1| + |X_0| + \eta||\psi_1||\psi_2(\varsigma).$$

Case 3: To prove that $\mathscr{Z}(B_{\zeta})$ is equi-continuous.
Let $x \in B_{\zeta}$ and $\zeta \in \mathscr{Z}(x)$ and a function $\psi \in \mathscr{Q}_{H,x}$, then

$$\begin{aligned}\zeta(\varpi) = {} & \frac{\varpi x_1 + x_0(b-\varpi)}{b} - \frac{\varpi(2-\mathfrak{F})}{b\mathscr{M}(\mathfrak{F}-1)} \int_0^b \Im(v)\,[E_1 w(\alpha), E_2 w(\alpha)]\,dv \\ & - \frac{\varpi(\mathfrak{F}-1)}{b\mathscr{M}(\mathfrak{F}-1)(\Gamma(\mathfrak{F}))} \int_0^b (b-v)^{(\mathfrak{F}-1)} \Im(v)\,[E_1 w(\alpha), E_2 w(\alpha)]\,dv \\ & + \frac{2-\mathfrak{F}}{\mathscr{M}(\mathfrak{F}-1)} \int_0^{\varpi} \Im(v)\,[E_1 w(\alpha), E_2 w(\alpha)]\,dv \\ & + \frac{(\mathfrak{F}-1)}{\mathscr{M}(\mathfrak{F}-1)(\Gamma(\mathfrak{F}))} \int_0^{\varpi} (\varpi - v)^{\mathfrak{F}-1} \Im(v)\,[E_1 w(\alpha), E_2 w(\alpha)]\,dv.\end{aligned}$$

Let $\varpi_1, \varpi_2 \in I < \varpi_2$. Then

$$\begin{aligned}
&|\zeta(\varpi_2)-\zeta(\varpi_1)| \\
&\quad\leq \frac{(\varpi_2-\varpi_1)(|x_1|+|x_0|)}{b}-\frac{(\varpi_2-\varpi_1)(2-\mathfrak{F})}{b\mathscr{M}(\mathfrak{F}-1)}\int_0^b |\Im(v)\,[E_1w(\alpha),E_2w(\alpha)]\,|dv \\
&\quad+\frac{(\varpi_2-\varpi_1)(\mathfrak{F}-1)}{b\mathscr{M}(\mathfrak{F}-1)\Gamma(\mathfrak{F})}\int_0^b (b-v)^{(\mathfrak{F}-1)}|\Im(v)\,[E_1w(\alpha),E_2w(\alpha)]\,|dv \\
&\quad+\frac{2-\mathfrak{F}}{\mathscr{M}(\mathfrak{F}-1)}\int_{\varpi_1}^{\varpi_2} |\Im(v)\,[E_1w(\alpha),E_2w(\alpha)]\,|dv \\
&\quad+\frac{(\mathfrak{F}-1)}{\mathscr{M}(\mathfrak{F}-1)\Gamma(\mathfrak{F})}\int_0^{\varpi_1}\left((\varpi_2-v)^{\mathfrak{F}-1}-(\varpi_1-v)^{\mathfrak{F}-1}\right)|\Im(v)\,[E_1w(\alpha),E_2w(\alpha)]\,|dv \\
&\quad+\frac{(\mathfrak{F}-1)}{\mathscr{M}(\mathfrak{F}-1)\Gamma(\mathfrak{F})}\int_{\varpi_1}^{\varpi_2}(\varpi_2-v)^{\mathfrak{F}-1}|\Im(v)\,[E_1w(\alpha),E_2w(\alpha)]\,|dv.
\end{aligned}$$

Similarly by using $(H_2)-(H_4)$, we get

$$\begin{aligned}
&|\zeta(\varpi_2)-\zeta(\varpi_1)| \\
&\leq \frac{(\varpi_2-\varpi_1)(|x_1|+|x_0|)}{b}+\frac{(\varpi_2-\varpi_1)||\psi_1||\psi_2(\varsigma)||\mathfrak{z}||}{\mathscr{M}(\mathfrak{F}-1)}+\frac{b^{\mathfrak{F}}(\varpi_2-\varpi_1)||\psi_1||\psi_2(\varsigma)||\mathfrak{z}||}{b\mathscr{M}(\mathfrak{F}-1)\Gamma(\mathfrak{F}+1)} \\
&\quad+\frac{(\varpi_2-\varpi_1)||\psi_1||\psi_2(\varsigma)||\mathfrak{z}||}{\mathscr{M}(\mathfrak{F}-1)}+\frac{(\varpi_2^{\mathfrak{F}}-\varpi_1^{\mathfrak{F}})||\psi_1||\psi_2(\varsigma)||\mathfrak{z}||}{\mathscr{M}(\mathfrak{F}-1)\Gamma(\mathfrak{F}+1)}.
\end{aligned}$$

As $\varpi_1 \to \varpi_2$, we obtain

$$|\zeta(\varpi_2)-\zeta(\varpi_1)| \to 0.$$

By Arzela-Ascoli theorem, $\mathfrak{Z}$ is completely continuous and $\mathfrak{Z}(B_\zeta)$ is equi-continuous. From [[31], Proposition 1.2], $\mathfrak{Z}$ has a closed graph, then consequently $\mathfrak{Z}$ is SVM.

Case 4: The graph of $\mathfrak{Z}$ is closed.
Let $x_n \to x_*, \zeta_n \in \mathfrak{Z}(x_n)$ and ζ_n converges to ζ_*.
To prove $\zeta_* \in \mathfrak{Z}(x_*)$.
Because $h_n \in \mathfrak{Z}(x_n)$, and $\psi_n \in \mathscr{Q}_{H,x_n}$,

$$\begin{aligned}
\zeta_n(\varpi) &= \frac{\varpi x_1+x_0(b-\varpi)}{b}-\frac{\varpi(2-\mathfrak{F})}{b\mathscr{M}(\mathfrak{F}-1)}\int_0^b \Im_n(v)\,[E_1w(\alpha),E_2w(\alpha)]\,dv \\
&\quad-\frac{\varpi(\mathfrak{F}-1)}{b\mathscr{M}(\mathfrak{F}-1)(\Gamma(\mathfrak{F}))}\int_0^b (b-v)^{(\mathfrak{F}-1)}\Im_n(v)\,[E_1w(\alpha),E_2w(\alpha)]\,dv \\
&\quad+\frac{2-\mathfrak{F}}{\mathscr{M}(\mathfrak{F}-1)}\int_0^{\varpi}\Im_n(v)\,[E_1w(\alpha),E_2w(\alpha)]\,dv \\
&\quad+\frac{(\mathfrak{F}-1)}{\mathscr{M}(\mathfrak{F}-1)(\Gamma(\mathfrak{F}))}\int_0^{\varpi}(\varpi-v)^{\mathfrak{F}-1}\Im_n(v)\,[E_1w(\alpha),E_2w(\alpha)]\,dv.
\end{aligned}$$

Thus, we need to show that $\psi_* \in \mathscr{Q}_{H,x_*}, \varpi \in I$,

$$\begin{aligned}
\zeta_*(\varpi) &= \frac{\varpi x_1+x_0(b-\varpi)}{b}-\frac{\varpi(2-\mathfrak{F})}{b\mathscr{M}(\mathfrak{F}-1)}\int_0^b \Im_*(v)\,[E_1w(\alpha),E_2w(\alpha)]\,dv \\
&\quad-\frac{\varpi(\mathfrak{F}-1)}{b\mathscr{M}(\mathfrak{F}-1)(\Gamma(\mathfrak{F}))}\int_0^b (b-v)^{(\mathfrak{F}-1)}\Im_*(v)\,[E_1w(\alpha),E_2w(\alpha)]\,dv \\
&\quad+\frac{2-\mathfrak{F}}{\mathscr{M}(\mathfrak{F}-1)}\int_0^{\varpi}\Im_*(v)\,[E_1w(\alpha),E_2w(\alpha)]\,dv \\
&\quad+\frac{(\mathfrak{F}-1)}{\mathscr{M}(\mathfrak{F}-1)(\Gamma(\mathfrak{F}))}\int_0^{\varpi}(\varpi-v)^{\mathfrak{F}-1}\Im_*(v)\,[E_1w(\alpha),E_2w(\alpha)]\,dv.
\end{aligned}$$

Define the continuous linear operator $\mathscr{P}: L^1(I,(-\infty,\infty)) \to C(I(-\infty,\infty))$ by,

$$\begin{aligned}\psi \to \mathscr{P}(\psi)(\varpi) = {} & \frac{\varpi x_1 + x_0(b-\varpi)}{b} - \frac{\varpi(2-\mathfrak{F})}{b\mathscr{M}(\mathfrak{F}-1)}\int_0^b \Im(v)\,[E_1 w(\alpha), E_2 w(\alpha)]\,dv \\ & - \frac{\varpi(\mathfrak{F}-1)}{b\mathscr{M}(\mathfrak{F}-1)(\Gamma(\mathfrak{F}))}\int_0^b (b-v)^{(\mathfrak{F}-1)}\Im(v)\,[E_1 w(\alpha), E_2 w(\alpha)]\,dv \\ & + \frac{2-\mathfrak{F}}{\mathscr{M}(\mathfrak{F}-1)}\int_0^{\varpi} \Im(v)\,[E_1 w(\alpha), E_2 w(\alpha)]\,dv \\ & + \frac{(\mathfrak{F}-1)}{\mathscr{M}(\mathfrak{F}-1)(\Gamma(\mathfrak{F}))}\int_0^{\varpi} (\varpi - v)^{\mathfrak{F}-1}\Im(v)\,[E_1 w(\alpha), E_2 w(\alpha)]\,dv.\end{aligned}$$

Observe that,

$$\begin{aligned}||\zeta_n - \zeta_*|| = || & - \frac{\varpi(2-\mathfrak{F})}{b\mathscr{M}(\mathfrak{F}-1)}\int_0^b \Im_n(v) + \Im_*(v)\,[E_1 w(\alpha), E_2 w(\alpha)]\,dv \\ & - \frac{\varpi(\mathfrak{F}-1)}{b\mathscr{M}(\mathfrak{F}-1)(\Gamma(\mathfrak{F}))}\int_0^b (b-v)^{(\mathfrak{F}-1)}\Im_n(v) - \Im_*(v)\,[E_1 w(\alpha), E_2 w(\alpha)]\,dv \\ & + \frac{2-\mathfrak{F}}{\mathscr{M}(\mathfrak{F}-1)}\int_0^{\varpi} \Im_n(v) - \Im_*(v)\,[E_1 w(\alpha), E_2 w(\alpha)]\,dv \\ & + \frac{(\mathfrak{F}-1)}{\mathscr{M}(\mathfrak{F}-1)(\Gamma(\mathfrak{F}))}\int_0^{\varpi} (\varpi - v)^{\mathfrak{F}-1}\Im_n(v) - \Im_2(*)\,[E_1 w(\alpha), E_2 w(\alpha)]\,dv \to 0||,\end{aligned}$$

From Lazota-Opial result [35],when $n \to \infty$ and $\mathscr{P} \circ \mathscr{Q}_{H,x}$ ia a closed graph operator,
we get

$$\zeta_n \in \mathscr{P}\left(\mathscr{Q}_{H,x_n}\right).$$

Because $x_n \to x_*$,

$$\begin{aligned}\zeta_*(\varpi) = {} & \frac{\varpi x_1 + x_0(b-\varpi)}{b} - \frac{\varpi(2-\mathfrak{F})}{b\mathscr{M}(\mathfrak{F}-1)}\int_0^b \Im_*(v)\,[E_1 w(\alpha), E_2 w(\alpha)]\,dv \\ & - \frac{\varpi(\mathfrak{F}-1)}{b\mathscr{M}(\mathfrak{F}-1)(\Gamma(\mathfrak{F}))}\int_0^b (b-v)^{(\mathfrak{F}-1)}\Im_*(v)\,[E_1 w(\alpha), E_2 w(\alpha)]\,dv \\ & + \frac{2-\mathfrak{F}}{\mathscr{M}(\mathfrak{F}-1)}\int_0^{\varpi} \Im_*(v)\,[E_1 w(\alpha), E_2 w(\alpha)]\,dv \\ & + \frac{(\mathfrak{F}-1)}{\mathscr{M}(\mathfrak{F}-1)(\Gamma(\mathfrak{F}))}\int_0^{\varpi} (\varpi - v)^{\mathfrak{F}-1}\Im_*(v)\,[E_1 w(\alpha), E_2 w(\alpha)]\,dv,\end{aligned}$$

for some $\Im_* \in \mathscr{Q}_{H,x_*}$.

Case 5: Let $\mathscr{V} \subseteq \mathfrak{E}$ be an open set with $x \notin \vee\mathfrak{Z}(x)$ for every $\vee \in (0,1)$ and $\forall x \in \imath\mathscr{V}$.
Let $\vee \in (0,1)$ and $x \in \vee\mathfrak{Z}(x)$. Then for $\Im \in \mathscr{Q}_{H,x}$,

$$\begin{aligned}|z(\varpi)| = \Big| & \frac{\vee\varpi x_1 + \vee x_0(b-\varpi)}{b} - \frac{\vee\varpi(2-\mathfrak{F})}{b\mathscr{M}(\mathfrak{F}-1)}\int_0^b \Im(v)\,[E_1 w(\alpha), E_2 w(\alpha)]\,dv \\ & - \frac{\vee\varpi(\mathfrak{F}-1)}{b\mathscr{M}(\mathfrak{F}-1)(\Gamma(\mathfrak{F}))}\int_0^b (b-v)^{(\mathfrak{F}-1)}\Im(v)\,[E_1 w(\alpha), E_2 w(\alpha)]\,dv \\ & + \frac{\vee(2-\mathfrak{F})}{\mathscr{M}(\mathfrak{F}-1)}\int_0^{\varpi} \Im(v)\,[E_1 w(\alpha), E_2 w(\alpha)]\,dv \\ & + \frac{\vee(\mathfrak{F}-1)}{\mathscr{M}(\mathfrak{F}-1)(\Gamma(\mathfrak{F}))}\int_0^{\varpi} (\varpi - v)^{\mathfrak{F}-1}\Im(v)\,[E_1 w(\alpha), E_2 w(\alpha)]\,dv\Big| \\ & \leq |x_1| + |x_0| + \eta||\psi_1||\psi_2(\varsigma)||\mathfrak{z}||.\end{aligned}$$

Thus, we have

$$|x(\varpi)| \leq |x_1| + |x_0| + \eta||\psi_1||\psi_2(x)||\mathfrak{z}||, \varpi \in I$$

and we obtain

$$\frac{||x||}{|x_1|+|x_0|+\eta||\psi_1||\psi_2(x)||_{\mathfrak{Z}}||} \leq 1.$$

By $[H_3]$, we have $\mathfrak{N} > 0$ is a constant, $||x|| \neq \mathfrak{N}$. Let the set $\mathscr{V}$ be defined as,

$$\mathscr{V} = \{x \in \mathfrak{E} : ||x|| < \mathfrak{N}\}.$$

By Case $1-4$, $\mathfrak{Z}\mathscr{V} \to \mathfrak{O}((E))$ is completely continuous.
$\therefore$ There is at least one solution to problem (1).

Next using a theorem of Covitz-Nadler [21], we derive an existence result for the inclusion problem (1), when H is a nonconvex-valued mapping.
Define $H_d : \mathfrak{O}(\varepsilon) \times \mathfrak{O}(\varepsilon) \to [0,\infty) \cup \infty$ by,

$$H_d(\widetilde{G},\widetilde{J}) = max\left\{\sup_{\widetilde{g}\in\widetilde{G}} d(\widetilde{G},\widetilde{J}), \sup_{\widetilde{j}\in\widetilde{J}} d(\widetilde{g},\widetilde{j})\right\},$$

where $d(\widetilde{G},\widetilde{J}) = inf_{\widetilde{g},\widetilde{G}} d(\widetilde{G},\widetilde{J})$ and $d(\widetilde{g},\widetilde{J}) = inf_{\widetilde{j},\widetilde{J}} d(\widetilde{G},\widetilde{J})$. Then $\left((O)_{c,cl}(\varepsilon), H_d\right)$ is a metric space.

Definition 3.3 $\mathfrak{Z} : \varepsilon \to \mathfrak{O}_{cl}(\varepsilon)$ is $\tau-$ Lipschitz iff there exists $\tau > 0$, so that

$$H_d(\mathfrak{Z}(\beta),\mathfrak{Z}(U_2)) \leq \tau d(\beta,U_2) \text{for any } \beta, U_2 \in \varepsilon.$$

In particular if, $\tau < 1$, we have that $\mathfrak{Z}$ is a contraction.

Theorem 3.4 Let,

(H5)$H : I \times R \to \mathscr{O}_{cp}(R)$ is a $H(x) : I \to \mathscr{O}_{cp}(R)$ is measurablefor any $x \in R$.
(H6)$H_d(H(\varpi,x),H(\varpi,\bar{x})) \leq \rho(\varpi)|x-\bar{x}| \forall \varpi \in I$ and $x,\bar{x} \in R$ with $\rho \in C(I,[0,\infty))$ and $d(0.H(\varpi,0)) \leq \rho(\varpi) \forall \varpi \in I$.

The FIDI of (1) has one solution on I, for when

$$\eta||\rho|| < 1,$$

η is given in equation (3.1).

Proof: From [H4] and [36], Theorem III H is measurable $\mathfrak{I} : I \to R, \mathfrak{I} \in L^1((I),R)$. $\mathscr{Q}_{H,x} \neq \oslash$. Let $\{\omega_n\}_n \geq 0 \in \mathfrak{Z}(x)$ be a $\omega_n \to \omega(n \to \infty)$ *in* $\mathfrak{E}.\omega \in \mathfrak{E}\&\mathfrak{I}_n\omega \in \mathscr{Q}_{H,x_n}$,

$$\begin{aligned}
\omega_n(\varpi) = {} & \frac{\varpi x_1 + x_0(b-\varpi)}{b} - \frac{\varpi(2-\mathfrak{F})}{b(\mathfrak{F}-1)} \int_0^b \mathfrak{I}_n(v)\,[E_1 w(\alpha), E_2 w(\alpha)]\,dv \\
& - \frac{\varpi(\mathfrak{F}-1)}{b\mathscr{M}(\mathfrak{F}-1)(\Gamma(\mathfrak{F}))} \int_0^b (b-v)^{(\mathfrak{F}-1)} \mathfrak{I}_n(v)\,[E_1 w(\alpha), E_2 w(\alpha)]\,dv \\
& + \frac{2-\mathfrak{F}}{\mathscr{M}(\mathfrak{F}-1)} \int_0^{\varpi} \mathfrak{I}_n(v)\,[E_1 w(\alpha), E_2 w(\alpha)]\,dv \\
& + \frac{(\mathfrak{F}-1)}{\mathscr{M}(\mathfrak{F}-1)(\Gamma(\mathfrak{F}))} \int_0^{\varpi} (\varpi-v)^{\mathfrak{F}-1} \mathfrak{I}_n(v)\,[E_1 w(\alpha), E_2 w(\alpha)]\,dv, \forall \varpi \in I.
\end{aligned}$$

Thus $\mathfrak{I} \in \mathscr{Q}_H, x$ and

$$\begin{aligned}
\omega_n(\varpi) \to \omega(\varpi) = {} & \frac{\varpi x_1 + x_0(b-\varpi)}{b} - \frac{\varpi(2-\mathfrak{F})}{b\mathscr{M}(\mathfrak{F}-1)} \int_0^b \mathfrak{I}(v)\,[E_1 w(\alpha), E_2 w(\alpha)]\,dv \\
& - \frac{\varpi(\mathfrak{F}-1)}{b\mathscr{M}(\mathfrak{F}-1)(\Gamma(\mathfrak{F}))} \int_0^b (b-v)^{(\mathfrak{F}-1)} \mathfrak{I}(v)\,[E_1 w(\alpha), E_2 w(\alpha)]\,dv \\
& + \frac{2-\mathfrak{F}}{\mathscr{M}(\mathfrak{F}-1)} \int_0^{\varpi} \mathfrak{I}(v)\,[E_1 w(\alpha), E_2 w(\alpha)]\,dv \\
& + \frac{(\mathfrak{F}-1)}{\mathscr{M}(\mathfrak{F}-1)(\Gamma(\mathfrak{F}))} \int_0^{\varpi} (\varpi-v)^{\mathfrak{F}-1} \mathfrak{I}(v)\,[E_1 w(\alpha), E_2 w(\alpha)]\,dv, \forall \varpi \in I.
\end{aligned}$$

Hence $\omega \in \mathfrak{Z}(x)$.
Now to show that, $0 < \varpi < 1, (\varpi = \eta||\rho||)$,

$$H_d(\mathfrak{Z}(x), \mathfrak{Z}(\bar{x}) \leq \varpi||x-\bar{x}||\text{for each}x, \bar{x} \in \mathscr{I}.$$

Here $x, \bar{x}$ and $\zeta_1 \in \mathfrak{Z}(x)$, and $\mathfrak{I}_1(\varpi) \in H(\varpi, x(\varpi))$, $\varpi \in I$

$$\begin{aligned}\zeta_1(\varpi) = &\frac{\varpi x_1 + x_0(b-\varpi)}{b} - \frac{\varpi(2-\mathfrak{F})}{b\mathscr{M}(\mathfrak{F}-1)}\int_0^b \mathfrak{I}_1(v)\,[E_1 w(\alpha), E_2 w(\alpha)]\,dv \\ &- \frac{\varpi(\mathfrak{F}-1)}{b\mathscr{M}(\mathfrak{F}-1)(\Gamma(\mathfrak{F}))}\int_0^b (b-v)^{(\mathfrak{F}-1)}\mathfrak{I}_1(v)\,[E_1 w(\alpha), E_2 w(\alpha)]\,dv \\ &+ \frac{2-\mathfrak{F}}{\mathscr{M}(\mathfrak{F}-1)}\int_0^{\varpi} \mathfrak{I}_1(v)\,[E_1 w(\alpha), E_2 w(\alpha)]\,dv \\ &+ \frac{(\mathfrak{F}-1)}{\mathscr{M}(\mathfrak{F}-1)(\Gamma(\mathfrak{F}))}\int_0^{\varpi} (\varpi - v)^{\mathfrak{F}-1}\mathfrak{I}_1(v)\,[E_1 w(\alpha), E_2 w(\alpha)]\,dv, \forall \varpi \in I.\end{aligned}$$

Using $[H_6]$

$$H_d(H(\varpi, x), H(\varpi, \bar{x})) \leq \rho(\varpi)|x(\varpi) - \bar{x}(\varpi)|.$$

Thus, $\xi(\varpi) \in H(\varpi, \bar{x})$,

$$|\mathfrak{I}_1(\varpi) - \xi| \leq \rho(\varpi)|x(\varpi) - \bar{x}(\varpi)|, \varpi \in I.$$

Let the operator $\mathscr{F} : I \to \mathfrak{O}(R)$ be defined as

$$\mathscr{F}(\varpi) = \xi \in R : |\mathfrak{I}_1(\varpi) - \xi| \leq \rho(\varpi)|x(\varpi) - \bar{x}(\varpi)|.$$

We find that $\mathfrak{I}_1$ and $\Lambda = \rho|x-\bar{x}|$ are measurable, so MVM $\mathscr{F}(\varpi) \cap H(\varpi, \bar{x})$ is measurable. Choosing $\mathfrak{I}_2(\varpi) \in H(\varpi, \bar{x})$, we have

$$|\mathfrak{I}_1(\varpi) - \mathfrak{I}_2(\varpi)| \leq \rho(\varpi)|x(\varpi) - \bar{x}(\varpi)|, \forall \varpi \in I.$$

Using

$$\begin{aligned}\zeta_2(\varpi) = &\frac{\varpi x_1 + x_0(b-\varpi)}{b} - \frac{\varpi(2-\mathfrak{F})}{b\mathscr{M}(\mathfrak{F}-1)}\int_0^b \mathfrak{I}_2(v)\,[E_1 w(\alpha), E_2 w(\alpha)]\,dv \\ &- \frac{\varpi(\mathfrak{F}-1)}{b\mathscr{M}(\mathfrak{F}-1)(\Gamma(\mathfrak{F}))}\int_0^b (b-v)^{(\mathfrak{F}-1)}\mathfrak{I}_2(v)\,[E_1 w(\alpha), E_2 w(\alpha)]\,dv \\ &+ \frac{2-\mathfrak{F}}{\mathscr{M}(\mathfrak{F}-1)}\int_0^{\varpi} \mathfrak{I}_2(v)\,[E_1 w(\alpha), E_2 w(\alpha)]\,dv \\ &+ \frac{(\mathfrak{F}-1)}{\mathscr{M}(\mathfrak{F}-1)(\Gamma(\mathfrak{F}))}\int_0^{\varpi} (\varpi - v)^{\mathfrak{F}-1}\mathfrak{I}_2(v)\,[E_1 w(\alpha), E_2 w(\alpha)]\,dv, \forall \varpi \in I.\end{aligned}$$

Also,

$$\begin{aligned}|\zeta_1(\varpi) - \zeta_2(\varpi)| = &\frac{\varpi(2-\mathfrak{F})}{b\mathscr{M}(\mathfrak{F}-1)}\int_0^b |\mathfrak{I}_1(v) - \mathfrak{I}_2(v)\,[E_1 w(\alpha), E_2 w(\alpha)]\,|dv \\ &- \frac{\varpi(\mathfrak{F}-1)}{b\mathscr{M}(\mathfrak{F}-1)(\Gamma(\mathfrak{F}))}\int_0^b (b-v)^{(\mathfrak{F}-1)}|\mathfrak{I}_1(v)\mathfrak{I}_2(v)\,[E_1 w(\alpha), E_2 w(\alpha)]\,|dv \\ &+ \frac{2-\mathfrak{F}}{\mathscr{M}(\mathfrak{F}-1)}\int_0^{\varpi} |\mathfrak{I}_1(v)\mathfrak{I}_2(v)\,[E_1 w(\alpha), E_2 w(\alpha)]\,|dv \\ &+ \frac{(\mathfrak{F}-1)}{\mathscr{M}(\mathfrak{F}-1)(\Gamma(\mathfrak{F}))}\int_0^{\varpi} (\varpi - v)^{\mathfrak{F}-1}|\mathfrak{I}_1(v)\mathfrak{I}_2(v)\,[E_1 w(\alpha), E_2 w(\alpha)]\,|dv \\ &\leq ||\alpha||||x-\bar{x}||\left(\frac{2b}{\mathscr{M}(\mathfrak{F}-1)} + \frac{2b^B}{\mathscr{M}(\mathfrak{F}-1)\Gamma(\mathfrak{F}+1)}\right).\end{aligned}$$

Hence

$$||\zeta_1 - \zeta_2|| \leq \eta||\rho||\,||x-\bar{x}||.$$

Now, swapping x and $\bar{x}$, one has

$$H_d(\mathfrak{Z}(x),\mathfrak{Z}(\bar{x})) \leq \eta||\rho||\,||x-\bar{x}||,$$

As I is a contraction, we can conclude that it has FP and hence according to Covitz-Nadler theorem problem (1) has a solution.

4 Examples

To demonstrate the validation of the results obtained in the previous section, we consider the following two examples.
Example 1: Suppose we have the following FIDI

$$\begin{aligned} &{}_0^{ABC}\mathscr{D}_{\varpi}^{\frac{3}{2}} z(\varpi) \in H\left(\varpi, z(\varpi), \int_0^b e(\varpi,s,z(s))ds, \int_0^{\varpi} h(\varpi,s,z(s))ds\right), \varpi \in I=(0,1) \\ &z(0)=z_0, z(1)=1, \mathscr{M}(\mathfrak{F}-1)=1 \end{aligned} \tag{4.1}$$

Here, $\mathfrak{F}=\frac{3}{2}, b=1 \& H:[0,1]\times R \to \mathscr{O}(R)$ is a MVM,

$$x \to H(\varpi,x)=\left[\frac{1}{10(\varpi^3+3exp(\varpi))}\frac{x^4}{(x^4+1)}, \frac{1}{\sqrt{\varpi+16}}\frac{|x|}{|x|+1}\right].$$

Obviously H fulfills $[H_1]$, and

$$\begin{aligned} ||H(\varpi,x)||_{\mathfrak{D}} &= sup\{|\odot|:\in H(\varpi,x)\} \\ &\leq \frac{1}{\sqrt{\varpi+16}} = \psi_1(\varpi)\psi_2(||x||)||\mathfrak{z}||, \end{aligned}$$

which implies $||\psi_1|| = \frac{1}{4}$ and $\psi_2(||x||)=1$.
By $[H_3]$ and in view of theorem 3.2, we get $\mathfrak{N} > 1.8761$. Thus $\exists$ a soln for (1) on $[0,1]$.

Example 2: Suppose we have the following FIDI

$$\begin{aligned} &{}_0^{ABC}\mathscr{D}_{\varpi}^{\frac{5}{4}} z(\varpi) \in H\left(\varpi, z(\varpi), \int_0^b e(\varpi,s,z(s))ds, \int_0^{\varpi} h(\varpi,s,z(s))ds\right), \varpi \in I=(0,1) \\ &z(0)=z_0, z(1)=1, \mathscr{M}(\mathfrak{F}-1)=1 \end{aligned} \tag{4.2}$$

Here, $\mathfrak{F}=\frac{5}{4}, b=1$ and $H:[0,1]\times R \to \mathscr{O}(R)$ is a MVM,

$$x \to H(\varpi,x)=\left[0, \frac{2sin(x^2)}{(\varpi^2+10)}+\frac{1}{14}\right].$$

$H_d(H(\varpi,x),H(\varpi,\bar{x})) \leq \rho(\varpi)|x-\bar{x}|$, where $\rho(\varpi)=\frac{2}{\varpi^2+10}$ as well $d(0,H(\varpi,0))=\frac{1}{14} \leq \rho(\varpi), \varpi \in [0,1]$.
$\therefore ||\rho||=\frac{1}{5}$ and $\eta||\rho|| \approx 0.75 < 1$.
By $[H_5]$ and in view of theorem 3.4, $\exists$ at least a solution for the problem (1) on $[0,1]$.

5 Conclusion

In this study we have analysed a class of FIDIs using the ABC derivative. Two cases of MVM with convex and non convex values were discussed wherein Leray-Schauder theorem was applied to study the former case and Covitz-Nadler theorem was applied to study the latter. The results obtained were then validated with the help of suitable examples.

Acknowledgment:
"The authors extend their appreciation to Prince Sattam bin Abdulaziz University for funding this research work through the project number (PSAU/2023/01/24878)"

References

[1] A. Ali, K. Shah, F. Jarad, V. Gupta and T. Abdeljawad, Existence and stability analysis to a coupled system of implicit type impulsive boundary value problems of fractional-order differential equations, *Adv. Differ. Equ.* **2019**, 21 (2019).

[2] M. M. Arjunan and S. Selvi, Existence results for impulsive mixed Volterra-Fredholm integro-differential inclusions with nonlocal conditions, *Int. J. Appl. Math.* **1**(2), 101-119 (2015).

[3] Y. Alruwaily, S. Aljoudi, L. Almaghamsi, A. B. Makhlouf and N. Alghamdi, Existence and uniqueness results for different orders coupled system of fractional integro-differential equations with anti-periodic nonlocal integral boundary conditions, *Symmetry.* **15**(1), 15 (2023).

[4] K. J. Basant, G. Dauda and M. A. Umar, Fractional order analysis of unsteady pressure-driven flow in an annulus with momentum slip, *Partial Differ. Equ. Appl. Math.* **7**, 100474 (2023).

[5] J. Bahram, J. Payam, S. Amirali and D. G. Davood, Rigid plate submerged in a newtonian fluid and fractional differential equation problems via Caputo fractional derivative, *Partial Differ. Equ. Appl. Math.* **6**, 100452 (2022).

[6] R. P Hem, R. P. Ganga and B. G. Dil, Vaccination effect on the dynamics of dengue disease transmission models in Nepal: a fractional derivative approach, *Partial Differ. Equ. Appl. Math.* **7**, 100476 (2023).

[7] M. Houas, S. M. Esmael and S. Rezapour, Solvability and stability for a fractional quantum jerk type problem including Riemann-Liouville-Caputo fractional q-derivatives, *Partial Differ. Equ. Appl. Math.* **7**, 100514 (2023).

[8] M. Kisielewicz, *Differential inclusions and optimal control.* Dordrecht, the Netherlands, Kluwer, 1991.

[9] Z. Laadjal and F. Jarad, Existence, uniqueness and stability of solutions for generalized proportional fractional hybrid integro-differential equations with Dirichlet boundary conditions, *AIMS Math.* **8**(1), 1172-1194 (2023).

[10] A. Lachouri, A. Ardjouni and A. Djoudi, Existence results for nonlinear sequential Caputo and Caputo-Hadamard fractional differential inclusions with three-point boundary conditions, *Math. Eng. Sci.* **12**(1), 163-179 (2021).

[11] A. Lachouri, A. Ardjouni and A. Djoudi, Investigation of the existence and uniqueness of solutions for higher order fractional differential inclusions and equations with integral boundary conditions, *J. Interdis. Math.* **24**(8), 2161-2179 (2021).

[12] K. S. Nisar, S. Alsaeed, K. Kaliraj, C. Ravichandran, W. Albalawi and Abdel-Haleem Abdel-Aty, Existence criteria for fractional differential equations using the topological degree method, *AIMS Math.* **8**(9), 21914-21928 (2023).

[13] K. S. Nisar, R. Jagatheeshwari, C. Ravichandran, P. Veeresha, High performance computational method for fractional model of solid tumour invasion, *Ain Shams. Eng. J.*, 102226 (2023).

[14] Y. Zhou, *Fractional evolution equations and inclusions: analysis and control*, Amsterdam, Elsevier, 2015.

[15] V. H. Le and D. K. Tran, Globally attracting solutions to impulsive fractional differential inclusions of Sobolev type, *Acta Math. Sci.* **37B**(5), 1295-1318 (2017).

[16] A. Pazy, *Semigroups of linear operators and applications to partial differential equations*, New York, Springer-Verlag, 1983.

[17] I. Podlubny, *Fractional differential equations: an introduction to fractional derivatives*, San Diego, CA: Academic Press, 1999.

[18] V. Vijayaraj, C. Ravichandran, S. Panumart and K. S. Nisar, Existence results of Atangana-Baleanu fractional integro-differential inclusions of Sobolev type, *Alex. Eng. J.* **66**, 249-255 (2023).

[19] C. Yong-Kui and P. Rodrigo, Properties of solution sets for Sobolev type fractional differential inclusions via resolvent family of operators, *Eur. Phys. J. Spec. Top.* **226**, 3391-3409 (2017).

[20] C. Ravichandran, K. Logeswari, A. Khan, T. Abdeljawad and J. F. Gomez-Aguilar, An epidemiological model for computer virus with Atangana-Baleanu fractional derivative, *Res. Phys.* **51**, 106601 (2023).

[21] H. Covitz and S. B. Nadler Jr, Multivalued contraction mappings in generalized metric spaces, *Isr. J. Math.* **8**, 5-11 (1970).

[22] M. Mallika Arjunan, T. Abdeljawad, V. Kavitha and A. Yousef, On a new class of Atangana-Baleanu fractional Volterra-Fredholm integro-differential inclusions with non-instantaneous impulses, *Chaos Soliton. Fract.* **148**, 111075 (2021).

[23] A. A. Noor, H. M. Osama and A. Y. Ahmed, A hybrid technique for approximating the solution of fractional order integro differential equations, *Partial Differ. Equ. Appl. Math.* **8**, 100552 (2023).

[24] X. J. Yang, *General fractional derivatives: theory, methods and applications*, 1st Edition. New York, CRC Press, 2019.

[25] E. Zeidler, *Nonlinear functional analysis and its application II/A*. New York, Springer, 1990.

[26] L. S. Daya, S. Biniyam, U. Faruk and D. P. Sunil, Caputo type fractional differentiation for the extended generalized Mittag-Leffler function, *Progr. Fract. Differ. Appl.* **9**(1), 135-143 (2023).

[27] A. Lachouri, Mohammed S. Abdo, A. Ardjouni, K. Shah and T. Abdeljawad, Investigation of fractional order inclusion problem with Mittag-Leffler type derivative, *J. Pseudo. Differ. Oper. Appl.* **14**, 43 (2023).

[28] A. Atangana and D. Baleanu, New fractional derivatives with non-local and non-singular kernel: theory and application to heat transfer model, *Therm. Sci.* **20**(2), 763-769 (2016).

[29] T. Abdeljawad, A Lyapunov type inequality for fractional operators with nonsingular Mittag-Leffler kernel, *J. Ineq. Appl.* **2017**, 130 (2017).

[30] S. Shabbir, K. Shah and T. Abdeljawad, Stability analysis for a class of implicit fractional differential equations involving Atangana-Baleanu fractional derivative, *Adv. Differ. Equ.* **2021**(1), 395 (2021).

[31] Soong, Cai-Juan, Rosshairy Abd Rahman, Razamin Ramli, Mohammed Suhaimee Abd Manaf, and Chek-Choon Ting. An Evolutionary Algorithm: An Enhancement of Binary Tournament Selection for Fish Feed Formulation. Complexity, **2022** Article ID 7796633: 1 -15 (2022). https://doi.org/10.1155/2022/7796633

K. Deimling, *Set-Valued Differential Equations*, Berlin, De Gruyter, 1992.

[32] S. Hu and N. Papageorgiou, *Handbook of Multivalued Analysis, Vol I: Theory*, Dordrecht, Kluwer, 1997.

[33] H. Khan, A. Khan, F. Jarad and A. Shah, Existence and data dependence theorems for solutions of an ABC-fractional order impulsive system, *Chaos Soliton. Fract.* **131**, 109477 (2020).
[34] A. Granas and J. Dugundji, *Fixed point theory*, New York, Springer, 2003.
[35] A. Lasota and Z. Opial, An application of the Kakutani-Ky Fan theorem in the theory of ordinary differential equations, *Bull. Acad. Polonaise Sci.* **13**, 781-786 (1965).
[36] C. Castaing and M. Valadier, *Convex analysis and measurable multifunctions; Lecture Notes in Mathematics 580*, Germany, New York, Springer, Berlin/Heidelberg, 1977.

AIMS Mathematics, 9(3): 8292–8310.
DOI: 10.3934/math.2024403
Received: 27 December 2023
Revised: 19 February 2024
Accepted: 20 February 2024
Published: 27 February 2024

http://www.aimspress.com/journal/Math

Research article

Results on generalized neutral fractional impulsive dynamic equation over time scales using nonlocal initial condition

Ahmed Morsy[1], C. Anusha[2], Kottakkaran Sooppy Nisar[3,4,*] and C. Ravichandran[2]

[1] Department of Mathematics, College of Arts and Sciences, Prince Sattam bin Abdulaziz University, Wadi Aldawaser 11991, Saudi Arabia
[2] Department of Mathematics, Kongunadu Arts and Science College, Coimbatore 641029, India
[3] Department of Mathematics, College of Science and Humanities in Alkharj, Prince Sattam bin Abdulaziz University, Alkharj 11942, Saudi Arabia
[4] Saveetha School of Engineering, SIMATS, Chennai, India

* **Correspondence:** Email: n.sooppy@psau.edu.sa.

Abstract: This paper explored the existence and uniqueness of a neutral fractional impulsive dynamic equation over time scales that included nonlocal initial conditions and employed the Caputo-nabla derivative (C∇D). The establishment of existence and uniqueness relies on the fine fixed point theorem. Furthermore, a comparison was conducted between the fractional order C∇D and the Riemann-Liouville nabla derivative (RL∇D) over time scales. Theoretical findings were substantiated through a numerical methodology, and an illustrative graph using MATLAB was presented for the provided example.

Keywords: neutral differential equations; C∇D; RL∇D; time scales
Mathematics Subject Classification: 26E70, 34K40, 34N05, 37C25

1. Introduction

Similar to how fractional exponents evolve from integer exponents, classical calculus concepts like integral and derivative operators serve as the foundation for fractional calculus [1, 2]. Many people are aware that depending on the geometrical and physical factors, integer-order derivatives and integrals have different meanings. This assumption, however, is disproved when dealing with fractional-order integration and differentiation, which covers a constantly expanding domain in both theory and practical applications to real-life challenges [3]. The study of fluid flow, rheology, diffusive transport, electrical networks, electromagnetic theory, probability, and research on viscoelastic materials are just a few of the scientific and engineering domains where it has lately been employed [4–6]. Fractional

differential equations (FDEs) have drawn attention from several researches as a result of its frequent occurrence in disciplines such as physics, chemistry, and engineering. The commonly used Laplace transform approach, the iterative method, the Fourier transform technique, and the operational method are just a few of the strategies developed to deal with FDEs [7–9]. The majority of these techniques, however, are only relevant to a few types of FDEs, particularly those that are linear and have constant coefficients. The existence of solutions for fractional semilinear differential or integrodifferential equations is one of the theoretical fields being investigated by many authors. There has been a significant development in nonlocal problems for FDEs or inclusions [10, 11]. Reimann-Liouvile fractional derivative-based linear FDEs with variable coefficients have been solved using the decomposition approach. FDEs have recently received a lot of attention from academics. This is because FDEs are frequently used in engineering and science, including in the study of diffusion in porous media, nonlinear earth oscillation, fractional biological neurons, traffic flow, polymer rheology, modeling of neural networks, and viscoelastic panels in supersonic gas flow [12–16].

In the real world, there may be situations that cannot be fully captured by either wholly continuous or entirely discrete phenomena. In these cases, we require a shared domain to adequately support both conditions. In order to unify continuous and discrete calculus, Stefan Hilger created a usual state known as time scale T [17–19]. This domain is based on the unification of these requirements [20–23]. To solve this type of model, which combines differential and difference equations, dynamic equations on a time scale were developed [24, 25]. Many scholars worked on dynamic equations that involve local beginning and boundary conditions and might be either linear or nonlinear. Because fractional calculus is accurate and has an advantage in the physical interpretation, several authors have studied the dynamic equation using this method [26–28].

We have seen a number of equations in the real world where the systems are permitted to experience a brief disturbance, the length of which may be insignificant compared to the overall process duration. In this situation, jump discontinuities may appear in the solution of these equations at time $\varsigma_1 < \varsigma_2 < \varsigma_3 < \cdots$, given in the form

$$p(\varsigma_k^+) - p(\varsigma_k^-) = \mathcal{I}_k(\varsigma_k, p(\varsigma_k^-)).$$

Impulsive dynamic equations are dynamic equations with jump discontinuities as solutions [29–31]. Dynamic impulsive equations on time scales have caught the attention of many academics recently. However, there are very few publications that investigate impulsive dynamic equations using fractional calculus on time scales with nonlocal initial conditions [32, 33].

Neutral differential equations [34, 35] appear when $\max\{n_1, n_2, \cdots, n_k\} = n$. The past and present values of the function are determined by Neutral differential equations, which differs from retarded differential equations in that they depend on derivatives with delays. Elastic networks are simulated by neutral type differential equations in high speed computers for the express purpose of joining switching circuits [36]. Due to their extensive use in practical mathematics, neutral differential equations have recently attracted a lot of attention [37, 38]. Many scientists have sought to create neutral differential systems, taking note of varied fixed point strategies, mild solutions, and nonlocal situations. Also, in recent years, neural networks have been extensively studied and have been applied in many fields, such as combinatorial optimization, multiagent systems, fault diagnosis, and industrial automation. However, the practical applications of neural networks have been limited due to some inherent dynamic properties, such as the information latching phenomenon [39–41].

While the authors of [24, 25] used the tools of the delta (Hilger) derivative to investigate the

fractional dynamic equation with local initial condition and instantaneous and non-instantaneous impulses, authors of [42] investigated the nonlocal initial condition's impulsive dynamic equation. In [43], the authors have discussed the impulsive fractional dynamic equation on time scales with a nonlocal initial condition. The exploration and elucidation of results pertaining to a generalized neutral fractional impulsive dynamic equation over time scales, specifically incorporating nonlocal initial conditions, is the main contribution of the this study.

As a result of the work described above, we assert that it's important to investigate the impulsive neutral fractional dynamic equation with nonlocal initial condition of the type:

$$\begin{cases} {}^{C}D^{\mathrm{w}}[u(\varsigma) - g(\varsigma, u)] = \mathfrak{Q}(\varsigma, u(\varsigma), {}^{C}D^{\mathrm{w}}u(\varsigma)), & \varsigma \in \mathscr{I},\ \varsigma \neq \varsigma_k \\ u(\varsigma_k^{+}) - u(\varsigma_k^{-}) = \mathcal{I}_k(\varsigma_k, u(\varsigma_k^{-})), & k = 1, 2, \cdots, m \\ u(0) = \varphi(u), \end{cases} \tag{1.1}$$

where $k \in \mathbb{N} \cup \{0\}$ and

$$\mathscr{I} = [0, \mathscr{T}] \cap \mathfrak{T}$$

for $\mathscr{T} \in \mathfrak{T}$. Let the left dense(ld) continuous function be

$$\mathfrak{Q} : \mathscr{I} \times \mathscr{R} \times \mathscr{R} \to \mathscr{R}$$

and ${}^{C}D^{\mathrm{w}}$ is Caputo nabla derivative (C∇D). We assume that

$$0 < \varsigma_o < \varsigma_1 < \varsigma_2 < \varsigma_3 < \cdots < \varsigma_n < \varsigma_{n+1} = \mathscr{T},$$

which indicates the impulse at specific time, and the terms

$$u(\varsigma_k^{+}) = lim_{d \to 0^{+}} u(\varsigma_k + d)$$

and

$$u(\varsigma_k^{-}) = lim_{d \to 0^{+}} u(\varsigma_k - d)$$

represent the function's right and left limits u at $\varsigma = \varsigma_k$ in relation to time scales. $\mathcal{I}_k$ are continuous real valued functions on $\mathscr{R}\ \forall\ k = 1, 2, \cdots, m$, and $\mathcal{I}_k(\varsigma_k, u(\varsigma_k^{-}))$ are the action of impulses on the time scale interval $\mathscr{I}$.

2. Preliminaries

Definition 2.1. *[44] A function ρ: $\mathfrak{T} \to \mathscr{R}$ defined by*

$$\rho(\varsigma) = inf\{\theta \in \mathfrak{T} : \theta < \varsigma\}$$

is said to be a backward jump operator. Any $\varsigma \in \mathfrak{T}$ is said to be ld if $\rho(\varsigma) = \varsigma$ and if $\rho(\varsigma) = \varsigma - 1$, then ς is said to be a left scattered point on $\mathfrak{T}$.

Remark 2.2. *If $\mathfrak{T}$ is a minimum right scattered point y, then set $\mathfrak{T}_\upsilon = \mathfrak{T}\backslash\{y\}$, otherwise $\mathfrak{T}_\upsilon = \mathfrak{T}$.*

Definition 2.3. *[42] A function*

$$x : \mathfrak{T} \times \mathscr{R} \times \mathscr{R} \to \mathscr{R}$$

is said to be an ld continuous function, if $x(\cdot, p, q)$ is ld continuous on $\mathfrak{T}$ for each ordered pair $(\varsigma, \theta) \in \mathscr{R} \times \mathscr{R}$ and $x(\varsigma, \cdot, \cdot)$ is continuous on $\mathscr{R} \times \mathscr{R}$ for fixed point $\varsigma \in \mathfrak{T}$.

Proposition 2.4. *[17] Assume g is an increasing continuous function on* $[0, \mathscr{T}] \cap \mathfrak{T}$. *If* $\mathbb{G}$ *is an addition to g in* $[0, \mathscr{T}]$, $\mathscr{T} \in \mathscr{R}$, *one can obtain*

$$\mathbb{G}(\varsigma) = \begin{cases} g(\varsigma), & if \varsigma \in \mathfrak{T}, \\ g(\theta), & if \varsigma \in (\varsigma, \rho(\varsigma)) \notin \mathscr{R}, \end{cases}$$

then,

$$\int_s^t g(\varsigma)\nabla\varsigma \leq \int_s^t g(\varsigma)d\varsigma, \tag{2.1}$$

for $s, t \in [0, \mathscr{T}] \cap \mathfrak{T}$, *such that* $s < t$.

Definition 2.5. *([44], Higher order nabla derivative) Consider an ld continuous function* $\mathfrak{H}$: $\mathfrak{T}_\upsilon \to \mathscr{R}$ *over* $\mathfrak{T}$. *Here,* $\mathfrak{H}_\nabla$ *is differentiable over* $\mathfrak{T}_\upsilon^{(2)} = \mathfrak{T}_{\upsilon\upsilon}$ *along*

$$\mathfrak{H}_\nabla^{(2)} = (\mathfrak{H})_\nabla : \mathfrak{T}_\upsilon^{(2)} \to \mathscr{R},$$

where $\mathfrak{H}_{\nabla\nabla} = \mathfrak{H}_\nabla^{(2)}$ *is the second order nabla derivative. Also, proceeding upto* n^{th} *order, one can get* $\mathfrak{H}_\nabla^{(n)}$: $\mathfrak{T}_\upsilon^{(n)} \to \mathscr{R}$.

Definition 2.6. *[44] Consider ld continuous function* $\mathfrak{H}$: $\mathfrak{T}_\upsilon^{(n)} \to \mathscr{R}$, *such that* $\mathfrak{H}_\nabla^{(n)}(\varsigma)$ *(*n^{th} *order of nabla derivative) appears, then the C*∇*D is*

$${}^{C}D_a^{\mathfrak{w}}\mathfrak{H}(\varsigma) = \frac{1}{\Gamma(n-\mathfrak{w})}\int_a^{\varsigma}(\varsigma - \rho(\theta))^{n-\mathfrak{w}-1}\mathfrak{H}_\nabla^n(\theta)\nabla\theta.$$

If $\mathfrak{w} \in (0, 1)$, *we obtain*

$${}^{C}D_a^{\mathfrak{w}}\mathfrak{H}(\varsigma) = \frac{1}{\Gamma(1-\mathfrak{w})}\int_a^{\varsigma}(\varsigma - \rho(\theta))^{-\mathfrak{w}}\mathfrak{H}_\nabla\nabla\theta.$$

Definition 2.7. *[44] On the set* $\mathfrak{T}_\upsilon$, *consider* $\mathfrak{H}$ *to be any ld continuous function, then the Riemann-Liouville nabla derivative (RL*∇*D) is*

$$D_{\varsigma_o}^{\mathfrak{w}}x(t) = \frac{1}{\Gamma(1-\mathfrak{w})}\Big(\int_{\varsigma_o}^{\varsigma}(\varsigma - \rho(\theta))^{-\mathfrak{w}}x(\theta)\nabla\theta\Big)^{\nabla}.$$

Definition 2.8. *[17] Assume* $\mathfrak{H}$: $\mathscr{I}_{\mathcal{J}} \to \mathscr{R}$, *then the RL*$\nabla$*D fractional integral of* $\mathfrak{H}$ *is*

$$D_{\varsigma_o}^{-\mathfrak{w}}\mathfrak{H}(\varsigma) = \mathbb{I}_{\varsigma_o}^{\mathfrak{w}}\mathfrak{H}(\varsigma) = \frac{1}{\Gamma(\mathfrak{w})}\int_{\varsigma_o}^{\varsigma}(\varsigma - \rho(\theta))^{\mathfrak{w}-1}\mathfrak{H}(\theta)\nabla\theta.$$

The RL∇*D integral always satisfies the condition*

$$\mathbb{I}_{\varsigma_o}^{\mathfrak{w}}\mathbb{I}_{\varsigma_o}^{u}\mathfrak{H}(\varsigma) = \mathbb{I}_{\varsigma_o}^{w+u}\mathfrak{H}(\varsigma).$$

Lemma 2.9. *[17] Assume the ld continuous function is* $u(\varsigma)$, *then*

$$\begin{cases} D^u\mathbb{I}^{\mathfrak{w}}\imath p(\varsigma) = u(\varsigma), \\ D^u\mathbb{I}^{\mathfrak{w}}\imath p(\varsigma) = \mathbb{I}^{w-u}u(\varsigma). \end{cases}$$

Theorem 2.10. *[25] Assume $D \subset \mathfrak{C}(\mathfrak{T}, \mathscr{R})$. Let D be bounded and equicontinuous simultaneously, then it is relatively compact.*

Theorem 2.11. *[42] A function $\mathfrak{H}(\mathcal{B})$ is relatively compact in $\mathcal{A}$ for $\mathfrak{H}$: $\mathcal{A} \to \mathcal{B}$, which is completely continuous.*

Theorem 2.12. *([24], Nonlinear alternatives Leray-Schauder's type) Let $C \subset \mathcal{X}$ be closed and convex and $\mathcal{X}$ be as Banach space. Let G: $\mathcal{U} \to C$ be a compact map and $\mathcal{U}$ be a relatively open subset of C with $0 \in \mathcal{U}$, then*

(i) G has a fixed point in $\mathcal{U}$; or

(ii) there is a point $\mathfrak{u} \in \delta U$ and $\gamma \in (0, 1)$ with $u = \gamma G(\mathfrak{u})$.

Theorem 2.13. *[42] For $\mathfrak{w} \in (0, 1)$, u is a solution for $\mathfrak{Q}$: $\mathscr{I}_{\mathcal{J}} \times \mathscr{R} \times \mathscr{R} \to \mathscr{R}$, then*

$$^{C}D^{\mathfrak{w}}u(\varsigma) = \mathfrak{Q}(\varsigma, u(\varsigma), {}^{C}D^{\mathfrak{w}}u(\varsigma)), \quad u(\varsigma)|_{\varsigma=0} = \varphi(u),$$

if u is the solution of equation

$$u(\varsigma) = \varphi(u) + \frac{1}{\Gamma(\mathfrak{w})}\int_{\varsigma_o}^{\varsigma} (\varsigma - \rho(x))^{\mathfrak{w}-1}\mathfrak{Q}(x, u(x), {}^{C}D^{\mathfrak{w}}u(x))\nabla x. \tag{2.2}$$

Definition 2.14. *[45] Let $\mathscr{X}$ be a Banach space and*

$$\mathscr{A} = \{\mathcal{L}(t) \in \mathscr{L}(\mathscr{X}) : t \geq 0\},$$

where $\mathscr{L}(\mathscr{X})$, a family of linear, bounded operators $\mathscr{L}(\mathscr{X})$: $\mathscr{X} \to \mathscr{X}$ for all $t \geq 0$. A is called a semigroup if, and only if,

$$\mathcal{L}(0) = \mathscr{I} \quad and \quad \mathcal{L}(s + t) = \mathcal{L}(s)\mathcal{L}(t), \quad \forall t, s \geq 0.$$

3. Analysis between RL∇D and C∇D

Proposition 3.1. *Let $m - 1 < \mathfrak{w} < m, m \in \mathbb{N}$ for any $\mathfrak{w} \in \mathscr{R}$, such that ${}^{C}D^{\mathfrak{w}}_{\varsigma_o}\mathbb{G}(\varsigma)$ exists over time scale $\mathfrak{T}$, then*

$${}^{C}D^{\mathfrak{w}}_{\varsigma_o}\mathbb{G}(\varsigma) = \mathbb{I}^{m-\mathfrak{w}}_{\varsigma_o}\mathbb{G}^{(m)}_{\nabla}(\varsigma).$$

Proof. The proof is evident from Theorems 2.12 and 2.13. □

Theorem 3.2. *For $m = [\mathfrak{w} + 1]$ and for any $\varsigma \in \mathfrak{T}_{v^n}$, the C∇D and RL∇D satisfies:*

$${}^{C}D^{\mathfrak{w}}_{\alpha}\mathbb{G}(\varsigma) = D^{\mathfrak{w}}_{\alpha}(\mathbb{G}(\varsigma) - \sum_{v=0}^{m-1}\frac{(\varsigma - \alpha)^{v}}{\Gamma(v + 1)}\mathbb{G}^{(v)}_{\nabla}(\alpha)),$$

for a fixed point $\alpha \in \mathfrak{T}$. Taylor's theorem defined in [27] proves this theorem.

Proof. Assume ld continuous function $\mathbb{G}$, then $\forall$ fixed $\alpha \in \mathfrak{T}$ and $m \in \mathbb{N} \cup \{0\}, m < n$. One can obtain

$$\begin{aligned}\mathbb{G}(\varsigma) &= \sum_{v=0}^{m-1} \frac{(\varsigma-\alpha)^v}{\Gamma(v+1)} \mathbb{G}_{\nabla}^{(v)}(\alpha) + \frac{1}{\Gamma(m)} \int_{\alpha}^{\varsigma} (\varsigma - \rho(\theta))^{\nabla\theta} \\ &= \sum_{v=0}^{m-1} \frac{(\varsigma-\alpha)^v}{\Gamma(v+1)} \mathbb{G}_{\nabla}^{(v)}(\alpha) + \mathbb{I}_{\alpha}^{m} \mathbb{G}_{\nabla}^{(m)}(\varsigma). \end{aligned} \tag{3.1}$$

Taking the Riemann-Liouville derivative $D_{\alpha}^{\mathfrak{w}}$ in each side of Eq (3.1), Lemma 2.9 and Proposition 3.1 are used below:

$$\begin{aligned} D_{\alpha}^{\mathfrak{w}} \mathbb{G}(\varsigma) &= D_{\alpha}^{\mathfrak{w}} \sum_{v=0}^{m-1} \frac{(\varsigma-\alpha)^v}{\Gamma(v+1)} \mathbb{G}_{\nabla}^{(v)}(\alpha) + D_{\alpha}^{\mathfrak{w}} \mathbb{I}_{\alpha}^{m} \mathbb{G}_{\nabla}^{(m)}(\varsigma) \\ &= D_{\alpha}^{\mathfrak{w}} \sum_{v=0}^{m-1} \frac{(\varsigma-\alpha)^v}{\Gamma(v+1)} \mathbb{G}_{\nabla}^{(v)}(\alpha) + \mathbb{I}_{\alpha}^{m-\mathfrak{w}} \mathbb{G}_{\nabla}^{(m)}(\varsigma) \\ &= D_{\alpha}^{\mathfrak{w}} \sum_{v=0}^{m-1} \frac{(\varsigma-\alpha)^v}{\Gamma(v+1)} \mathbb{G}_{\nabla}^{(v)}(\alpha) + {}^{C}D_{\alpha}^{\mathfrak{w}} \mathbb{G}(\varsigma). \end{aligned} \tag{3.2}$$

From the above equation, we obtain

$$\begin{aligned} {}^{C}D_{\alpha}^{\mathfrak{w}} \mathbb{G}(\varsigma) &= D_{\alpha}^{\mathfrak{w}} \mathbb{G}(\varsigma) - D_{\alpha}^{\mathfrak{w}} \sum_{v=0}^{m-1} \frac{(\varsigma-\alpha)^v}{\Gamma(v+1)} \mathbb{G}_{\nabla}^{(v)}(\alpha) \\ &= D_{\alpha}^{\mathfrak{w}} (\mathbb{G}(\varsigma) - \sum_{v=0}^{m-1} \frac{(\varsigma-\alpha)^v}{\Gamma(v+1)} \mathbb{G}_{\nabla}^{(v)}(\alpha)). \end{aligned} \tag{3.3}$$

□

Proposition 3.3. *If* $\mathfrak{w} \in (0,1)$, *then* $m = 1$. *Hence, from the Eq (3.3),*

$$ {}^{C}D_{\alpha}^{\mathfrak{w}}(\varsigma) = D_{\alpha}^{\mathfrak{w}}(\mathbb{G}(\varsigma) - \mathbb{G}(\alpha)).$$

Case 1. *If* $\mathbb{G}(\alpha) \to 0$, *as* $\alpha \to 0$, *then*

$$ {}^{C}D_{\alpha}^{\mathfrak{w}}(\varsigma) = D_{\alpha}^{\mathfrak{w}} \mathbb{G}(\varsigma). \tag{3.4}$$

Hence, C∇D and the Riemann-Liouville derivative coincide with each other.

Case 2. *If* $\mathfrak{w} \in \mathbb{N}$, *by applying Eq (3.1) in Eq (3.2) and applying Lemma 2.9, one can get*

$$\begin{aligned} {}^{C}D_{\alpha}^{\mathfrak{w}} \mathbb{G}(\varsigma) &= D_{\alpha}^{\mathfrak{w}} (\mathbb{G}(\varsigma) - \sum_{v=0}^{m-1} \frac{(\varsigma-\alpha)^v}{\Gamma(v+1)} \mathbb{G}_{\nabla}^{(v)}(\alpha)) \\ &= D_{\alpha}^{\mathfrak{w}} \mathbb{I}_{\alpha}^{m} \mathbb{G}_{\nabla}^{(m)}(\varsigma) \\ &= \mathbb{G}^{(m)}(\varsigma). \end{aligned}$$

∴ C∇D coincides with the nabla derivative.

4. Existence and uniqueness of impulsive neutral fractional dynamic equation

A population dynamics model featuring a stop-start phenomenon can be used to compare the dynamic Eq (1.1) to that model. If we take into account a negative impact on that particular species, we can observe the population change, that the C∇D ${}^{C}D^{\mathfrak{w}}u(\varsigma)$ presents (at the initial stage of time), with respect to ς on

$$\mathscr{I} = [0, \mathscr{T}] \cap \mathfrak{T}.$$

We investigate a scenario in specific times $\varsigma_1, \varsigma_2, \varsigma_3, \cdots$ such that

$$0 < \varsigma_1 < \varsigma_2 < \varsigma_3, \cdots, \varsigma_m < \varsigma_{m+1} = \mathscr{T}, \quad lim_k = \infty.$$

Impulse effects have an impact on people " momentarily," so there is a surge in the population $u(\varsigma)$, and $u(\varsigma_k^+)$ and $u(\varsigma_k^-)$ show the species population at the time ς_k before and after the impulsive effect.

Assume a collection of every ld continuous function $\mathfrak{C}(\mathscr{I}, \mathscr{R})$. Put $\mathscr{I}_o = [0, \varsigma_1]$ and $\mathscr{I}_k = [\varsigma_k, \varsigma_{k+1}]$ for each $k = 1, 2, \cdots, m$. Let

$$\mathfrak{PC}(\mathscr{I}, \mathscr{R}) = \{u : \mathscr{I}_k \to \mathscr{R}, u \in \mathfrak{C}(\mathscr{I}, \mathscr{R}) \text{ and } u(\varsigma_k^+) \text{ and } u(\varsigma_k^-) \text{ exist with } u(\varsigma_k^-) = u(\varsigma_k), k = 1, 2, \cdots, m\}$$

and

$$\mathfrak{PC}^1(\mathscr{I}, \mathscr{R}) = \{u : \mathscr{I}_k \to \mathscr{R}, u \in \mathfrak{C}^1(\mathscr{I}, \mathscr{R}), k = 1, 2, \cdots, m\},$$

where $\mathfrak{PC}^1(\mathscr{I}, \mathscr{R})$ is collection of every function from $\mathscr{I}_k$ to $\mathscr{R}$, i.e., ld continuously ∇ differentiable function.

The set $\mathfrak{PC}(\mathscr{I}, \mathscr{R})$ is a Banach space

$$\|u\|_{\mathfrak{PC}} = sup_{\varsigma \in \mathscr{I}} |u(\varsigma)|.$$

Definition 4.1. *A function $u \in \mathfrak{PC}^1(\mathscr{I}, \mathscr{R})$ is a solution of the Eq (1.1), if u satisfies the Eq (1.1) on $\mathscr{I}$ having*

$$u(\varsigma_k^+) - u(\varsigma_k^-) = \mathscr{I}_k(\varsigma_k, u(\varsigma_k^-)) \text{ and } u(0) = \varphi(\mathscr{T}).$$

Lemma 4.2. *Assume an ld continuous function $\mathscr{H}: \mathscr{I} \to \mathscr{R}$, such that solution (1.1) is*

$$\begin{cases} {}^{C}D^{\mathfrak{w}}[u(\varsigma) - g(\varsigma, u)] = \mathscr{H}(\varsigma), & \varsigma \in \mathscr{I}, \ \varsigma \neq \varsigma_k \\ u(\varsigma_k^+) - u(\varsigma_k^-) = \mathscr{I}_k(\varsigma_k, u(\varsigma_k^-)), & k = 1, 2, 3, \cdots, m \\ u(0) = \varphi(u), \end{cases} \tag{4.1}$$

where the integral equation specifies

$$u(\varsigma) \begin{cases} \varphi(u) + g(\varsigma) + \frac{g(0)}{\Gamma(\mathfrak{w})} \int_0^{\varsigma} (\varsigma - \rho(\theta))^{\mathfrak{w}-1} \mathscr{H}(\theta) \nabla\theta, & \varsigma \in \mathscr{I}_o, \\ \varphi(u) + g(\varsigma) + \frac{g(0)}{\Gamma(\mathfrak{w})} \sum_{i=1}^{k} \int_{\varsigma_{i-1}}^{\varsigma_i} (\varsigma_i - \rho(\theta))^{\mathfrak{w}-1} \mathscr{H}(\theta) \nabla\theta \\ + \frac{g(0)}{\Gamma(\mathfrak{w})} \int_{\varsigma_k}^{\varsigma} (\varsigma - \rho(\theta))^{\mathfrak{w}-1} \mathscr{H}(\theta) \nabla\theta + \sum_{i=1}^{k} \mathscr{I}_{\mathfrak{i}}(\varsigma_{\mathfrak{i}}, u(\varsigma_{\mathfrak{i}}^-)), & \varsigma \in \mathscr{I}_k. \end{cases} \tag{4.2}$$

Proof. If $\varsigma \in \mathscr{I}_o$, then the solution of the Eq (4.1) is given by

$$u(\varsigma) = \varphi(p) + g(\varsigma) + \frac{g(0)}{\Gamma(\mathfrak{w})} \int_0^{\varsigma} (\varsigma - \rho(\theta))^{\mathfrak{w}-1} \mathscr{H}(\theta) \nabla\theta. \tag{4.3}$$

For $\varsigma \in \mathscr{I}_1$, the problem

$$\begin{cases} {}^{C}D^{\mathfrak{w}}[u(\varsigma) - g(\varsigma, u)] = \mathscr{H}(\varsigma), \\ u(\varsigma_1^+) - u(\varsigma_1^-) = \mathcal{I}_1(\varsigma_1, u(\varsigma_1^-)), \end{cases}$$

holds the solution

$$u(\varsigma) = u(\varsigma_1^+) + g(\varsigma) + \frac{g(0)}{\Gamma(\mathfrak{w})} \int_{\varsigma_1}^{\varsigma} (\varsigma - \rho(\theta))^{\mathfrak{w}-1} \mathscr{H}(\theta) \nabla\theta. \tag{4.4}$$

Again,

$$u(\varsigma_1^+) - u(\varsigma_1^-) = \mathcal{I}_1(\varsigma_1, u(\varsigma_1^-)). \tag{4.5}$$

Applying Eq (4.5) in Eq (4.4), then

$$u(\varsigma) = u(\varsigma_1^-) + \mathcal{I}_1(\varsigma_1, u(\varsigma_1^-)) + g(\varsigma) + \frac{g(0)}{\Gamma(\mathfrak{w})} \int_{\varsigma_1}^{\varsigma} (\varsigma - \rho(\theta))^{\mathfrak{w}-1} \mathscr{H}(\theta) \nabla\theta,$$

which follows that

$$\begin{aligned} u(\varsigma) =& \varphi(p) + \mathcal{I}_1(\varsigma_1, u(\varsigma_1^-)) + g(\varsigma) + \frac{g(0)}{\Gamma(\mathfrak{w})} \int_{\varsigma_1}^{\varsigma} (\varsigma - \rho(\theta))^{\mathfrak{w}-1} \mathscr{H}(\theta) \nabla\theta \\ &+ \frac{g(0)}{\Gamma(\mathfrak{w})} \int_{0}^{\varsigma} (\varsigma - \rho(\theta))^{\mathfrak{w}-1} \mathscr{H}(\theta) \nabla\theta, \qquad \varsigma \in \mathscr{I}_1. \end{aligned}$$

Using the idea of mathematical induction and generalizing in this way for $\varsigma \in \mathscr{I}_k$, $k = 1, 2, \cdots, m$, one can say,

$$\begin{aligned} u(\varsigma) =& \varphi(u) + g(\varsigma) + \frac{g(0)}{\Gamma(\mathfrak{w})} \int_{0}^{\varsigma} (\varsigma - \rho(\theta))^{\mathfrak{w}-1} \mathscr{H}(\theta) \nabla\theta \\ &+ \frac{g(0)}{\Gamma(\mathfrak{w})} \sum_{i=1}^{k} \int_{\varsigma_{i-1}}^{\varsigma_i} (\varsigma_i - \rho(\theta))^{\mathfrak{w}-1} \mathscr{H}(\theta) \nabla\theta + \sum_{i=1}^{k} \mathcal{I}_{\mathfrak{i}}(\varsigma_{\mathfrak{i}}, u(\varsigma_{\mathfrak{i}})), \qquad k = 1, 2, 3, \cdots, m. \end{aligned}$$

□

The following hypotheses are necessary in order to prove the existence and uniqueness of the solution to Eq (1.1):

(A1) $\mathfrak{L}$: $\mathscr{I} \times \mathscr{R} \times \mathscr{R} \to \mathscr{R}$ is ld continuous and there should be a constant $\mathcal{K} > 0$ and $0 < \mathscr{G} < 1$, which contents

$$|\mathfrak{L}(\varsigma, \theta_1, \theta_2) - \mathfrak{L}(\varsigma, \zeta_1, \zeta_2)| \leq \mathcal{K}|\theta_1 - \zeta_1| + \mathscr{G}|\theta_2 - \zeta_2|, \qquad \forall \varsigma \in \mathbb{I},$$

$\theta_i, \zeta_i \in \mathscr{R}$ for $\mathfrak{i} = 1, 2$.

(A2) There exist constants $\mathcal{A} > 0, \mathcal{F} > 0$, and $0 < \mathcal{E} < 1$, such that

$$|\mathfrak{L}(\varsigma, \theta, \zeta)| \leq \mathcal{A} + \mathcal{F}|\theta| + \mathcal{E}|\zeta|, \qquad \forall \theta, \zeta \in \mathscr{R}.$$

(A3) $\mathcal{I}_k(\varsigma, u)$ is continuous $\forall\ k = 1, 2, \cdots m$ and contents:

(i) There exists a "+" ve constant $\mathcal{M}_k$ for $k = 1, 2, \cdots, m$ such that

$$|\mathcal{I}_k(\varsigma, u)| \leq \mathcal{M}_k, \qquad \forall \varsigma \in \mathcal{J}_k, u \in \mathcal{R}.$$

(ii) There exists a "+" ve constatnt $\mathcal{L}_k$, for $k = 1, 2, 3, \cdots, m$ such that

$$|\mathcal{I}_k(\varsigma, u) - \mathcal{I}_k(\varsigma, \mathfrak{h})| \leq \mathcal{L}_k|u - \mathfrak{h}|, \qquad \forall \varsigma \in \mathcal{J}_k, u, \mathfrak{h} \in \mathcal{R}.$$

(A4) There must be a non "-" ve increasing function μ: $\mathcal{R}^+ \to \mathcal{R}^+$ such that

$$|\varphi(\varsigma) - \varphi(\theta)| \leq \mathcal{H}|\varsigma - \theta|, \qquad \forall \varsigma \in \mathcal{J},$$

and a "+" ve constant $\mathcal{H}$ such that

$$|\varphi(\varsigma) - \varphi(\theta)| \leq \mathcal{H}|\varsigma - \theta|, \qquad \forall \varsigma, \theta \in \mathcal{J}.$$

(A5) For $\varsigma \in \mathcal{J}_o$ in a time scale interval, let the function $u(\varsigma)$ be

$$u(\varsigma) = \varphi(p) + g(\varsigma) + \frac{g(0)}{\Gamma(\mathfrak{w})} \int_0^{\varsigma} (\varsigma - \rho(\theta))^{\mathfrak{w}-1} \mathfrak{Q}(\varsigma, u(\varsigma), {}^{C}D^{\mathfrak{w}} u(\varsigma)) \nabla\theta.$$

The Banach contraction theorem forms the basis of the following theorem.

Theorem 4.3. *If all conditions (A1)–(A4) and*

$$\sum_{i=1}^{m} \mathcal{L}_{\mathfrak{i}} + \mathcal{H} + g(\varsigma) + \frac{g(0)\mathcal{K}\mathcal{T}^{\mathfrak{w}}(m+1)}{(1-\mathcal{G})(\mathfrak{w}+1)} < 1$$

hold, then Eq (1.1) must contain a solution on $\mathcal{J}$.

Proof. Assume

$${}^{C}D^{\mathfrak{w}}[u(\varsigma) - g(\varsigma, u)] = \mathfrak{h}(\varsigma).$$

Let $\Pi \subseteq \mathfrak{PC}(\mathcal{J}_k, \mathcal{R})$ such that

$$\Pi = \{u \in \mathfrak{PC}^1(\mathcal{J}_k, \mathcal{R}) : \|u\|_{\mathfrak{PC}} \leq \omega\}$$

and χ: $\Pi \to \Pi$ such that

$$(\chi u)(\varsigma) = \varphi(u) + g(\varsigma) + \frac{g(0)}{\Gamma(\mathfrak{w})} \int_0^{\varsigma} (\varsigma - \rho(\theta))^{\mathfrak{w}-1} \mathfrak{Q}(\varsigma, u(\varsigma), {}^{C}D^{\mathfrak{w}} u(\varsigma)) \nabla\theta,$$

for $\varsigma \in \mathcal{J}_o$, and

$$\begin{aligned}(\chi u)(\varsigma) =& \varphi(u) + g(\varsigma) + \frac{g(0)}{\Gamma(\mathfrak{w})} \sum_{i=1}^{k} \int_{\varsigma_{i-1}}^{\varsigma_i} (\varsigma - \rho(\theta))^{\mathfrak{w}-1} \mathfrak{Q}(\varsigma, u(\varsigma), \mathfrak{h}(\varsigma)) \nabla\theta + \sum_{i=1}^{k} \mathcal{I}_{\mathfrak{i}}(\varsigma_{\mathfrak{i}}, u(\varsigma_{\mathfrak{i}}^{-})) \\ &+ \frac{g(0)}{\Gamma(\mathfrak{w})} \int_{\varsigma_k}^{\varsigma} (\varsigma - \rho(\theta))^{\mathfrak{w}-1} \mathfrak{Q}(\varsigma, u(\varsigma), {}^{C}D^{\mathfrak{w}} u(\varsigma)) \nabla\theta,\end{aligned}$$

for $\varsigma \in \mathscr{I}_k$, then $k = 1, 2, 3, \cdots, m$.

Case 1. Let $\varsigma \in \mathscr{I}_k$, then $u \in \Pi$,

$$\begin{aligned}|(\chi u)(\varsigma)| =&|\varphi(u)| + |g(\varsigma)| + |\frac{g(0)}{\Gamma(\mathfrak{w})}\sum_{i=1}^{k}\int_{\varsigma_{i-1}}^{\varsigma_i}(\varsigma-\rho(\theta))^{\mathfrak{w}-1}\mathfrak{h}(\theta)\nabla\theta| + |\sum_{i=1}^{k}\mathcal{I}_{\mathfrak{i}}(\varsigma_{\mathfrak{i}}, u(\varsigma_{\mathfrak{i}}^{-}))|\\ &+|\frac{g(0)}{\Gamma(\mathfrak{w})}\int_{\varsigma_k}^{\varsigma}(\varsigma-\rho(\theta))^{\mathfrak{w}-1}\mathfrak{h}(\theta))\nabla\theta|,\end{aligned}$$

where $\mathfrak{h} \in \Pi$, $\varsigma \in \mathscr{I}$. By Eq (1.1), one can get

$$\mathfrak{h} = \mathfrak{L}(\varsigma, u, \mathfrak{h}),$$

and

$$\begin{aligned}|\mathfrak{h}| &= |\mathfrak{L}(\varsigma, u, \mathfrak{h})|\\ &\leq \mathcal{A} + \mathcal{F}|u(\varsigma)| + \mathcal{E}|\mathfrak{h}(\varsigma)|\\ &\leq \frac{\mathcal{A}+\mathcal{F}\omega}{1-\mathcal{E}}.\end{aligned} \tag{4.6}$$

Again, taking the norm of $\mathfrak{PC}(\mathscr{I}, \mathscr{R})$ in (4.6),

$$\|u\|_{\mathfrak{PC}} \leq \frac{\alpha+\mathcal{F}\omega}{1-\mathcal{E}},$$

where

$$\|\mathcal{A}\|_{\mathfrak{PC}} = \alpha.$$

Using the condition of Case 1 and Proposition 2.4, we obtain

$$\begin{aligned}\|\chi\|_{\mathfrak{PC}} =&sup_{\varsigma\in\mathbb{I}}|\chi u(\varsigma)|\\ &\leq \mu|u| + g(\varsigma) + \sum_{i=1}^{m}\mathscr{M}_i + \frac{g(0)[\mathcal{A}+\mathcal{F}|u|]}{(1-\mathcal{E})\Gamma(\mathfrak{w})}\Big[\sum_{i=1}^{m}\int_{\varsigma_{i-1}}^{\varsigma_i}(\varsigma-\theta)^{(\mathfrak{w}-1)}d\theta + \int_{\varsigma_k}^{\varsigma}(\varsigma-\theta)^{(\mathfrak{w}-1)}d\theta\Big]\\ &\leq \mu\omega + g(\varsigma) + \sum_{i=1}^{m}\mathscr{M}_i + \frac{g(0)\mathscr{T}^{\mathfrak{w}}(\alpha+\mathcal{F}\omega)(m+1)}{\Gamma(\mathfrak{w}+1)(1-\mathcal{E})}\\ &\leq \omega,\end{aligned} \tag{4.7}$$

where

$$\omega = \frac{\sum_{i=1}^{m}\mathscr{M}_i + g(\varsigma) + \frac{g(0)(m+1)\mathscr{T}^{\mathfrak{w}}\alpha}{\Gamma(\mathfrak{w}+1)(1-\mathcal{E})}}{1-\mu+\frac{(m+1)\mathscr{T}^{\mathfrak{w}}\mathcal{F}g(0)}{\Gamma(\mathfrak{w}+1)(1-\mathcal{E})}}.$$

Case 2. If $\varsigma \in \mathscr{I}_o$, by a similar way, one can obtain

$$\begin{aligned}\|\chi_u\|_{\mathfrak{PC}} &\leq \mu\omega + g(\varsigma) + \frac{g(0)\mathscr{T}^{\mathfrak{w}}(\alpha+\mathcal{F}\omega)}{\Gamma(\mathfrak{w}+1)}\\ &\leq \omega.\end{aligned} \tag{4.8}$$

Thus, from (4.8), $\|\chi_u\|_{\mathfrak{P}\mathfrak{C}} \leq \omega$. Hence, $\chi(\Pi)$ is bounded. Also, for $u, v \in \Pi$,

$$\begin{aligned}\|\chi_u - \chi_v\|_{\mathfrak{P}\mathfrak{C}} =& sup_{\varsigma\in\mathscr{I}_k}|(\chi_u)(\varsigma) - (\chi_v)(\varsigma)| \\ &\leq \sum_{i=1}^{k} |\mathcal{I}_{\mathfrak{i}}(\varsigma_{\mathfrak{i}}, u(\varsigma_{\mathfrak{i}}^-)) - \mathcal{I}_{\mathfrak{i}}(\varsigma_{\mathfrak{i}}, v(\varsigma_{\mathfrak{i}}^-))| + |g(\varsigma)| + \frac{g(0)}{\Gamma(\mathfrak{w})}\Big| \int_{\varsigma_k}^{\varsigma} (\varsigma - \rho(\theta))^{\mathfrak{w}-1}(\mathfrak{h}(\theta) - \mathfrak{i}(\theta))\nabla\theta\Big| \\ &+ \frac{g(0)}{\Gamma(\mathfrak{w})}\Big| \sum_{i=1}^{k} \int_{\varsigma_{i-1}}^{\varsigma_i} (\varsigma_i - \rho(\theta))^{\mathfrak{w}-1}(\mathfrak{h}(\theta) - \mathfrak{i}(\theta))\nabla\theta\Big| + |\varphi(u) - \varphi(v)|, \end{aligned} \tag{4.9}$$

where $\mathfrak{i} \in \Pi$, then $\mathfrak{i}(\varsigma) = \mathfrak{L}(\varsigma, v(\varsigma), \mathfrak{i}(\varsigma))$. For $\varsigma \in \mathscr{I}$, one can get

$$\begin{aligned}|\mathfrak{h}(\varsigma) - \mathfrak{i}(\varsigma)| &= |\mathfrak{L}(\varsigma, u(\varsigma), \mathfrak{h}(\varsigma)) - \mathfrak{L}(\varsigma, v(\varsigma), \mathfrak{i}(\varsigma))| \\ &\leq \mathcal{K}|u(\varsigma) - v(\varsigma)| + \mathscr{G}|\mathfrak{h}(\varsigma) - \mathfrak{i}(\varsigma)| \\ &\leq \frac{\mathcal{K}|u(\varsigma) - v(\varsigma)|}{1 - \mathscr{G}}. \end{aligned} \tag{4.10}$$

Taking the norm of $\mathfrak{P}\mathfrak{C}(\mathscr{I}, \mathscr{R})$, (4.10) becomes

$$\|\mathfrak{h} - \mathfrak{i}\|_{\mathfrak{P}\mathfrak{C}} \leq \frac{\mathcal{K}\|u - v\|_{\mathfrak{P}\mathfrak{C}}}{1 - \mathscr{G}}. \tag{4.11}$$

Using (4.11) in (4.9) and applying the Proposition 2.4,

$$\begin{aligned}\|\chi_u - \chi_v\|_{\mathfrak{P}\mathfrak{C}} \leq& \sum_{i=1}^{m} \mathcal{L}_i|u(\varsigma_i^-) - v(\varsigma_i^-)| + g(\varsigma) + \frac{\mathcal{K}g(0)|u(\theta) - v(\theta)|}{(1 - \mathscr{G})\Gamma(\mathfrak{w})} \int_{\varsigma_k}^{\varsigma} (\varsigma - \theta)^{\mathfrak{w}-1}d\theta \\ &+ \frac{\mathcal{K}g(0)|u(\theta) - v(\theta)|}{(1 - \mathscr{G})\Gamma(\mathfrak{w})} \sum_{i=1}^{m} \int_{\varsigma_i-1}^{\varsigma_i} (\varsigma - \theta)^{\mathfrak{w}-1}d\theta + \mathscr{H}|u - v| \\ \leq& \|u - v\|_{\mathfrak{P}\mathfrak{C}} \sum_{i=1}^{m} \mathcal{L}_i + g(\varsigma) + \frac{\mathcal{K}\mathcal{T}^{\mathfrak{w}}g(0)\|u - v\|_{\mathfrak{P}\mathfrak{C}}}{(1 - \mathscr{G})\Gamma(\mathfrak{w} + 1)} \\ &+ \frac{m\mathcal{K}\mathcal{T}^{\mathfrak{w}}g(0)\|u - v\|_{\mathfrak{P}\mathfrak{C}}}{(1 - \mathscr{G})\Gamma(\mathfrak{w} + 1)} + \mathscr{H}\|u - v\|_{\mathfrak{P}\mathfrak{C}} \\ \leq& \Big(\sum_{i=1}^{m} \mathcal{L}_i + g(\varsigma) + \frac{\mathcal{K}\mathcal{T}^{\mathfrak{w}}g(0)(m + 1)}{(1 - \mathscr{G})\Gamma(\mathfrak{w} + 1)} + \mathscr{H}\Big)\|u - v\|_{\mathfrak{P}\mathfrak{C}}. \end{aligned} \tag{4.12}$$

Similarly, for $\varsigma \in \mathscr{I}_o$,

$$\|\chi_u - \chi_v\|_{\mathfrak{P}\mathfrak{C}} \leq \Big(\mathscr{H} + g(\varsigma) + \frac{\mathcal{K}\mathcal{T}^{\mathfrak{w}}g(0)}{(1 - \mathscr{G})\Gamma(\mathfrak{w} + 1)}\Big)\|u - v\|_{\mathfrak{P}\mathfrak{C}}. \tag{4.13}$$

Thus, from (4.12) and (4.13), we obtain

$$\|\chi_u - \chi_v\|_{\mathfrak{P}\mathfrak{C}} \leq \mathcal{U}\|u - v\|_{\mathfrak{P}\mathfrak{C}},$$

where

$$\mathcal{U} = \sum_{i=1}^{m} \mathcal{L}_i + g(\varsigma) + \frac{\mathcal{K}\mathcal{T}^{\mathfrak{w}}g(0)(m + 1)}{(1 - \mathscr{G})\Gamma(\mathfrak{w} + 1)} + \mathscr{H}.$$

Here, $\mathcal{U} < 1$, then χ: $\Pi \to \Pi$ is a contraction operator. According to the Banach contraction theorem, it has a fixed point, which is the solution to Eq (1.1). □

Equation (1.1)'s adequate condition for a solution is based on the nonlinear alternative to Leray-Schauder's fixed point theorem.

Theorem 4.4. *If (A1) through (A4) are true and there is a positive constant β, then*

$$\mu\beta + \sum_{i=1}^{m} \mathscr{M}_i + g(\varsigma) + \frac{(m+1)\mathscr{T}^{\mathfrak{w}} g(0)(\mathscr{A} + \mathscr{F}\beta)}{\Gamma(\mathfrak{w}+1)(1-\mathscr{E})} < \beta. \tag{4.14}$$

Therefore, there is at least one solution to Eq (1.1) in $\mathscr{I}$.

Proof. The following steps are used to demonstrate the theorem's proof.

Step 1. χ: $\Pi \to \Pi$ is continuous.

Assume $\{u_n\}$ is a sequence of Π such that $u_n \to u$, then $\varsigma \in \mathscr{I}_k, k = 1, 2, 3, \cdots, m$.

$$\begin{aligned}
\|\chi_{u_n} - \chi_v\|_{\mathfrak{PC}} =& sup_{\varsigma\in\mathscr{I}_k}|(\chi_{u_n})(\varsigma) - (\chi_v)(\varsigma)| \\
&\leq \sum_{i=1}^{m} |\mathcal{I}_i(\varsigma_i, u_n(\varsigma_i^-)) - \mathcal{I}_i(\varsigma_i, u(\varsigma_i^-))| + |g(\varsigma)| + \frac{g(0)}{\Gamma(\mathfrak{w})}\left| \int_{\varsigma_k}^{\varsigma} (\varsigma-\theta)^{\mathfrak{w}-1}(\mathfrak{h}_n(\theta) - \mathfrak{h}(\theta))d\theta \right| \\
&\quad + \frac{g(0)}{\Gamma(\mathfrak{w})}\left| \sum_{i=1}^{m} \int_{\varsigma_{i-1}}^{\varsigma_i} (\varsigma_i-\theta)^{\mathfrak{w}-1}(\mathfrak{h}_n(\theta) - \mathfrak{h}(\theta))d\theta \right| + |\varphi(u_n) - \varphi(u)|,
\end{aligned} \tag{4.15}$$

where $\mathfrak{h}_n \in \Pi$, such that

$$\mathfrak{h}_n = \mathfrak{L}(\varsigma, u_n, \mathfrak{h}_n),$$

and for $\varsigma \in \mathscr{I}_k$, we obtain

$$\begin{aligned}
|\mathfrak{h}_n - \mathfrak{h}| &= |\mathfrak{L}(\varsigma, u_n, \mathfrak{h}_n) - \mathfrak{L}(\varsigma, u, \mathfrak{h})| \\
&\leq \mathcal{K}|u_n - u| + \mathscr{G}|\mathfrak{h}_n - \mathfrak{h}| \\
&\leq \frac{\mathcal{K}|u_n - u|}{1-\mathscr{G}}.
\end{aligned} \tag{4.16}$$

Taking the norm of $\mathfrak{PC}(\mathscr{I}, \mathscr{R})$, (4.16) becomes

$$\|\mathfrak{h}_n - \mathfrak{h}\|_{\mathfrak{PC}} \leq \frac{\mathcal{K}\|u_n - u\|_{\mathfrak{PC}}}{1-\mathscr{G}}. \tag{4.17}$$

Using (4.17) in (4.15), we obtain

$$\|\chi_{u_n} - \chi_v\|_{\mathfrak{PC}} \leq \|u_n - u\|_{\mathfrak{PC}} \leq \left(\sum_{i=1}^{m} \mathcal{L}_i + g(\varsigma) + \frac{\mathcal{K}\mathscr{T}^{\mathfrak{w}} g(0)(m+1)}{(1-\mathscr{G})\Gamma(\mathfrak{w}+1)} + \mathscr{H} \right)$$

As $n \to \infty$, let $u_n \to u$ such that

$$\|\chi_{u_n} - \chi_v\|_{\mathfrak{PC}} \to 0.$$

As a result, χ is continuous.

Also, for $\varsigma \in \mathscr{I}_o$, the proof is similar.

Step 2. The operator χ map Π to $\mathfrak{PC}(\mathscr{I}, \mathscr{R})$.

Assume $x_1, x_2 \in \mathscr{I}_k, k = 1, 2, \cdots, m$, such that $x_1 < x_2$, then

$$\begin{aligned}
\|\chi_u(x_2) - \chi_v(x_1)\|_{\mathfrak{PC}} =& sup_{\varsigma\in\mathscr{I}_k}|(\chi_u)(x_2) - (\chi_v)(x_1)| \\
\leq& \frac{g(0)}{\Gamma(\mathfrak{w})}\left|\int_{\varsigma_k}^{x_1}(x_2-\rho(\theta))^{\mathfrak{w}-1} - (x_1-\rho(\theta)^{\mathfrak{w}-1})\mathfrak{h}(\theta)\nabla\theta\right| + |g(\varsigma)| \\
&+ \frac{g(0)}{\Gamma(\mathfrak{w})}\left|\int_{x_1}^{x_2}(x_2-\rho(\theta))^{\mathfrak{w}-1}\mathfrak{h}(\theta)\nabla\theta\right| + \sum_{0<\varsigma_k<x_2-x_1}|\mathcal{I}_{\varsigma_k}(\varsigma_k, u(\varsigma_k^-))| \\
\leq& \frac{g(0)}{\Gamma(\mathfrak{w})}\left|\int_{\varsigma_k}^{x_1}(x_2-(\theta))^{\mathfrak{w}-1} - (x_1-(\theta)^{\mathfrak{w}-1})\mathfrak{h}(\theta)\nabla\theta\right| + |g(\varsigma)| \\
&+ \frac{g(0)}{\Gamma(\mathfrak{w})}\left|\int_{x_1}^{x_2}(x_2-(\theta))^{\mathfrak{w}-1}\mathfrak{h}(\theta)\nabla\theta\right| + \sum_{0<\varsigma_k<x_2-x_1}|\mathcal{I}_{\varsigma_k}(\varsigma_k, u(\varsigma_k^-))| \\
\leq& \frac{(\mathcal{A}+\mathcal{F}\omega)g(o)}{(1-\mathcal{E})\Gamma(\mathfrak{w})}\Big(\left|\int_{\varsigma_k}^{x_1}(x_2-(\theta))^{\mathfrak{w}-1} - (x_1-(\theta)^{\mathfrak{w}-1})\mathfrak{h}(\theta)\nabla\theta\right| \\
&+ \frac{g(0)}{\Gamma(\mathfrak{w})}\left|\int_{x_1}^{x_2}(x_2-(\theta))^{\mathfrak{w}-1}\mathfrak{h}(\theta)\nabla\theta\right|\Big) + |g(\varsigma)| + \sum_{0<\varsigma_k<x_2-x_1}|\mathcal{I}_{\varsigma_k}(\varsigma_k, u(\varsigma_k^-))|.
\end{aligned}$$

Since $(x-(\theta))^{\mathfrak{w}-1}$ is continuous, if $x_1 \to x_2$, then

$$\|\chi_u(x_2) - \chi_v(x_1)\|_{\mathfrak{PC}} \to 0.$$

Thus, the operator χ is equicontinuous in $\mathscr{I}_k$. Since the result at $x_1, x_2 \in \mathscr{I}_o$ is comparable, the evidence is left out.

Step 3. Let χ map Π be a bounded set of $\mathfrak{PC}(\mathscr{I}, \mathscr{R})$.

From (4.7), it is clear that $\|\chi(p)\| \leq \omega$ for $\omega \in \mathscr{R}$. As a consequence of Steps 1–3, using the Arzela-Ascoli theorem, one can discover that χ is entirely continuous.

Step 4. Let $\gamma \in (0, 1)$,

$$k = \{u \in \mathfrak{PC}(\mathscr{I}_k, \mathscr{R}) : u = \gamma\chi(u), 0 < \gamma < 1\}$$

be bounded.

Also, by $\varsigma \in \mathscr{I}_k, k = 1, 2, 3, \cdots, m$, one can obtain

$$\begin{aligned}
|u(\varsigma)| = |\gamma\chi(u)\varsigma| =& \Big|\gamma\Big(\varphi(u) + g(\varsigma) + \frac{g(0)}{\Gamma(\mathfrak{w})}\sum_{i=1}^{k}\int_{\varsigma_i-1}^{\varsigma_i}(\varsigma-\rho(\theta))^{\mathfrak{w}-1}\mathfrak{h}(\theta)\nabla\theta \\
&+ \frac{g(0)}{\Gamma(\mathfrak{w})}\int_{\varsigma_k}^{\varsigma}(\varsigma-\rho(\theta))^{\mathfrak{w}-1}\mathfrak{h}(\theta)\nabla\theta + \sum_{i=1}^{k}\mathcal{I}_{\mathfrak{i}}(\varsigma_{\mathfrak{i}}, u(\varsigma_{\mathfrak{i}}^-))\Big)\Big| \\
\leq& \mu\|u\|_{\mathfrak{PC}} + \sum_{i=1}^{n}\mathscr{M}_{iti} + +g(\varsigma)\frac{(\mathcal{A}+\mathcal{F}\|u\|_{\mathfrak{PC}})g(0)\mathscr{T}^{\mathfrak{w}}(m+1)}{\Gamma(\mathfrak{w}+1)(1-\mathcal{E})}.
\end{aligned}$$

Thus,

$$\frac{\|u\|_{\mathfrak{PC}}}{\mu\|u\|_{\mathfrak{PC}} + \sum_{i=1}^{n}\mathscr{M}_{iti} + +g(\varsigma)\frac{(\mathcal{A}+\mathcal{F}\|u\|_{\mathfrak{PC}})g(0)\mathscr{T}^{\mathfrak{w}}(m+1)}{\Gamma(\mathfrak{w}+1)(1-\mathcal{E})}} \leq 1.$$

From Eq (4.14), we get a "+" ve constant β such that $\|u\|_{\mathfrak{PC}} \neq \beta$. Consider a set

$$\psi = \{u \in \mathfrak{PC}(\mathscr{I}, \mathscr{R}) : \|u\|_{\mathfrak{PC}} < \beta\},$$

such that

$$\chi : \tilde{\psi} \to \mathfrak{PC}(\mathscr{I}, \mathscr{R})$$

is continuous and completely continuous.

Thus, no $u \in \partial(\psi)$ can be found such that $u = \gamma\chi(u), \gamma \in (0,1)$. Hence, a nonlinear alternative of Leray Schauder's fixed point theorem gives that the answer to Eq (1.1) is a fixed point for χ.

The outcome for $\varsigma \in \mathscr{I}_o$ is almost identical, thus it is not included. □

5. Example

Example 5.1. *Take into account a nonlocal initial condition over time scale in a neutral impulsive fractional dynamic equation*

$$\mathfrak{T} = [0, \frac{1}{5}] \cup [\frac{1}{4}, 1],$$

and we get

$$\begin{cases} {}^{C}D^{\frac{1}{4}}[u(\varsigma) - g(\varsigma, u)] = \dfrac{e^{-5\varsigma}[4 + g(0)(|u(\varsigma)| + |{}^{C}D^{\mathfrak{w}}u(\varsigma)|) + g(\varsigma)]}{25e^{2\varsigma}(1 + |u(\varsigma)|)}, & \varsigma \in [0,1] \cap \mathscr{T},\ \varsigma \neq \frac{1}{5} \\ u(\frac{1}{5}^{+}) - u(\frac{1}{5}^{-}) = \dfrac{1 + u(\frac{1}{5})}{15}, & \varsigma_1 = \frac{1}{5} \\ u(0) = \dfrac{u}{10}. \end{cases} \tag{5.1}$$

We set

$$\mathfrak{L}(\varsigma, u, v) = \frac{e^{-5\varsigma}[4 + g(0)(|u(\varsigma)| + |v(\varsigma)|) + g(\varsigma)]}{25e^{2\varsigma}(1 + |u(\varsigma)|)}. \tag{5.2}$$

It is evident that (5.2)'s right side is continuous for $u, v \in \mathscr{R}$ in relation to time scale. Again, $\forall$ $\varsigma \in [0,1] \cap \mathfrak{T}$ and $\mathfrak{h}, \mathfrak{i} \in \mathscr{R}$. We obtain

$$\begin{aligned} \mathfrak{L}(\varsigma, u, v) &\leq \frac{4 + g(0)(|u(\varsigma)| + |v(\varsigma)|) + g(\varsigma)}{25e^2} \\ &\leq \frac{4}{25e^2} + \frac{1}{25e^2}|u(\varsigma)| + \frac{1}{25e^2}|v(\varsigma)| + \frac{2}{25e^2}, \end{aligned}$$

then, we get

$$\mathcal{A} = \frac{4}{25e^2},\ \mathcal{F} = \frac{1}{25e^2},\ \mathcal{E} = \frac{1}{25e^2},\ g(0) = 1,\ g(\varsigma) = \frac{2}{25e^2}.$$

Next,

$$\begin{aligned} |\mathfrak{L}(\varsigma, u, v) - \mathfrak{L}(\varsigma, \mathfrak{h}, \mathfrak{i})| &\leq \frac{1}{25e^2}|u - \mathfrak{h}| + \frac{1}{25e^2}|v - \mathfrak{i}|, \\ |\mathcal{I}_1(\varsigma, u) - \mathcal{I}_1(\varsigma, v)| &\leq \frac{1}{15}|u - \mathfrak{h}|, \end{aligned}$$

$$|\varphi(u) - \varphi(\mathfrak{h})| \leq \frac{1}{10}|u - \mathfrak{h}|,$$
$$|\varphi(u)| \leq \frac{1}{10}.$$

Thus, one can obtain

$$\mathcal{K} = \frac{1}{25e^2}, \ \mathscr{G} = \frac{1}{25e^2}, \ \mathcal{L} = \frac{1}{15}, \ \mathscr{H} = \frac{1}{10}.$$

From the above data, we can say that the Eq (5.1) satisfies all the conditions of (A1)–(A4).

Again, for m = 1 we get

$$\mathcal{L} + g(\varsigma) + \frac{\mathcal{K}\mathscr{T}^{\mathfrak{w}} g(0)(m+1)}{(1-\mathscr{G})\Gamma(\mathfrak{w}+1)} + \mathscr{H} \leq \frac{1}{15} + \frac{1}{10} + \frac{1}{25e^2} + \frac{4\frac{1}{25e^2}}{(1-\frac{1}{25e^2})\Gamma(\frac{1}{4}+1)}$$
$$\leq 1.$$

As a result, the requirements of Theorem 4.3 are met. Consequently, we came to the conclusion that the solution to Eq (5.1) is unique.

Below Table 1 represents the numerical approach for the theoretical results.

Table 1. Variation of $u(\varsigma)$ value for different values of $\mathcal{L}$ and g.

$g \downarrow$	$\mathcal{L}$=1/15	$\mathcal{L}$=1/25	$\mathcal{L}$ = 1/35	$\mathcal{L}$=1/45	$\mathcal{L}$=1/55
1/50	0.6778	0.6511	0.6397	0.6333	0.6293
1/40	0.6828	0.6561	0.6447	0.6383	0.6343
1/30	0.6911	0.6645	0.6530	0.6467	0.6426
1/20	0.7078	0.6811	0.6697	0.6633	0.6593
1/10	0.7578	0.7311	0.7197	0.7133	0.7093

Figure 1 reveals a commendable correspondence between the numerical solution & exact solution across the entire interval.

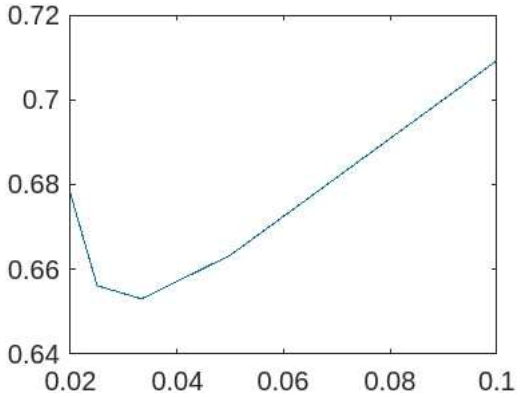

Figure 1. Graph of the approximate solution of $u(\varsigma)$.

6. Conclusions

In this article, we examine both operators in the setting of time scales and analyze the C∇D and RL∇D. Additionally, the C∇D of the fractional dynamic equation including instantaneous impulses and a nonlocal initial condition are also examined. Later, the numerical technique is followed by an example based on all theoretical findings on the existence and uniqueness of the solution. A graph using MATLAB is also represented for the example.

Futher, in modeling the spread of infectious diseases like COVID-19, a dynamic equation in time scales can be used to capture the various stages of infection, transmission rates, and the impact of interventions over time. Mathematical models, often expressed as differential equations or agent-based models, can be adapted to include time scales that represent different temporal aspects of the disease dynamics.

Similarly, in cancer modeling, incorporating a dynamic equation in time scales allows for the consideration of the progression of the disease, the growth of tumors, and the response to treatments over time. This can lead to more accurate predictions and insights into the evolution of the disease and the effectiveness of different therapeutic interventions.

Use of AI tools declaration

The authors declare they have not used Artificial Intelligence (AI) tools in the creation of this article.

Acknowledgments

The authors extend their appreciation to Prince Sattam bin Abdulaziz University for funding this research work through the project number (PSAU/2023/01/26285).

Conflict of interest

The authors declare that they have no conflicts of interest.

References

1. T. Linitda, K. Karthikeyan, P. R. Sekar, T. Sitthiwirattham, Analysis on controllability results for impulsive neutral Hilfer fractional differential equations with nonlocal conditions, *Mathematics*, **11** (2023), 1071. https://doi.org/10.3390/math11051071
2. K. Kaliraj, P. K. L. Priya, C. Ravichandran, An explication of finite-time stability for fractional delay model with neutral impulsive conditions, *Qual. Theory Dyn. Syst.*, **21** (2022), 161. https://doi.org/10.1007/s12346-022-00694-8
3. B. Gogoi, U. K. Saha, B. Hazarika, Existence of solution of a nonlinear fractional dynamic equation with initial and boundary conditions on time scales, *J. Anal.*, **32** (2023), 85–102. https://doi.org/10.1007/s41478-023-00597-0

4. K. Jothimani, C. Ravichandran, V. Kumar, M. Djemai, K. S. Nisar, Interpretation of trajectory control and optimization for the nondense fractional system, *Int. J. Appl. Comput. Math.*, **8** (2022), 273. https://doi.org/10.1007/s40819-022-01478-z
5. K. Jothimani, N. Valliammal, S. Alsaeed, K. S. Nisar, C. Ravichandran, Controllability results of Hilfer fractional derivative through integral contractors, *Qual. Theory Dyn. Syst.*, **22** (2023), 137. https://doi.org/10.1007/s12346-023-00833-9
6. I. Podlubny, *Fractional differential equations*, San Diego: Academic Press, 1999.
7. L. Byszewski, Theorems about the existence and uniqueness of solutions of a semilinear evolution nonlocal Cauchy problem, *J. Math. Anal. Appl.*, **162** (1991), 494–505. https://doi.org/10.1016/0022-247X(91)90164-U
8. K. Munusamy, C. Ravichandran, K. S. Nisar, R. Jagatheeshwari, N. Valliammal, Results on neutral integrodifferential system using Krasnoselskii-Schaefer theorem with initial conditions, *AIP Conf. Proc.*, **2718** (2023), 040001. https://doi.org/10.1063/5.0137023
9. P. Veeresha, D. G. Prakasha, C. Ravichandran, L. Akinyemi, K. S. Nisar, Numerical approach to generalized coupled fractional Ramani equations, *Int. J. Mod. Phys. B*, **36** (2022), 2250047. https://doi.org/10.1142/S0217979222500473
10. A. Debbouche, J. J. Nieto, Relaxation in controlled systems described by fractional integro-differential equations with nonlocal control conditions, *Electron. J. Differ. Equations*, **89** (2015), 1–18.
11. V. E. Fedorov, A. Debbouche, A class of degenerate fractional evolution systems in banach spaces, *Differ. Equations*, **49** (2013), 1569–1576. https://doi.org/10.1134/S0012266113120112
12. R. P. Agarwal, M. Bohner, D. O'Regan, A. Peterson, Dynamic equations on time scales: a survey, *J. Comput. Appl. Math.*, **141** (2002), 1–26. https://doi.org/10.1016/S0377-0427(01)00432-0
13. K. S. Nisar, K. Munusamy, C. Ravichandran, Results on existence of solutions in nonlocal partial functional integrodifferential equations with finite delay in nondense domain, *Alex. Eng. J.*, **73** (2023), 377–384. https://doi.org/10.1016/j.aej.2023.04.050
14. H. Vu, N. D. Phu, N. V. Hoa, A survey on random fractional differential equations involving the generalized Caputo fractional-order derivative, *Commun. Nonlinear Sci. Numer. Simul.*, **121** (2023), 107202. https://doi.org/10.1016/j.cnsns.2023.107202
15. J. Zuo, J. Yang, Approximation properties of residual neural networks for fractional differential equations, *Commun. Nonlinear Sci. Numer. Simul.*, **125** (2023), 107399. https://doi.org/10.1016/j.cnsns.2023.107399
16. A. Khatoon, A. Raheem, A. Afreen, Approximate solutions for neutral stochastic fractional differential equations, *Commun. Nonlinear Sci. Numer. Simul.*, **125** (2023), 107414. https://doi.org/10.1016/j.cnsns.2023.107414
17. N. Benkhettou, A. Hammoudi, D. F. M. Torres, Existence and uniqueness of solution for a fractional Riemann-Liouville initial value problem on time scales, *J. King Saud Univ. Sci.*, **28** (2016), 87–92. https://doi.org/10.1016/j.jksus.2015.08.001
18. M. Bohner, A. Peterson, *Dynamic equations on time scales: an introduction with application*, Birkhauser, 2001. https://doi.org/10.1007/978-1-4612-0201-1

19. M. Bohner, A. Peterson, *Advances in dynamic equations on time scales*, Birkhauser, 2003. https://doi.org/10.1007/978-0-8176-8230-9

20. K. Zhao, Generalized UH-stability of a nonlinear fractional coupling ($\mathscr{P}_1$, $\mathscr{P}_2$)-Laplacian system concerned with nonsingular Atangana-Baleanu fractional calculus, *J. Inequal. Appl.*, **96** (2023), 96. https://doi.org/10.1186/s13660-023-03010-3

21. K. Zhao, Solvability, approximation and stability of periodic boundary value problem for a nonlinear Hadamard fractional differential equation with $\mathcal{P}$-Laplacian, *Axioms*, **12** (2023), 733. https://doi.org/10.3390/axioms12080733

22. K. Zhao, Study on the stability and its simulation algorithm of a nonlinear impulsive ABC-fractional coupled system with a Laplacian operator via F-contractive mapping, *Adv. Contin. Discrete Models*, **2024** (2024), 5. https://doi.org/10.1186/s13662-024-03801-y

23. K. Zhao, Existence and uh-stability of integral boundary problem for a class of nonlinear higher-order Hadamard fractional Langevin equation via Mittag-Leffler functions, *Filomat*, **37** (2023), 1053–1063. https://doi.org/10.2298/FIL2304053Z

24. V. Kumar, M. Malik, Existence, uniqueness and stability of nonlinear implicit fractional dynamical equation with impulsive condition on time scales, *Nonauton. Dyn. Syst.*, **6** (2019), 65–80. https://doi.org/10.1515/msds-2019-0005

25. V. Kumar, M. Malik, Existence and stability of fractional integro differential equation with non-instantaneous integrable impulses and periodic boundary condition on time scales, *J. King Saud Univ. Sci.*, **31** (2019), 1311–1317. https://doi.org/10.1016/j.jksus.2018.10.011

26. G. A. Anastassiou, Foundations of nabla fractional calculus on time scales and inequalities, *Comput. Math. Appl.*, **59** (2010), 3750–3762. https://doi.org/10.1016/j.camwa.2010.03.072

27. J. Zhu, L. Wu, Fractional Cauchy problem with Caputo nabla derivative on time scales, *Abstr. Appl. Anal.*, **2015** (2015), 486054. https://doi.org/10.1155/2015/486054

28. J. Zhu, Y. Zhu, Fractional Cauchy problem with Riemann-Liouville fractional delta derivative on time scales, *Abstr. Appl. Anal.*, **2013** (2013), 401596. https://doi.org/10.1155/2013/401596

29. R. Knapik, Impulsive differential equations with non local conditions, *Morehead Electron. J. Appl. Math.*, **2** (2003), 1–6.

30. K. Shah, B. Abdalla, T. Abdeljawad, R. Gul, Analysis of multipoint impulsive problem of fractional-order differential equations, *Bound. Value Probl.*, **2023** (2023), 1. https://doi.org/10.1186/s13661-022-01688-w

31. A. K. Tripathy, S. S. Santra, Necessary and sufficient conditions for oscillations to a second-order neutral differential equations with impulses, *Kragujevac J. Math.*, **47** (2023), 81–93.

32. Y. K. Chang, W. T. Li, Existence results for impulsive dynamic equations on time scales with nonlocal initial conditions, *Math. Comput. Modell.*, **43** (2006), 377–384. https://doi.org/10.1016/j.mcm.2005.12.015

33. M. Xia, L. Liu, J. Fang, Y. Zhang, Stability analysis for a class of stochastic differential equations with impulses, *Mathematics*, **11** (2023), 1541. https://doi.org/10.3390/math11061541

34. H. M Ahmed, Fractional neutral evolution equations with nonlocal conditions, *Adv. Differ. Equations*, **2013** (2013), 117. https://doi.org/10.1186/1687-1847-2013-117

35. H. Boularesy, A. Ardjouniz, Y. Laskri, Existence and uniqueness of solutions to fractional order nonlinear neutral differential equations, *Appl. Math. E-Notes*, **18** (2018), 25–33.

36. H. M. Ahmed, Semilinear neutral fractional stochastic integro-differential equations with nonlocal conditions, *J. Theor. Probab.*, **28** (2015), 667–680. https://doi.org/10.1007/s10959-013-0520-1

37. A. Chadha, D. N. Pandey, Existence and approximation of solution to neutral fractional differential equation with nonlocal conditions, *Comput. Math. Appl.*, **69** (2015), 893–908. https://doi.org/10.1016/j.camwa.2015.02.003

38. A. Morsy, K. S. Nisar, C. Ravichandran, C. Anusha, Sequential fractional order neutral functional integro differential equations on time scales with Caputo fractional operator over Banach spaces, *AIMS Math.*, **8** (2023), 5934–5949. https://doi.org/10.3934/math.2023299

39. G. Tan, Z. Wang, Reachable set estimation of delayed Markovian jump neural networks based on an improved reciprocally convex inequality, *IEEE Trans. Neural Networks Learn. Syst.*, **33** (2022), 2737–2742. https://doi.org/10.1109/TNNLS.2020.3045599

40. G. Tan, Z. Wang, Stability analysis of recurrent neural networks with time-varying delay based on a flexible negative-determination quadratic function method, *IEEE Trans. Neural Networks Learn. Syst.*, 2023. https://doi.org/10.1109/TNNLS.2023.3327318

41. J. Hu, G. Tan, L. Liu, A new result on H∞ state estimation for delayed neural networks based on an extended reciprocally convex inequality, *IEEE Trans. Circuits Syst.*, 2023. https://doi.org/10.1109/TCSII.2023.3323834

42. S. Tikare, Nonlocal initial value problems for first order dynamic equations on time scale, *Appl. Math. E-Notes*, **21** (2021), 410–420.

43. B. Gogoi, B. Hazarika, U. K. Saha, Impulsive fractional dynamic equation with nonlocal initial condition on time scales, *ArXiv*, 2022. https://doi.org/10.48550/arXiv.2207.01517

44. B. Gogoi, U. K. Saha, B. Hazarika, D. F. M. Torres, H. Ahmad, Nabla fractional derivative and fractional integral on time scales, *Axioms*, **10** (2021), 317. https://doi.org/10.3390/axioms10040317

45. M. Bragdi, A. Debbouche, D. Baleanu, Existence of solutions for fractional differential inclusions with separated boundary conditions in Banach space, *Adv. Math. Phys.*, **2013** (2013), 426061. https://doi.org/10.1155/2013/426061

ScienceDirect

Ain Shams Engineering Journal
Volume 14, Issue 12, December 2023, 102226

High performance computational method for fractional model of solid tumour invasion ☆

Kottakkaran Sooppy Nisar [a], R. Jagatheeshwari [b], C. Ravichandran [c], P. Veeresha [d]

Show more

Outline | Share | Cite

https://doi.org/10.1016/j.asej.2023.102226
Get rights and content

Abstract

The behaviour of the solid tumour invasion system in the sense of Caputo fractional with time ζ and space x is analyzed by the high performance computational method: q-Homotopy Analysis Transform method (q-HATM). The existence of the solutions has been verified with the assist of fixed point theorem and derived numerical solution for different values of $\alpha, \zeta, \hbar$. The novel simulation for all cases is explained through figures. We derived that the method is very efficient for analyzing the behaviour of the epidemiological system.

Previous Next

Keywords

Fractional derivative and integrals; Homotopy; Fixed point techniques; Mathematical models

2020 MSC

92–10; 26A33; 37C25; 55P15

1. Introduction

Cancer has a major repercussion on human society across the globe. Malignant tumours and Neoplasms are generally known as cancer. There are some cancer surgeries, namely radiation therapy, chemotherapy, hormone therapy and immunotherapy. However, it cause the leading non-communicable deaths according to the Indian National Cancer Registry Program report 2020[1].In 1889, an English surgeon, Stephen Paget, stated that cancer spread via blood circulation. It stimulated researchers to study cancer growth, cause, stage, size, components and evolution etc. A detailed study of different types of solid tumours has been explained [2]. Many researchers modelled solid tumour growth mathematically using the biological components tumour cells, macro molecules adative enzymes[3], [4].These researchers misapprehend the contribution of oxygen. A deeper

Typesetting math: 91%

ARTICLES
Archives of Veterinary Science
UFPR
https://www.ufpr.br/

Determination of heavy metals in various tissues of locally reared (country) chicken in major districts of Karnataka, India: Assessment of potential health risks.

Shashank Ajjigudde Shreenivasa[1], *Krishnakumar Velayudhannair*[2*], *John Paul Arockiasamy*[1], *Ganesh Shama*[4], *Rajeshkumar Sivakumar*[5]

Submitted *21/07/2023*
Accepted *20/10/2023*

[1]*Department of Life Sciences, CHRIST (Deemed to be University), Bangalore Central Campus, Hosur Road, Dharmaram Post, Bengaluru- 560 029, Karnataka, India. ORCID: http://orcid.org/0000-0003-3870-5842.*
[2]*Department of Life Sciences, CHRIST (Deemed to be University), Bangalore Central Campus, Hosur Road, Dharmaram Post, Bengaluru- 560 029, Karnataka, India. ORCID: https://orcid.org/0000-0002-2183-4632.*
[3]*Department of Zoology, St. Joseph's College, 36 Lalbagh Road, Bengaluru, Karnataka, India. ORCID: http://orcid.org/0000-0002-0998-1736*
[4]*Department of Life Sciences, CHRIST (Deemed to be University), Bangalore Central Campus, Hosur Road, Dharmaram Post, Bengaluru- 560 029, Karnataka, India. ORCID: http://orcid.org/0009-0007-7524-2046*
[5]*Department of Zoology, Kongunadu Arts and Science College (Autonomous), GN Mills, Coimbatore – 641029, Tamilnadu, India. ORCID: http://orcid.org/0000-0002-0054-3633*

Correspondence email: krishnakumar.v@christuniversity.in

Abstract: Food is one of the most prevalent ways that humans are exposed to metals. Heavy metals including cadmium, iron, zinc, lead, and mercury are harmful to humans and have a detrimental impact on health because they accumulate in biological organs. The concentration levels of these heavy metals were tested in different edible parts of the country (locally raised) chicken from various districts in Karnataka, India, namely Bengaluru, Tumakuru, Mangaluru, and Udupi, using an Atomic-Absorption Spectrophotometer (AAS). Heavy metal concentrations in various chicken parts were found to be below detectable limits (BDL)-0.0062, 0.027-3.178, and 0.262-2.103 ppm for Cd, Fe, and Zn, respectively, whereas Hg and Pb were BDL. The content of Zn was found to be significantly higher in all chicken samples from all examined districts, followed by Fe and Cd. Hg and Pb concentrations, on the other hand, were below the detection level in all samples. The estimated daily intakes (EDIs) of the observed metals from country chicken consumption were found to be lower than their respective FAO/WHO reference oral doses (RfD). The non-carcinogenic health hazards posed by the tested metals to the target population were estimated using the Hazard Quotient (HQ) and Hazard Index (HI) values. The HQ and HI values observed in this estimation were less than one, indicating that exposure to these heavy metals through the consumption of country chicken is unlikely to provide possible health concerns to the examined region's human population.

Keywords Metal exposure, Country chicken, Food safety, Toxicity, Health hazards, Permissible Limit.

1. Introduction

The chicken industry (Poultry) is one of India's most rapidly increasing agro-based industries, and it is a major supplier of critical nutrients, namely protein (Burel and Valat, 2009). In India, two chicken varieties, broiler and country chicken (village-reared), are consumed. Country chicken is raised locally by people in their homes and is identifiable by its more diminutive stature and different colours. Country chicken consumption by the native population is substantial, particularly in our research area. However, it is lower than broiler chicken consumption due to the latter's ease of availability and low cost. Chicken meat is relatively less expensive than other meats, making up about 45% of the total meat consumed in India (Russell et al., 2001; Chatterjee and Rajkumar, 2015). Recently, the high demand for chicken meat has substantially affected production, leading to increased production and extensive modification of poultry feeds to meet the increased demand. It has been reported that poultry feeds, whether local, natural or improved modifications from unique manufacturing processes, are affected by the content of heavy metals (Chatterjee and Rajkumar, 2015). The primary way that heavy metals bioaccumulation in chicken is via consuming contaminated food.

Heavy metal food poisoning is a significant health hazard globally, especially in developing nations like India (Mohammed et al., 2013). Heavy metals commonly poison chickens through contaminated water, poultry feed, industrial effluents, sewage water, agricultural activities, and aerial spraying in chicken breeding zones. Several studies on the heavy metal level in meat samples indicate that bioaccumulation of heavy metals in animal feeds is the main source of intake (Das and Das, 2018; Korish and Attia, 2020). Heavy metals like Cadmium (Cd), Iron (Fe), Zinc (Zn), Mercury (Hg) and Lead (Pb) are plentiful in the environment and can also be found in small amounts in fishes and chickens. Humans are exposed to these heavy metals through the consumption of contaminated food, particularly livestock (Khan et al., 2015; Mathiyan et al., 2021). Furthermore, other heavy metals such as Hg, Cd, and Pb are not required for the body's health and operation (Ayar et al., 2009). In general, increasing toxic element intake endangers all living organisms (Qin et al., 2009). The International Research Agency on Cancer and the United States National Toxicology Program have both classified increased human Cd consumption as a carcinogen (Congeevaram et al., 2007). Cd is a typical additive toxic compound that can build up in the kidneys over the years. It poses acute toxicity in humans due to taking more than the limit from contaminated food and beverages (Khan et al., 2015). Fe and Zn are useful and necessary elements in human development; Zn deficiency will cause abnormal growth, skin eruption, hair loss, etc., and excessive intake will Pb to nausea, cramps, and diarrhoea (Sharma and Agarwal, 2005). A deficiency of Fe causes anaemia in humans and the high accumulation leads to dangerous problems with the liver, pancreas, heart diseases, and diabetes (Whittaker, 1998). Hg and Pb are non-essential metals

"Women empowerment through Beekeeping Programme",

Date: 16th October, 2024

Venue: ICAR- Krishi Vigyan Kendra (KVK), Vivekanandhapuram, Karamadai Black, Coimbatore -641 113.

The guest lecture with hands on training was organized by the **Mrs. Gomathi, Assistant Director of Horticulture (ADH),** Department of Horticulture Plantation Crop, Karamadai Block, Tribal People, Coimbatore, Sponsored by National Bee Board, NBHM, GOL New Delhi. The resource person of the programme was **Dr. S Rajeshkumar**, Assistant Professor, Department of Zoology, and Diploma in Apiculture, Kongunadu Arts and Science College who enlightened the participants about the fundamentals of Biology, Types of Honey bee and its importance in agriculture for sustainable livelihood. This workshop was focused on the practical skills and techniques necessary for successful beekeeping practices. The session was headed by **Dr. P. Kumaravadivelu,** Senior Scientist and Head, ICAR-KVK, Coimbatore and **Dr. P Gomathi,** Assistant Senior Scientist, ICAR-KVK, Coimbatore. The Presidential address was given by **Mrs. Gomathi, ADH**, Department of Horticulture Plantation crop, Coimbatore district. Madam created insight about the various sustainable practices which will be useful for the betterment of society. The women self help group (tribal People) Karamadai block, women's was trained on Beekeeping during this programme and equipped them to develop their own projects for the future betterment. The resource person **Dr. S Rajeshkumar**, enlighten the participants with theoretical, practical demonstration and the hands on training in the beekeeping practices. Participants had the opportunity to observe hive inspections, beekeeping equipment handling, and observed various bees in a colony under the guidance of experienced beekeepers. The beekeeping workshop provided participants with a comprehensive understanding of beekeeping principles, practices, and entrepreneurial opportunities. By enlightens the

participants with practical skills and knowledge on Beekeeping, the workshop fulfilled its aim to encourage sustainable beekeeping practices and promote the conservation of bee populations. Participants expressed enthusiasm and eagerness to apply their newfound knowledge in establishing and managing their beekeeping ventures.

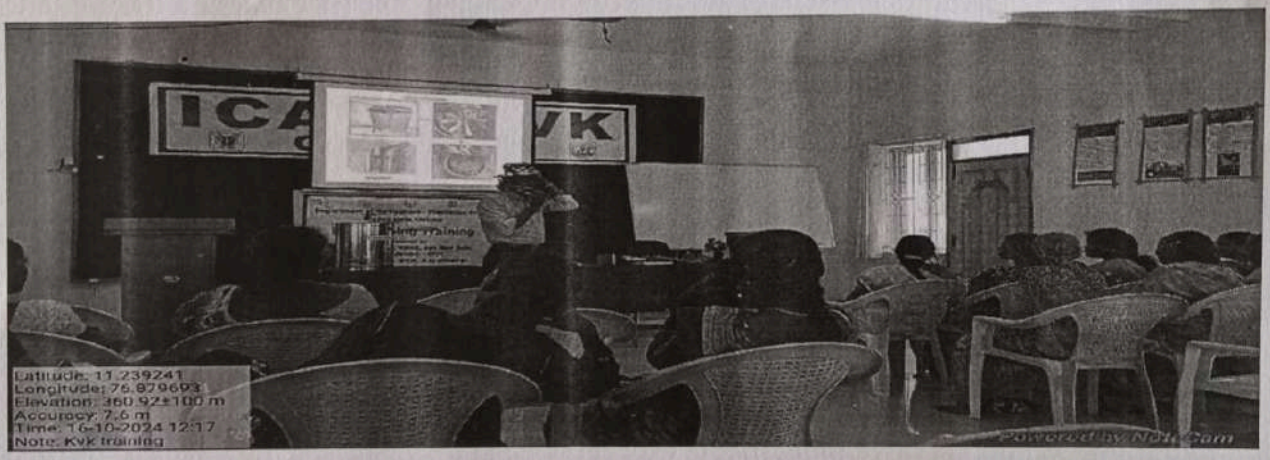

THE COVAI MAIL
Tamil & English Weekly News Paper
Postal Reg.No: CB/123/24-26.
www.covaimail.com www.facebook.com/THE COVAI MAIL
Date: 17.10.2024

Beekeeping programme to empower women

(From left) Suchindra, Assistant Director of Horticulture, Karamadai; Gomathi, Assistant Senior Scientist, ICAR- Krishi Vigyan Kendra and Rajeshkumar, Assistant Professor, Department of Zoology, and Diploma in Apiculture, Kongunadu Arts and Science College.

The Covai Mail

Krishi Vigyan Kendra (KVK), Department of Horticulture Plantation Crop, Karamadai Block and Kongunadu Arts and Science College jointly organised a one-week awareness programme with hands-on training on Beekeeping with the sponsorship of the National Bee Board recently at ICAR- Krishi Vigyan Kendra (KVK), Vivekanandhapuram, Karamadai Block.

The resource person of the programme was Rajeshkumar, Assistant Professor, Department of Zoology, and Diploma in Apiculture, Kongunadu Arts and Science College who enlightened the participants about the fundamentals of Biology, types of honey bees and their importance in agriculture for sustainable livelihood.

This workshop was focused on the practical skills and techniques

Rajeshkumar, Assistant Professor, Department of Zoology, and Diploma in Apiculture, Kongunadu Arts and Science College addressing the gathering on beekeeping.

necessary for successful beekeeping practices. The session was headed by Kumaravadivelu, Senior Scientist and Head of the venue and Gomathi, Assistant Senior Scientist.

The presidential address was given by Gomathi who created insight about the various sustainable practices which will be useful for the betterment of society.

Rajeshkumar enlightens the participants with theoretical, and practical demonstrations and hands-on training in beekeeping practices.

At the programme, 30 women of a self-help group (tribal People) at Karamadai block were trained in Beekeeping and equipped to develop their projects for future betterment.

With this programme, participants had the opportunity to observe hive inspections and beekeeping equipment handling and observed various bees in a colony under the guidance of experienced beekeepers. The event also provided participants with a comprehensive understanding of beekeeping principles, practices, and entrepreneurial opportunities.

The beekeeping workshop fulfilled its aim to encourage sustainable beekeeping practices and promote the conservation of bee populations. Participants expressed enthusiasm and eagerness to apply their newfound knowledge in establishing and managing their beekeeping ventures.

University of Madras
Department of Inorganic Chemistry
Guindy Campus, Chennai-600 025
Email: jeevapandian@yahoo.co.uk

Dr.K.PANDIAN, M.Sc.; Ph.D
Professor

21st July 2023

It is with great enthusiasm and interest that I support and collaborate with Dr. K. Kalpanadevi, Associate Professor and Head, PG and Research Department of Chemistry, Kongunadu Arts and Science College, Coimbatore. I had a long-time association with that august institution as Board of Studies in Chemistry, resource person in various seminars and workshops, Doctoral committee member and Ph.D. viva examiner. Therefore, I would like to extend my research collaboration in the area of nanomaterials with the Department of Chemistry in both student exchange programme and joint publications. As our research interests are alike, I believe that the proposed collaboration will have the potential to contribute a significantly production of novel materials in recent applications. I look forward to collaborating with you on all phases of research.

(K.PANDIAN)

Journal of Solid State Chemistry 325 (2023) 124158

Contents lists available at ScienceDirect

Journal of Solid State Chemistry

journal homepage: www.elsevier.com/locate/jssc

Structural and Multi-functional properties of isoelectronic guanyl hydrazinium picolinic derivatives exhibit centric and non-centric space group

S. Packiaraj [a,b,*], N. Angamuthu [c,b], S. Poornima [d,b], A. Pushpaveni [e,b], L. Kousalya [f], J.M. Rawson [g], S. Govindarajan [b,**]

[a] Department of Science and Humanities (Chemistry), Sri Krishna College of Engineering & Technology, Coimbatore, 641 008, Tamil Nadu, India
[b] Department of Chemistry, Bharathiar University, Coimbatore, 641 046, Tamil Nadu, India
[c] Department of Chemistry, Dr. R.K.Shanmugam College of Arts and Science, Kallakurichi, Tamil Nadu, India
[d] Department of Science and Humanities (Chemistry), Sree Sakthi Engineering College, Karamadai, Coimbatore, 641 104, India
[e] Department of Chemistry, Kongunadu Arts and Science College, Coimbatore, 641 049, Tamil Nadu, India
[f] Department of Botany, Nirmala College for Women, Coimbatore, 641018, Tamil Nadu, India
[g] Department of Chemistry and Biochemistry, The University of Windsor, Ontario, N9B3P4, Canada

ARTICLE INFO

Keywords:
Picolinic derivatives
Guanyl hydrazine bicarbonate
Crystal structure
Supramolecular synthons
Antioxidant activity
Photoluminescent studies

ABSTRACT

The equimolar reaction mixture of isoelectronic picolinic acid N-oxide (PAHNO) and/or 3-hydroxy picolinic acid (3-HPAH) with guanyl hydrazine bicarbonate (AgunH.HCO_3) in aqueous medium at room temperature produce 1:1 salt. Irrespective of the molar ratios (1; 1, 1:2 & 2:1) and reaction conditions maintained, invariably gives the same product in the form of polycrystalline nature except 1:1 ratio which yields a single crystal. The isoelectronic salts were characterized by spectroscopic, PXRD, thermal study and single crystal X-ray diffraction techniques. In general, most of the salts were crystallized in a centric space group rather than a non-centric, the prevailing factors are nature of the organic species and reaction conditions like pH, pKa, solvent effects, temperature and molar ratio *etc*,. Surprisingly, in the present case, the isoelectric salt of $[AgunH]^+[PANO]^-$ crystalized in centric ($P2_1/n$), where in case of $[AgunH]^+[3\text{-}HPA]^-$ crystalized in non-centric ($Pca2_1$) space group even though in the same reaction conditions. This may be due to the presence of the 3rd position of hydroxyl group and non-covalent interactions in $[AgunH]^+[3\text{-}HPA]^-$ that facilitate non-centric space group. Both salts are stabilized by the variety of hydrogen bond features leading to intra- and intermolecular N-H···O, N-H···N, and C-H···N hydrogen bonds and π-π stacking interactions along with homo- and hetero ring motifs [two $R_2^2(8)$, $R_1^1(6)$, and two $R_2^2(9)$]. These interactions render them an appropriate acid-base ion pair for the formation of sturdy hydrogen-bonded supramolecular synthons. Thermal studies on these salts reveal that the thermal degradation occurs *via* melting followed by complete loss of organic species. The solid-state emission spectra of free acids and its salts were recorded and compared. The materials exhibit a prominent luminescent character towards red shift than the starting compounds. Further, these materials show enhanced secondary antioxidant and antimicrobial activities, this is due to the crucial role of hydrazine species in guanyl hydrazinium cation.

1. Introduction

Guanyl hydrazine (Agun) also known as aminoguanidine, a versatile cation, dibasic in nature displays a similar fashion as like hydrazine (NH_2-NH_2), forming mono- $[AgunH]^+$ and di-cationic $[AgunH]^{2+}$ salts with various inorganic anions [1–7] including few carboxylic systems [8–15]. As expected, the guanyl hydrazinium salts exhibit mono-rather than di-cationic form due to the imine nitrogen (-C═NH, pKa1 = 11.5) appear as a more basic site than hydrazine end (-NH-NH_2, pKa2 = 0.7) in the guanyl hydrazine molecule. However, a meager number of results

* Corresponding author. Department of Science and Humanities (Chemistry), Sri Krishna College of Engineering & Technology, Coimbatore, 641 008, Tamil Nadu, India.
** Corresponding author.
E-mail addresses: srajguru1987@gmail.com (S. Packiaraj), drsgovind@yahoo.co.in (S. Govindarajan).

https://doi.org/10.1016/j.jssc.2023.124158
Received 11 April 2023; Received in revised form 3 June 2023; Accepted 7 June 2023
Available online 12 June 2023

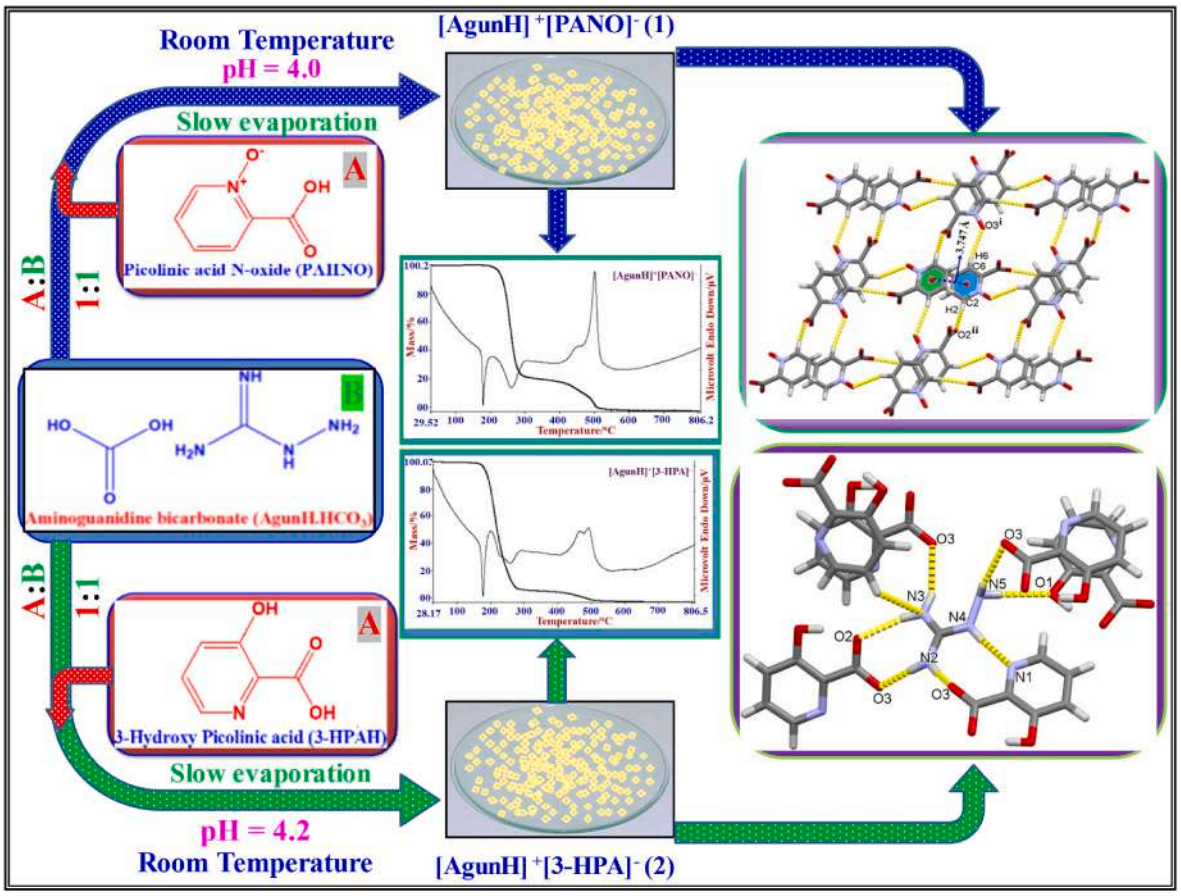

Scheme 1. The structure of starting compounds (free acids and base), detailed experimental procedure and reaction conditions are shown in Scheme.

are noticed in the di-cationic form confirming the protonation occurring at imine (C═NH) and hydrazinic (-NH-NH_2) nitrogens in the Agun molecule [6,7]. Furthermore, the number of preparative and computational studies on the synthesis and energetics of guanyl hydrazinium salts resulting from inorganic acids, have been well studied [7]. Meanwhile, the physical properties of guanidinium salts have attracted considerable interest in biotechnology, medicine, *etc.,* since the guanidine group is biologically significant and acts as a key functional group in few amino acids [16] such as creatinine, arginine, *etc,*.

The syntheses of guanyl hydrazinium salts of aliphatic organic acids especially oxalic, tartaric, squaric, succinic, fumaric, oxamic, malonic, sulfoacetic, maleic and formic acids [9–15] have been well studied by various researchers including our team. From our best knowledge, there are no reports available in the literature for the crystal structures of guanyl hydrazinium with heteroaromatic carboxylic systems except our own previous reports [17–19]. In specific, guanyl hydrazinium salts of dipicolinate, quinolinate [17], pyrazole 3,5-dicarboxylate [18] and pyrazine-2-carboxylate [19] are exists solely in the mono-protonated form $[AgunH]^+$. In recent years our research team were focusing to prepare the guanyl hydrazinium salts of organic acids, in particular, the multifunctional nature of the heteroaromatic mono- and dicarboxylic systems, namely, pyrazole, pyridine and pyrazine carboxylic acids.

In this line, the search of literature survey towards pyridine related systems shows countable reports, namely 3-hydroxy picolinic acid (3-HPAH) with N^6-benzyladenine [20], N6-benzoyladenine [21] and 6-Amino-5-fluoro-1H-pyrimidin-2-one [22] are studied and structurally characterized. Surprisingly we couldn't find any reports in the salts of the isoelectronic picolinic acid N-oxide (PAHNO) system. This made our interest to fulfill the research gap by studying the salt forming ability and multifunctional behavior of isoelectronic picolinic acids, namely, picolinic acid N-oxide and 3-hydroxy picolinic acid with dibasic nature of the guanyl hydrazine. Hence, we made a first attempt to study the isoelectronic guanyl hydrazinium picolinic derivatives with respect to their spectral, thermal and emission properties including single crystal determination. Also, this manuscript focuses on identifying the secondary antioxidant and antimicrobial studies of these materials, and have been compared with free acids and base. For clarity, the structures of the isoelectronic acids, base and detailed reaction conditions of the salts are shown in Scheme 1.

2. Experimental section

2.1. Materials and physical measures

All of the chemicals were of A.R. grade (AgunH.HCO_3: CAS No.-2582-30-1; PAHNO: CAS No.- 824-40-8 & 3-HPAH: CAS No.- 874-24-8) and were utilized directly without further purification. The hydrazine content of the synthesized compounds was determined volumetrically using a 0.025 M KIO_3 solution under Andrews' conditions [23]. A Vario-ELIII elemental analyzer was employed to perform the elemental analyses for C, H, N, and S. The IR spectra were recorded using a JACSO-4100 spectrophotometer as KBr pellets in the range of 4000–400 cm^{-1}. Melting points were determined using the MR–VIS, LABINDIA visual melting range apparatus and are uncorrected. On a PerkinElmer SII thermal analyzer, the simultaneous TG-DTA studies were carried out. The curves were obtained in air using platinum cup sample holders containing 5–10 mg of the sample at a heating rate of 10 °C per minute.

Using Mo-Kα radiation at room temperature, the single crystal data for compound **1** were collected using a Bruker APEX CCD diffractometer. Data was collected with the use of the SMART software [24], integrated using SAINT [25], and corrected for absorption using SADABS [26]. The structure was solved using direct methods, and the

Table 1
Crystal data and structure refinement parameters for salts **1** and **2.**

Compounds Name	$[AgunH]^+[PANO]^-$ **1**	$[AgunH]^+[3\text{-}HPA]^-$ **2**
Empirical formula	$C_7H_{11}N_5O_3$	$C_7H_{11}N_5O_3$
Formula weight	213.21	213.21
Temperature/K	296(2)	296(2)
Crystal system	monoclinic	orthorhombic
Space group	$P2_1/n$	$Pca2_1$
a/Å	7.4194(7)	19.003(7)
b/Å	10.3401(12)	6.357(2)
c/Å	12.9840(16)	7.943(3)
α/°	90	90
β/°	103.280(4)	90
γ/°	90	90
Volume/Å^3	969.46(19)	959.531
Z	4	1
ρ_{calc}g/cm^3	1.461	1.462
μ/mm^{-1}	0.117	0.138
F(000)	448	252
Crystal size/mm^3	0.5 × 0.35 × 0.3	0.35 × 0.25 × 0.25
2Θ range for data collection/°	5.1 to 56.96	3.48 to 56.44o
Index ranges	$-9 \le h \le 9$, $-13 \le k \le 13$, $-17 \le l \le 17$	$-8 \le h \le 9$, $-9 \le k \le 9$, $-10 \le l \le 15$
Reflections collected	11394	3024
Independent reflections	2394 [$R_{int} = 0.0300$, $R_{sigma} = 0.0213$]	2392 [$R_{int} = 0.0132$, $R_{sigma} = 0.0215$]
Data/restraints/ parameters	2394/3/153	2392/8/140
Goodness-of-fit on F^2	1.039	1.043
Final R indexes [$I \ge 2\sigma$ (I)]	$R_1 = 0.0358$, w$R_2 = 0.0951$	$R_1 = 0.0379$, w$R_2 = 0.1123$
Final R indexes [all data]	$R_1 = 0.0487$, w$R_2 = 0.1037$	$R_1 = 0.0477$, w$R_2 = 0.1187$
Largest diff. peak/ hole/e Å^{-3}	0.26/-0.20	0.30/-0.22

SHELXL-2014/7 programme [27] was used to do full least-squares refinement against F2. N-H bond constraints and a riding model for their U_{iso} were used to refine the coordinates of the H atoms in subsequent difference maps. Using Mo-Kα radiation at room temperature (298 K), the single crystal X-ray data for compound **2** were collected using a Bruker APEX-II CCD diffractometer. Data was collected with the use of the APEX-II software [28], integrated using SAINT [25], and corrected for absorption using SADABS [26]. SIR-92 was used to solve the structures [29], and full least-squares refinement undertaken against F^2 refined using SHELXL-2014/7 program [27]. CCDC deposit numbers: 2067481 and 2067482. Table 1 summarizes the crystallographic data as well as the specifics of the final refinement parameters. The powder XRD pattern of the prepared salts in present study was recorded on a JEOL JDX 8030 and Phillips X-ray diffractometer using Cu-Kα radiation with nickel filters. The JASCO-FP-6600 spectrophotometer was used to record the solid-state luminescence spectra of the free acid and its salts; the excitation and emission slit widths were 2.5 and 5 nm, respectively.

2.2. Preparation of Guanylhydrazinium pyridine-2-carboxylate N-oxide {$[AgunH]^+[PANO]^-$} (1)

The title salt was prepared by mixing the equimolar ratios of commercially available picolinic acid N-oxide (0.139 g, 0.001 mol) and guanyl hydrazine bicarbonate (0.136 g, 0.001 mol) in aqueous medium under laboratory conditions. The resulting mixture was mechanically stirred well till the effervescence ceased, and the solution kept over water bath for a few minutes to afford a clear solution (pH = 4.0), and continued to concentrate the solution over a water-bath to reduce one-fourth of its initial volume. After a day, the crystalline compound began to appear and the crystallization process sustained for another two days. Finally, the transparent light-yellow crystals were then separated, washed with ethanol, and allowed to dry in the air. After this process, the good quality single crystals were selected by naked-eye using a lens for SCXRD analysis; the remaining crystals were used for powder XRD study to verify the formation of a new phase and compare the polymorphic nature of the compound.

Micro-analysis for the crystalline solid $[AgunH]^+[PANO]^-$. Yield: 75%. m.p. 160–162 °C. $^a\Lambda_m$: 121 $\Omega^{-1}cm^2mol^{-1}$. Anal. calcd. for $C_7H_{11}N_5O_3$ (Mr = 213.21): C, 39.44%; H, 5.20%; N, 32.85%. Found: C, 39.45%; H, 5.22%; N, 32.85%. By titration of the hydrazinic part of AgunH: calcd. 15.01%, found 15.05%. FT-IR (KBr, cm^{-1}): 3450(br, s), 1640(s), 1613(m), 1512(s), 1479(m), 1385(s), 1240(m), 1119(s), 1054 (w), 956(m), 860(m), 730(m), 741(m), 663(m), 630(m), 562(m), 535 (m), 440(m).

2.3. Preparation of Guanylhydrazinium 3-Hydroxy-pyridine-2-carboxylate {$[AgunH]^+[3\text{-}HPA]^-$} (2)

Here, the same procedure was followed as in the preparation of salt **1** described above. The isoelectronic species of 3-hydroxy picolinic acid is used (0.139 g, 0.001 mol) instead of picolinic acid N-oxide. Irrespective of the mole ratios (1:1, 1:2, 2:1), pale yellow square-shaped crystals of $[AgunH]^+[3\text{-}HPA]^-$ (**2**) were isolated after 2 days and air dried. Whereas in salt **1**, among the three ratios (1:1, 1:2, 2:1), the 1:1 ratio alone affords single crystal as a product, remaining ratios also yield the same product but polycrystalline in nature.

Micro-analysis for the crystalline solid $[AgunH]^+[3\text{-}HPA]^-$. Yield: 75%. m.p. 162–165 °C. $^a\Lambda_m$: 122 $\Omega^{-1}cm^2mol^{-1}$. Anal. calcd. for $C_7H_{11}N_5O_3$ (Mr = 213.21): C, 39.44%; H, 5.20%; N, 32.85%. Found: C, 39.43%; H, 5.21%; N, 32.84%. By titration of the hydrazinic part of AgunH: calcd. 15.01%, found 15.06%. FT-IR (KBr, cm^{-1}): 3450(br, s), 1645(s), 1611(m), 1515(s), 1480(m), 1381(s), 1244(m), 1120(s), 1054 (w), 957(m), 862(m), 730(m), 745(m), 665(m), 632(m), 562(m), 530 (m), 441(m).

2.4. Antimicrobial activity

The Clinical Laboratory at the PSG Institute of Medical Science and Research provided gram positive and gram-negative pathogenic strains of *E. coli*, *Shigella dysenteriae*, *Staphylococcus aureus* and *B. Substilis*, which were sub-cultured in nutrient agar slants at 37 °C for 24 h and stored in a refrigerator. Nutrient agar media was sterilized before being put into a sterile petri dish and allowed to set up at room temperature [18,30,31]. A saline suspension of bacteria with an absorbance of 0.1 at 600 nm in a spectrophotometer was swiped across the surface of the solution and left too dry for a short time. The agar plates were punctured with 5 mm holes using a sterile gel puncher, and salt solutions were then applied to the wells at varying concentrations. The zones of inhibition were then looked at after the plates had been incubated for 24 h at 37 °C. The minimal inhibitory concentration (MIC) was established as the lowest concentration of a compound solution that inhibited the corresponding strains' plates from displaying any evidence of noticeable growth [18,30,31].

2.5. Total antioxidant activity

The assay is based on the reduction of Mo^{VI} to Mo^{V} through extraction and the subsequent formation of a green phosphate/Mo^{V} complex at an acidic pH [32]. The samples were mixed with 3 mL of reagent solution (0.6 M sulphuric acid, 28 mM sodium phosphate and 4 mM ammonium molybdate) at various concentrations ranging from 50 to 250 g/mL. The reaction solution-filled tubes underwent a 90-min incubation period at 90 °C. After the solution had cooled to room temperature, its absorbance was measured at 695 nm in comparison to a blank methanol solution. A standard graph of ascorbic acid was used to compute the equivalents of ascorbic acid. Values are reported as equivalents of ascorbic acid in g per mg of sample for all tests, which were carried out in triplicate.

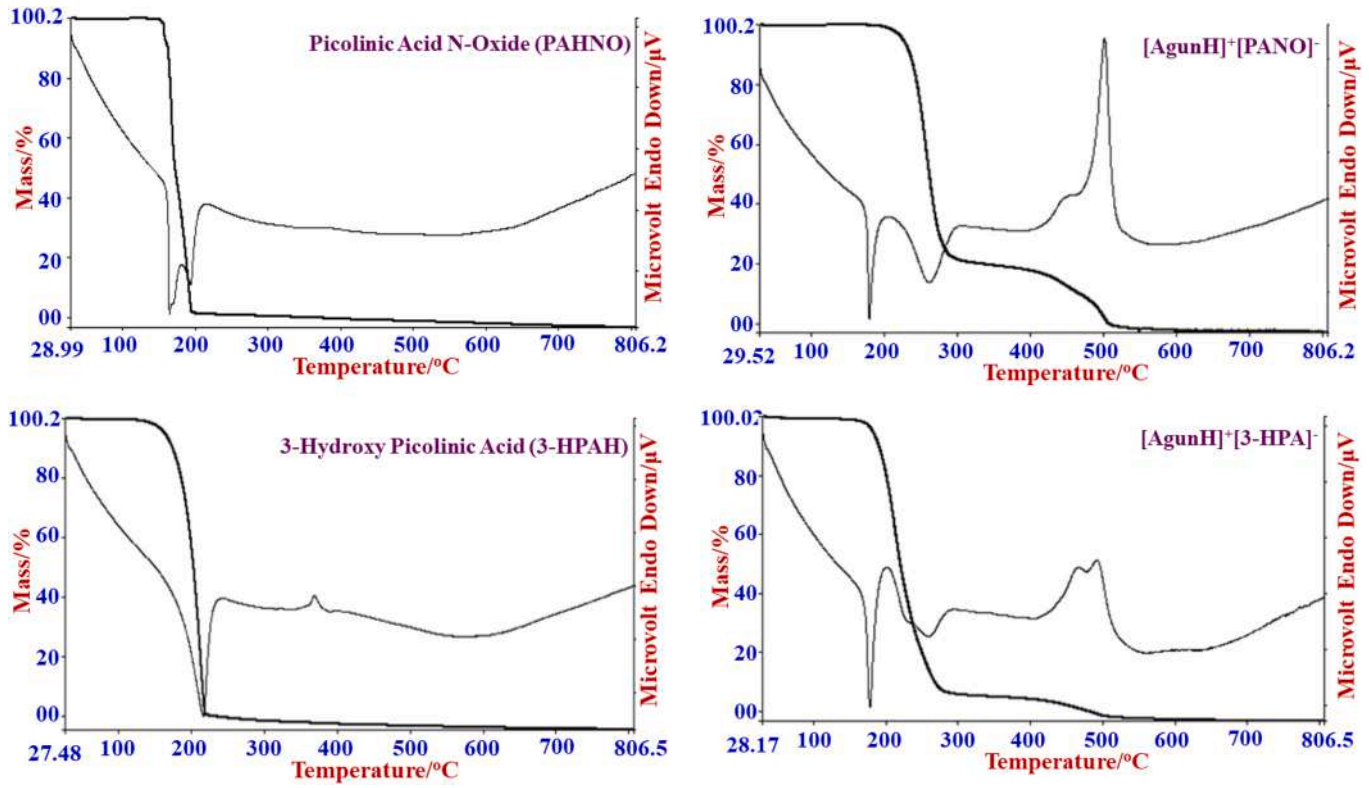

Fig. 1. Simultaneous TG-DTA of free acids [PAHNO & 3-HPAH] and its slats {$[AgunH]^+[PANO]^-$ (**1**) & $[AgunH]^+[3\text{-}HPA]^-$ (**2**)}.

2.6. 1,1-Diphenyl-2-picrylhydrazyl (DPPH) radical scavenging activity

In order to assess how well different antioxidant compounds, scavenge free radicals, DPPH has been employed extensively. The antioxidants were able to convert the stable radical DPPH in the DPPH assay into the yellow-colored diphenyl-picryl hydrazine. The approach is based on the reduction of DPPH in an alcoholic solution in the presence of an antioxidant that donates hydrogen because of the reaction's production of the non-radical form of DPPH-H [33]. DPPH is typically used as a reagent to assess the ability of antioxidants to scavenge free radicals. A stable free radical called DPPH can accept an electron or a hydrogen radical to transform into a stable diamagnetic molecule. It is believed that antioxidants' capacity to donate hydrogen accounts for their impact on DPPH. The study revealed that the materials are the better proton-donating ability and it could act as free radical inhibitors or scavengers, and its potentially acting as secondary antioxidants [18,19], even though the DPPH radical scavenging abilities of the samples were lower than those of ascorbic acid at 100 μg/ml. The following equation was used to calculate the DPPH radical scavenging activity:

$$\text{DPPH scavenging activity (\%)} = (A^0 - A^1)/A^1 \text{ X } 100$$

Where, A^0 was the absorbance of the control and A^1 was the absorbance in the presence of the test sample.

2.7. Results and Discussion

The isoelectronic species of picolinic acid N-oxide and/or 3-hydroxy picolinic acid coupled with guanyl hydrazine in equimolar ratio under aqueous medium afforded the 1:1 salt, $[AgunH]^+[PANO]^-$ and $[AgunH]^+[3\text{-}HPA]^-$, respectively. The pKa value of guanyl hydrazine is 11.5 [14,17], while the picolinic acid derivatives (pKa) lie in the range 2.5–5.5, a pKa difference is more than 3 [pKa(base)-pKa(acid)]. As expected, this lifts proton transfer from the acid to the base, which favors the formation of salt rather than a co-crystal [18,19]. Electrolytic behavior of the free acids and its salts were obtained in aqueous medium at ambient conditions. The free acids, being a slowly soluble substance, afford a value around 118 $\Omega^{-1}cm^2mol^{-1}$ which corresponds to 1:1 electrolyte. The poor solubility of acids in water may be the reason for these slight lower conductance values as expected [19]. The $[AgunH]^+[PANO]^-$ and $[AgunH]^+[3\text{-}HPA]^-$ salts, which is completely dissociated in aqueous medium and show a molar conductance value at 121 $\Omega^{-1}cm^2mol^{-1}$ for salt **1** and 122 $\Omega^{-1}cm^2mol^{-1}$ for salt **2**, respectively, indicating 1:1 electrolytic nature [18,19].

2.8. Infrared spectra

FT-IR spectra have been recorded to identify the molecular interaction of guanyl hydrazine bicarbonate with isoelectronic picolinic acids [PAHNO or 3-HPAH]. The spectra of the free acids [PAHNO & 3-HPAH] and their salts [$[AgunH]^+[PANO]^-$ (**1**) and $[AgunH]^+[3\text{-}HPA]^-$ (**2**)] are depicted in ESI (Fig. 1), and their characteristic band assignments are given in the preparation part. The IR spectra of the free acids show a peak in the region of 3480 to 3380 cm^{-1}. Here, the picolinic acid N-oxide shows a strong and distinct peak at 3380 cm^{-1} corresponds to hydroxyl group in –COOH [34], whereas 3-hydroxy picolinic acid exhibits a broad peak is due to overlapping of hydroxyl and carboxyl groups [35]. By examining the carbonyl stretching mode (C═O) of the free acid, it is possible to confirm the proton transfer from acid to base or co-crystal [18,19]. As expected, the free carbonyl group (C═O) shows a strong stretching frequency at 1690 cm^{-1} [18,19]. This stretching vibration mode totally disappeared from the ionized forms of salts **1** and **2**, and formation of two new peaks appeared in the range of 1640–1645 cm^{-1} ($\nu_{asym.}$ (COO-)) and 1475-1480 cm^{-1} ($\nu_{sym.}$ (COO-)), respectively (ESI, Fig. 1), which clearly indicates the formation of salt rather than co-crystal [18,19]. A sharp peak at 1230 cm^{-1} along with two additional peaks at 1238 and 1250 cm^{-1} is assigned to the N-O stretching vibrations of the PAHNO acid [36]. These vibrations are accompanied by a significant change in dipole moment and polarizability of the nitrogen & oxygen atoms. In the case of 3-HPAH acid, the above peaks are markedly

Table 2
Thermal data for free acids [PAHNO & 3-HPAH] and its salts {[AgunH]$^+$[PANO]$^-$ (**1**) & [AgunH]$^+$[3-HPA]$^-$ (**2**)}.

Compound	DTA Peak Temp./ ^{o}C	Thermogravimetry			Decomposition products
		Temp. range/ ^{o}C	Mass loss/ %		
			Obsd.	Calcd.	
PAHNO	(+) 175	-	-	-	Melting
	(+) 195	180 – 250	100	100	Complete decomposition
3-HPAH	(+) 220	180 – 250	100	100	Complete decomposition
[AgunH]$^+$[PANO]$^-$ (**1**)	(+) 185	-	-	-	Melting
	(+) 280	210 – 300	80.20	80.30	Formation of NH=C=NH
	(-) 500	300 – 550	100	100	Complete decomposition
[AgunH]$^+$[3-HPA]$^-$ (**2**)	(+) 185	-	-	-	Melting
	(+) 275 (-) 480 (-) 500	195 – 510	100	100	Complete decomposition

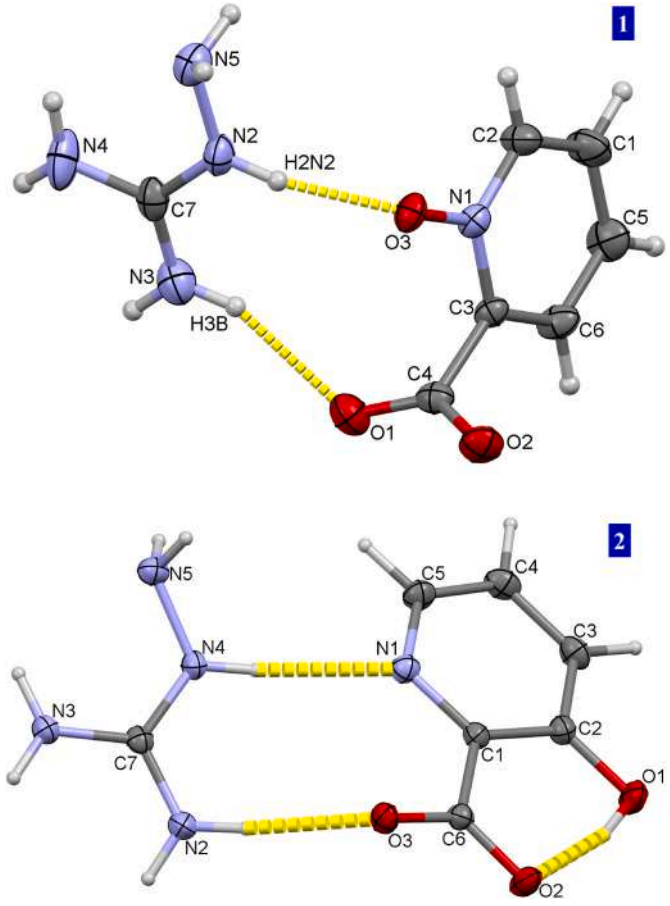

Fig. 2. Asymmetric units and atom labelling schemes for the salts **1** & **2** with thermal ellipsoids for non-H atoms drawn at 50% probability. Intramolecular H-bonded interactions between cation and anion are highlighted in yellow dashed lines.

absent, which infers the absence of the N-O group.

In salt **1**, the strong blue shifted IR band at 1258 cm^{-1} supports ν(N-O) stretching vibration and the existence of N-H···O hydrogen bond contacts with [AgunH]$^+$ cation [36], which is further confirmed by single-crystal XRD. The salts **1** and **2** show a broad peak in the range of 3400–3350 cm^{-1} is attributed to the combined vibrations of the amine (NH_2) and imine (NH) groups in the AgunH$^+$ cation [17–19]. Also, the hydrogen atoms in the pyridine ring of picolinic acids show three different vibrations for =C-H stretching, in plane bending and out of plane deformation which enhances the broad peak in the above region [36]. The intense peak that appears at 1600-1550 cm^{-1} infers that the ring vibration and C=N in the pyridine ring [17–19]. The sharp peak observed around 1112 cm^{-1}, is due to hydrazine moiety (-NH-NH_2) in guanyl hydrazinium cation, confirming the presence of cation in these salts [17–19,37].

2.9. Thermal decomposition studies

Thermal analysis is one of the most valid analytical techniques undergone to predict the purity, stability, molecular composition, and possible intermediates including physical changes of the substance are measured as the function of temperature [17–19]. The absorption (endothermic) or emission (exothermic) of energy levels in thermograms leads to the change in weight of the substance [17–19]. The energy change is not always accompanied by gain or loss in weight, indicating the phase transition (*i.e.,* melting/crystallization) of compounds [17–19]. To understand the thermal stability of the prepared compounds, the simultaneous TG-DTA analysis was carried out from 50 to 750 °C in air. The thermograms and thermal data are given in Fig. 1 and Table 2 respectively. The thermogravimetric results are in good agreement with the DTA data.

In TG, 2-picolinic acid N-oxide (PAHNO) shows horizontal plateau up-to 175 °C without change in weight, corresponding to a sharp endothermic peak at 165 °C in DTA. This infers that the compound undergoing melting is best fit with experimental value given in the preparation part. After melting, the compound completely decomposes to give gaseous products. Unlike PAHNO, the 3-hydroxy picolinic acid (3-HPAH) experiences single step endothermic decomposition in the temperature range of 190–500 °C along with melting as seen in Fig. 1. Thermograms of the free acids are entirely differ from its isolated salts. Salt **1** displays three step decomposition patterns, whereas the salt **2** shows melting (185 °C) followed by complete decomposition as shown in Fig. 1.

The former salt, [AgunH]$^+$[PANO]$^-$ (**1**), undergoes melting (0% weight loss) in the first step with a sharp endothermic peak in DTA at

Table 3
Selected bond lengths [Å] for salts **1** and **2**.

Compounds	1			2	
Atom	Atom	Length/Å	Atom	Atom	Length/Å
C1	C2	1.359(2)	N1	C1	1.343(3)
C1	C5	1.375(2)	N1	C5	1.337(3)
C2	N1	1.344(17)	C1	C2	1.408(3)
C3	C4	1.509(17)	C1	C6	1.506(3)
C3	C6	1.373(17)	C2	C3	1.398(3)
C3	N1	1.344(15)	C2	O1	1.348(2)
C4	O1	1.233(17)	C3	C4	1.373(3)
C4	O2	1.241(15)	C4	C5	1.391(3)
C5	C6	1.372(2)	C6	O2	1.265(2)
C7	N2	1.313(18)	C6	O3	1.259(2)
C7	N3	1.319(2)	C7	N2	1.321(2)
C7	N4	1.312(19)	C7	N3	1.325(3)
N1	O3	1.323(13)	C7	N4	1.336(3)
N2	N5	1.405(17)	N4	N5	1.405(2)

Table 4
Selected bond angles [°] for salts **1** and **2**.

Compounds	1				2			
Atom	Atom	Atom	Angle/°	Atom	Atom	Atom	Angle/°
C2	C1	C5	120.25 (14)	N1	C1	C2	121.79 (11)
N1	C2	C1	120.14 (13)	C1	C2	C3	119.43 (10)
C6	C3	C4	124.46 (11)	C2	C3	C4	118.05 (9)
N1	C3	C4	115.98 (10)	C5	C4	C3	119.21 (13)
N1	C3	C6	119.56 (11)	C4	C5	N1	123.67 (15)
O1	C4	C3	117.21 (11)	N1	C1	C6	117.05 (10)
O1	C4	O2	127.58 (12)	C6	C1	C2	121.16 (12)
O2	C4	C3	115.20 (11)	C1	C2	O1	121.89 (12)
C6	C5	C1	118.64 (13)	O1	C2	C3	118.68 (14)
C5	C6	C3	120.22 (13)	O2	C6	O3	123.84 (16)
N2	C7	N3	119.95 (12)	C5	N1	C1	117.82 (13)
N4	C7	N2	119.22 (15)	N2	C7	N3	120.68 (14)
N4	C7	N3	120.83 (15)	N3	C7	N4	121.47 (15)
C2	N1	C3	121.18 (11)	N2	C7	N4	117.82 (11)
O3	N1	C2	119.86 (10)	C6	N4	N5	118.17 (13)
O3	N1	C3	118.96 (10)	C1	C6	O2	119.82 (10)
C7	N2	N5	118.34 (11)	C1	C6	O3	116.34 (11)

185 °C. The value of melting shows slightly higher temperature than free acid (PAHNO) and is deducing that the salt involving strong H-bond contacts between the $[AgunH]^+$ cation and $[PANO]^-$ anion is confirmed by single crystal study. In the second step, the formation of a stable intermediate carbodiimide (NH═C═NH) [38,39] with weight loss of 80.20% in TG and is in good agreement with calculated value (80.30%). The corresponding endothermic peak in DTA shows at 280 °C. In the last step, the stable intermediate completely decomposes and shows an intense exothermic peak at 500 °C along with a shoulder peak in DTA to release the gaseous products. In contrast, the salt **2** shows a similar melting point followed by complete rupture of the whole molecule with exothermic peaks (doublet) is observed in DTA to form the gaseous products. The rapid breakdown of molecules is due to the presence of multiple strong N-H···O and N-H···N hydrogen bond contacts between $[AgunH]^+$ cation and $[3\text{-HPA}]^-$ anion, and these contacts are noticed from SCXRD.

2.10. Structural description

The nitrogen-rich organic base, namely, guanyl hydrazine readily forms salt rather than co-crystal with mono- and di-carboxylic systems, due to large pKa difference (>3) in between organic base and acid, which favours proton transfer [18,19]. During crystallization, the suitable crystals were isolated from compounds **1** and **2** and determined by X-ray diffraction analysis. Most of the salts are crystallized in centric space groups rather than non-centric depending on the temperature, solvents effect, pH and starting compounds, *etc,*. In the present study, salt **1** is crystallized in a centric space group ($P2_1/n$) whereas salt **2** is non-centric ($Pca2_1$) even though the same experimental conditions are maintained. The molecular structure of $[AgunH]^+[PANO]^-$ (**1**) and $[AgunH]^+[3\text{-HPA}]^-$ (**2**) are depicted in Fig. 2. Crystal data refinement details and bond parameters (bond lengths and bond angles) including hydrogen bonding contacts observed from the X-ray analysis are given in Tables 1, 3–5.

The anhydrous 1:1 salt $[AgunH]^+[PANO]^-$ is crystallized in a monoclinic crystal system with centric ($P2_1/n$) space group. The asymmetric unit consists of one each of guanyl hydrazinium cation and picolinate N-oxide anion (Fig. 2). The lengths of the C-N bonds on the $[AgunH]^+$ cation and the C-O bonds on the carboxylate group in the $[PANO]^-$/$[3\text{-HPA}]^-$ anion are crucial in determining a salt or co-crystal formation [18,19]. The standard C-N bond lengths of the imine (NH) and amine (NH_2) groups in a free guanyl hydrazine molecule are 1.28 Å and 1.47 Å, respectively [18,19]. The length of the imine C-N bond shows a minor variation after the protonation of the guanidinic core, which was precisely observed from the structural analysis.

The guanidine core (CN3) of the guanyl hydrazinium moiety seems to have the following observed C-N bond lengths: C7-N2 = 1.313(18); C7-N3 = 1.319(2); C7-N4 = 1.312(19) for **1** and C7-N2 = 1.321(2); C7-N3 = 1.325(3); C7-N4 = 1.336(3) for **2**, respectively. The fact that the bond lengths of C7-N2 and C7-N4 are nearly identical to those of C7-N3 implies that protonation can take place at either C7-N2 or C7-N4. Since the C7-N4 bond is just slightly shorter than the C7-N2 bond, it may be concluded that N4 has the protonation site. Whereas, in salt **2**, the bond lengths of C7-N2 and C7-N3 have almost equal values than C7-N4 indicates that protonation can occur either at C7-N2 or C7-N3. Therefore, it may be inferred that N2 has the protonation site and N4 extends the hydrazinic end (–NH–NH_2), since the C7-N2 bond is just a little bit shorter than the C7-N3 bond. The aforementioned statements are in good agreement with our previously reported works [18,19].

The C-O bond lengths of anions $[PANO^-$ and $3\text{-HPA}^-]$ are 1.233(17) & 1.241(15) Å for **1**; 1.265(2) & 1.259(2) Å for **2**, respectively, which is used to determine the deprotonation site. In most cases, the free carboxylic group of C-O is longer than C═O by at least 0.08 Å [18,19]. Bond length is reduced by deprotonation of a carboxyl group (-COOH), and the difference is ~ 0.02 Å or less. In the present study, the difference d(C-O) is 0.008 Å for **1** and 0.006 Å for **2**, respectively, showing that the formation of a salt is implied by the deprotonation of the carboxyl ($PANO^-$ or 3-HPA^-) group. Additionally, the hydrogen atoms in the electron-density difference map shows that proton transfer from the carboxyl group of PAHNO /3-HPAH to the guanyl hydrazine moiety has occurred, indicating the formation of a salt rather than a co-crystal [17–19]. The guanidinium core (CN3) present in the $[AgunH]^+$ cation appears to be conjugated, even though the terminal NH_2 group of the hydrazinic portion (-NH-NH_2) of the guanyl hydrazine cation possesses sp^3 character [14,15,17–19]. The conjugate structure of the guanidinium core and it being a basic prevents the N lone pair for the further protonation, but the terminal NH_2 groups might still act as bases.

Furthermore, the $AgunH^+$ cations in salts **1** & **2** have almost planar structure with a slight deviation from planarity due to the terminal

Table 5
Hydrogen bonding for $[AgunH]^+[PANO]^-$ (**1**) and $[AgunH]^+[3\text{-}HPA]^-$ (**2**).

$[AgunH]^+[PANO]^-$ (1)					$[AgunH]^+[3\text{-}HPA]^-$ (2)				
D-H…A	D-H (Å)	H…A (Å)	D-H…A (Å)	D-H…A (°)	D-H…A	D-H (Å)	H…A (Å)	D-H…A (Å)	D-H…A (°)
N3–H3A…O2^{i}	0.860	2.132	2.958	160.70	O1–H1···O2^{i}	0.918	1.633	2.528	164.00
N4–H4A…O2^{i}	0.811	2.629	3.301	141.31	N2–H2A…O3^{i}	0.872	1.995	2.844	164.24
N4–H4A…O3^{i}	0.811	2.273	2.864	130.15	N4–H4A…N1^{i}	0.865	2.116	2.979	175.10
N5–H5A…O2^{ii}	0.837	2.238	3.014	163.70	C4–H4···N3^{ii}	1.008	2.733	3.476	130.70
N5–H5B···O1 ^{iii}	0.936	2.167	3.076	154.09	N2–H2B···O3^{iii}	0.871	2.040	2.890	165.10
C2–H2···O2^{ii}	0.930	2.321	3.216	161.42	N3–H3A…O2^{iii}	0.869	2.109	2.960	166.02
C6–H6···O3^{iii}	0.930	2.686	3.527	150.73	N3–H3B···O3^{iv}	0.861	2.320	3.128	156.38
N2–H2N2···O3^{iv}	0.860	1.849	2.699	169.63	N5–H5A…O1^{v}	0.882	2.292	3.158	167.11
N3–H3B···O1^{iv}	0.860	2.139	2.959	159.25	N5–H5B···O3 ^{vi}	0.870	2.425	3.210	150.24
Symmetry code: (**i**) 1 + x, y, z (**ii**) 1/2 + x, 1/2-y, 1/2 + z (**iii**) 1.5-x, 1/2 + y, 1/2-z (**iv**) x, y, z.					**Symmetry code:** (**i**) x, y, z (**ii**) 1/2 + x, -y, z (**iii**) -x, 1-y, 1/2 + z (**iv**) -x, -y, 1/2 + z (**v**) 1/2-x, 1 + y, 1/2 + z (**vi**) x, −1+y, z.				

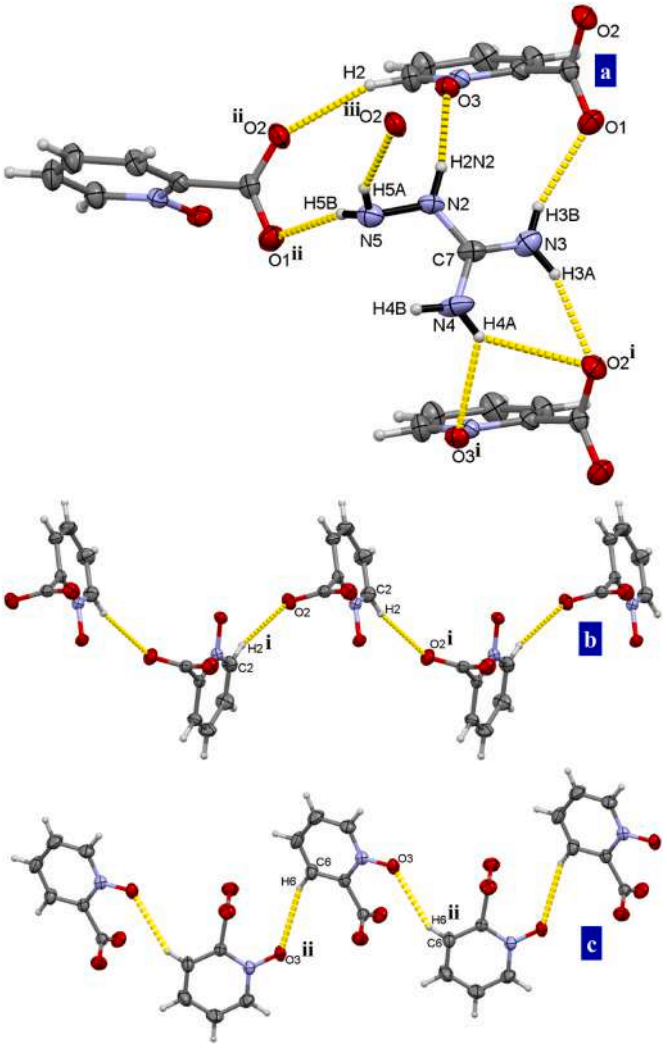

Fig. 3. (**a**) View of salt **1** revealing hydrogen bonding networks between $[AgunH]^+$ and $[PANO]^-$ [Symmetry Code: (**i**) 1+x, y, z; (**ii**) ½+x, ½-y, ½+z; (**iii**) 1.5-x, ½+y, ½-z]; (**b** & **c**) Wave-like 1D structure is created by weak C2-H2···O2 and C6-H6···O3 hydrogen bonding interactions between the $[PANO]^-$ anions [Symmetry Code: (**i**) ½+x, ½-y, ½+z, (**ii**) 1.5-x, -½+y, ½-z].

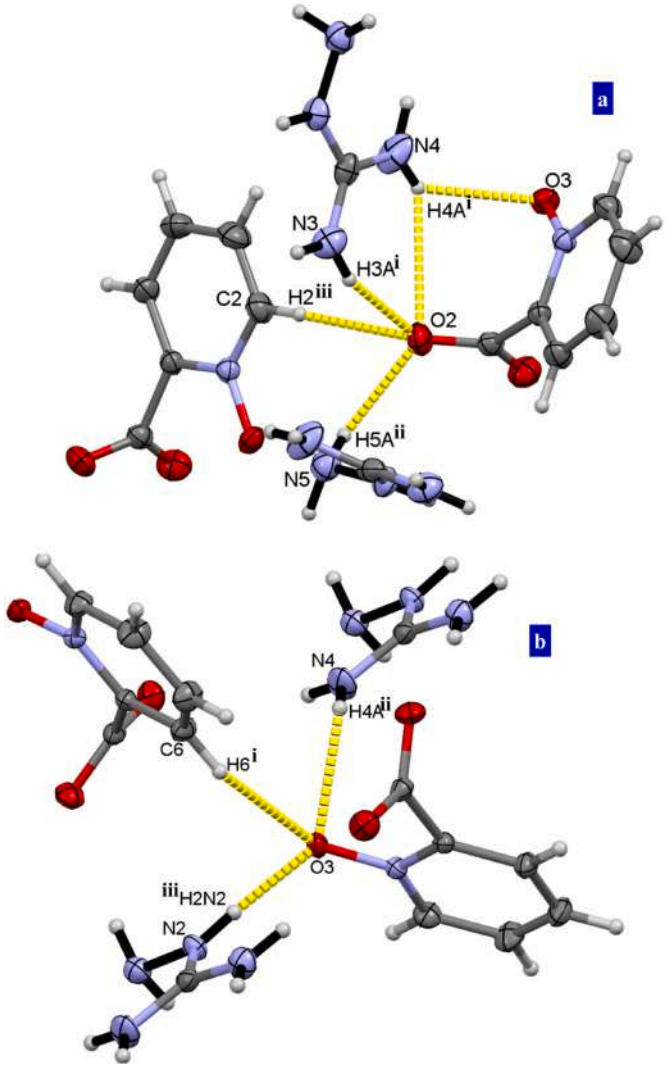

Fig. 4. (**a**) Tetrafurcated (C4-O2) acceptor and bifurcated (N4A-H4A) donor hydrogen bonding interactions *via* $[PANO]^-$ anions and $[AgunH]^+$ cations [Symmetry operation: (**i**) 1-x, y, z; (**ii**) 1.5-x, -½+y, ½-z; (**iii**) -½+x, ½-y, -½+z]; (**b**) Trifurcate hydrogen bonding acceptor (O3) atom in $[PANO]^-$ anion and shown in yellow dashed lines [Symmetry operation: (**i**) 1.5-x, ½+y, ½-z; (**ii**) -1+x, y, z; (**iii**) x, y, z].

hydrogen atoms of the hydrazine ($-NH_2$) entity of guanyl hydrazine (Fig. 2). Meanwhile, the deprotonated carboxylate group in $PANO^-$ anion is twisted out of the molecular plane (angle between $-COO^-$ and pyridyl ring planes is 84.44°) in order to form hydrogen bonds to $[AgunH]^+$ cation and $PANO^-$ anion is illustrated in Fig. 3a. Conversely, in $3\text{-}HPA^-$ anion, the deprotonated carboxylate ($-COO^-$) and hydroxyl groups (-OH) are lie in the same plane with pyridyl ring permitting π-conjugation and forming on intramolecular O1-H1···O2 (d(H … A) =

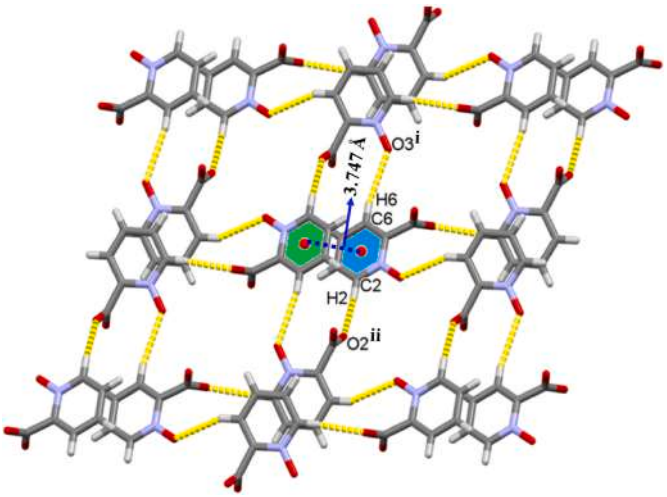

Fig. 5. View of H-bonded interactions between the sheets forming a bilayer structure by weak C-H···O hydrogen bonding networks, and Sandwich π-π stacking interaction (3.75 Å) by adjacent [PANO]$^-$ anions [Symmetry operation: **(i)** 1.5-x, -½+y, ½-z; **(ii)** -½+x, ½-y, -½+z].

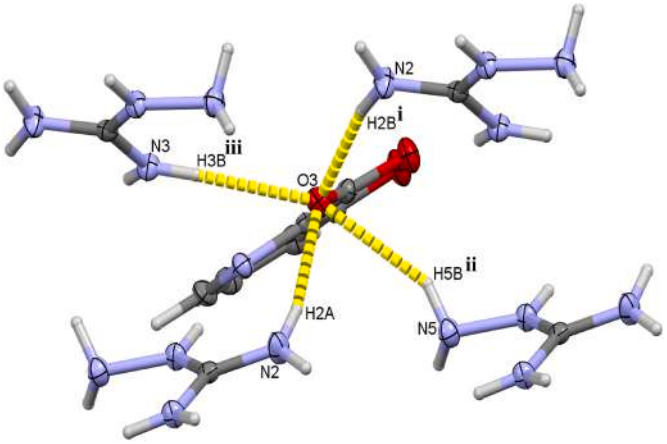

Fig. 6. Detail of the hydrogen bonds involving the tetrafurcated carboxylate-O3 atom as acceptor in 3-HPA$^-$ anion and donor atoms (N2-H2A, N2-H2B, N3-H3B and N5-H5B) in [AgunH]$^+$ cations [Symmetry operation: **(i)** 1-x, -y, -½+z; **(ii)** x, -1+y, z; **(iii)** 1-x, 2-y, -½+z].

1.633 Å) contact to the hydroxyl group as shown in Fig. 2.

As shown in Fig. 3, all N-H hydrogen bond donors (6 N-H) in the cationic moiety of salt **1** apart from N4-H4B are actively established with acceptors moiety (PANO$^-$ anion) through various symmetrical contacts and are showed in yellow dashed lines. The one dimensional wave like structures is formed by weak C2-H2···O2 (d(H … A) = 2.321 Å) and C6-H6···O3 (d(H … A) = 2.686 Å) hydrogen bonds as shown in Fig. 3b & c. Notably, the picolinate N-oxide (PANO$^-$) anion has three oxygen atoms: one N-Oxide oxygen (O3), and two carboxylate oxygens (O1, O2) atoms. Fig. 4a and b shows how the tetrafurcated and trifurcated N-H···O hydrogen bonding contacts have been achieved by the carboxylate (O2) and N-oxide oxygen atoms (O3) connecting with two molecules of AgunH cations and a PANO$^-$ anion. Two dimensional sheet is achieved by weak C-H···O [C2-H2···O2 (d(H … A) = 2.321 Å) and C6-H6···O3 (d (H … A) = 2.686 Å)] hydrogen bond contacts between the PANO$^-$ anions. Further, the centroid-centroid distance between the two planar heterocycles of PANO$^-$ anions (seen in Fig. 5; 3.75 Å) is significantly longer than the inter-layer contacts in graphite (3.35 Å) [17]. This stacking motif appears to result from an extensive array of hydrogen bonds where anions are strongly held together by bridging AgunH$^+$ units

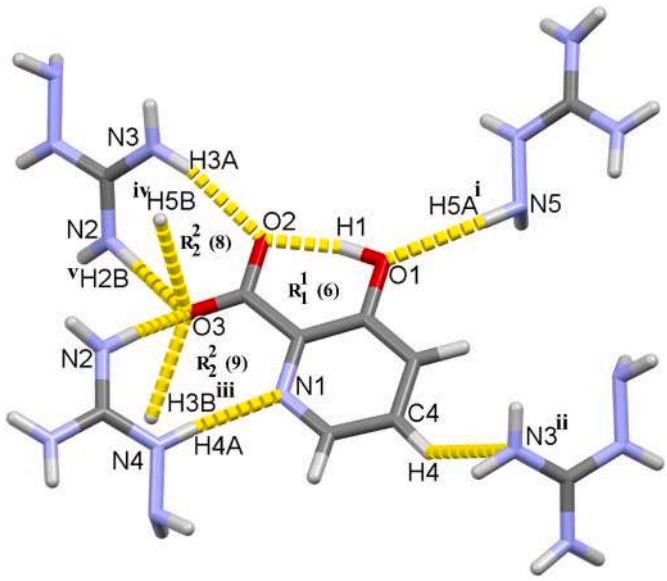

Fig. 7. Tetrafurcated and bifurcated carboxylate (O3 & O2) oxygen atoms in 3-HPA-anion and act as acceptor hydrogen bonding contacts with [AgunH]$^+$ cations, and viewing homo- and hetero-ring motifs [$R_1^1(6)$, $R_2^2(8)$ & $R_2^2(9)$] are highlighted in yellow dashed lines [Symmetry operation: **(i)** ½-x, -1+y, -1/2z; **(ii)** -½+x, 2-y, z; **(iii)** 1-x, 2-y, -½+z; **(iv)** 1-x, 1-y, -½+z; **(v)** x, -1+y, z].

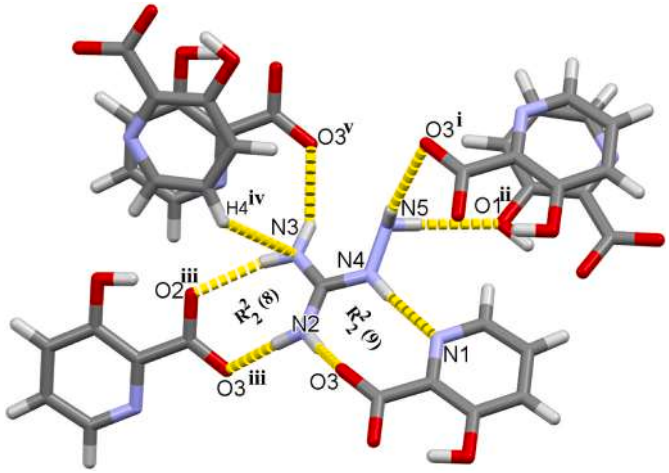

Fig. 8. View of versatile hydrogen bonding contacts in [AgunH]$^+$ cation, i.e., all the donor atoms in [AgunH]$^+$ cation involving H-bonding interactions with 3-HPA$^-$ anions, and showing hetero-ring motifs [$R_2^2(8)$ and $R_2^2(9)$] [Symmetry operation: **(i)** x, 1+y, z; **(ii)** ½-x, 1/2+y, ½+z; **(iii)** 1-x, 1-y, ½+z; **(iv)** ½+x, 2-y, z; **(v)** 1-x, 2-y, ½+z].

and pi-pi interactions to generate third-dimensionality as depicted in Fig. 5.

Contrary to salt **1**, anhydrous 1:1 salt **2** crystallizes in an ortho-rhombic crystal system with a non-centric (*Pca21*) space group even under the same experimental conditions. Guanyl hydrazinium cation and 3-hydroxy picolinate anion are both present in the asymmetric unit in 1:1 ratio as shown in Fig. 2. The 3-HPA$^-$ anion, which has the same structural formula as in **1**, with –OH group in the third position, resulting more complex packing motif than that observed in **1**. In **1**, the [AgunH]$^+$ cation with 6 hydrogen bond donors [6 N-H] can only partially fulfill the six H-bond acceptors [6 O lone pairs] from the PANO$^-$ anion as shown in Fig. 3a. While in **2**, there are more hydrogen bond donors [7 N-H and 1 *O*-H groups] than potential acceptors [6 O lone pairs and 1 N lone pair on the 3-HPA-anion] to form seven

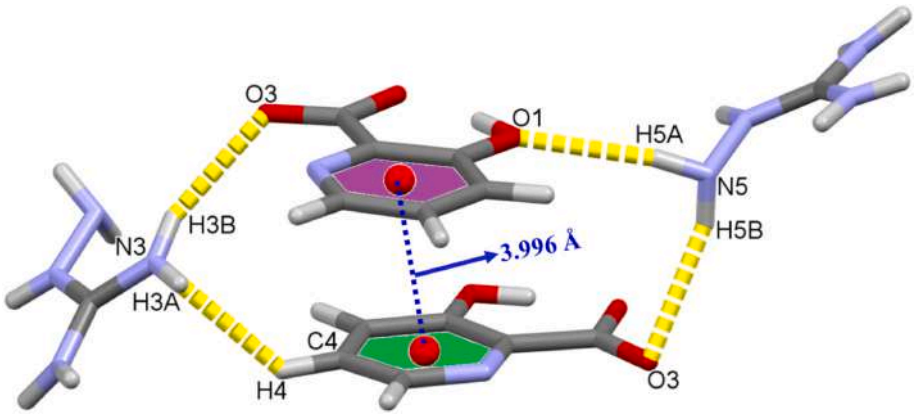

Fig. 9. View of hydrogen bonding contacts in $[AgunH]^+$ cationic molecules and π-π stacking between adjacent 3-HPA$^-$ anions [Symmetry operation: (**i**) ½-x, -1+y, -1/2+z; (**ii**) 1-x, 2-y, -½+z; (**iii**) ½-x, -1+y, -1/2+z].

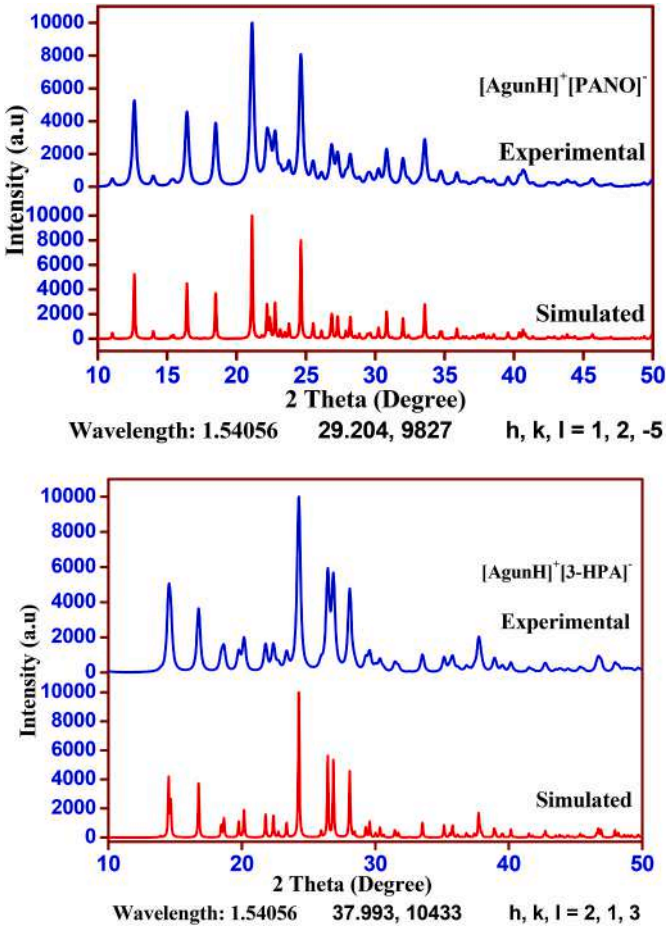

Fig. 10. Experimental and simulated PXRD patterns (derived from single-crystal XRD) of salts $[AgunH]^+[PANO]^-$ (**1**) & $[AgunH]^+[3\text{-}HPA]^-$ (**2**), are shown for comparison.

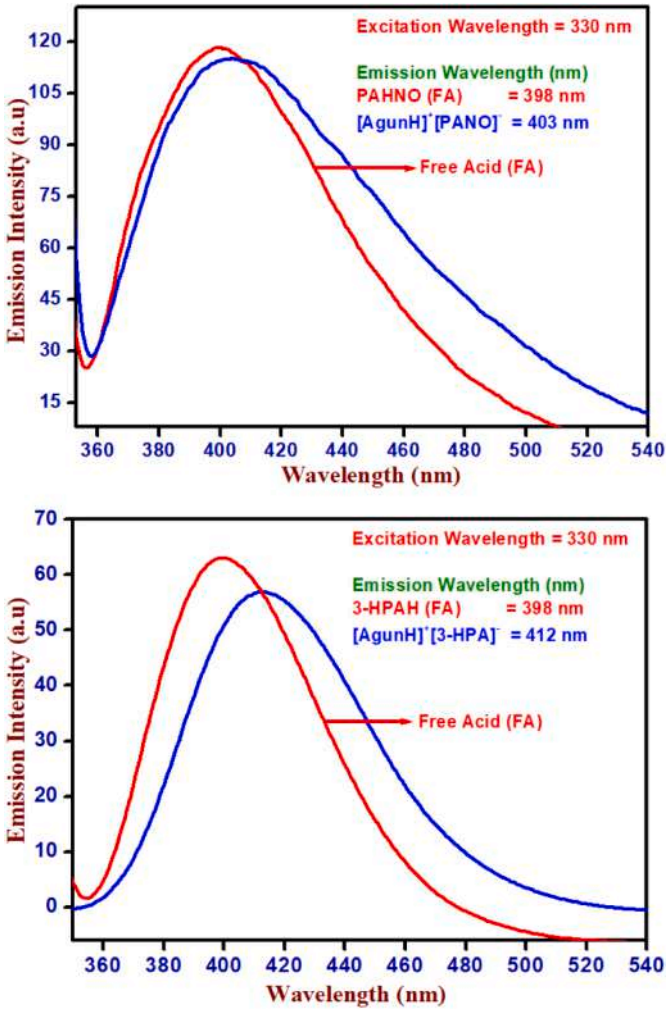

Fig. 11. Photoluminescent spectra of free acids [PAHNO & 3-HPAH] and its salts {$[AgunH]^+[PANO]^-$ (**1**) & $[AgunH]^+[3\text{-}HPA]^-$} (**2**). The excitation wavelength of free acids (PAHNO & 3-HPAH) and its salts is 330 nm in solid state at room temperature."

intermolecular H-bonds as shown in Fig. 7.

Multiple N-H-O and N-H-N hydrogen bonding contacts between the cations and anions are employed to form a stable crystal. This stability is reflected in thermograms of TG-DTA analysis without showing distinct step for melting and continuous rapture of whole molecule is observed. The 3-hydroxy picolinate (3-HPA$^-$) anion is notable for having four electronegative atoms: one hydroxyl oxygen (O1), two carboxylate oxygens (O2, O3), and one pyridine N-atom involving in strong hydrogen bonding. In Figs. 6 and 7, it is seen how the carboxylate oxygens (O2 & O3) connected with $AgunH^+$ cations to form bifurcated and tetrafurcated N-H···O hydrogen bonding contacts, respectively. Another noteworthy characteristic of this crystal system is the formation of different

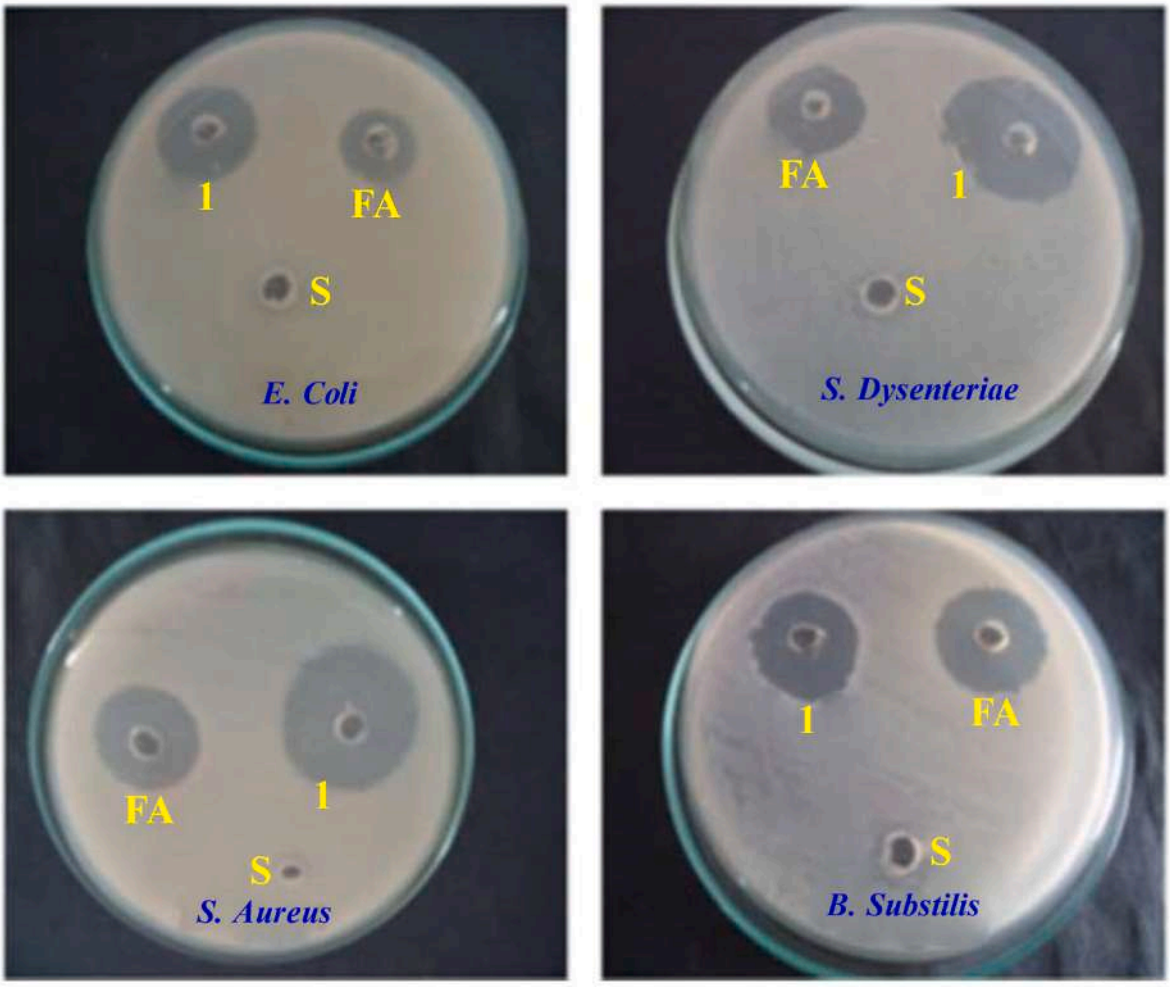

Fig. 12. Antibacterial activity of picolinic acid N-oxide (FA) and $[AgunH]^+[PANO]^-$ (**1**) ['S' stands for Solvent/Control; 'FA' stands for Free acid (PAHNO); **1** = $[AgunH]^+[PANO]^-$].

homo- and hetero-ring motifs [two R_2^2 (8), R_1^1 (6), and two R_2^2 (9)] that were observed using the graph set tool and are depicted in Figs. 7 and 8. These ring motifs formed by hydrogen bond interactions are essential for stabilizing the supramolecular architecture between the cations and anions. The two planar 3-HPA^- heterocycles have a significantly longer (centroid⋯centroid distance is 3.996 Å) π–π stacking interactions than salt **1** (3.747 Å; seen in Fig. 5) is depicted in Fig. 9. This stacked motif appears to result from a complex hydrogen-bonded network in which anions are held together *via* bridging $AgunH^+$ units (Fig. 9): the one of the $[AgunH]^+$ molecule creates two N-H⋯O hydrogen bonds between anions with O⋯H contacts of 2.292 and 2.425 Å. The other $AgunH^+$ cation joins with weak C4-H4⋯N3 at 2.733 Å and N3-H3B⋯O3 at 2.320 Å contacts to create the second bridge (Fig. 9).

One more remarkable finding was noticed from these structures, especially in the strong N-H⋯O and N-H⋯N hydrogen bonds [very strong N2-H2⋯O3 (N1-O3 oxide) hydrogen bonds in **1**, d(H … A) = 1.846 Å, seen in Fig. 3a & Table 5, and N-H⋯N in **2**; d(H … A) = 2.094 Å, seen in Fig. 7 & Table 5]; this was due to the pyridine N atom being free in the ring and readily forming N-H⋯N hydrogen bonds with guanyl hydrazinium cation. As a whole, N-H⋯O, N-H⋯N, weak C-H⋯N hydrogen bonds, and other non-covalent weak forces like π-π interaction (π-π = 3.996 Å, Fig. 9) between two planar 3-HPA^- anions (all of the N-H atoms in the $AgunH^+$ cation operate as donors and the carboxylate oxygen and ring nitrogen atoms in the 3-HPA^- anion act as acceptors) to create three-dimensional supramolecular networks.

2.11. Powder X-ray diffraction studies

The main X-ray diffraction applications of powder X-ray (PXRD) and single-crystal X-ray diffraction (SCXRD) methods is to explore the structural analysis for the prepared compounds [18,19]. Powder X-ray diffraction is used to characterize bulk materials is a quick and efficient approach for identifying polymorphs or polymorphic mixture of the compounds. Whereas the precise structural and molecular conformation of the prepared crystalline compounds are determined by single-crystal X-ray diffraction method. Fig. 10 correlates the simulated XRD patterns derived from SCXRD and the experimental powder XRD patterns for the synthesized crystalline compounds. The XRD patterns show sharp lines with a slight change in peak position/intensity of the 2θ values, indicating a typically crystalline, polymorphic nature of the products and free from impurities [18,19,37]. The bulk nature or particle size of the crystalline compounds could be responsible for the small variation in the peak position of the 2θ values in the experimental powder pattern.

2.12. Photoluminescence studies

In general, pyridine derivatives, particularly pyridine substituted mono- and dicarboxylic systems are well known to exhibit luminescent properties and have been extensively studied by various groups [40–43], including our reports [17,44]. In this present study, we compare and focus on the photoluminescent properties of isoelectronic acids (PAHNO & 3-HPAH) and their salts, $[AgunH]^+[PANO]^-$ (**1**) and

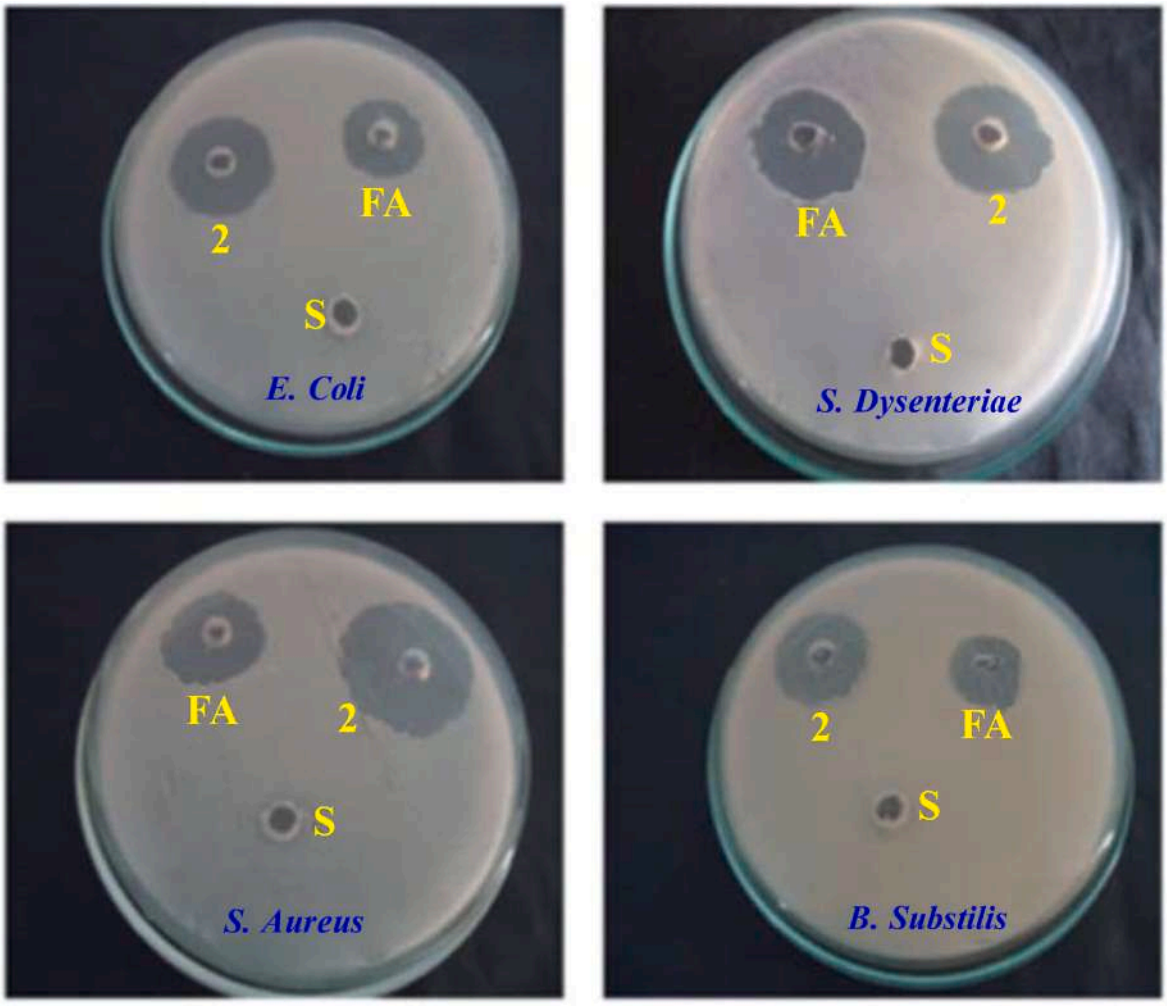

Fig. 13. Antibacterial activity of 3-hydroxy picolinic acid (FA) and $[AgunH]^+[3\text{-}HPA]^-$ (**2**) ['S' stands for Solvent/Control; 'FA' stands for Free acid (3-HPAH); **2** = $[AgunH]^+[3\text{-}HPA]^-$].

Table 6
The range of inhibitory concentration (MIC) values of the free acids [PAHNO & 3-HPAH], base [$AgunH.HCO_3$] and its salts {$[AgunH]^+[PANO]^-$ (**1**) & $[AgunH]^+[3\text{-}HPA]^-$ (**2**)}.

Compounds	Minimum Inhibitory Concentration (μg mL^{-1})			
	E. Coli	*S. Dysenteriae*	*S. Aureus*	*B. Substilis*
PAHNO	>250	185	180	95
3-HPAH	170	90	>250	>250
Salt 1	**90**	**70**	**65**	**75**
Salt 2	**95**	**65**	**75**	**80**
Ciprofloxacin	**25**	**20**	**30**	**20**
Control	NI	NI	NI	NI

[a]NI: No inhibition; ">" above the (MIC) activities; values in red – standard, and in green – relatively more active for salts than free acids

$[AgunH]^+[3\text{-}HPA]^-$ (**2**), have been studied in solid state at room temperature. The emission spectra of free acids and their salts are illustrated in Fig. 11. The free acids exhibit weak luminescence with an emission maximum at 398 nm (excitation wavelength at 330 nm), which is attributed to the intra-ligand π* - n transition [17–19,44]. When excited at the same wavelength as free acids (330 nm), the isoelectronic salts (**1** & **2**) differ in the emission intensity and exhibit a slightly broad red shift at 403 nm for **1** and 412 nm for **2**, respectively. The enhancement of red shift and intensity variation of emission peaks in $[PANO]^-$ and $[3\text{-}HPA]^-$ anions compared to that of the free acids is attributed to the

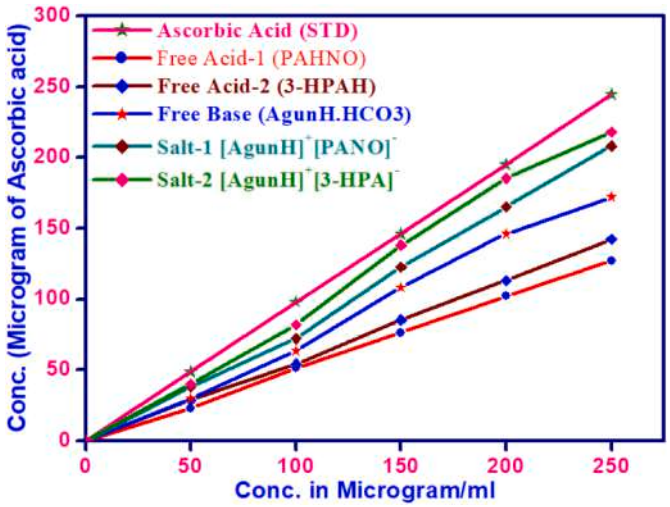

Fig. 14. Total antioxidant activity of standard (Ascorbic acid), starting compounds (PAHNO, 3-HPAH & AgunH.HCO_3) and its salts **1** & **2** at different concentrations (50–250 μg/ml). The experiments were performed in triplicates.

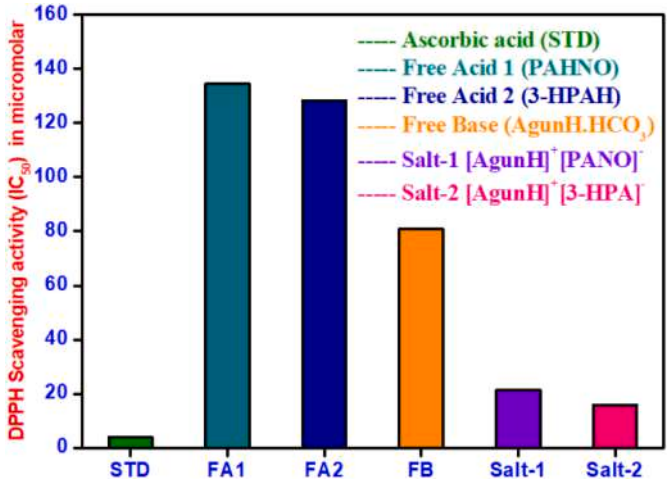

Fig. 15. DPPH scavenging activity of free acids (PAHNO & 3-HPAH), base (AgunH.HCO_3) and its salts **1** & **2** at different concentrations. Ascorbic acid was taken as the standard. Sample was taken from the range of 50–250 μg/ml. Assay was done in triplicates.

deprotonation of the carboxylic group leading to a conjugation between carboxylate group (-COO^-) and pyridine ring [17–19]. The solid-state structure of the ligands [[PANO]$^-$ or [3-HPA]$^-$] also exhibit non-covalent contacts, namely, hydrogen bonding and π-π stacking interactions further inducing the red shift (Fig. 11). As expected, the emission of free acids caused by the π*–n transition is very weak when compared to the π*–π transition of the carboxylate anions {[PANO]$^-$ & [3-HPA]$^-$} [17–19]. From our earlier reports [17–19], we conclude the free guanyl hydrazine bicarbonate and protonated $[AgunH]^+$ molecules do not exhibit emission spectra emphasizing the luminescent property is only due to free acids and its anions. Finally, the preliminary emission spectral results show that the salts (**1** & **2**) exhibit relatively strong emission bands (red shift) at room temperature, indicating that they may be good candidates for photoactive materials.

3. Biological studies

3.1. Antibacterial activity

Four pathogenic microbes namely (i) *Escherichia Coli* (E.C) (ii) *Shigella Dysenteriae* (S.D) (iii) *Staphylococcus Aureus* (S.A) and (iv) *Bacillus Substilis* (B.S) were used to assess the antibacterial potential of the picolinic acid N-oxide, 3-hydroxy picolinic acid and their salts *via., in vitro* using disc diffusion method [18,19,30,31]. Among the four pathogenic strains two are gram negative (E.C and S.D) and two are gram positive (S.A and B.S). The zone of inhibition is provided in Figs. 12 and 13. Further the Minimum Inhibitory Concentration (MIC) values of the salts were compared with the standard *Ciprofloxacin* by using 10% DMSO as control and the metrics are displayed in Table 6. Salts 1 and 2 revealed superior inhibitory effects than free acids (MIC ≤180 μg/mL) against *S. Dysenteriae*, *S. aureus* and *B. subtilis* with MIC values around or between 65 and 80 μg/mL. From the results, the activity appears to strongly correlate with the presence of the hydrazine moiety in the guanyl hydrazinium cation, which is consistent with our previous reports [18,19]. In contrast, the bacterial activity of the free base is diminished may be due to poor solubility of guanyl hydrazine bicarbonate.

3.2. Antioxidant activity

Radical scavenging research is the emerging trend in science. The total antioxidant and DPPH scavenging activity of the free acids, PAHNO & 3-HPAH, and its salts (**1** & **2**) of different concentrations have been determined and are displayed in Figs. 14 and 15. DPPH is the one of the commercially available common probes to analyze the radical scavenging process in antioxidants. Our research group proposed a mechanistic model [18,19] by Hydrogen Atom Transfer (HAT) reaction from an antioxidant or oxidant to $DPPH^▪$ radical. Here we propose the similar path of mechanism for the precursors [free acids (FA) & base (Agun)] and are elucidated in Scheme 2. Based on our proposed model, it appears that there are three mechanistic pathways for free acids (FA) and base (Agun) with $DPPH^▪$ radical. In the first step (a) the free Agun/FA moiety is transformed into $Agun^▪$/$FA^▪$ radical after donation of H-atom. In the second step (b) one each of $Agun^▪$ and $FA^▪$ radicals combined to give a combination product. Further in step (c) involves unstable complex reaction between $Agun^▪$/$FA^▪$ with $DPPH^▪$ to form Agun-DPPH/FA-DPPH as shown in Scheme 2.

According to the reaction sequence, each one species of $Agun^▪$ and $FA^▪$ are required to form combination products leading to better scavenging activity. Furthermore, the experimental results show that the total antioxidant activity can be attributed to the increasing number of amine groups appended to the guanidine core. Thus, the present proposed model and experimental results show that the total antioxidant and DPPH scavenging activity was obtained in the following order: PAHNO < 3-HPAH < $[AgunH]^+[PANO]^-$ (**1**) < $[AgunH]^+[3\text{-HPA}]^-$ (**2**). The salt **2** appears to have better total antioxidant and DPPH scavenging activities than the salt **1** and starting compounds, which could be attributed to the presence of one free –OH group in the third position of the pyridine ring in $[3\text{-HPA}]^-$ anion, as shown in Figs. 14 and 15. This enhanced activity of these salts seems to be similar to our earlier reports [18,19]. Finally, we concluded that the order of radical scavenging efficiency is more likely to be in the antibacterial study.

4. Conclusions

The reaction mixture of isoelectronic picolinic acids, namely, picolinic acid N-oxide and 3-hydroxy picolinic acid with guanyl hydrazine bicarbonate in equimolar ratio has yielded 1:1 salt of $[AgunH]^+[PANO]^-$ (**1**) and $[AgunH]^+[3\text{-HPA}]^-$ (**2**) respectively. The literature survey shows three reports related to salts of 3-hydroxy picolinic acid with N^6-Benzyladeninium [20], N^6-benzoyladenine [21] and

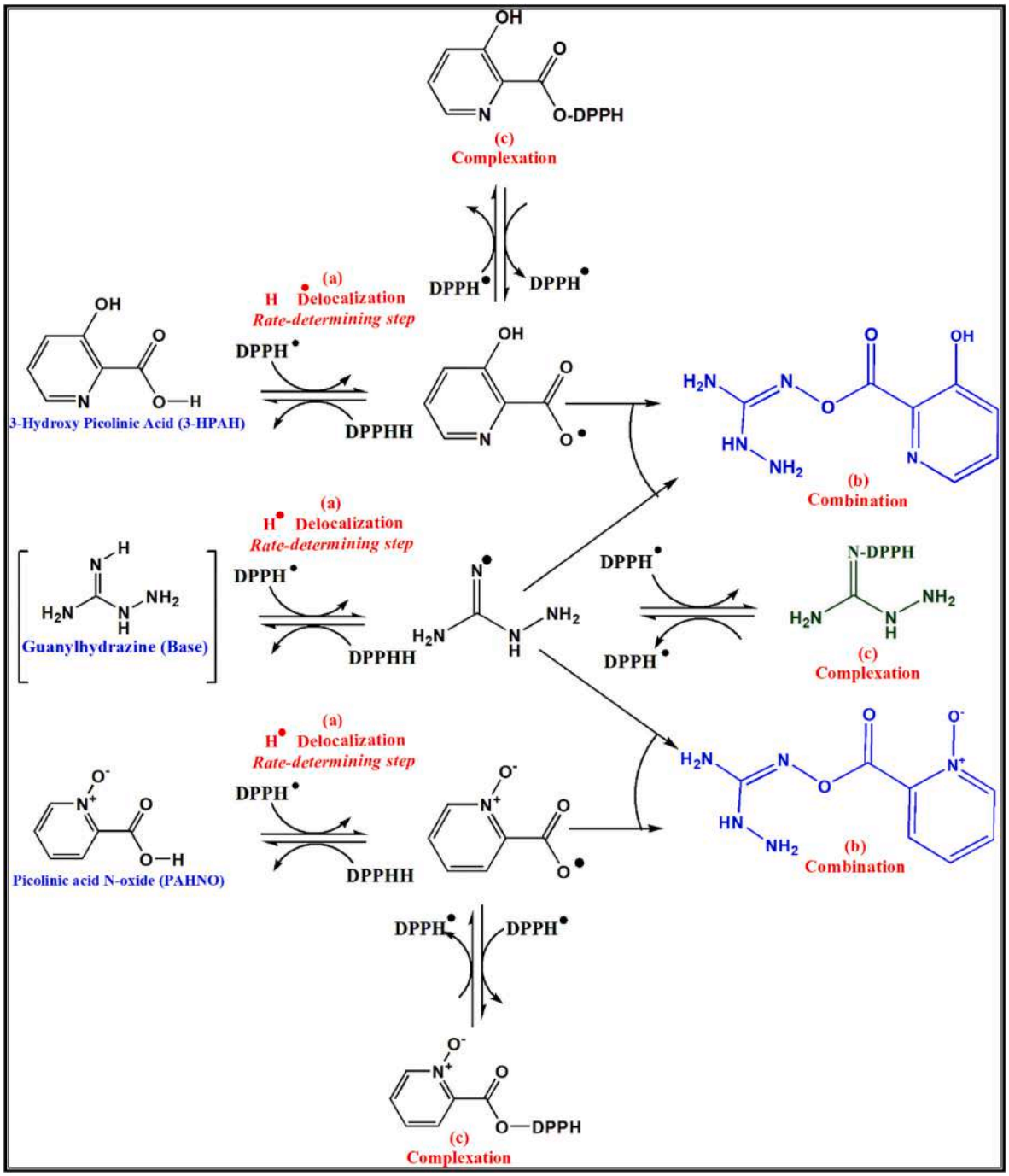

Scheme-2. Proposed mechanism for free acids (PAHNO & 3-HPAH), base (Agun) and its salts {$[AgunH]^+[PANO]^-$ & $[AgunH]^+[3\text{-}HPA]^-$} with DPPH radical reaction.

6-Amino-5-fluoro-1H-pyrimidin-2-one [22] bases using a mixture of solvents by slow evaporation method. Meanwhile, there is no report on salts of picolinic acid N-oxide with organic bases. Based on the literature reports, our work on the salt forming ability of isoelectronic picolinic acid derivatives with organic bases, in particular, nitrogen rich guanyl hydrazine has been taken. First time, we successfully synthesized the title salts in aqueous medium under template method and structurally characterized. The structural result reveals that salt **1** crystallized in centric ($P2_1/n$), whereas, **2** is in non-centric ($Pca2_1$) space group, even though in the same reaction conditions. This may be due to the presence of hydroxyl group in 3rd position of $3\text{-}HPA^-$ anion. Different hydrogen bonded features, such as intra- and intermolecular hydrogen bonds and π-π stacking interactions, as well as homo- and hetero ring motifs [two $R_2^2(8)$, $R_1^1(6)$, and two $R_2^2(9)$], acting as a main driving force to stabilize the crystal packing of salts **1** and **2**. These observations emphasize the significance of anions [$PANO^-$ & $3\text{-}HPA^-$] and $AgunH^+$ cation, which potentially acting as a suitable acid-base ion pair in the formation of robust hydrogen bonded supramolecular synthons [17–19]. In terms of properties, the emission spectra of the parent acids have shown relatively low luminescence behavior than the salts, whereas the antibacterial and antioxidant properties are in the following order: $[AgunH]^+[3\text{-}HPA]^- > [AgunH]^+[PANO]^- > AgunH.HCO_3 >$ 3-HPAH > PAHNO, which is consistent with the presence of hydrazine functionalities paving for the dominant antibacterial and antioxidant activities. Overall, it is expected that the results of this investigation will be useful in the development of new potent water-soluble guanyl hydrazinium

salts with effective antibacterial and antioxidant materials using a simple in-situ method. With these acids, single crystals of higher analogues of guanidinium salts are being grown and will be reported in due course.

Ethical approval

Not Applicable.

Data and code availability

Not Applicable.

CRediT authorship contribution statement

S. Packiaraj: Methodology, Writing – original draft, Visualization, Writing – review & editing. **N. Angamuthu:** Investigation, Formal analysis, Validation. **S. Poornima:** Data checking, Visualization, Writing – review & editing, Reviewing & Editing. **A. Pushpaveni:** Data checking, Visualization, Writing – review & editing, Reviewing & Editing. **L. Kousalya:** Writing- Antioxidant result interpretation. **J.M. Rawson:** Data Collection of single crystal and refinements. **S. Govindarajan:** Supervision.

Declaration of competing interest

There is no conflict of interest to declare.

Data availability

Data will be made available on request.

Acknowledgements

S. P. wishes to thank URF for the award of a research fellowship in science for meritorious students under the University Research Fellowship. The authors A. P and S. G. thanks to the UGC-SAP-DRS II, New Delhi (India), for financial support. S. G. is also thankful for the award of UGC-Emeritus Fellowship by UGC, New Delhi, India.

Appendix A. Supplementary data

Supplementary data to this article can be found online at https://doi.org/10.1016/j.jssc.2023.124158.

References

[1] J.H. Bryd, et al., The Crystal Structure of Aminoguanidine Hydrochloride Acta Crystallogr, 1957.
[2] A. Akella, et al., Aminoguanidinium Nitrate Acta Crystallogr, C50, 1994.
[3] E.R. Khomaa, et al., Synthesis and structure of aminoguanidinium sulfite monohydrate Russ, J. Inorg. Chem. (2013).
[4] I. Nemec, et al., The structural phase transitions of aminoguanidinium(1+) dihydrogen phosphate-study of crystal structures, vibrational spectra and thermal behavior, J. Solid State Chem. (2004).
[5] J.N. Adams, The Crystal Structure of Aminoguanidinium Dihydrogen Orthophosphate Acta Crystallogr, 1997.
[6] M. Koskinen, et al., Aminoguanidinium (+2) - sulphate, Z. Naturforsch. (1994).
[7] J.T. Koskinen, et al., Experimental and computational studies on aminoguanidine free base, monocation and dication, Part I: the crystal and molecular structure of aminoguanidine monohydrochloride and the ab initio structure of the endiamine tautomer of aminoguanidine free base, Z. Naturforsch. (1996).
[8] M. Gobel, et al., Potassium-, ammonium-, hydrazinium-, guanidinium-, aminoguanidinium-, diaminoguanidinium-, triaminoguanidinium- and melaminium nitro formate synthesis, characterization and energetic properties Z, fur. Anorg. Allg. Chem. (2007).
[9] M. Koskinen, et al., Structure of aminoguanidine hemioxalate. implications for the synthesis of amidinohydrazones Monatsh, Fur. Chem. (1997).
[10] Z. Machackova, et al., The crystal structure, vibrational spectra, thermal behavior and second harmonic generation of aminoguanidinium (+1) hydrogen (L)-tartrate monohydrate, J. Mol. Struct. (2007).
[11] T. Kolev et al. Aminoguanidinium Squarate Acta Crystallogr. Doi.org/10.1107/S0108270197099460.
[12] S. Murugavel, et al., Aminoguanidinium Hydrogen Succinate Acta Crystallogr, 2009.
[13] S. Murugavel, et al., Aminoguanidinium Hydrogen Fumarate Acta Crystallogr, 2009.
[14] R. Selvakumar, et al., The chemistry of aminoguanidine derivatives – preparation, crystal structure, thermal properties, and molecular docking studies of aminoguanidinium salts of several carboxylic acids, J. Phys. Chem. Solid. (2015).
[15] G. Radha, et al., Synthesis and Experimental Studies on Supramolecular Synthons of Aminoguanidinium Carboxylates: A Case Study of π-Hole Bonded Carbon Bonding via Theoretical Approaches Chemistry Select, 2018.
[16] P.P. Deyn (Ed.), Guanidino Compounds in Biology and Medicine London, England, J. Libbey, 1992.
[17] S. Packiaraj, et al., Preparation, thermal behavior, luminescent properties, and crystal structures of aminoguanidinium 2, n-pyridine-dicarboxylate (n= 3, 4, 5, and 6) salts, J. Therm. Anal. Calorim. (2015).
[18] S. Packiaraj, et al., Structural and antioxidant properties of guanidinium pyrazole-3,5-dicarboxylates Cryst, Eng. Commun. (2016).
[19] S. Packiaraj, et al., Structural and antioxidant properties of guanylhydrazinium pyrazine-2-carboxylate, J. Mater. Sci. Mater. Electron. (2021).
[20] J.S. Nirmalram, et al., Hydrogen bonded supramolecular assembly in N6-benzyladeninium nitrate and N6-benzyladeninium 3-hydroxy picolinate: a synthetic cytokinin, J. Chem. Crystallogr. (2011).
[21] Ammasai Karthikeyan, et al., Supramolecular hydrogen-bonding patterns in two cocrystals of the N(7)–H tautomeric form of N6-benzoyladenine: N6-benzoyladenine–3-hydroxypyridinium-2-carboxylate (1/1) and N6-benzoyladenine–DL-tartaric acid, Acta Crystallogr. (1/1) (2015).
[22] Ammasai Karthikeyan, et al., Crystal Structure of 4-Amino-5-Fluoro-2-Oxo-2,3-Dihydropyrimidin-1-Ium 3-Hydroxypyridine-2-Carboxylate Acta Cryst, 2014.
[23] G.H. Jeffery, et al., "Vogel's Textbook of Quantitative Chemical, Analysis" fifth ed., 1985.
[24] SMART, Bruker AXS, Wisconsin, 2001. USA.
[25] SAINT, Bruker AXS, Wisconsin, 2001. USA.
[26] SADABS, Bruker AXS, Wisconsin, USA, 2007.
[27] G.M. Sheldrick, Crystal Structure Refinement with SHELXL Acta Crystallogr. Sect *C*, 2015.
[28] APEX-II, Bruker AXS, Wisconsin, USA.
[29] A. Altomare, et al., SIR92 - a program for automatic solution of crystal structures by direct methods, J. Appl. Crystallogr. (1994).
[30] T. Premkumar, et al., Antimicrobial study on trivalent lighter rare-earth complexes of 2-pyrazinecarboxylate with hydrazinium cation World, J. Microbiol. Biotechnol. (2006).
[31] K. Rajavelu, et al., Synthesis and photophysical, electrochemical, antibacterial, and DNA binding studies of triazinocalix[2]arenes, J. Mater. Chem. (2015).
[32] P. Prieto, et al., Spectrophotometric quantization of antioxidant capacity through the formation of a phosphomolybdenum complex: specific application to the determination of vitamin E, Anal. Biochem. (1992).
[33] K. Nagendra Prasad, et al., Identification of phenolic compounds and appraisal of antioxidant and antityrosinase activities from litchi (Litchi sinensis Sonn.) seeds, Food Chem. (2009).
[34] R.H. Wiley, et al., Pyrimidine N-Oxides and their infrared absorption characteristics, J. Am. Chem. Soc. (1957).
[35] D.P. Mohanty, et al., Synthesis of diorganosilicon (IV) complexes of 3-hydroxy-2-pyridine carboxylic acid and 2-pyridine carboxylic acid, J. Adv. Sci. Technol. (2013).
[36] S. Youssif, Recent trends in the chemistry of pyridine N-oxides, ARKIVOC (Gainesville, FL, U. S.) (2001).
[37] A. Pushpaveni, et al., Structural and multi-functional properties of novel thorium complex bearing higher analogue of guanidine base Mater, Chem. Phys. (2022).
[38] S. Packiaraj, et al., New insight for the estimation of sulfur content from guanidinium tris(thiodipropionato) lanthanate(III) trihydrate: synthesis, thermal, and photoluminescent studies, Monatshefte fur Chemie - Chemical Monthly (2021).
[39] S. Packiaraj, et al., Synthesis, thermal behaviour, XRD, and luminescent properties of lighter lanthanidethiodipropionate hydrates containing aminogunidine as neutral ligand, Open J. Inorg. Chem. (2014).
[40] C.G. Wang, et al., A Series of Three-Dimensional Lanthanide-Rigid-Flexible Frameworks: Synthesis, Structure, and Luminescent Pro^{P}*erties* of Coordination Polymers with 2,5-Pyridine Dicarboxylic Acid and Adipic Acid Cryst, Growth Des, 2009.
[41] Y.G. Huang, et al., Synthesis, structure and luminescent properties of lanthanide–organic frameworks based on pyridine-2,6-dicarboxylic acid, J. Mol. Struct. (2008).
[42] S. Demir, et al., Metal–organic Frameworks Based on copper(I) Iodide and Pyridine-3,5-Dicarboxylic Acid: Synthesis, Crystal Structures and Luminescent Properties Polyhedron, 2016.
[43] V.F. Zolin, et al., Spectroscopy of europium and terbium pyridine-carboxylates, J. Alloys Compd. (2004).
[44] A. Pushpaveni, et al., Structural resemblance and variation in transition metal complexes derived from dipicolinic acid and guanylhydrazine Inorganica, Chim. Acta (2018).

separations

MDPI

Article

Phyto-Mediated Green Synthesis of Silver Nanoparticles Using an Aqueous Leaf Extract of *Momordica cymbalaria*: Antioxidant, Cytotoxic, Antibacterial, and Photocatalytic Properties

Madasamy Sundar [1], Gopalan Rajagopal [2], Ambikapathi Nivetha [3], Seetharaman Prabu Kumar [4,*] and Selvaraj Muthukumar [1,*]

[1] Centre for Research and Postgraduate Studies in Botany, Ayya Nadar Janaki Ammal College (Affiliated to Madurai Kamaraj University, Madurai), Sivakasi 626124, Tamil Nadu, India; sundarcrpb@gmail.com
[2] Postgraduate and Research Department of Zoology, Ayya Nadar Janaki Ammal College (Affiliated to Madurai Kamaraj University, Madurai), Sivakasi 626124, Tamil Nadu, India; rajagopalzoology@gmail.com
[3] Post Graduate and Research Department of Chemistry, Kongunadu Arts and Science College, Coimbatore-641029, Tamilnadu, India; nivethaambikapathi@gmail.com
[4] Laboratory of Functional Molecules and Materials, School of Physics and Optoelectronic Engineering, Shandong University of Technology, Xincun West Road 266, Zibo 255000, China
* Correspondence: drspk1989@gmail.com (S.P.K.); muthukumargowsic@gmail.com (S.M.)

Abstract: In this study, we biosynthesized the stable silver nanoparticles (AgNPs) from *Momordica cymbalaria* leaves to evaluate their antioxidant, antibacterial, cytotoxic, and photocatalytic properties. Initially, we screened the bioactive compounds from *M. cymbalaria* extract using GC-MS. The biosynthesis of *Mc*-AgNPs was confirmed using instruments, such as UV-visible spectroscopy FT-IR, XRD, SEM with EDX, and HR-TEM analyses. The UV-visible spectrum indicated absorbance at 425 nm. The crystallite size of the *M. cymbalaria*-stabilized nanoparticles was determined to be 20.14 nm. The morphology and size of the synthesized *Mc*-AgNPs were confirmed via SEM-EDX and HR-TEM analyses, with a size range from 16 to 22 nm. The synthesized *Mc*-AgNPs exhibited a photocatalytic yield of 60%. The biosynthesized *Mc*-AgNPs demonstrated strong antioxidant properties and prominent antibacterial activity against human pathogenic bacteria. The cytotoxicity study revealed that *Mc*-AgNPs were effective against MCF-7 cells in a dose-dependent manner. The recognized bioactivities confirm that the synthesized *Mc*-AgNPs act as effective catalysts in oxidation and serve as potent antioxidant, anticancer, and antibacterial agents.

Keywords: *M. cymbalaria*; silver nanoparticle; antioxidant; antibacterial; anticancer and photocatalytic activity

Citation: Sundar, M.; Rajagopal, G.; Nivetha, A.; Prabu Kumar, S.; Muthukumar, S. Phyto-Mediated Green Synthesis of Silver Nanoparticles Using an Aqueous Leaf Extract of *Momordica cymbalaria*: Antioxidant, Cytotoxic, Antibacterial, and Photocatalytic Properties. *Separations* **2024**, *11*, 61. https://doi.org/10.3390/separations11020061

Academic Editor: Alessandra Bonamore

Received: 28 December 2023
Revised: 8 February 2024
Accepted: 14 February 2024
Published: 17 February 2024

1. Introduction

Nanotechnology has evolved into a significant and intriguing field of research due to its unique characteristics and wide range of applications in sectors, such as agriculture, food, and health [1]. A different approach to addressing some of the most urgent issues facing the world today, such as cancer and multi-drug resistance (MDR), is Nanotherapy. When a microbe naturally becomes resistant to an antibiotic that was once useful for treating infections it caused, this is known as multi-drug resistance (MDR) [2]. With the few antimicrobial drugs now on the market, treating these drug-resistant bacterial strains, also known as "superbugs", is quite challenging. According to Shankar (2016), if appropriate measures are not taken to address this problem, multi-drug resistance (MDR) is predicted to claim up to 10 million lives by 2050, with over 4 million of those fatalities occurring in Asia [3]. Therefore, the World Health Organization (WHO) has asked researchers worldwide to perform research and create innovative anti-MDR agents, particularly antibacterial medications, to solve this exceedingly worrisome topic [4].

Cancer is another serious illness that has long plagued humanity and stands out as one of the deadliest diseases in the contemporary world. Among women, breast cancer has consistently ranked as a prominent contributor to mortality. According to their report, the World Health Organization (WHO) anticipates a staggering 16.3 million fatalities from these ailments by 2040 [5]. Most cancer treatments and controls include surgery, chemotherapy, targeted therapy, immunotherapy, radiation therapy, and hormone therapy. Traditional therapy may cause drug resistance, recurrence, metastasis, and toxicity. Nanotechnology in medicine has offered hope to biological and therapeutic fields [6–8]. While surgery, radiation, and chemotherapy are effective conventional cancer treatments, their severe side effects lower patients' quality of life. In addition, the patient might potentially acquire resistance to MDR strains posing severe hurdles in treating cancer [9]. The development of novel treatments utilizing nanotechnology has the potential to enhance the inadequacies of existing cancer treatments.

Due to their intense color and persistent breakdown, synthetic dyes used in plastic, food, paper, paint, and cosmetics pollute the environment [10]. Most of the standard procedures to address this contamination, including reverse osmosis, coagulation, adsorption and ultra-filtration, etc., fail to decolorize and mineralize these dyes due to their high stability and complicated aromatic structures [11]. Thus, a new treatment approach is needed to destroy and deprive these crucial hazardous chemicals or convert them into environmentally friendly products [12]. Metal nanoparticles act as catalysts in several chemical processes in nano-catalysis, a fast-growing nanotechnology field [13].

Nanoparticles exhibit potential as antibiotics, antioxidants, and anticancer agents due to their small size, large surface-area-to-volume ratio, and diverse optical, chemical, magnetic, and mechanical properties [14]. Noble metal nanoparticles, such as those made from zinc, silver, copper, gold, platinum, magnesium, and titanium, have received considerable attention in biological applications due to their multifunctional diagnostics [15]. While recent advances in nanotechnology and the increasing use of nanoparticles have brought attention to previously untapped natural resources, they have also highlighted cutting-edge methods for exploiting them. The physical and chemical processes for synthesizing nanoparticles are widely known [16]. However, these techniques often produce toxic by-products during synthesis. Consequently, researchers are exploring natural biological resources, such as microbes, amino acids, polymers, sugars, vitamins, and plant extracts, to rapidly and efficiently fabricate metal nanoparticles [17,18].

Plant-mediated nanoparticle synthesis is gaining importance due to its low toxicity, efficiency, eco-friendliness, and shorter processing times [19]. This exploration into plant-based nano-synthesis delves into the diverse range of plants employed, highlighting their unique phytochemical compositions and properties. Medicinal plants' leaves, stems, and roots and the seeds and fruits of crops are harnessed to create a sustainable platform for nanomaterial synthesis. These green-synthesized nanoparticles show promise across multiple applications, driven by their biocompatibility, tunable physicochemical properties, and renewable sources [20,21]. Plants provide a rich source of bioactive compounds that can reduce, stabilize, and cap metabolites, converting metal ions into nanoparticles. This can lead to the synthesis of nanoparticles with predefined characteristics, such as flaviolin, polysaccharides, alkaloid amines, proteins, terpenoids, polyphenols, tannins, and aldehydes [22].

M. cymbalaria has been used in various Asian herbal medicine systems for an extended duration [23]. *Momordica* plants are known for their biologically active compounds [24]. The identified alkaloids, flavonoids, and saponins are particularly noteworthy, as these compounds have been associated with a range of beneficial biological activities. Alkaloids, for instance, are known for their antimicrobial and anticancer properties [25]. Flavonoids are recognized for their antioxidant and anti-inflammatory effects, contributing to potential health benefits [26]. Saponins, on the other hand, have demonstrated antidiabetic properties in various studies [26]. The potential biological benefits of phytochemicals found in *Momordica* have attracted significant interest in recent studies, focusing on compounds

related to diabetes mellitus, cardioprotective properties, cancer, ulcers, and diabetic neuropathy [27–30]. It has also been documented that the herb possesses wound-healing, hypoglycemic, hypolipidemic, anti-infertility, nephroprotective, hepatoprotective, and antioxidant properties [31–35].

Silver nanoparticles (AgNPs) have emerged as a leading type among biosynthesized metal nanoparticles over the past two decades due to their distinct physical, chemical, and biological properties [36]. While $AgNO_3$ can be toxic at high concentrations, studies have demonstrated increased catalytic activity, chemical stability, biocompatibility, and therapeutic potential at lower concentrations of $AgNO_3$ [37]. The potential anti-cancer and antibacterial actions of silver nanoparticles are well-documented [38], with the controlled release of silver being a notable advantage over bulk metals and their salts [39]. The concept of new-age bio-nano formulations espouses nanotechnology with traditional medicine [40,41]. Many studies have highlighted the green synthesis of AgNPs with plant leaves, but there has been limited exploration of green synthesis using wild and native plant species with biomedical applications [42–45]. Silver nanoparticles have shown considerable promise in counteracting reactive oxygen species, indicating a potential role in reducing oxidative stress [46]. Their selective cytotoxicity against cancer cells also ignites interest in their anti-cancer mechanisms, leading to the development of novel, targeted cancer treatments [47,48]. Moreover, the broad-spectrum antimicrobial effectiveness of silver nanoparticles against a variety of pathogens underscores their importance in tackling infectious diseases and antibiotic resistance [49]. This extensive study aims to decipher the complex molecular mechanisms underlying these critical aspects, offering a comprehensive view of silver nanoparticles' therapeutic prospects and aiding progress in nanomedicine [50]. The aforementioned points indicate that synthesizing metal nanoparticles using a green chemical approach is an intriguing and underexplored opportunity, which has sparked interest in the current study.

This research examines the antibacterial, cytotoxic, and photocatalytic potential of *M. cymbalaria*-mediated silver nanoparticle synthesis. By integrating the properties of the *Momordica* genus with nanotechnology, this study seeks to demonstrate the potential applications of these nanoparticles in various medicinal and environmental contexts. Exploring green synthesis using wild species and native plants, particularly those with anti-cancer and antibacterial activities, represents a novel and underexplored opportunity, potentially leading to new insights and applications in nanomedicine and environmental sustainability.

2. Materials and Methods

Most of the chemicals utilized in this investigation were procured from various suppliers. All analytical-grade experimental chemicals were obtained from HI Media, located in Mumbai, India. These included Muller Hinton agar, Nutrient broth, Modified Eagle Medium (MEM), fetal bovine serum (FBS), trypsin, silver nitrate ($AgNO_3$), iodine, potassium iodide, magnesium ribbon, lead acetate, chloroform, concentrated sulfuric acid (Conc. H_2SO_4), potassium sodium tartrate, sodium hydroxide (NaOH), methanol, glacial acetic acid, ferric chloride ($FeCl_3$), dimethyl sulfoxide (DMSO), and hydrochloric acid (HCl). Additionally, two specific chemicals, 2,2 diphenyl 1 picrylhydrazyl (DPPH) and 3-(4,5-dimethylthiazol-2-yl)-2,5-diphenyl tetrazolium bromide (MTT), were purchased from Sigma Aldrich in Bangalore, India.

2.1. Preparation of Plant Extract

M. cymbalaria plant leaves were collected from Srivilliputtur, Tamil Nadu, India. Upon collection, the plants were immediately placed in sterilized Ziplock bags and transported to the laboratory. The specimens were authenticated by taxonomists at the Centre for Research and Postgraduate Studies in Botany, Ayya Nadar Janaki Ammal College, Sivakasi, Tamil Nadu, India. The leaves were then selected for further processing. To prepare the leaf samples, they were initially rinsed with water and subsequently left to dry under a sunshade. Once dried, the leaves were ground into a fine powder. For the extraction

process, 10 g of this powdered *M. cymbalaria* leaves was steeped in conical flasks containing 100 mL of double-distilled water. The mixture was agitated thoroughly and left undisturbed for five hours to ensure sufficient extraction. Following the extraction, the solution was filtered through a Whatman No. 1 filter paper to obtain a clear filtrate, which was then used to synthesize the *Mc*-AgNPs.

2.2. Phytochemical Analysis

The crude leaf extracts of *M. cymbalaria* were subjected to qualitative analysis to detect the presence of phytochemicals. Phytoconstituents, such as alkaloids [51], flavonoids [52], carbohydrates [53], phenols, and tannins [54], along with steroids, cardiac glycosides [55], terpenoids, and phlobatannins [56], were analyzed using the following established standard procedures.

2.3. Gas Chromatography-Mass Spectrometry (GC-MS) Analysis

Chemical analysis of the *M. cymbalaria* leaf extract was performed using a Gas Chromatography-Mass Spectrometry (GC-MS, Shimadzu, Tokyo, Japan) system equipped with a Thermal Desorption (TD) unit. The GC-MS apparatus featured an Rtx-5 capillary column (30 m $\times$ 0.25 mm, with a film thickness of 0.25 µm) and employed helium as the carrier gas at a constant flow rate of 1.21 mL/min. The oven temperature was programmed to rise from 60 °C to 200 °C at a rate of 5 °C per minute before a final ramp to 280 °C. Scans were carried out at m/z values ranging from 50 to 450. The mass fragmentation patterns of the compounds were identified using the NIST library, with the mass spectrometer operating at 70 eV.

2.4. Synthesis of AgNPs from M. cymbalaria

Silver nitrate served as the precursor for the synthesis of AgNPs. As detailed in a previous report, a 1 mM $AgNO_3$ solution (100 mL) was prepared by dissolving the silver nitrate in deionized water. This solution was then combined with the *M. cymbalaria* leaf extract at a 2:10 ratio and incubated in a dark area. After incubation, the sample was centrifuged at 10,000$\times$ *g* rpm for 15 min at 4 °C to obtain a clear supernatant. The resulting pellet was washed three times with deionized water [57].

2.5. Characterization of Mc-AgNPs

2.5.1. UV-Vis Spectroscopy

A noticeable color change occurred after incubating the *M. cymbalaria* (*Mc*) aqueous extract with the $AgNO_3$ solution. UV-visible spectroscopy (Shimadzu, Japan) was utilized to analyze the peaks of *Mc*-AgNPs within the wavelength range of 200 to 800 nm.

2.5.2. Fourier-Transform Infrared Spectroscopy (FT-IR) Analysis

The functional groups present in the green-synthesized *Mc*-AgNPs were characterized using Fourier Transform Infrared (FT-IR) spectroscopy to investigate the plant compounds responsible for the reduction of silver ions. The dried nanoparticle powders and the plant extract were mixed with KBr to form pellets, which were then analyzed with an FT-IR spectrometer (Spectrum 65, PerkinElmer, WA, USA).

2.5.3. X-ray Diffraction (XRD) Analysis

XRD analysis was conducted to determine the crystallinity, phase, and average crystallite size of the *Mc*-AgNPs. The synthesized nanoparticles were dispersed in ethanol and deposited onto a glass substrate for XRD analysis. The analysis was carried out using an Ultima IV-Rigaku diffractometer equipped with CuKα radiation (λ = 1.540 Å) at 45 kV and 30 mA, in Tokyo, Japan.

2.5.4. SEM and EDX Analysis

The dimensions and morphology of the *Mc*-AgNPs were analyzed using a Scanning Electron Microscope (SEM), specifically the Carl Zeiss Microscopy GmbH, EVO18 model from the Jena, Germany. To prepare the samples, the *Mc*-AgNPs were dispersed in 100% ethanol through ultrasonication. The solution was then deposited onto a glass slide and left to air-dry, allowing the solvent to evaporate completely. Subsequently, a thin layer of gold, approximately 3 nm in thickness, was sputtered onto the sample using a vacuum sputter coater. The SEM was equipped with an integrated Energy-Dispersive X-ray (EDX) analysis system (Quantax 200 with X Flash® 6130) to determine the elemental composition.

2.5.5. HR-TEM and SAED Analysis

The research utilized a high-resolution transmission electron microscope (HR-TEM) and the selected area diffraction pattern (SAED), specifically the JEOL-2100 model from JEOL India Pvt. Ltd., in New Delhi, India, with a magnification capability of 46,000×. Samples were prepared using the Formvar resin grid technique: a suspension of the synthesized nanoparticles at a weight-to-volume ratio of 0.5% was deposited onto a TEM grid coated with Formvar resin. The grid was air-dried for ten minutes before being examined. Photographs were captured to document the morphology of the nanoparticle aggregates.

2.6. DPPH-Radical-Scavenging Assay

A DPPH-radical-scavenging assay was developed to evaluate antioxidant properties by measuring the free-radical-scavenging activity. *Mc*-AgNPs were dissolved in deionized water at concentrations ranging from 200 to 1000 µg/mL. Ascorbic acid was used as a positive control. The assay commenced by mixing 0.1 mL of the *Mc*-AgNPs solution with 1 mL of a freshly prepared 0.1 mM DPPH solution in ethanol. After 20 min of vigorous shaking at room temperature, the absorbance at a wavelength of 517 nm was measured. A control sample, devoid of silver nanoparticles, was also prepared [58]. The radical-scavenging activity was calculated by measuring the reduction in DPPH absorbance using the following formula (Equation (1)):

$$Scavenging\ effect\ (\%) = \left[\frac{\mathrm{Ac} - \mathrm{As}}{\mathrm{Ac}}\right] \times 100 \quad (1)$$

where, Ac is the abs of the control, and As is the abs of the sample or standard.

2.7. Cytotoxicity Assay

The MCF-7 (breast cancer) and Vero cell line (non-cancerous) were cultured in DEME medium supplemented with 10% fetal bovine serum, 100 units/mL of penicillin, and streptomycin at 37 °C with 5% CO_2 and 95% relative humidity. The culture media were replaced twice a week. The in vitro cytotoxicity activity *Mc*-AgNPs was evaluated against the MCF-7 human breast cancer cell line and Vero cell lines using the 3-(4,5-dimethylthiazol-2-yl)-2,5-diphenyl tetrazolium bromide (MTT) assay [59]. Initially, 1×10^5 cells were seeded in a 96-well plate and allowed to attach for 24 h. The previous culture medium was then replaced with a medium containing various concentrations of *Mc*-AgNPs (1.95 to 1000 µg/mL), and the assay was triplicated. Doxorubicin was used as the reference drug (0.1 g/mL). After a 24 h incubation, the cells were washed three times with 1× PBS buffer, and MTT solution (5 mg/mL) was added. Following a 2 h incubation at 37 °C, the formed formazan crystals were diluted in 1 mL of dimethylsulfoxide (DMSO), and the absorbance was measured at 570 nm using a microplate reader (BMG Labtech in Ortenberg, Germany). The percentage of viability was calculated using the following formula [60] (Equation (2)).

$$\text{Cell viability}(\%) = [(\mathrm{OD}_{\text{sample}} - \mathrm{O.D.}_{\text{blank}})/\mathrm{O.D.}_{\text{conrtol}}] \times 100 \quad (2)$$

2.8. Antibacterial Activity

The bacterial strains, such as methicillin-resistant *Staphylococcus aureus* ATCC-43300 (MRSA), vancomycin-resistant *Enterococcus faecium* ATCC 49624 (VREF), *Escherichia coli* ATCC-25922, and *Serratia marcescens* ATCC-27137, were obtained from the American Type Culture Collection (ATCC). Muller Hinton Agar (MHA) was used as the medium to test the antibacterial efficacy of *Mc*-AgNPs via the Kirby-Bauer well-diffusion methods. The process involved pouring sterilized MHA onto sterile Petri plates and waiting for it to solidify. After the medium was ready, bacteria were inoculated onto the surface using a sterile cotton swab. In the well-diffusion method, wells were punched into the agar using a cork borer 15 min later. *Mc*-AgNPs were introduced into three separate wells at concentrations of 50 µg/mL, 100 µg/mL, and 150 µg/mL, which were made from a stock solution dissolved in 50% DMSO. The plates were incubated at 37 °C, and the inhibition zones were measured 24 h later to evaluate the antibacterial activity of *Mc*-AgNPs [61].

Microbial Growth Assay

The assessment of the antibacterial efficacy of *Mc*-AgNPs against bacterial pathogens was conducted by subjecting 10^7 colony-forming units (CFUs) of bacterial isolates to individual treatments with varying concentrations of *Mc*-AgNPs (100, 80, 60, 40, and 20 µg/mL). Following an initial incubation period of 1 h at 30 °C, bacterial colonies were quantified using an automated colony counter [62].

2.9. Photocatalytic Activity

The photodegradation of methylene blue dye solution was investigated under sunlight in a batch reactor system, utilizing the synthesized *Mc*-AgNPs as the catalyst [63]. An open-type rectangular tray measuring 16 × 15 × 5 cm and made of borosilicate glass was employed as a reactor to sustain the dye solution in sunlight-mediated photocatalysis. Methylene blue dye (0.159 g) was dissolved in distilled water to produce a 1 molar solution of 1 L. From this, 50 mL was taken and diluted to a 250 mL solution (500 ppm). This prepared solution was transferred to the rectangular tray and *Mc*-AgNPs (50 mg or 0.05 g) were added. One molar NaOH/HCl was used to maintain a neutral pH. The mixture of the 250 mL dye solution with a known concentration and the synthesized *Mc*-AgNPs nanocomposite was stirred vigorously using a magnetic stirrer at a medium rotation to attain equilibrium. After allowing the adsorption process to equilibrate, the mixture was exposed to sunlight for 30 min. UV-visible spectroscopy was used to analyze the solution to obtain the maximum absorption range. Then, the solution was irradiated in sunlight for 180 min with continuous stirring. Initially, the irradiated dye solution was collected within 10 min, and the remaining dye solution was collected at intervals every 20 min and then analyzed using a UV-Visible spectrophotometer. The ideal conditions for the photodegradation investigation were maintained under direct sunlight. Every 30 min, the amount of solar light was monitored, and the average amount of light over the course of each experiment was computed. The UV-Vis spectrophotometer measured the residual concentration of the dye solution at 665 nm. A digital lux meter was used to measure the intensity of light and sunshine throughout the reaction time, which was around 820 lux. Throughout the studies, the intensity remained almost constant.

The formula below was used for calculating the degradation percentage (Equation (3)).

$$\%\ \text{of degradation} = ((C0 - Ct)/(C0)) \times 100 \quad (3)$$

Where C0 was the initial absorbance of the dye solution and Ct was the absorbance at time intervals.

2.10. Statistical Analysis

All experiments were conducted in triplicate to ensure reproducibility. Statistical analyses were performed to assess the significance of differences between the measured

mean values using a two-tailed Student's *t*-test. A *p*-value of less than 0.05 was deemed to indicate statistical significance. All statistical calculations were performed using SPSS software (version 21.0; I.B.M. Corp., New York, NY, USA).

3. Results and Discussion

The presence of diverse phytochemicals in *M. cymbalaria* underscores its potential as a valuable source of bioactive compounds in Table 1. While our results support the potential pharmacological relevance of *M. cymbalaria* extracts, it is crucial to highlight the need for further investigations, including detailed chemical isolation and mechanistic studies. Identifying the compounds responsible for the observed bioactivities would provide a more comprehensive understanding of the plant's therapeutic potential. Moreover, contrary to some previous studies, the absence of tannins in the extract warrants additional exploration to elucidate the variability in the phytoconstituent compositions among different plant samples. The phytochemical profile of *M. cymbalaria* showcases its richness in bioactive compounds, opening avenues for future research on its medicinal and therapeutic applications. However, further studies are necessary to unravel the mechanisms underlying its observed pharmacological activities.

Table 1. Preliminary phytochemical analysis of *M. cymbalaria* extract.

S.No.	Phytochemical Class	*M. cymbalaria* Leaf Extract
1	Alkaloids	++
2	Flavonoids	++
3	Tannins	−
4	Phenols	+
5	Steroids	+
6	Saponin	++
7	Terpenoids	+
8	Carbohydrates	+
9	Phlobatannins	−

++ Indicates the presence of a high amount; + indicates the presence; − indicates the absence of the phytochemical.

3.1. GC-MS Analysis

The GC-MS analysis of the leaf extract of *M. cymbalaria* leaves provided valuable insights into the composition of phytocompounds present in the plant (Figure 1 and Table 2). Oleic acid emerged as the predominant compound, constituting 39.37% of the total composition. This finding aligns with previous studies highlighting the prevalence of oleic acid in various plant extracts, showcasing its significance in plant metabolism and potential health benefits [64–66]. *n*-Hexadecanoic acid (20.86%) and octadecanoic acid (11.26%) further contributed to the fatty acid profile of the extract. Fatty acids play crucial roles in plant development and are known for their diverse physiological functions [67,68]. Additionally, the presence of 5-hydroxymethylfurfural (8.49%), known for its antioxidant properties, adds another layer of potential health benefits associated with the extract [69]. The diverse classes of compounds, including esters, steroids, fatty acids, terpenes, aliphatic alcohols, and flavonoids, suggest the complex chemical composition of *Momordica cymbalaria*, contributing to its pharmacological significance [70]. It is noteworthy that while the identified compounds provide valuable information, further research is essential to explore the specific biological activities and potential synergistic effects of these phytocompounds. Comparative studies with other *Momordica* species may reveal unique chemical signatures and therapeutic potentials. Future studies should delve into the bioactivities associated with these compounds and their practical applications in medicine and nutrition.

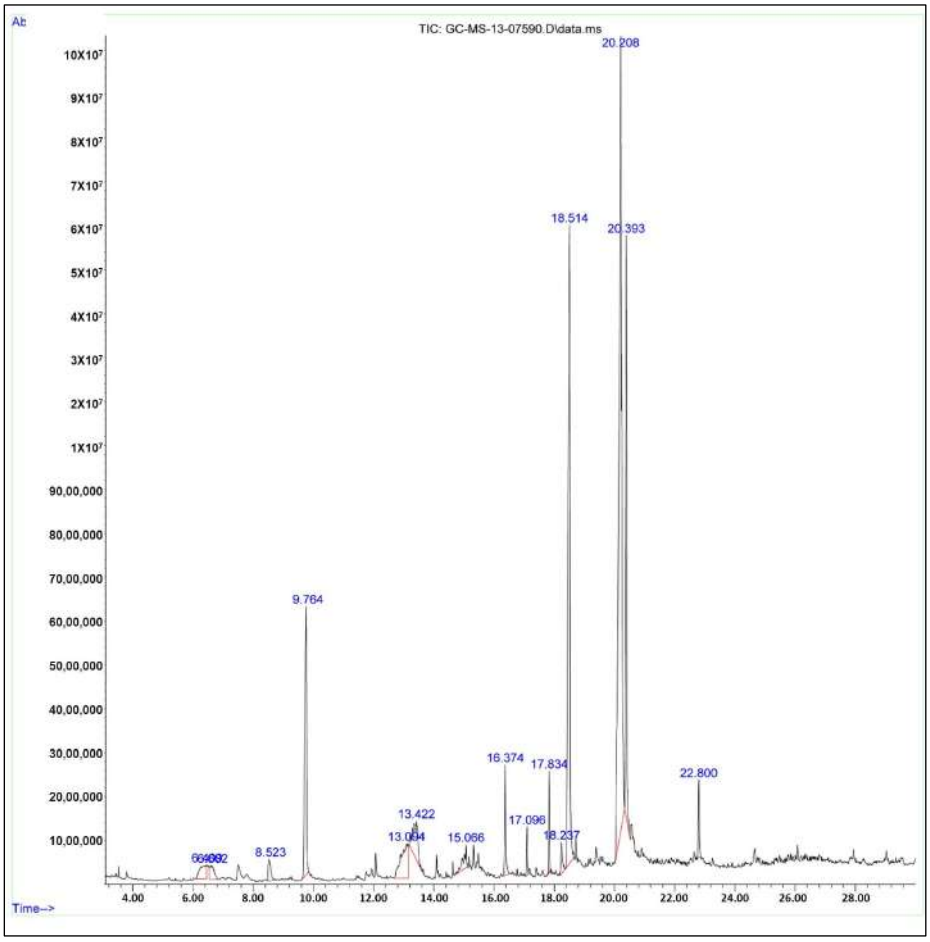

Figure 1. Analysis of bioactive compounds from *M. cymbalaria* via GC-MS.

Table 2. GC-MS profile of phytocompounds in *M. cymbalaria* extract.

Peak	R. Time	Area	Area%	Name
1	6.409	4,709,431	1.66	S-Methyl-L-cysteine, N-(ethoxyca…
2	6.602	3,217,202	1.14	S-Methyl-L-cysteine, N-(ethoxyca…
3	8.523	2,997,683	1.06	4H-Pyran-4-one, 2, 3-dihydro-3,5-…
4	9.764	24,034,843	8.49	5-Hydroxymethylfurfural
5	13.094	13,332,417	4.71	2-Isopropoxyethyl propionate
6	13.422	10,307,348	3.64	1,3-Dioxane, 4,4-dimethyl-
7	15.066	3,657,786	1.29	Humulenol-II
8	16.374	5,827,800	2.06	Tetradecanoic acid
9	17.096	2,281,005	0.81	Cyclohexanol, 3-ethenyl-3-methyl…
10	17.834	3,981,804	1.41	(3S,3aS,6R,7R,9aS)-1, 1, 7-Trimeth…
11	18.237	2,697,462	0.95	Palmitoleic acid
12	18.514	59,065,176	20.86	n-Hexadecanoic acid
13	20.208	111,488,797	39.37	Oleic Acid
14	20.393	31,876,258	11.26	Octadecanoic acid
15	22.800	3,678,672	1.30	Dehydroabietic acid

3.2. Green Synthesis of Mc-AgNPs

The silver nitrate was mixed with the plant extract, the silver ions from $AgNO_3$ bound to the plant proteins, and water-soluble compounds using –OH and –COOH groups, leading to conformational changes in the protein molecule, which contributed to the captured metal ion transformation into a silver nanoparticle [71]. In general, a metal nanoparticle synthesis mechanism using plants and plant extracts contains three main steps: (1) the phase of activation wherein metal ions are reduced and reduced metal atoms are nucleated; (2) the growth phase that is characterized by an increase in the thermodynamic stability of nanoparticles and the spontaneous coalescence of small adjacent nanoparticles into larger particles (direct formation of nanoparticles through heterogeneous nucleation and growth, and further metal ion reduction; a process referred to as an Ostwald ripening); (3) the final shape of the nanoparticles is determined at the process termination step.

3.3. Characterization of Mc-AgNPs

3.3.1. UV-Vis Spectroscopic Analysis

The aqueous leaf extract of *M. cymbalaria* was mixed with an $AgNO_3$ solution and initially turned into a pale yellow color. Then, after incubation at 8 h, the solution turned dark brown, indicating the synthesis of *Mc*-AgNPs. Similar observations were reported by other investigators who used plant extracts as a reducing agent [72,73]. Further, the UV-Vis spectroscopy, widely employed for identifying the structural properties of nanoparticles, revealed a distinct peak at 425 nm, indicating the broad size distribution and presence of AgNPs on the surface of the nanoparticles in the solution (Figure 2). This peak is attributed to the surface plasmon resonance of electrons [74]. The transformation of silver ions into silver nanoparticles began as soon as the reaction was initiated, with the complete reduction occurring within about two minutes at ambient conditions, which signifies the quick biosynthesis of the silver nanoparticles [75].

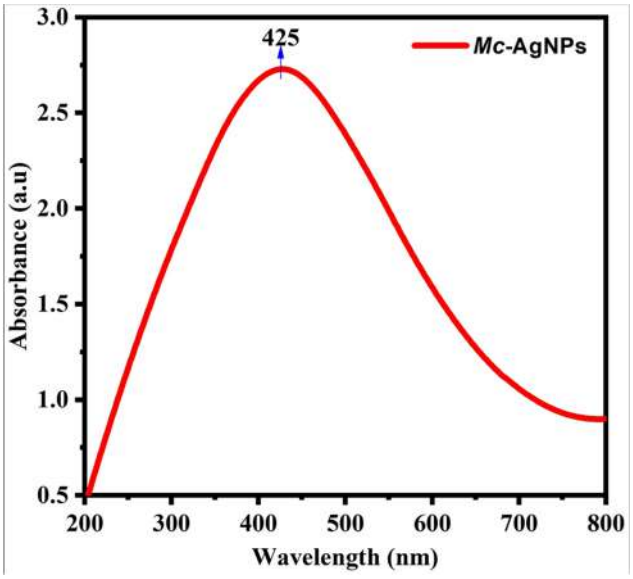

Figure 2. UV analysis of synthesized *Mc*-AgNPs. A peak of 425 nm demonstrates the production of AgNPs on the surface of nanoparticles in the solution due to the surface-plasma resonance (SPR) electrons.

3.3.2. FT-IR Analysis

The chemical composition and functional groups present in *Mc*-AgNPs were investigated using FT-IR spectroscopy. The probable biomolecules responsible for the capping and reduction of silver nanoparticles were determined using FT-IR spectroscopy. Figure 3 displays the FT-IR spectrum for the *Mc* aqueous extract and *Mc*-AgNPs. The strong and broad absorption peak observed at 3412.13 cm^{-1} represents the O-H stretching of water molecules. The characteristic peaks at 2930.79 cm^{-1} and 2854.58 cm^{-1} are attributed to

C-H stretching vibrations [14]. The peak at 2923.79 cm^{-1} corresponds to the medium C-H stretching of alkanes. The absorption at 2164.07 cm^{-1} is indicative of the strong C-N stretching of thiocyanate. The peaks at 2387.24 cm^{-1}, 2059.09 cm^{-1}, and 1745.72 cm^{-1} correspond to strong C=O stretching in the compound. The smaller peaks at 1626.27, 1403.57 cm^{-1}, and 1654.74 cm^{-1} are credited to the medium C=C stretching of disubstituted alkenes (cis) and medium O-H bending and medium C=N stretching of imines/oximes. The functional group C=C stretching of cyclic alkenes was observed at 1563.54 cm^{-1}. The minor peaks at 1250.38 and 1118.19 cm^{-1} were strongly related to the C-O stretching of aromatic esters and aliphatic/aryl ethers, respectively. The C-N stretching of amine groups was recorded at 1160.18 cm^{-1}. The sharp peaks at 1076.20 cm^{-1} correspond to the strong C-O stretching of primary alcohols. The presence of flavanones and terpenoids in the plants are evidenced by the absorption by AgNPs, confirmed by the presence of carbonyl (C=O) groups. These carbonyl groups strongly bind to AgNPs and act as stabilizing molecules [76].

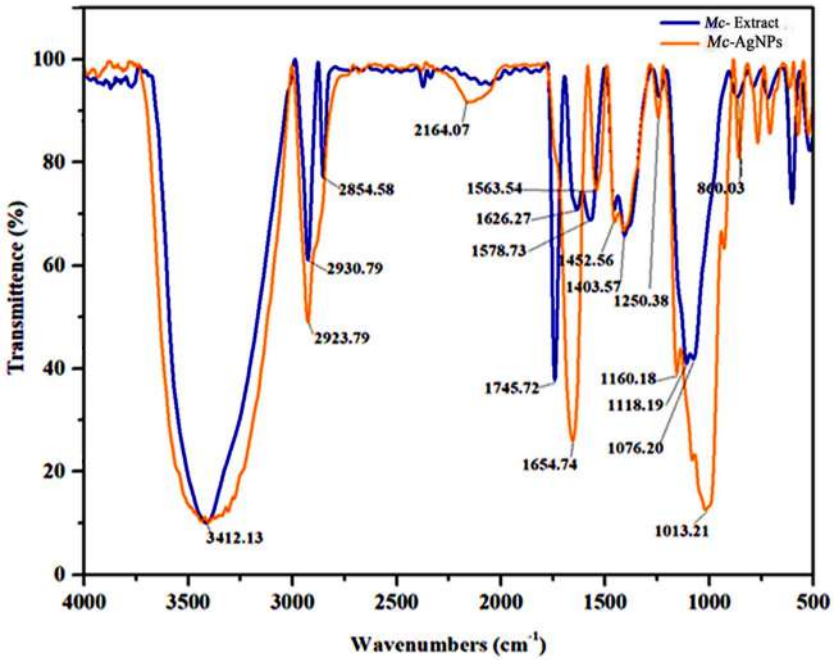

Figure 3. FT-IR spectrum of *Mc* and *Mc*-AgNPs.

3.3.3. XRD Analysis

The crystallographic characteristics of the *Mc*-AgNPs were determined through X-ray diffraction (XRD) analysis. The XRD spectrum highlighted several distinct peaks corresponding to the Bragg reflections, notably at 2θ angles of 38.15°, 44.48°, 64.56°, and 77.64°. These peaks were attributed to the (111), (200), (220), and (311) lattice planes, respectively, as shown in Figure 4. These lattice planes indicate the face-centered cubic (F.C.C.) structure, confirming the crystalline nature of the *Mc*-AgNPs, which is in alignment with the standard JCPDS card no: 84-0713. The presence of these peaks suggests that the plant-based synthesis approach yields well-defined crystalline nanoparticles, likely due to the presence of natural stabilizing compounds in the plant extracts that aid in maintaining the structural integrity of the nanoparticles. Comparative analysis suggests that the diffraction patterns of the *Mc*-AgNPs show remarkable similarity to those reported for nanoparticles synthesized using *Euphorbia antiquorum* and *Corallocarpus epigaeus*, which exhibit analogous diffraction features corresponding to the same indexed planes [77,78]. This similarity underscores a consistent crystalline structure among plant-mediated synthesized silver nanoparticles [79].

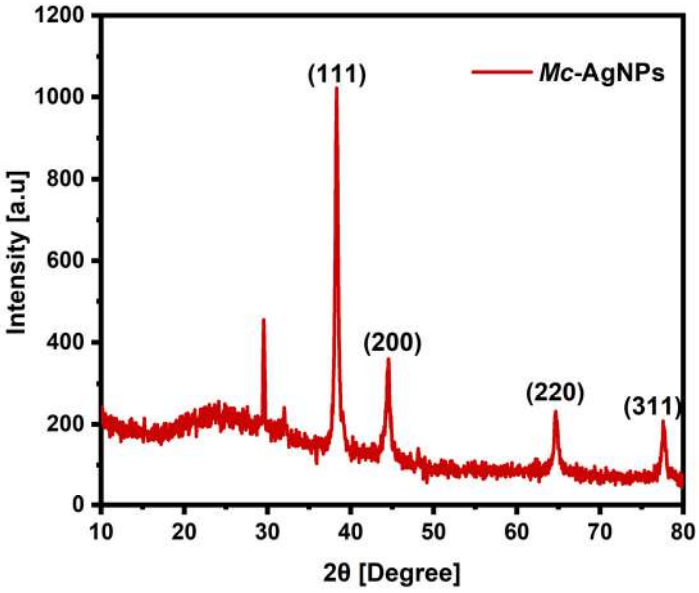

Figure 4. XRD analysis of *Mc*-AgNPs. The XRD revealed the formation of metallic Ag from Ag+ using the *M. cymbalaria* leaf extract.

3.3.4. SEM and E.D.X. Analysis

The SEM analysis was used to determine the size and shape of the *Mc*-AgNPs. According to the SEM analysis, the synthesized *Mc*-AgNPs had a cluster-like shape and significantly agglomerated. The SEM analysis of *Mc*-AgNPs is shown in Figure 5. Additionally, the dehydration that occurred during sample preparation for SEM analysis most likely contributed to the substantial aggregation of the biosynthesized AgNPs [80]. E.D.X. analysis determined the elemental makeup, atomic composition and weight percentage of the *Mc*-AgNPs. The E.D.X. analysis of *Mc*-AgNPs is shown in Figure 5. The study revealed certain contaminants, including carbon, oxygen, silicon, and very minute amounts of calcium and sodium. Oxygen and carbon were also present in the spectra. These elements were found to be essential for stabilizing and reducing biosynthesized AgNPs and were associated with the organic substances of the leaf extract on the surfaces of *Mc*-AgNPs [81].

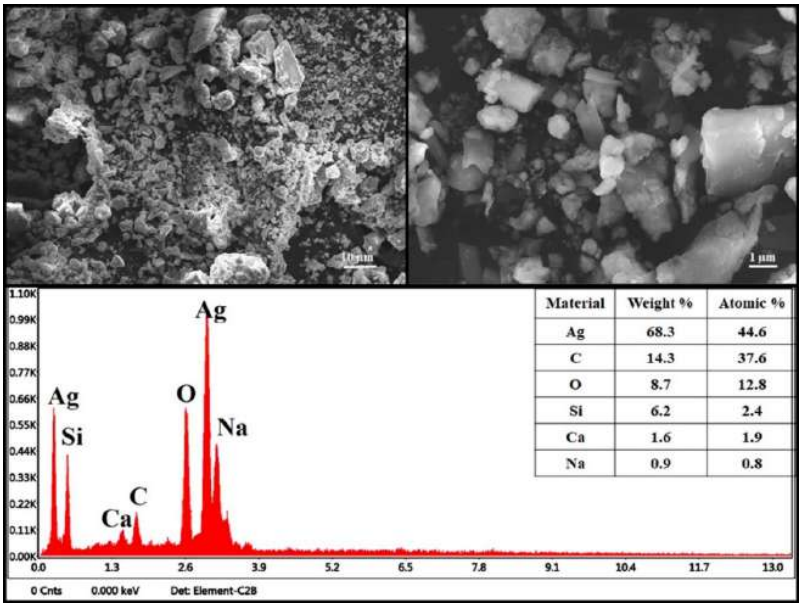

Figure 5. SEM and EDX analysis of *Mc*-AgNPs.

3.3.5. HR-TEM with SAED Analysis

Figure 6A displays the HR-TEM analysis of *Mc*-AgNPs. Most of the nanoparticles had a spherical shape in their morphology. It was discovered that some of the nanoparticles had an oval or elliptical shape. It is uncommon for biological systems to produce nanoparticles with varying degrees of sphericity and dimensionality. The noticeable distinction of lighter edges compared to the centers of the particles led researchers to hypothesize that proteins or other biomolecules enveloped the Ag nanoparticles [82]. HR-TEM examination revealed that most particles had a size of around 16 to 22 nm. Figure 6B presents an overview of the SAED pattern for the *Mc*-AgNPs. The synthesized silver nanoparticle (AgNP) crystallinity was confirmed through selected area electron diffraction (SAED) pattern analysis. The diffraction rings observed in the SAED patterns corresponded to the (111), (200), (220), and (311) planes, which are indicative of the fcc lattice structure commonly associated with *Mc*-AgNPs. This observation perfectly correlated with the XRD results, underscoring the spherical and crystalline nature of the NPs. High-resolution SAED images further substantiated the crystalline structure of the AgNPs, as demonstrated by the clear and consistent diffraction patterns across multiple magnifications [83].

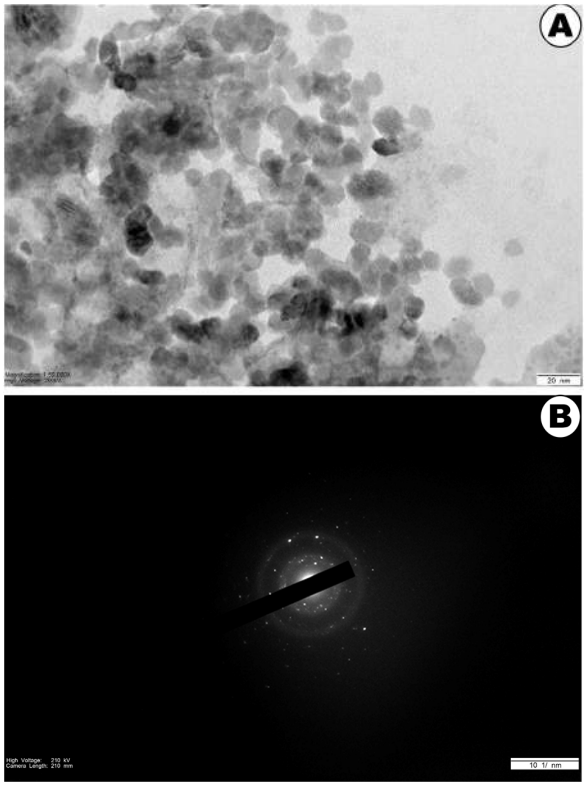

Figure 6. (**A**) HRTEM analysis for *Mc*-AgNPs (the synthesized nanoparticle was a cluster in morphology and highly agglomerated); (**B**) SAED analysis of Mc-AgNPs.

3.4. DPPH Assay

The antioxidant capacities of *Mc*-AgNPs were assessed using the DPPH assay. It is understood that DPPH-scavenging activities are related to hydrogen's ability to donate to different antioxidant molecules. Figure 7 depicts how the behavior of DPPH in radical scavenging is affected by various *Mc*-AgNP concentrations. *Mc*-AgNPs and ascorbic acid produced a potent inhibitory activity against DPPH radicals, a source of antioxidants. With higher concentrations, *Mc*-AgNPs' free radical scavenging ability seems to improve. Notably, at 1000 µg/mL, *Mc*-AgNPs showed more decisive antioxidant action, with a 67.77% inhibition rate, compared to ascorbic acid at 73.31%. Previous research has also indicated that as treatment doses are increased, antioxidant activity progressively rises [84–86]. As a result, the potential antioxidant capability of our synthesized *Mc*-AgNPs was evident.

Examining the ability of nanoparticles to quench neutrals revealed that *Mc*-AgNPs could produce free, stable neutral radicals from DPPH. Different facets of the antioxidant process were highlighted in the experimental investigations used. The DPPH assay showed that AgNPs donate electrons to neutralize the free radicals of unstable DPPH within the reaction medium [87].

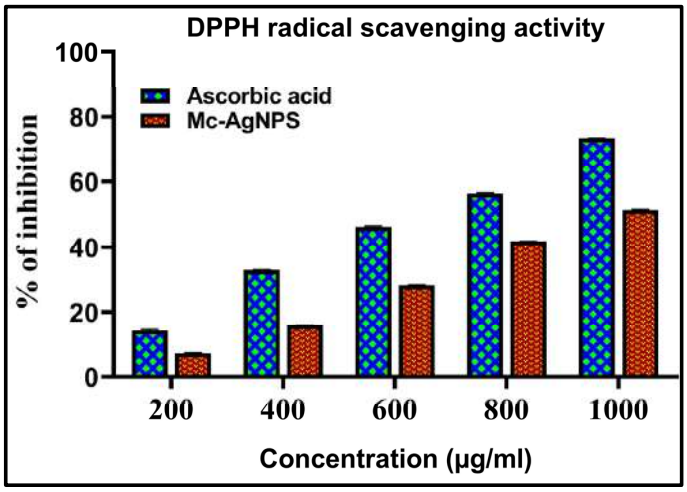

Figure 7. DPPH analysis of green synthesized *Mc*-AgNPs.

3.5. Cytotoxicity Activity

The cytotoxic effects of *Mc*-AgNPs were investigated on both MCF-7 cells and Vero cells. *Mc*-AgNPs had a dose-dependent cytotoxic impact on breast cancer cells. The IC_{50} values were 54.89 µg/mL for MCF-7 breast cancer cells and 160.74 µg/mL for the non-malignant Vero cells. Cytotoxicity assays indicated that Mc-AgNPs are more cytotoxic to cancer cells than to non-tumorigenic cells. Doxorubicin, used as a comparative standard, exhibited IC_{50} values of 2.04 µg/mL for MCF-7 cells and 3.08 µg/mL for Vero cells, as depicted in Figures 8 and 9 [88,89]. Likewise, the leaf extract of the *A. vulgaris*-mediated synthesis of AgNPs (*AV*-AgNPs) demonstrated an IC_{50} value of approximately 60 µg/mL for MCF-7 cells [87]. Due to improved cellular uptake and the retention of nanoparticles, *Cp*-AgNPs demonstrated a cytotoxicity gap in MCF-7 cell lines [90]. Despite their small size, nanoparticles resist P-glycoprotein efflux and can enter cells via endocytosis [91].

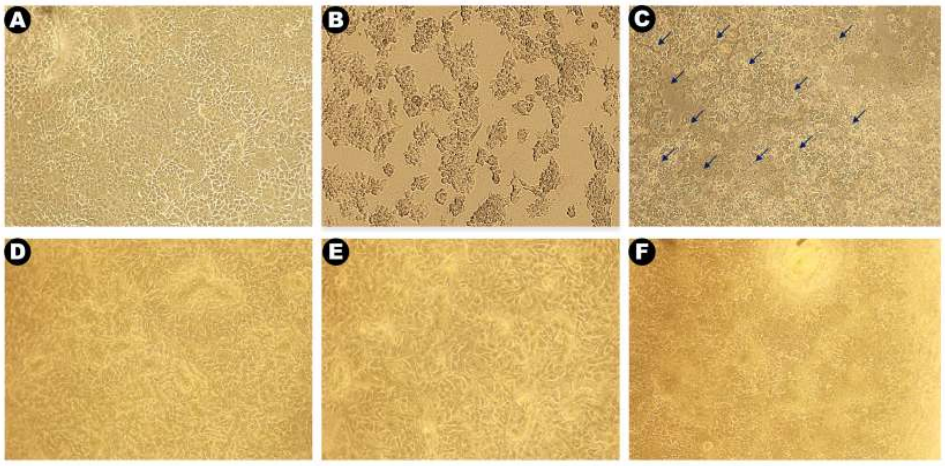

Figure 8. Anticancer activity of green synthesized *Mc*-AgNPs. (**A**) MCF-7 control; (**B**) MCF-7 treated with doxorubicin; (**C**) MCF-7 treated with *Mc*-AgNPs; (**D**) Vero cell line control, and (**E**) Vero cell line treated with doxorubicin; (**F**) Vero cell line treated with *Mc*-AgNPs.

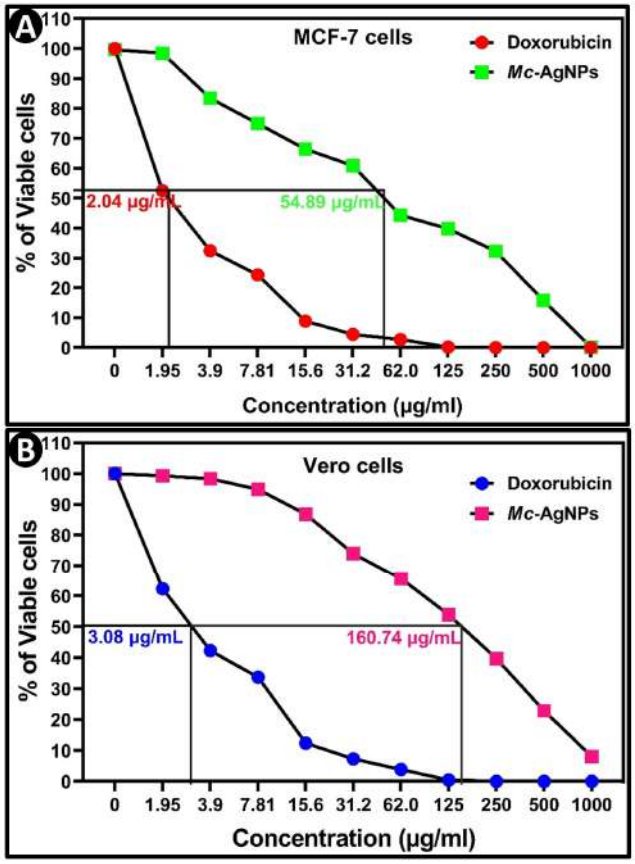

Figure 9. Determination of the IC_{50} value for *Mc*-AgNPs and Dox via an MTT assay; (**A**) MCF-7 cells (**B**) Vero cells.

3.6. Antibacterial Activity

Multi-drug resistance has been a significant obstacle to promising antibiotic therapeutics and necessitates the development of a medication with nanoforumulations to tackle resistant bacterial strains [92]. In this study, the antibacterial activity of biosynthesized *Mc*-AgNPs was evaluated by using the well-diffusion method, against a selection of four bacterial pathogens: Gram-positive (*E. coli* ATCC-25922, and *S. marcescens* ATCC-27137) and Gram-negative (MRSA ATCC-43300, and VREF ATCC-49624). Concerning the zone of inhibition for each strain of bacteria, *Mc*-AgNPs exhibited a significant level of inhibition of *E. coli*, followed by *S. marcescens*, MRSA, and VREF, respectively. The maximum zone of inhibition observed for *E. coli* at the highest dose of *Mc*-AgNPs was 17.33 mm (Figure 10). *Mc*-AgNPs exhibited dose-dependent antibacterial efficacy against all the bacterial pathogens. In the present study, the inhibitory action of *Mc*-AgNPs was comparatively low for Gram-negative bacteria. This difference in susceptibility is often attributed to the structural variations in the cell walls of these two types of bacteria [93]. Gram-positive bacteria have a thick peptidoglycan layer in their cell walls, making them more susceptible to the action of nanoparticles. On the other hand, Gram-negative bacteria have a thinner peptidoglycan layer and an outer membrane made up of LPS, lipoproteins, and phospholipids that act as a penetration barrier and only permit the entry of macromolecules [94]. The silver ions from the nanoparticles are attracted to the negative charge of the bacterial cell wall. When they encounter electrostatic attraction, they migrate and bind to the bacterial cell wall, influencing the permeability of the cell wall and altering its structure [75]. The DNA of microorganisms loses its ability to replicate and to produce cellular proteins, such as ribosome subunits. After exposure to Ag+ ions, most of the enzymes necessary to produce ATP become inactive [95]. In our study, chloramphenicol was used as a positive control. The synthesized *Mc*-AgNPs had low antibacterial efficacy, when compared to

chloramphenicol. Contreras and Vazquez (1977) reported that chloramphenicol inhibited translation by preventing the peptidyl transferase reaction or translocation step on the 50S component of the bacterial ribosome [96].

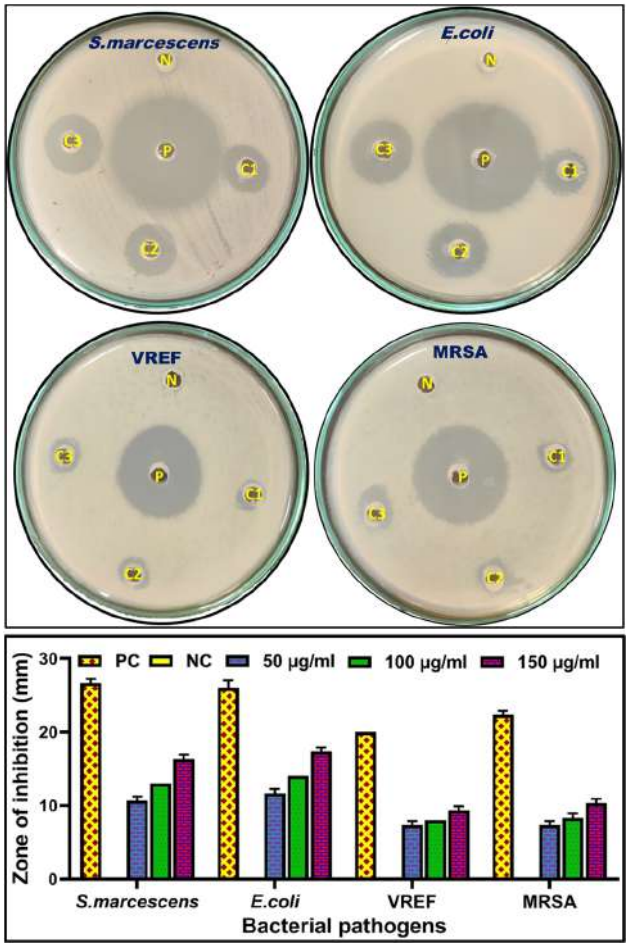

Figure 10. Antibacterial activity of green synthesized *Mc*-AgNPs against different clinical pathogenic bacteria.

Microbial Growth Assay

Microbial growth assays were conducted to evaluate the bactericidal activity of *Mc*-AgNPs against MRSA, VREF, *E. coli*, and *S. marcescens*. Bacterial isolates, numbering approximately 10^7 colony-forming units (CFUs), were exposed to varying concentrations of Ag-NPs (100, 80, 60, 40, and 20 µg/mL) and cultured on Mueller-Hinton agar (MHA) plates. Following treatment, a notable reduction in the colony count was observed for all four pathogens after 24 h, particularly with concentrations of 60 and 80 µg/mL of *Mc*-AgNPs. The observed reduction in colony numbers suggests the bactericidal efficacy of AgNPs against the tested microbial strains (Figure 11). The mechanism of action of *Mc*-AgNPs involves anchoring to the bacterial cell wall at multiple sites, followed by penetration and the induction of structural changes. This process leads to cell wall perforations, resulting in intracellular substance leakage [97]. Dizaj et al. (2014) suggested that AgNPs interact with the cell wall, causing disruptive effects [98]. Moreover, upon penetration, *Mc*-AgNPs release silver ions, which, in turn, generate reactive oxygen species. This oxidative stress affects membrane proteins and disrupts the electron transport chain [99]. The cumulative effect of these processes contributes to the observed bactericidal activity of *Mc*-AgNPs against bacteria, providing insights into their potential as antibacterial agents.

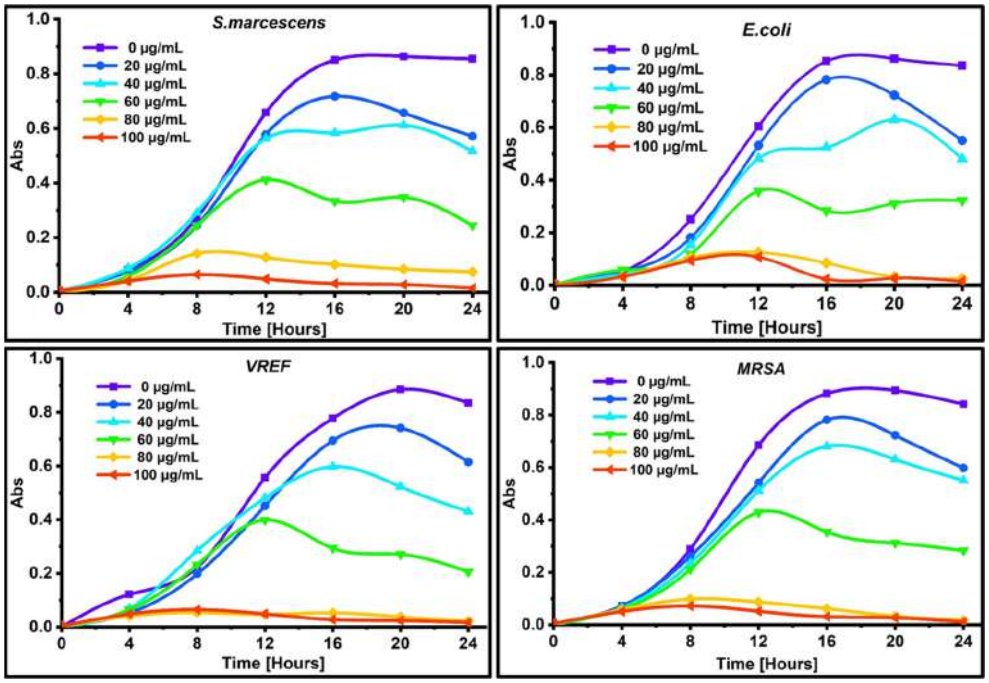

Figure 11. Microbial growth assay using *Mc*-AgNPs.

3.7. Photocatalytic Studies

For the past several years, the photocatalytic degradation of hazardous organic pollutants has drawn significant interest from researchers worldwide. Particularly toxic and non-biodegradable, colored organic dyes from the textile and paper industries harm the environment. Seventy percent of the dye material, sourced from azo dyes, severely pollutes the environment by dispersing potentially harmful particles into the aquatic system [100]. However, the conventional bio-treatment methods for degrading dye wastewater have recently been costly and ineffective due to the stability and aromatic complex structures of these organic dyes [101]. As a photocatalyst, metal oxide nanoparticles have shown remarkable effectiveness in mineralizing various environmental contaminants, including detergents, dyes, and volatile organic compounds [102]. Various metal oxides, such as Ag_2O, TiO_2, ZnO, WO_3, Fe_2O_3, and CuO, have recently been used as essential photocatalysts for degrading organic dye pollutants in water and air [103].

The environmental concern of the photocatalytic nature and efficiency of the synthesized nanocomposite was evaluated effectively. Figure 12A shows the UV-Vis absorption spectra of an organic dye molecule, like methylene blue, when exposed to sunlight with a maximum light intensity of approximately 860–980 lux from 11.30 am to 2.30 pm. The sample solutions were collected at several time intervals, such as 0, 10, 30, 50, 70, 90, 120, and 180 min, in the presence of *Mc*-AgNPs nanocomposites as the photocatalysts. Decolorization was observed during the degradation study and may be due to damage to the sulfur-nitrogen bonds in the MB solution. After the degradation study, CO_2 and H_2O were formed along with degraded products. From the studies, the maximum photodegradation percentage obtained for methylene blue for each sample in the presence of the synthesized catalyst, *Mc*-AgNPs, was found to be around 60%. The photodegradation percentage values of MB dye in the presence of the *Mc*-AgNPs nanocomposites after 180 min of exposure are shown in Figure 12B. From Table 3, *Mc*-AgNPs have higher photocatalytic activity against M.B. dye than some other reported plant-mediated silver nanoparticles.

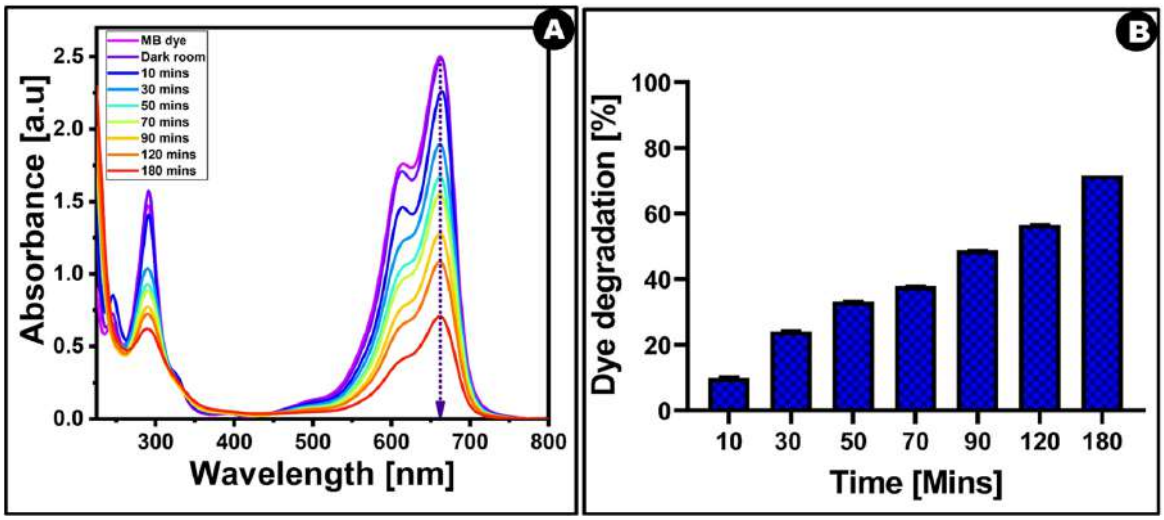

Figure 12. (**A**) Photocatalytic activity of green synthesized *Mc*-AgNPs; (**B**) Photodegradation of methylene blue dye in the presence of the green synthesized *Mc*-AgNPs.

Table 3. Comparison of photocatalytic activity of some silver nanoparticles against MB dye.

S.No	Catalyst	Pollutant	Degradation Efficiency (%) and Time	References
1	*Morinda tinctoria*-Ag	MB	95.3% & 72 h	[104]
2	Honey-Ag	MB	92% & 72 h	[105]
3	*Imperata cylindrical*-Ag	MB	92.06% & 14 min	[106]
4	*Gymnema sylvestre*-Ag	MB	95% & 7 h	[107]
5	*Peltophorum pterocarpu*m-Ag	MB	82% & 6 min	[108]
6	*Camellia sinensis*-Ag	MB	95% & 72 h	[109]
7	*Momordica cymbalaria*-Ag	MB	60% & 3 h	Present work

The photocatalytic degradation process induces the degradation of MB. The destruction of MB was probable owing to the production of an electron and hole pair on the catalyst surface during light-source radiation. The electron and hole pair intermingled with a water molecule, generating hydroxyl radicals. This is accountable for breaking the harmful MB components. Electrons in the conduction band on the catalyst's surface alter the molecular oxygen to superoxide ions and ultimately form hydrogen peroxide. The hole generates a hydroxyl radical, which plays an important role in the breakage of MB molecules [110].

$$Mc - \text{AgNPS} + h\nu \rightarrow Mc - \text{AgNPS}\left(e^-_{CB} + h^+_{VB}\right) \qquad h^+_{VB} + \text{MB} \rightarrow \text{MB}^+ \rightarrow \text{Oxidation of MB}$$

$$h^+_{VB} + H_2O\left(OH^-\right) \rightarrow OH + H^+$$

$$OH + \text{MB dye} \rightarrow CO_2 + H_2O$$

Reusability Test and Stability Analysis of Mc-AgNPs

Regeneration and reusability are significant factors in the field of catalysis for an environmental friendly and cost-effective point of view. To evaluate the stability of the *Mc*-AgNPs, a reusability study was performed on the degradation of methylene blue dye. The catalyst was collected after the completion of the degradation study and washed, dried, and used for the reusability study. The degradation efficiency was slightly decreased during the degradation study and may be due to the loss of catalyst weight while washing and

drying. The degradation efficiency was found to be 60% in cycle I and gradually decreased after cycle IV, which was found to be 51%. Figure 13A shows the reusability study of the *Mc*-AgNPs against MB dye.

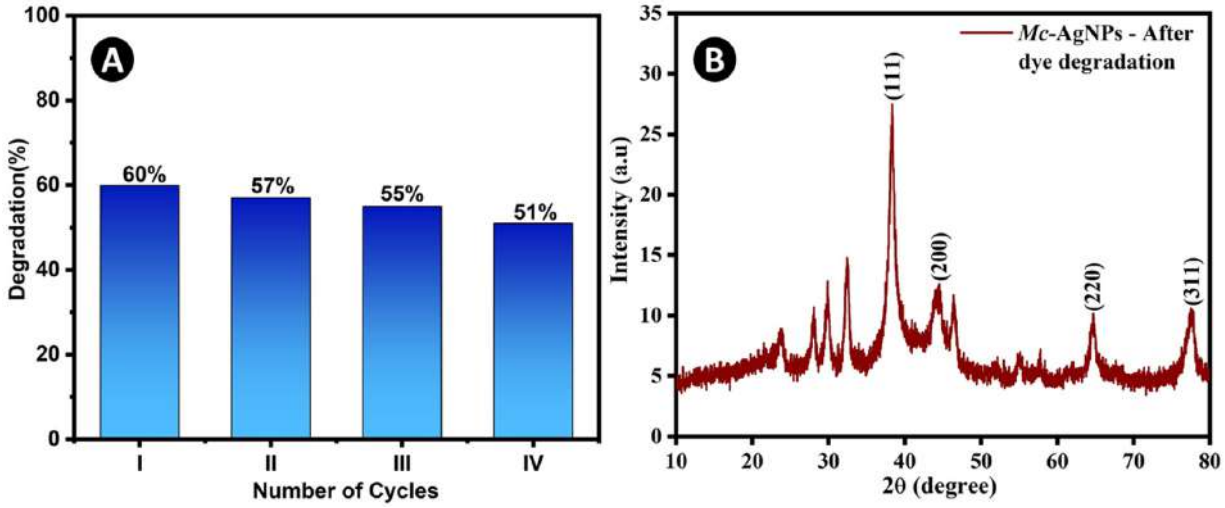

Figure 13. (**A**) Reusability test of *Mc*-AgNPs; (**B**) XRD analysis of *Mc*-AgNPs after recycling.

The *Mc*-AgNPs are moderately stable up to the IV cycle in the degradation of MB. However, the stability of the catalyst after the degradation process was investigated using XRD (Figure 13B). The results confirmed that the crystallinity of the *Mc*-AgNPs became lower, and impurity peaks appeared after the 4th cycle. This may be due to the catalyst's photo corrosion and photo dissolution.

4. Conclusions

In this study, an aqueous leaf extract from *M. cymbalaria* was successfully utilized to synthesize silver nanoparticles, where the extract plays an important role as a capping agent. In addition, the synthesized *Mc*-AgNPs show bacterial-inhibitory effects against MDR bacterial strains. The synthesized *Mc*-AgNPs exhibit potent scavenging properties and act as a defense activator against MCF-7 cells while exhibiting lower toxicity to *Mc*-AgNP-treated Vero cells. According to the results of the photocatalytic analysis, *Mc*-AgNPs were effective at degrading methylene blue dye when exposed to sunlight. As a result, the textile and water purification industries stand to gain a great deal from this. Our findings unequivocally corroborate the theory that plant-mediated nanoparticles will soon be able to be used as potent therapeutic agents against human pathogens to treat diseases brought on by free radicals and purify wastewater by eliminating harmful dyes.

Author Contributions: Conceptualization: M.S., G.R., S.P.K. and S.M.; Methodology: S.P.K. and S.M.; Investigation: M.S., G.R. and A.N.; Validation: M.S., G.R., and A.N.; Writing—Original draft preparation: M.S., G.R. and A.N.; Writing—review and editing: S.P.K. and S.M. All authors reviewed the results and approved the final version of the manuscript.

Funding: This research received no external funding.

Data Availability Statement: On request, the author will provide the data.

Conflicts of Interest: The authors declare no conflicts of interest.

References

1. He, X.; Deng, H.; Hwang, H.M. The current application of nanotechnology in food and agriculture. *J. Food Drug Anal.* **2019**, *27*, 1–21. [CrossRef] [PubMed]
2. Mariappan, V.; Vellasamy, K.M.; Mohamad, N.A.; Subramaniam, S.; Vadivelu, J. OneHealth approaches contribute towards antimicrobial resistance: Malaysian perspective. *Front. Microbiol.* **2021**, *12*, 718774. [CrossRef] [PubMed]
3. Shankar, P.R. Book review: Tackling drug-resistant infections globally. *Arch. Pharm. Pract.* **2016**, *7*, 110–111. [CrossRef]

4. Sánchez-López, E.; Gomes, D.; Esteruelas, G.; Bonilla, L.; Lopez-Machado, A.L.; Galindo, R.; Cano, A.; Espina, M.; Ettcheto, M.; Camins, A.; et al. Metal-based nanoparticles as antimicrobial agents: An overview. *Nanomaterials* **2020**, *10*, 292. [CrossRef] [PubMed]
5. Ferlay, J.; Colombet, M.; Soerjomataram, I.; Mathers, C.; Parkin, D.M.; Piñeros, M.; Znaor, A.; Bray, F. Estimating the global cancer incidence and mortality in 2018: GLOBOCAN sources and methods. *Int. J. Cancer* **2019**, *144*, 1941–1953. [CrossRef] [PubMed]
6. Curigliano, G.; Criscitiello, C. Successes and limitations of targeted cancer therapy in breast cancer. *Successes Limit. Target. Cancer Ther.* **2014**, *41*, 15–35.
7. Kumari, P.; Ghosh, B.; Biswas, S. Nanocarriers for cancer-targeted drug delivery. *J. Drug Target.* **2016**, *24*, 179–191. [CrossRef]
8. Tang, X.; Cai, S.; Zhang, R.; Liu, P.; Chen, H.; Zheng, Y.; Sun, L. Paclitaxel-loaded nanoparticles of star-shaped cholic acid-core PLA-TPGS copolymer for breast cancer treatment. *Nanoscale Res. Lett.* **2013**, *8*, 420. [CrossRef]
9. Abdalla, A.M.; Xiao, L.; Ullah, M.W.; Yu, M.; Ouyang, C.; Yang, G. Current challenges of cancer anti-angiogenic therapy and the promise of nanotherapeutics. *Theranostics* **2018**, *8*, 533. [CrossRef] [PubMed]
10. Khan, A.U.; Yuan, Q.; Khan, Z.U.H.; Ahmad, A.; Khan, F.U.; Tahir, K.; Shakeel, M.; Ullah, S. An eco-benign synthesis of AgNPs using aqueous extract of Longan fruit peel: Antiproliferative response against human breast cancer cell line MCF-7, antioxidant and photocatalytic deprivation of methylene blue. *J. Photochem. Photobiol. B Biol.* **2018**, *183*, 367–373. [CrossRef] [PubMed]
11. Alsukaibi, A.K. Various approaches for the detoxification of toxic dyes in wastewater. *Processes* **2022**, *10*, 1968. [CrossRef]
12. Khan, A.U.; Yuan, Q.; Wei, Y.; Tahir, K.; Khan, S.U.; Ahmad, A.; Khan, S.; Nazir, S.; Khan, F.U. Ultra-efficient photocatalytic deprivation of methylene blue and biological activities of biogenic silver nanoparticles. *J. Photochem. Photobiol. B Biol.* **2016**, *159*, 49–58. [CrossRef]
13. Narayan, N.; Meiyazhagan, A.; Vajtai, R. Metal nanoparticles as green catalysts. *Materials* **2019**, *12*, 3602. [CrossRef]
14. Tanase, C.; Berta, L.; Coman, N.A.; Roșca, I.; Man, A.; Toma, F.; Mocan, A.; Jakab-Farkas, L.; Biró, D.; Mare, A. Investigation of in vitro antioxidant and antibacterial potential of silver nanoparticles obtained by biosynthesis using beech bark extract. *Antioxidants* **2019**, *8*, 459. [CrossRef]
15. Behboodi, S.; Baghbani-Arani, F.; Abdalan, S.; Sadat Shandiz, S.A. Green engineered biomolecule-capped silver nanoparticles fabricated from *Cichorium intybus* extract: In vitro assessment on apoptosis properties toward human breast cancer (MCF-7) cells. *Biol. Trace Elem. Res.* **2019**, *187*, 392–402. [CrossRef] [PubMed]
16. Alqudami, A.; Annapoorni, S. Fluorescence from metallic silver and iron nanoparticles prepared by exploding wire technique. *Plasmonics* **2007**, *2*, 5–13. [CrossRef]
17. Jyoti, K.; Baunthiyal, M.; Singh, A. Characterization of silver nanoparticles synthesized using *Urtica dioica* Linn. leaves and their synergistic effects with antibiotics. *J. Radiat. Res. Appl. Sci.* **2016**, *9*, 217–227. [CrossRef]
18. Sharma, N.K.; Vishwakarma, J.; Rai, S.; Alomar, T.S.; AlMasoud, N.; Bhattarai, A. Green route synthesis and characterization techniques of silver nanoparticles and their biological adeptness. *ACS Omega* **2022**, *7*, 27004–27020. [CrossRef] [PubMed]
19. Gengan, R.M.; Anand, K.; Phulukdaree, A.; Chuturgoon, A. A549 lung cell line activity of biosynthesized silver nanoparticles using *Albizia adianthifolia* leaf. *Colloids Surf. B Biointerfaces* **2013**, *105*, 87–91. [CrossRef] [PubMed]
20. Kumar, D.; Kumar, P.; Singh, H.; Agrawal, V. Biocontrol of mosquito vectors through herbal-derived silver nanoparticles: Prospects and challenges. *Environ. Sci. Pollut. Res.* **2020**, *27*, 25987–26024. [CrossRef] [PubMed]
21. Adeyemi, J.O.; Oriola, A.O.; Onwudiwe, D.C.; Oyedeji, A.O. Plant extracts mediated metal-based nanoparticles: Synthesis and biological applications. *Biomolecules* **2022**, *12*, 627. [CrossRef]
22. Rajan, R.; Chandran, K.; Harper, S.L.; Yun, S.I.; Kalaichelvan, P.T. Plant extract synthesized silver nanoparticles: An ongoing source of novel biocompatible materials. *Ind. Crops Prod.* **2015**, *70*, 356–373. [CrossRef]
23. Jeyadevi, R.A.; Sivasudha, T.; Rameshkumar, A.; Sangeetha, B.; Ananth, D.A.; Aseervatham, G.S.B. Nutritional constituents and medicinal values of *Momordica cymbalaria* (Athalakkai)–A review. *Asian Pac. J. Trop. Biomed.* **2012**, *2*, S456–S461. [CrossRef]
24. Gopu, C.; Chirumamilla, P.; Kagithoju, S.; Taduri, S. Green synthesis of silver nanoparticles using *Momordica cymbalaria* aqueous leaf extracts and screening of their antimicrobial activity: AgNPs studies in *Momordica cymba-laria*. *Proc. Natl. Acad. Sci. India Sect. B Biol. Sci.* **2022**, *92*, 771–782. [CrossRef]
25. Sundar, M.; Suresh, S.; Lingakumar, K. Influence of *Caralluma adscendens* Var. *attenuata* cold cream on UV-B damaged skin epidermal cells: A novel approach. *3 Biotech* **2021**, *11*, 155. [CrossRef]
26. Anand, T.; Sundararajan, M.; Anbukkarasi, M.; Thomas, P.A.; Geraldine, P.A. methanolic extract of *Ocimum basilicum* exhibits antioxidant effects and prevents selenite-induced cataract formation in cultured lenses of Wistar rats. *Pharmacogn. J.* **2019**, *11*, 496–504. [CrossRef]
27. Swamy, M.K.; Akhtar, M.S.; Mohanty, S.K.; Sinniah, U.R. Synthesis and characterization of silver nanoparticles using fruit extract of *Momordica cymbalaria* and assessment of their in vitro antimicrobial, antioxidant and cytotoxicity activities. *Spectrochim. Acta A Mol. Biomol. Spectrosc.* **2015**, *151*, 939–944. [CrossRef] [PubMed]
28. Jha, D.K.; Koneri, R.; Samaddar, S. Potential bio-resources of *Momordica dioica* roxb: A review. *Int. J. Pharm. Sci. Rev. Res.* **2017**, *45*, 203–209.
29. Kumar, A.; Dubey, A.; Singh, R. Investigation on Anti-Ulcer Activity of *Momordica dioica* Fruits in Wistar Rat. *Int. J. Res. Appl. Sci. Biotechnol.* **2022**, *9*, 105–111. [CrossRef]
30. Choudhary, B.R.; Berwal, M.K.; Ram, H.; Choudhary, M.K.; Singh, D. Momordica balsamina L.: An unexploited vegetable crop rich in medicinal and nutritional properties. *J. Agric. Ecol.* **2022**, *14*, 84–92. [CrossRef]

31. Elangovan, A.; Subramanian, A.; Durairaj, S.; Ramachandran, J.; Lakshmanan, D.K.; Ravichandran, G.; Nambirajan, G.; Thilagar, S. Antidiabetic and hypolipidemic efficacy of skin and seed extracts of *Momordica cymbalaria* on alloxan induced diabetic model in rats. *J. Ethnopharmacol.* **2019**, *241*, 111989. [CrossRef]
32. Ramesh, M.; Rao, Y.N.; Rao, A.A.; Prabhakar, M.C.; Rao, C.S.; Muralidhar, N.; Reddy, B.M. Antinociceptive and anti-inflammatory activity of a flavonoid isolated from *Caralluma attenuata*. *J. Ethnopharmacol.* **1998**, *62*, 63–66. [CrossRef]
33. Jia, R.B.; Wu, J.; Li, Z.R.; Ou, Z.R.; Lin, L.; Sun, B.; Zhao, M. Structural characterization of polysaccharides from three seaweed species and their hypoglycemic and hypolipidemic activities in type 2 diabetic rats. *Int. J. Biol. Macromol.* **2020**, *155*, 1040–1049. [CrossRef]
34. Jain, A.; Soni, M.; Deb, L.; Jain, A.; Rout, S.P.; Gupta, V.B.; Krishna, K.L. Antioxidant and hepatoprotective activity of ethanolic and aqueous extracts of *Momordica dioica* Roxb. leaves. *J. Ethnopharmacol.* **2008**, *115*, 61–66. [CrossRef]
35. Jha, D.K.; Koneri, R.; Samaddar, S. Medicinal use of an ancient herb *Momordica cymbalaria*: A review. *Int. J. Pharm. Sci. Res.* **2018**, *9*, 432–441.
36. Ahn, E.Y.; Jin, H.; Park, Y. Assessing the antioxidant, cytotoxic, apoptotic and wound healing properties of silver nanoparticles green-synthesized by plant extracts. *Mater. Sci. Eng. C* **2019**, *101*, 204–216. [CrossRef] [PubMed]
37. Fahimirad, S.; Ajalloueian, F.; Ghorbanpour, M. Synthesis and therapeutic potential of silver nanomaterials derived from plant extracts. *Ecotoxicol. Environ. Saf.* **2019**, *168*, 260–278. [CrossRef] [PubMed]
38. Haggag, E.G.; Elshamy, A.M.; Rabeh, M.A.; Gabr, N.M.; Salem, M.; Youssif, K.A.; Samir, A.; Bin Muhsinah, A.; Alsayari, A.; Abdelmohsen, U.R. Antiviral potential of green synthesized silver nanoparticles of *Lampranthus coccineus* and *Malephora lutea*. *Int. J. Nanomed.* **2019**, *14*, 6217–6229. [CrossRef] [PubMed]
39. Totaro, P.; Rambaldini, M. Efficacy of antimicrobial activity of slow release silver nanoparticles dressing in post-cardiac surgery mediastinitis. *Interact. Cardiovasc. Thorac. Surg.* **2009**, *8*, 153–154. [CrossRef] [PubMed]
40. Bobo, D.; Robinson, K.J.; Islam, J.; Thurecht, K.J.; Corrie, S.R. Nanoparticle-based medicines: A review of FDA-approved materials and clinical trials to date. *Pharm. Res.* **2016**, *33*, 2373–2387. [CrossRef]
41. Buniyamin, I.; Akhir, R.M.; Asli, N.A.; Khusaimi, Z.; Malek, M.F.; Mahmood, M.R. Nanotechnology applications in biomedical systems. *Curr. Nanomater.* **2022**, *7*, 167–180. [CrossRef]
42. Waghchaure, R.H.; Adole, V.A. Biosynthesis of metal and metal oxide nanoparticles using various parts of plants for antibacterial, antifungal and anticancer activity: A review. *J. Indian Chem. Soc.* **2023**, *100*, 100987. [CrossRef]
43. Chandrasekharan, S.; Chinnasamy, G.; Bhatnagar, S. Sustainable phyto-fabrication of silver nanoparticles using *Gmelina arborea* exhibit antimicrobial and biofilm inhibition activity. *Sci. Rep.* **2022**, *12*, 156. [CrossRef] [PubMed]
44. Shreyash, N.; Bajpai, S.; Khan, M.A.; Vijay, Y.; Tiwary, S.K.; Sonker, M. Green synthesis of nanoparticles and their biomedical applications: A review. *ACS Appl. Nano Mater.* **2021**, *4*, 11428–11457. [CrossRef]
45. Jabeen, S.; Qureshi, R.; Munazir, M.; Maqsood, M.; Munir, M.; Shah, S.S.H.; Rahim, B.Z. Application of green synthesized silver nanoparticles in cancer treatment—A critical review. *Mater. Res. Express* **2021**, *8*, 092001. [CrossRef]
46. Sanpui, P.; Chattopadhyay, A.; Ghosh, S.S. Induction of apoptosis in cancer cells at low silver nanoparticle concentrations using chitosan nanocarrier. *ACS Appl. Mater. Interfaces* **2011**, *3*, 218–228. [CrossRef] [PubMed]
47. Kumar, H.; Bhardwaj, K.; Nepovimova, E.; Kuča, K.; Singh Dhanjal, D.; Bhardwaj, S.; Bhatia, S.K.; Verma, R.; Kumar, D. Antioxidant functionalized nanoparticles: A combat against oxidative stress. *Nanomaterials* **2020**, *10*, 1334. [CrossRef] [PubMed]
48. Kashyap, B.K.; Singh, V.V.; Solanki, M.K.; Kumar, A.; Ruokolainen, J.; Kesari, K.K. Smart Nanomaterials in Cancer Theranostics: Challenges and Opportunities. *ACS Omega* **2023**, *8*, 14290–14320. [CrossRef] [PubMed]
49. Saravanan, H.; Subramani, T.; Rajaramon, S.; David, H.; Sajeevan, A.; Sujith, S.; Solomon, A.P. Exploring nanocomposites for controlling infectious microorganisms: Charting the path forward in antimicrobial strategies. *Front. Pharmacol.* **2023**, *14*, 1282073. [CrossRef] [PubMed]
50. Zykova, M.V.; Volikov, A.B.; Buyko, E.E.; Bratishko, K.A.; Ivanov, V.V.; Konstantinov, A.I.; Logvinova, L.A.; Mihalyov, D.A.; Sobolev, N.A.; Zhirkova, A.M.; et al. Enhanced Antioxidant Activity and Reduced Cytotoxicity of Silver Nanoparticles Stabilized by Different Humic Materials. *Polymers* **2023**, *15*, 3386. [CrossRef]
51. Wagner, H. *Pharmazeutische Biology AUFI*; Gustav Fisher Verlag: Stuttgart, Germany, 1993; p. 184, 15 BN 3-437-20 498-X.
52. Harborne, J.B.; Williams, C.A. Anthocyanins and other flavonoids. *Nat. Prod. Rep.* **1998**, *15*, 631–652. [CrossRef]
53. Little, E.; Ramakrishnan, M.; Roy, B.; Gazit, G.; Lee, A.S. The glucose-regulated proteins (GRP78 and GRP94): Functions, gene regulation, and applications. *Crit. Rev. Eukaryot. Gene Expr.* **1994**, *4*, 1–18. [CrossRef]
54. Raaman, N. *Phytochemical Techniques*; New India Publishing: Pitampura, India, 2006.
55. Kokate, C.K.; Purohit, A.P.; Gokhale, S.B. Pharmacognosy, Nirali Prakashan, Pune. *Med. J.* **2002**, *43*, 77–85.
56. Edeoga, H.O.; Okwu, D.E.; Mbaebie, B.O. Phytochemical constituents of some Nigerian medicinal plants. *Afr. J. Biotechnol.* **2005**, *4*, 685–688. [CrossRef]
57. Rajagopal, G.; Manivannan, N.; Sundararajan, M.; Kumar, A.G.; Senthilkumar, S.; Mathivanan, N.; Ilango, S. Biocompatibility assessment of silver chloride nanoparticles derived from *Padina gymnospora* and its therapeutic potential. *Nano Express* **2021**, *2*, 010010. [CrossRef]
58. Anand, T.; Anbukkarasi, M.; Thomas, P.A.; Geraldine, P.A. Comparison between plain eugenol and eugenol-loaded chitosan nanoparticles for prevention of in vitro selenite-induced cataractogenesis. *J. Drug Deliv. Sci. Technol.* **2021**, *65*, 102696. [CrossRef]

59. Rajagopal, G.; Nivetha, A.; Sundar, M.; Panneerselvam, T.; Murugesan, S.; Parasuraman, P.; Kumar, S.; Ilango, S.; Kunjiappan, S. Mixed phytochemicals mediated synthesis of copper nanoparticles for anticancer and larvicidal applications. *Heliyon* **2021**, *7*, e07360. [CrossRef]
60. Mosmann, T. Rapid colorimetric assay for cellular growth and survival: Application to proliferation and cytotoxicity assays. *J. Immunol. Methods* **1998**, *65*, 55–63. [CrossRef] [PubMed]
61. Rajagopal, G.; Nivetha, A.; Ilango, S.; Muthudevi, G.P.; Prabha, I.; Arthimanju, R. Phytofabrication of selenium nanoparticles using *Azolla pinnata*: Evaluation of catalytic properties in oxidation, antioxidant and antimicrobial activities. *J. Environ. Chem. Eng.* **2021**, *9*, 105483. [CrossRef]
62. Kasithevar, M.; Saravanan, M.; Prakash, P.; Kumar, H.; Ovais, M.; Barabadi, H.; Shinwari, Z.K. Green synthesis of silver nanoparticles using *Alysicarpus monilifer* leaf extract and its antibacterial activity against MRSA and CoNS isolates in HIV patients. *J. Interdiscip. Nanomed.* **2017**, *2*, 131–141. [CrossRef]
63. Nivetha, A.; Prabha, I. Surfactant-Enhanced Nano Spinel Oxide for Applications in Catalysis, Dye Degradation and Antibacterial Activity. *ChemistrySelect* **2022**, *7*, e202202389. [CrossRef]
64. Dilika, F.; Bremner, P.D.; Meyer, J.J.M. Antibacterial activity of linoleic and oleic acids isolated from *Helichrysum pedunculatum*: A plant used during circumcision rites. *Fitoterapia* **2000**, *71*, 450–452. [CrossRef]
65. Abubacker, M.N.; Devi, P.K. In vitro antifungal potentials of bioactive compound oleic acid, 3-(octadecyloxy) propyl ester isolated from *Lepidagathis cristata* Willd. (*Acanthaceae*) inflorescence. *Asian Pac. J. Trop. Med.* **2014**, *7*, S190–S193. [CrossRef] [PubMed]
66. Habeeb Rahuman, H.B.; Dhandapani, R.; Narayanan, S.; Palanivel, V.; Paramasivam, R.; Subbarayalu, R.; Thangavelu, S.; Muthupandian, S. Medicinal plants mediated the green synthesis of silver nanoparticles and their biomedical applications. *IET Nanobiotechnol.* **2022**, *16*, 115–144. [CrossRef]
67. De Carvalho, C.C.; Caramujo, M.J. The various roles of fatty acids. *Molecules* **2018**, *23*, 2583. [CrossRef] [PubMed]
68. Sundar, M.; Lingakumar, K. Investigating the efficacy of topical application of *Ipomoea carnea* herbal cream in preventing skin damage induced by UVB radiation in a rat model. *Heliyon* **2023**, *9*, e19161. [CrossRef]
69. Zhang, L.; Zhang, W.; Zhang, F.; Jiang, J. Xylo-oligosaccharides and lignin production from *Camellia oleifera* shell by malic acid hydrolysis at mild conditions. *Bioresour. Technol.* **2021**, *341*, 125897. [CrossRef] [PubMed]
70. Mukherjee, P.K.; Singha, S.; Kar, A.; Chanda, J.; Banerjee, S.; Dasgupta, B.; Haldar, P.K.; Sharma, N. Therapeutic importance of Cucurbitaceae: A medicinally important family. *J. Ethnopharmacol.* **2022**, *282*, 114599. [CrossRef]
71. Mikhailova, E.O. Silver nanoparticles: Mechanism of action and probable bio-application. *J. Funct. Biomater.* **2020**, *11*, 84. [CrossRef]
72. Ansari, M.; Ahmed, S.; Abbasi, A.; Khan, M.T.; Subhan, M.; Bukhari, N.A.; Hatamleh, A.A.; Abdelsalam, N.R. Plant mediated fabrication of silver nanoparticles, process optimization, and impact on tomato plant. *Sci. Rep.* **2023**, *13*, 18048. [CrossRef]
73. Radzikowska-Büchner, E.; Flieger, W.; Pasieczna-Patkowska, S.; Franus, W.; Panek, R.; Korona-Głowniak, I.; Suśniak, K.; Rajtar, B.; Świątek, Ł.; Żuk, N.; et al. Antimicrobial and Apoptotic Efficacy of Plant-Mediated Silver Nanoparticles. *Molecules* **2023**, *28*, 5519. [CrossRef] [PubMed]
74. Bilal, M.; Rasheed, T.; Iqbal, H.M.; Li, C.; Hu, H.; Zhang, X. Development of silver nanoparticles loaded chi-tosan-alginate constructs with biomedical potentialities. *Int. J. Biol. Macromol.* **2017**, *105*, 393–400. [CrossRef] [PubMed]
75. Ahmed, S.; Ahmad, M.; Swami, B.L.; Ikram, S. Green synthesis of silver nanoparticles using *Azadirachta indica* aqueous leaf extract. *J. Radiat. Res. Appl. Sci.* **2016**, *9*, 1–7. [CrossRef]
76. Dipankar, C.; Murugan, S. The green synthesis, characterization and evaluation of the biological activities of silver nanoparticles synthesized from *Iresine herbstii* leaf aqueous extracts. *Colloids Surf. B Biointerfaces* **2012**, *98*, 112–119. [CrossRef] [PubMed]
77. Rajkuberan, C.; Prabukumar, S.; Sathishkumar, G.; Wilson, A.; Ravindran, K.; Sivaramakrishnan, S. Facile synthesis of silver nanoparticles using *Euphorbia antiquorum* L. latex extract and evaluation of their biomedical perspectives as anticancer agents. *J. Saudi Chem. Soc.* **2017**, *21*, 911–919. [CrossRef]
78. Veera, S.; Chirumamilla, P.; Dharavath, S.B.; Maduru, N.; Taduri, S. Facile green synthesis of silver nanoparticles using *Coral-locarpus epigaeus* leaf extract: Structural, photoluminescence and antibacterial properties. *Chem. Data Collect.* **2023**, *45*, 101032. [CrossRef]
79. Jeeva, K.; Thiyagarajan, M.; Elangovan, V.; Geetha, N.; Venkatachalam, P. *Caesalpinia coriaria* leaf extracts mediated biosynthesis of metallic silver nanoparticles and their antibacterial activity against clinically isolated pathogens. *Ind. Crops Prod.* **2014**, *52*, 714–720. [CrossRef]
80. Sigamoney, M.; Shaik, S.; Govender, P.; Krishna, S.B.N. African leafy vegetables as bio-factories for silver nano-particles: A case study on *Amaranthus dubius* C Mart. Ex Thell. *S. Afr. J. Bot.* **2016**, *103*, 230–240. [CrossRef]
81. Jagtap, U.B.; Bapat, V.A. Green synthesis of silver nanoparticles using *Artocarpus heterophyllus* Lam. seed extract and its antibacterial activity. *Ind. Crops Prod.* **2013**, *46*, 132–137. [CrossRef]
82. Khan, M.J.; Shameli, K.; Sazili, A.Q.; Selamat, J.; Kumari, S. Rapid green synthesis and characterization of silver nanoparticles arbitrated by *curcumin* in an alkaline medium. *Molecules* **2019**, *24*, 719. [CrossRef]
83. Moond, M.; Singh, S.; Sangwan, S.; Devi, P.; Beniwal, A.; Rani, J.; Kumari, A.; Rani, S. Biosynthesis of silver nano-particles utilizing leaf extract of *Trigonella foenum-graecum* L. for catalytic dyes degradation and colorimetric sensing of Fe^{3+}/Hg^{2+}. *Molecules* **2023**, *28*, 951. [CrossRef] [PubMed]

84. Khuda, F.; Jamil, M.; Khalil, A.A.K.; Ullah, R.; Ullah, N.; Naureen, F.; Abbas, M.; Khan, M.S.; Ali, S.; Farooqi, H.M.U.; et al. Assessment of antioxidant and cytotoxic potential of silver nanoparticles synthesized from root extract of *Reynoutria japonica* Houtt. *Arab. J. Chem.* **2022**, *15*, 104327. [CrossRef]
85. Ajaykumar, A.P.; Sabira, O.; Binitha, V.S.; Varma, S.R.; Mathew, A.; Jayaraj, K.N.; Janish, P.A.; Zeena, K.V.; Sheena, P.; Venugopal, V.; et al. Bio-Fabricated Silver Nanoparticles from the Leaf Extract of the Poisonous Plant, *Holigarna arnottiana*: Assessment of Antimicrobial, Antimitotic, Anticancer, and Radical-Scavenging Properties. *Pharmaceutics* **2023**, *15*, 2468. [CrossRef] [PubMed]
86. Hamida, R.S.; Ali, M.A.; Alfassam, H.E.; Momenah, M.A.; Alkhateeb, M.A.; Bin-Meferij, M.M. One-Step Phytofabrication Method of Silver and Gold Nanoparticles Using *Haloxylon Salicornicum* for Anticancer, Antimicrobial, and Antioxidant Activities. *Pharmaceutics* **2023**, *15*, 529. [CrossRef] [PubMed]
87. Rasheed, T.; Bilal, M.; Iqbal, H.M.; Li, C. Green biosynthesis of silver nanoparticles using leaves extract of *Artemisia vulgaris* and their potential biomedical applications. *Colloids Surf. B Biointerfaces* **2017**, *158*, 408–415. [CrossRef] [PubMed]
88. Bordoni, V.; Sanna, L.; Lyu, W.; Avitabile, E.; Zoroddu, S.; Medici, S.; Kelvin, D.J.; Bagella, L. Silver nanoparticles derived by artemisia arborescens reveal anticancer and apoptosis-inducing effects. *Int. J. Mol. Sci.* **2021**, *22*, 8621. [CrossRef] [PubMed]
89. Mariadoss, A.V.A.; Ramachandran, V.; Shalini, V.; Agilan, B.; Franklin, J.H.; Sanjay, K.; Alaa, Y.G.; Tawfiq, M.A.A.; Ernest, D. Green synthesis, characterization and antibacterial activity of silver nanoparticles by *Malus domestica* and its cytotoxic effect on (MCF-7) cell line. *Microb. Pathog.* **2019**, *135*, 103609. [CrossRef]
90. Ingale, S.; Gaykar, B.; Pagar, K.; Shelke, D. Green Synthesis of Silver Nanoparticles from *Cyathocline purpurea* (Don) O. Kuntze and Its Efficacy Against MCF-7 Cancer Cell Line. *BioNanoScience* **2023**, *13*, 1197–1212. [CrossRef]
91. Halder, J.; Pradhan, D.; Kar, B.; Ghosh, G.; Rath, G. Nano therapeutics approaches to overcome P-glycoprotein-mediated multi-drug resistance in cancer. *Nanomed. NBM* **2022**, *40*, 102494. [CrossRef]
92. Odonkor, S.T.; Addo, K.K. Bacteria resistance to antibiotics: Recent trends and challenges. *Int. J. Biol. Med. Res.* **2011**, *2*, 1204–1210.
93. Khan, S.; Rukayadi, Y.; Jaafar, A.H.; Ahmad, N.H. Antibacterial potential of silver nanoparticles (SP-AgNPs) synthesized from *Syzygium polyanthum* (Wight) Walp. against selected foodborne pathogens. *Heliyon* **2023**, *9*, e22771. [CrossRef]
94. Netai, M.M.; Stephen, N.; Musekiwa, C. Synthesis of silver nanoparticles using wild *Cucumis anguria*: Characterization and antibacterial activity. *Afr. J. Biotechnol.* **2017**, *16*, 1911–1921.
95. Franci, G.; Falanga, A.; Galdiero, S.; Palomba, L.; Rai, M.; Morelli, G.; Galdiero, M. Silver nanoparticles as potential antibacterial agents. *Molecules* **2015**, *20*, 8856–8874. [CrossRef]
96. Contreras, A.; Vazquez, D. Cooperative and antagonistic interactions of peptidyl-tRNA and antibiotics with bacterial ribosomes. *Eur. J. Biochem.* **1977**, *74*, 539–547. [CrossRef]
97. Haseef, H.M.A.; Dinesh, S.; Prakash, J.; Marvaan, M.S.; Madasamy, S.; Pannerselvam, B.; Venkatasubbu, G.D. Calcium oxide/silica nanocomposite and *L. coromandelica* bark incorporated κ-carrageenan/sodium alginate hy-drogel for rapid hemostasis. *Int. J. Biol. Macromol.* **2024**, *254*, 127951. [CrossRef] [PubMed]
98. Dizaj, S.M.; Lotfipour, F.; Barzegar-Jalali, M.; Zarrintan, M.H.; Adibkia, K. Antimicrobial activity of the metals and metal oxide nanoparticles. *Mater. Sci. Eng. C* **2014**, *44*, 278–284. [CrossRef] [PubMed]
99. Ahmed, S.; Ahmad, M.; Swami, B.L.; Ikram, S. A review on plants extract mediated synthesis of silver nanoparticles for antimicrobial applications: A green expertise. *J. Adv. Res.* **2016**, *7*, 17–28. [CrossRef] [PubMed]
100. Torkaman, M.; Moradi, R.; Keyvani, B. Photocatalytic degradation azo dye Direct Red 23 using carbon nanotubes particles by UV/H2O2 process in batch photoreactor. *Rev. Roum. Chim.* **2016**, *61*, 763–772.
101. Ismail, M.; Akhtar, K.; Khan, M.I.; Kamal, T.; Khan, M.A.; Asiri, A.; Seo, J.; Khan, S.B. Pollution, toxicity and carcinogenicity of organic dyes and their catalytic bio-remediation. *Curr. Pharm. Des.* **2019**, *25*, 3645–3663. [CrossRef]
102. Yogalakshmi, K.N.; Das, A.; Rani, G.; Jaswal, V.; Randhawa, J.S. Nano-bioremediation: A new age technology for the treatment of dyes in textile effluents. In *Bioremediation of Industrial Waste for Environmental Safety: Volume I: Industrial Waste and Its Management*; Springer: Berlin/Heidelberg, Germany, 2020; pp. 313–347.
103. Lidia, F.; Maria, H. TiO2/Fly Ash nanocomposite for photodegradation of organic pollutant. In *Handbook of Nano-Materials and Nanocomposites for Energy and Environmental Applications*; Springer: Cham, Switzerland, 2020; pp. 1–24.
104. Vanaja, M.; Paulkumar, K.; Baburaja, M.; Rajeshkumar, S.; Gnanajobitha, G.; Malarkodi, C.; Sivakavinesan, M.; Annadurai, G. Degradation of methylene blue using biologically synthesized silver nanoparticles. *Bioinorg. Chem. Appl.* **2014**, *19*, 2014. [CrossRef]
105. Al-Zaban, M.I.; Mahmoud, M.A.; AlHarbi, M.A. Catalytic degradation of methylene blue using silver nanoparticles synthesized by honey. *Saudi J. Biol. Sci.* **2021**, *28*, 2007–2013. [CrossRef]
106. Fairuzi, A.A.; Bonnia, N.N.; Akhir, R.M.; Abrani, M.A.; Akil, H.M. 2018, January. Degradation of methylene blue using silver nanoparticles synthesized from *Imperata cylindrica* aqueous extract. *IOP Conf. Ser. Earth Environ. Sci.* **2018**, *105*, 012018. [CrossRef]
107. Kumar, M.S.; Supraja, N.; David, E. Photocatalytic degradation of methylene blue using silver nanoparticles synthesized from *Gymnema sylvestre* and antimicrobial assay. *Nov. Res. Sci.* **2019**, *2*, 1–7.
108. Ogundare, S.A.; Adesetan, T.O.; Muungani, G.; Moodley, V.; Amaku, J.F.; Atewolara-Odule, O.C.; Yussuf, S.T.; Sanyaolu, N.O.; Ibikunle, A.A.; Balogun, M.S.; et al. Catalytic degradation of methylene blue dye and antibacterial activity of biosynthesized silver nanoparticles using *Peltophorum pterocarpum* (DC.) leaves. *Environ. Sci. Adv.* **2023**, *2*, 247–256. [CrossRef]

109. Trieu, Q.A.; Le, C.T.B.; Pham, C.M.; Bui, T.H. Photocatalytic degradation of methylene blue and antibacterial activity of silver nanoparticles synthesized from *Camellia sinensis* leaf extract. *J. Exp. Nanosci.* **2023**, *18*, 2225759. [CrossRef]
110. Alam, M.W.; Aamir, M.; Farhan, M.; Albuhulayqah, M.; Ahmad, M.M.; Ravikumar, C.R.; Dileep Kumar, V.G.; Ananda Murthy, H.C. Green synthesis of Ni-Cu-Zn based nanosized metal oxides for photocatalytic and sensor applications. *Crystals* **2021**, *11*, 1467. [CrossRef]

DEVELOPMENT OF NATURAL JELLY FROM BEETROOT PEEL: ANALYZE ITS STABILITY AND SENSORY PROPERTIES

B Vishnupriya*[1], M Manjudevi[2], V Agalya[3]

[1]Assistant Professor, PG and Research Department of Biotechnology, Kongunadu Arts and Science College, Coimbatore, Tamilnadu

[2]Research Scholar, PG and Research Department of Biotechnology, Kongunadu Arts and Science College, Coimbatore, Tamilnadu

[3]Associate Professor, IEEE Senior Member, Department of EEE, CMR Institute of technology, Bangalore – 37

ABSTRACT

The present research work was made to formulate and evaluate natural jelly from Beetroot peel. Beet root (*Beta vulgaris*) is a vegetable with high amount of biologically active substances and inorganic nitrogen. Ultra sonication assisted aqueous extraction of pigment from beetroot peel was done and total betalain pigments were measured by pH differential method. FTIR results confirm the presence of amine and carboxyl group which indicates the medicinal and nutritive value of beetroot peel. In this study two different formulations (FI and FII) were prepared by using agar agar (Food grade), brown sugar, honey, citric acid and salt. Stability of the betalain pigment was analyzed at various temperature (5, 10, 15, 20, 25 and 30°C) also evaluated antimicrobial and antioxidant property. The results of the storage properties revealed that the developed jelly can be stored under refrigerated and ambient conditions for a period of 15days respectively without addition of any artificial preservative. Based on the sensory quality characteristics viz., color, texture, shape, flavor and overall acceptability FI can be used in development of jelly successfully.

Keywords: Beetroot peel, Jelly, Betalain, Antimicrobial, Antioxidant, Sensory analysis

INTRODUCTION

Beetroot (*B. vulgaris*) is biennial plant grown in temperate countries and it is an alkaline food with pH in range of 7.5 to 8.0 [33]. Beet root are the excellent source of beta carotene, calcium ion and nitrogen. In India it is mainly grown for its juice and vegetable value which contains vitamin A, B1, B2, B6 and C also it is the good source of various minerals [24]. Recent report indicates that beet root extract possesses anti-hypertensive, hypoglycemic, anti-oxidant, anti-inflammatory, and hepatic protective activity additionally beetroot is the natural source of dye and it is used for many food processing unit. The pigment present in the beet root is betalain, an alkaline pigment and is a glucoside that hydrolyzes into sugar glucose and betanidin [42]. Generally, betalain has excellent stability at various pH, light and temperature.

Most of the beet products are made from sugar beet and most importantly beet cellulose works as a bulk residue, increasing peristalsis and making stool passage easier, hence constipation is prevented by using it on a regular basis also, lowers blood pressure in hypertensive persons. Gastric ulcer can be treated with beetroot wine. It increases the urinary output due to its rich potassium content and cures hypo-glycaemia. It is also helpful in various treatment of piles, tuberculosis, cholera, diarrhea, dysentery and lowered state of body resistant after major surgical operation etc [41]. The beet root juice is a natural cure for erectile dysfunction and the removal of kidney and bladder stones [37].

Waste material of beet root peel high concentration of phenolic compounds, it is a rich source of phytochemicals and antioxidants. [15]. Vulgaxanthin I, Vulgaxanthin II, indicaxanthin, betanin, prebetanin, isobetanin, and neobetanin were among the betalains discovered in beetroot peel extract. cyclodopa glucoside, V-formylcyclodopa glucoside, dihydroxyindolcarboxylic acid glucoside, betalamic acid, L-tryptophan, p-coumaric acid, ferulic acid, and quantities of unidentified flavonoids are also present. [21]. In the recent report, green synthesis of nanoplates from aqueous extract of beet root peel was investigated for anisotropic noble metal research (Deokar and Ingale, 2018). Due to higher antioxidant level and nitrogen is used as a good quality fertilizer than that of standard antioxidants [3].

Tomato pastes, soups, sauces, desserts, jams, jellies, candies, and morning cereals all benefit from beet root peel extract. Jellies are made by cooking fruit juice with sugar. It is made from juice or aqueous extract of one or more fruits or vegetables with sweetening properties with or without

the addition of water [13]. Kids of all ages like jelly but commercial jellies containing high amounts of artificial colorants, sugar or high fructose corn syrup can be detrimental to one's health.

The purpose of this research was to develop and assess natural jelly from beet root peel with the help of sweeting agent and gelling agent and thereby sensory analysis carried out.

MATERIALS AND METHODS

Collection and Storage of Samples

Beetroot (Vitamin A, C and B6), Agar agar (Gelling agent), citric acid or lemon, brown sugar and Honey (Sweetening agent) procured from Reliance fresh Mart, Coimbatore, Tamilnadu, India. The peel was removed and dried under hot air oven at 75ºC for 2 days. The dried peel was finely powdered in a grinder and stored in a container for further studies [12].

Pigment Extraction

In a conical flask, ten grams of powder were concentrated with 50 ml of deionized water. The mixture was then processed under sonicator for about 6 hrs under proper conditions and observed in proper intervals of time. The aqueous extract was then centrifuged for 10 minutes at 5000 rpm and the supernatant is collected and stored in refrigerator [1].

Phytochemical analysis

Phytochemical analysis of the beetroot peel extract was carried out in accordance with standard Protocol [18].

Total pigment content Estimation

Total amount of Betalain pigment was measured by the [8] method with modified dilution.

$$\textbf{Total pigment content } \left(\frac{mg}{g}\right) = \frac{A \times DF \times MW \times 1000}{\varepsilon \times L}$$

Chemical Structure Analysis

FTIR (Fourier Transform Infrared Spectroscopy)

The extracted pigments' Fourier transform-infrared spectrum was obtained from pellets made with 1 mg of sample and 100 mg of dry potassium bromide (KBr). The spectra were taken with a Perkin Elmer FT-IR Spectrum GX (USA) infrared spectrophotometer between 700 and 4000 cm^{-1}. [9].

Antimicrobial Activity

The agar well diffusion method was used to test the antimicrobial activity of the peel extract (1.0 mg). The activity was evaluated against two Gram- Negative bacteria (*Escherichia coli* MTCC 1687, *Serratia marcescens* MTCC 4822), two Gram-positive bacteria (*Bacillus cereus* MTCC 6840 and *Staphylococcus* aureus MTCC 96), two microscopic filamentous fungi (*Aspergillus flavus* MTCC 535 *and A. versicolor* MTCC 698). The Bacteria and fungi were collected from Microbial Type Culture Collection, Chandigarh**.** Microbial growth inhibition was measured around the impregnated discs. When the zone diameter is > 10 mm, 5–10 mm, or 2–5 mm, antimicrobial activity is termed high, moderate, or trace, respectively, and minimal effect when the value is less than 2 mm and % of inhibition was computed. [9].

Anti-oxidant Property

DPPH Radical Scavenging Method

DPPH scavenging activity of Betalain pigment was tested by the method of Sanchéz-Moréno *et al*., (1998). For anti-oxidant study, dried extract was used and the method was described in [19]. DPPH solution in methanol (0.1mM) was mixed with different concentration of extract (20 to 100mg/l) and read the absorbance at 518 nm. The standard utilized in this investigation was 1, 4-dithioerythritol, and the results were given in milligrams per liter. [16].

Thin Layer Chromatography

Separation of Betalain pigment was done by cellulose coated TLC plate with the sequential use of two different polar system (Less PS I - Ethanol: Acetic acid: Isopropanol: water: 20:5:55:20 ml) and More PS II - Isopropanol: Ethanol: Water: HCl: 55: 20: 24: 1 ml). A hundred milliliters of beetroot extract were combined with two milliliters of water. and applied on the TLC plate and allowed the solvents moved 10cm then dried under atmosphere and run twice in two different solvents in the same direction. This method was done with modified procedure of [6].

Preparation of Formulation for organoleptic evaluation

Two different formulations were prepared with various concentrations of the ingredients for organoleptic evaluation studies (Tab 1).

Table 1. Formulation based various combination of the extract

S.No	Sample	FI	FII
1.	Beet root extract (ml)	5	10
2.	Agar agar (g)	2	2
3.	Honey (ml)	10	5
4.	Brown Sugar	10	5
5.	Water (ml)	3	3
	Total	20	20

Preparation of Jelly

Based on organoleptic evaluation the selected formulation was heated and filled in small cups (preferably used for jelly preparation) and stored in refrigerator for 1 hr. The prepared jellies can be scooped from the cups and can be consumed directly [10].

Stability and Storage Study

The selected formulation was checked for stability at various temperatures (5, 10, 15, 20, 25 and 30˚C) samples were placed in capped glass vials wrapped with aluminium foil and sealed with parafilm during the storage test for 30 days by measuring the samples in colorimeter at 535nm. The reading was taken at the interval of 5 days once until 30 days.

Statistical Analysis

For significant differences at $p<0.05$, the data were subjected to one-way ANOVA followed by post hoc Duncan's Multiple Range Test (DMRT) using SPSS 17.

RESULTS AND DISCUSSION

Sample Extraction & Preliminary Screening

The beetroot peel was finely powdered and extracted with d.H_2O under ultrasonicator for 6h, centrifuged and stored the supernatant under refrigeration (Plate 1). The Extract was subjected for different chemical analysis for preliminary screening and the results indicated the presence of various compounds and shown in table 2. It has been reported extensively, that betalain pigment

was extracted from beetroot peel by ultra-sonication method with the extraction time of 3h and stored at low temperature [38]. Similarly, ultrasonication assisted distilled water extraction was carried out and reported as this method was not significantly influence on pH, soluble solids and total solids but yield of pigment was significantly higher [27]. According to the method of [39] ultrasound-assisted extraction showed better results in betalain extraction than orbital shaking extraction. Our report is extensively correlated with the results of [18, 30] for the presence of flavonoids, saponins, sterols and triterpenes in beetroot extracts after phyto-chemical screening. This type of biochemical profile has been observed in another study using GC-MS that dealt with *Satureja khuzistanica* for preserving vegetable oils [4]. Phytochemicals of different beetroot's vegetation extract were analyzed and reported [5].

Plate 1: Ultrasonicated Aqueous Extract

Phytoconstituents	Qualitative Analysis
Tannins	+
Saponins	+
Flavonoid	+
Reducing sugars	+
Terpenoids	+
Triterpenes	+
Anthraquinones	-

Table 2: Phytochemical analysis of the extract

Chemical structural analysis

The FTIR images showed two strong bands at 3309.39 cm^{-1}, and 1635.40 cm^{-1}corresponding to N-H stretch for 1º, 2ºamines and C=O stretch for carboxyl group respectively were observed. (Figure 1).

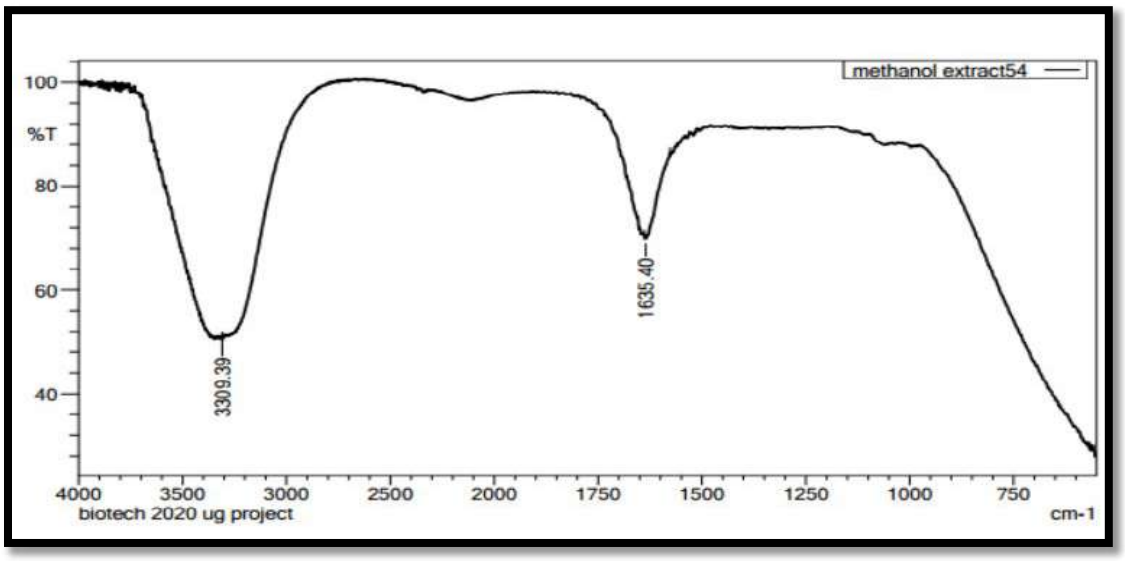

Figure 1. FTIR analysis

From figure 1, amines & carboxyl groups present in the extract possessed the use of medicines, food product preparation and source of good preservatives respectively. Also, the incidence of nitrogen functional groups confirmed the existence of betalains which is similar to the findings of [11] at 1,415 $cm^{-1.}$ The transmittance results at 3319 and 1637 cm1 were consistent with our findings, indicating asymmetric and symmetric stretching vibrations of OH groups and H-O-H due to moisture content [26]. In beet juice lyophilization study, show the stretching of -OH group and NH at 3300 and 1620 cm^{-1}. The same method was used to detect the vibration frequencies of betalain functional groups, which revealed that the band at 3359 cm-1 was caused by the stretching vibration of the N-H bond. [22].

Anti-microbial activity

The antimicrobial effect of is shown in table 3. *E. coli* exhibited the maximum antimicrobial activity with inhibition of about 90.2±0.2 compared with the standard disc of Chloramphenicol (100%). *S. marcescens, B. cereus, A. flavus* and *A. versicolor* of fungi showed clear zone formation

of growth inhibition, the percentage was calculated with standard fluconazole. The extract showed trace amount of inhibition on *S. aureus* compared to other strains. The antimicrobial activity of one of the major ingredients for jelly preparation was quantified in terms of their ability to restrict the growth of the test strains. Beetroots' antibacterial action has been linked to the presence of phenolic chemicals, which prevent the growth of undesirable microbes. There have been a few researches on the antibacterial effectiveness of beetroot. [13] suggested that beetroot extracts showed excellent activity against tested microbes *E. coli, P. vulgaris, S. aureus, K. pneumonia and P. mirabilis*. The extract of 100 µl demonstrated inhibitory efficacy against all Gram–negative bacteria tested, with *Salmonella typhimurium* and *Citrobacter freundii* being the most vulnerable strains, with 50 µl of the extract inhibiting their growth [42]. Endometabolites of sugarbeet seed residues, such as phenols, flavonoids, and their glycosides, have antibacterial properties in some circumstances and can be exploited as natural biologically active chemicals. [28].

Microorganism	**Inhibition Zone (mm)**	**Inhibition (%)**
Bacteria		
Escherichia coli	H	90.2±0.2
Serratia marcescens	M	52.3±0.4
Bacillus cereus	M	58.3±0.3
Staphylococcus aureus	T	35.4±0.2
Fungi		
Aspergillus flavus	M	49.1±0.2
A. versicolor	M	47.2±0.4

Values are mean±standard of the three replicates

Legend: H > than 10 mm, M > 5–10 mm, T > 2–5 mm.

Table 3 Antimicrobial effect of Beetroot peel extract

DPPH Radical Scavenging Method

Aqueous extract of beetroot peel exhibited potent free radical scavenging activity by increasing the concentration from 20 to 100mg/l. It showed similar potential as standard 1, 4-dithioerythritol (20 to 100mg/l). IC_{50} value of the beetroot peel extract was 80 mg/l and for standard 91 mg/l

concentration. DPPH is dark purple color changes into yellow color by accepting hydrogen from donor and becomes a non-radical form (Figure 2). Similar to our study [34] reported, Methanol and ethanol beetroot extract displayed increasing DPPH scavenging activity when the concentration was increased and its IC50 values were 0.129 and 0.254 mg/ml. According to [23], increasing the concentration of beetroot peel extract boosted scavenging activity (4 to 20%).

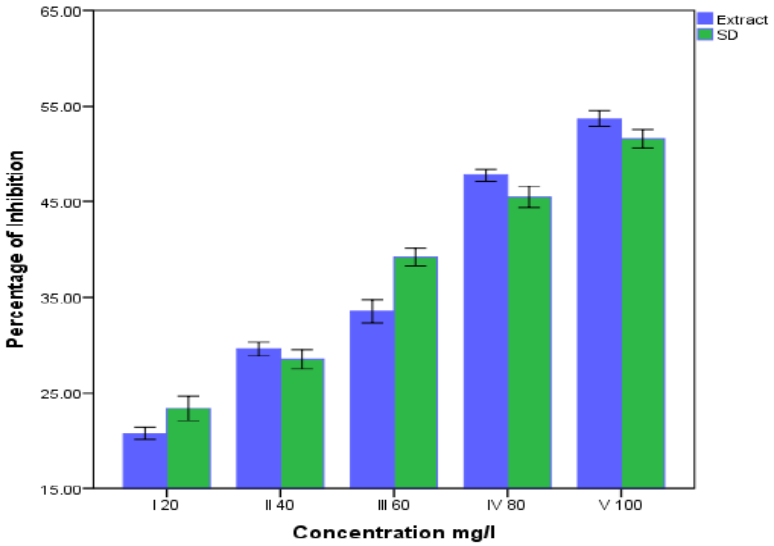

Legend: SD-Standard

Figure 2: DPPH scavenging property of Extract

Thin Layer Chromatography

TLC was used to validate the presence of betalain throughout the separation process. The separated pigment bands seen on a TLC plate by running with PS I and their corresponding visible spectra were identified as betacyanin pigment with identified red spot chromatogram by calculating the R_f value 0.80 and pink spot chromatogram identified as anthocyanin, R_f value found as 0.44. For PS II pink spot was identified with R_f value 0.82. By Interpreting the result with [18] the compound was confirmed to be betacyanin, R_f value was 0.98. Similar work was conducted on dragon fruit, different fraction has been shown, two have not been identified due to unavailable information. Known colored pigments betacyanin and anthocyanin was obtained with R_f value of 0.45 and 0.85 [31].

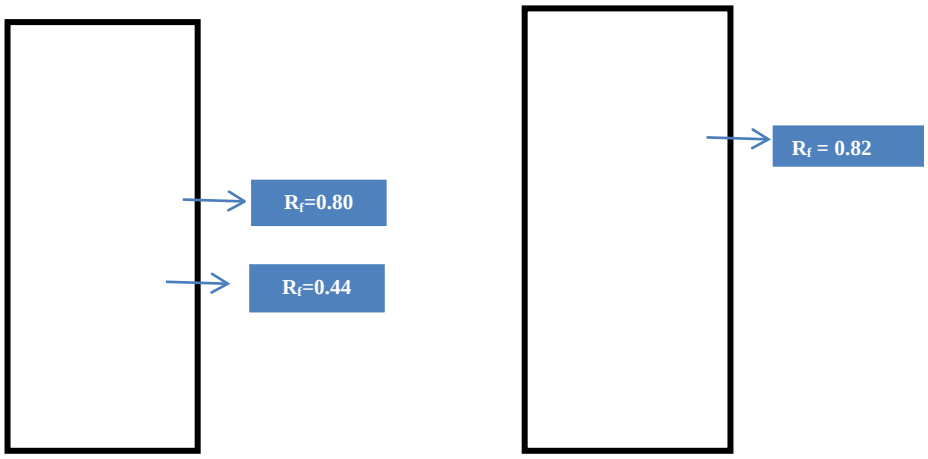

Legend: PS - Polar Systems

Plate 2: TLC of aqueous extract of beet root peel extract

Preparation of Jelly and Sensory Analysis

Two different formulations of jelly were prepared mentioned above in the method section. Mixed the ingredients and heated for 100°C 4 min or desired consistency was reached. Jelly was prepared and filled in small cup PS I y used for jelly preparation) a PS II n refrigerator for 1 hr and illustrated in figure 3. Previously, jelly preparation was done with beet root juice, pectin, citric acid and sugar and the highest evaluation score was 8.3 [10]. According to [38] natural jelly was prepared from citrus waste and analyzed carotenoid content. In another study, natural jellies were prepared with carrot, papaya and beet root with different ratios and its nutritive values were analyzed [17]. Different Sensory attributes like appearance, color, flavor, shape, texture and overall acceptability was analyzed by panel of 5 trained members having experience in sensory evaluations of the product with 9-point hedonic scale. Based on the average score formulation I was selected for further studies (Figure 4).

F1 **F2**

Figure 3 Jelly Preparation

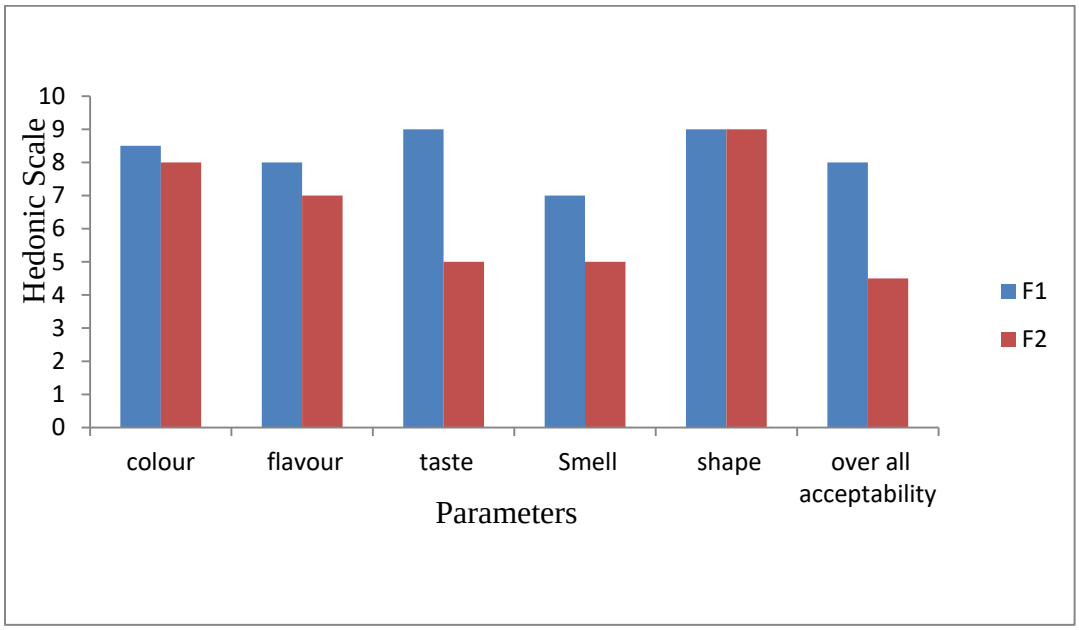

Legend: F1- Formulation I; F2- Formulation II

Figure 4: Sensory Analysis of the formulations

Stability and Storage Test

Stability test of betalain for formulation I was performed at various temperatures and read the absorbance at 535nm for every 5th day until 30 days. Based on the report, the pigment was found to be stable up to 15ºC for 15 days and the stability decreases when the temperature and days increases above 15ºC and 15th day respectively. The hypochromic shifts occurs when the other components of

the sample react to the temperatures. The absorbance of samples stored at room temperature decreased gradually as the day increased but the jellies stored in refrigerator showed degradation of pigment after 15th day. Hence natural extract can be recommended to be used at or below 25ºC with minimum loss in pigments for 20 days (Figure 5). Previously the stability was tested with sugar free grape jelly for 60days at 4°C for diabetic patients or for individuals who desire to reduce their body weight [20]. The impacts of storage temperature and time of jam and juice from two varieties of monkey kola stored at different temperatures 29 to 32°C, there were no significant changes in specific gravity of the jam and juice samples stored for four weeks ($p>0.05$) [29].

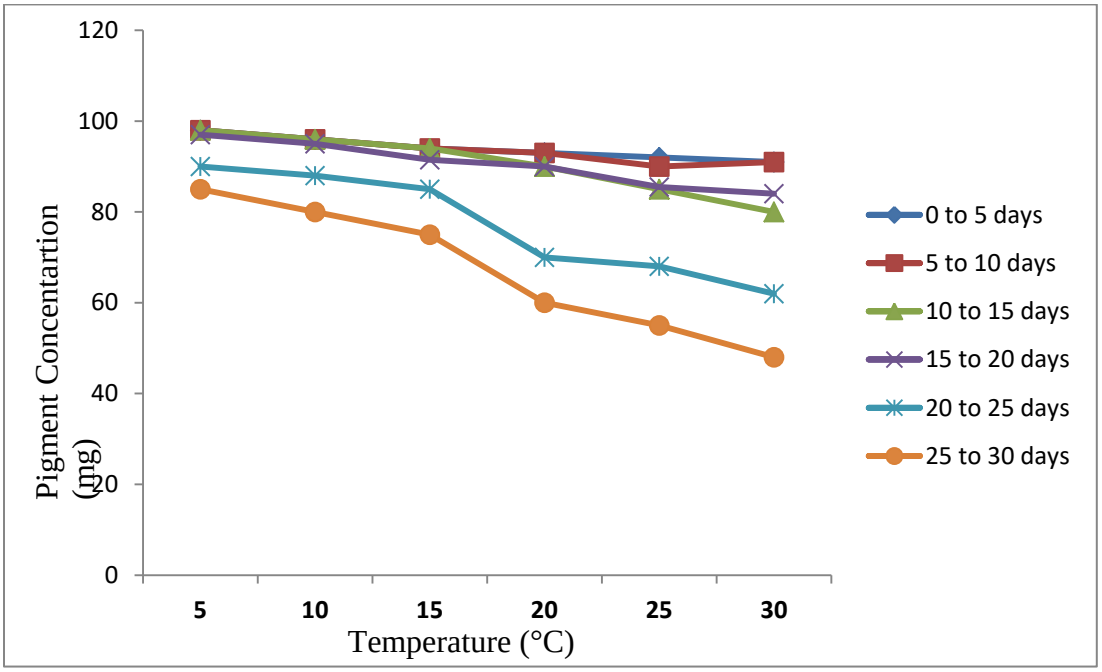

Figure 5: Stability study of the sample at various temperatures

PATENT DETAILS

B Vishnupriya, V Agalya "Fiber to Sugar free Jelly from By - Product of Beetroot", "202141025316", June 7, 2021.

Available: https://ipindiaservices.gov.in/PublicSearch/PublicationSearch/PatentDetails, Accessed on: June 11, 2021.

CONCLUSION

The focus of this research was on making jelly from beetroot peel. Because of the high concentration of phenolic compounds, the by-product of beet root peel contains rich source of phytochemicals and antioxidants. For the successful preparation of jelly, the formulation I was standardized as beetroot extract (5 ml), agar agar (2 g), honey (10 ml) and brown sugar (10 ml). The stability was checked at different temperature. The jellies stored in refrigerator and ambient condition showed pigment stability until 15^{th} and 5^{th} day respectively without addition of any artificial preservative. In sensory examination, the beetroot jelly formulation received the maximum score of 8.0 overall acceptance. The nutritional properties of the formulation will be analyzed in future.

REFERENCE

1. Aggarwal, P., Kaur, S. and Kaur, N., 2022. Intermediate moisture kinnow bar from low grade kinnow mandarins: Phytonutritional profile, morphological characterization, and storage stability. *Food Bioscience*, p.101837.
2. Alihosseini F, Ju KS, Lango J, Hammock BD, Sun G. Antibacterial colorants: characterization of prodiginines and their applications on textile materials. Biotechnology progress. 2008 May;24(3):742-7.
3. Andronopoulou E, Vorgias CE. Multiple components and induction mechanism of the chitinolytic system of the hyperthermophilic archaeon *Thermococcus chitonophagus*. Applied microbiology and biotechnology. 2004 Nov;65(6):694-702.
4. Babagil A, Tasgin E, Nadaroglu H, Kaymak HC. Antioxidant and antiradical activity of beetroot (Beta vulgaris L. var. conditiva Alef.) grown using different fertilizers. Journal of Chemistry. 2018 Jan 1;2018.
5. Bahrami B, Mahboubi M, Yari R, Mehran M. The antimicrobial and antioxidant potencies of Satureja Khuzistanica essential oil for preserving of vegetable oils. Journal of Microbiology, Biotechnology and Food Sciences. 2021 Jan 6; 2021:979-82.
6. Bilyk A. Thin-Layer Chromatographic Separation of Beet Pigments. Journal of Food Science. 1981 Jan;46(1):298-9.

7. Bonyadian M, Moshtaghi H. Bacteriocidal activity of some plant's essential oils against Bacillus cereus, Salmonella typhimurium, Listeria monocytogenes and Yersinia enterocolitica. Research Journal of Microbiology. 2008;3(11):648-53.
8. Castellar R, Obon JM, Alacid M, Fernández-Lopez JA. Color properties and stability of betacyanins from Opuntia fruits. Journal of Agricultural and Food Chemistry. 2003 Apr 23;51(9):2772-6.
9. Chan-Higuera JE, Carbonell-Barrachina AA, Cardenas-Lopez JL, Kacaniova M, Burgos-Hernández A, Ezquerra-Brauer JM. Jumbo squid (Dosidicus gigas) skin pigments: Chemical analysis and evaluation of antimicrobial and antimutagenic potential. Journal of Microbiology, Biotechnology and Food Sciences. 2021 Jan 6; 2021:349-53.
10. Chaudhari SN, Nikam MP. Development and sensory analysis of beetroot jelly. International Journal of Science and Research. 2015;4(10):827-30.
11. Chhikara N, Kushwaha K, Jaglan S, Sharma P, Panghal A. Nutritional, physicochemical, and functional quality of beetroot (Beta vulgaris L.) incorporated Asian noodles. Cereal Chemistry. 2019 Jan;96(1):154-61.
12. Codex Alimentarius. Codex standard: Standard for Jams, Jellies and Marmalades Website: 2009:296.
13. Deokar GK, Ingale AG. Unveiling an unexpected potential of beetroot waste in green synthesis of single crystalline gold nanoplates: A mechanistic study. Arabian journal of chemistry. 2018 Sep 1;11(6):950-8.
14. Din, S.N., Mubarak, A., Lani, M.N., Yahaya, M.Z. and Wan Abdullah, W.Z., 2022. Development of pastilles from flesh and rind of watermelon. *Food Research*, *6*(3), pp.288-297.
15. Dos S Baiao D, da Silva DV, Paschoalin VM. Beetroot, a remarkable vegetable: Its nitrate and phytochemical contents can be adjusted in novel formulations to benefit health and support cardiovascular disease therapies. Antioxidants. 2020 Oct;9(10):960.
16. Goldfein K. Added Sugars: Why It is Added to Food and the Challenges of Labeling it.
17. Goulas V, Manganaris GA. Exploring the phytochemical content and the antioxidant potential of Citrus fruits grown in Cyprus. Food Chemistry. 2012 Mar 1;131(1):39-47.

18. Ivanisova E, Czakoova M, Kacaniova M, Tvrda E. Nutritional and technological properties of selected kinds of coffee. Journal of Microbiology, Biotechnology and Food Sciences. 2021 Jan 6; 2021:400-3.
19. Jyothi Sri S, Sahoo NK, Kusuma D and Uma Shankar CH. Fabrication and Evaluation of Non-Medicated Jellies of Carrot, Beetroot and Papaya, J Pharm Res,3(4): 000187.
20. Kezi J, Sumathy JH. Betalain-a boon to the food industry. Discov. 2014; 20:51-8.
21. Khalaf NA, Shakya A, Al-olhman A, El-Agbar Z, Farah H. Antioxidant and anti-inflammatory activity of Ethanolic extract of Beta–vulgaris Linn roots. Turkish Journal of Biology. 2008: 51-5.
22. Kim SK, Chojnacka K, editors. Marine algae extracts: processes, products, and applications. John Wiley & Sons; 2015 Jan 30.
23. Kujala T, Loponen J, Pihlaja K. Betalains and phenolics in red beetroot (Beta vulgaris) peel extracts: extraction and characterisation. Zeitschrift für Naturforschung C. 2001 Jun 1;56(5-6):343-8.
24. Lucia Aztatzi-Rugerio, Sulem Yali Granados-Balbuena1, Yimi Zainos-Cuapio2, Erik Ocaranza-Sa´nchez1, Marlon Rojas-Lo´pez1. Analysis of the degradation of betanin obtained from beetroot using Fourier transform infrared spectroscopy. Journal of Food Science and Technology .56, 3677–3686. 2019.
25. Mahato N, Sinha M, Sharma K, Koteswararao R, Cho MH. Modern extraction and purification techniques for obtaining high purity food-grade bioactive compounds and value-added co-products from citrus wastes. Foods. 2019 Nov;8(11):523.
26. Maqbool H, Safeena MP, Sathish Kumar K, Zynudheen AA, Ninan G, Kumar BM. Beetroot peel extract as a natural preservative for shelf-life extension of deccan mahseer (Tor khudree) Steaks during chill storage.
27. Mathlouthi M. Water content, water activity, water structure and the stability of foodstuffs. Food control. 2001 Oct 1;12(7):409-17.
28. Mudgal, D., 2022. Nutritional composition and value-added products of beetroot: A review. *Journal of Current Research in Food Science*, *3*(1), pp.01-09.
29. Nashihah S, Mun'im A, Saputri FC. Formulation and characterization of rice bran oil in alginate microcapsules. Journal of Young Pharmacists. 2018;10(1):37.

30. Nesakumar N, Baskar C, Kesavan S, Rayappan JB, Alwarappan S. Analysis of moisture content in beetroot using Fourier transform infrared spectroscopy and by principal component analysis. Scientific reports. 2018 May 22;8(1):1-0.
31. Ngamwonglumlert L, Devahastin S, Chiewchan N. Natural colorants: Pigment stability and extraction yield enhancement via utilization of appropriate pretreatment and extraction methods. Critical reviews in food science and nutrition. 2017 Oct 13;57(15):3243-59.
32. Nikoo, M. and Gavlighi, H.A., 2022. Natural Antioxidants and Flavorings for Clean Label Foods. In *The Age of Clean Label Foods* (pp. 73-102). Springer, Cham.
33. Oksana K, Artur L. Biological Activity of Endometabolites from Sugar Beet (Beta Vulgaris L.) Pericarps. Journal of Microbiology, Biotechnology and Food Sciences. 2021 Jan 6; 2021:1303-6.
34. Okudu H, Ene-Obong H. Evaluation of the effect of storage time and temperature on some physicochemical properties of juice and jam developed from two varieties of monkey kola (Cola parchycarpa, Cola lepidota). African Journal of Food Science and Technology. 2015;6(7):194-203.
35. Onkar PR, Powar PV, Sharma PH, Avari JG. Evaluation of phytochemical and pharmacological activity of beetroot extracts (Beta vulgaris). Biochemistry & Pharmacology. 2013;2(4).
36. Pangesty DRH, Andarwulan N, Adawiyah DR. Identification of Pigment and its Antioxidant Activity of Several Species of Indonesian Dragon Fruit. Asian Journal of Chemistry. 2018; 30(9);1983-1988.
37. Pavlovic R, Mladenovic J, Radovanovic B, Maskovic P, Acamovic-Dokovic G. Biological activity of beetroot extracts.
38. Prieto-Santiago V, Cavia MM, Alonso-Torre SR, Carrillo C. Relationship between color and betalain content in different thermally treated beetroot products. Journal of Food Science and Technology. 2020 Sep;57(9):3305-13.
39. Quintana, S.E., Torregroza-Fuentes, E. and García Zapateiro, L.A., 2022. Development of Dressing-Type Emulsion with Hydrocolloids from Butternut Squash Seed: Effect of Additives on Emulsion Stability. *Gels*, *8*(4), p.209.
40. Saani M, Lawrence R. Evaluation of pigments as antioxidant and antibacterial agents from beta vulgaris Linn. International Journal of Current Pharmaceutical Research. 2016;8(3).

41. Saiki RK, Gelfand DH, Stoffel S, Scharf SJ, Higuchi R, Horn GT, Mullis KB, Erlich HA. Primer-directed enzymatic amplification of DNA with a thermostable DNA polymerase. Science. 1988 Jan 29;239(4839):487-91.
42. Sánchez-Moreno C, Larrauri JA, Saura-Calixto F. A procedure to measure the antiradical efficiency of polyphenols. Journal of the Science of Food and Agriculture. 1998 Feb;76(2):270-6.
43. Sharma N, Tanwer BS, Vijayvergia R. Study of medicinal plants in Aravalli regions of Rajasthan for treatment of kidney stone and urinary tract troubles. International Journal of PharmTech Research. 2011;3(1):110-3.
44. Silva JP, Bolanho BC, Stevanato N, Massa TB, da Silva C. Ultrasound-assisted extraction of red beet pigments (Beta vulgaris L.): Influence of operational parameters and kinetic modeling. Journal of Food Processing and Preservation. 2020 Oct;44(10): e14762.
45. Sivakumar V, Anna JL, Vijayeeswarri J, Swaminathan G. Ultrasound assisted enhancement in natural dye extraction from beetroot for industrial applications and natural dyeing of leather. Ultrasonics Sonochemistry. 2009 Aug 1;16(6):782-9.
46. Thakur V, Gupta DK. Studies on the clarification and concentration of beetroot juice. Journal of food processing and preservation. 2006 Apr;30(2):194-207.
47. Velicanski AS, Cvetkovic DD, Markov SL, Vulic JJ, Dilas SM. Antibacterial activity of Beta vulgaris L. pomace extract. Acta periodica technologica. 2011(42):263-9.
48. Vulvic JJ, Cebovic TN, Canadanovic-Brunet JM, Cetkovic GS, Canadanovic VM, Djilas SM, Saponjac VT. In vivo and in vitro antioxidant effects of beetroot pomace extracts. *Journal of Functional Foods*. 2014 Jan 1; 6:168-75.

International Journal of Biological Macromolecules xxx (xxxx) 127027

Contents lists available at ScienceDirect

International Journal of Biological Macromolecules

journal homepage: www.elsevier.com/locate/ijbiomac

Photocatalytic degradation of fluoroquinolone antibiotics using chitosan biopolymer functionalized copper oxide nanoparticles by facile sonochemical method

M. Ganeshbabu [a], J. Shiva Priya [a], G. Murali Manoj [b], N. Prasanna Naga Puneeth [a], C. Shobana [c], H. Shankar [b, *], R. Kalai Selvan [a, *]

[a] Energy Storage and Conversion Devices Laboratory, Department of Physics, Bharathiar University, Coimbatore 641046, Tamil Nadu, India
[b] Department of Physics, KPR Institute of Engineering and Technology, Coimbatore 641407, India
[c] Department of Zoology, Kongunadu Arts and Science College, Coimbatore 641 029, India

ARTICLE INFO

Keywords:
Chitosan
Copper oxide
Photocatalyst
Antibiotics
Sonochemical method

ABSTRACT

Photocatalytic degradation is an excellent method for removing pharmaceutical residues due to their simplicity, ecological benignity, high efficiency, and exceptional stability. Herein, we demonstrate the chitosan biopolymer functionalized copper oxide nanoparticles as an efficient photocatalyst synthesized by the facile sonochemical method. The X-ray diffraction Rietveld refinement revealed the formation of single-phase copper oxide with a monoclinic structure. The presence of biopolymer functionalization was corroborated by Fourier Transform Infrared spectroscopy by observing the -NH_2 and -OH functional groups. The high-resolution transmission electron microscopic images inferred that Chitosan functionalized copper oxide particles are nano-sized with a smooth texture and aggregation-free particles. The strong absorbance and the broad photoluminescence emission in the ultraviolet-visible region confirm the suitability of copper oxide (CuO) and Chitosan functionalized (C-CuO) nanoparticles for photocatalytic applications. The catalytic activity was studied against fluoroquinolone-based antibiotics such as ciprofloxacin and norfloxacin under direct sunlight illumination. Interestingly, the C-CuO catalyst demonstrated 71.07 % and 71.9 % degradation for ciprofloxacin and norfloxacin, respectively. The obtained photocatalytic activity of the prepared CuO and C-CuO catalysts was superior to the CuO particles prepared by the coprecipitation method (CC-CuO).

1. Introduction

Rapid industrialization and urbanization have increased environmental pollution in the past few decades. Out of three basic pollutions, water pollution is more significant due to the release of untreated/incompletely treated wastewater from the industries [1–4]. Apart from industrial waste like dyes and heavy metal-containing slags, the amount of pharmaceutical residues found in water sources has exceeded the threshold limits worldwide [5]. Most of the time, antibiotics are improperly released from medical lines, and partially metabolized antibiotics taken by humans and animals are excreted into water bodies [6–8]. So, they can create detrimental effects on aquatic ecosystems, including disrupting microorganisms that help the nitrogen cycle [9,10], promoting the growth of antibiotic-resistant bacteria in the human body [11], blocking sewage through the development of bacterial biofilms [12], bioaccumulation in the food chain [13] and other ecological processes [14]. Available antibiotic residues mainly observed in wastewater are fluoroquinolones, carbapenems, and cephalosporins [15]. Ciprofloxacin (CIP) and norfloxacin (NOR) are fluoroquinolone antibiotics that are routinely used to treat a variety of bacterial diseases [15]. Hence, there is a pressing need to remediate this wastewater to avoid high environmental risk.

Physical, chemical, and biological approaches are commonly used to remove pollutants from wastewater [9,10]. The physical (sorption and membrane filtration) and the chemical methods, such as coagulation/flocculation along with filtration, floatation, and precipitation, decrease the concentration of the antibiotics instead of degradation [17]. Therefore, the sludge produced from the above processes has to be subjected to further treatment for safe disposal [17]. On the other hand, biological methods are slow and must maintain certain external conditions for occurring reactions. Through some of the organic molecules degraded by the microorganisms, some are recalcitrant due to the com-

* Corresponding authors.
E-mail addresses: shankarnh@gmail.com (H. Shankar), selvankram@buc.edu.in (R.K. Selvan).

https://doi.org/10.1016/j.ijbiomac.2023.127027
Received 14 May 2023; Received in revised form 31 August 2023; Accepted 20 September 2023
0141-8130/

plexity of their chemical structure and resistant to degradation under aerobic conditions [18].

Interestingly, photocatalytic degradation is one of the versatile techniques to degrade toxic pollutants under visible regions. In this method, the photocatalyst absorbs the light quanta and mediates the chemical transformation of the reactants by photoreaction [19]. Among the homogeneous and heterogeneous catalysts [20,21], the heterogenous catalysts completely mineralize the dye/antibiotics molecules into CO_2 and other harmless by-products [22–24]. Further, the advantages of heterogeneous photocatalysts are chemical stability, non-toxicity, recyclability, and easy separation [25]. Various simple metal oxides, including TiO_2, ZnO, CeO_2, SnO_2, Bi_2O_3, V_2O_5, Fe_2O_3, and WO_3, have been used as photocatalysts for antibiotic and synthetic dye degradation [26]. Metal oxides are suitable photocatalysts due to their favorable electronic structure, capacity to create charge carriers, charge transport characteristics, and light absorption properties [27,28]. Moreover, they are biocompatible and have a simple composition with stoichiometric diversity.

The current study focused on the fabrication of copper oxide (CuO) nanoparticles and chitosan-functionalized CuO for the degradation of ciprofloxacin (CIP) and norfloxacin (NOR) in the presence of sunlight. It is well known that CuO is a p-type semiconductor with a bandgap of ~1.2 eV, and its absorption lies in the visible light region. Since 43 % of the solar spectrum is made up of visible light, the CuO photocatalyst remains active under sunlight irradiation [29–32]. CuO NPs tend to absorb molecular oxygen and scavenge photoelectrons that restrict the electron-hole recombination at the interface [33]. However, they have been combined with metals, nonmetals, and polymers to further improve the light absorption capabilities of metal oxide nanoparticles via the synergistic effect [34]. Significantly, when metal oxides are composited/functionalized with macromolecules, the particle size is reduced, allowing the produced photoelectrons and holes to be trapped on the particle surface and reducing the chance of electron-hole recombination [35]. Polymers like polyethylene glycol, polyvinyl pyrrolidone, polyvinyl alcohol, polypyrrole (PPy), etc., have been used to enhance the photocatalytic properties of metal oxide like TiO_2, ZnO, and associated nanocomposites [36]. Since Chitosan is the second-most prevalent biopolymer after cellulose and is a non-toxic biopolymer made from chitin, it was chosen for functionalization in this study [37]. Recently, chitosan composites with TiO_2, ZnO, and CdS have been used for the degradation of dye present in aqueous solution [38–40]. Because of the unique properties of CuO and Chitosan, the chitosan-CuO system has been investigated for a variety of applications, including antifouling coatings, oxidative degradation of azoic dye, microbial-resistant nanocomposite films for antimicrobial application, and non-enzymatic (electrochemical sensing) hydrogen peroxide sensing [41–44].

The CuO NPs have been prepared using a variety of approaches, including chemical precipitation, hydrothermal, solution combustion, sonochemical, and electrochemical procedures [45]. Among these, the sonochemical process is an efficient and fast technique that offers good control over the morphology and crystallite size of the nanostructures in comparison to other methods [46]. Ultrasound is regarded as a better tool for promoting mass transport during synthesis using acoustic streaming and turbulent mixing. The improved mass transport favors the desired reaction conditions for nanomaterial synthesis. The microjets and shockwaves generate defects or damage to the solid surface when they impinge on it. These defects can capture photoelectrons and decrease the bandgap energy, which enhances the photocatalytic process [47]. Nanoparticles produced by ultrasonic irradiation exhibited better photocatalytic efficiency over the nanoparticles prepared by other methods due to larger specific surface area and smaller crystallite size [48,49].

Hence, to achieve the aforementioned benefits, photodegradation of ciprofloxacin and norfloxacin antibiotic drugs (fluoroquinolone class drugs) by chitosan-functionalized CuO nanoparticles, synthesized by sonochemical method was studied under direct sunlight irradiation in the present work. To determine the benefits of chitosan functionalization, the pristine CuO is likewise synthesized using the same sonochemical process, and the results are compared. Similarly, to assess the influence of the sonochemical approach, the coprecipitation method is employed to synthesize and study the characteristics of chitosan-functionalized CuO.

2. Materials and methods

Copper acetate monohydrate ($Cu(CH_3COO)_2.H_2O$) (Merck), sodium hydroxide (NaOH) (HiMedia), Chitosan ($C_{56}H_{103}N_9O$) (low molecular weight), ciprofloxacin ($C_{17}H_{18}FN_3O_3HCl$), and Norfloxacin ($C_{16}H_{18}FN_3O_3$) (Sigma-Aldrich) were of analytical grade and were used without any further purification. All the solutions were prepared using double distilled water.

To synthesize CuO NPs, 1 M Cu $(CH_3COO)_2.H_2O$ was dissolved in 10 ml of double distilled water under constant agitation using a magnetic stirrer (500 rpm at room temperature). 2 M NaOH solution was added dropwise to the above solution under ultrasound irradiation for 1 h. (9 s on and 1 s off) until a black precipitate was formed. The temperature was constantly monitored using a thermostat during the sonication process. The obtained precipitate was washed with distilled water and ethanol and dried in a hot air oven. Later, the brown precipitate was ground using mortar and pestle. The resulting powder was calcined for 3 h at 500 °C under an argon atmosphere to get CuO nanoparticles. The sample thus prepared was labeled CuO. The same procedure was followed for synthesizing chitosan-functionalized CuO NPs except for the first step. 1 M $Cu(CH_3COO)_2.H_2O$ was added to 10 ml chitosan solution (1 g of chitosan in 1 % glacial acetic acid) instead of water. All the other steps were the same as mentioned in the above process. The biopolymer chitosan is composed of glucosamine and *N*-acetylglucosamine units. At about 270 °C, Chitosan starts to degrade thermally. The *N*-acetylglucosamine and glucosamine units disintegrate at the above temperature, producing carbon dioxide, water, and ammonia. As the temperature rises, the degradation rate accelerates until the Chitosan is totally broken down at about 500 °C. In the meantime, the surfaces of the CuO nanoparticles were grafted with the amine and hydroxyl functional groups [50–52]. The Chitosan functionalized CuO thus obtained was labeled C-CuO.

The X-ray diffraction technique was used to analyze the crystallographic structure and phase of the nanoparticles (D8 Advance diffractometer, BRUKER). The functional groups or bending and stretching of bonds were determined from the Fourier Transform Infrared (FTIR) spectra using JASCO FT-IR-6600 instruments. UV–visible absorption spectra were measured on a JASCO V-650 spectrophotometer. Photoluminescence spectra were obtained using FluoroMax Plus (HORIBA) instrument. HRTEM was performed by JEOL JEM 2100 plus a High-resolution transmission microscope for the assessment of the morphology of nanoparticles.

The photocatalytic activity of the samples was evaluated by the photodegradation of fluoroquinolone antibiotics (Ciprofloxacin and Norfloxacin) for 140 and 60 min. For the experiment, 40 mg of the prepared samples (CuO and C-CuO) was added with 50 ml of aqueous solution of antibiotics (25 mg/L). The solutions were kept in the dark and constantly stirred for 60 min to obtain the absorption-desorption equilibrium. The blank solution (Without photocatalyst) was also exposed to direct sunlight. Aliquots of 5 ml from each beaker were collected at an interval of 20 min and centrifuged to remove the photocatalyst. The concentration of dye present in each sample is evaluated using a UV–vis absorption spectrometer. The degradation percentage was calculated using the following equation.

$$\text{Degradation } (\%) = \frac{C_0 - C}{C_0} \times 100 \quad (1)$$

where C_0 is the initial dye concentration, and C is the concentration of antibiotics at time t. The concentration of the CIP/NOR in the solution is found from the absorbance as it is directly proportional to the concentration.

3. Results and discussion

3.1. Structural and optical properties

The crystallinity and the phase formation of the synthesized pristine and Chitosan functionalized CuO nanoparticles are analysed using the XRD technique. Fig. 1 (a,b) shows the corresponding XRD Rietveld refinement pattern using the FullProf program. The observed sharp, intense, well-defined peaks indicate the high crystalline nature of the materials. The absence of characteristic peaks related to impurities shows that the synthesized samples are highly phase-pure. The Rietveld refinement revealed that the measured pattern and the predicted values agreed well based on the low values of the residuals for the weighted pattern R_{wp}, R_p, and the structural factor R_f (Table 1). The XRD patterns are indexed in the monoclinic system with the lattice parameters of a = 4.686 Å, b = 3.428 Å, c = 5.131 Å, and β = 99.4◦ for C-CuO and a = 4.684 Å, b = 3.428 Å, c = 5.131 Å, and β = 99.39°for CuO. The peak positions and lattice parameters are comparable with the JCPDS (PDF No. 89–5899) and the reported pristine CuO [53]. However, the peak intensity of C-CuO is higher than the pristine CuO, which reveals the high crystallinity. This suggests that the decomposition of the polymer over calcination enhances the crystalline formation and hence improves the crystallinity of the nanoparticles [54]. Usually, the polymers are organic compounds, which provide additional thermal energy for compound formation through the exothermic reaction during the calcination. The decomposition of the polymer removes any impurities, residual solvents, etc., [55]. Additionally, the high-temperature calcination promotes the diffusion and rearrangement of atoms, forming more ordered and crystalline structures [55,56]. It is believed that the high crystallinity of the photocatalyst favors the catalytic process [57,58].

Subsequently, the grain size, lattice strain, lattice density, dislocation density, and surface area were calculated using the following equations and are given in Table 1.

$$D = \frac{0.9\lambda}{\beta cos\theta} \quad (2)$$

$$\epsilon = \frac{\beta cos\theta}{4} \quad (3)$$

$$\rho = \frac{Z\,M}{N\,V} \quad (4)$$

$$s = \frac{6}{\rho \text{ x } D} \quad (5)$$

where D is the grain size, β is the full-width half maximum, ρ is the lattice density, Z is the number of atoms present in the cell, M is the molecular weight, N is the Avagadros number, V is the cell volume, and s is the surface area. The peaks broadening indicates that the grains are

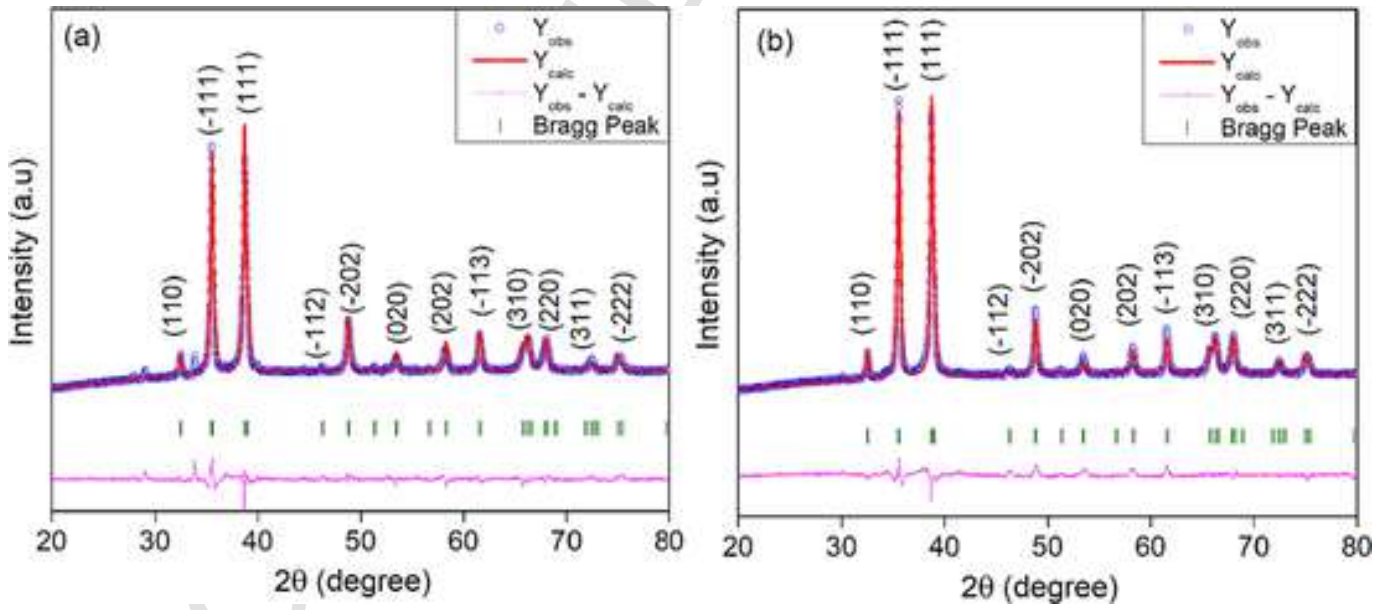

Fig. 1. XRD Rietveld refinement pattern of (a) CuO and (b) C-CuO.

Table 1
XRD Rietveld refinement lattice parameters.

Sample	Lattice Constants	Cell volume ($Å^3$)	R_p	R_{wp}	χ^2	Grain size (nm)	Lattice strain	Lattice Density (g/cm^3)	Dislocation density ($\times 10^{15}$ lines/m^2)	Surface area (m^2/g)
CuO	a = 4.686 Å b = 3.428 Å c = 5.131 Å β = 99.42◦	81.34	18.1	14.1	5.49	26	0.001298	6.55	1.338	34
C-CuO	a = 4.684 Å b = 3.428 Å c = 5.131 Å β = 99.39◦	81.29	17.2	12.4	4.69	21	0.001195	6.52	1.038	42

in the nanoscale dimensions. Usually, grain size and lattice defects influence peak broadening significantly. The grain size calculated using the Scherrer equation (Eq. (2)) is 26 nm for CuO and 21 nm for the C-CuO catalysts, respectively. Lattice strain for CuO and C-CuO is 0.001298 and 0.001195, respectively. From the lattice strain and grain size values, it is evident that grain size is directly proportional to lattice strain [59]. These relations correlated with Previous reports by Avinash et al. 2019, prepared *aloe vera latex*-assisted CuO particles, and Badri et al. 2021, obtained from prickly pear leaf extract gaped CuO nanoparticles [60,61]. The obtained lattice density [62] matches the JCPDS (PDF No. 89–5899). Similarly, the calculated specific surface area of CuO and Chitosan functionalized CuO is 34 and 42 m^2/g. M. P. Geetha et al. 2020 made a similar observation of higher surface area while functionalizing CuO nanoparticles (CuO NPs) with carboxylic acid and silane functional groups using the reagents EDTA (Ethylenediamine tetraacetic acid) and APTES (Aminopropyl triethoxysilane) [62]. A significantly higher surface area implies that the Chitosan functionalized CuO can be a suitable catalyst.

Fig. 2a shows the FTIR spectra of CuO and C-CuO samples. For the C-CuO catalyst, the peaks observed at 2973 cm^{-1} and 2887 cm^{-1} correspond to C—H stretching vibration [63], and the band at 1625 cm^{-1} indicates the C—O stretching along with N—H deformation [64]. The band confirms the presence of carboxylic acid at 1398 cm^{-1} [65]. The band at 1152 cm^{-1} indicates the asymmetric stretching of C-O-C that corresponds to the β(1–4) glycosidic linkage of Chitosan [66]. All of these functional groups support the existence of chitosan residues in the CuO nanoparticles. It is widely assumed that the presence of $-NH_2$ and -OH functional groups in the catalyst aids in anchoring dye molecules. The observed band between 900 cm^{-1} and 600 cm^{-1} represents the elongation vibrations of the transition metal-oxygen bond corresponding to CuO. The characteristic peaks of Cu—O occurred at 546 cm^{-1}, 593 cm^{-1}, and 700 cm^{-1} [57,67,68]. Stabilization of CuO nanoparticles by Chitosan is evident from the increase in the intensity of peaks in the fingerprint region of the spectra.

UV–visible absorbance spectra are collected to elucidate the optical properties of CuO and C-CuO nanoparticles. Fig. 2b shows that the prepared CuO and C-CuO catalysts have strong absorbance characteristics in UV and the entire visible region. The absorbance peak of C-CuO is slightly blue-shifted than that of the CuO nanoparticles due to the quantum confinement effect [69]. Using a Tauc plot (Fig. 2b inset), the calculated band gap for CuO and C-CuO are 1.58 eV and 1.75 eV, respectively. The minor enhancement of the band energy gap is due to the lowering of particle size, which will be discussed later in the HRTEM analysis [70,71]. However, the obtained band gap value of Chitosan functionalized CuO is most favorable for photocatalytic application under visible light conditions.

3.2. Morphological and particle size analysis

The morphology and size of the nanoparticles are visualized using High-Resolution Transmission Electron Microscopic (HRTEM) images. Fig. 3 shows the TEM/HRTEM images and SAED pattern of CuO and C-CuO catalysts. The TEM images (Fig. 3a and d) revealed that CuO exhibits more agglomeration than C-CuO particles. C-CuO samples have spherical and rod-like particle morphologies with particle sizes ranging from 70 to 110 nm. The surface of functionalized CuO has a smooth texture, and the addition of Chitosan regulates particle aggregation. The obtained well-defined parallel lattice fringes show that the synthesized crystals are highly crystalline (Fig. 3b and e). The lattice spacing for CuO (CuO) and functionalized CuO (C-CuO) is calculated as 0.2680 nm and 0.2528 nm, respectively. The lattice spacing of the latter is in good agreement with the (0 0 2) plane of monoclinic CuO, which is in accordance with the XRD results. The selective area diffraction (SAED) pattern reveals the polycrystalline nature of the synthesized catalysts. The lattice planes obtained from the pattern are consistent with the XRD data (Fig. 3c and f).

Further, the size distribution of the prepared CuO and C-CuO nanoparticles was investigated using the dynamic light scattering (DLS) method (Fig. 4). The DLS spectra show that the Sonochmeically made Chitosan functionalized CuO (C-CuO) particle size is smaller. The average particle size of CuO and C-CuO particles are 383 nm and 150 nm, respectively. It further substantiates the larger active surface area of C-CuO for catalytic applications.

3.3. Photocatalytic activity of CuO and C-CuO catalysts

The photocatalytic activity of the prepared CuO and C-CuO catalysts is determined by monitoring the degradation of ciprofloxacin (CIP) and norfloxacin (NOR) for a reaction time of 140 min and 60 min under the irradiation of sunlight at an interval of 20 min. The characteristic absorption band of CIP (Fig. 5) and NOR (Fig. 6) at 275 and 272 nm gradually decreases as a function of irradiation time. Figs. 5a and 6a show the photolysis of the blank solution (without catalyst) as well as Fig. 5 (b, c) and Fig. 6(b, c) elucidate the degradation activity of CuO and C-CuO catalysts for CIP and NOR degradation, respectively. In both cases, as the reaction time increases, the peak intensity decreases, i.e., the concentration of the fluoroquinolone antibiotics decreases in the aqueous solution. Comparatively, the C-CuO catalyst provides higher photocatalytic activity than the CuO catalyst in both antibiotics degradation.

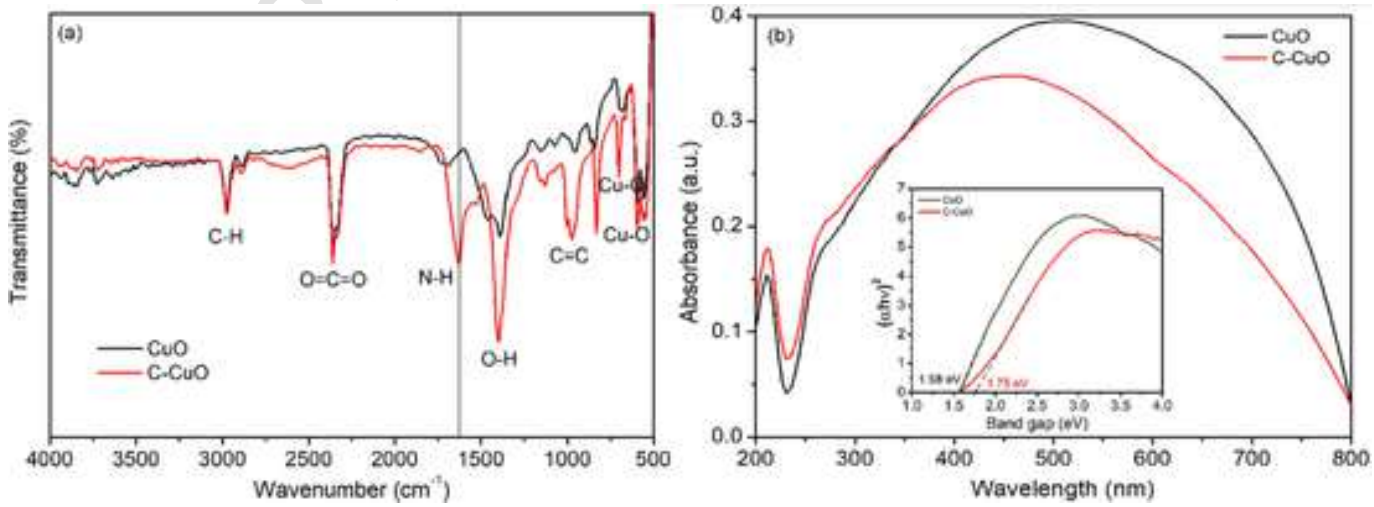

Fig. 2. (a) FTIR and (b) UV–Vis spectra of CuO and C-CuO catalyst (inset: Tauc Plot).

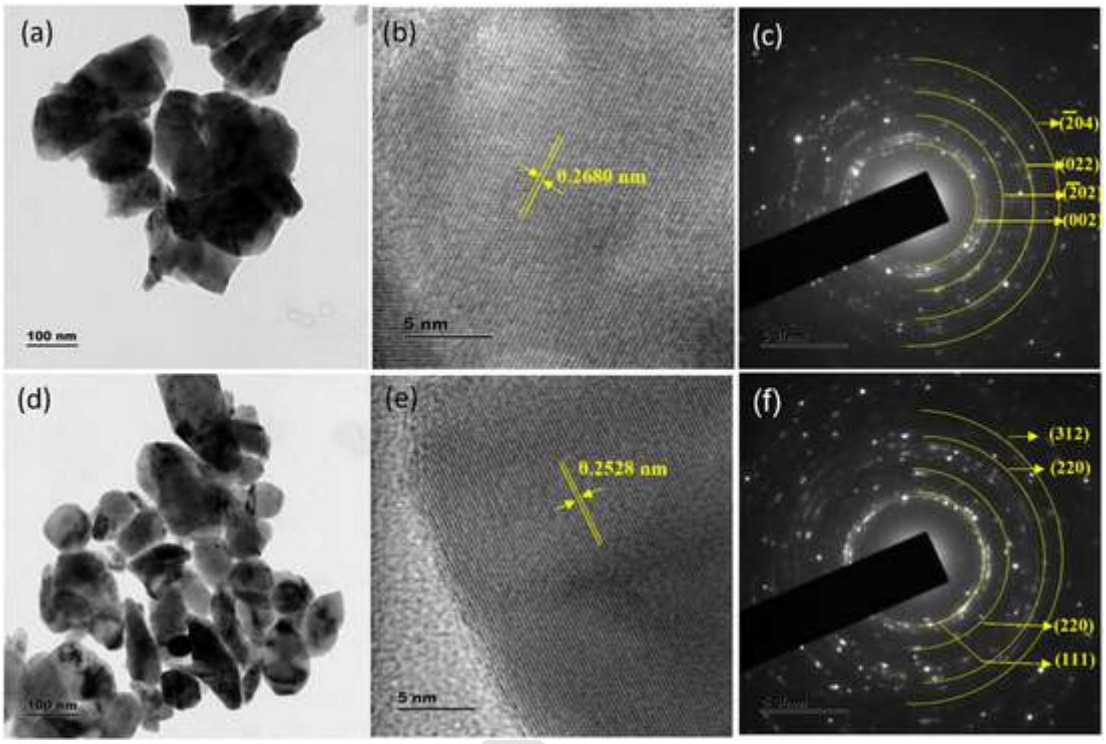

Fig. 3. TEM, HRTEM, and SAED patterns of (a-c) CuO and (d-f) C-CuO nanoparticles, respectively.

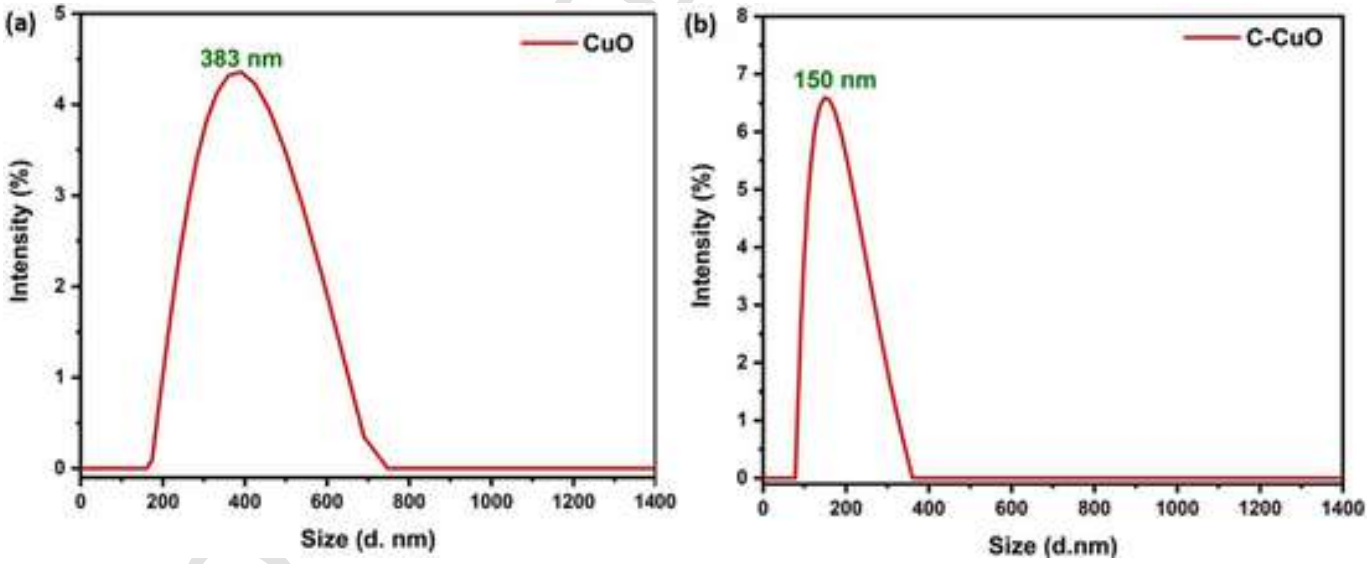

Fig. 4. DLS spectra of (a) CuO and (b) C-CuO.

The CIP degradation percentage of C-CuO, CuO, and the blank are 71.07 %, 54.37 %, and 8.31 %, respectively. Similarly, the C-CuO catalyst provides the activity of 71.9 % degradation against NOR after 60 min of sunlight illumination, which is 1.24 times larger than CuO (57.6 %). Fig. 7a provides evidence that the photolysis-induced NOR degradation is negligible. The photocatalyst-assisted reaction has more degradation against the pharmaceutical pollutant, indicating that the photocatalytic process outperforms photolysis than the blank solution.

Antibiotics' photocatalytic degradation mechanism can occur in three steps. The 1st step is the adsorption of CIP/NOR pollutant molecules by the surface of the C-CuO nanoparticles, as observed in the TEM images. Since the nanoparticles with a high surface area can adsorb more CIP/NOR molecules, making the degradation faster [72]. 2nd step is the production of photoelectrons. The nanoparticles absorb the photons from the sunlight, and the electrons get excited to the conduction band from the valence band, leaving behind a hole. The reduced size of the catalyst nanoparticles prevents the recombination of the electron-hole pairs [73]. 3rd step is producing reactive oxygen species (ROS) like superoxide and hydrogen peroxide. Electrons in the conduction band react with oxygen in the water to form superoxide. The H^+ ions with the superoxide produce H_2O_2, which decomposes into hydroxyl ions with good oxidizing properties. These ions break the bonds of the CIP/NOR pollutant molecules and reduce them to CO_2 and other harmless products [74]. The possible reaction equations are given below (Eqs. (6)–(11)).

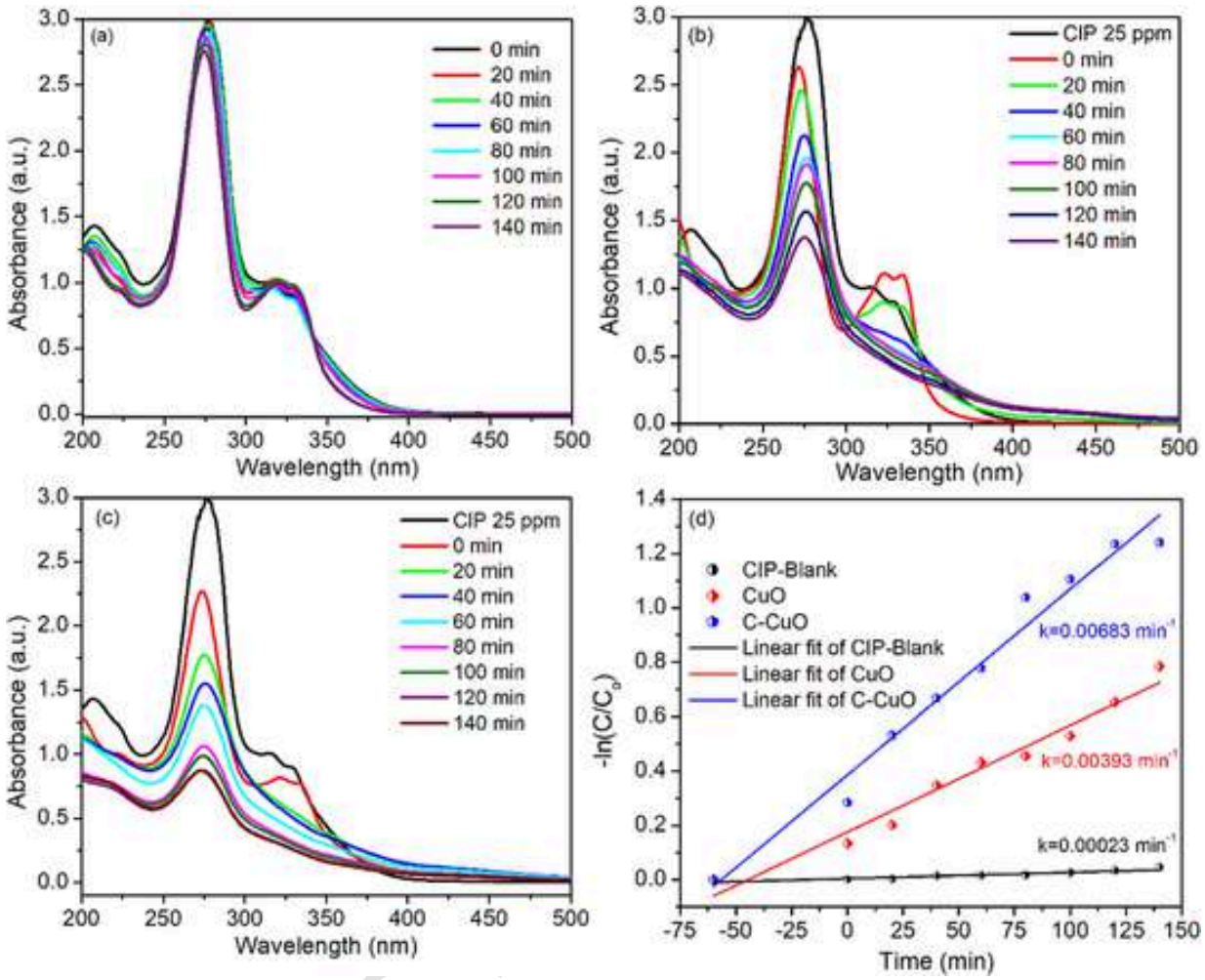

Fig. 5. UV–Vis spectra of the photocatalytic degradation of CIP using (a) without catalyst, (b, c) with catalysts of CuO and C-CuO, and (d) the corresponding Pseudo-first order kinetics plot.

$$CuO + h\gamma \rightarrow CuO\ \left(e^{-}_{cb} + h^{+}_{vb}\right) \quad (6)$$

$$H_2O \rightarrow H^{+} + OH^{-} \quad (7)$$

$$O_2 + 2e^{-} \rightarrow O_2^{*} \quad (8)$$

$$O_2^{*} + 2H^{+} \rightarrow H_2O_2 \quad (9)$$

$$H_2O_2 \rightarrow 2OH^{-} \quad (10)$$

$$OH^{-} + \text{Antibiotics} \rightarrow CO_2 + H_2O \quad (11)$$

Subsequently, the reaction kinetics and the rate constant are calculated using Eq. (12). It reveals that photocatalysis obeys pseudo-first-order kinetics.

$$k = \frac{1}{t}\ \ln\ \left(C_o/C\right) \quad (12)$$

where k is the rate constant in min^{-1}, C_o is the dye concentration at $t = 0$, and C is the dye concentration at time t. Figs. 5d and 6d depict the rate-constant determination for the photodegradation by CuO, CuO, and blank solution. It is observed that the rate constants of CuO and C-CuO are 0.00393 min^{-1} and 0.00683 min^{-1}, respectively, for CIP disintegration. Similarly, the CuO and C-CuO rate constant is 0.0070 min^{-1} and 0.0103 min^{-1} for NOR degradation. From the rate constants, it is evident that C-CuO exhibits better photocatalytic properties than CuO catalyst. Subsequently, the obtained parameters are compared with the reported metal oxide and polymer composites (Tables 2 and 3), which further confirms the catalytic performance of C-CuO nanoparticles is relatively high [75–77].

The improved photocatalytic activity of C-CuO may be due to the following reasons. The biopolymer chitosan used during the sonochemical synthesis of CuO served as a bio-stabilizer, increasing the material's crystallinity and purity. Also, the sonochemical approach produced more active sites with an increased surface area. The smaller particle size observed from TEM images and the wide range of visible light absorption confirmed by UV and PL play an important role in the photocatalytic degradation of CIP and NOR. Furthermore, the presence of amine and the hydroxyl functional groups generated by chitosan mediation, which was corroborated by FTIR, may have some advantageous effects on the subsequent processes during photocatalytic degradation. The amine and hydroxyl functional groups improve the ability of CuO to absorb light and can facilitate the transfer of electrons between the nanoparticles and the pollutant. Since amino and hydroxyl functional groups can serve as electron donors or acceptors, they facilitate the transport of electrons between the nanoparticles and the contaminants. In order to enable anchoring/absorbing additional pollutant molecules, the Chitosan functionalized CuO (C-CuO) comprises more amino and hydroxyl groups. Moreover, the increased photocatalytic activity of C-CuO against pharmaceutical pollutants (CIP & NOR) is due to the higher point contact, surface smoothness, more surface-active sites, and superior charge separation capability.

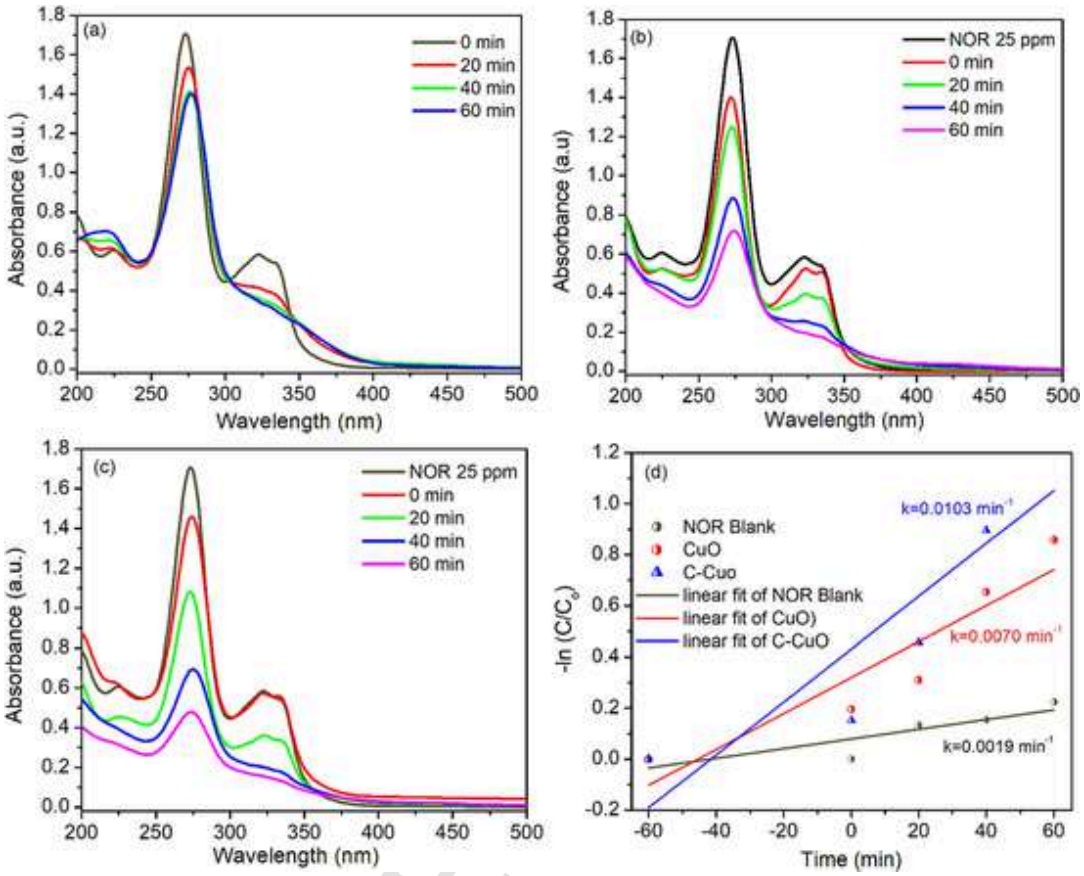

Fig. 6. UV–Vis spectra of the photocatalytic degradation of NOR using (a) without catalyst, (b, c) with CuO and C-CuO catalysts, and (d) the corresponding Pseudo-first order kinetics plot.

3.4. Analysis of chitosan functionalized CuO synthesized by coprecipitation method

To identify the role of the sonochemical method in the degradation of the antibiotic, the C-CuO is prepared by a conventional coprecipitation approach (without sonication), labeled as CC-CuO. Fig. 7 shows the structural, optical, and morphological properties of the CC-CuO catalyst. The distinctive Braggs peaks correspond to the monoclinic phase of CuO (JCPDS PDF No. 89-5899) without any additional impurities (Fig. 7a). The presence of Chitosan during the preparation of CC-CuO is the factor that causes the phase purity and high crystallinity, as observed in C-CuO nanoparticles. The crystallite size of CC-CuO is 34 nm, which is larger than the sonochemically synthesized CuO and C-CuO. The unit cell parameters of CC-CuO are a = 4.7032, b = 3.4225, c = 5.0492, and = 100.05°. The CC-CuO catalyst has a lattice strain of 0.06064. The lattice density and surface area of CC-CuO are 6.524 g/cm^3 and 34 m^2/g, respectively. The FTIR spectrum further infers the presence of amine and hydroxyl functional groups, substantiating that the prepared catalyst functionalized with chitosan molecules (Fig. 7b). The CC-CuO catalyst has random morphologies with an average particle size is around 170 nm observed from the TEM image (Fig. 7b inset). The UV–visible absorbance spectrum (Fig. 7c) elucidates the broad range of visible light responses with the energy gap of 1.54 eV measured using the Tauc plot (Fig. 7c inset).

Fig. 7d shows the comparative acquired PL emission spectra for C-CuO and CC-CuO nanoparticles at a 300 nm excitation wavelength. The broad emission on both catalysts in the visible spectra supports the UV–Visible results. The observed peak around 330 nm corresponds to the band edge emission in the UV region. The defect associated with deep-level emission (DLE) caused by structural defects such as oxygen vacancies is the leading cause of the peak at 466 nm in C-CuO catalysts. The trapped electrons at the Cu interstitial site underwent a radiative transition to the valence band, resulting in the blue emission (DLE) [69]. However, the difference in PL intensity and peak shift was detected for CC-CuO over C-CuO. The blue shift and enhanced peak intensity of CC-CuO shows better photogenerated charge recombination [32]. Therefore, these optical characteristics further confirm the suitability of Chitosan functionalized sonochemically prepared CuO (C-CuO) for photocatalytic application.

Fig. 8 (a,b) shows the photocatalytic degradation properties of CC-CuO of CIP and NOR antibiotics. The degradation efficiency of CC-CuO for NOR and CIP antibiotics is 21.05 % and 22.52 % after the measured reaction time. Similarly, the rate constants of NOR and CIP degradations are 0.00342 min^{-1} and 0.00133 min^{-1}, respectively. The rate constant of CC-CuO for NOR and CIP is roughly 2 and 5.3 times lower than the value obtained for C-CuO, respectively. Compared to C-CuO, CC-CuO has a significantly larger size, and its band gap value of 1.54 eV is located in the near-infrared range. Since the surface-to-volume ratio is lower and the photoactive zone for CC-CuO is substantially smaller, there is less possibility for the potential photocatalytic process. Overall, C-CuO outperformed CC-CuO in photocatalytic performance. The main factors contributing to the superiority of the C-CuO photocatalyst may be the functionalization of CuO by biopolymer, the smaller particle size, the significant number of defect sites during intense ultrasonic irradiation by the sonochemical process, and the appropriate bandgap [87].

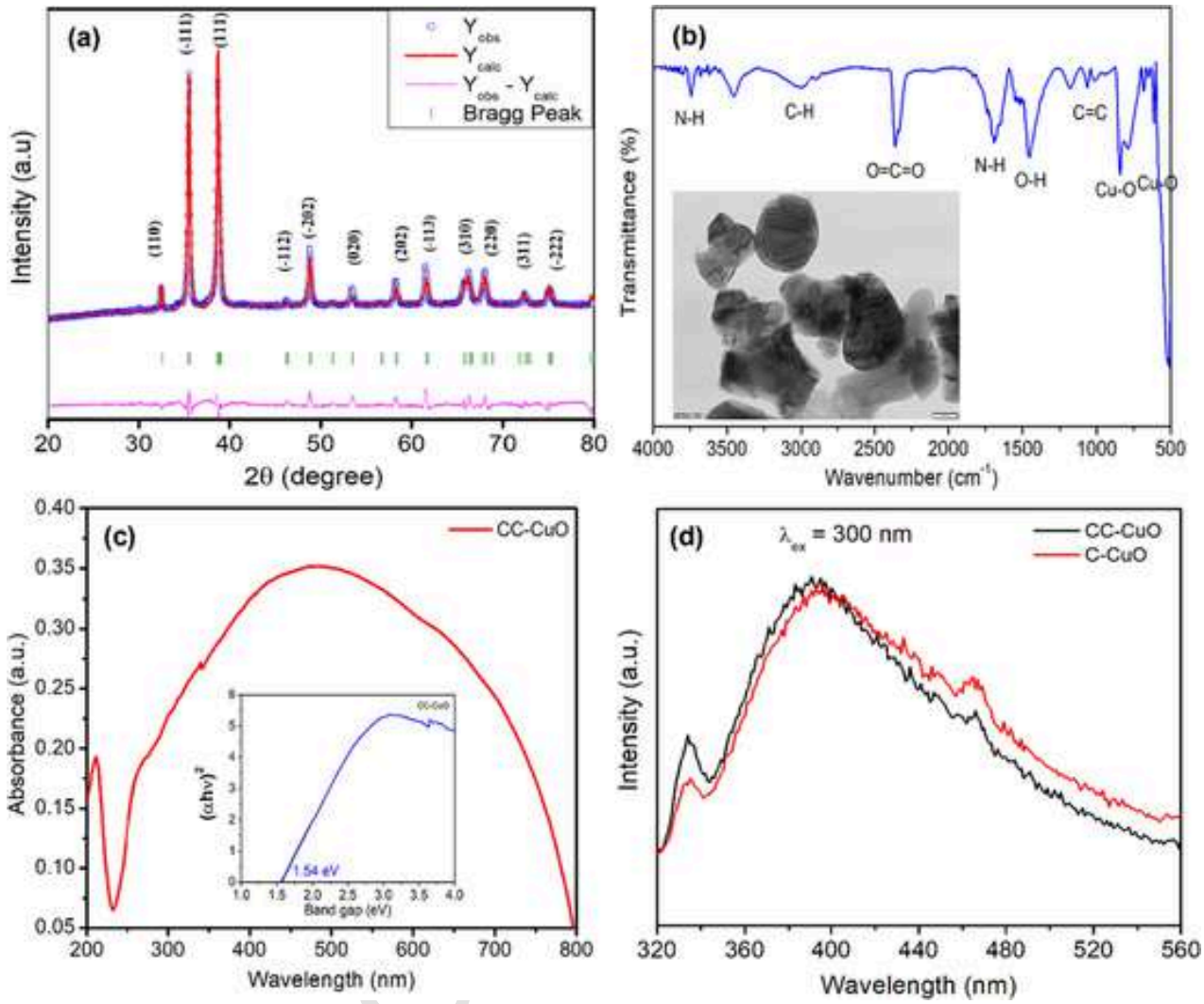

Fig. 7. (a) XRD Rietveld refinement, (b) FTIR spectrum (inset: TEM image), and (c) UV- vis spectrum (inset: Tauc Plot) of CC-CuO catalyst. (d) Comparative PL emission spectra of C-CuO and CC-CuO catalysts.

Table 2
Comparison of ciprofloxin photocatalytic degradation by C-CuO with other reported catalysts.

Catalyst	Dose	Light source	Ciprofloxin concentration	Degradation time	Percentage of degradation	Reference
$Ag/Fe_2O_3/ZnO$	30 mg/L	Sun light	10 ppm	210 min	76.4 %	[78]
Fe-ZnO	150 mg/L	Sun light	10 ppm	210 min	66 %	[79]
$g\text{-}C_3N_4/RGO/WO_3$	0.1 g/L	500 W Xenon lamp	20 ppm	180 min	85 %	[80]
$N,S\text{-}TiO_2$	0.05 g	500 W Halogen lamp	30 ppm	150 min	78.7 %	[81]
Er-BiOBr	0.01 g	300 W Xe lamp	10 ppm	360 min	61 %	[82]
C-CuO	40 mg	Sun light	25 ppm	140 min	71.07 %	This work

Table 3
Comparison of Norfloxin photocatalytic degradation by C-CuO with other reported catalysts.

Catalyst	Dose	Light source	Norfloxin concentration	Degradation time	Percentage of degradation	Reference
$TiO_2/Bi_2WO_6/rGO$	50 mg	500 W xenon lamp	20 ppm	60 min	84.13 %	[83]
$AgBr/LaNiO_3/g\text{-}C_3N_4$	20 mg	500 W xenon lamp	20 ppm	120 min	87 %	[84]
ZnO/ZnS@BC	0.5 g/L	UV lamp	25 ppm	3 h	55 %	[85]
rGO/Ag_2PO_4	–	250 W xenon lamp	15 ppm	100 min	83.68 %	[86]
C-CuO	40 mg	Sun light	25 ppm	60 min	71.9 %	This work

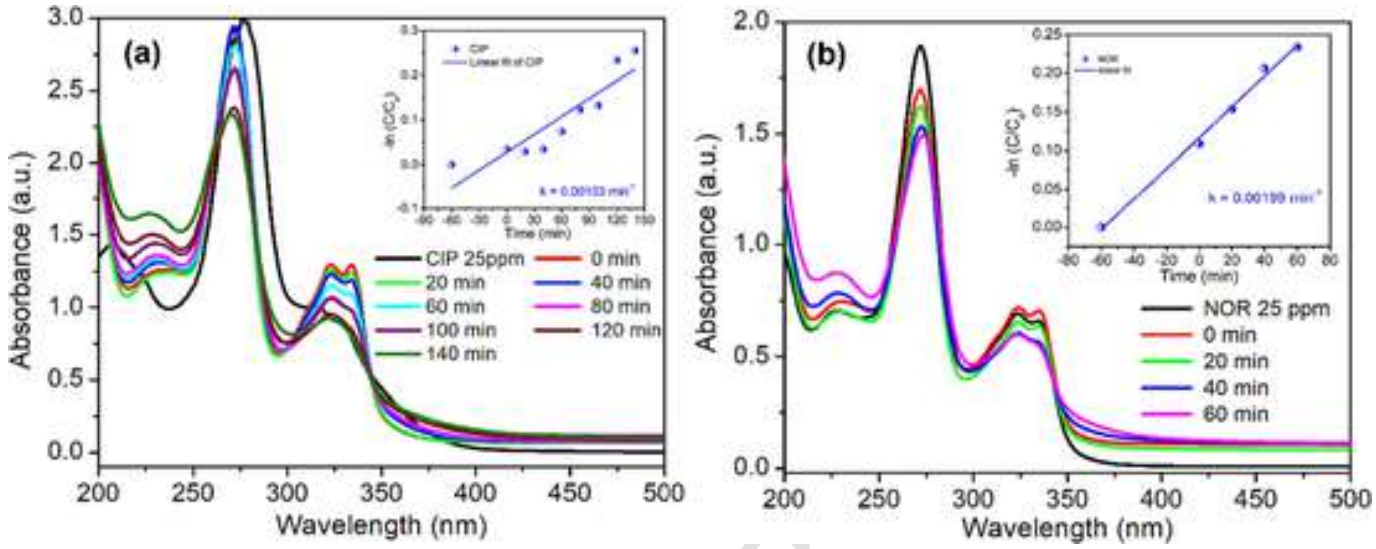

Fig. 8. UV–Vis spectra of the photocatalytic degradation of (a) CIP and (b) NOR using CC-CuO as catalyst (inset: Corresponding pseudo-first-order kinetics plot).

4. Conclusion

This study uses a sonochemical approach to create highly crystalline chitosan-functionalized CuO nanoparticles. For comparison, the coprecipitation method was also employed to prepare Chitosan functionalized CuO nanoparticles. The XRD pattern supports the purity and monoclinic structure of the synthesized CuO nanoparticles. Chitosan functionalization is confirmed by the presence of -NH_2 and -OH functional groups in FTIR spectra. Based on the strong UV–visible spectral absorption and broad PL emission in the UV and visible region, it is confirmed that CuO and C-CuO are beneficial for photocatalytic applications. According to HRTEM examination, the nanoparticles have a smooth texture, and adding Chitosan reduces particle aggregation significantly. Under direct sunlight, the photocatalytic activity of the nanoparticles is tested against the fluoroquinolone-based drugs Ciprofloxacin and Norfloxacin. The first order rate constant for the degradation of CIP and NOR are 0.00683 min^{-1} and 0.0103 min^{-1}, respectively. Chitosan functionalized CuO (C-CuO) prepared by the sonochemical method outperformed the degradation of antibiotics because of its enriched functional group, more active sites, and smaller particle size.

Uncited reference

[16]

Declaration of competing interest

The authors declare that they have no known competing financial interests or personal relationships that could have appeared to influence the work reported in this paper.

Data availability

Data will be made available on request.

References

[1] K.K. Kesari, R. Soni, Q.M.S. Jamal, P. Tripathi, J.A. Lal, N.K. Jha, M.H. Siddiqui, P. Kumar, V. Tripathi, J. Ruokolainen, Wastewater treatment and reuse: a review of its applications and health implications, Water. Air. Soil Pollut. 232 (2021), https://doi.org/10.1007/s11270-021-05154-8.

[2] Z. Wang, L. Hu, M. Zhao, L. Dai, D. Hrynsphan, S. Tatsiana, J. Chen, Bamboo charcoal fused with polyurethane foam for efficiently removing organic solvents from wastewater: experimental and simulation, Biochar. 4 (2022), https://doi.org/10.1007/s42773-022-00153-2.

[3] B. Guo, Y. Wang, Y. Feng, C. Liang, L. Tang, X. Yao, F. Hu, The effects of environmental tax reform on urban air pollution: a quasi-natural experiment based on the Environmental Protection Tax Law, Front. Public Heal. 10 (2022), https://doi.org/10.3389/fpubh.2022.967524.

[4] G. Zhang, Z. Zhao, X.A. Yin, Y. Zhu, Impacts of biochars on bacterial community shifts and biodegradation of antibiotics in an agricultural soil during short-term incubation, Sci. Total Environ. 771 (2021) 144751, https://doi.org/10.1016/j.scitotenv.2020.144751.

[5] B.H. Schafhauser, L.A. Kristofco, C.M.R. de Oliveira, B.W. Brooks, Global review and analysis of erythromycin in the environment: occurrence, bioaccumulation and antibiotic resistance hazards, Environ. Pollut. 238 (2018) 440–451, https://doi.org/10.1016/j.envpol.2018.03.052.

[6] D.G.J. Larsson, C.F. Flach, Antibiotic resistance in the environment, Nat. Rev. Microbiol. 20 (2022) 257–269, https://doi.org/10.1038/s41579-021-00649-x.

[7] S. Pang, C. Zhou, Y. Sun, K. Zhang, W. Ye, X. Zhao, L. Cai, B. Hui, Natural wood-derived charcoal embedded with bimetallic iron/cobalt sites to promote ciprofloxacin degradation, J. Clean. Prod. 414 (2023) 137569, https://doi.org/10.1016/j.jclepro.2023.137569.

[8] Z. Liu, B. Fan, J. Zhao, B. Yang, X. Zheng, Benzothiazole derivatives-based supramolecular assemblies as efficient corrosion inhibitors for copper in artificial seawater: formation, interfacial release and protective mechanisms, Corros. Sci. 212 (2023) 110957, https://doi.org/10.1016/j.corsci.2022.110957.

[9] A. Alam, W.U. Rahman, Z.U. Rahman, S.A. Khan, Z. Shah, K. Shaheen, H. Suo, M.N. Qureshi, S.B. Khan, E.M. Bakhsh, K. Akhtar, Photocatalytic degradation of the antibiotic ciprofloxacin in the aqueous solution using Mn/co oxide photocatalyst, J. Mater. Sci. Mater. Electron. 33 (2022) 4255–4267, https://doi.org/10.1007/s10854-021-07619-2.

[10] J.E. Sosa-Hernández, L.I. Rodas-Zuluaga, I.Y. López-Pacheco, E.M. Melchor-Martínez, Z. Aghalari, D.S. Limón, H.M.N. Iqbal, R. Parra-Saldívar, Sources of antibiotics pollutants in the aquatic environment under SARS-CoV-2 pandemic situation, Case Stud. Chem. Environ. Eng. 4 (2021), https://doi.org/10.1016/j.cscee.2021.100127.

[11] Y. Ben, C. Fu, M. Hu, L. Liu, M.H. Wong, C. Zheng, Human health risk assessment of antibiotic resistance associated with antibiotic residues in the environment: a review, Environ. Res. 169 (2019) 483–493, https://doi.org/10.1016/j.envres.2018.11.040.

[12] I. Chattopadhyay, R.B. J., T.M.M. Usman, S. Varjani, Exploring the role of microbial biofilm for industrial effluents treatment, Bioengineered. 13 (2022) 6420–6440, https://doi.org/10.1080/21655979.2022.2044250.

[13] Z. Xie, G. Lu, Z. Yan, J. Liu, P. Wang, Y. Wang, Bioaccumulation and trophic transfer of pharmaceuticals in food webs from a large freshwater lake, Environ. Pollut. 222 (2017) 356–366, https://doi.org/10.1016/j.envpol.2016.12.026.

[14] A.H. Khan, H.A. Aziz, N.A. Khan, M.A. Hasan, S. Ahmed, I.H. Farooqi, A. Dhingra, V. Vambol, F. Changani, M. Yousefi, S. Islam, N. Mozaffari, M.S. Mahtab, Impact, disease outbreak and the eco-hazards associated with pharmaceutical residues: a critical review, Int. J. Environ. Sci. Technol. 19 (2022) 677–688, https://doi.org/10.1007/s13762-021-03158-9.

[15] N. Hanna, P. Sun, Q. Sun, X. Li, X. Yang, X. Ji, H. Zou, J. Ottoson, L.E. Nilsson, B. Berglund, O.J. Dyar, A.J. Tamhankar, C. Stålsby Lundborg, Presence of antibiotic residues in various environmental compartments of Shandong province in eastern China: its potential for resistance development and ecological and human risk, Environ. Int. 114 (2018) 131–142, https://doi.org/10.1016/j.envint.2018.02.003.

[16] K. Sathya, K. Nagarajan, G. Carlin Geor Malar, S. Rajalakshmi, P. Raja Lakshmi, A comprehensive review on comparison among effluent treatment methods and modern methods of treatment of industrial wastewater effluent from different sources, Appl. Water Sci. 12 (2022) 1–27. doi:https://doi.org/10.1007/s13201-022-01594-7.

[17] M.P.C. Mora-Gamboa, S.M. Rincón-Gamboa, L.D. Ardila-Leal, R.A. Poutou-Piñales, A.M. Pedroza-Rodríguez, B.E. Quevedo-Hidalgo, Impact of antibiotics as waste, physical, chemical, and enzymatical degradation: use of laccases, Molecules. 27 (2022) 1–44, https://doi.org/10.3390/molecules27144436.
[18] A. Fiaz, D. Zhu, J. Sun, Environmental fate of tetracycline antibiotics: degradation pathway mechanisms, challenges, and perspectives, Environ. Sci. Eur. 33 (2021), https://doi.org/10.1186/s12302-021-00505-y.
[19] V.N. Lad, Z.V.P. Murthy, Advanced Materials for Photocatalytic Applications: The Challenge Ahead, Inc, 2020, https://doi.org/10.1016/B978-0-12-819051-7.00001-4.
[20] M. Antonopoulou, C. Kosma, T. Albanis, I. Konstantinou, An overview of homogeneous and heterogeneous photocatalysis applications for the removal of pharmaceutical compounds from real or synthetic hospital wastewaters under lab or pilot scale, Sci. Total Environ. 765 (2021) 144163, https://doi.org/10.1016/j.scitotenv.2020.144163.
[21] C. Huang, J. Wen, Y. Shen, F. He, L. Mi, Z. Gan, J. Ma, S. Liu, H. Ma, Y. Zhang, Dissolution and homogeneous photocatalysis of polymeric carbon nitride, Chem. Sci. 9 (2018) 7912–7915, https://doi.org/10.1039/c8sc03855d.
[22] R. Pelosato, I. Bolognino, F. Fontana, I.N. Sora, Applications of heterogeneous photocatalysis to the degradation of oxytetracycline in water: a review, Molecules. 27 (2022), https://doi.org/10.3390/molecules27092743.
[23] M. Ganeshbabu, N. Kannan, P.S. Venkatesh, G. Paulraj, K. Jeganathan, Synthesis and characterization of BiVO4 nanoparticles for environmental applications, RSC Adv. 10 (2020) 18315–18322, https://doi.org/10.1039/d0ra01065k.
[24] S. Vijayalakshmi, E. Kumar, P.S. Venkatesh, A. Raja, Preparation of zirconium oxide with polyaniline nanocatalyst for the decomposition of pharmaceutical industrial wastewater, Ionics (Kiel). 26 (2019) 1507–1513, https://doi.org/10.1007/s11581-019-03323-8.
[25] F. Silerio-Vázquez, M.T. Alarcón-Herrera, J.B. Proal-Nájera, Solar heterogeneous photocatalytic degradation of phenol on TiO2/quartz and TiO2/calcite: a statistical and kinetic approach on comparative efficiencies towards a TiO2/glass system, Environ. Sci. Pollut. Res. 29 (2022) 42319–42330, https://doi.org/10.1007/s11356-022-19379-5.
[26] N.M. Izzudin, A.A. Jalil, F.F.A. Aziz, M.S. Azami, M.W. Ali, N.S. Hassan, A.F.A. Rahman, A.A. Fauzi, D.V.N. Vo, Simultaneous remediation of hexavalent chromium and organic pollutants in wastewater using period 4 transition metal oxide-based photocatalysts: a review, Environ. Chem. Lett. 19 (2021) 4489–4517, https://doi.org/10.1007/s10311-021-01272-1.
[27] C. Karthikeyan, P. Arunachalam, K. Ramachandran, A.M. Al-Mayouf, S. Karuppuchamy, Recent advances in semiconductor metal oxides with enhanced methods for solar photocatalytic applications, J. Alloys Compd. 828 (2020) 154281, https://doi.org/10.1016/j.jallcom.2020.154281.
[28] Y. Zheng, Y. Liu, X. Guo, Z. Chen, W. Zhang, Y. Wang, X. Tang, Y. Zhang, Y. Zhao, Sulfur-doped g-C3N4/rGO porous nanosheets for highly efficient photocatalytic degradation of refractory contaminants, J. Mater. Sci. Technol. 41 (2020) 117–126, https://doi.org/10.1016/j.jmst.2019.09.018.
[29] N.A.A. Review, H.G. Attiya, W.J. Fendi, Z.A. Al-dulaimy, A. Farooq, A.M. Mohammed, Characterization synthesis of copper oxide, J. Pharm. Negat. Results. 14 (2023) 250–256, https://doi.org/10.47750/pnr.202.
[30] A. Waris, M. Din, A. Ali, M. Ali, S. Afridi, A. Baset, A. Ullah Khan, A comprehensive review of green synthesis of copper oxide nanoparticles and their diverse biomedical applications, Inorg. Chem. Commun. 123 (2021) 108369, https://doi.org/10.1016/j.inoche.2020.108369.
[31] N. Verma, N. Kumar, Synthesis and biomedical applications of copper oxide nanoparticles: an expanding horizon, ACS Biomater Sci. Eng. 5 (2019) 1170–1188, https://doi.org/10.1021/acsbiomaterials.8b01092.
[32] P. Raizada, A. Sudhaik, S. Patial, V. Hasija, A.A. Parwaz Khan, P. Singh, S. Gautam, M. Kaur, V.H. Nguyen, Engineering Nanostructures of CuO-Based Photocatalysts for Water Treatment: Current Progress and Future Challenges, The Author(s), 2020, https://doi.org/10.1016/j.arabjc.2020.06.031.
[33] M. Rafique, F. Shafiq, S.S. Ali Gillani, M. Shakil, M.B. Tahir, I. Sadaf, Eco-friendly green and biosynthesis of copper oxide nanoparticles using Citrofortunella microcarpa leaves extract for efficient photocatalytic degradation of Rhodamin B dye form textile wastewater, Optik (Stuttg). 208 (2020) https://doi.org/10.1016/j.ijleo.2019.164053, 164053.
[34] J. Ge, Y. Zhang, Y.J. Heo, S.J. Park, Advanced Design and Synthesis of Composite Photocatalysts for The Remediation of Wastewater: A Review, 2019, https://doi.org/10.3390/catal9020122.
[35] T. Borjigin, M. Schmitt, F. Morlet-Savary, P. Xiao, J. Lalevée, Low-cost and recyclable Photocatalysts: metal oxide/polymer composites applied in the catalytic breakdown of dyes, Photochem. 2 (2022) 733–751, https://doi.org/10.3390/photochem2030047.
[36] A.R. Wassel, M.E. El-Naggar, K. Shoueir, Recent advances in polymer/metal/metal oxide hybrid nanostructures for catalytic applications: a review, J. Environ. Chem. Eng. 8 (2020) 104175, https://doi.org/10.1016/j.jece.2020.104175.
[37] G. Ali, M. Sharma, E.S. Salama, Z. Ling, X. Li, Applications of chitin and chitosan as natural biopolymer: potential sources, pretreatments, and degradation pathways, Biomass Convers. Biorefinery. (2022), https://doi.org/10.1007/s13399-022-02684-x.
[38] R. Jiang, H.Y. Zhu, Y.Q. Fu, S.T. Jiang, E.M. Zong, J.Q. Zhu, Y.Y. Zhu, L.F. Chen, Colloidal CdS sensitized nano-ZnO/chitosan hydrogel with fast and efficient photocatalytic removal of Congo red under solar light irradiation, Int. J. Biol. Macromol. 174 (2021) 52–60, https://doi.org/10.1016/j.ijbiomac.2021.01.077.
[39] M. Malekkiani, A. Heshmati Jannat Magham, F. Ravari, M. Dadmehr, Facile fabrication of ternary MWCNTs/ZnO/Chitosan nanocomposite for enhanced photocatalytic degradation of methylene blue and antibacterial activity, Sci. Rep. 12 (2022) 1–22, https://doi.org/10.1038/s41598-022-09571-5.
[40] A. Spoială, C.I. Ilie, G. Dolete, A.M. Croitoru, V.A. Surdu, R.D. Truşcă, L. Motelica, O.C. Oprea, D. Ficai, A. Ficai, E. Andronescu, L.M. Diţu, Preparation and characterization of chitosan/TiO2 composite membranes as adsorbent materials for water purification, Membranes (Basel). 12 (2022), https://doi.org/10.3390/membranes12080804.
[41] A. Arena, G. Scandurra, C. Ciofi, Copper oxide chitosan nanocomposite: characterization and application in non-enzymatic hydrogen peroxide sensing, Sensors. 17 (2017) 2198, https://doi.org/10.3390/s17102198.
[42] T. Jayaramudu, K. Varaprasad, R.D. Pyarasani, K.K. Reddy, K.D. Kumar, A. Akbari-Fakhrabadi, R.V. Mangalaraja, J. Amalraj, Chitosan capped copper oxide/copper nanoparticles encapsulated microbial resistant nanocomposite films, Int. J. Biol. Macromol. 128 (2019) 499–508, https://doi.org/10.1016/j.ijbiomac.2019.01.145.
[43] S. Ltaief, M. Jabli, S. Ben Abdessalem, Immobilization of copper oxide nanoparticles onto chitosan biopolymer: application to the oxidative degradation of Naphthol blue black, Carbohydr. Polym. 261 (2021) 117908, https://doi.org/10.1016/j.carbpol.2021.117908.
[44] T. Abiraman, E. Ramanathan, G. Kavitha, R. Rengasamy, S. Balasubramanian, Synthesis of chitosan capped copper oxide nanoleaves using high intensity (30 kHz) ultrasound sonication and their application in antifouling coatings, Ultrason. Sonochem. 34 (2017) 781–791, https://doi.org/10.1016/j.ultsonch.2016.07.013.
[45] M.E. Grigore, E.R. Biscu, A.M. Holban, M.C. Gestal, A.M. Grumezescu, Methods of synthesis, properties and biomedical applications of CuO nanoparticles, Pharmaceuticals. 9 (2016) 1–14, https://doi.org/10.3390/ph9040075.
[46] A. Gedanken, I. Perelshtein, Power Ultrasound for the Production of Nanomaterials, Elsevier Ltd., 2015, https://doi.org/10.1016/B978-1-78242-028-6.00018-1.
[47] S. Wang, X. Zhang, L. Pan, F.M. Zhao, J.J. Zou, T. Zhang, L. Wang, Controllable sonochemical synthesis of Cu2O/Cu2(OH)3NO3 composites toward synergy of adsorption and photocatalysis, Appl. Catal. Environ. 164 (2015) 234–240, https://doi.org/10.1016/j.apcatb.2014.09.033.
[48] J. Guo, S. Zhu, Z. Chen, Y. Li, Z. Yu, Q. Liu, J. Li, C. Feng, D. Zhang, Ultrasonics Sonochemistry Sonochemical synthesis of TiO 2 nanoparticles on graphene for use as photocatalyst, Ultrason. - Sonochemistry. 18 (2011) 1082–1090, https://doi.org/10.1016/j.ultsonch.2011.03.021.
[49] M.T. Noman, M. Petru, J. Militkỳ, M. Azeem, M.A. Ashraf, One-Pot sonochemical synthesis of ZnO nanoparticles for photocatalytic applications, modelling and optimization, Materials (Basel). 13 (2020) 14, https://doi.org/10.3390/ma13010014.
[50] C. Peniche-Covas, W. Argüelles-Monal, J. San Román, A kinetic study of the thermal degradation of chitosan and a mercaptan derivative of chitosan, Polym. Degrad. Stab. 39 (1993) 21–28, https://doi.org/10.1016/0141-3910(93)90120-8.
[51] A. Pellis, G.M. Guebitz, G.S. Nyanhongo, Chitosan: sources, processing and modification techniques, Gels. 8 (2022) 5–25, https://doi.org/10.3390/gels8070393.
[52] J. Lu, Y. Chen, M. Ding, X. Fan, J. Hu, Y. Chen, J. Li, Z. Li, W. Liu, A 4arm-*extraction, structure and Immunoregulatory* chitosan hydrogels as antibacterial wound dressing, Carbohydr. Polym. 277 (2022) 118871, https://doi.org/10.1016/j.carbpol.2021.118871.
[53] V. Jagadeesan, V. Subramaniam, Impact of molarity on structural, optical, morphological and electrical properties of copper oxide thin films prepared by cost effective jet nebulizer spray pyrolysis technique, J. Mater. Sci. Mater. Electron. 30 (2019) 1571–1578, https://doi.org/10.1007/s10854-018-0428-8.
[54] A.H. Naseri, M.G. Saion, E.B. Shaari, The amazing effects and role of PVP on the phase composition and morphology of manganese ferrite nanoparticles prepared by thermal treatment method, 2nd Int. Conf. Environ. Sci. Biotechnol. 48 (2012) 169–173.
[55] R. Javed, M. Zia, S. Naz, S.O. Aisida, N. Ul Ain, Q. Ao, Role of capping agents in the application of nanoparticles in biomedicine and environmental remediation: recent trends and future prospects, J. Nanobiotechnology. 18 (2020) 1–15, https://doi.org/10.1186/s12951-020-00704-4.
[56] Q.P. Zhang, X.N. Xu, Y.T. Liu, M. Xu, S.H. Deng, Y. Chen, H. Yuan, F. Yu, Y. Huang, K. Zhao, S. Xu, G. Xiong, A feasible strategy to balance the crystallinity and specific surface area of metal oxide nanocrystals, Sci. Rep. 7 (2017) 1–12, https://doi.org/10.1038/srep46424.
[57] J. Akter, K.P. Sapkota, M.A. Hanif, M.A. Islam, H.G. Abbas, J.R. Hahn, Kinetically controlled selective synthesis of Cu2O and CuO nanoparticles toward enhanced degradation of methylene blue using ultraviolet and sun light, Mater. Sci. Semicond. Process. 123 (2021) 105570, https://doi.org/10.1016/j.mssp.2020.105570.
[58] V.D. Nithya, R.K. Selvan, L. Vasylechko, C. Sanjeeviraja, Effect of carbon coating on the electrochemical properties of Bi2WO6 nanoparticles by PVP-assisted sonochemical method, J. Appl. Electrochem. 45 (2015) 473–485, https://doi.org/10.1007/s10800-015-0822-3.
[59] R. Shashanka, Investigation of optical and thermal properties of CuO and ZnO nanoparticles prepared by crocus Sativus (saffron) flower extract, J. Iran. Chem. Soc. 18 (2021) 415–427, https://doi.org/10.1007/s13738-020-02037-3.
[60] B. Avinash, C.R. Ravikumar, M.R.A. Kumar, H.P. Nagaswarupa, M.S. Santosh, A.S. Bhatt, D. Kuznetsov, Nano CuO: electrochemical sensor for the determination of paracetamol and D-glucose, J. Phys. Chem. Solid 134 (2019) 193–200, https://doi.org/10.1016/j.jpcs.2019.06.012.
[61] A. Badri, S. Slimi, M. Guergueb, H. Kahri, X. Mateos, Green synthesis of copper oxide nanoparticles using prickly pear peel fruit extract: characterization and catalytic activity, Inorg. Chem. Commun. 134 (2021) 109027, https://doi.org/10.1016/j.inoche.2021.109027.

[62] A. Shanmugavani, S. Gowrimeena, P. Rupa Kasturi, S. Yuvaraj, L. John Berchmans, R. Kalai Selvan, Effect of zinc precursors on the hydrogen evolution reaction and electrochemical corrosion studies of ZnWO4 nanoparticles synthesized by hot injection method, J. Phys. Chem. Solid 119 (2018) 210–219, https://doi.org/10.1016/j.jpcs.2018.03.005.
[63] S. Dhanavel, E.A.K. Nivethaa, V. Narayanan, A. Stephen, Photocatalytic activity of chitosan/ZnO nanocomposites for degrading methylene blue, Int. J. ChemTech Res. 6 (2014) 1880–1882.
[64] K. Araya-Castro, T.C. Chao, B. Durán-Vinet, C. Cisternas, G. Ciudad, O. Rubilar, Green synthesis of copper oxide nanoparticles using protein fractions from an aqueous extract of brown algae macrocystis pyrifera, Processes. 9 (2021) 1–10, https://doi.org/10.3390/pr9010078.
[65] S.C. Boyatzis, A.M. Douvas, V. Argyropoulos, A. Siatou, M. Vlachopoulou, Characterization of a water-dispersible metal protective coating with fourier transform infrared spectroscopy, modulated differential scanning calorimetry, and ellipsometry, Appl. Spectrosc. 66 (2012) 580–590, https://doi.org/10.1366/11-06371.
[66] M.F. Queiroz, K.R.T. Melo, D.A. Sabry, G.L. Sassaki, H.A.O. Rocha, Does the use of chitosan contribute to oxalate kidney stone formation? Mar. Drugs 13 (2015) 141–158, https://doi.org/10.3390/md13010141.
[67] D.J. Manasa, K.R. Chandrashekar, D.J. Madhu Kumar, M. Niranjana, K.M. Navada, Mussaenda frondosa L. mediated facile green synthesis of copper oxide nanoparticles – characterization, photocatalytic and their biological investigations, Arab. J. Chem. 14 (2021) https://doi.org/10.1016/j.arabjc.2021.103184, 103184.
[68] S. Sathiyavimal, S. Vasantharaj, V. Veeramani, M. Saravanan, G. Rajalakshmi, T. Kaliannan, F.A. Al-Misned, A. Pugazhendhi, Green chemistry route of biosynthesized copper oxide nanoparticles using Psidium guajava leaf extract and their antibacterial activity and effective removal of industrial dyes, J. Environ. Chem. Eng. 9 (2021) 105033, https://doi.org/10.1016/j.jece.2021.105033.
[69] E. Bruno, M. Haris, A. Mohan, M. Senthilkumar, Temperature effect on CuO nanoparticles via facile hydrothermal approach to effective utilization of UV–visible region for photocatalytic activity, Appl. Phys. A Mater. Sci. Process. 127 (2021) 1–14, https://doi.org/10.1007/s00339-021-05081-9.
[70] M.A. Khan, N. Nayan, M.K. Ahmad Shadiullah, C.F. Soon, Surface study of cuo nanopetals by advanced nanocharacterization techniques with enhanced optical and catalytic properties, Nanomaterials. 10 (2020) 1–18, https://doi.org/10.3390/nano10071298.
[71] R. Nayak, F.A. Ali, D.K. Mishra, D. Ray, V.K. Aswal, S.K. Sahoo, B. Nanda, Fabrication of CuO nanoparticle: an efficient catalyst utilized for sensing and degradation of phenol, J. Mater. Res. Technol. 9 (2020) 11045–11059, https://doi.org/10.1016/j.jmrt.2020.07.100.
[72] M. El-Kemary, H. El-Shamy, I. El-Mehasseb, Photocatalytic degradation of ciprofloxacin drug in water using ZnO nanoparticles, JOL 130 (2010) 2327–2331, https://doi.org/10.1016/j.jlumin.2010.07.013.
[73] X. Hu, X. Hu, Q. Peng, L. Zhou, X. Tan, L. Jiang, C. Tang, H. Wang, S. Liu, Y. Wang, Z. Ning, Mechanisms underlying the photocatalytic degradation pathway of ciprofloxacin with heterogeneous TiO2, Chem. Eng. J. 380 (2020), https://doi.org/10.1016/j.cej.2019.122366.
[74] S. Xing, W. Li, B. Liu, Y. Wu, Y. Gao, Removal of ciprofloxacin by persulfate activation with CuO: a pH-dependent mechanism, Chem. Eng. J. 382 (2020), https://doi.org/10.1016/j.cej.2019.122837.
[75] R. Kaushik, P.K. Samal, A. Halder, Degradation of fluoroquinolone-based pollutants and bacterial inactivation by visible-light-active aluminum-doped TiO2 Nanoflakes, ACS Appl. Nano Mater. 2 (2019) 7898–7909, https://doi.org/10.1021/acsanm.9b01913.
[76] M. Sayed, M. Ismail, S. Khan, S. Tabassum, H.M. Khan, Degradation of ciprofloxacin in water by advanced oxidation process: kinetics study, influencing parameters and degradation pathways, Environ. Technol. (United Kingdom). 37 (2016) 590–602, https://doi.org/10.1080/09593330.2015.1075597.
[77] S. Vijayalakshmi, E. Kumar, P.S. Venkatesh, A. Raja, Preparation of zirconium oxide with polyaniline nanocatalyst for the decomposition of pharmaceutical industrial wastewater, Ionics (Kiel). 26 (2020) 1507–1513, https://doi.org/10.1007/s11581-019-03323-8.
[78] A. Kaur, W.A. Anderson, S. Tanvir, S.K. Kansal, Solar light active silver/iron oxide/zinc oxide heterostructure for photodegradation of ciprofloxacin, transformation products and antibacterial activity, J. Colloid Interface Sci. 557 (2019) 236–253, https://doi.org/10.1016/j.jcis.2019.09.017.
[79] S. Das, S. Ghosh, A.J. Misra, A.J. Tamhankar, A. Mishra, C.S. Lundborg, S.K. Tripathy, Sunlight assisted photocatalytic degradation of ciprofloxacin in water using fe doped zno nanoparticles for potential public health applications, Int. J. Environ. Res. Public Health 15 (2018) 2240, https://doi.org/10.3390/ijerph15112440.
[80] N. Lu, P. Wang, Y. Su, H. Yu, N. Liu, X. Quan, Construction of Z-scheme g-C3N4/RGO/WO3 with in situ photoreduced graphene oxide as electron mediator for efficient photocatalytic degradation of ciprofloxacin, Chemosphere. 215 (2019) 444–453, https://doi.org/10.1016/j.chemosphere.2018.10.065.
[81] L.T. Nguyen, H.T. Nguyen, T.D. Pham, T.D. Tran, H.T. Chu, H.T. Dang, V.H. Nguyen, K.M. Nguyen, T.T. Pham, B. Van der Bruggen, UV–visible light driven photocatalytic degradation of ciprofloxacin by N,S co-doped TiO2: the effect of operational parameters, Top. Catal. 63 (2020) 985–995, https://doi.org/10.1007/s11244-020-01319-7.
[82] J. Xia, M. Ji, W. Li, J. Di, H. Xu, M. He, Q. Zhang, H. Li, Synthesis of erbium ions doped BiOBr via a reactive ionic liquid with improved photocatalytic activity, Colloids Surfaces A Physicochem. Eng. Asp. 489 (2016) 343–350, https://doi.org/10.1016/j.colsurfa.2015.10.037.
[83] L. Ma, J. Duan, B. Ji, Y. Liu, C. Li, C. Li, W. Zhao, Z. Yang, Ligand-metal charge transfer mechanism enhances TiO2/Bi2WO6/rGO nanomaterials photocatalytic efficient degradation of norfloxacin under visible light, J. Alloys Compd. 869 (2021) 158679, https://doi.org/10.1016/j.jallcom.2021.158679.
[84] J. Zhang, Z. Zhu, J. Jiang, H. Li, Synthesis of novel ternary dual Z-scheme AgBr/LaNiO3/g-C3N4 composite with boosted visible-light Photodegradation of Norfloxacin, Molecules. 25 (2020) 3706, https://doi.org/10.3390/molecules25163706.
[85] W. Liu, T. He, Y. Wang, G. Ning, Z. Xu, X. Chen, X. Hu, Y. Wu, Y. Zhao, Synergistic adsorption-photocatalytic degradation effect and norfloxacin mechanism of ZnO/ZnS@BC under UV-light irradiation, Sci. Rep. 10 (2020) 11903, https://doi.org/10.1038/s41598-020-68517-x.
[86] B. Ji, W. Zhao, J. Duan, L. Fu, L. Ma, Z. Yang, Immobilized Ag3PO4/GO on 3D nickel foam and its photocatalytic degradation of norfloxacin antibiotic under visible light, RSC Adv. 10 (2020) 4427–4435, https://doi.org/10.1039/c9ra08678a.
[87] S.S. Warule, N.S. Chaudhari, B.B. Kale, M.A. More, Novel sonochemical assisted hydrothermal approach towards the controllable synthesis of ZnO nanorods, nanocups and nanoneedles and their photocatalytic study, CrystEngComm. 11 (2009) 2776–2783, https://doi.org/10.1039/b909916f.

Thalassas: An International Journal of Marine Sciences
https://doi.org/10.1007/s41208-024-00692-4

RESEARCH

Meticulous Taxonomic Evidence and Molecular Confirmation of *Sphyraena forsteri* Cuvier, 1829 (Carangiformes: Sphyraenidae) from the Southeast coast of India

Sivaranjani Sekar[1] · Kannan Karuppiah[2] · Kumar Rajendran[3] · Madhuri Krishnamoorthy[1] · Divya Dharmaraj[1] · Kannapiran Ethiraj[3,4]

Received: 21 April 2023 / Revised: 30 December 2023 / Accepted: 23 February 2024

Abstract
Bigeye barracuda is a commercially valued species as food and game fish in the Indo-Pacific region. The taxonomic details of bigeye barracuda *Sphyraena forsteri* Cuvier, 1829 is poorly reported in the literature from Indian waters. The current taxonomic study identifies the *S. forsteri* based on different sizes of the specimens ranging from 255 to 376 mm total length and 83–271 g weight collected from three different landing stations along the Southeast coast of India. Totally, forty-five specimens were examined which include 21 males (46.67%) and 24 females (53.33%). *Sphyraena forsteri* is diagnosed with enlarged eyes; covered with very tiny cycloid scales all over the body; 101–120 lateral line scales; cheek scales 5–6.5; seven branchiostegal rays. *Sphyraena forsteri* differs from its congeners by having the gill raker counts; upper limb rough with tiny bony setae, 10–20 small tubercle spines on the first-gill arch (in lower limb) uniformly arranged with 4 to 5 bony setae in a single group with one large spine, gill raker absent. The genetic confirmation of *S. forsteri* was investigated using 668 bp sequences of mitochondrial cytochrome oxidase subunit I gene. The species *S. forsteri* formed a stoutly supported clade against the five other congeneric species within the same family Sphyraenidae. This study provides a better taxonomic interpretation of *S. forsteri* with the molecular and combination of comprehensive morphological with detailed description of scale, otolith, vertebral characters of specimens from the Southeast coast of India.

Keywords Bigeye barracuda · DNA barcoding · Morphology · Southeast coast of India · Taxonomy

Introduction

The family Sphyraenidae (Rafinesque 1815) belongs to the order Carangiformes and comprises a single genus *Sphyraena* (Rose 1793). Globally, twenty-seven valid species and two new species in the last decade have been documented (Fricke et al. 2023). In Indian waters, eleven species have been reported namely, *Sphyraena barracuda* (Edwards 1771), *S. forsteri* (Cuvier 1829), *S. jello* (Cuvier 1829), *S. obtusata* (Cuvier 1829), *S. flavicauda* (Ruppell 1838), *S. novaehollandiae* (Gunther 1860), *S. qenie* (Klunzinger 1870), *S. acutipinnis* (Day 1876), *S. chrysotaenia* (Klunzinger 1870), *S. putnamae* (Jordan and Seale 1905) and *S. arabiansis* (Abdussamad et al. 2015). Sphyraenidae is the foremost largest coastal pelagic piscivore, especially on the coral reefs (Rose 1984) and plays a major role in the marine food chain. These are commercially important fishes due to their delicacy and great flavours (Smith 1956). Sphyraenids are commonly referred to as barracuda for their ferocious behaviours and predatory habit. They are distributed globally in tropical and sub-tropical waters of the Indo-Pacific region (Ballen 2019). Barracudas commonly occur at the depth of 6–300 m (Myers 1991).

✉ Kannapiran Ethiraj
ekannapiran@gmail.com

1 Department of Animal Health and Management, Alagappa University, Karaikudi, Tamil Nadu 630003, India

2 Department of Zoology, Kongunadu Arts and Science College, Coimbatore, Tamil Nadu 641029, India

3 Department of Fisheries Science, Alagappa University, Karaikudi, Tamil Nadu 630003, India

4 Department of Zoology, Center for Distance and Online Education, Alagappa University, Karaikudi 630003, India

Published online: 29 February 2024

The genus *Sphyraena* (Rose 1793) had been characterized by an elongated body; dorsal fins widely separated; pointed snout, lower jaw larger; strong and sharp canine teeth. According to the gill raker structure and count (one, two, or absence of gill raker), *Sphyraena* is separated into three groups: the first group with largest body and absence of gill raker reported in six species *Sphyraena arabiansis, S. barracuda, S. forsteri, S. qenie, S. jello, S. putnamae* (Morishita et al. 2020); the second group with the presence of two gill rakers on the first gill arch reported in three species *viz., S. obtusata, S. chrysotaenia, S. flavicauda* and the third group with single gill raker on the first gill arch noticed in *S. accutipinnis* and *S. novaehollandidae* (Australian species). Scale and otolith morphology are efficient for growth studies, species recognition, age determination, migration-related to previous environmental details, genetic population, and phylogenetic assessment of species in taxonomy (Dapar et al. 2012). Sphyraenids are one of the least investigated species in the Southeast Coast of India. Due to the lack of taxonomic and molecular information from the Indian coast, the present study was carried out to describe the detailed taxonomic and molecular record of *S. forsteri*.

Materials and Methods

Sample Collection

Totally 45 fish samples were collected from the Southeast coast of India viz., Gulf of Mannar and Chennai coast landing centres during August 2021 to September 2022. The GPS-coordinate point of the sampling places is shown in the map (Fig. 1). Fish specimens were trapped by using the gillnet (length of 40–45 mm), caught along 15 to 27 nautical miles distance from the depth of 45 to 72 m. Fresh specimens were photographed with Nikon P950 camera, subjected to external morphological measurement by using a digital vernier caliper with a precision length of 0.1 mm and weight using a digital weighing balance with a precision of 0.01 g (Doiuchi and Nakabo 2007; Kannan et al.

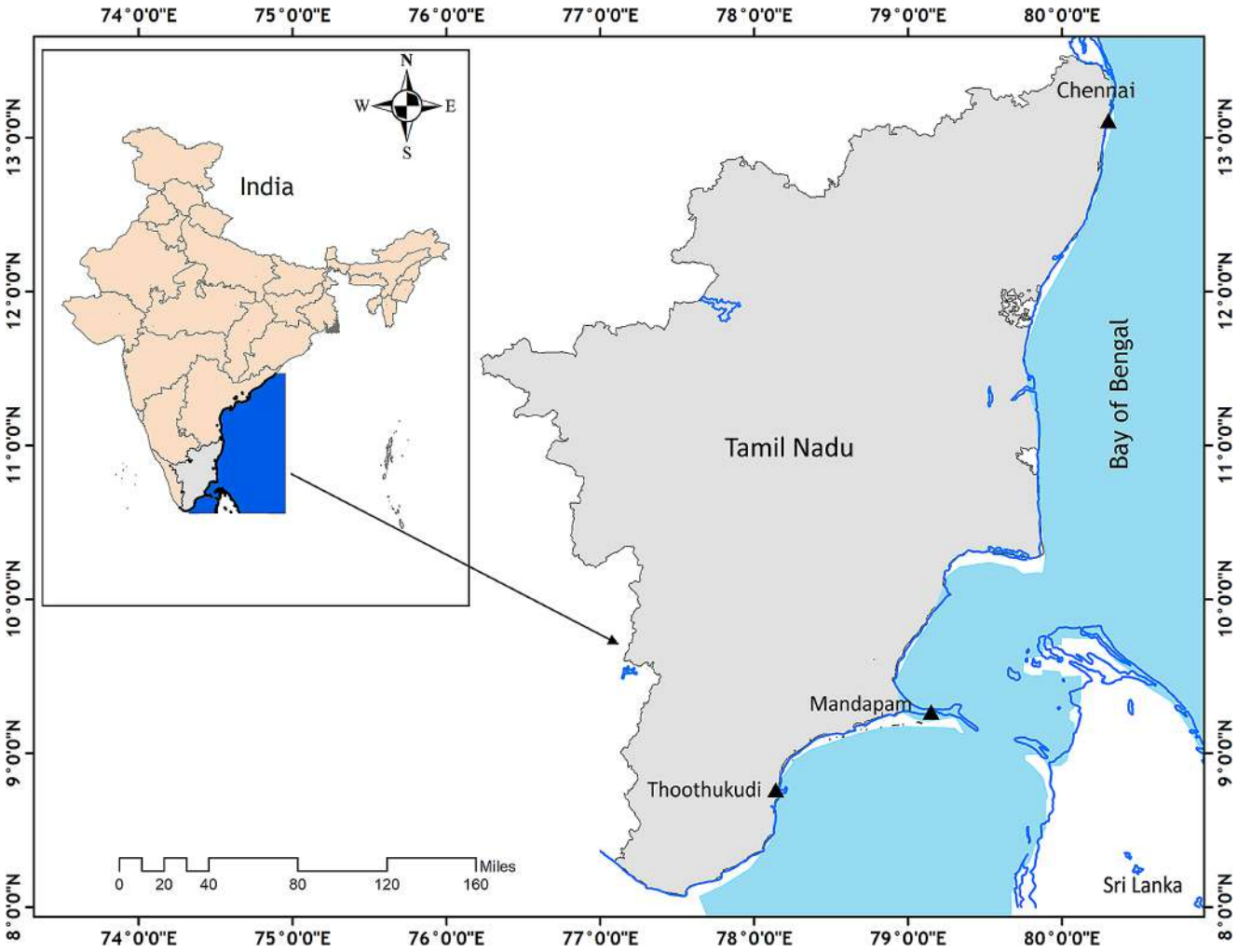

Fig. 1 Map showing the collection site of the specimen *Sphyraena forsteri*

2021a, b). The total length (TL) was measured from the anterior edge of the snout to the utmost edge of the caudal fin and standard length (SL) was measured from the tip of the snout to the last vertebra, other measurement characters are shown (Table 1). The muscle was collected from the caudal region on the right side of the fish sample and stored in 99.9% ethanol for molecular study and specimens were preserved in 10% formalin for taxonomical studies (Diaz-Viloria et al. 2005). Representative specimen was deposited in the National Repository for Fish Cell lines (NRFC) of the ICAR-National Bureau of Fish Genetic Resources (NBFGR), Lucknow, India with the accession number-SPHSFOR/NBFGR (Fig. 2).

Collection and Processing of Scales

The scales were collected from eight different parts of the individual fish including head region, lateral line scales along the lateral line, Inter-dorsal (between the two dorsal fins), insertion points of the pectoral and pelvic fins, mid portion of the body, origin of anal fin and caudal peduncle region these all are collected from the left portion of the fish (Casteel 1976). The scales were washed with distilled water by using a fine brush. Then, the scales were put into 1% Potassium hydroxide solution for 30 min incubation for removing the excess tissues on the surface to the root region of the scales followed by treatment with 70% ethanol (10–20 min) for dehydration. The scales were kept between the two hard slides and allowed to dry for 24 h (Lippitsch

Table 1 Count and proportional measurements of *Sphyraena forsteri* collected from Southeast Coast of India (n = 45)

Morphometric parameters (mm)		
Total length	255–376	
Standard length	202–306	
Meristic characters		
First dorsal fins/rays	V	
Second dorsal fins/ rays	II + 7–8	
Pectoral fins/rays	II + 12–13	
Pelvic fins/rays	I + 5	
Anal fins/rays	II + 7–8	
Branchiostegal rays	7	
Scales above lateral line	9.5–17	
Scales below the lateral line	14.5–17	
Lateral line scales	101–120	
Cheek scales	5–6.5	
Body band	Absent	
GR absent but minute bony setae are presents	13–20	
Body weight (g)	83–271	
Upper (minute) bony setae	16	
Lower (minute) spines	14	
Morphometric characters	**Proportion range as SL**	**Proportion range as SL%**
Body depth at pelvic fin origin	5.4–7.9	12.6–18.4
Body width	7.4–13.4	7.5–13.5
Interdorsal fin length	5.3–6.3	15.9–18.9
Prepectoral length	2.9–3.3	30.6–34.9
Prepelvic length	2.4–2.6	38.3–41.9
Upper-jaw length	5.8–8.2	12.3–17.4
Lower jaw length	5.3–7.2	13.9–18.8
1st dorsal fin base	8.4–11.1	9.0–11.9
2nd dorsal fin base	9.1–15.1	6.6–10.9
Pectoral fin base	33.9–39.5	2.5–3.0
Pelvic fin base	18.0–20.7	4.8–5.6
Anal fin base	9.6–14.8	6.8–10.4
Length of caudal peduncle	5.5–6.6	15.2–18.1
Distance between D1 origin to anal fin origin	2.7–3.1	31.8–37.5
Pectoral to pelvic insertion	8.1–13.3	7.5–12.3
Pelvic insertion to anal fin origin	2.7–3.0	33.1–37.3
Snout to head dorsal line edge region	3.7–4.5	22.0–27.2
Nostril to snout length	6.1–10.0	10.0–16.4
Nostril to eye diameter	9.1–13.8	7.2–11.0

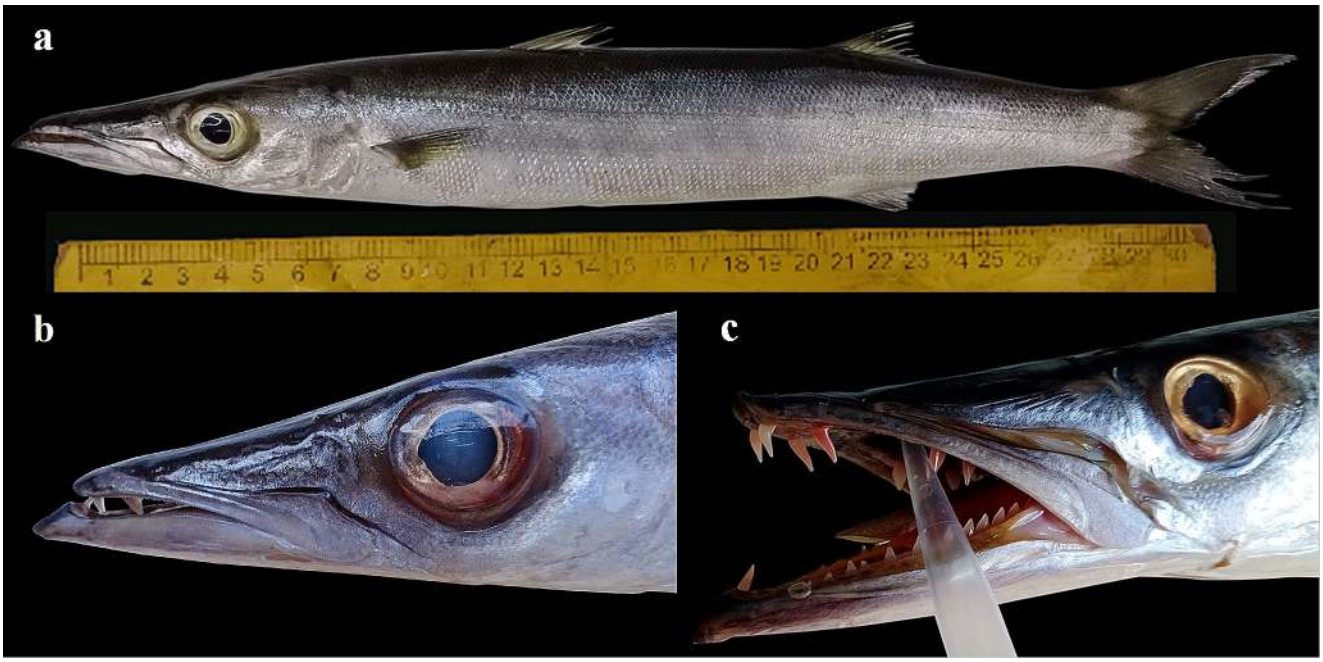

Fig. 2 Fresh specimens of **a***Sphyraena forsteri* (Non-type SPHSFOR/NBFGR, 320 mm TL, Gulf of Mannar) **b** maxilla quite reaching the anterior margin of the eye **c** very sharp and canine teeth are represented, lower jaw projecting teeth are directly backwards and size are increasing contiguous

1995). Thereafter, the sample was observed under the QUASMO (Model Name/Number: STAR 4) microscope for digital imaging.

Otolith Preparation and Imaging

Both the right and left otolith were dissected and collected from the dorsal region of the head, near the brain cavity. The collected otolith was cleaned with distilled water and treated with 5% Potassium hydroxide solution for 1 h to remove the tissues attached to the otolith and washed once again with distilled water using a brush. Subsequently, the samples were allowed to dry for 30 min (Secor et al. 1992). Then the otolith images were taken through the stereomicroscope (Stereomicroscope Nikon SMZ1000, Japan). Each otoliths rostrum was placed in the vertical (top) direction. Depending on the size of the otolith the magnification lens was adjusted to focus. Freshly preserved specimens (–20 °C) are used for vertebral studies. The vertebral counts were observed by using the X-ray radiograph image (Siemens 300 mA X-Ray machine).

Molecular Analysis

Single fish was chosen for molecular studies and the same specimen was deposited in the museum (Accession number-SPHSFOR/NBFGR). DNA extraction was carried out by the Phenol-chloroform based protocol with few modifications (Kumar and Aswath 2016). Briefly, 20 mg of tissue sample was taken in a 2 ml eppendorf tube, 100 µl lysis buffer and 400 µl of sodium dodecyl sulphate were mixed well and incubated for 15–20 min at room temperature. After incubation the DNA was extracted by using Phenol: chloroform: isoamyl alcohol (25:24:1) solution. Finally, the precipitated DNA pellet was washed with 70% ethanol (cold condition). The DNA quality and integrity were confirmed by using the agarose gel electrophoresis.

For amplification of the mitochondrial COI gene, universal primer combinations, forward primer (FishF1 5′-TCAACCAACCACAAAGACATTGGCAC-3′) and reverse primer (FishR1 5′-TAGACTTCTGGGTGGCCAAAGAATCA-3′) were used (Ward et al. 2005). Amplifications were performed using a prime 96 ^{PLUS} Thermal cycler. The thermal regime consisted of an initial denaturation step of 2 min at 94 °C followed by 1 cycle and 35 cycles for 30 s at 94 °C, annealing of 40 s at 52 °C and of 1 min at 72 °C, followed by a final extension of 10 min at 72 °C followed by 1 cycle. The PCR products were visualized under gel documentation on 2% agarose gel by using the stains (Ethidium bromide), the loading dyes contains Xylene cyanol and Bromophenol blue and purified for further sequencing using PCR purification kit (Sigma Aldrich, Bangalore). The amplified COI genes finally resulted with 668 bp fragment, respectively.

Phylogenetic Analysis

The raw sequence data was aligned and compared with the known species to check the genetic affinity and integrity of the sequence using Basic Local Alignment Search Tool. The analysis was completed using a single out-group (*Scomberomorus commerson*) and other sequences of voucher specimens and aligned with 32 sequences of COI genes collected from the GenBank database. After sequencing, gene alignment was done by using the Bio edit version 7.1.3.0 software (Hall 1999). The evolutionary history was inferred using the Neighbour-Joining method (Saitou and Nei 1987). The percentage of replicate trees in which the associated taxa clustered together in the bootstrap test is shown below the branches (Felsenstein 1985). Evolutionary analyses and the divergences of the sequence were assessed using MEGAX (Kumar et al. 2018; Kannan et al. 2023). The nucleotide sequence of the mitochondrial COI gene was deposited in the NCBI GenBank with the Accession No: OP024182.

Results

Sphyraena forsteri Cuvier 1829 (type locality: Tahiti Island in French Polynesia).

(English name: Big eye barracuda)

Non–type SPHSFOR/NBFGR forty-five specimens of *Sphyraena forsteri* were measured, males 42.85% and females 57.14% in the range of 255–376 mm TL from Southeast Coast of India during August 2021- September 2022.

Diagnosis

Body fusiform with lightly compressed; body lacks distinct markings; First dorsal fin with V spines, Second dorsal fin II spines with 7–8 rays, Anal fin spines II with 7–8 rays, Pelvic fin spine I with 5 rays, Pectoral fin rays 12–13; Lateral line scales numbered between 101 and 120; Branchiostegal rays 7. Scales above the lateral line 9.5–17; Scales below the lateral line 14.5–17; Cheek scales 5–6.5. Gill raker absent, but 10–20 min bony setae dispersed on the lower arm of the first gill arch; the group of minute short spines are present uniformly on the upper gill arm (Fig. 3). Body depth 6.9–7.7; Head depth 2.9–3.2 in Standard length. Preoperculum rounded; 2 flattened spines on operculum, lower angle pointed and reach at the level of pectoral fin insertion. Black with yellowish dusky blotch existing underneath the pectoral fin region; enlarged eyes, maxilla quite reaching the anterior margin of eye; small sensory canal lines are present on the suborbital region and needle-like marker is visible (in the form of zigzag); tip of pectoral fin does not reaching beyond first dorsal fin origin; the pelvic fin origin is situated in front of first dorsal fin origin; the last ray of anal fin and 2nd dorsal fin is well elongated; caudal fin typically forked without a pair of lobes; upper and lower tip of caudal fin slightly bent; lateral line initiated with end of the head to caudal fin region (start with a straight line, slightly curved above pectoral fin tip, continuously form a straight line and reach the caudal fin), papillae on dorsal region originates from the snout and ends behind the inter dorsal cavity. In the dorsal region, the upper snout is sharp, and in the ventral region, the lower snout is narrowed, scales are very small; cycloid type and covered all over the body (except the dorsal head and ventral snout). Lower jaw relatively large than the upper jaw with the length of 1.7–2.3 in of Head Length (HL); orbit diameter 9.8–13.7 in HL; pelvic, pectoral, and anal fin base 5.9–6.9, 10.6–12.7 and 3.0–5.0 in HL respectively; length of caudal peduncle 1.7–2.2 in HL; last ray of the second dorsal and anal fin 4.6–6.8 and 4.8–7.7 in HL; distance between 1st dorsal fin origin to the last ray of the 2nd dorsal 0.9–1.2 in HL; nostril to eye 2.9–4.7 in HL; maxillary depth 13.0–16.0 in HL.

Teeth

Compared to the other species, teeth are very sharp and canine directly backwards, and size increasing contiguous; lower jaw projecting, strong and pointed. In the front of upper jaw, two pairs of teeth: the first pair of teeth is smaller than the second pair, then a series of widely spaced minute teeth was observed. Within the upper jaw 4 pairs of teeth are visible, the first pair of teeth is very small, the 2nd pair of teeth is slightly larger than the first one then a series of the size of the teeth decreasing contiguously (palatine tooth patches also present on the roof of the upper jaw). In the lower jaw, the teeth are small to moderate, anterior edges of the lower jaw contain one canine tooth; sides of the lower jaw well spaced started with five pairs of small teeth, after 25.4 mm, 12–13 pair of teeth are present in the posterior region; these are increasing in size; directed backward.

Colouration

Body with no crossbars and marks; black blotch is presented underneath the pectoral fin; inside of the jaw is dark grey with a brownish colour. The second dorsal fin and pectoral fin are black with yellowish dusky colour. The pelvic fin and anal fins are whitish (but the tip of the anal fin is blackish dusky). The caudal and first dorsal fins are duskish black. The inner margin of the upper and lower jaw black with brownish dusky. The tongue is oval shaped with black and

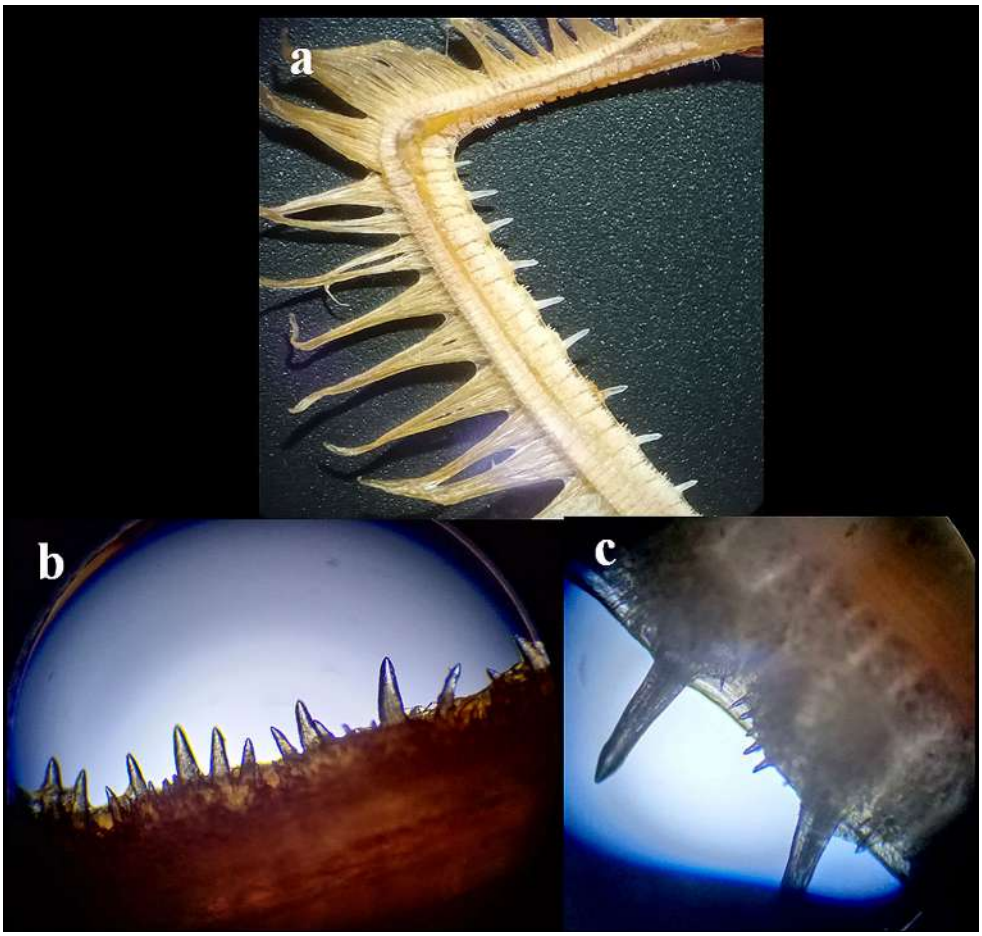

Fig. 3 **a** First gill filament **b** upper arm with minute bony setae **c** lower arm with 13–20 distinct spines are presents uniformly

greyish spots on the upper region. The dorsal region of the body is slightly yellowish black colour, ventral region of the body is pure white with silver reflection (seen only in the fresh condition), in the preserved condition, these types of species are dull white colour; the pre-operculum region has silver reflection.

Distribution

S. forsteri is distributed from Micronesia regions to the Gulf of Suez. These are widely distributed from the subtropical Indo-Pacific and tropical regions of the Marquesas Islands (Rose 1984) to East Africa (Fowler 1904) and Southern Japan, South to New Caledonia (Rose 1984). In the present study, specimens were collected from the two major landing centres along the Southeast Coast of India. The first sampling station were collected between the Thoothukudi and Mandapam, Gulf of Mannar. The second sampling station was reaches to the Kasimedu landing centre from the Chennai Coast.

A total of 24 vertebrae were observed in the X-ray image. In the first pre-dorsal region, two vertebrates then the second pre-dorsal region ten vertebrates and the pre-anal region eleven vertebrates were numbered. Subsequently, the bases of the first dorsal fin vertebrae are 4, second dorsal fin vertebrae is six and the anal fin have six vertebrates numbered sequentially.

Otoliths were observed under the stereomicroscope. The rostrum is well developed, and the anterior and posterior rostrum is slightly bent down to the left and right sides of the otolith. It represented the 3–4 annular rings (Fig. 4). The upper and lower limb of the gill counts were observed under the microscope (Fig. 3).

Scale images were observed under the stereomicroscope. The most common scale type in the studied species was cycloid. The scale demonstrated variations in morphology from the different body regions. The shape of the scale was of four different types: round shape being the most common, inter-dorsal, anal, head and caudal scales are round in shape except the pelvic scale (oval in shape), centre of the body scales are square shape, pectoral scale (semi-rectangle shape), with 10–12 radii, lateral line scale (slightly hexagon shape) having the large size of focus (Fig. 5).

The molecular analysis of the mtDNA barcoding results showed that the species *Sphyraena forsteri* as valid. The pairwise sequence comparison between entire clades of

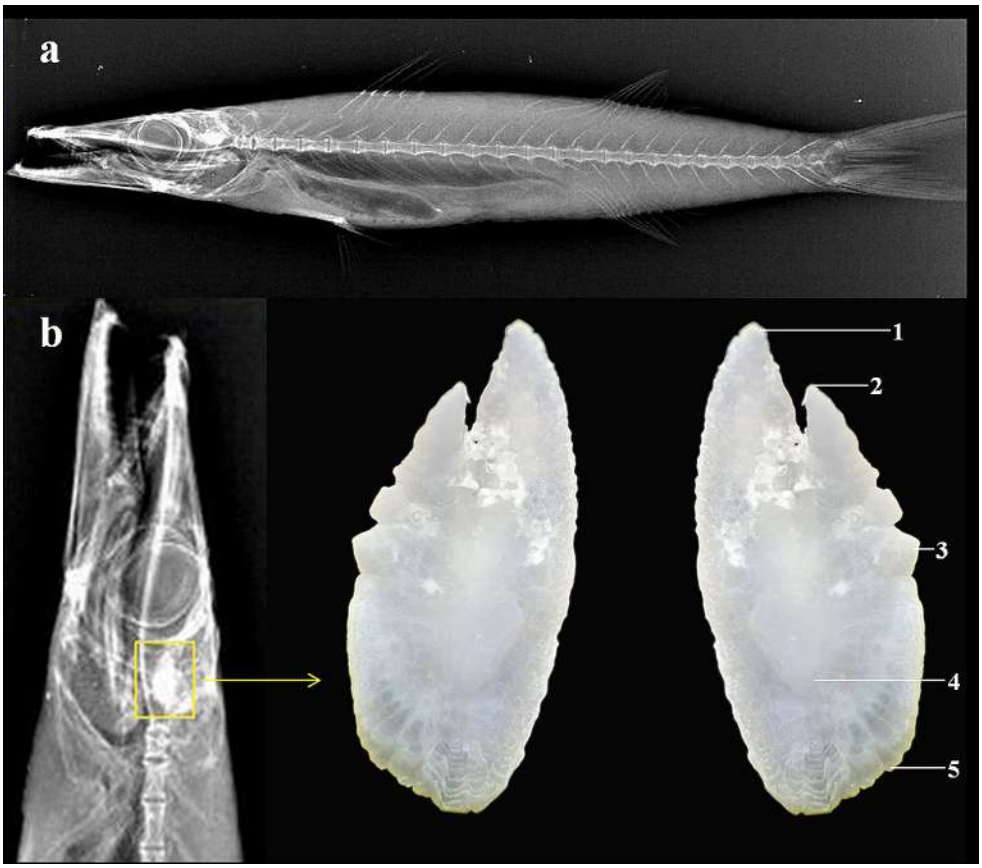

Fig. 4 Radiograph image of **a** *Sphyraena forsteri*, Non-type SPHSFOR/NBFGR with 24 vertebrae (11-abdominal region and 13-caudal region) **b** otolith morphology of *Sphyraena forsteri*, collected from the left and right sides of the dorsal region;1 rostrum, 2 antirostrum, 3 lobes 4 sulcus acusticus, 5 Postrostrum

the same genus *Sphyraena* clearly elucidate the phylogenic analysis with highest bootstrap values 100% and 0.2% K2P distance value (Fig. 6).

Comparisons

The morphometric measurements and meristic counts of the collected samples confirmed the species *S. forsteri* and compared based on the earlier reports (Table 2). It is most similar to *Sphyraena qenie* with the traits of last ray of the anal fin and the second dorsal fin distinctly elongated, caudal fin is completely black (Senou 2001). *S. forsteri* (Cuvier 1829) is distinguished from *S. qenie* by having the four major considerable characters: an inky blotch under the base of the pectoral fin vs. absence of inky blotches; Body with 18–20 lateral bands vs. absence of body markers; absence of gill raker on the first gill arch vs. 10–20 small peculiar spines present on the first-gill arch respectively; comparing to other species *S. forsteri* have enlarged eyes.

Remarks

The species *Sphyraena forsteri* was originally described in Cuvier's (1829) report based on Esox sphyraenoides bank library followed by Bleeker (1854) and Gunther (1860). The barracudas (Pisces: Sphyraenidae) was first reported from the Indian Ocean as *Sphyraena toxeuma* (Fowler 1903) ranging from 243 to 640 mm in SL. But this name was not accepted in the World Register of Marine Species. The comparative data for *Sphyraena toxeuma* was reported mistakenly by several authors (Fowler 1903; Jordan and Seale 1905; Weber and de Beaufort 1922; Fowler 1928; Schultz 1953; Fourmanoir 1954). Finally, the species was validated as *Sphyraena forsteri* (Smith 1956; Fourmanoir 1957) by Eschmeyer's Catalog of Fishes (Fricke et al. 2023). *Sphyraena forsteri* was remarkable as the absence of gill raker in the first gill arch; body markers are absent. *S. forsteri* is distinguished from the closely related species *Sphyraena qenie* by the tiny size of the body scales and comparing to the other congeners of the species; eyes are enlarged in size and gill raker is absent despite the presence of minute spines on the first gill arch.

Discussion

The lack of detailed taxonomy studies of *Sphyraena* genus from Indian waters need detailed study in the area. Further, molecular studies are required to resolve the complexity in the identification of species, understand the status of

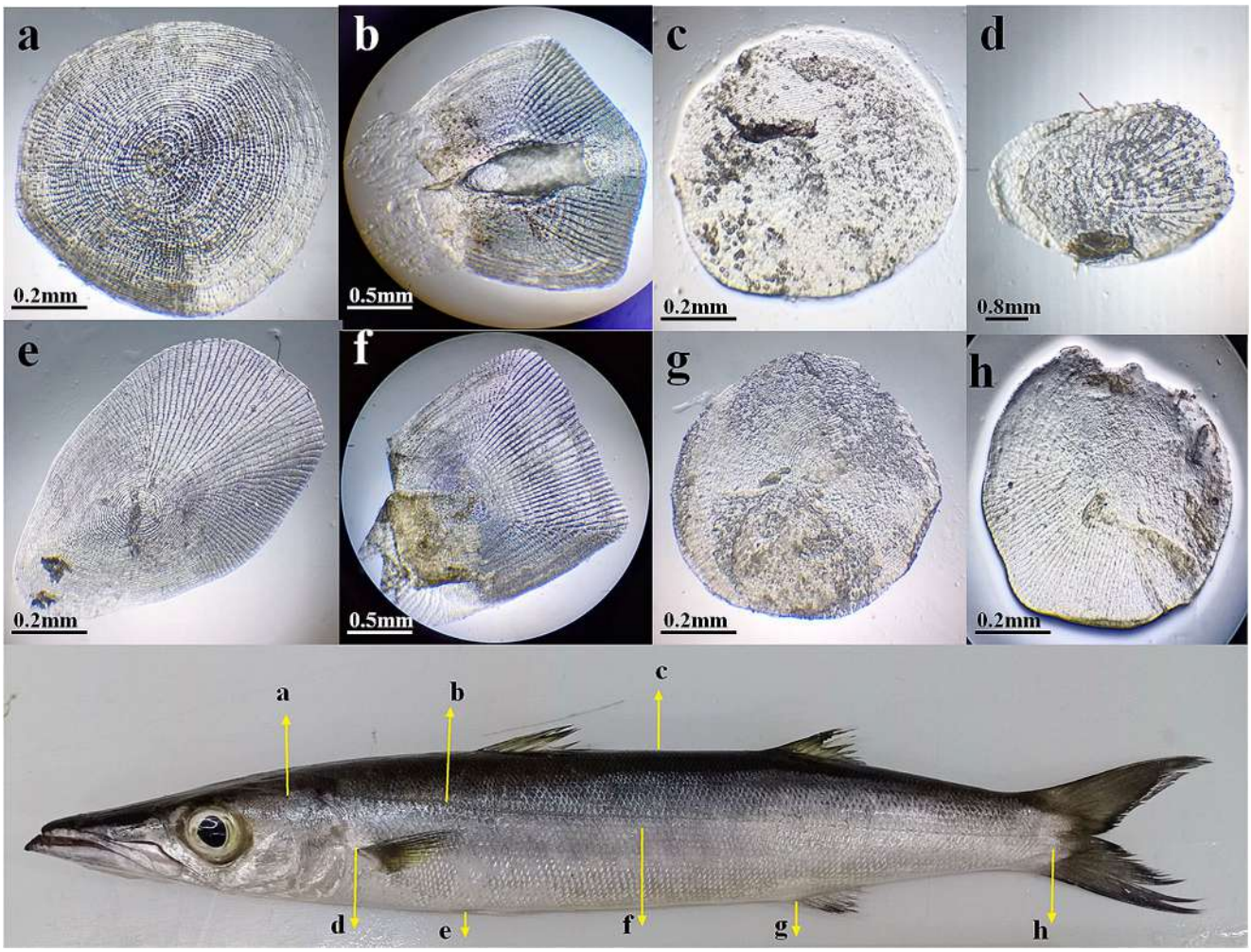

Fig. 5 Body scales of *Sphyraena forsteri* were collected from various parts **a** Collected from the head region **b** Lateral line scale-collected on the LL **c** Inter-dorsal scale were collected between the two dorsal fins **d** Pectoral scale -collected from the insertion point of the pectoral fin **e** Pelvic scale -collected from the insertion point of the pelvic region **f** Body scale -collected from the centre region of the trunk **g** Anal scale -collected from the anal origin of anal fin **h** Caudal scale- collected from the caudal peduncle region

Sphyraena forsteri diversity. *Sphyraena forsteri* is one of the least morphologically and genetically investigated species in Indian waters. Studies on taxonomical and molecular approach of the species are not reported. This species was initially described by Cuvier in the year 1829. The first mistakable description of big eye barracuda was relevant due to the wide geographical areas and age and maturity stage of the specimen to report (Fowler 1903) in the Museum of National d'Histoire Naturelle, Paris. Although, the species were discussed by many authors (Weber and de Beaufort 1922) for certain noticeable corrections, they were designated as a neotype (Fowler 1928; Schultz 1953; Smith 1956; Klausewitz and Bauchot 1967). The species was distributed along the West (Kapoor et al. 2022) and east coast (Mostly in subareas) abundant from a depth of 50–70 m. Our measurement description closely resembles the descriptions of Fowler (1928) from the East African, Schultz (1953) from Western Pacific and Smith (1956) from Western Indian Ocean.

Among the 29 extant species more than four have the molecular document (Doiuchi and Nakabo 2007) including *S. barracuda* with 630 bp of mt-Cytb gene (Rabosky et al. 2014), S. *obtusata* with 800 bp fragments of Cytb (Daly-Engel et al. 2012), ray – finned fishes of 14 *Sphyraena* species with their megaphylogeny, nevertheless 90% of missing data. Currently, no molecular studies are focused on *Sphyraena forsteri.* The molecular approach of the present study was fully supported to the monophyletic species, the nuclear markers like cytochrome oxidase subunit I (COI) are used to analyse the phylogenetic relationship of the species *S. forsteri*. Conventionally barracuda's are mostly relavent to mackerals, allies and tunas for based on their morphological characters. Hence, in the present study Scombriformes: suborder Scombroidei (Johnson 1986) was considered as a sister

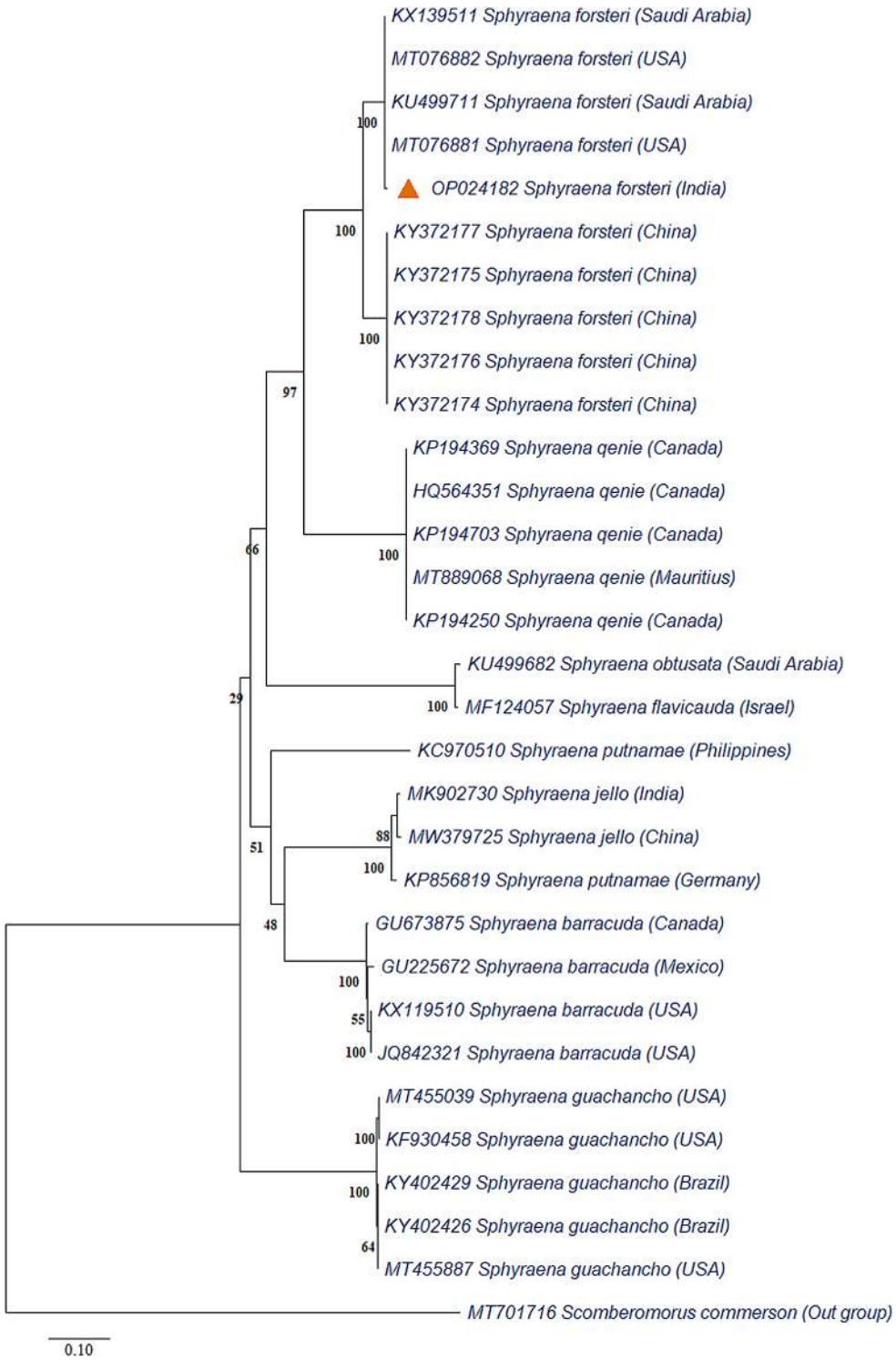

Fig. 6 *Sphyraena forsteri* is related based on phylogenetic tree with partial mitochondrial COI gene sequences (668 bp) Support values indicated along branches. Each node labelled with GenBank accession number and their collected countries

clade of the evolutionary history. The specimens of *S. forsteri* were characterized using mtDNA (COI gene sequencing). This analysis involved 31 nucleotide sequences and one out group (Family: Scombridae). The BLAST result shows 99.8% sequence similarity with another sequence of *Sphyraena forsteri* (Ac. No- KU499711) collected from Saudi Arabia with highest bootstrap value of 0.2% pair wise K2P genetic distance value. In the maximum like hood tree the species *S. forsteri* (Cuvier 1829) forms a sister clade of the same species *S. forsteri* (Cuvier 1829) with 0.2% and 3.3% distance value collected from USA, Saudi Arabia and China respectively. The next clade were formed by other species within the genus *S. qenie* (Klunzinger 1870) with 9.0% distance value collected from Canada and Mauritius,16.0%

Table 2 Comparison of proportional range between the *Sphyraena forsteri*

% of Standard Length	Sphyraena forsteri	Sphyraena toxeuma (Fowler 1928)	
	Present Study	Western Indian Ocean Smith (1956)	East African Coast (Fowler, 1925)
Head length	30.1–34.9	32–33	31.7–34.4
Body depth	13.1–16.9	13–14	13.0–14.4
Eye diameter	5.9–9.8	4.8–5.4	4.8–5.7
Snout length	12.0–16.8	14.5–16	13.7–15.6
Inter-orbital	4.0–5.0	4.2–5.5	6.2–7.8
Postorbital	11.1–13.1	11–12	10–11.0
Depth of caudal peduncle	6.6–9.2	5.6–6.2	5.5–6.4
Snout to 1st dorsal	40.9–48.7	40–43	40.7–43.9
In standard length (SL)	**Present Study**	***S. toxeuma*** (Fowler 1928) **East African Specimen**	***S. forsteri*** **C.V Western Pacific** (Schultz 1953)
Head	2.9–3.3 (3.1)	2.90–3.15	3
Depth	5.9–7.7 (6.6)	6.94–7.68	6.4–7
Snout to first dorsal	2.1–2.4 (2.2)	2.26–2.44	–
Distance between origin of dorsal fins	2.9–3.8 (3.5)	3.30–3.72	–
In Head length	3.3–5.5 (4.1)	5.5–6.47	4.5–4.7
Eye diameter	2.0–2.7 (2.3)	2.18–2.36	–
Snout length	6.8–8.6 (7.7)	6.42–7.91	–
Inter-orbital length	2.4–2.9 (2.7)	2.61–3.31	–
Postorbital length	3.5–5.0 (4.6)	4.9–2-6	–
Depth of caudal peduncle	2.6–4.5 (3.3)	2.8–3.41	–
Pectoral to pelvic	1.66–1.45	1.45–2.10	1.3–1.4
In Postorbital Eye Pectoral to Pelvic	1.35–1.05	1.20–1.54	–

and 18.3% with *Sphyraena putnamae* (Jordan and Seale 1905) collected from Germany and Philipines, *Sphyraena barracuda* (Edwards 1771) with 16.2% and 16.5% collected from USA, Canada and Mexico respectively, *Sphyraena jello* (Cuvier 1829) with 16.5% distance value from India and China18.0% and 18.4% with other species *Sphyraena guachancho* (Cuvier 1829) collected from Brazil and USA. Finally, the lowest genetic distance value was observed in *Sphyraena flavicauda* (Ruppell 1838) with 21.4% and *Sphyraena obtusata* (Cuvier 1829) with 21.7% collected from Israel and Saudi Arabia.

The present result provides the detailed taxonomic description along with the genetic information of *Sphyraena forsteri* (bigeye barracuda) from Indian water. The results can be used to validate the *Sphyraena forsteri* taxonomical identification and to conserve the fisheries resources along the Southeast coast of India. The present study brings a new insight and inference for the researchers and for conservation of the species from Southeast coast of India.

Acknowledgements Authors are thankful for the RUSA Scheme Phase 2.0 grant [F-24-51/2014–U, Policy (TN Multi-Gen), Department of Education, Govt. of India. Dt. 09.10.2018]. Authors acknowledge Indian Council of Agricultural Research - National Bureau of Fish Genetic Resources (ICAR-NBFGR), Cochin for accepting the sample as non-type specimen. The authors thank the fisher people for providing samples and useful information. Ms. Sivaranjani would like to express thankfulness to the Head, Department of Fisheries Science, Alagappa University for the financial support under RUSA TBRP-Project Fellow.

Author Contributions SS: Conceptualization, methodology, resources, investigation, software, writing—original draftKK: Methodology, data curation, formal analysis RK: Reviewing MK: MethodologyDD: AssistingKE: Supervision, administration.

Funding RUSA Scheme Phase 2.0 grant [F-24-51/2014–U, Policy (TN Multi-Gen), Department of Education, Govt. of India. Dt. 09.10.2018].

Data Availability The data that support the findings of this study are available from the corresponding author upon request.

Declarations

Ethical Approval Fishes used in this study are commercially available edible fishes. This research did not include the use of live animals. All fish used in this study were sampled as part of ongoing commercial and recreational fisheries sampling. This sampling project collected data to monitor commercial and recreational fisheries to promote sustainable fisheries management. As no fish was harvested intentionally for this study, no approval of research ethics committee was required to accomplish the goals of this study.

Competing Interests The authors have no relevant financial or non-financial interests to disclose.

References

Abdussamad EM, Retheesh TB, Thangaraja R, Bineesh KK, Prakasan D (2015) *Sphyraena arabiansis* a new species of Barracuda (Family: Sphyraenidae) from the south-west coast of India. Indian J Fish 62(2):1–6

Ballen GA (2019) Nomenclature of the Sphyraenidae (Teleostei: Carangaria): a synthesis of fossil-and extant-based classification systems. Zootaxa 4686(3):397–408
Bleeker P (1854) Nalezingen op de Ichthyologie van Japan. Bijdrage tot de kennis der Sphyraenoiden van den Indischen Archipel. Batavia, 22 p
Casteel RW (1976) Fish remains in archaeology and paleo-environmental studies. Academic, London
Cuvier G (1829) Achille valenciennes Histoire naturelle des poisons, Bertrand
Daly-Engel TS, Randall JE, Bowen BW (2012) Is the great Barracuda (Sphyraena barracuda) a reef fish or a pelagic fish? The phylogeographic perspective. Mar Biol 159:975–985
Dapar MLG, Torres MAJ, Fabricante PK, Demayo CG (2012) Scale morphology of the Indian goatfish, *Parupeneus indicus* (Shaw, 1803) (Perciformes: Mullidae). Adv Environ Biol 6(4):1426–1432
Day F (1876) The fishes of India; being a natural history of the fishes known to inhabit the seas and fresh waters of India, Fishes India Part 2, Burma and Ceylon
Diaz-Viloria N, Sanchez-Velasco L, Perez-Enriquez R (2005) Inhibition of DNA amplification in marine fish larvae preserved in formalin. J Plankton Res 27:787–792
Doiuchi R, Nakabo T (2007) Molecular evidence for the taxonomic status of three species of the *Sphyraena obtusata* group (Perciformes: Sphyraenidae) from East Asia. Ichthyol Res 54:313–316
Edwards M (1771) Appendix. In: Catesby M (ed) The natural history of California, Florida and the Bahama, Islands. Third edition. Printed by author, London
Felsenstein J (1985) Confidence limits on phylogenies: an approach using the bootstrap. Evol 39(4):783–791
Fourmanoir P (1954) Ichthyologie et pêche aux, Comores
Fourmanoir P (1957) Poissons Téléostéens des eaux malgaches du canal de Mozambique (vol:1). Institut scientifique de, Madagascar
Fowler HW (1903) New and little known Mugilidae and Sphyraenidae. Proc Acad Nat 743–752
Fowler HW (1904) A collection of fishes from Sumatra. J Acad Nat Sci Phila (Ser 2) 12:495–560
Fowler HW (1928) The fishes of Oceania, Mem. Bish Mus 10:1–540
Fricke R, Eschmeyer WN, Fong JD (2023) Eschmeyer's Catalog of Fishes: Genera/Speciesby Family/Subfamily.http://researcharchive.calacademy.org/research/ichthyology/catalog/Species, Accessed 15th December 2023
Gunther A (1860) Squamipinnes, Cirrhitidae, Triglidae, Trachinidae, Sciaenidae, Polynemidae, Sphyraenidae, Trichiuridae, Scombridae, Carangidae, Xiphiidae. Catalogue of the acanthopterygian fishes in the collection of the British Museum. Natural History), London
Hall TA (1999) BioEdit: a user-friendly biological sequence alignment editor and analysis program for Windows 95/98/NT. Nucleic Acids Symp Ser 41:95–98
Johnson GD (1986) Scombroid Phylogeny: an alternative hypothesis. Bull Mar Sci 39(1):1–41
Jordan DS, Seale A (1905) The fishes of Samoa: description of the species found in the Archipelago, with a provisional check-list of the fishes of Oceania. Bull Bureau Fisheries 25:173–455
Kannan K, Kodeeswaran P, Kumar R, Madhuri K, Divya D, Kannapiran E (2021a) Length-weight relationship of Coral reef-associated fishes from Gulf of Mannar and Palk Bay, Southeast Coast of India. J Appl Ichthyol 37(1):162–164
Kannan K, Sivaranjani S, Kumar R, Karuppasamy K, Prabhu NM, Kannapiran E (2021b) Length-weight relationship of six demersal fish species from Gulf of Mannar, Bay of Bengal, Eastern Indian Ocean. J Appl Ichthyol 37(2):367–369
Kannan K, Kumar R, Raja S, John S, Kannapiran E (2023) Molecular taxonomy and distribution status of *Odontanthias perumali* (Talwar, 1976) from Bay of Bengal. East Indian Ocean Thalassas 39:1039–1045
Kapoor D, Dayal R, Ponniah AG (2002) Fish biodiversity of India. National Bureau of Fish Genetic Resources Lucknow, India
Klausewitz W, Bauchot ML (1967) Rehabilitation De *Sphyraena forsteri* Cuvier in Cuv. Val 1829 et designation d'un ngotype (Pisces, Mugiliformes, Sphyraenidae). Bull Mus Nat Hist Nat 39:117–120
Klunzinger KB (1870) Synopsis Der fische des Rothen Meeres. C. Ueberreuter'she Buchdruckerei, Germany
Kumar STP, Aswath N (2016) DNA isolation from teeth by organic extraction and identification of sex of the individual by analyzing the AMEL gene marker using PCR. J Forensic Dent 8(1):18
Kumar S, Stecher G, Li M, Knyaz C, Tamura K (2018) MEGA X: Molecular Evolutionary Genetics Analysis across computing platforms. Mol Biol Evol 35(6):1547–1549
Lippitsch E (1995) Scale and squamation character polarity and phyletic assessment in the family Cichlidae. J Fish Biol 47(1):91–106
Morishita S, Miki R, Wada H, Itou M, Motomura H (2020) Morphological comparisons of *Sphyraena qenie* with *S.putnamae*, with a revised key to Indo-Pacific species of Sphyraena lacking gill rakers (Sphyraenidae). Ichthyol Res 67:456–463
Myers RF (1991) Micronesian reef fishes, Second edn. Coral Graphics, Barrigada, Guam
Rabosky DL, Hutchinson MN, Donnellan SC, Talaba AL, Lovette IJ (2014) Phylogenetic disassembly of species boundaries in a widespread group of Australian skinks (Scincidae: Ctenotus). Mol Phylogenet Evol 77:71–82
Rafinesque CS (1815) Analyse de la nature, ou tableau de l'univers et des corps organises. Aux depens de l'auteur. (No. 177)
Rose AF (1793) Petri Artedi Angermannia–Sueci synonymia nominum piscium fere omnium. Ichthyologiae pars IV, editio II, AF Röse, Grypeswald (Greifswald), Germany
Rose JH (1984) Sphyraenidae. In W. Fischer and G. Bianchi (eds.) FAO species identification sheets for fishery purposes. Western Indian Ocean (Fishing Area 51). FAO, Rome
Ruppell WPES (1838) Fische des rothen Meeres.[Fische aus dem rothen Meere.]. Ruppell WPES Neue Wirbelthiere zu der Fauna von Abyssinien gehorig. Siegmund Schmerber, Frankfurt am Main. 148 pages and 33 figure plates
Saitou N, Nei M (1987) The neighbor-joining method: a new method for reconstructing phylogenetic trees. Mol Biol Evol 4(4):406–425
Schultz LP (1953) Family Sphyraenidae: Barracudas. Families from Asymmetrontidae through Siganidae
Secor DH, Dean JM, Laban EH (1992) Otolith removal and preparation for microstructural examination. Otolith microstructure examination and analysis. Can J Fish Aquat 117:19–57
Senou H (2001) Sphyraenidae. Barracudas. In: Carpenter KE, Niem V (eds) FAO species identification guide for fishery purposes. The living marine resources of the Western Central Pacific. Bony fishes part 4 (Labridae to Latimeriidae), estuarine crocodiles. FAO, Rome, pp 3685–3697
Smith JLB (1956) The fishes of the family Sphyraenidae in the western Indian Ocean. Ichthyol.Bull. Rhodes Univ. (3): 37–46 fig pls 1–2
Ward RD, Zemlak TS, Innes BH, Last PR, Hebert PD (2005) DNA barcoding Australia's fish species. Philos Trans R Soc Lond B Biol Sci 360(1462):1847–1857
Weber M, De Beaufort LF (1922) The fishes of the Indo-Australian Archipelago. IV. Heteromi, Solenichthyes, Synentognathi, Percesoces, Labyrinthici, Microcyprini. E J Brill Leiden 4:1–410

ANNA UNIVERSITY
REGIONAL CAMPUS COIMBATORE

Dr. K. RAJASEKAR, Ph.D.,
BOYSCAST Fellow (MIT, Boston, USA)
Assistant Professor – Chemistry

Phone (Off): 0422 6942501
Mobile:9442392728

Letter of Appreciation for Successful Collaboration

To: **08.04.2024**

Dr. M. Santhoshkumar
Assistant Professor, Department of Biochemistry
Kongunadu Arts and Science College (Autonomous)
Coimbatore - 641029

Dear Dr. M. Santhoshkumar,

I am writing to convey my heartfelt appreciation for the successful research collaboration between Anna University Regional Campus, Coimbatore, and Kongunadu Arts and Science College, Coimbatore

The research projects undertaken by Ms. Kavya M. (Reg. No. 222BC004) and Ms. Sneha R. (Reg. No. 222BC005) on the topics *"Smart Nanocarrier: Graphene Oxide Decorated with Nickel Nanowire for Optimized Delivery of Herbal Medicinal Agent 'Plumbago Indica' for Breast Cancer (MCF-7)"* and *"Graphene Oxide Nickel Nanowire Composite for the Targeted and Sustained Delivery of Semecarpus Anacardium—The Herbal Drug for Breast Cancer (MCF-7)"*, respectively, are excellent examples of innovative and impactful research.

I deeply appreciate the dedication and hard work of the students, who spent three months at our campus to complete the experimental phases of their projects. Your mentorship, Dr. M. Santhoshkumar, has been invaluable in guiding them throughout their research journey. Your expertise and unwavering support have significantly contributed to the successful completion of their dissertations.

Furthermore, this collaboration has been a testament to the strong research bond between our institutions. Dr. M. Santhoshkumar, your efforts in fostering interdisciplinary research and promoting innovative ideas have been instrumental in achieving these outstanding results.

I am confident that this partnership will continue to grow, leading to even more groundbreaking research in the future. Thank you once again for your exceptional contributions, and I look forward to further strengthening our collaboration.

Warm regards,

Dr. K. Rajasekar
Assistant Professor, Department of Chemistry
Anna University Regional Campus, Coimbatore
Coimbatore - 641046

Fwd: Acceptance of Laboratory Works Proposal for PG Students

2 messages

222BC005 Sneha Rajagopal <222bc005@kongunaducollege.ac.in> Tue, Dec 19, 2023 at 11:36 AM
To: "M.Santhoshkumar Assistant Professor" <msanthoshkumar_bc@kongunaducollege.ac.in>

---------- Forwarded message ---------
From: **Rajasekar K** <rajasekar@aurcc.ac.in>
Date: Tue, Dec 19, 2023, 10:45 AM
Subject: Acceptance of Laboratory Works Proposal for PG Students
To: <222bc005@kongunaducollege.ac.in>

Dear Dr. Santhosh,
We appreciate your interest in conducting laboratory works in our Nanotechnology Lab at Anna university regional campus, Coimbatore.

After careful consideration, we are pleased to inform you that your proposal has been accepted. Your PG students are welcome to commence their laboratory works in Nanotechnology Lab starting from December 20, 2023, for a duration of one month.

Please ensure that all necessary arrangements are made, and our team will be available to assist as needed. We look forward to a productive collaboration.

Best regards,
Rajasekar

Sent from my iPhone

M.Santhoshkumar Assistant Professor <msanthoshkumar_bc@kongunaducollege.ac.in> Tue, Dec 19, 2023 at 12:13 PM
To: rajasekar@aurcc.ac.in

Dear Prof. Rajasekar Sir,
I am very much grateful for your kind acceptance. I am sure that my students will work sincerely to synthesize the drug compounds in your laboratory. I will arrange necessary On-Duty for my students to commence the project work.
I am hereby acknowledging your email communication.
[Quoted text hidden]

CERTIFICATE

This is certified that the dissertation entitled "Graphene oxide nickel nanowire composite for the targeted and sustained delivery of *Semecarpus anacardium*- the herbal drug for breast cancer (MCF-7)" submitted by **SNEHA. R (222BC005)** to the Department of Biochemistry, Kongunadu Arts and Science College (Autonomous), Affiliated to Bharathiyar University, in partial fulfillment of the requirement for the **Degree of Master of Science in Biochemistry** is a record of bonafide and original research work carried out by his during the period of 2023-2024 of his study, under the supervision and guidance of **Dr. M. SANTHOSHKUMAR., M.Sc., Ph.D., (SET)., B.Ed., PGDCRP., PGDBI., Assistant professor,** Department of Biochemistry, Kongunadu Arts and Science College (Autonomous),Coimbatore-641 029. The results embodied in this dissertation is new and has not been submitted for the award of any Degree/Diploma/Associate/Fellowship or any other similar title to any candidate.

M. Santhoshkumar

Signature of the Guide

Dr. M. SANTHOSHKUMAR M.Sc.,Ph.D.,
Assistant Professor of Biochemistry
Kongunadu Arts and Science College
G.N.Mills Post, Coimbatore - 641029.

Place: Coimbatore

Date: 27/3/24

27/3/24

Head
Department of Biochemistry
(PG & Research)
Kongunadu Arts and Science College
Coimbatore - 641 029

Head of the Department

Counter signed by

27/3/24

Signature of the Principal

PRINCIPAL
Kongunadu Arts & Science College

Submitted for the Viva-Voce examination held on 29/4/2024 at Kongunadu Arts and Science College (Autonomous), Coimbatore-641029.

Examiners

1. 22/4/24
(Dr. G. KARTHIKEYAN)

2. M. Santhoshkumar 22/4/24
(Dr. M. SANTHOSHKUMAR)

CERTIFICATE

This is certified that the dissertation entitled "Graphene oxide nickel nanowire composite for the targeted and sustained delivery of *Semecarpus anacardium*- the herbal drug for breast cancer (MCF-7)" submitted by **SNEHA. R (222BC005)** to the Department of Biochemistry, Kongunadu Arts and Science College (Autonomous), Affiliated to Bharathiyar University, in partial fulfillment of the requirement for the **Degree of Master of Science in Biochemistry** is a record of bonafide and original research work carried out by his during the period of 2023-2024 of his study, under the supervision and guidance of **Dr. M. SANTHOSHKUMAR., M.Sc., Ph.D., (SET)., B.Ed., PGDCRP., PGDBI., Assistant professor,** Department of Biochemistry, Kongunadu Arts and Science College (Autonomous),Coimbatore-641 029. The results embodied in this dissertation is new and has not been submitted for the award of any Degree/Diploma/Associate/Fellowship or any other similar title to any candidate.

M. Santhoshkumar

Signature of the Guide

Dr. M. SANTHOSHKUMAR M.Sc.,Ph.D.,
Assistant Professor of Biochemistry
Kongunadu Arts and Science College
G.N.Mills Post, Coimbatore - 641029.

Place: Coimbatore

Date: 27/3/24

27/3/24

Head
Department of Biochemistry
(PG & Research)
Kongunadu Arts and Science College
Coimbatore - 641 029

Head of the Department

Counter signed by

27/3/24

Signature of the Principal

PRINCIPAL
Kongunadu Arts & Science College

Submitted for the Viva-Voce examination held on 29/4/2024 at Kongunadu Arts and Science College (Autonomous), Coimbatore-641029.

Examiners

1. 22/4/24
(Dr. G. KARTHIKEYAN)

2. M. Santhoshkumar 22/4/24
(Dr. M. SANTHOSHKUMAR)